

This electronic thesis or dissertation has been downloaded from the King's Research Portal at <https://kclpure.kcl.ac.uk/portal/>



The rich conformational landscape of musks and their precursors revealed by broadband rotational spectroscopy

Burevschi, Cate

Awarding institution:
King's College London

The copyright of this thesis rests with the author and no quotation from it or information derived from it may be published without proper acknowledgement.

END USER LICENCE AGREEMENT



Unless another licence is stated on the immediately following page this work is licensed

under a Creative Commons Attribution-NonCommercial-NoDerivatives 4.0 International

licence. <https://creativecommons.org/licenses/by-nc-nd/4.0/>

You are free to copy, distribute and transmit the work

Under the following conditions:

- Attribution: You must attribute the work in the manner specified by the author (but not in any way that suggests that they endorse you or your use of the work).
- Non Commercial: You may not use this work for commercial purposes.
- No Derivative Works - You may not alter, transform, or build upon this work.

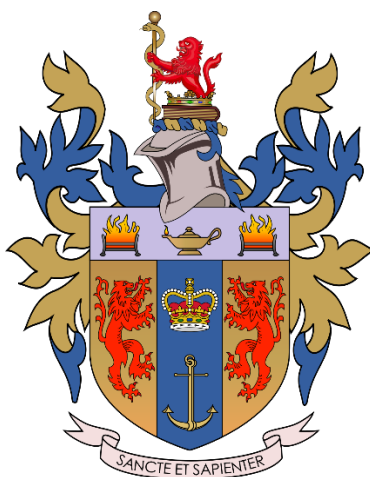
Any of these conditions can be waived if you receive permission from the author. Your fair dealings and other rights are in no way affected by the above.

Take down policy

If you believe that this document breaches copyright please contact librarypure@kcl.ac.uk providing details, and we will remove access to the work immediately and investigate your claim.

The Rich Conformational Landscape of Musks and their Precursors Revealed by Broadband Rotational Spectroscopy

Ecaterina Burevschi



PhD Thesis submitted in compliance with King's
College London regulations for Doctor of
Philosophy degree

Department of Chemistry
Faculty of Natural & Mathematical Sciences
King's College London

ACKNOWLEDGEMENTS

I would like to sincerely thank my supervisor Dr. Maria Sanz, who has inspired this work and believed in my ability to deliver it. I would also like to thank Maria for the constant support, guidance and motivation over these years, it wouldn't have been possible without her.

I would like to thank and acknowledge Firmenich and specifically Dr. Alec Birkbeck, for providing samples and insightful discussions on the behaviour and smell of musk odorants.

Sending big thanks to the rest of the team Shefali Saxena and Seema (Indy) Murugachandran, who have always been there to help me in the lab, coming up with solutions whenever things went wrong and for all our insightful discussions. Many thanks to Dr. Donatella Loru and Dr. Isabel Pena for training me to use the instrument and teaching me the fundamentals in the field. I would also like to thank other temporary members of the group: Safia Hussain, Sanjana Panchagnula, Dr. Elena R. Alonso.

I would like to send my thanks to the rest of the Britannia House and the Chemistry Department for being a supportive and inclusive community.

Many thanks to the Microwave community for appreciating my work at conferences and meetings, and especially I would like to thank Dr. Pascal Drean and Dr. Qian Gou groups for our collaborations in the past years.

I would also like to thank King's College and the funding body EPSRC for financially supporting my research.

Last but not least, I would like to send huge thanks to my family and friends who have been there for me during these four years: my parents who have never stopped believing in me and to who I owe all my successes; Callum, Anna and Henry who have always been there to celebrate my achievements and to support me during the most challenging times; Magd, Caleb, Jackson, Camille, Maddy, Doina and Sorina for staying good friends over the years.

Many thanks to all the people I met during my academic life at King's, in conferences, outreach and academic events and outside academia.

LIST OF PUBLICATIONS

Burevschi, E., Pena, I., Sanz, M. E., Medium-sized rings: conformational preferences in cyclooctanone driven by transannular repulsive interactions. *Phys. Chem. Chem. Phys.*, 2019, **21**, 4331-4338.

Burevschi, E., Alonso, E. R., Sanz, M. E., Binding Site Switch by Dispersion Interactions: Rotational Signatures of Fenchone–Phenol and Fenchone–Benzene Complexes. *Chemistry – A European Journal*, 2020, **26**, 49, 11327-11333.

LIST OF TABLES

CHAPTER 2

Table 2.1. Selection rules for the quantum numbers K_{-1} and K_{+1} for each dipole moment.

CHAPTER 4

Table 4.1. Ab initio spectroscopic parameters for conformers of cyclooctanone.

Table 4.2. Experimental spectroscopic parameters of the three observed conformers of cyclooctanone compared with those obtained in a previous work.

Table 4.3. Experimental spectroscopic parameters for all singly substituted ^{13}C and ^{18}O isotopic species of the **BC1** conformer of cyclooctanone.

Table 4.4. Substitution coordinates of the heavy atoms of cyclooctanone **BC1**.

Table 4.5. Experimental bond lengths (\AA), angles and dihedral angles ($^\circ$) of **BC1** cyclooctanone (r_s and r_o structures), theoretical MP2 structural parameters, and structural parameters of cyclooctane.

Table 4.6. Comparison of bond lengths (\AA) and bond angles ($^\circ$) of cyclopentanone, cyclohexanone, cycloheptanone, and cyclooctanone.

CHAPTER 5

Table 5.1. Theoretical spectroscopic parameters and relative energies for the isomers of cyclooctanone- H_2O within 1000 cm^{-1} .

Table 5.2. Binding energy decomposition analysis in kJ mol^{-1} for the complexes of cyclooctanone- (H_2O) on their MP2 and B3LYP-D3BJ geometries, using SAPT(0)/jun-cc-pDVZ calculations within Psi4.

Table 5.3. Theoretical spectroscopic parameters and relative energies for the isomers of cyclooctanone- $(\text{H}_2\text{O})_2$ within 600 cm^{-1} .

Table 5.4. Experimental spectroscopic constants of the observed isomers of cyclooctanone-water.

Table 5.5. Experimental spectroscopic parameters for all singly substituted ^{13}C and ^{18}O isotopic species of the water complexes of **BC1**.

Table 5.6. Comparison of the bond lengths (in Å) and angles (in degrees) of the heavy atoms of complexes of BC1–H₂O determined experimentally with the experimental structural parameters of BC1 monomer.

Table 5.7. Comparison of the bond lengths (in Å) and angles (in degrees) of the heavy atoms of complexes of BC1–(H₂O)₂ determined experimentally with the experimental structural parameters of BC1 monomer.

Table 5.8. Substitution coordinates of the heavy atoms of water complexes of BC1 in Å.

Table 5.9. B3LYP-D3BJ and MP2 spectroscopic parameters and relative energies for the gem-diol species within 1000 cm⁻¹. All calculations were performed with the 6-311++G(d,p) basis set.

CHAPTER 6

Table 6.1. Ab initio^a spectroscopic parameters for the conformers cyclododecanone within 850 cm⁻¹.

Table 6.2. Experimental spectroscopic parameters of the seven observed conformers of cyclododecanone.

Table 6.3. Experimental spectroscopic parameters for all singly substituted ¹³C isotopic species of conformer 1 of cyclododecanone.

Table 6.4. Substitution coordinates of the heavy atoms of conformer 1 of cyclododecanone in Å.

Table 6.5. Benchmarking of the theoretical rotational constants against the experimental ($A_{calc} - A_{exp}$)/ $A_{exp} \times 100\%$.

Table 6.6. Substitution and effective experimental bond lengths (Å), angles and dihedral angles (°) of conformer 1 of cyclododecanone, and B3LYP-D3BJ/6-311++G(d,p) equilibrium structural parameters of all observed conformers of cyclododecanone.

CHAPTER 7

Table 7.1. Experimental spectroscopic parameters of the conformers of muscone belonging to class I.

Table 7.2. B3LYP-D3BJ/6-311++G(d,p) theoretical spectroscopic parameters and relative energies of the conformers of muscone belonging to class I.

Table 7.3. *MP2/6-311++G(d,p) theoretical spectroscopic parameters and relative energies of the conformers of muscone belonging to class I.*

Table 7.4. *wB97XD/6-311++G(d,p) theoretical spectroscopic parameters and relative energies of the conformers of muscone belonging to class I.*

Table 7.5. *B2PLYP-D3BJ/def2TZVP theoretical spectroscopic parameters and relative energies of the conformers of muscone belonging to class I.*

Table 7.6. *Experimental spectroscopic parameters of the conformers of muscone belonging to class II.*

Table 7.7. *B3LYP-D3BJ/6-311++G(d,p) theoretical spectroscopic parameters and relative energies of the conformers of muscone belonging to class II.*

Table 7.8. *MP2/6-311++G(d,p) theoretical spectroscopic parameters and relative energies of the conformers of muscone belonging to class II.*

Table 7.9. *wB97XD/6-311++G(d,p) theoretical spectroscopic parameters and relative energies of the conformers of muscone belonging to class II.*

Table 7.10. *B2PLYP-D3BJ/def2TZVP theoretical spectroscopic parameters and relative energies of the conformers of muscone belonging to class II.*

Table 7.11. *Experimental spectroscopic parameters of the conformers of muscone belonging to class III.*

Table 7.12. *B3LYP-D3BJ/6-311++G(d,p) theoretical spectroscopic parameters and relative energies of the conformers of muscone belonging to class III.*

Table 7.13. *MP2/6-311++G(d,p) theoretical spectroscopic parameters and relative energies of the conformers of muscone belonging to class III.*

Table 7.14. *wB97XD/6-311++G(d,p) theoretical spectroscopic parameters and relative energies of the conformers of muscone belonging to class III.*

Table 7.15. *B2PLYP-D3BJ/6-311++G(d,p) theoretical spectroscopic parameters and relative energies of the conformers of muscone belonging to class III.*

Table 7.16. *Experimental spectroscopic parameters of the conformers of muscone belonging to class IV.*

Table 7.17. *B3LYP-D3BJ/6-311++G(d,p) theoretical spectroscopic parameters and relative energies of the conformers of muscone belonging to class IV.*

Table 7.18. MP2/6-311++G(d,p) theoretical spectroscopic parameters and relative energies of the conformers of muscone belonging to class IV.

Table 7.19. wB97XD/6-311++G(d,p) theoretical spectroscopic parameters and relative energies of the conformers of muscone belonging to class IV.

Table 7.20. B2PLYP-D3BJ/def2TZVP theoretical spectroscopic parameters and relative energies of the conformers of muscone belonging to class IV.

Table 7.21. Rotational constants of the assigned conformers predicted by B3LYP-D3BJ, MP2 and wB97XD levels of theory with 6-311++G(d,p), and B2PLYP-D3BJ with def2TZVP and the % errors calculated from experimental rotational constants as $(A_{THEOR} - A_{EXP})/A_{EXP}$.

CHAPTER 8

Table 8.1. B3LYP-D3BJ/6-311++G(d,p) spectroscopic parameters of the conformers of civetone within 450 cm^{-1} .

Table 8.2. wB97XD/6-311++G(d,p) spectroscopic parameters of the conformers of civetone within 450 cm^{-1} .

Table 8.3. MP2/6-311++G(d,p) spectroscopic parameters of the conformers of civetone within 450 cm^{-1} .

Table 8.4. Experimental spectroscopic parameters of the observed rotamers of civetone.

Table 8.5. Experimental and predicted rotational constants by B3YP-D3BJ, wB97XD and MP2, including deviation from the experiment; calculated as $(A_{THEOR} - A_{EXP})/A_{EXP} \times 100\%$.

CHAPTER 9

Table 9.1. Spectroscopic parameters of the conformers of civetone within 450 cm^{-1} predicted at the B3LYP-D3BJ/6-311++G(d,p) level of theory.

Table 9.2. Spectroscopic parameters of the conformers of civetone within 450 cm^{-1} predicted at the MP2/6-311++G(d,p) level of theory.

Table 9.3. Spectroscopic parameters of the conformers of civetone within 450 cm^{-1} predicted at the wB97XD/6-311++G(d,p) level of theory.

Table 9.4. Experimental spectroscopic parameters of the observed conformers of exaltolide.

Table 9.5. Intramolecular distances in the oblate conformers of exaltolide.

Table 9.6. Intramolecular distances in the prolate conformers of exaltolide.

Table 9.7. Theoretical rotational constants and the % deviation from experiment by B3LYP-D3BJ, MP2 and wB97XD levels of theory with 6-311++G(d,p) basis set.

CHAPTER 10

Table 10.1. B3LYP-D3BJ/6-311++G(d,p) spectroscopic rotational parameters, relative raw and ZPC energies for romandolide conformations within 700 cm^{-1} .

Table 10.2. B3LYP-D3BJ/def2-TZVP spectroscopic rotational parameters, relative raw and ZPC energies for romandolide conformations within 700 cm^{-1} .

Table 10.3. B3LYP-D3BJ/def2-QZVP spectroscopic rotational parameters and relative raw energies for romandolide conformations within 700 cm^{-1} .

Table 10.4. MP2/6-311++G(d,p) spectroscopic rotational parameters and relative raw energies for romandolide conformations within 700 cm^{-1} .

Table 10.5. B2PLYP-D3BJ/6-311++G(d,p) spectroscopic rotational parameters and relative raw energies for romandolide conformations within 700 cm^{-1} .

Table 10.6. Experimental spectroscopic constants of the observed conformers of romandolide.

Table 10.7. Theoretical rotational constants and the % deviation from experiment by B3LYP-D3BJ, MP2 and B2PLYP-D3BJ levels of theory with 6-311++G(d,p) basis set.

CHAPTER 11

Table 11.1. B3LYP-D3BJ/6-311++G(d,p) spectroscopic rotational parameters, relative raw and ZPC energies for helvetolide conformations within 500 cm^{-1} .

Table 11.2. MP2/6-311++G(d,p) spectroscopic rotational parameters, relative raw and ZPC energies for helvetolide conformations within 500 cm^{-1} .

Table 11.3. Experimental spectroscopic constants of the observed conformers of helvetolide.

Table 11.4. Theoretical rotational constants and the % deviation from experiment by B3LYP-D3BJ and MP2 with 6-311++G(d,p) basis set.

APPENDIX I

Table S4.1. Measured frequencies and residuals (in MHz) for the rotational transitions of the parent species of cyclooctanone BC1.

Table S4.2. Measured frequencies and residuals (in MHz) for the rotational transitions of the $^{13}\text{C}_1$ isotopologue of cyclooctanone BC1.

Table S4.3. Measured frequencies and residuals (in MHz) for the rotational transitions of the $^{13}\text{C}_2$ isotopologue of cyclooctanone BC1.

Table S4.4. Measured frequencies and residuals (in MHz) for the rotational transitions of the $^{13}\text{C}_3$ isotopologue of cyclooctanone BC1.

Table S4.5. Measured frequencies and residuals (in MHz) for the rotational transitions of the $^{13}\text{C}_4$ isotopologue of cyclooctanone BC1.

Table S4.6. Measured frequencies and residuals (in MHz) for the rotational transitions of the $^{13}\text{C}_5$ isotopologue of cyclooctanone BC1.

Table S4.7. Measured frequencies and residuals (in MHz) for the rotational transitions of the $^{13}\text{C}_6$ isotopologue of cyclooctanone BC1.

Table S4.8. Measured frequencies and residuals (in MHz) for the rotational transitions of the $^{13}\text{C}_8$ isotopologue of cyclooctanone BC1.

Table S4.9. Measured frequencies and residuals (in MHz) for the rotational transitions of the $^{13}\text{C}_9$ isotopologue of cyclooctanone BC1.

Table S4.10. Measured frequencies and residuals (in MHz) for the rotational transitions of the $^{13}\text{O}_7$ isotopologue of cyclooctanone BC1.

Table S4.11. Measured frequencies and residuals (in MHz) for the rotational transitions of cyclooctanone TBC1.

Table S4.12. Measured frequencies and residuals (in MHz) for the rotational transitions of cyclooctanone BC2.

APPENDIX II

Table S5.1. Measured frequencies and residuals (in MHz) for the rotational transitions of the parent species of BC1-1w-1 complex.

Table S5.2. Measured frequencies and residuals (in MHz) for the rotational transitions of the $^{13}\text{C}_1$ isotopologue of BC1-1w-1.

Table S5.3. Measured frequencies and residuals (in MHz) for the rotational transitions of the $^{13}\text{C}_2$ isotopologue of BC1-1w-1.

Table S5.4. Measured frequencies and residuals (in MHz) for the rotational transitions of the $^{13}\text{C}_3$ isotopologue of BC1-1w-1.

Table S5.5. Measured frequencies and residuals (in MHz) for the rotational transitions of the $^{13}\text{C}_4$ isotopologue of BC1-1w-1.

Table S5.6. Measured frequencies and residuals (in MHz) for the rotational transitions of the $^{13}\text{C}_5$ isotopologue of BC1-1w-1.

Table S5.7. Measured frequencies and residuals (in MHz) for the rotational transitions of the $^{13}\text{C}_6$ isotopologue of BC1-1w-1.

Table S5.8. Measured frequencies and residuals (in MHz) for the rotational transitions of the $^{18}\text{O}_7$ isotopologue of BC1-1w-1.

Table S5.9. Measured frequencies and residuals (in MHz) for the rotational transitions of the $^{13}\text{C}_8$ isotopologue of BC1-1w-1.

Table S5.10. Measured frequencies and residuals (in MHz) for the rotational transitions of the $^{13}\text{C}_9$ isotopologue of BC1-1w-1.

Table S5.11. Measured frequencies and residuals (in MHz) for the rotational transitions of the $^{18}\text{O}_{10}$ isotopologue of BC1-1w-1.

Table S5.12. Measured frequencies and residuals (in MHz) for the rotational transitions of the parent species of BC1-1w-2 complex.

Table S5.13. Measured frequencies and residuals (in MHz) for the rotational transitions of the $^{13}\text{C}_1$ isotopologue of BC1-1w-2.

Table S5.14. Measured frequencies and residuals (in MHz) for the rotational transitions of the $^{13}\text{C}_2$ isotopologue of BC1-1w-2.

Table S5.15. Measured frequencies and residuals (in MHz) for the rotational transitions of the $^{13}\text{C}_3$ isotopologue of BC1-1w-2.

Table S5.16. Measured frequencies and residuals (in MHz) for the rotational transitions of the $^{13}\text{C}_4$ isotopologue of BC1-1w-2.

Table S5.17. Measured frequencies and residuals (in MHz) for the rotational transitions of the $^{13}\text{C}_5$ isotopologue of BC1-1w-2.

Table S5.18. Measured frequencies and residuals (in MHz) for the rotational transitions of the $^{13}\text{C}_6$ isotopologue of BC1-1w-2.

Table S5.19. Measured frequencies and residuals (in MHz) for the rotational transitions of the $^{18}\text{O}_7$ isotopologue of BC1-1w-2.

Table S5.20. Measured frequencies and residuals (in MHz) for the rotational transitions of the $^{13}\text{C}_8$ isotopologue of BC1-1w-2.

Table S5.21. Measured frequencies and residuals (in MHz) for the rotational transitions of the $^{13}\text{C}_9$ isotopologue of BC1-1w-2.

Table S5.22. Measured frequencies and residuals (in MHz) for the rotational transitions of the $^{18}\text{O}_{10}$ isotopologue of BC1-1w-2.

Table S5.23. Measured frequencies and residuals (in MHz) for the rotational transitions of the parent species of BC1-2w-2a complex.

Table S5.24. Measured frequencies and residuals (in MHz) for the rotational transitions of the $^{13}\text{C}_1$ isotopologue of BC1-2w-2a.

Table S5.25. Measured frequencies and residuals (in MHz) for the rotational transitions of the $^{13}\text{C}_2$ isotopologue of BC1-2w-2a.

Table S5.26. Measured frequencies and residuals (in MHz) for the rotational transitions of the $^{13}\text{C}_3$ isotopologue of BC1-2w-2a.

Table S5.27. Measured frequencies and residuals (in MHz) for the rotational transitions of the $^{13}\text{C}_4$ isotopologue of BC1-2w-2a.

Table S5.28. Measured frequencies and residuals (in MHz) for the rotational transitions of the $^{13}\text{C}_5$ isotopologue of BC1-2w-2a.

Table S5.29. Measured frequencies and residuals (in MHz) for the rotational transitions of the $^{13}\text{C}_6$ isotopologue of BC1-2w-2a.

Table S5.30. Measured frequencies and residuals (in MHz) for the rotational transitions of the $^{18}\text{O}_7$ isotopologue of BC1-2w-2a.

Table S5.31. Measured frequencies and residuals (in MHz) for the rotational transitions of the $^{13}\text{C}_8$ isotopologue of BC1-2w-2a.

Table S5.32. Measured frequencies and residuals (in MHz) for the rotational transitions of the $^{13}\text{C}_9$ isotopologue of BC1-2w-2a.

Table S5.33. Measured frequencies and residuals (in MHz) for the rotational transitions of the $^{18}\text{O}_{10}$ isotopologue of BC1-2w-2a.

Table S5.34. Measured frequencies and residuals (in MHz) for the rotational transitions of the $^{18}\text{O}_{11}$ isotopologue of BC1-2w-2a.

Table S5.35. Measured frequencies and residuals (in MHz) for the rotational transitions of the parent species of BC1-2w-5a complex.

Table S5.36. Measured frequencies and residuals (in MHz) for the rotational transitions of the $^{13}\text{C}_1$ isotopologue of BC1-2w-5a.

Table S5.37. Measured frequencies and residuals (in MHz) for the rotational transitions of the $^{13}\text{C}_2$ isotopologue of BC1-2w-5a.

Table S5.38. Measured frequencies and residuals (in MHz) for the rotational transitions of the $^{13}\text{C}_3$ isotopologue of BC1-2w-5a.

Table S5.39. Measured frequencies and residuals (in MHz) for the rotational transitions of the $^{13}\text{C}_4$ isotopologue of BC1-2w-5a.

Table S5.40. Measured frequencies and residuals (in MHz) for the rotational transitions of the $^{13}\text{C}_5$ isotopologue of BC1-2w-5a.

Table S5.41. Measured frequencies and residuals (in MHz) for the rotational transitions of the $^{13}\text{C}_6$ isotopologue of BC1-2w-5a.

Table S5.42. Measured frequencies and residuals (in MHz) for the rotational transitions of the $^{18}\text{O}_7$ isotopologue of BC1-2w-5a.

Table S5.43. Measured frequencies and residuals (in MHz) for the rotational transitions of the $^{13}\text{C}_8$ isotopologue of BC1-2w-5a.

Table S5.44. Measured frequencies and residuals (in MHz) for the rotational transitions of the $^{13}\text{C}_9$ isotopologue of BC1-2w-5a.

Table S5.45. Measured frequencies and residuals (in MHz) for the rotational transitions of the $^{18}\text{O}_{10}$ isotopologue of BC1-2w-5a.

Table S5.46. Measured frequencies and residuals (in MHz) for the rotational transitions of the $^{18}\text{O}_{11}$ isotopologue of BC1-2w-5a.

APPENDIX III

Table S6.1. Measured frequencies and residuals (in MHz) for the rotational transitions of the parent species of conformer 1.

Table S6.2. Measured frequencies and residuals (in MHz) for the rotational transitions of the $^{13}\text{C}_1$ isotopologue of conformer 1.

Table S6.33. Measured frequencies and residuals (in MHz) for the rotational transitions of the $^{13}\text{C}_2$ isotopologue of conformer 1.

Table S6.4. Measured frequencies and residuals (in MHz) for the rotational transitions of the $^{13}\text{C}_3$ isotopologue of conformer 1.

Table S6.5. Measured frequencies and residuals (in MHz) for the rotational transitions of the $^{13}\text{C}_4$ isotopologue of conformer 1.

Table S6.6. Measured frequencies and residuals (in MHz) for the rotational transitions of the $^{13}\text{C}_5$ isotopologue of conformer 1.

Table S6.7. Measured frequencies and residuals (in MHz) for the rotational transitions of the $^{13}\text{C}_6$ isotopologue of conformer 1.

Table S6.8. Measured frequencies and residuals (in MHz) for the rotational transitions of the $^{13}\text{C}_7$ isotopologue of conformer 1.

Table S6.9. Measured frequencies and residuals (in MHz) for the rotational transitions of the $^{13}\text{C}_8$ isotopologue of conformer 1.

Table S6.10. Measured frequencies and residuals (in MHz) for the rotational transitions of the $^{13}\text{C}_9$ isotopologue of conformer 1.

Table S6.11. Measured frequencies and residuals (in MHz) for the rotational transitions of the $^{13}\text{C}_{10}$ isotopologue of conformer 1.

Table S6.12. Measured frequencies and residuals (in MHz) for the rotational transitions of the $^{13}\text{C}_{11}$ isotopologue of conformer 1.

Table S6.13. Measured frequencies and residuals (in MHz) for the rotational transitions of the $^{13}\text{C}_{12}$ isotopologue of conformer 1.

Table S6.14. Measured frequencies and residuals (in MHz) for the rotational transitions of conformer 7.

Table S6.15. Measured frequencies and residuals (in MHz) for the rotational transitions of conformer 9.

Table S6.16. Measured frequencies and residuals (in MHz) for the rotational transitions of conformer 11.

Table S6.17. Measured frequencies and residuals (in MHz) for the rotational transitions of conformer 13.

Table S6.18. Measured frequencies and residuals (in MHz) for the rotational transitions of conformer 4.

Table S6.19. Measured frequencies and residuals (in MHz) for the rotational transitions of conformer 14.

APPENDIX IV

Table S7.1. Measured frequencies and residuals (in MHz) for the rotational transitions of the conformer **3f** of muscone.

Table S7.2. Measured frequencies and residuals (in MHz) for the rotational transitions of the conformer **33l** of muscone.

Table S7.3. Measured frequencies and residuals (in MHz) for the rotational transitions of the conformer **13f** of muscone.

Table S7.4. Measured frequencies and residuals (in MHz) for the rotational transitions of the conformer **37a** of muscone.

Table S7.5. Measured frequencies and residuals (in MHz) for the rotational transitions of the conformer **8g** of muscone.

Table S7.6. Measured frequencies and residuals (in MHz) for the rotational transitions of the conformer **2f** of muscone.

Table S7.7. Measured frequencies and residuals (in MHz) for the rotational transitions of the conformer **31d** of muscone.

Table S7.8. Measured frequencies and residuals (in MHz) for the rotational transitions of the conformer **19c** of muscone.

Table S7.9. Measured frequencies and residuals (in MHz) for the rotational transitions of the conformer **1h** of muscone.

Table S7.10. Measured frequencies and residuals (in MHz) for the rotational transitions of the conformer **6j** of muscone.

Table S7.11. Measured frequencies and residuals (in MHz) for the rotational transitions of the conformer **2l** of muscone.

Table S7.12. Measured frequencies and residuals (in MHz) for the rotational transitions of the conformer **1f** of muscone.

Table S7.13. Measured frequencies and residuals (in MHz) for the rotational transitions of the conformer **9i** of muscone.

Table S7.14. Measured frequencies and residuals (in MHz) for the rotational transitions of the conformer **4h** of muscone.

Table S7.15. Measured frequencies and residuals (in MHz) for the rotational transitions of the conformer **15k** of muscone.

Table S7.16. Measured frequencies and residuals (in MHz) for the rotational transitions of the conformer **13h** of muscone.

Table S7.17. Measured frequencies and residuals (in MHz) for the rotational transitions of the conformer **7b** of muscone.

Table S7.18. Measured frequencies and residuals (in MHz) for the rotational transitions of the conformer **16g** of muscone.

Table S7.19. Measured frequencies and residuals (in MHz) for the rotational transitions of the conformer **3h** of muscone.

Table S7.20. Measured frequencies and residuals (in MHz) for the rotational transitions of the conformer **18j** of muscone.

Table S7.21. Measured frequencies and residuals (in MHz) for the rotational transitions of the conformer **24g** of muscone.

Table S7.22. Measured frequencies and residuals (in MHz) for the rotational transitions of the conformer **15h** of muscone.

Table S7.23. Measured frequencies and residuals (in MHz) for the rotational transitions of the conformer **7d** of muscone.

Table S7.24. Measured frequencies and residuals (in MHz) for the rotational transitions of the conformer **14g** of muscone.

Table S7.25. Measured frequencies and residuals (in MHz) for the rotational transitions of the conformer **12i** of muscone.

Table S7.26. Measured frequencies and residuals (in MHz) for the rotational transitions of the conformer **48b** of muscone.

Table S7.27. Measured frequencies and residuals (in MHz) for the rotational transitions of the conformer **42g** of muscone.

Table S7.28. Measured frequencies and residuals (in MHz) for the rotational transitions of the conformer **21c** of muscone.

Table S7.29. Measured frequencies and residuals (in MHz) for the rotational transitions of the conformer **43n** of muscone.

Table S7.30. Measured frequencies and residuals (in MHz) for the rotational transitions of the conformer **19h** of muscone.

APPENDIX V

Table S8.1. Measured frequencies and residuals (in MHz) for the rotational transitions of the conformer **5a** of civetone.

Table S8.2. Measured frequencies and residuals (in MHz) for the rotational transitions of the conformer **6b** of civetone.

Table S8.3. Measured frequencies and residuals (in MHz) for the rotational transitions of the conformer **12a** of civetone.

Table S8.4. Measured frequencies and residuals (in MHz) for the rotational transitions of the conformer **6a** of civetone.

Table S8.5. Measured frequencies and residuals (in MHz) for the rotational transitions of the conformer **11a** of civetone.

Table S8.6. Measured frequencies and residuals (in MHz) for the rotational transitions of the conformer **10d** of civetone.

Table S8.7. Measured frequencies and residuals (in MHz) for the rotational transitions of the conformer **1a** of civetone.

Table S8.8. Measured frequencies and residuals (in MHz) for the rotational transitions of the conformer **2a** of civetone.

Table S8.9. Measured frequencies and residuals (in MHz) for the rotational transitions of the conformer **3a** of civetone.

Table S8.10. Measured frequencies and residuals (in MHz) for the rotational transitions of the conformer **20d** of civetone.

Table S8.11. Measured frequencies and residuals (in MHz) for the rotational transitions of the conformer **8a** of civetone.

Table S8.12. Measured frequencies and residuals (in MHz) for the rotational transitions of the conformer **4a** of civetone.

Table S8.13. Measured frequencies and residuals (in MHz) for the rotational transitions of the conformer **20b** of civetone.

Table S8.14. Measured frequencies and residuals (in MHz) for the rotational transitions of the conformer **67b** of civetone.

Table S8.15. Measured frequencies and residuals (in MHz) for the rotational transitions of the conformer **24c** of civetone.

Table S8.16. Measured frequencies and residuals (in MHz) for the rotational transitions of the conformer **30a** of civetone.

Table S8.17. Measured frequencies and residuals (in MHz) for the rotational transitions of the conformer **85a** of civetone.

APPENDIX VI

Table S9.1. Measured frequencies and residuals (in MHz) for the rotational transitions of the conformer **2b** of exaltolide.

Table S9.2. Measured frequencies and residuals (in MHz) for the rotational transitions of the conformer **53a** of exaltolide.

Table S9.3. Measured frequencies and residuals (in MHz) for the rotational transitions of the conformer **49a** of exaltolide.

Table S9.4. Measured frequencies and residuals (in MHz) for the rotational transitions of the conformer **6c** of exaltolide.

Table S9.5. Measured frequencies and residuals (in MHz) for the rotational transitions of the conformer **21d** of exaltolide.

Table S9.6. Measured frequencies and residuals (in MHz) for the rotational transitions of the conformer **4b** of exaltolide.

Table S9.7. Measured frequencies and residuals (in MHz) for the rotational transitions of the conformer **4a** of exaltolide.

Table S9.8. Measured frequencies and residuals (in MHz) for the rotational transitions of the conformer **7b** of exaltolide.

Table S9.9. Measured frequencies and residuals (in MHz) for the rotational transitions of the conformer **3b** of exaltolide.

APPENDIX VII

Table S10.1. Measured frequencies and residuals (in MHz) for the rotational transitions of the conformer **2** of romandolide.

Table S10.2. Measured frequencies and residuals (in MHz) for the rotational transitions of the conformer **30** of romandolide.

Table S10.3. Measured frequencies and residuals (in MHz) for the rotational transitions of the conformer **3** of romandolide.

Table S10.4. Measured frequencies and residuals (in MHz) for the rotational transitions of the conformer **9** of romandolide.

Table S10.5. Measured frequencies and residuals (in MHz) for the rotational transitions of the conformer **48** of romandolide.

Table S10.6. Measured frequencies and residuals (in MHz) for the rotational transitions of the conformer **50** of romandolide.

Table S10.6. Measured frequencies and residuals (in MHz) for the rotational transitions of the rotamer **VII**.

APPENDIX VIII

Table S11.1. Measured frequencies and residuals (in MHz) for the rotational transitions of the conformer **1** of helvetolide.

Table S11.2. Measured frequencies and residuals (in MHz) for the rotational transitions of the conformer **2** of helvetolide.

Table S11.3. Measured frequencies and residuals (in MHz) for the rotational transitions of the conformer **37** of helvetolide.

Table S11.4. Measured frequencies and residuals (in MHz) for the rotational transitions of the conformer **34** of helvetolide.

Table S11.5. Measured frequencies and residuals (in MHz) for the rotational transitions of the conformer **12** of helvetolide.

Table S11.6. Measured frequencies and residuals (in MHz) for the rotational transitions of the conformer **19** of helvetolide.

LIST OF FIGURES

Chapter 1

Figure 1.1. Prototypical musk odorants from the main four structural classes.

Figure 1.2. Representatives of the macrocyclic musks class.

Figure 1.3. Representatives of the alicyclic musks class.

Figure 1.4. The evolution of the musk olfactophore.

Chapter 2

Figure 2.1. Examples of different rotors.

Figure 2.2. Diagram showing the sequence of the rotational levels and corresponding absorption lines for a linear top rotor.

Chapter 3

Figure 3.1. CP-FTMW spectrometer at King's College London.

Figure 3.2. Schematic representation of the 2-8 GHz CP-FTMW spectrometer at King's College London.

Figure 3.3. Schematic set-up and sequence of events of the 2-8 GHz CP-FTMW spectrometer at King's College London.

Figure 3.4. Graphical representation of a supersonic jet of water seeded into a backing gas (the gas molecules are omitted).

Figure 3.5. Scheme of the injection line.

Figure 3.6. The design and dimensions of the new external receptacle.

Chapter 4

Figure 4.1. Conformers of cyclooctanone predicted at MP2/6-311++G(d,p)+ZPC level of theory.

Figure 4.2. 2-8 GHz spectrum of cyclooctanone in neon.

Figure 4.3. Comparison of the r_s structure of conformer **BC1** (purple spheres) with *ab initio* MP2 structure (grey framework).

Figure 4.4. Intramolecular distances for the observed boat-chair and twisted boat-chair conformers **BC1**, **TBC1** and **BC2**, and the higher-energy boat-chair conformers **BC3** and **BC4** at MP2/6-311++G(d,p) level.

Chapter 5

Figure 5.1. Top view of some cyclooctanone-H₂O structures from B3LYP-D3BJ and MP2 calculations.

Figure 5.2. r_s structures for the assigned complexes of cyclooctanone-(H₂O)_{1,2}. The blue dots are the experimental r_s positions of the heavy atoms overlapped with the MP2 electronic structures.

Figure 5.3. NCI and RDG plots of the observed isomers of **BC1-1w**.

Figure 5.4. NCI plots of the observed isomers of **BC1-2w**.

Figure 5.5. Overlapped spectra of normal water (black) and ¹⁸O isotopically enriched water (grey) showing the presence of the ¹⁸O=C species in the later for **BC1-1w-2** complex.

Figure 5.6. Overlapped spectra of normal water (black) and ¹⁸O isotopically enriched water (red) showing the presence of the ¹⁸O=C species in the later for **BC1-2w-5a** complex.

Figure 5.7. Reaction scheme of the ketone hydration via the gem-diol formation step.

Chapter 6

Figure 6.1. Relative conformational abundances (in brackets) of the seven assigned conformers.

Figure 6.2. r_s structure (blue spheres indicating the position of the C atoms) overlapped with B3LYP-D3BJ/6-311++G(d,p) (grey framework), including atom labelling.

Figure 6.3. Intramolecular interactions in the observed conformers of cyclododecanone.

Chapter 7

Figure 7.1. Molecular structure of (*R*)-muscone, 15-membered ring ketone.

Figure 7.2. Broadband rotational spectrum of muscone collected in neon at 5 bar, temperature of 437 K, 1M FIDs.

Figure 7.3. Overlay of experimental spectrum (upper trace) and predicted spectrum of **3f** conformer using the experimental parameters (lower trace).

Figure 7.4. Top and side views of the assigned conformers of muscone in decreasing order of their conformational abundance. The relative conformational abundance ratio with respect to the least abundant conformer is indicated in parentheses.

Figure 7.5. Intramolecular interactions in conformers of muscone with high, medium and low abundance.

Figure 7.6. The NCI and RDG plots of all assigned conformers of muscone with top and side views. NCI plotted with 0.5 isosurfaces.

Figure 7.7. Comparison of the six most abundant conformations of muscone with Bersuker's and Kansey's olfactophore models.

Chapter 8

Figure 8.1. Molecular structure of civetone, cis double bond at position 9.

Figure 8.2. Experimental rotational spectrum of civetone (top trace, black) overlaid with the predicted spectrum of **1a** (low trace, blue) using its experimental parameters.

Figure 8.3. Top and side views of the identified conformations of civetone optimised at the B3LYP-D3BJ/6-311++G(d,p) level of theory, in decreasing order of relative conformational abundance (in parentheses).

Figure 8.4. Intramolecular interactions in conformers of civetone with different abundances from high to low (indicated in parentheses).

Figure 8.5. NCI plots of the 17 identified conformations of civetone plotted on the B3LYP-D3BJ/6-311++G(d,p) structures.

Figure 8.6. Comparison of **1a**, **8a** and **67b** with Bersuker's and Kansy's models. The blue frame indicates the elliptical shape suggested by both models.

Chapter 9

Figure 9.1. Structures of (R)-muscone, cis-civetone and exaltolide studied in this thesis.

Figure 9.2. Top and side views of the assigned conformers of exaltolide in decreasing order of conformational abundance (indicated in brackets).

Figure 9.3. The NCI plots of the nine assigned conformers of exaltolide in their decreasing order of conformational abundance.

Figure 9.4. Intramolecular interactions in oblate (6c) and prolate (4b) conformers of exaltolide.

Figure 9.5. The most abundant conformations of muscone, civetone and exaltolide.

Chapter 10

Figure 10.1. Structures of cyclomusk, romandolide and helvetolide from acyclic family of musks.

Figure 10.2. Methyl rotation barrier heights of the four methyl groups calculated for conformer 2 at the B3LYP-D3BJ/6-311++G(d,p) level of theory.

Figure 10.3. a. Segments of the spectrum with c-type transitions of conformer 30. **b.** Segments of the spectrum with a- and b-type transitions of conformer 30.

Figure 10.4. Conformations of romandolide with aliphatic tails **above** the cyclohexane ring optimised at B3LYP-D3BJ/6-311++G(d,p), with side and top views.

Figure 10.5. Conformations of romandolide with aliphatic tails **below** the cyclohexane ring optimised at B3LYP-D3BJ/6-311++G(d,p), with side and top views.

Figure 10.6. Conformations of romandolide with aliphatic tails **around (front)** the cyclohexane ring optimised at B3LYP-D3BJ/6-311++G(d,p), with side and top views.

Figure 10.7. Conformations of romandolide with aliphatic tails **around (back)** the cyclohexane ring optimised at B3LYP-D3BJ/6-311++G(d,p) within 600 cm^{-1} , with side and top views.

Figure 10.8. Conformations of romandolide with aliphatic tails **away** from the cyclohexane ring predicted by B3LYP-D3BJ/6-311++G(d,p), with side and top views.

Figure 10.10. Oxygen labels in the structure of romandolide.

Figure 10.11. Intramolecular interactions in the assigned conformers of romandolide.

Figure 10.12. The most abundant conformations of muscone, civetone, exaltolide and romandolide.

Chapter 11

Figure 11.1. Molecular structures of romandolide and helvetolide.

Figure 11.2. Methyl rotation barrier heights of the six methyl groups of conformer **1** of helvetolide at the B3LYP-D3BJ/6-311++G(d,p) level of theory.

Figure 11.3. Top and side views of the conformations of helvetolide with aliphatic tails **below** the cyclohexane ring optimised at B3LYP-D3BJ/6-311++G(d,p) level.

Figure 11.4. Top and side views of the conformations of helvetolide with aliphatic tails **above** the cyclohexane ring optimised at B3LYP-D3BJ/6-311++G(d,p) level.

Figure 11.5. Top and side views of the conformations of helvetolide with aliphatic tails **around** the cyclohexane ring on the same side as the dimethyl groups optimised at B3LYP-D3BJ/6-311++G(d,p) level.

Figure 11.6. Top and side views of the conformations of helvetolide with aliphatic tails **around** the cyclohexane ring on the opposite side to the dimethyl groups and one conformation with the tail **away** from the cyclohexane ring optimised at B3LYP-D3BJ/6-311++G(d,p).

Figure 11.7. Experimental broadband rotational spectrum between 3000-3650 MHz (black, upper trace), and simulated spectrum (lower trace) of conformers **1** (blue) and **2** (orange) using their experimental rotational constants.

Figure 11.8. Oxygen labels in the structure of helvetolide.

Figure 11.9. Intramolecular interactions (B3LYP-D3BJ distances in Å) in the observed conformers of helvetolide. Those in blue represent C–H···O attractive interactions, and those in orange represent H···H interactions.

Figure 11.10. Non-covalent interactions (NCI) analysis of the six observed conformers of helvetolide.

Figure 11.11. The most abundant conformations of muscone, civetone, exaltolide, romandolide and helvetolide.

ABSTRACT

Musk odorants represent a class of fragrances which exhibit a warm, sensual, animalistic and natural scent, and were introduced into the perfume industry at the beginning of the 20th century. Structurally, musk odorants are remarkably diverse, including macrocyclic molecules, polycyclic benzene derivatives, nitro arenes, and linear aliphatic compounds, and therefore there is lack of knowledge of the molecular determinants that lead to musk odour. Moreover, some classes of musks such as nitro musks have been proved to be toxic, while others such as polycyclic musks resulted in bioaccumulation and biomagnification through the food chain. Macrocyclic musks, which are biodegradable and exhibit strong olfactory and fixative properties, have an expensive and complex synthesis. The alicyclic class was discovered most recently and so far constitutes the most suitable replacement for macrocyclic musks at commercial scale. There is interest in the perfume industry to develop new musks, but these molecules are conformationally rich and there is very limited knowledge of their active conformations.

In this project, we have investigated the conformational landscapes of several musk odorants from alicyclic and macrocyclic classes using broadband rotational spectroscopy. Rotational spectroscopy is a high-resolution technique directly dependent on molecular mass distribution, and therefore able to distinguish minute structural changes. Together with theoretical computations, rotational spectroscopy allows unambiguous identification of co-existing conformers in molecular jets. As part of this project, two alicyclic musks, romandolide and helvetolide, both widely used in the perfume industry, have been investigated. From the macrocyclic musk class the spectra of muscone, civetone and exaltolide have been analysed. Their conformational landscapes have been found to be extraordinarily rich and complex. To understand conformational changes as ring size increases, smaller cyclic ketones of 8-, 11- and 12-membered rings have also been analysed. A clear trend emerges that with the increase in the ring size the number of low energy conformers increases considerably. From the comparison between the observed conformations of all musks, information on conformational preferences, intramolecular interactions, and the structural features responsible for the musky scent has been obtained. The results have been compared to previous work on musks, including the musk olfactophore models, and are essential for understanding odorant identification and for a rational design of new musk odorants.

TABLE OF CONTENTS

1. INTRODUCTION	30
1.1. Musk odorants	30
1.2. Macrocyclic musks	31
1.3. Alicyclic musks.....	33
1.4. Olfaction theories	34
1.5. Musk olfactory receptors.....	35
1.6. Structure-odour relationships in musks and the musk olfactophore	36
1.7. Analysis of conformationally complex molecules: rotational spectroscopy	38
1.8. Investigated molecular systems.....	39
1.9. Bibliography	40
2. THEORETICAL BACKGROUND.....	45
2.1. Fundamentals of rotational spectroscopy	45
2.1.2. Classical angular momenta, moments of inertia and rotational energy	46
2.1.3. The rigid rotor	48
2.1.4. Linear top rotor	50
2.1.5. Spherical top rotor	51
2.1.6. Symmetric top rotor.....	52
2.1.7. Asymmetric top rotor.....	53
2.1.8. Centrifugal distortion	55
2.2. Structural determination methods	57
2.2.1. The equilibrium structure	57
2.2.2. The effective structure.....	58
2.2.3. The substitution structure	59
2.3. Bibliography	60
3. EXPERIMENTAL SET-UP AND INSTRUMENT DEVELOPMENT	63
3.1. Sequence of operation.....	63
3.1.1. Molecular pulse.....	65
3.1.2. Chirped pulse generation.....	67
3.1.3. Interaction between the molecular jet and the MW chirped pulse	67
3.1.4. FID detection.....	68
3.2. External receptacle development.....	68
3.3. Bibliography	70
4. MEDIUM-SIZED RINGS: CONFORMATIONAL PREFERENCES IN CYCLOOCTANONE DRIVEN BY TRANSANNULAR REPULSIVE INTERACTIONS	72

4.1.	Introduction	72
4.2.	Methods	73
4.2.1.	Theoretical	73
4.2.2.	Experimental	73
4.3.	Results and Discussion	74
4.3.1.	Conformational landscape of cyclooctanone	74
4.3.2.	Rotational spectrum.....	75
4.3.3.	Structural determination of BC1.....	78
4.3.4.	Intramolecular interactions	82
4.4.	Conclusions	83
4.5.	Bibliography	84
5.	STRUCTURES OF THE COMPLEXES OF CYCLOOCTANONE WITH WATER.....	89
5.1.	Introduction	89
5.2.	Methods	90
5.2.1.	Theoretical	90
5.2.2.	Experimental	90
5.3.	Results and Discussion	91
5.3.1.	Theoretical results.....	91
5.3.2.	Spectral assignment.....	96
5.3.3.	Experimental structures.....	100
5.3.4.	Non-covalent interactions and conformational abundances	106
5.3.5.	Ketone hydration: Geminal-diol formation	109
5.4.	Conclusions	112
5.5.	Bibliography	112
6.	CONFORMATIONAL INVESTIGATION OF CYCLODODECANONE.....	115
6.1.	Introduction	115
6.2.	Methods	117
6.2.1.	Theoretical	117
6.2.2.	Experimental	117
6.3.	Results.....	119
6.3.1.	Rotational spectrum.....	119
6.3.2.	Experimental structure of conformer 1	123
6.4.	Discussion.....	125
6.5.	Conclusions	127
6.6.	Bibliography	128
7.	THE RICH CONFORMATIONAL LANDSCAPE OF MUSCONE	132
7.1.	Introduction	132

7.2.	Methods	133
7.2.1.	Theoretical	133
7.2.2.	Experimental	135
7.3.	Results	136
7.3.1.	Spectral assignment	136
7.4.	Discussion.....	156
7.4.1.	Theoretical methods and benchmarking	156
7.4.2.	Conformational features in muscone	160
7.4.3.	Non-covalent interactions	165
7.5.	Conclusions	177
7.6.	Bibliography	179
8.	CIVETONE: THE INFLUENCE OF A DOUBLE BOND IN THE CONFORMATIONS OF A KETONE MACROCYCLE	183
8.1.	Introduction	183
8.2.	Methods	184
8.2.1.	Computational	184
8.2.2.	Experimental	184
8.3.	Spectral assignment	188
8.4.	Discussion.....	196
8.4.1.	Theoretical benchmarking	196
8.4.2.	Identified conformations of civetone	198
8.4.3.	Non-covalent interactions	199
8.4.4.	Civetone within Bersuker's and Kansy's olfactophore models.....	203
8.5.	Conclusions	204
8.6.	Bibliography	204
9.	THE PREFERRED CONFORMATIONS OF THE MACROCYCLIC LACTONE EXALTOLIDE	207
9.1.	Introduction	207
9.2.	Methods	208
9.2.1.	Theoretical	208
9.2.2.	Experimental	208
9.3.	Results and discussion	212
9.3.1.	Rotational spectrum.....	212
9.3.2.	Conformational abundance and structural comparison.....	214
9.3.3.	Non-covalent interactions	217
9.3.4.	Benchmarking of theoretical methods	220
9.3.5.	Comparison with the other muscone and civetone macrocycle ketone	222
9.4.	Conclusions	223

9.5.	Bibliography	223
10.	EXPERIMENTALLY OBSERVED HORSESHOE CONFIGURATIONS OF THE ALICYCLIC MUSK ROMANDOLIDE	226
10.1.	Introduction	226
10.2.	Methods	227
10.2.1.	Theoretical	227
10.2.2.	Experimental	228
10.3.	Results	231
10.3.1.	Rotational spectrum.....	231
10.3.2.	Theoretical results.....	234
10.4.	Discussion.....	238
10.4.1.	Conformational preferences and intramolecular interactions	238
10.4.2.	Benchmarking of computational methods	245
10.4.3.	Comparison with macrocycles	247
10.4.4.	Kraft's olfactophore model	248
10.5.	Conclusions	248
10.6.	Bibliography	249
11.	CONFORMATIONAL INVESTIGATION OF AN ALICYCLIC MUSK: HELVETOLOLIDE	252
11.1.	Introduction	252
11.2.	Methods	253
11.2.1.	Theoretical	253
11.2.2.	Experimental	253
11.3.	Results	255
11.3.1.	Theoretical results.....	255
11.3.2.	Spectral assignment.....	258
11.4.	Discussion.....	261
11.4.1.	Benchmarking of computational methods	261
11.4.2.	Conformational preferences and intramolecular interactions	262
11.4.3.	Comparison with romandolide and macrocycles	267
11.5.	Conclusions	268
11.6.	Bibliography	269
12.	CONCLUSIONS AND PERSPECTIVES.....	272



INTRODUCTION

Chapter 1



1. INTRODUCTION

1.1. Musk odorants

The musk smell is known as the most complex and exquisite aroma produced by nature, often described as sensual, earthy, warm and woody. Structurally, musk odorants are very diverse and can be classified into several groups: macrocyclic, nitro, polycyclic and alicyclic.¹⁻³ Macrocyclic musks are of natural origin and have been extracted from musk pods for centuries. They have been used in perfumery but also as a universal drug in Chinese and pre-historic Indian medicine, for their benefits in promoting blood circulation, and for their anti-inflammatory, antitumor and antifungal properties.⁴⁻⁷ The scarcity of musk pods and the difficulties involved in the extraction and synthesis of macrocyclic compounds reduced their usage in perfumery, driving the fragrance chemists towards developing synthetic musks, which resulted in the discovery of nitro arenes, polycyclic and alicyclic musks. The nitro musks have been removed from the perfume and cosmetic industries due to phototoxic and carcinogenic effects,⁸ whilst the polycyclic musks are being eliminated because of their bioaccumulation and environmental concerns.⁹ This makes macrocyclic and alicyclic musks the most suitable for current industrial applications. The structural diversity of musks makes it difficult for fragrance chemists to understand and rationalise the relationship between their structure and the olfactory response.

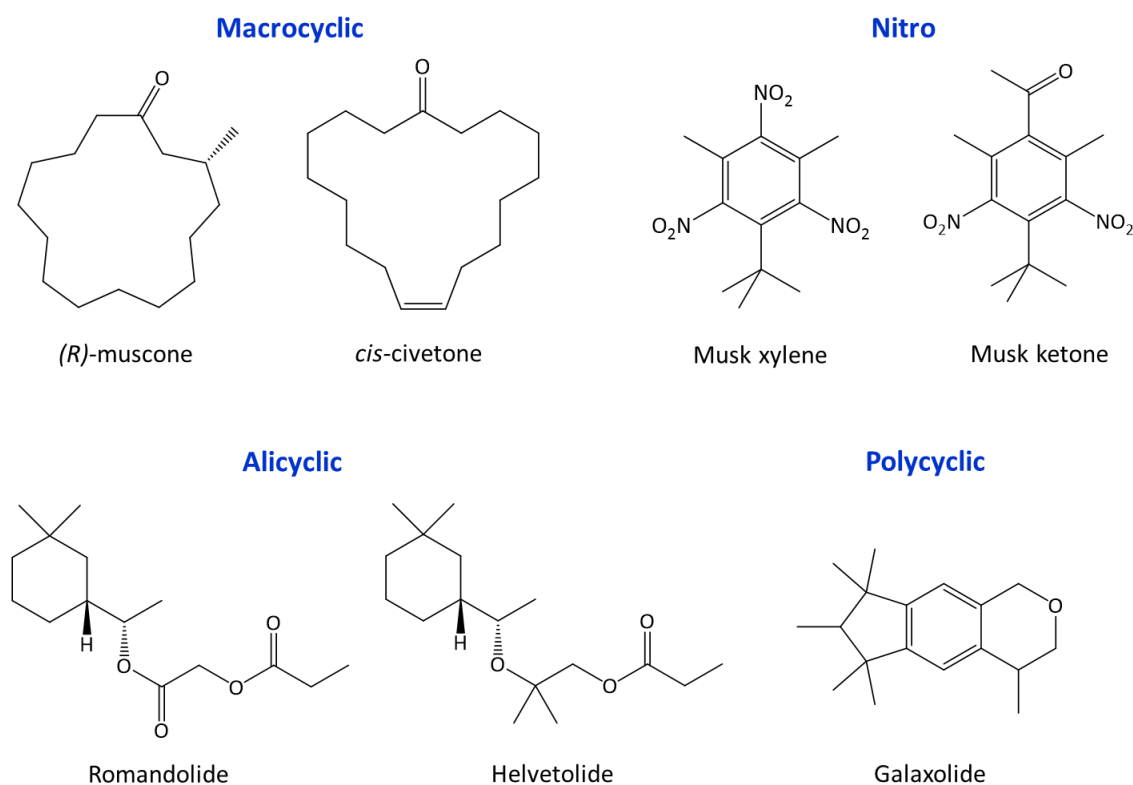


Figure 1.1. Prototypical musk odorants from the main four structural classes.

1.2. Macrocyclic musks

The macrocyclic musks, also known as natural musks, are usually 15- to 17-membered cycles with carbonyl or lactone functional groups.¹⁰ The name “musk” originates from the substance with a strong smell produced by a gland of the male musk deer. For hundreds of years the musk pods were accessed by killing musk deer. The musk pod was further dried and its contents (musk “grains”), were diluted in alcoholic tinctures. By significantly reducing the concentration of the musk solution, an exquisite aroma was achieved. The use of musk dates to pre-historic India and ancient China, where it was used in traditional medicine as a universal drug. Due to the scarcity and the complex process of obtaining musk, it used to be only affordable for the upper social classes as it was more expensive than gold.¹

It was not until 1906 that the main component contributing to the musk scent in the musk pod was isolated and named *muscone*.¹¹ In 1915 Sack isolated the active component from the secretion of civet cat and named it *civetone*.¹ In 1926 Ružička characterised both compounds and identified their structures, *muscone* as 3-methyl-1-cyclopentadecanone, and *civetone* as cycloheptadeca-9-en-1-one. He confirmed their structures by synthesis, introducing for the first time the macrocyclic class of compounds.¹²⁻¹⁵ Until Ruzicka’s discovery, macrocycles were considered unstable and hence not expected to exist in nature according to Baeyer’s strain theory.¹⁶ In 1927, the musk smelling compounds from angelica root oil and ambrette seed oil were isolated for the first time.¹⁷ One year later Stoll and Ruzicka synthesised them and determined their structures as macrocyclic lactones, *exaltolide* (cyclopentadecenolide) and *ambrettolide* (cyclohexadecanolide), respectively.¹ After this advancement in synthetic chemistry, other macrocyclic compounds with musk-like scents were isolated from natural sources and routes for their synthesis developed. The macrocyclic compounds isolated from animal sources were generally ketones, and the ones from plant sources were usually lactones.^{1,18}

The developments in synthetic chemistry, introduced by Ružička and others,^{12-15,19} and the demand for macrocyclic musks inspired the perfume chemists to develop synthetic replacements. Therefore, there have been numerous attempts to optimise syntheses of natural macrocyclic musks for industrial applications and to develop new compounds with similar structures, olfactory and fixative properties. This led to the discovery of other substances, not observed in nature previously.^{1,18} Towards the end of the 20th century, various industrial routes to macrocyclic musk compounds were known. These included ring expansions from smaller cycles such as cyclododecanone,^{2,10} acyloin condensations,^{20,21} alkyl peroxide rearrangements,²² polymerisation-depolymerisation^{10,23} and transesterification reactions.^{2,10} The suggested routes were not scalable enough and often involved multiple steps; hence they could not be

implemented at industrial level. Therefore, the discovery of polycyclic musks in mid-20th century led to their domination in the global market, satisfying the economic and industrial standards, while macrocyclic musks covered only 5 % of the global production.^{1,24}

Whilst syntheses of macrocyclic musks remain challenging, significant progress has been achieved in the past decades, which includes more sophisticated chemistry, such as ring-closing olefin metathesis reactions involving metal catalysts.^{25–28} However, there is still a need to find faster and more cost-effective solutions to produce these valuable macrocyclic compounds, including more selective catalysts for stereoselective synthesis, renewable substrates and upscaling.²⁸

Because of the large number of single bonds in the macrocyclic musks, they are conformationally very flexible and hence could not be studied structurally or conformationally to understand the structure-odour relationship. In order to derive information about their structures, substituted analogues have been studied, such as 2,4-dinitrophenyl hydrazine (DNP) derivatives. DNP analogues of both muscone and civetone have been subjected to structural studies by X-ray crystallography.^{29–31} The reason behind the choice of the substituent was its bulkiness and polarity, which was intended to reduce the conformational flexibility of the macrocycles and to enable their crystallisation. The analysis of DNP derivatives revealed significant disorder, which was expected for such large rings. Other studies on macrocycles involving conformational constrains consisted in introducing one or two –CF₂ groups in various positions.³² The fluorinated carbon, being bulkier than –CH₂, occupies a corner position and thus significantly reduces the flexibility of the macrocycle, making it possible to be analysed by X-ray crystallography. Further studies on the structure-odour relationship in macrocyclic musks involved methylene bridged macrocycles, where the focus was on the effect of conformational constrains on olfactory potency.³³ Despite the efforts in studying substituted and modified macrocyclic musks, there is a lack of understanding of the structure-odour relationship in this class of compounds.

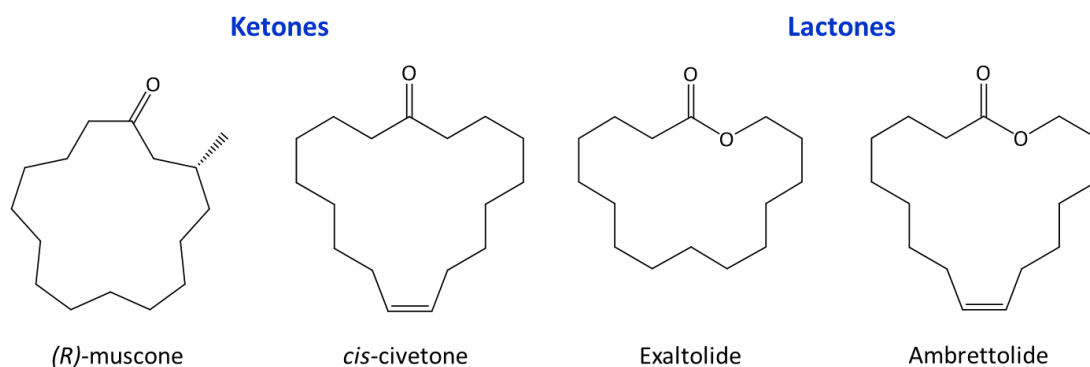


Figure 1.2. Representatives of the macrocyclic musks class.

1.3. Alicyclic musks

The alicyclic musks were introduced in 1975 with the discovery of *cyclomusk* by Hoffmann and von Fraunberg of BASF.³⁴ The scent of cyclomusk was described as fruity and strawberry-like. In 1990, *helvetolide*, another prototypical representative of this class, was discovered by Giersch and Schulte-Elte at Firmenich.³⁵ It exhibits a musky-floral, fruity, pear-like odour. In 2000, Williams at Firmenich found that by substitution of the *gem*-dimethyl ether moiety of helvetolide with an ester a slight change in scent is induced.³⁶ The resulting musk odorant was named *romandolide*, which is less fruity and more ambrette-like compared to helvetolide. Since their discovery, both romandolide and helvetolide have been successfully used in the perfume industry. For example, helvetolide constitutes the base notes of the Miracle perfume by Lancome at 6.1%, and of the Emporio White Her by Armani at 8.8%, both popular fragrances. Romandolide is used in Absolu by Rochas, and Murmure by Van Cleef & Arples.³⁶

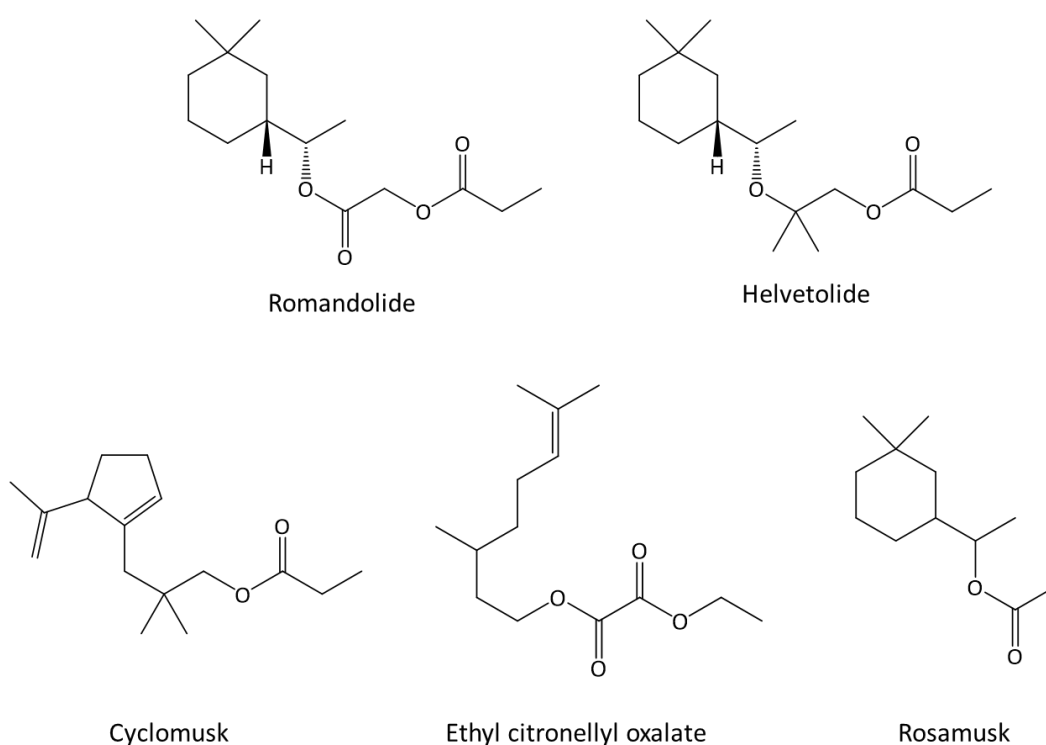


Figure 1.3. Representatives of the alicyclic musks class.

The olfactory properties of helvetolide and romandolide are thought to be related to the *gem*-dimethyl group and the additional carbonyl group, respectively. Attempts to add these moieties to macrocyclic ketones and lactones resulted in significant decrease of muskiness, which suggests that alicyclic and macrocyclic musks form different conformations or interact in different ways with the olfactory receptors.^{37,38} Nevertheless, Kraft proposed in 2004 that

alicyclic musks adopt a horse-shoe shape³⁶, which resembles the shape of macrocyclic musks. This triggered new questions: do alicyclic musks occupy the same conformational space as the macrocyclic ones? Is this related to the way in which they interact with olfactory receptors? Other alicyclic musks include *rosamusk* and *ethyl citronellyl oxalate*. Whilst structurally they are part of the same family as helvetolide and romandolide, their scent is more floral, rosy- and geranium-like and are not used in perfumery as musks. Similar to the macrocyclic musks, the alicyclic family has not been studied structurally or conformationally, because of the high degree of flexibility of the aliphatic tails in their structures.

1.4. Olfaction theories

Olfaction is the least understood and debated senses. The human olfactory system is built of approximately 400 olfactory receptors (OR)³⁹ which are able to detect about one trillion odours.⁴⁰ A combinatorial system is generally accepted to be in place to discriminate such a large number of odours with a limited number of receptors, where instead of allocating an individual OR to a specific odour, combinations of receptors are used to detect various odorants and the same odorant can be recognised by different receptors.⁴¹

Along the years two theories trying to explain olfaction at the molecular level became popular: the *docking theory*, based on physicochemical characteristics of the odorant triggering a respond from the ORs upon establishing weak bonding interactions, and the *vibrational theory*, which states that receptors can identify molecular vibrational frequencies.⁴²

The docking theory was introduced by Moncrieff in 1944,⁴³ and later by Pauling in 1946.⁴² In some way their suggested theory is accepted nowadays: receptors have a bonding landscape with different shapes, and odorants will bind selectively to different receptors depending on their shape and size. The vibrational theory was introduced in 1927 by Dyson,^{42,43} and later revived by Turin in 1997.⁴⁴ Based on this theory, an odorant is recognised by the receptors only if it has the right vibrational frequency. The vibrational theory has been tested on muscone by Block *et al.* in 2015 and was eliminated as the possible mechanism of odorant recognition.⁴⁵ To assess the theory, the authors used deuterated and ¹³C substituted species of muscone and tested the olfactory response against the human musk receptor OR5AN1, and other mouse musk receptors. However, no differences in receptor response were noted, and therefore the vibrational theory was proved implausible.

Most recently, in 2020, the importance of odorant's conformational flexibility has been recognised in a new theory for molecular recognition in olfaction.⁴⁶ The study found that

different conformations of a conformationally flexible odorant generated different olfactory receptor responses and concluded that overall odorant recognition is a complex effect of the different conformations activating and partly activating the receptor. This theory supports the combinatorial coding system of olfaction.

The newly suggested theory adds further complexity to the olfaction process, highlighting the role of odorants' conformations. The most successful musk odorants (macrocyclic and alicyclic) are highly flexible and expected to coexist in multiple conformations. Thus, the question arises: do we smell only one conformation of a musk odorant or the olfactory response is produced by an assembly of conformations binding to multiple receptors? In order to answer this question, we first need to know what the possible conformations of odorants are. The aim of this thesis is to advance our understanding of the structure-odour relationship by characterising the conformational landscapes of the most prototypical musk odorants from the macrocyclic and alicyclic classes.

1.5. Musk olfactory receptors

An important drawback in our understanding of olfaction is the lack of knowledge on ORs. In 1991, Buck and Axel revealed that ORs are G-protein coupled receptors (GPCRs).⁴⁷ Whilst approximately 400 ORs⁴⁸ have been discovered in the human olfactory system up to date, there are no X-ray crystallographic or NMR data on ORs, and their amino acid sequence is still unknown. This prevents further advancements in predicting and understanding odorant-receptor interactions.

In 2018, two structural models of human ORs for muscone and nitro musks were proposed, OR5AN1 and OR1A1.⁴⁹ These were modelled using quantum mechanics/molecular mechanics (QM/MM) hybrid methods based on a series of musky smelling compounds, such as constrained structures of (*R*)-muscone, 15-membered ring sulfoxide compounds and nitromusks. The models were validated with experimental activation profiles of the receptor on ligand binding, in addition to site-directed mutagenesis analysis. The authors concluded that OR1A1 receptor responds only to nitromusks, whilst OR5AN1 responds to macrocyclic sulfoxides and fluorine-substituted muscone. The investigation also generated 3D-QSAR (quantitative structure-activity relationship) models, which confirm that the non-polar parts of the odorant influence the response of OR5AN1 as much as the H-bond acceptor. The conformations of macrocyclic and alicyclic musks identified and presented in this thesis could be further tested against the reported ORs.

1.6. Structure-odour relationships in musks and the musk olfactophore

Given the small number of human ORs, it seemed unlikely that four ORs will be allocated to detect musk odorants from the four different classes discovered up to date. Therefore, it has been assumed that the musks from all classes activate the same olfactory receptor. A few studies have focused on developing an olfactophore model which describes the structural features of a musk odorant and the main interactions between the musk odorant and the binding pocket of the receptor.^{36,50-53}

The first musk olfactophore model was developed in 1991 by Bersuker *et al.* by comparing 352 structures of musk odorants from the nitro, polycyclic and macrocyclic classes. This model, with an accuracy of 54%, could predict musk scented odorants based on a few features. It proposed that in order to smell musky an odorant had to have a pseudo-rectangular shape, with a shorter horizontal axis of 5-6 Å, compared to a vertical axis of 6.2-7.2 Å. The second feature was the presence of a H-bonding acceptor such as -C=O, -NO₂ or -CN group along the shorter axis.^{2,36,50}

In 1995, Kansy *et al.* evaluated and improved Bersuker's model to 65% accuracy by including the distances of the hydrophobic moieties from the H-bonding acceptor in the odorant.³⁶ According to this model three hydrophobic moieties should be at 5.5, 6.5 and 8.0 Å from the H-bonding acceptor in order for a compound to have musky odour, similar to the positions of the methyl groups with respect to the oxygen in galaxolide.³⁶ Macrocyclic musks, such as pentadecane-15-lactone, were also included in the development of the model.

Due to the high potency of galaxolide as a musk odorant and its rigid structure, it became the structure of choice in further investigating the musk olfactophore model. Comparing all the four stereoisomers of galaxolide, in 2001 Kraft *et al.* determined that the enantioselectivity of the methyl group in the 3rd position with respect to the oxygen is essential for the musk odour.^{36,51} Based on this additional feature Kraft *et al.* constructed a more complete musk olfactophore model and presented the first potential interactions formed between a musk odorant and the binding pocket of the olfactory receptor. The model suggests that the H-bonding acceptor moiety has the role of an osmophore in the odorant, which is to insert the odorant in the binding pocket, hence forming stronger interactions with the residues in the pocket. The middle part of the odorant should be less bulky not to interfere with the insertion, whilst the spatial arrangement in the hydrophobic site is of less significance for the musky odour as it is situated just outside the binding pocket.^{36,51}

The most recent model, developed by Zou *et al.* in 2012⁵⁴ and further improved in 2016,⁵³ suggests that 2 hydrogen-bond acceptors separated by 6.96 Å and 2 aliphatic hydrophobes positioned at a distance of 7.51 Å are required for musky scent. This model has been developed on structurally modified and theoretical data of alicyclic and cyclic musks comprising more than one hydrogen-bond acceptor. Further structural and conformational studies of musks are essential to develop a more accurate olfactophore model, which could be used to design other musk odorants.

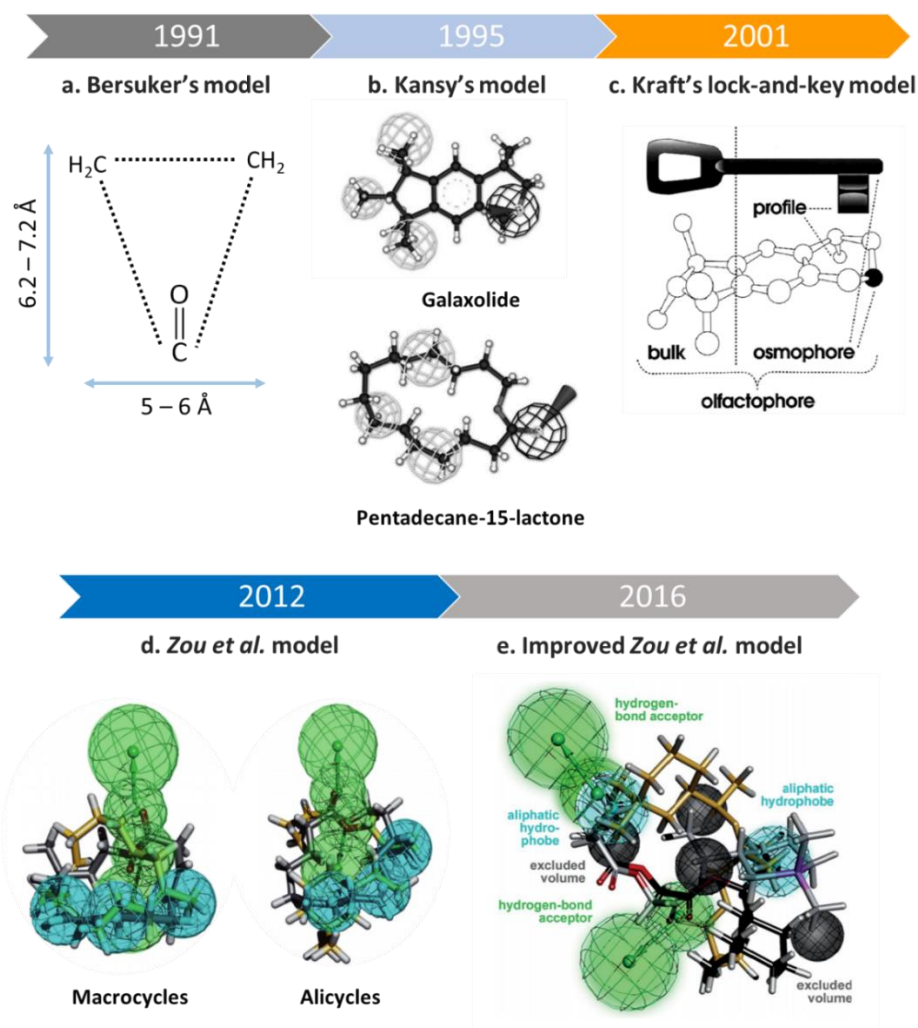


Figure 1.4. The evolution of the musk olfactophore. **a.** Bersuker's model⁵⁰ developed on 352 structures, with 54 % accuracy. Hydrogen-bond acceptor (C=O, NO₂, CN). **b.** Kansy's model,³⁶ 65% accuracy, 3 hydrophobic moieties & 1 hydrogen-bond acceptor. **c.** Kraft's lock-and-key model, odorant – odorant receptor interactions. **d.** Zou *et al.* model,⁵² 3 hydrophobic moieties & 2 hydrogen-bond acceptors, 54% correlation. **e.** Improved Zou *et al.* model,⁵³ 2 hydrophobic moieties & 2 hydrogen-bond acceptors, 80% correlation.

1.7. Analysis of conformationally complex molecules: rotational spectroscopy

Unlike rigid molecules, analysis of conformationally flexible molecules is challenging. Traditional techniques used for structural studies are X-ray crystallography, NMR and electron diffraction. X-ray crystallography is performed in solid state, which prevents observation of multiple conformations due to crystal packing. Whilst studies on musk odorants using X-ray crystallography have been attempted, they have not been successful without introducing conformational constraints in the systems investigated, as the high flexibility of macrocyclic and alicyclic musks impedes formation of suitable crystals. X-ray crystallography has thus provided only limited information on the structures and conformational flexibility of musks. NMR spectroscopy is conducted in liquid state as well as in solid state, and is widely used in conformational studies. However, due to the timescale of the technique, interconvertible conformations with low barriers are usually observed as broad peaks, and their spectroscopic signatures cannot be distinguished.⁵⁵ Further disadvantages of the techniques above are the environment in which they are conducted, which interferes with the intrinsic conformational properties of the molecules under study and whose effects are difficult to disentangle. This is overcome in the gas phase where the molecular systems are probed isolated in a collision-free environment. Gas phase techniques such as UV and IR coupled with supersonic expansions, and electron diffraction⁵⁶ offer some conformational information, however with limited resolution. Rotational spectroscopy is one of the most sensitive gas phase techniques, able to distinguish minute changes in molecular structure because of the direct dependence of the rotational spectrum to the moments of inertia. The only requirement is that molecules must possess a permanent dipole moment to interact with the electric field of the microwave radiation, making rotational spectroscopy applicable to a vast range of molecular systems.

Microwave spectroscopy is a high-resolution technique consisting in the excitation of molecules in gas phase using microwave radiation within the frequency range of 1 to 1000 GHz, or wavelengths of 30 cm to 0.3 mm. It was introduced at the beginning of the 20th century by Cleeton & Williams with the development of the absorption spectrometer.⁵⁷ Experiments in absorption spectrometers are performed in gas cells, producing complicated spectra arising from the distribution of the molecular population over several rotational and vibrational states. In 1981, Balle and Flygare demonstrated that the Fourier transform microwave (FTMW) technique can be used with a Fabry-Pérot resonator in combination with molecular beams.^{58,59} In Fabry-Pérot spectrometers microwave pulses are applied instead of a tuneable microwave source. This technique allows for the sample to be probed milliseconds after the supersonic expansion, where the molecular rotational temperatures are as low as a few K. This was a ground-breaking development because it allowed concentration of molecular population on the ground

vibrational state and the lower rotational energy levels, simplifying considerably the spectra. Further advantages were the improved sensitivity and resolution, and the possibility to study weakly bound complexes.⁵⁹ However, Fabry-Perot spectrometers have a small bandwidth of approximately 1 MHz, which results in time-consuming spectral searches, which typically cover several hundred MHz.

Taking advantage of technological progress in electronics, in 2008 B.H. Pate at the University of Virginia designed a spectrometer which retains the benefits of the Balle-Flygare FTMW spectrometer whilst adding new features.⁶⁰ The main addition to this technique is the "chirped" microwave polarisation, which is a linear sweep over a broad frequency range allowing for acquisition of broadband spectrum in a few microseconds. The instrument uses a high-speed oscilloscope where the molecular free induction decay is collected, digitised, and amplified in the time domain. The broadband addition to the instrument is highly complementary to the Fabry-Perot design, allowing to preserve the high sensitivity and resolution whilst reducing the time for spectrum acquisition and facilitating the identification of spectral patterns belonging to different conformers coexisting in the sample. These features are particularly important for conformationally flexible molecules such as musk odorants. We have applied the CP-FTMW spectrometer at King's College London,^{61,62} based on Pate's design, to the study of the musk odorants presented in this thesis.

1.8. Investigated molecular systems

In this thesis, broadband rotational spectroscopy has been applied to the study of musks belonging to the macrocyclic and alicyclic classes, along with other relevant cycles. Before presenting the data on musks, the thesis begins with two chapters explaining the fundamentals of rotational spectroscopy and the design and operation of our broadband rotational spectrometer. The investigation of cyclooctanone, an 8-membered ring ketone, and a precursor to macrocycle musks, is presented in Chapter 4. The conformational preferences of the cycloketone have been determined, as well as the experimental structure of the most abundant conformation. In Chapter 5 follows with the study of cyclooctanone-water complexes. The full experimental structures of the complexes of cyclooctanone with one and two water molecules are presented. We also obtained indirect evidence of geminal diol formation upon complexation of the ketone with water. With the aim of understanding the behaviour of larger rings, the conformational landscape of cyclododecanone was characterised (Chapter 6).

The most prototypical representatives from the macrocyclic and alicyclic musk were chosen for their study, with muscone (Chapter 7), civetone (Chapter 8) and exaltolide (Chapter 9) belonging to the macrocyclic class, and romandolide (Chapter 10) and helvetolide (Chapter 11) to the alicyclic class. The choice of macrocycles was intended to give an insight into the role of the size the ring and the different functional groups on the conformational preferences. Muscone is a 15-membered ring ketone, civetone an unsaturated 17-membered ketone, and exaltolide a 16-membered ring lactone, all showing rich and complex conformational landscapes. By comparing the conformational preferences of all three, several features were identified which could help understand the structure-odour relationship in this class. Investigation of romandolide and helvetolide has shown the tendency of these compounds to form horse-shoe shapes, which partially resemble the appearance and the conformational space of the macrocyclic musks. Further comparison between the two classes could lead towards an improved olfactophore model which could be used in designing new musk odorants. Moreover, the results presented in this thesis could provide valuable information on how musks bind to the olfactory receptors.

1.9. Bibliography

1. Sommer, C. The role of musk and musk compounds in the fragrance industry. *Handbook of Environmental Chemistry* **3**, 1–16 (2004).
2. Fráter, G., Bajgrowicz, J. A. & Kraft, P. Fragrance chemistry. *Tetrahedron* **54**, 7633–7703 (1998).
3. Homes, V. & Traffic, E. *On the Scent: Conserving Musk Deer: the Uses of Musk and Europe's Role in Its Trade*. (1999).
4. Cen, W., Chen, Z., Gu, N. & Hoppe, R. Prevention of AMI Induced Ventricular Remodeling: Inhibitory Effects of Heart-Protecting Musk Pill on IL-6 and TNF-Alpha. *Evidence-based Complementary and Alternative Medicine* **2017**, 1–7 (2017).
5. Wang, X. *et al.* Beneficial effects of muscone on cardiac remodeling in a mouse model of myocardial infarction. *International Journal of Molecular Medicine* **34**, 103–111 (2014).
6. Liang, Q. Q., Zhang, M., Zhou, Q., Shi, Q. & Wang, Y. J. Muscone protects vertebral end-plate degeneration by antiinflammatory property. *Clinical Orthopaedics and Related Research* **468**, 1600–1610 (2010).
7. Asada, R., Kageyama, K., Tanaka, H., Saitoh, Y. & Miwa, N. Antitumor and anti-invasive effects of diverse musk-fragrant macrocyclic ketones and their enhancement by hyperthermia. *Molecular Medicine Reports* **5**, 148–152 (2012).
8. David, O. R. P. Artificial Nitromusks, Stories of Chemists and Businessmen. *European Journal of Organic Chemistry* **2017**, 4–13 (2017).
9. Fromme, H., Otto, T. & Pilz, K. Polycyclic Musk Fragrances in the Aquatic Environment. *ACS Symposium Series* **773**, 203–222 (2001).

10. Williams, A. S. The synthesis of macrocyclic musks. *Synthesis* **10**, 1707–1723 (1999).
11. Walbaum, H. Das natirliche Moschusaroma. in 488–493 (1906).
12. Ruzicka, L. Zur Kenntnis des Kohlenstoffringes. *Helv. Chim. Acta* **715**, 1008–1017 (1926).
13. Ruzicka, L. Zur Kenntnis des Kohlenstoffringes I. Über die Konstitution des Zibetons. *Helvetica Chimica Acta* **9**, 230–248 (1926).
14. Ruzicka, L. Zur Kenntnis des Kohlenstoffringes VIII. Weitere Beiträge zur Konstitution des Muscons. *Helvetica Chimica Acta* **9**, 1008–1017 (1926).
15. Ruzicka, L., Stoll, M. & Schinz, H. Zur Kenntnis des Kohlenstoffringes II. Synthese der carbocyclischen Ketone vom Zehner- bis zum Achtzehnering. *Helvetica Chimica Acta* **9**, 249–264 (1926).
16. Baeyer, A. Ueber Polyacetylenverbindungen. *Berichte der deutschen chemischen Gesellschaft* **18**, 2269–2281 (1885).
17. Kerschbaum, M. Über Lactone mit großen Ringen - die Träger des vegetabilischen Moschus-Duftes. *Berichte der deutschen chemischen Gesellschaft (A and B Series)* **60**, 902–909 (1927).
18. Gautschi, M., Bajgrowicz, J. A. & Kraft, P. Fragrance chemistry - Milestones and perspectives. *Chimia* **55**, 379–387 (2001).
19. Ruzicka, L. & Stoll, M. Gewinnung einiger mit der Untersuchung des Muscons zusammenhängender Methyl-polymethylen-dicarbonensäuren II. Über eine Synthese der 2-Methyl-tridecan-1,13-dicarbonensäure. *Helvetica Chimica Acta* **10**, 691–694 (1927).
20. Finley, K. T. & Finley, K. T. Acyloin cyclization. 573–589 (1964).
21. Finley, K. T. The acyloin condensation as a cyclization method. *Chemical Reviews* **64**, 573–589 (1964).
22. Story, P. R., Denson, D. D., Bishop, C. E., Clark, B. C. & Farine, J. C. A New General Synthesis of Macrocyclic Compounds. *Journal of the American Chemical Society* **90**, 817–818 (1968).
23. Spanagel, E. W. & Carothers, W. H. Preparation of Macrocyclic Lactones by Depolymerization. *Journal of the American Chemical Society* **58**, 654–656 (1936).
24. Berger, R. G. Scent and Chemistry. The Molecular World of Odors. *Angewandte Chemie International Edition* **51**, 3058–3058 (2012).
25. Sytniczuk, A., Milewski, M., Kajetanowicz, A. & Grela, K. Preparation of macrocyclic musks via olefin metathesis: comparison with classical syntheses and recent advances. *Russian Chemical Reviews* **89**, 469–490 (2020).
26. Gradillas, A. & Pérez-Castells, J. Macrocyclization by ring-closing metathesis in the total synthesis of natural products: Reaction conditions and limitations. *Angewandte Chemie - International Edition* vol. 45 6086–6101 (2006).
27. Fu, A. Ring closing alkyne metathesis : stereoselective synthesis of civetone. **606**, 75–78 (2000).
28. Michrowska, A., Wawrzyniak, P. & Grela, K. Synthesis of macrocyclic carbonates with musk odor by ring-closing olefin metathesis. *European Journal of Organic Chemistry* **9**, 2053–2056 (2004).

29. Bernardinelli, G. & Gerdil, R. Structures cristallines et moléculaires des muscs macrocycliques. II. La trans-civettone et sa 2,4-dinitrophénylhydrazone. *Helvetica Chimica Acta* **65**, 730–738 (1982).
30. Bernardinelli, G. & Gerdil, R. Structures cristallines et moléculaires des muscs macrocycliques. I. La cis-civettone et les variétés polymorphes α et β de sa 2,4-dinitrophénylhydrazone. *Helvetica Chimica Acta* **65**, 558–572 (1982).
31. Bernardinelli, G. & Gerdil, R. Structures cristallines et moléculaires des muscs macrocycliques') 111. La muscone et sa 2,4-dinitrophénylhydrazone. *Helvetica Chimica Acta* **4**, 1310–1317 (1982).
32. Callejo, R. *et al.* Fluorinated Musk Fragrances: The CF₂ Group as a Conformational Bias Influencing the Odour of Civetone and (R)-Muscone. *Chemistry - A European Journal* **22**, 8137–8151 (2016).
33. McAndrew, B. A. & Russell, S. W. Bicyclic analogues of exaltone (cyclopentadecanone) and muscone (3-methylcyclopentadecanone). *Journal of the Chemical Society, Perkin Transactions 1* **12**, 1172–1180 (1975).
34. Kraft, P., Bajgrowicz, J. A., Denis, C. & Fráter, G. Odds and trends: Recent developments in the chemistry of odorants. *Angewandte Chemie - International Edition* **39**, 2980–3010 (2000).
35. Eh, M. New Alicyclic Musks: The Fourth Generation of Musk Odorants. *Perspectives in Flavor and Fragrance Research* **1**, 145–154 (2007).
36. Kraft, P. “Brain aided” musk design. *Chemistry and Biodiversity* **1**, 1957–1974 (2004).
37. Kraft, P. & Cadalbert, R. 4-substituted 1,7-dioxacycloalkan-8-ones: Preparation and olfactory properties. *Synthesis* **11**, 1662–1669 (1998).
38. Kraft, P. Aroma Chemicals IV: Musks. in *Chemistry and Technology of Flavours and Fragrances* 143–168 (2009).
39. Trimmer, C. *et al.* Genetic variation across the human olfactory receptor repertoire alters odor perception. *Proceedings of the National Academy of Sciences of the United States of America* **116**, 9475–9480 (2019).
40. Morrison, J. Human nose can detect 1 trillion odours. *Nature* (2014).
41. Grabe, V. & Sachse, S. Fundamental principles of the olfactory code. *BioSystems* **164**, 94–101 (2018).
42. Horsfield, A. P., Haase, A. & Turin, L. Molecular recognition in olfaction. *Advances in Physics: X* **2**, 937–977 (2017).
43. Jones, F. N. & Jones, M. H. Modern Theories of Olfaction: A Critical Review. *Journal of Psychology: Interdisciplinary and Applied* **36**, 207–241 (1953).
44. Turin, L. A spectroscopic mechanism for primary olfactory reception. *Chemical Senses* **21**, 773–791 (1996).
45. Block, E. *et al.* Implausibility of the vibrational theory of olfaction. *Proceedings of the National Academy of Sciences of the United States of America* **112**, E2766–E2774 (2015).
46. Liu, M. T., Na, M., Li, Y., Biscoe, M. R. & Ryan, K. Conformational Sensing by a Mammalian Olfactory Receptor. *Chemistry - A European Journal* **26**, 11462–11469 (2020).
47. Buck, L. & Axel, R. A novel multigene family may encode odorant receptors: A molecular basis for odor recognition. *Cell* **65**, 175–187 (1991).

48. Green, E. D. & Chakravarti, A. The human genome sequence expedition: Views from the "base camp." *Genome Research* **11**, 645–651 (2001).
49. Ahmed, L. *et al.* Molecular mechanism of activation of human musk receptors OR5AN1 and OR1A1 by (R)-muscone and diverse other musk-smelling compounds. *Proceedings of the National Academy of Sciences of the United States of America* **115**, E3950–E3958 (2018).
50. Bersuker, I., Dimoglo, A., Gorbachov, M. & Vlad, P. Origin of musk fragrance activity: the electron -topologic approach. *New Journal of Chemistry* **15**, 307–320 (1991).
51. Kraft, P. & Fráter, G. Enantioselectivity of the musk odor sensation. *Chirality* **13**, 388–394 (2001).
52. Zou, Y. *et al.* Efficient macrocyclization by a novel oxy-oxonia-cope reaction: Synthesis and olfactory properties of new macrocyclic musks. *Chemistry - A European Journal* **18**, 7010–7015 (2012).
53. Liu, J. *et al.* Synthesis and Olfactory Properties of Silicon-Containing Analogs of Rosamusk, Romandolide, and Applelide: Insights into the Structural Parameters of Linear Alicyclic Musks. *European Journal of Organic Chemistry* **2016**, 976–982 (2016).
54. Zou, Y. *et al.* Efficient macrocyclization by a novel oxy-oxonia-cope reaction: Synthesis and olfactory properties of new macrocyclic musks. *Chemistry - A European Journal* **18**, 7010–7015 (2012).
55. Tormena, C. F. Conformational analysis of small molecules: NMR and quantum mechanics calculations. *Progress in Nuclear Magnetic Resonance Spectroscopy* **96**, 73–88 (2016).
56. Spiridonov, V. P., Vogt, N. & Vogt, J. Determination of molecular structure in terms of potential energy functions from gas-phase electron diffraction supplemented by other experimental and computational data. *Structural Chemistry* **12**, 349–376 (2001).
57. Cleeton, C. E. & Williams, N. H. Electromagnetic waves of 1.1 cm wave-length and the absorption spectrum of ammonia. *Physical Review* **45**, 234–237 (1934).
58. Balle, T. J. & Flygare, W. H. Fabry-Perot cavity pulsed Fourier transform microwave spectrometer with a pulsed nozzle particle source. *Review of Scientific Instruments* **52**, 33–45 (1981).
59. Balle, T. J., Campbell, E. J., Keenan, M. R. & Flygare, W. H. A new method for observing the rotational spectra of weak molecular complexes: KrHCl. *The Journal of Chemical Physics* **72**, 922–932 (1980).
60. Brown, G. G. *et al.* A broadband Fourier transform microwave spectrometer based on chirped pulse excitation. *Review of Scientific Instruments* **79**, 053103–13 (2008).
61. Loru, D., Bermúdez, M. A. & Sanz, M. E. Structure of fenchone by broadband rotational spectroscopy Structure of fenchone by broadband rotational spectroscopy. *The Journal of Chemical Physics* **145**, 074311–8 (2016).
62. Loru, D., Peña, I. & Sanz, M. E. Ethanol dimer: Observation of three new conformers by broadband rotational spectroscopy. *Journal of Molecular Spectroscopy* **335**, 93–101 (2017).



THEORETICAL BACKGROUND

Chapter 2



2. THEORETICAL BACKGROUND

2.1. Fundamentals of rotational spectroscopy

2.1.1. The Born-Oppenheimer approximation

The Hamiltonian operator of a diatomic or polyatomic molecule, similar to the Hamiltonian of an atom, can be described as:

$$H = T + V \quad (2.1)$$

where T is kinetic energy operator and V is the potential energy operator. The kinetic energy comprises T_e and T_n contributions from the electrons and nuclear motions, respectively.^{1,2} The potential energy includes three terms: V_{ee} and V_{nn} , due to coulombic repulsions between the electrons and between the nuclei, respectively, and an additional term V_{ne} , due to attractive forces between the electrons and nuclei.

$$H = T_e + T_n + V_{ee} + V_{nn} + V_{ne} \quad (2.2)$$

The Schrödinger equation for a fixed molecule, describing the motion of the electrons, can be written as:

$$H_e \psi_e = E_e \psi_e \quad (2.3)$$

$T_n = 0$, due to fixed nuclei, and V_{nn} is constant, and therefore H_e becomes:

$$H_e = T_e + V_{ee} + V_{ne} \quad (2.4)$$

Due to the V_{ne} term, H_e , and hence E_e , depend on the coordinates of the nuclei. In 1927, Max Born and J. Robert Oppenheimer proposed that since the nuclei are much heavier than the electrons, they must move significantly slower. Hence the two motions can be treated separately. As a result of the Born–Oppenheimer approximation, the T_e and V_{ee} can also be regarded as constant, because the electrons adjust immediately to any nuclear motion. For this reason, E_e is part of the potential field of the nuclear motion, so that:

$$H_n = T_n + V_{nn} + E_e \quad (2.5)$$

and the Schrödinger equation describing the motion of the nuclei is:

$$H_n \psi_n = E_n \psi_n \quad (2.6)$$

Based on the Born–Oppenheimer approximation that the total wave function ψ can be factorized as:

$$\psi = \psi_e \psi_n \quad (2.7)$$

where ψ_e is a function of nuclear and electron motion terms, and ψ_n a function of nuclear motion. The total molecular energy is therefore:

$$E = E_e + E_n \quad (2.8)$$

The ψ_n function can be further factorised into ψ_{vib} and ψ_{rot} parts as:

$$\psi_n = \psi_{vib}\psi_{rot} \quad (2.9)$$

Therefore, the total nuclear energy E_n can be written as:

$$E_n = E_{vib} + E_{rot} \quad (2.10)$$

Substituting equation (2.10) into (2.8), the total energy of a molecular system becomes:

$$E = E_e + E_{vib} + E_{rot} \quad (2.11)$$

and the total wavefunction ψ :

$$\psi = \psi_e\psi_{vib}\psi_{rot} \quad (2.12)$$

Classical angular momenta, moments of inertia and rotational energy

The quantum mechanical properties of a molecular rotor can be derived from the classical terms for the angular momenta and rotational energy. The classical angular momentum P of a rigid system can be described as:¹

$$P = I\omega \quad (2.13)$$

where ω is the angular velocity and I is the moment of inertia tensor. In dyadic notation moment of inertia can be expanded as:

$$\begin{aligned} I = & I_{xx}ii + I_{xy}ij + I_{xz}ik \\ & + I_{yx}ji + I_{yy}jj + I_{yz}jk \\ & + I_{zx}ki + I_{zy}kj + I_{zz}kk \end{aligned} \quad (2.14)$$

Each of the terms in equation (2.14) can be expressed in terms of the mass (m) and the x, y, z coordinates referring to an axis system fixed on the molecular rotor and centred on its centre of mass as:

$$\begin{aligned} I_x = I_{xx} &= \sum m(y^2 + z^2) \\ I_y = I_{yy} &= \sum m(z^2 + x^2) \\ I_z = I_{zz} &= \sum m(x^2 + y^2) \\ I_{xy} = I_{yx} &= -\sum mxy \\ I_{zx} = I_{xz} &= -\sum mxz \\ I_{yz} = I_{zy} &= -\sum myz \end{aligned} \quad (2.15)$$

The inertia tensor is given by the 3×3 matrix:

$$I = \begin{vmatrix} I_{xx} & I_{xy} & I_{xz} \\ I_{yx} & I_{yy} & I_{yz} \\ I_{zx} & I_{zy} & I_{zz} \end{vmatrix} \quad (2.16)$$

where the diagonal elements of the matrix are the *principal moments of inertia*, whilst the other off-diagonal elements are the *products of inertia*. It is always possible to choose the coordinate axes in a way that the products of inertia are removed, leaving only the diagonal elements. This can be achieved by diagonalisation of the matrix multiplying it by an orthogonal matrix giving:

$$I = \begin{vmatrix} I_{aa} & 0 & 0 \\ 0 & I_{bb} & 0 \\ 0 & 0 & I_{cc} \end{vmatrix} \quad (2.17)$$

The I_a , I_b and I_c principal moments of inertia are chosen so that:

$$I_a \leq I_b \leq I_c \quad (2.18)$$

The relationship between I_a , I_b and I_c determine the geometry of the rotor in the following way:¹

Rotor	Moments of inertia
Linear top	$I_a = 0, I_b = I_c$
Spherical top	$I_a = I_b = I_c$
Oblate symmetric top	$I_a = I_b < I_c$
Prolate symmetric top	$I_a < I_b = I_c$
Asymmetric top	$I_a < I_b < I_c$

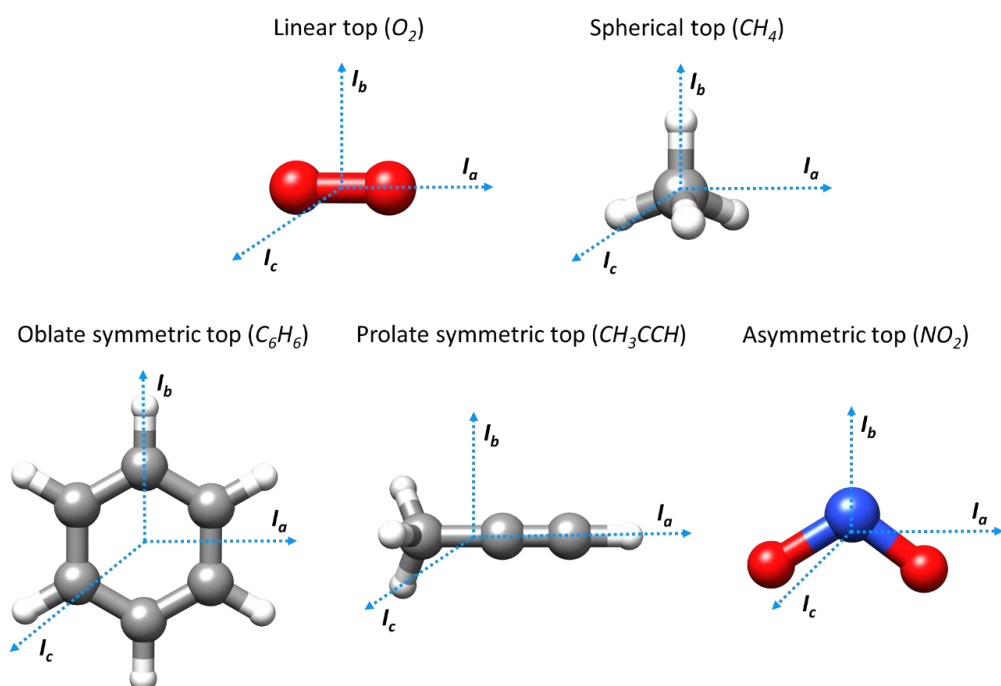


Figure 2.1. Examples of different rotors.

The rigid rotor

In an isotropic environment (free of external forces), the total energy of a rigid molecule is only dependent on the kinetic energy. The kinetic energy of a rigid rotor is described as:

$$E_{rot} = \frac{1}{2} \omega I \omega \quad (2.19)$$

$$= \frac{1}{2} (I_{xx} \omega_x^2 + I_{yy} \omega_y^2 + I_{zz} \omega_z^2 + 2I_{xz} \omega_x \omega_z + 2I_{yz} \omega_y \omega_z + 2I_{zx} \omega_z \omega_x)$$

In the principal axis system, it can be written as:

$$E_{rot} = \frac{1}{2} (I_x \omega_x^2 + I_y \omega_y^2 + I_z \omega_z^2) \quad (2.20)$$

When the notation x, y, z coordinates represent the principal axis system, the angular momentum components are:

$$P_x = I_x \omega_x, \quad P_y = I_y \omega_y, \quad P_z = I_z \omega_z \quad (2.21)$$

And the rotational energy in angular momentum terms can be described as:

$$E_{rot} = \frac{1}{2} \left(\frac{P_x^2}{I_x} + \frac{P_y^2}{I_y} + \frac{P_z^2}{I_z} \right) \quad (2.22)$$

If the system is not subjected to a torque, then the components P_x^2 , P_y^2 and P_z^2 are constant and hence, the total angular momentum (P^2) is constant:

$$P^2 = P_x^2 + P_y^2 + P_z^2 = \text{constant} \quad (2.23)$$

The kinetic energy of the rotor is also constant:

$$E_{rot} = \frac{1}{2} \left(\frac{P_x^2}{I_x} + \frac{P_y^2}{I_y} + \frac{P_z^2}{I_z} \right) = \text{constant} \quad (2.24)$$

The rotational energy levels resulting from the eigenvalues of the Hamiltonian. The eigenvalues can be expressed in terms of the angular momentum operators of a molecular system. In space-fixed rectangular coordinates X, Y, Z the classical angular momentum of a system can be expressed as:

$$P = iP_X + jP_Y + kP_Z \quad (2.25)$$

The component angular momentum operators are:

$$P_X = \sum_n \frac{\hbar}{i} \left[Y \left(\frac{\partial}{\partial Z} \right) - Z \left(\frac{\partial}{\partial Y} \right) \right]_n$$

$$P_Y = \sum_n \frac{\hbar}{i} \left[Z \left(\frac{\partial}{\partial X} \right) - X \left(\frac{\partial}{\partial Z} \right) \right]_n \quad (2.26)$$

$$P_Z = \sum_n \frac{\hbar}{i} \left[X \left(\frac{\partial}{\partial Y} \right) - Y \left(\frac{\partial}{\partial X} \right) \right]_n$$

where $i = (-1)^{\frac{1}{2}}$ and $\hbar = h/2\pi$.

The quantum mechanical rotational energy operator is obtained by substituting the classical angular momentum with the corresponding angular momentum operator.

$$\hat{H} = \frac{1}{2} \left(\frac{P_x^2}{I_x} + \frac{P_y^2}{I_y} + \frac{P_z^2}{I_z} \right) \quad (2.27)$$

where:

$$\begin{aligned} P_x &= \sum_n \frac{\hbar}{i} \left(y \frac{\partial}{\partial z} - z \frac{\partial}{\partial y} \right) \\ P_y &= \sum_n \frac{\hbar}{i} \left(z \frac{\partial}{\partial x} - x \frac{\partial}{\partial z} \right) \\ P_z &= \sum_n \frac{\hbar}{i} \left(x \frac{\partial}{\partial y} - y \frac{\partial}{\partial x} \right) \end{aligned} \quad (2.28)$$

It is easy to notice from expression (2.23) that P^2 commutes with its constituent operators. Whilst the component operators do not commute among themselves, the following commutations are possible:

$$\begin{aligned} P_x P_y - P_y P_x &= i\hbar P_z \\ P_y P_z - P_z P_y &= i\hbar P_x \\ P_z P_x - P_x P_z &= i\hbar P_y \end{aligned} \quad (2.29)$$

According to a principle of quantum mechanics, operators which commute have common sets of eigenfunctions. Hence, P^2 , P_z and P_x share common eigenfunctions, which we label as $\psi_{J,M,K}$ and can be expressed as:

$$\begin{aligned} P^2 \psi_{J,M,K} &= k_J \psi_{J,M,K} \\ P_z \psi_{J,M,K} &= k_M \psi_{J,M,K} \\ P_x \psi_{J,M,K} &= k_K \psi_{J,M,K} \end{aligned} \quad (2.30)$$

where k_J , k_M and k_K are eigenvalues of P^2 , P_z and P_x and through a sequence of derivations can be quantised as:

$$\begin{aligned} k_J &= \hbar^2 J(J+1) \\ k_M &= \hbar M \\ k_K &= \hbar K \end{aligned} \quad (2.31)$$

where:

$$\begin{aligned} J &= 0, 1, 2, \dots \\ M &= J, J-1, J-2, \dots, -J \\ K &= J, J-1, J-2, \dots, -J \end{aligned} \quad (2.32)$$

Expression (2.27) can be presented in terms of the rotational constants as:

$$H = AP_a^2 + BP_b^2 + CP_c^2 \quad (2.33)$$

where $A, B,$ and C are the rotational constants which are dependent of the principal moments of inertia I_a, I_b and I_c as following:

$$A = \frac{h}{8\pi^2 I_a} \quad B = \frac{h}{8\pi^2 I_b} \quad C = \frac{h}{8\pi^2 I_c} \quad (2.34)$$

Due to the inverse proportionality relationship between the rotational constants and the moments of inertia:

$$A \geq B \geq C \quad (2.35)$$

The relationship between the three rotational constants lead to the classification of different rotors, which will be described in more detail in the following sections.

Linear top rotor

A linear polyatomic molecule, similar to the diatomic molecule, has no angular momentum along the a inertial axis ($I_a = 0, I_b = I_c$). Therefore, the total angular momentum P^2 is:

$$P^2 = P_b^2 + P_c^2 \quad (2.36)$$

and the rotational Hamiltonian of a linear rotor can be expressed as:

$$H = \frac{1}{2I} (P_b^2 + P_c^2) = \frac{P^2}{2I} \quad (2.37)$$

The rotational energy, resulting from the nonvanishing matrix elements, can be derived by substituting the P^2 in equation (2.36) with the corresponding eigenvalue:

$$E_{rot} = \frac{h^2 J(J+1)}{8\pi^2 I} \quad (2.38)$$

Considering that the rotational constant $B = (h/8\pi^2 I)$, equation 2.38 can be expressed as:

$$E_{rot} = hBJ(J+1) \quad (2.39)$$

Besides having a permanent dipole moment, the selection rules of a linear top are:

$$\Delta J = \pm 1 \quad \Delta M = 0, \pm 1 \quad (2.40)$$

The selection rule of quantum number M has physical significance only when an electric or magnetic external field is applied.

Therefore, the frequency (in units of Hz or cm^{-1}) corresponding to the transition $J \rightarrow J+1$ can be converted from equation (2.39) to:

$$\nu_{rot} = 2B(J + 1) \quad (2.41)$$

According to expression (2.40), the rotational spectrum of a linear molecule consists of a harmonic series of lines separated by $2B$ with frequencies:¹

$$\nu = 2B, 4B, 6B, \dots \quad (2.42)$$

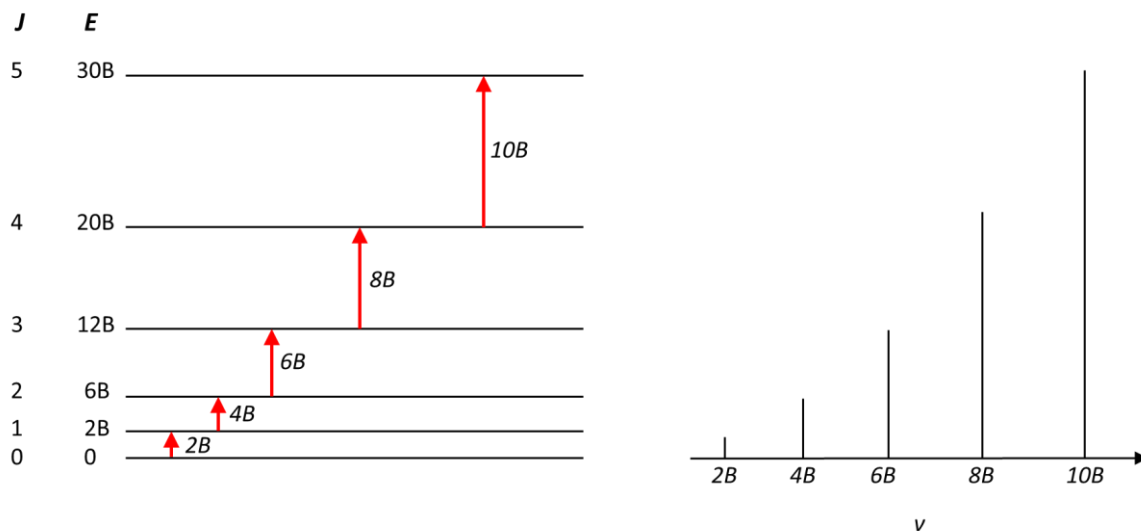


Figure 2.2. Diagram showing the sequence of the rotational levels and corresponding absorption lines for a linear top rotor.

Spherical top rotor

Spherical top rotors have equal moments of inertia along the three principal inertial axes. Therefore:

$$I_a = I_b = I_c \quad (2.43)$$

This usually results in the three dipole moment components μ_a , μ_b , and μ_c being equal to zero. Hence, spectra of spherical top rotors are not generally observable by microwave spectroscopy. Nevertheless, in 1971 James Watson observed for the first time the rotational spectrum of CH_4 , which was allowed by a dipole moment being created as a result of centrifugal distortion.³

The Hamiltonian expression of spherical tops can be written as:

$$H = \frac{1}{2I}(P_a^2 + P_b^2 + P_c^2) = \frac{P^2}{2I} \quad (2.44)$$

The expressions for the rotational energy are the same as for the linear top, equations (2.38) and (2.39). Therefore, all selection rules for linear top rotors apply for spherical top rotors as well, equation (2.40).

Symmetric top rotor

A symmetric top rotor is a molecule with two equal principal moments of inertia. This condition is normally satisfied when the molecule has one of the moments of inertia as axis of symmetry. If the I_a principal moment of inertia lies along the symmetry axis, the molecule is a *prolate symmetric top*, and if the I_c principal moment of inertia axis lies along the symmetry axis, then the molecule is a *oblate symmetric top*.

From section 2.1.2, a *prolate symmetric top* rotor has the three principal moments of inertia as following:

$$I_a < I_b = I_c \quad (2.45)$$

whilst an *oblate symmetric top*:

$$I_a = I_b < I_c \quad (2.46)$$

Their corresponding rotational Hamiltonian expressions are

$$H = \frac{P^2}{2I_b} + \frac{1}{2} \left(\frac{1}{I_a} - \frac{1}{I_b} \right) P_a^2 \quad (2.47)$$

for the *prolate symmetric top* rotor, and

$$H = \frac{P^2}{2I_b} + \frac{1}{2} \left(\frac{1}{I_c} - \frac{1}{I_b} \right) P_c^2 \quad (2.48)$$

for the *oblate symmetric top* rotor.

The rotational energy of each of the two types of rotors can be derived from equations (2.47) and (2.48) in the same way as for linear and spherical tops. For the *prolate symmetric top* rotor the corresponding rotational energy is:

$$E_{rot} = \left(\frac{h^2}{8\pi^2 I_b} \right) J(J+1) + \left(\frac{h^2}{8\pi^2} \right) \left(\frac{1}{I_a} - \frac{1}{I_b} \right) K^2 \quad (2.49)$$

whilst for the *oblate symmetric top* rotor it is:

$$E_{rot} = \left(\frac{h^2}{8\pi^2 I_b} \right) J(J+1) + \left(\frac{h^2}{8\pi^2} \right) \left(\frac{1}{I_c} - \frac{1}{I_b} \right) K^2 \quad (2.50)$$

Both equations (2.49) and (2.50) can be written in terms of rotational constants A, B and C as follows:

$$E_{rot}(J, K) = h[BJ(J+1) + (A - B)K^2] \quad (2.51)$$

and:

$$E_{rot}(J, K) = h[BJ(J+1) + (C - B)K^2] \quad (2.52)$$

respectively.

Because of the relation (2.35), $(A - B)$ in equation (2.51) for a *prolate symmetric top* is a positive term, and therefore the energy of rotational levels increases with the increase in K . However, $(C - B)$ in equation (2.52) for an *oblate symmetric top* is a negative term and the energy of rotational energy decreases with the increase in K .

The selection rules of a symmetric top rotor are:

$$\Delta J = 0, \pm 1 \quad \Delta K = 0 \quad \Delta M = 0, \pm 1 \quad (2.53)$$

The quantum number K may take values up to J : $K = 0, 1, 2, \dots, J$. It can not be greater than J , as I_c is not able to exceed the magnitude of P . All levels with $K = 0$ are non-degenerate and the ones with $K \neq 0$ are doubly degenerate. The latter can be explained classically, as being a result of clockwise and anticlockwise rotation with the same angular momentum.¹ In the absence of any external field, similar to linear and spherical-top rotors, the degeneracy in M will remain as $2J + 1$.

The corresponding frequency relation for a symmetric top rotor is the same as for the linear and the spherical tops:

$$\nu_{rot} = 2B(J + 1) \quad (2.54)$$

With addition of the first order centrifugal distortion stretching constants to the rigid rotor, the expression of the rotational energy in (2.51) becomes:

$$E_{rot}(J, K) = h[B_0J(J + 1) + (A_0 - B_0)K^2 - D_JJ^2(J + 1)^2 - D_{JK}J(J + 1)^2 + DK^4] \quad (2.55)$$

For the oblate rotor the second term $(A_0 - B_0)$ becomes $(C_0 - B_0)$.

The frequency relation for expression (2.55) with selection rules of $J + 1 \leftarrow J$ and $K \leftarrow K$ is:

$$\nu_{rot} = 2B_0(J + 1) - 4D_J(J + 1)^3 - 2D_{JK}(J + 1)K^2 \quad (2.56)$$

Asymmetric top rotor

An asymmetric top rotor is a molecule with all the moments of inertia different and non-zero.

$$I_a \neq I_b \neq I_c \quad (2.57)$$

This increases considerably the complexity of the rotational spectrum, as there the rotational frequencies can no longer be expressed in convenient expressions as in linear or symmetric top. Nevertheless, the asymmetric tops form the largest group of molecules. The only way to determine the rotational terms of an asymmetric tops is by matrix diagonalization of each value of J , which remains a relevant quantum term. M is still a good quantum number, whilst K

quantum number cannot be used anymore to describe the energy of the rotational levels. King et al. introduced a double subscript system to help describe the system, known as K_{-1} and K_{+1} pseudo-quantum numbers, which are related to the prolate and oblate symmetric rotors described above.⁴

The behaviour of an asymmetric rotor can be described using Ray's parameter (κ):

$$\kappa = \frac{2B - A - C}{A - C} \quad (2.58)$$

which is a measure of the asymmetry of the rotor. κ can take values between -1 and $+1$, which correspond to the prolate and oblate symmetric top limits, respectively.

The rotational problem in asymmetric rotors is overcome by using a Cartesian axis system x, y , and z , with its origin at the center of mass of the molecule that coincides with the principal axes of inertia a, b and c . The Hamiltonian describing the rotation of a rigid asymmetric rotor is:

$$H = AP_a^2 + BP_b^2 + CP_c^2 \quad (2.59)$$

Including the Rays parameter (2.56) into the expression (2.57):

$$H = \frac{1}{2}(A + C)P^2 + \frac{1}{2}(A - C)H(\kappa) \quad (2.60)$$

where $H(\kappa)$ is the reduced Hamiltonian:

$$H(\kappa) = P_a^2 + \kappa P_b^2 + P_c^2 \quad (2.61)$$

$H(\kappa)$ does not depend on the rotational constants, allowing to treat the asymmetry as a perturbation.

The total rotational energy can be written as:

$$E_{rot} = \frac{1}{2}(A + C)J(J + 1) + \frac{1}{2}(A - C)E_{JK_aK_b} \quad (2.62)$$

with $E_{JK_aK_b}$ being $2J + 1$ solutions for each J level.

The selection rule for the J quantum number, similar to the symmetric body is:

$$\Delta J = 0, \pm 1 \quad (2.63)$$

where $\Delta J = +1$ gives rise to R -branch transitions, $\Delta J = -1$ to P -branch, and $\Delta J = 0$ are Q -branch transitions.

Asymmetric top can have non-zero dipole moment components along all three inertial axes. The existence of different dipole moment components μ_a, μ_b and μ_c give rise to different transitions, of a -, b - and c -type, respectively. The selections rules for each a -, b - and c -types can be expressed in terms of the K_{-1} and K_{+1} quantum numbers, using $J''_{K_{-1}K_{+1}} \leftarrow J'_{K_{-1}K_{+1}}$ notation:

Table 2.1. Selection rules for the quantum numbers K_{-1} and K_{+1} for each dipole moment.

Dipole moment component	Permitted transitions $J''_{K_{-1}K_{+1}} \leftarrow J'_{K_{-1}K_{+1}}$	Selection rule $\Delta K_{-1}, \Delta K_{+1}$
$\mu_a \neq 0$	$ee \leftarrow eo$ $oe \leftarrow oo$	$\Delta K_{-1} = 0, \pm 2, \dots$ $\Delta K_{+1} = \pm 1, \pm 3, \dots$
$\mu_b \neq 0$	$ee \leftarrow oo$ $oe \leftarrow eo$	$\Delta K_{-1} = \pm 1, \pm 3, \dots$ $\Delta K_{+1} = \pm 1, \pm 3, \dots$
$\mu_c \neq 0$	$ee \leftarrow oe$ $eo \leftarrow oo$	$\Delta K_{-1} = \pm 1, \pm 3, \dots$ $\Delta K_{+1} = 0, \pm 3, \dots$

The magnitude of the dipole moment μ is usually quoted in Debye units, and it can be determined experimentally using the Stark effect.

Centrifugal distortion

In the previous description of symmetric and asymmetric rotors the systems were considered rigid. Whilst this is a useful approximation, the nuclei in molecule are held together by a certain degree of restoring forces. Therefore, when the molecule rotates a centrifugal force is produced which affects its bond distances and angles. The rotating molecule changes from an equilibrium to a distorted configuration. The effects of the centrifugal distortion are large for light linear and symmetric top molecules because of the small moments of inertia. However, the theory of centrifugal distortion is considerably more complex for asymmetric rotors. The effect of centrifugal distortion can be quantified from the analysis of the microwave spectrum, which allows high precision measurements.^{4,5}

Although the effects of distortion can be quite dramatic in a rotational spectrum, distortion represents only a small part of the rotational energy. Therefore, it is usually treated as a perturbation of the rigid rotor Hamiltonian:

$$H = H_{rot} + H_d \quad (2.64)$$

where H_d is:

$$H_d = \frac{\hbar^2}{4} \sum_{\alpha, \beta, \gamma, \delta} \tau_{\alpha\beta\gamma\delta} P_\alpha P_\beta P_\gamma P_\delta \quad (2.65)$$

The $\tau_{\alpha\beta\gamma\delta}$ term represents the distortion constants, also called the fourth order centrifugal constants. The distortion contribution includes angular momentum along all three axes.

$$\tau_{\alpha\beta\gamma\delta} = -\frac{1}{2} \sum_{ij} \mu_{\alpha\beta}^{(i)} (f^{-1})_{ij} \mu_{\gamma\delta}^{(j)} \quad (2.66)$$

where f^{-1} is a matrix element inverse to the matrix of force constants.

The inverse proportional dependence of the distortion constants to the molecular force constant matrix is expected, as weaker bonds with small force constants would experience larger distortion effects compared to the strong bonds with large force constants.

The total energy including the centrifugal distortion contribution can be written as:

$$E = E_{rot} + E_d \quad (2.67)$$

where E_d is the centrifugal distortion energy and in a symmetric rotor can be expressed as:

$$E_d = -[D_J J^2 (J + 1)^2 + D_{JK} J (J + 1) K^2 + D_K K^2] \quad (2.68)$$

where D_J , D_{JK} and D_K are the distortion coefficients of the first order energy expression, and E_r is the energy of the rigid rotor.

The expression (2.65) describes the Hamiltonian independent of the rotational and vibrational coordinates. Whilst this approximation is valid for a rigid rotor, in an actual molecule vibrational motion will affect the rotational and distortion constants, even in the ground state. Experimentally determined rotational and centrifugal constants take this effect into account and depend on the vibrational state in which the rotational spectrum is observed.

$$D_J = \frac{\hbar^4}{2h} \frac{m}{f(I^e)^3} = \frac{4B_e^3}{\omega_e^2} \quad (2.69)$$

where m is the reduced mass, B_e is the equilibrium rotational constant, ω_e^2 is the vibrational frequency of the molecule in wavenumbers. D_J is always positive, whilst the others can take both negative and positive values.

In an asymmetric determination of centrifugal distortion is more complex than in symmetric top molecules. Unlike the linear description of the centrifugal distortion constants for symmetric rotor described in equation (2.68), in the case of an asymmetric top rotor the linear combinations of the centrifugal distortion constants are unknown. Watson^{5,6} changed the semirigid rotor Hamiltonian in the reduced Hamiltonian by introducing the unitary operator U :

$$\tilde{H} = U^{-1} H U \quad (2.70)$$

which results in two different reductions: A and S . The A -reduction is usually used for the asymmetric top molecules and can be expressed as:

$$\begin{aligned}
H^A = & \frac{1}{2}(B^{(A)} + C^{(A)})P^2 + \left[A^{(A)} - \frac{1}{2}(B^{(A)} + C^{(A)}) \right] P_z^2 + \frac{1}{2}(B^{(A)} - C^{(A)})(P_x^2 - P_y^2) \\
& - D_J P^4 - D_{JK} P^2 P_x^2 - D_K J_z^4 - 2\delta_J J^2 (P_x^2 - P_y^2) \\
& + \delta_K [P_z^2 (P_x^2 - P_y^2) + (P_x^2 - P_y^2) P_z^2]
\end{aligned} \tag{2.71}$$

The reduced Hamiltonian for S -reduction, which is more suitable for only slightly asymmetric tops is described by Gordy and Cook in chapter 8.¹ Both reductions A and S have been used in the data analysis of the molecules in this thesis.

2.2. Structural determination methods

Due to its high accuracy and high-resolution, microwave spectroscopy is widely applicable to the evaluation of molecular structures. Structural information, such as bond lengths and bond angles, is derived from I_b and I_c , which are inversely proportional to the rotational constants A, B and C , respectively. One challenge in deriving the structural parameters is the vibrational energy, which affects the molecular structure even in ground states. Therefore, the experimentally obtained moments of inertia must be corrected to account for this effect. Generally, the spectrum of isotopically substituted species is studied to provide adequate data for structural determination. The improved sensitivity of spectrometers and recent technological advancements have allowed for more structural studies.^{1,6}

Over the years, a few methods have been introduced which correct for the vibrational effects. The ones applied in the structural determination of molecules presented in this thesis are:

1. r_e is the *equilibrium structure*, which corresponds to the theoretically calculated structure and does not include any effects of vibrational motion.
2. r_0 is the *effective structure*, which is calculated for the ground vibrational state.
3. r_s is the *substitution structure*, which is derived from the isotopically substituted species.

The equilibrium structure

To account for the vibration-rotation interaction, the r_e structure uses the approximation that the rotational constant characterises the rotation as a slow motion averaged over a rapid vibration motion. Using a diatomic model, this can be presented in the equation of the effective rotational constant B at any vibrational level v :

$$B_v = \frac{h}{8\pi^2 I_b^v} = \frac{h}{8\pi^2 \mu} \left\langle \frac{1}{r^2} \right\rangle \quad (2.72)$$

In which μ is the reduced mass of the diatomic molecule and $\langle 1/r^2 \rangle$ is the average over the vibrational wave function. The latter can be expanded in vibrational coordinate terms as:

$$\frac{1}{r^2} = \frac{1}{r_e^2} (1 + \xi)^{-2} \quad (2.73)$$

where $\xi = (r - r_e)/r_e$.

The effective rotational constant of a vibrating rotator B_v can be written as:

$$B_v = B_e - \alpha_e \left(v + \frac{1}{2} \right) \quad (2.74)$$

with:

$$\alpha_e = -\left(\frac{6B_e^2}{\omega_e} \right) (1 + a_1) \quad (2.75)$$

It has been proved that expression (2.66) is an accurate approximation to the effective rotational constant.

The expressions describing the rotational constants of a polyatomic molecule are:

$$\begin{aligned} A_v &= A_e - \sum_s \alpha_s^a \left(v_s + \frac{d_s}{2} \right) \\ B_v &= B_e - \sum_s \alpha_s^b \left(v_s + \frac{d_s}{2} \right) \\ C_v &= C_e - \sum_s \alpha_s^c \left(v_s + \frac{d_s}{2} \right) \end{aligned} \quad (2.76)$$

The equilibrium structures of the molecules analysed in this thesis have been derived from *ab initio* calculations.

The effective structure

The effective structure refers to structure calculated directly from the B_v for a certain vibrational level. Structural parameters are selected in order to reproduce the effective moments of inertia. The effective structure for a diatomic structure can be written as:

$$r_0 = \left(\frac{h}{8\pi^2 \mu B_0} \right)^{1/2} = \left(\frac{I_b^0}{\mu} \right)^{1/2} \quad (2.77)$$

Any bond distance calculated from B_0 will be different from the r_e bond distance, since r_0 is a reciprocal of square root of the inverse squared internuclear distance:

$$r_0 = \left\langle \frac{1}{r^2} \right\rangle^{-1/2} \neq r_e \quad (2.78)$$

r_0 is larger than r_e and is also expected to change with isotopic substitution. The difference between the two is more significant in light atoms, such as hydrogen, which causes a large effect on the amplitude of vibrations. The effect of isotopic substitution on heavier atoms is almost not observable.

In a polyatomic molecule Coriolis contributions affect the r_0 structure, which is no longer $(r^{-2})^{-1/2}$, and assumptions such as structural parameters being independent of the mass changes are needed for structural determination. Moreover, different r_0 structures can be calculated depending on the isotopic substitutions considered. The limitation of this method remains the neglect of the zero-point vibrational effects, which can lead to low accuracy. Nevertheless, it is convenient for complicated molecular systems. The linear representation of the least-square fitting method is:

$$I_i = I_i^0 + \sum_j \left(\frac{\partial I_i}{\partial p_j} \right)_0 \Delta p_j \quad (2.79)$$

where I_i is the experimental moment of inertia, I_i^0 is the calculated or predicted moment of inertia, and p_j is the structural parameter. The derivative $\left(\frac{\partial I_i}{\partial p_j} \right)$ is calculated by keeping the other parameters fixed.

The effective structures presented in this thesis have been calculated using STRFIT program which is available on PROSPE website.⁷

The substitution structure

In 1953, Kraitchman suggested a method for to determine the coordinates of an atom in the molecule principal axis system, which uses moments of inertia differences resulting from single isotopic substitution of the atom. In order to calculate the full structure, it is evident that mono-substituted species of all atoms are required. Moreover, the structural parameters such as bond lengths and angles are considered to be fixed and not affected by the substitution, hence the system is assumed to be rigid.⁸

Previously, the I_x , I_y and I_z moments of inertia of the parent species have been described in equation (2.15). Similarly, the moments of inertia of the isotopic species I'_x , I'_y and I'_z can be defined as:

$$\begin{aligned}
 I'_x &= I_x + \mu(y^2 + z^2) \\
 I'_y &= I_y + \mu(x^2 + z^2) \\
 I'_z &= I_z + \mu(x^2 + y^2) \\
 I'_{xy} &= -\mu xy \\
 I'_{xz} &= -\mu xz \\
 I'_{yz} &= -\mu yz
 \end{aligned}
 \tag{2.80}$$

where μ is the reduced mass of the isotopic substitution and can be expressed as:

$$\mu = \frac{M\Delta m}{M + \Delta m}
 \tag{2.81}$$

with M as total mass of the parent species and Δm as the mass of the isotopically substituted atom.

Diagonalization of the inertial matrix allows determination of the principal moments of inertia of the substituted molecule, which are identified experimentally from the spectral analysis of the isotopologues.

The absolute coordinates of the substituted atom in a linear molecule, where $I_z = 0$ and $I_x = I_y$, can be easily derived from equation (2.76). The z coordinates will be the only non-zero ones, and therefore equation (2.76) becomes:

$$\begin{aligned}
 I'_{xy} &= I'_{xz} = I'_{yz} = 0 \\
 I'_x &= I_x + \mu z^2 \\
 I'_y &= I_y + \mu z^2 \\
 I'_z &= I_z = 0
 \end{aligned}
 \tag{2.82}$$

From I'_x and I'_y the absolute value of the distance of substituted atom $|z|$ can be determined as:

$$|z| = \left[\frac{1}{\mu} (I'_x - I_x) \right]^{1/2} = \left[\frac{1}{\mu} (I'_y - I_y) \right]^{1/2}
 \tag{2.83}$$

Whilst the method allows for the accurate position of the substitution atoms to be calculated, the signs of the coordinates cannot be identified, so theoretical structures are used to obtain them.

2.3. Bibliography

1. Gordy, W. & Cook, R. L. *Microwave molecular spectra*. (JOHN WILEY & SONS, 1984).

2. Bauder, A. Fundamentals of Rotational Spectroscopy. in *Handbook of High-resolution Spectroscopy* (2011).
3. Watson, J. K. G. Forbidden rotational spectra of polyatomic molecules. *Journal of Molecular Spectroscopy* **40**, 536–544 (1971).
4. King, G. W., Hainer, R. M. & Cross, P. C. I. Calculation and symmetry classification of energy levels. *The Journal of Chemical Physics* **11**, 27–42 (1943).
5. Watson, J. K. G. Determination of centrifugal distortion coefficients of asymmetric-top molecules. *The Journal of Chemical Physics* **46**, 1935–1949 (1967).
6. Watson, J. K. G. Simplification of the molecular vibration-rotation Hamiltonian. *Molecular Physics* **15**, 479–490 (1968).
7. Kisiel, Z. PROSPE-Programs for Rotational spectroscopy. 91–106 (2001).
8. Kraitchman, J. Determination of Molecular Structure from Microwave Spectroscopic Data. *American Journal of Physics* **21**, 17–24 (1953).



EXPERIMENTAL SET-UP AND INSTRUMENT DEVELOPMENT

Chapter 3



3. EXPERIMENTAL SET-UP AND INSTRUMENT DEVELOPMENT

Chirped pulse Fourier Transform Microwave (CP-FTMW) spectrometers, not being generally commercially available, were usually designed to adapt to the research needs. Nowadays they can be purchased from BrightSpec, a company founded by Brooks Pate. Our CP-FTMW spectrometer (Figure 3.1), was designed based on Pate's model^{1,2} and operates in the 2-8 GHz frequency range, which is suitable for the study of large molecular systems, such as the cycles and musk odorants presented in this thesis.³ This chapter provides the description of the technique, our instrumental set-up and further details on each of the events in the operation cycle.

3.1. Sequence of operation

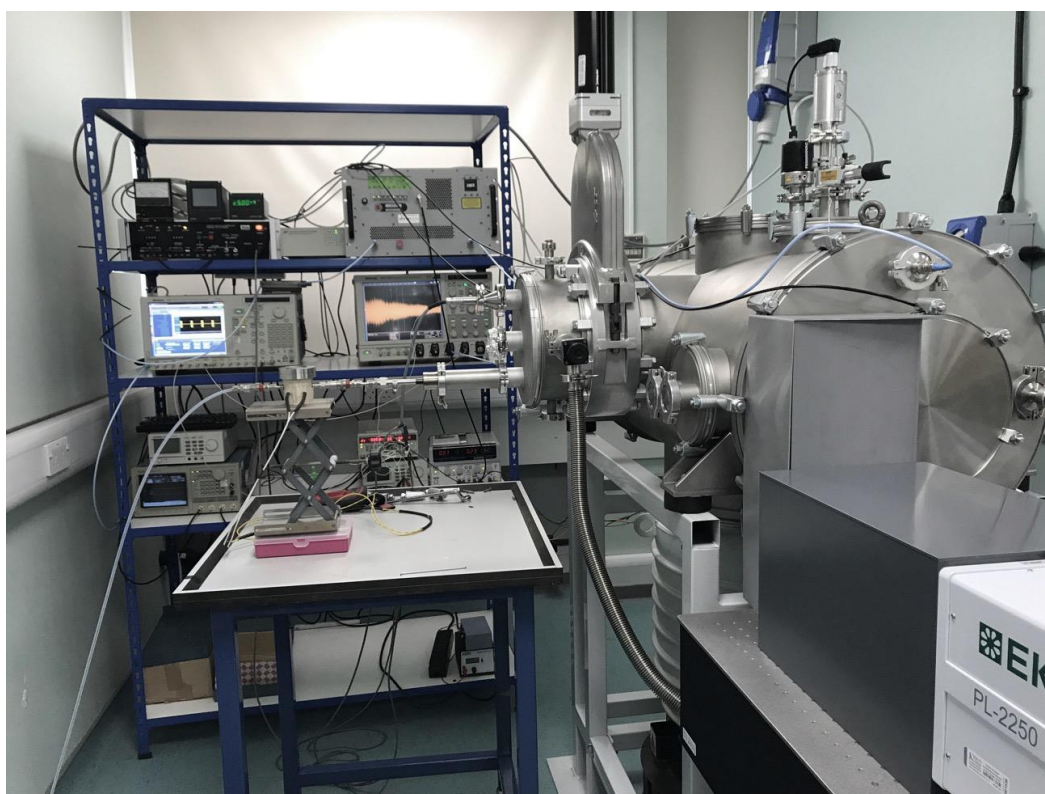


Figure 3.1. CP-FTMW spectrometer at King's College London.

Our CP-FTMW spectrometer operates in a cyclic manner. Each cycle starts with the generation of a molecular pulse, followed by polarisation with a 2-8 GHz chirped pulse. The chirped pulse is created by an arbitrary waveform generator (AWG) and amplified using a travelling wave tube amplifier (TWTA) before interacting with the molecular pulse. In our set-up the MW pulse interacts perpendicularly with molecular pulse. The MW pulse is conducted inside the vacuum chamber via a standard horn antenna. Upon interaction with the excitation pulse,

molecules undergo polarisation and create a macroscopic dipole moment. When the MW radiation excitation is interrupted, molecules relax and emit the absorbed energy. The molecular emission signal is collected by a second standard horn antenna which is at the opposite side of the vacuum chamber. The emission signal, which is very weak due to the small population difference between rotational levels, is amplified using a low noise amplifier and recorded by an oscilloscope as a free induction decay (FID) in the time domain. The FID is Fourier-transformed to the frequency domain using a fast Fourier transform algorithm. The final spectrum is obtained by repeating the cycle until the sum of FIDs offers a satisfactory signal-to-noise (S/N) ratio.

The different components of our spectrometer and their connections are illustrated in Figure 3.2. The four main steps of the experimental cycle: (1) molecular pulse generation, (2) the MW chirp pulse generation, (3) the interaction between the molecular and MW pulses, and (4) FID detection are depicted in Figure 3.3 and explained further below.

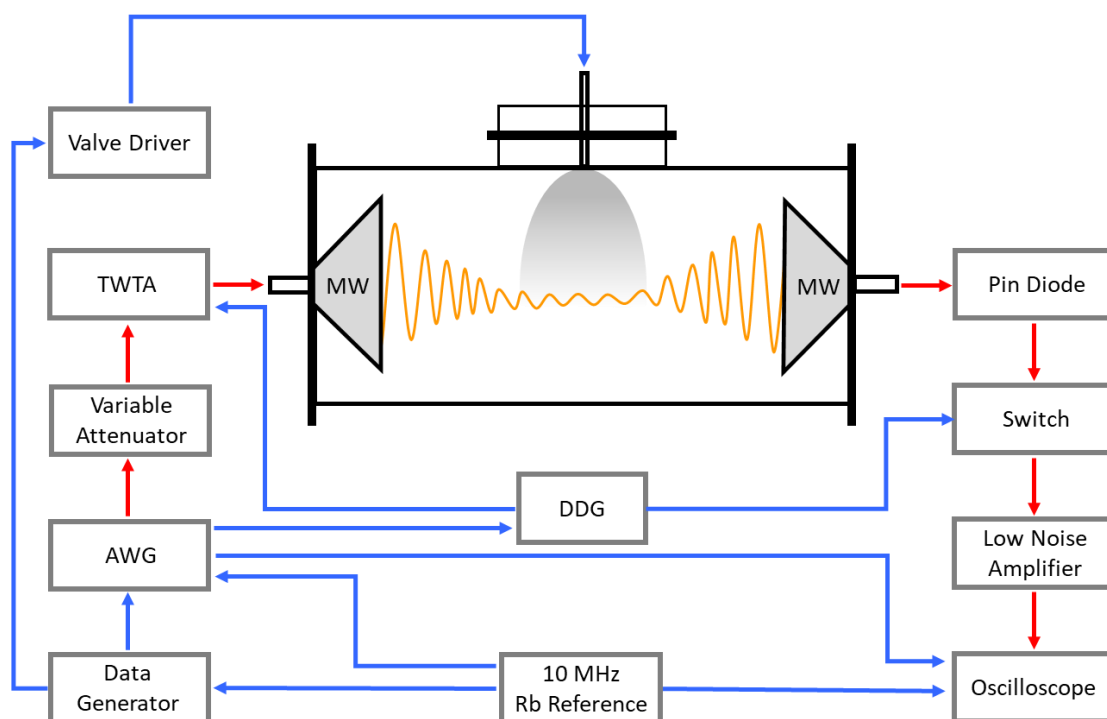


Figure 3.2. Schematic representation of the 2-8 GHz CP-FTMW spectrometer at King's College London. Red lines represent the path of the MW radiation; blue lines are the TTL signals. The MW chirped pulse is created by a 24 GS/s arbitrary waveform generator (AWG), amplified by a 200 W travelling wave tube amplifier (TWTA) and transmitted inside the vacuum chamber by a standard horn antenna. The emission signal is collected at the second horn antenna, amplified using a low noise amplifier and collected in the time domain using a 100 GS/s oscilloscope. All components are locked to a 10 MHz Rubidium reference.

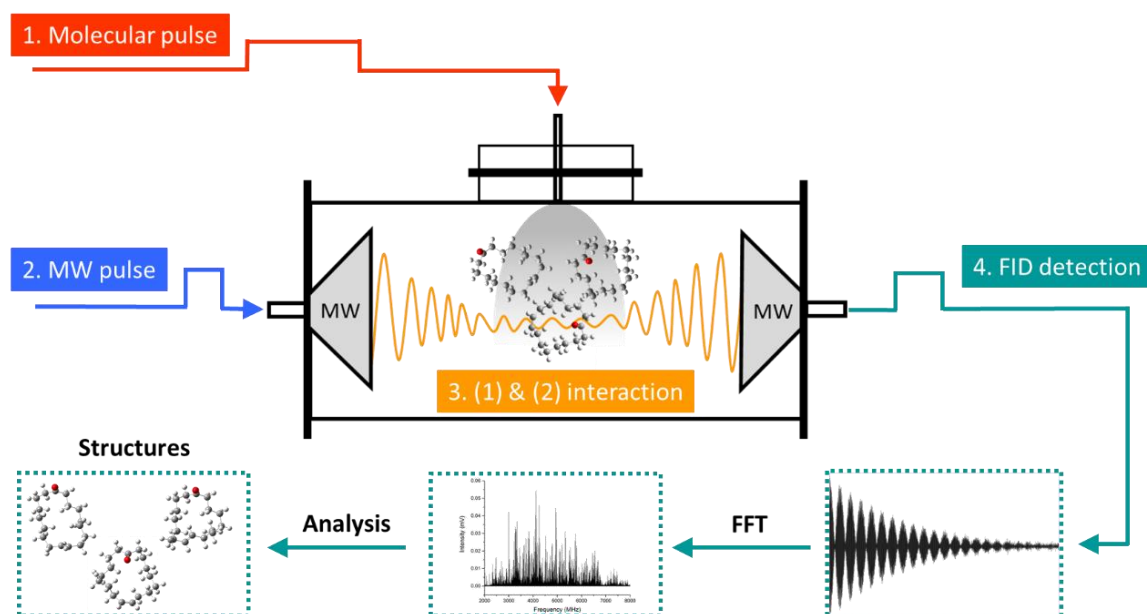


Figure 3.3. Schematic set-up and sequence of events of the 2-8 GHz CP-FTMW spectrometer at King's College London. (1) The molecular pulse supersonically expands into the vacuum chamber. (2) The amplified MW chirped pulse is broadcast into the chamber via a horn antenna. (3) Interaction between the molecular jet and the MW pulse. (4) Detection of the emission signal.

Molecular pulse

In our experimental set-up we use a supersonic expansion to create a molecular jet. Supersonic expansions are widely used in combination with other techniques for their numerous advantages, which are discussed below.

A supersonic jet is created by expanding a gas through a small orifice from a very high pressure region to very low pressure region, Figure 3.4.⁴ During the early stages of the supersonic expansion, the molecules in the gas undergo adiabatic cooling, which consists in the almost complete conversion of their internal energy to kinetic energy. This results in low translational, rotational and vibrational temperatures, which leads to a narrow velocity distribution and narrow line shapes. An additional benefit of a supersonic expansion is population of only the lower energy levels, which contributes to more intense and simplified spectra. Moreover, the frequency of collisions decreases considerably moving away from the nozzle and after the first stages of the expansion the molecules do not interact anymore. This allows for the molecules to be investigated isolated, allowing for the study of their fundamental molecular properties. Furthermore, supersonic expansion makes possible the study of weakly bound complexes, which are formed during the collisions in the throat of nozzle. If the complexes subsist the first stages of the supersonic expansion they can be observed in the

spectrum. These large number of advantages offered by supersonic expansions make them a popular technique in combination with other spectroscopic techniques.^{5–14}

In our set-up, the molecular jet is supersonically expanded by using a backing gas, usually Ne, He or Ar, and pulsing the sample mixture from the heating nozzle (yellow receptacle in Figure 3.5.B) to the vacuum chamber (grey region in Figure 3.4). We probe the molecular sample in the zone of silence, where due to the low rotational temperatures only a few rotational states are populated. The length of the molecular pulse is chosen depending on the seeding gas. When Ne is used, we typically employ molecular pulses of 1000 μs length. When Ar or He are used, 600 μs length pulses are created.

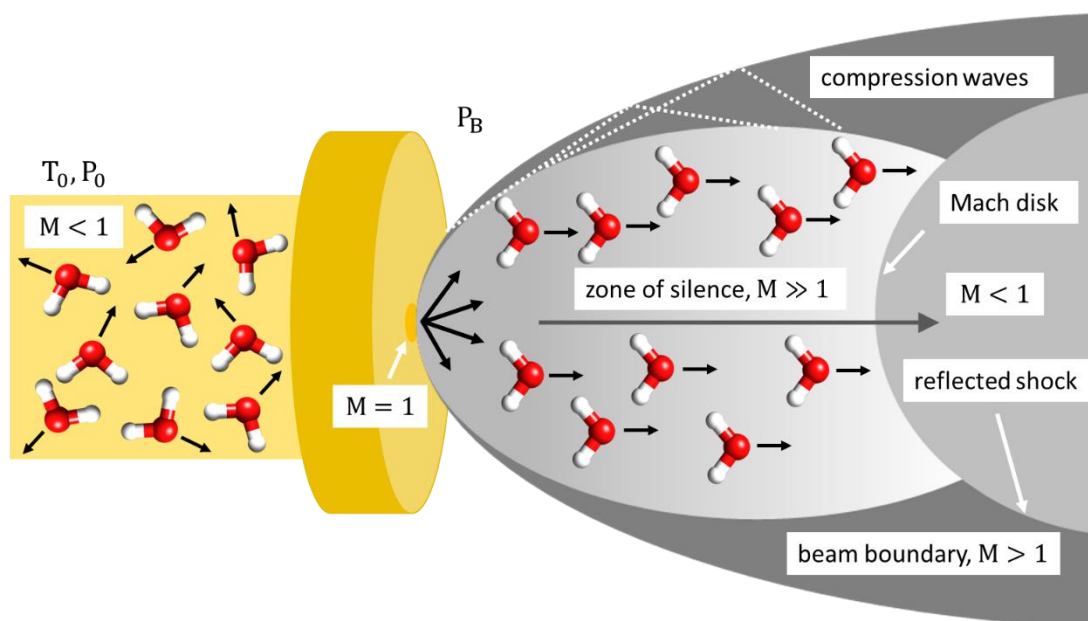


Figure 3.4. Graphical representation of a supersonic jet of water seeded into a backing gas (the gas molecules are omitted). M is the Mach number: $M = v/c$, where v is velocity of the beam and c is the local speed of sound.⁴ In the reservoir before the expansion, the sample gas is defined by temperature T_0 and pressure P_0 . Due to the large number of collisions in this area the velocity of the gas is small and leads to a Mach number $M < 1$. The pressure difference ($P_0 - P_B$) between the two areas leads to an increase in the velocity as the volume of the reservoir decreases, reaching a Mach number $M = 1$ at the orifice exit. With the increase in the volume, the density of the molecules decreases as well as the number of collisions, leading to an increase in velocity and hence a much greater Mach number $M \gg 1$. At this point the beam can be treated as a supersonic beam. This section of the supersonic expansion is also called “zone of silence”, as there are no collisions or interactions between the molecules. The supersonic expansion has a barrel shape and at the boundaries shock waves are created as collisions with the warmer environment occur.

Chirped pulse generation

The fast passage technique, which allows for the macroscopic polarisation of the sample, was introduced in rotational spectroscopy in 1974 by McGurk *et al.*^{15,16} With the technology advancements in recent years and introduction of arbitrary wave generators (AWG), Pate *et al.* applied the fast passage excitation technique in 2008 to develop the new broadband technique Chirped-pulse Fourier transform microwave (CP-FTMW) spectroscopy.¹

Our spectrometer is based on Pate's design with the main component being the 24 GS/s arbitrary waveform generator (Tektronix AWG 7122C), which creates the microwave excitation pulses linearly swept in frequency range from 2 to 8 GHz and with a length of 4 μs .³ The generated MW pulse is first adjusted by a variable attenuator (Agilent 8494B) and further amplified by a 200 W pulsed travelling wave tube amplifier (TWTA, IFI GT82-200) to achieve the desired degree of polarisation. It is essential to optimise the length of the MW chirped pulse so that it is long enough to increase the level of polarisation of the sample, whilst keeping it short enough so the polarisation occurs faster than the relaxation time.

Interaction between the molecular jet and the MW chirped pulse

We create the supersonic jet by seeding the sample into a carrier gas (Ne, Ar or He) using a solenoid valve, which is controlled by a valve driver (IOTA ONE, Parker Hannifin). The latter is triggered by our DG2040 data generator. The molecular jet interacts with in the MW radiation in the vacuum chamber, where vacuum, with an ultimate pressure of the order of 10^{-7} mbar, is created using a vacuum system composed of a roots, a rotary and a diffusion pump. The MW radiation is transmitted inside the vacuum chamber and collected on the other side by standard horn antennas, which are separated by approximately 40 cm and positioned perpendicularly to the molecular beam.

The intensity of the emission signal depends on the interaction between the molecular and the MW pulses. The molecular pulse should be long enough to allow for the largest molecular density in the jet, but also short enough to allow the vacuum to be regenerated in the chamber by the pumps. The best emission signal is obtained when the largest number of molecules are captured and polarised by the excitation pulse. The optimal overlap between the pulses is achieved by regulating the duration of the molecular pulse and the delay between the molecular pulse and the MW pulse. Therefore, delays are provided from the beginning of each pulse. In our set-up the MW pulses are delayed by 100 μs from the end of the molecular pulse in experiments conducted with Ne, and 200 μs for Ar and He experiments.

FID detection

In our set-up the weak emission signal emitted by the molecules after the excitation is amplified by a low noise amplifier and then digitised by a 100 GS/s digital oscilloscope (Tektronix DPO71604C) in the time domain. To obtain the frequency domain spectrum a fast Fourier transform algorithm implemented in a python script is used. To protect the detection site, a pin diode (Advanced Control Components ACLM-4540) and a microwave switch (Advanced control Components S1S3R) have been added between the low noise amplifier and the second horn antenna.

Collection of the FID starts 2.5 μs after the end of the polarisation pulse in our instrument, which was found to be optimal. If the emission signal is collected whilst the molecules are being irradiated it leads to inaccurate frequency measurements, but also can damage the detection components resulting from the high power of the excitation pulse. The FID acquisition time is 20 μs , which provides a good compromise for frequency resolution and intensity. To optimise the sample consumption and time required for the spectral recording, we use the fast frame feature of the oscilloscope. This allows for multiple FIDs to be collected and averaged for each molecular pulse. In our current set-up, four FIDs are collected for each molecular pulse, and the instrument works at a repetition rate of 4 Hz. This results in a total of 57600 FIDs collected over an hour.¹⁷

3.2. External receptacle development

Part of this PhD project was the improvement of the external receptacle (Figure 3.5. A and Figure 3.6), which is used in the study of complex presented in this thesis and in related studies. The previously used receptacle was quite big, with relatively thick walls, and it took a long time to reach the desired temperature. Therefore, a new receptacle, smaller in size and with thinner walls, was designed and built. The overall volume of the reservoir was reduced approximately four times compared to the original design, and the thickness of the walls was reduced by half, optimising the required heating time. The new reservoir is made of stainless steel to minimise possible reactions of the target samples when the temperature is increased. Heating is achieved by using resistance wires, allowing for heating up to 100 °C. Alternative heating elements were tested, specifically silicone heater mats, but the best option to heat up the receptacle remained resistive heating.

The external reservoir (Figure 3.5. A) is used in the investigation of complexes between two different compounds. Generally, water or the more volatile compound is placed in the external

reservoir, whilst the odorant which usually requires heating to higher temperatures is placed in the heating nozzle (Figure 3.5. B) which can heat up to 200 °C. This allows for both samples to be heated at different temperatures and achieve the desired vapour pressures. The carrier gas (Ne, Ar or He) passing through the injection line picks first the molecules from the external reservoir and conducts them to the heating nozzle where both samples mix. The weakly bound complexes are formed by collisions in the first stages of the supersonic expansion.

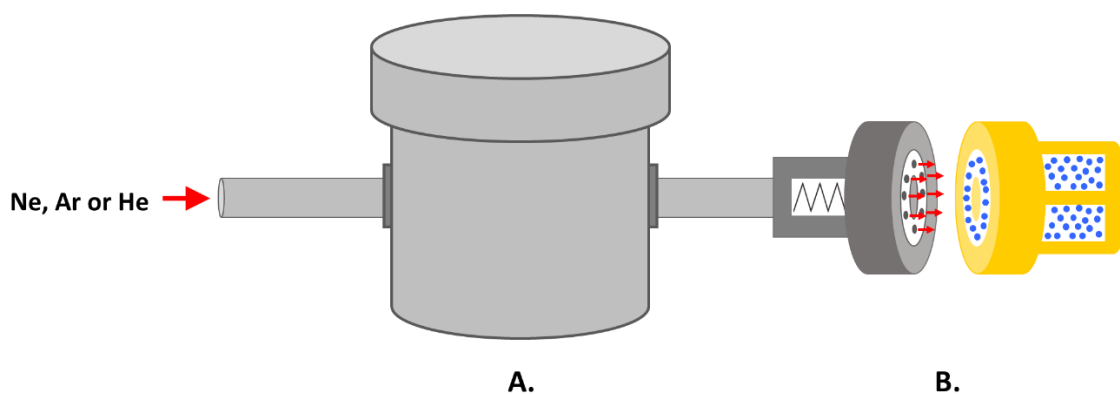


Figure 3.5. Scheme of the injection line. **A.** External receptacle where water (and other compounds of interest) is placed. **B.** Heating nozzle where the odorant is placed.

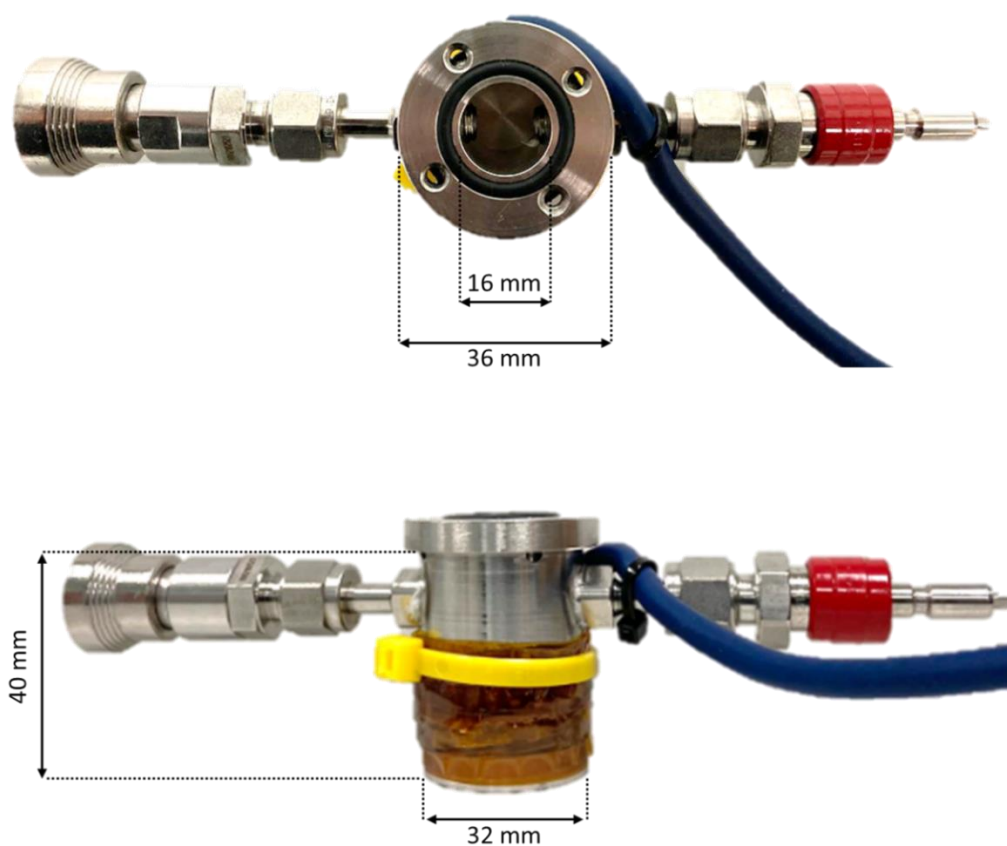


Figure 3.6. The design and dimensions of the new external receptacle.

3.3. Bibliography

1. Brown, G. G. *et al.* A broadband Fourier transform microwave spectrometer based on chirped pulse excitation. *Review of Scientific Instruments* **79**, 053103–13 (2008).
2. Neill, J. L. *et al.* Rotational spectroscopy of iodobenzene and iodobenzene-neon with a direct digital 2-8 GHz chirped-pulse Fourier transform microwave spectrometer. *Journal of Molecular Spectroscopy* **269**, 21–29 (2011).
3. Loru, D., Bermúdez, M. A. & Sanz, M. E. Structure of fenchone by broadband rotational spectroscopy. *Journal of Chemical Physics* **145**, 07114311–8 (2016).
4. Miller, D. R. Free jet sources. in *Atomic Molecular Beam Methods* (ed. Scoles, G.) 14–54 (Oxford University Press, 1988).
5. Levy, D. H. Laser Spectroscopy of Cold Gas-Phase Molecules. *Annual Review of Physical Chemistry* **31**, 197–225 (1980).
6. LeGreve, T. A., Baquero, E. E. & Zwier, T. S. Infrared and ultraviolet spectral signatures and conformational preferences of jet-cooled serotonin. *Journal of the American Chemical Society* **129**, 4028–4038 (2007).
7. Johnston, M. Supersonic jet expansions in analytical spectroscopy. *Trends in Analytical Chemistry* **3**, 58–61 (1984).
8. Paul, J. B., Collier, C. P., Saykally, R. J., Scherer, J. J. & O’Keefe, A. Direct measurement of water cluster concentrations by infrared cavity ringdown laser absorption spectroscopy. *Journal of Physical Chemistry A* **101**, 5211–5214 (1997).
9. Hager, J. W. & Wallace, S. C. Two-Laser Photoionization Supersonic Jet Mass Spectrometry of Aromatic Molecules. *Analytical Chemistry* **60**, 5–10 (1988).
10. McDaniel, J. C. & Graves, J. Laser-induced-fluorescence visualization of transverse gaseous injection in a nonreacting supersonic combustor. *Journal of Propulsion and Power* **4**, 591–597 (1988).
11. Paul, P. H., Lee, M. P. & Hanson, R. K. Molecular velocity imaging of supersonic flows using pulsed planar laser-induced fluorescence of NO. *Optics Letters* **14**, 417 (1989).
12. Lesarri, A., Mata, S., López, J. C. & Alonso, J. L. A laser-ablation molecular-beam Fourier-transform microwave spectrometer: The rotational spectrum of organic solids. *Review of Scientific Instruments* **74**, 4799–4804 (2003).
13. Steimle, T. C., Costen, M. L., Hall, G. E. & Sears, T. J. Transient frequency modulation absorption spectroscopy of molecules produced in a laser ablation supersonic expansion source. *Chemical Physics Letters* **319**, 363–367 (2000).
14. Katzy, R., Singer, M., Izadnia, S., Laforge, A. C. & Stienkemeier, F. Doping He droplets by laser ablation with a pulsed supersonic jet source. *Review of Scientific Instruments* **87**, 013105–6 (2016).
15. McGurk, J. C., Schmalz, T. G. & Flygare, W. H. Fast passage in rotational spectroscopy: Theory and experiment. *The Journal of Chemical Physics* **60**, 4181–4188 (1974).
16. Caminati, W. & Grabow, J. U. Microwave Spectroscopy: Molecular Systems. in *Frontiers of Molecular Spectroscopy* 455–552 (2009).
17. Loru, D., Peña, I. & Sanz, M. E. Ethanol dimer: Observation of three new conformers by broadband rotational spectroscopy. *Journal of Molecular Spectroscopy* **335**, 93–101 (2017).



**MEDIUM-SIZED RINGS:
CONFORMATIONAL
PREFERENCES IN
CYCLOOCTANONE DRIVEN
BY TRANSANNULAR
REPULSIVE INTERACTIONS**

Chapter 4



4. MEDIUM-SIZED RINGS: CONFORMATIONAL PREFERENCES IN CYCLOOCTANONE DRIVEN BY TRANSANNULAR REPULSIVE INTERACTIONS

Published Article: *Phys. Chem. Chem. Phys.*, 2019, **21**, 4331-4338.

4.1. Introduction

Characterization of the conformations and structural features of cyclic alkanes and their derivatives has attracted a great deal of attention over the years, as a testing ground for theories on chemical bond, intramolecular forces and reactivity. Molecular conformation is determined by the balance of intramolecular forces, which in cycloalkanes include angular strain, torsional strain and non-bonded transannular interactions. The structural properties of small rings have been extensively studied.¹⁻⁶ Large amplitude motions such as ring-puckering and pseudorotation have been thoroughly characterised in four- and five-membered rings, including cycloalkanes, cycloalkanones and their substituted heterocycles.⁷⁻¹⁴ These investigations showed that angular strain is dominant, and provided information on how replacement of a methylene group by a heteroatom or a carbonyl group in the ring affects conformation and the balance of intramolecular interactions. Six-membered cycloalkanes and their derivatives were found to prefer a chair conformation,^{6,15-19} while seven-membered rings suffer some ring strain and undergo pseudorotation.^{20,21}

Fewer structural investigations have been reported on medium-sized eight- to twelve-membered cycloalkanes and their derivatives, including cycloalkanones. Conformational analysis of these larger cycles is more complicated as flexibility increases with ring size. Torsional strain and non-bonded transannular interactions are expected to be more important in determining ring conformation.²² Several studies of medium-sized rings were conducted using X-ray crystallography,^{23,24} NMR spectroscopy²⁵⁻²⁸ and electron diffraction,^{17,29} mostly during the 70s and 80s. These techniques provide very valuable structural information, but they have limitations to characterize multi-conformational systems. An alternative is the use of microwave spectroscopy, which due to its high resolution has the advantage of being able to distinguish without ambiguity between different conformations simultaneously present in the sample.

In this work we report the investigation of the eight-membered ketone cyclooctanone using broadband rotational spectroscopy³⁰ in combination with quantum-chemistry calculations. Cyclooctanone is used as a precursor in the synthesis of more complex cyclic compounds, such as amber-³¹ and violet-smelling odorants³², and 14-membered cyclic lactones³³, and it is a structural motif present in natural compounds belonging to the terpenoid and lignin classes.³⁴⁻³⁶ The conformational landscape of cyclooctanone has been the subject of some computational studies³⁷⁻³⁹, which predict several conformers within 10 kJ/mol. Previous experimental NMR

data and vibrational and rotational spectroscopic studies⁴⁰ were consistent with the presence of one conformation of cyclooctanone in a boat-chair configuration. However, the rotational study was conducted at low resolution, and the rotational constants were estimated to large uncertainties, of up to 100 MHz.

Our conformational analysis of cyclooctanone aimed to establish whether one or more conformations coexist, and to get an insight on the intramolecular forces dictating conformational preferences. Are they different from those playing a key role in smaller rings? We have identified three conformers of cyclooctanone showing boat-chair and twisted boat-chair configurations. The structure of the lowest-energy boat-chair conformation has been determined and compared with those reported for cyclooctane and smaller cycloalkanones. The driving force for the preferred conformations of cyclooctanone is to minimise non-bonded repulsive interactions across the ring; the conformational energy ordering is inversely proportional to the extent of these interactions.

4.2. Methods

Theoretical

The conformational landscape of cyclooctanone was first sampled using molecular mechanics MM1 method with the energy limit of 84 kJ/mol, which produced eleven conformations. The geometry of the conformational minima was then optimized at the M062X, B3LYP-D3BJ and MP2 levels of theory with the 6-311++G(d,p) basis set using Gaussian09.⁴¹ The DFT and *ab initio* calculations have returned ten distinct conformations (Fig. 1), as one of the initial crown conformers converged to distorted crown. Harmonic vibrational calculations at the three levels of theory were also carried out to determine whether all the minima are local minima in the potential energy surface, and obtain zero-point corrections and Gibbs free energies of the conformers. Rotational constants, dipole moments and relative energies of all predicted conformers are collected in Table 1 and Tables S1-S2.

Experimental

The rotational spectrum of cyclooctanone was recorded using the CP-FTMW spectrometer at King's College London, which operates in the 2-8 GHz frequency range.^{42,43} Optimal signals were obtained by placing cyclooctanone (98%, m.p. 313 K) in a bespoke heated nozzle at 347 K. Gas-phase cyclooctanone was seeded in neon at stagnation pressures of 5 bar and conducted to the vacuum chamber, where it was polarised with 4 chirped microwave pulses of 4 μ s length. After each excitation pulse, molecular relaxation signals (free inductions decays, FIDs) were

collected for 20 μs by our digital oscilloscope. The time domain spectrum was converted to the frequency domain using a fast Fourier-transform algorithm with a Kaiser-Bessel window. 1.4 million FIDs were coherently added to produce the spectrum of Fig. 2. The spectra of cyclooctanone seeded in helium and argon as carrier gases were collected with the same set up. Molecular pulses of 1000 μs duration were used when neon was used as carrier gas, and of 600 μs duration when helium and argon were used.

4.3. Results and Discussion

Conformational landscape of cyclooctanone

Our investigation of the conformational landscape of cyclooctanone, carried out at different levels of theory and using a larger basis set than previous investigations (see details in the Experimental Section), yielded 10 distinct conformers within 50 kJ/mol, which are grouped in four classes according to the configuration of the ring (see Figure 4.1): boat-chair (BC), twisted boat-chair (TBC), crown (CR), and boat-boat (BB). This set of conformers and their energy ordering are different from those reported in earlier theoretical studies. The global minimum is predicted to be the same, the boat chair conformation **BC1** in our nomenclature (Figure 4.1). However, the second conformer in energy is predicted as a twisted boat chair conformer (**TBC1**), followed by a boat chair conformer (**BC2**) and a distorted crown conformer (**CR1**). At all the levels of theory used in this work the boat-chair conformers previously labelled 2³⁷ or CB-2³⁹ converged to the twisted boat-chair conformer **TBC1**, and the formerly reported crown conformation converged to the distorted crown **CR1**. Our computational results yielded an additional boat-boat conformation **BB2**, which is the highest in energy. Rotational constants, dipole moments and relative energies of all predicted conformers are collected in Table 4.1 and Tables S1-S2, and their Cartesian coordinates from MP2/3-611++G(d,p) included in Tables S3-12.

Table 4.1. *Ab initio*^[a] spectroscopic parameters for conformers of cyclooctanone.

	BC1	TBC1	BC2	CR1	BC3	TBC2	BB1	TBC3	BC4	BB2
$A^{[b]}$ (MHz)	1912	1991	2032	1919	1915	2114	1946	2007	2264	2175
B (MHz)	1692	1641	1648	1731	1679	1538	1627	1695	1450	1515
C (MHz)	1175	1100	1124	1128	1233	1118	1243	1118	1017	1126
μ_a (D)	-2.0	2.4	2.4	0.6	1.2	2.0	-2.2	1.9	-3.1	2.9
μ_b (D)	-0.1	0.2	-0.5	-0.6	0.0	-0.5	-0.3	-1.0	0.0	-0.8
μ_c (D)	2.1	-1.7	-1.6	2.1	2.5	2.1	2.1	-1.7	-0.8	-0.9
$\Delta E^{[c]}$ (cm^{-1})	0	737	724	878	1196	1198	1261	1286	1684	2151
$\Delta E_0^{[d]}$ (cm^{-1})	0	673	789	830	1212	1198	1248	1357	1716	2205
$\Delta G^{347 [e]}$ (cm^{-1})	0	494	753	716	1074	1115	1101	1341	1606	2132

[a] MP2/6-311++G(d,p); [b] A , B , C are the rotational constants; μ_a , μ_b and μ_c are the electric dipole moment components; [c] Relative electronic energies; [d] Relative electronic energies including the zero-point correction; [e] Gibbs free energies at 347 K at the MP2/6-311++G(d,p) level.

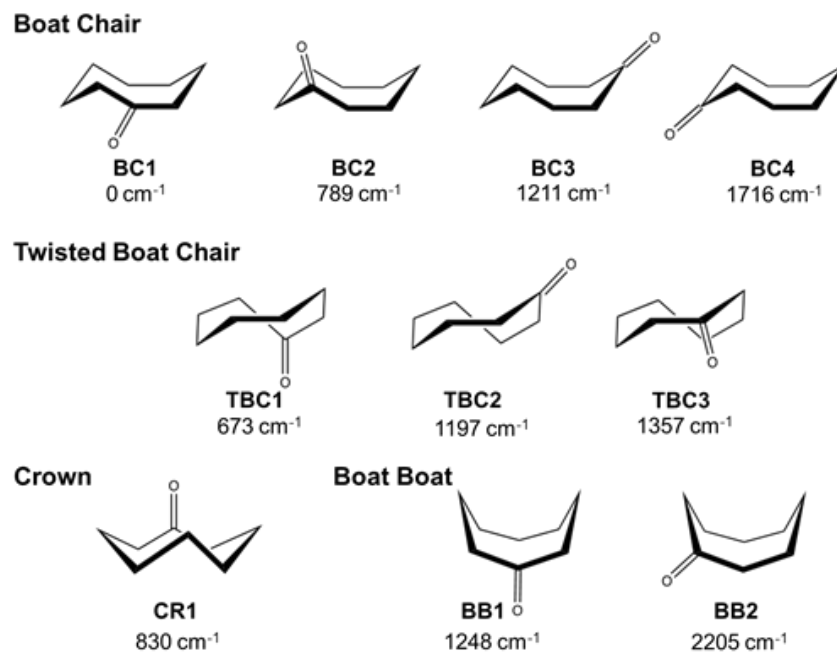


Figure 4.1. Conformers of cyclooctanone predicted at MP2/6-311++G(d,p)+ZPC level of theory.

Rotational spectrum

The broadband rotational spectrum of cyclooctanone was collected in the 2-8 GHz region (Figure 4.2). It is very intense and on first inspection it does not seem to contain a lot of transitions. The most intense lines were quickly identified as a- and c-type $J+1 \leftarrow J$ transitions corresponding to the **BC1** conformation of cyclooctanone (Figure 4.1), predicted to be the global minimum, and observed in a previous microwave study.⁴⁴ A total of 69 transitions (Appendix I) were fit to the Watson Hamiltonian in the A reduction and III representation⁴⁵ using Pickett's SPFIT/SPCAT programs.⁴⁶ They yielded the rotational and centrifugal distortion constants of Table 4.2, which improve the former estimated values by several orders of magnitude.

Since the rotational transitions of **BC1** were very intense, transitions arising from its ¹³C and ¹⁸O isotopologues in natural abundance (ca. 1.1% and 0.2%, respectively), were searched for and observed at the expected frequency shifts from the parent species. The measured transitions (Appendix I) were fit to the same Hamiltonian⁴⁷ as the parent species and the determined rotational constants are shown in Table 4.3.

Once transitions from **BC1** cyclooctanone were removed from the spectrum, further inspection led to the assignment of two other conformers of cyclooctanone, and determination of their rotational constants following the same procedure as outlined above (see Table 4.2, and

Appendix I for the fits of measured transitions). From the comparison between experimental and theoretical rotational constants, these conformers were identified as **TBC1** and **BC2**. The transitions corresponding to the next conformer in the energy ordering, **CR1**, could not be observed in the spectrum, probably because it is not sufficiently populated in our supersonic expansion.

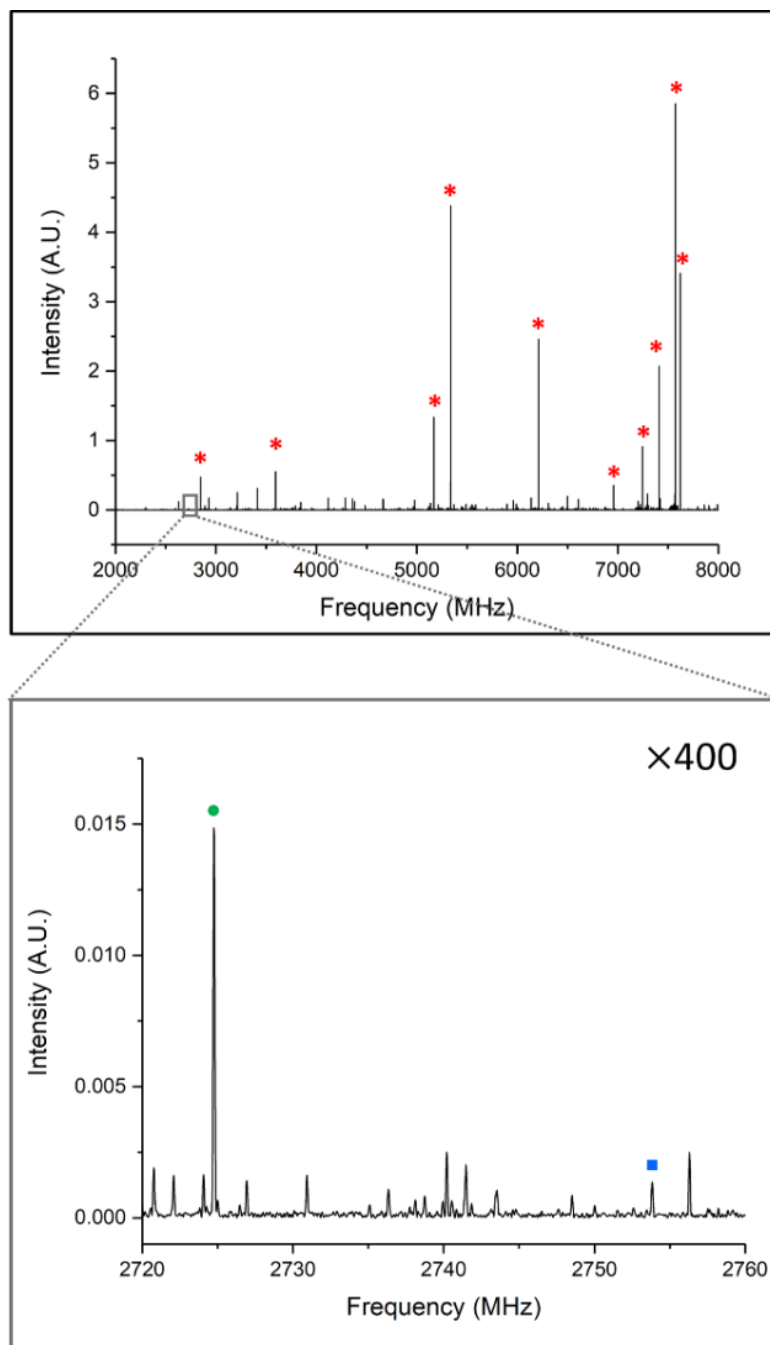


Figure 4.2. 2-8 GHz spectrum of cyclooctanone in neon. The red stars indicate the rotational transitions of conformer **BC1**. The enlarged region 2720-2760 MHz shows the $1_{01} \leftarrow 0_{00}$ rotational transition of **TBC1** (green circle) and **BC2** (blue square).

Table 4.2. Experimental spectroscopic parameters of the three observed conformers of cyclooctanone compared with those obtained in a previous work.⁴⁴

	BC1	TBC1	BC2	Ref. [44]
$A^{[a]}$ (MHz)	1909.57246(33) ^[f]	1984.4524(10)	2026.75087(52)	1910(5)
B (MHz)	1683.01292(32)	1632.66619(89)	1638.36289(48)	1680(30)
C (MHz)	1162.36489(30)	1092.10687(92)	1115.46660(42)	1100(100)
$\kappa^{[b]}$	0.4	0.2	0.1	0.4
Δ_J (kHz)	0.3269(95)	1.246(61)	0.110(28)	-
Δ_{JK} (kHz)	-0.6958(45)	-3.820(38)	-	-
Δ_K (kHz)	0.5212(51)	2.908(28)	-	-
δ_J (kHz)	0.01984(77)	-0.0563(76)	-	-
δ_K (kHz)	0.7584(57)	3.926(50)	-	-
$a/b/c^{[c]}$	$\gamma/\gamma/\gamma$	$\gamma/n/\gamma$	$\gamma/n/\gamma$	$n/n/\gamma$
$\sigma^{[d]}$ (kHz)	4.0	5.7	2.0	-
$N^{[e]}$	69	37	13	-

[a] A , B and C are the rotational constants. Δ_J , Δ_{JK} , Δ_K , Δ_J and Δ_K are the centrifugal distortion constants; [b] Ray's asymmetry parameter; [c] a , b and c are the type of transitions observed; [d] σ is the rms deviation of the fit; [e] N is the number of the fitted transitions; [f] Standard error in parentheses in units of the last digit.

Table 4.3. Experimental spectroscopic parameters for all singly substituted ¹³C and ¹⁸O isotopic species of the **BC1** conformer of cyclooctanone.

Parameter	A (MHz)	B (MHz)	C (MHz)	σ (kHz)	N
¹³ C ₁	1908.60080(73)	1673.55905(65)	1157.51096(34)	2.6	10
¹³ C ₂	1899.58571(93)	1670.95299(83)	1156.96807(43)	3.3	10
¹³ C ₃	1883.0199(10)	1682.14826(91)	1152.42858(47)	3.7	10
¹³ C ₄	1892.69070(73)	1674.58818(64)	1152.13583(33)	2.6	10
¹³ C ₅	1902.61094(53)	1666.47311(34)	1156.13498(17)	1.3	9
¹³ C ₆	1903.6868(13)	1663.15703(81)	1151.05925(41)	3.2	9
¹³ C ₇	1890.43352(81)	1675.00266(71)	1154.59819(37)	2.9	10
¹³ C ₈	1889.67383(27)	1680.82408(24)	1154.35408(12)	0.9	9
¹⁸ O	1894.2963(14)	1627.6585(13)	1140.30796(67)	5.1	10

All three methods, MP2, B3LYP-D3BJ and M062X with the 6-311++G(d,p) basis set, predict the rotational constants of the three observed conformers reasonably well. MP2 is the best performing method with an average percentage difference of 0.54%, followed by B3LYP-D3BJ with 0.62% and M062X with 0.74%. MP2 consistently overestimates the B and C constants, while B3LYP-D3BJ underestimates them. The theoretical A rotational constant of conformer **TBC1** shows the largest deviation from the experimental value, 1.7% using M062X.

The relative abundances of the observed conformers have been calculated considering that conformational abundance is directly proportional to the intensity of its transitions and inversely proportional to the square of the corresponding dipole moment component. Since all of the assigned conformers have a-type spectrum, we estimated conformational relative abundances by comparing common a -type transitions. The results show that **BC1** is significantly more abundant than **TBC1** and **BC2**. Using Ne as a carrier gas, relative conformational abundances are

BC1 : **TBC1** : **BC2** = 525 : 12 : 1. In addition to Ne, we have collected the spectrum of cyclooctanone seeded in He and in Ar, which produce different degrees of conformational relaxation. He is the least effective relaxant among the three noble gases, whilst Ar is the most effective and sometimes leads to the observation of just the lowest-energy conformation.⁴⁸ In He, the relative conformational abundances change to **BC1** : **TBC1** : **BC2** = 210 : 6 : 1. In Ar, where **BC2** could not be detected as the S/N ratio was lower compared to the other two spectra, the relative abundances of the other two conformers are **BC1** : **TBC1** = 40 : 1.

In all carrier gases conformer **BC1** is about 40 times more abundant than conformer **TBC1**, the second most abundant conformer. This shows that conformer **BC1** is the global minimum and that there is a very strong preference of cyclooctanone to adopt this boat-chair configuration. The change in the relative conformational abundances of **BC2** : **BC1** when changing carrier gas indicates that **BC2** relaxes in our supersonic jet. The paths for interconversion are very complicated involving a large number of coordinates changes, and including pseudorotation and inversion motions. However, their calculation is out of the scope of this paper. Previously reported barriers for pseudorotation and ring inversion of cyclooctanone were calculated from vibrational and structural data as having upper bounds of 33 kJ/mol and 36 kJ/mol, respectively,⁴⁰ and from NMR measurements as 26 kJ/mol and 31 kJ/mol, respectively.⁴⁹ These barriers are too high to allow for conformational relaxation in a supersonic jet considering the typical limit of 13 kJ/mol ascribed to multipath molecular systems.^{48,50} However, a complete exploration of the potential energy surface may reveal other lower-energy paths for conformational interconversion.

Structural determination of BC1

The observation of the ¹³C and ¹⁸O monosubstituted isotopic species of conformer **BC1** permitted to calculate the coordinates of these heavy atoms in the principal inertial axes system using Kraitchman's equations^{51,52} (Table 4.4), and to determine the substitution structure r_s . The effective structure r_0 was determined from a least-square fit of all the experimental moments of inertia,⁵³ where the structural parameters of the hydrogen atoms were fixed to the MP2/6-311++G(d,p) theoretical values. The bond lengths, bond angles and dihedral angles of the **BC1** conformer for both r_s and r_0 structures are collected in Table 4.4 (see Figure 4.3 for atom numbering).

Table 4.4. Substitution coordinates of the heavy atoms of cyclooctanone **BC1**.

	a	b	c
C ₁	-1.8597(8)	-0.9109(17)	-0.2614(58)
C ₂	-1.4720(10)	0.4191(36)	-0.9043(17)
C ₃	-1.1883(13)	1.5703(10)	0.0746(201)
C ₄	0.2775(54)	1.9202(8)	0.2661(56)
C ₅	1.1736(13)	0.8064(19)	0.8824(17)
C ₆	1.3014(12)	-0.3715(40)	-0.0616(244)
O ₇	2.0275(7)	-0.3199(47)	-1.0233(15)
C ₈	-0.8901(17)	-1.4608(10)	0.7812(19)
C ₉	0.5368(28)	-1.6557(9)	0.2869(53)

Table 4.5. Experimental bond lengths (Å), angles and dihedral angles (°) of **BC1** cyclooctanone (r_s and r_0 structures), theoretical MP2 structural parameters, and structural parameters of cyclooctane.

	Cyclooctanone		Cyclooctane	
	r_s	r_0^a	MP2 6-311++G(d,p)	Electron Diffraction ⁵⁴
$r(\text{C}_2\text{-C}_1)$	1.527(5)	1.539(6)	1.536	–
$r(\text{C}_3\text{-C}_2)$	1.538(13)	1.544(6)	1.545	–
$r(\text{C}_4\text{-C}_3)$	1.519(6)	1.540(6)	1.535	–
$r(\text{C}_5\text{-C}_4)$	1.557(4)	1.541(6)	1.540	–
$r(\text{C}_6\text{-C}_5)$	1.515(16)	1.520(9) ^c	1.522	–
$r(\text{O}_7\text{-C}_6)$	1.206(19)	1.215(9)	1.223	–
$r(\text{C}_9\text{-C}_6)$	1.535(7)	1.520(9)	1.519	–
$r(\text{C}_9\text{-C}_8)$	1.523(4)	1.535(6)	1.533	–
$r(\text{C}_8\text{-C}_1)$	1.526(4)	1.533(6)	1.531	–
Avg. $r(\text{C-C})$	1.530(7)	1.534(7)	–	1.540(1)
$\angle(\text{C}_3\text{-C}_2\text{-C}_1)$	115.5(6)	115.2(3)	114.8	117.0(20)
$\angle(\text{C}_4\text{-C}_3\text{-C}_2)$	115.5(6)	114.8(2)	114.5	116.1(18)
$\angle(\text{C}_5\text{-C}_4\text{-C}_3)$	116.1(3)	115.7(2)	115.7	120.2(10)
$\angle(\text{C}_6\text{-C}_5\text{-C}_4)$	111.0(6)	111.8(4) ^[c]	111.7	116.1(18)
$\angle(\text{O}_7\text{-C}_6\text{-C}_5)$	121.0(4)	120.4(5) ^[c]	120.1	–
$\angle(\text{C}_9\text{-C}_6\text{-C}_5)$	117.8(13)	118.8(6) ^[c]	118.3	117.0(20)
$\angle(\text{C}_9\text{-C}_6\text{-O}_7)$	121.1(10)	120.7(8)	121.6	–
$\angle(\text{C}_8\text{-C}_9\text{-C}_6)$	115.7(3)	115.6(3)	115.2	116.0(15)
$\angle(\text{C}_9\text{-C}_8\text{-C}_1)$	114.8(3)	114.5(4)	114.1	116.1
$\angle(\text{C}_8\text{-C}_1\text{-C}_2)$	116.1(1)	116.0(2)	115.7	116.0(15)
$\tau(\text{C}_4\text{C}_3\text{C}_2\text{C}_1)$	104.7(9)	105.1(2)	105.8	98.4(35)
$\tau(\text{C}_9\text{C}_8\text{C}_1\text{C}_2)$	-56.7(3)	-57.4(5)	-58.6	-68.3
$\tau(\text{C}_8\text{C}_1\text{C}_2\text{C}_3)$	-54.4(3)	-53.6(5)	-53.0	-42.0
$\tau(\text{C}_8\text{C}_9\text{C}_6\text{O}_7)$	-140.3(7)	-139.7(4)	-138.2	–
$\tau(\text{C}_6\text{C}_9\text{C}_8\text{C}_1)$	66.8(10)	67.4(10)	67.6	68.3

[a] The substitution structure has been determined from the atomic coordinates including Costain's error, and with signs taken from *ab initio* calculations; [b] Effective structure; non fitted parameters were fixed to the MP2/6-311++G(d,p) value; [c] Derived from the determined r_0 structure, not fitted directly.

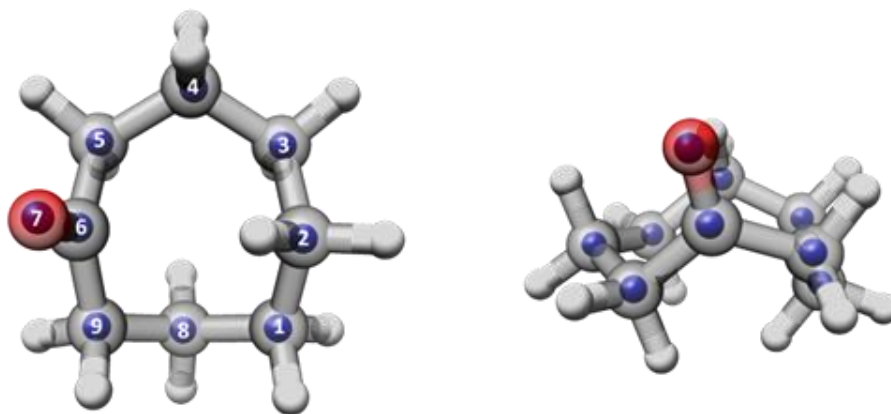


Figure 4.3. Comparison of the r_s structure of conformer **BC1** (purple spheres) with *ab initio* MP2 structure (grey framework).

The resulting structural parameters from both calculations agree well with each other. There is a relatively large discrepancy in the $r(\text{C}_4\text{--C}_3)$ bond length that is likely due to the large uncertainty of the c substitution coordinate of C_3 , very close to zero. The internuclear distances $r(\text{C}_6\text{--C}_5)$ and $r(\text{C}_9\text{--C}_6)$ involving the carbonyl carbon C_6 are quite different from each other, which can be ascribed to the uncertainty in the c coordinate of C_6 . Bond angles and dihedral angles from substitution and effective structures are within 1° . The $\angle(\text{C--C--C})$ angles, not including the $\angle(\text{C--CO--C})$ angle, have all very similar values of *ca.* 115° , except for $\angle(\text{C}_6\text{--C}_5\text{--C}_4)$ which is about 4° more acute. The lower value of $\angle(\text{C}_6\text{--C}_5\text{--C}_4)$ is consistent across r_s and r_0 structures and it is also predicted by quantum mechanical calculations. Both r_0 and r_s structures are in very good agreement with the theoretical ones. An overlay of the experimental substitution r_s and *ab initio* MP2 coordinates (Figure 4.3) shows their excellent match.

We have compared the structure of cyclooctanone with that of cyclooctane, previously studied by electron diffraction,⁵⁴ to determine the effect of inserting a carbonyl group in the ring. Structural studies of cyclooctane in the liquid and gas phases indicate that it exists predominantly in a boat-chair conformation.^{54,55} Cyclooctanone maintains a strong preference for being in a boat-chair conformation, thus indicating that the overall conformational preference of an eight-membered ring is not affected by substituting a methylene by a carbonyl group. The electron diffraction study of cyclooctane only provided an average $\text{sp}^3\text{--sp}^3$ C–C bond length of $1.540(1)$ Å. Bond lengths for cyclooctanone are slightly shorter, with average values of $1.530(7)$ Å and $1.534(7)$ Å for the r_s and r_0 structures, respectively. The values of the bond angles of cyclooctane and cyclooctanone are the same within experimental uncertainties, except for the angles $\angle(\text{C}_6\text{--C}_5\text{--C}_4)$ and $\angle(\text{C}_5\text{--C}_4\text{--C}_3)$, which are about 4° more acute in cyclooctanone, probably to accommodate the carbonyl group in the ring. The largest changes occur on the

dihedral angles, where there are differences of up to 10°, which collectively result in the boat part of the ring being less “puckered” in cyclooctanone than in cyclooctane. This behaviour on including a carbonyl group in the ring has been observed for smaller cycles.⁵⁶

The structure of cyclooctanone can be compared with those of related cyclic ketones previously reported by microwave spectroscopy and electron diffraction.^{17,29,57} The average value of 1.534(7) Å for the sp³-sp³ C–C internuclear distance of cyclooctanone is similar to those reported for cycloheptanone, cyclohexanone and cyclopentanone (Table 4.6). The sp²-sp³ C–C internuclear distance shows a greater variation, with similar values for cyclooctanone and cycloheptanone, a shorter distance in cyclohexanone and a longer one in cyclopentanone. The sp²-sp³ C–C internuclear distances for cyclooctanone and cycloheptanone are closer to that determined for acetone, 1.517(3) Å,⁵⁸ probably a reflection of the reduced ring strain in the larger cyclic ketones. The C–O internuclear distances are very similar for all cyclic ketones studied so far, with the exception of cyclohexanone, that exhibits a slightly larger distance. They are also similar to the value determined for acetone 1.210(4) Å. The bond angles show clear trends as the size of the ring increases. In going from cyclopentanone to cyclooctanone, the ∠(C–CO–C) angle becomes more obtuse and closer to the typical sp²-hybridized angle of 120°. The ∠(C–CO–C) angle of the six-, seven- and eight-membered cyclic ketones are, within uncertainties, essentially the same as that of acetone, of 116.0(15)°. Cyclopentanone presents a considerably more acute angle of 108.6(2)°, reflecting its larger ring strain. Changes in the ∠(C–C–C) angles are dictated by structural requirements due to ring size. The average ∠(C–C–C) angle in cyclooctanone, calculated without including ∠(C₆–C₅–C₄) (see above) and ∠(C–CO–C), is 115.3(3)°, very similar to the average value of 115.5(5)° for cycloheptanone. Cyclohexanone has an average angle of 111.1(2)°, closer to the tetrahedral angle of 109.5°, and cyclopentanone of 103.8(2)°. Dihedral angles cannot be directly compared.

Table 4.6. Comparison of bond lengths (Å) and bond angles (°) of cyclopentanone,^[a] cyclohexanone,^[b] cycloheptanone^[c] and cyclooctanone.^[d]

Parameter	Cyclopentanone	Cyclohexanone	Cycloheptanone	Cyclooctanone
$r(\text{C}-\text{C})$ sp ² -sp ³	1.531(4)	1.503(4)	1.517	1.520(9)
$r(\text{C}-\text{C})$ sp ³ -sp ³	1.542(3)	1.542(2)	1.536(2)	1.534(7)
$r(\text{C}=\text{O})$	1.213(4)	1.229(3)	1.219(12)	1.215(9)
∠(C–CO–C)	108.6(2)	115.3(3)	117.3(18)	118.8(6)*
Avg ∠(C–C–C)	-	110.8(2)	-	114.8

[a] ED+MW⁵⁷; [b] ED+MW¹⁷; [c] ED²⁹; [d] This work, r_o.

Intramolecular interactions

There is a huge difference in abundance between conformer **BC1** and the other observed conformations of cyclooctanone, which can be rationalized in terms of the various non-bonded interactions at play (Figure 4.4). All observed conformers show attractive C–H···O interactions between the oxygen in the carbonyl group and neighboring hydrogen atoms, eclipsed configurations of hydrogen atoms, and repulsive interactions CH···HC across the ring. **BC1**, **TBC1** and **BC2** display very similar C–H···O interactions (green). The HCCH eclipsed conformations (blue) are also essentially the same for all three conformers. The main difference lies on the CH···HC repulsive interactions (red), which are stronger in **TBC1** and **BC2** than in **BC1** because the H atoms are located at shorter distances. The differences in these interactions are larger between **TBC1** and **BC2** than between **BC1** and **TBC1**, which can be taken as an indication that, for the same position of the carbonyl group in the ring, boat-chair configurations are more energetically favoured than twisted boat chain configurations.

If we compare the theoretical structures for all boat-chair conformations (Figure 4.4) it can be seen that **BC3** and **BC4**, although benefiting from having two C–H···O interactions, also have two HCCH eclipsed interactions, and a higher number of short CH···HC interactions across the ring than **BC1** and **BC2** and therefore they lie at higher energies. The shorter CH···HC interactions for **BC4** explain its higher relative energy with respect to **BC3**.

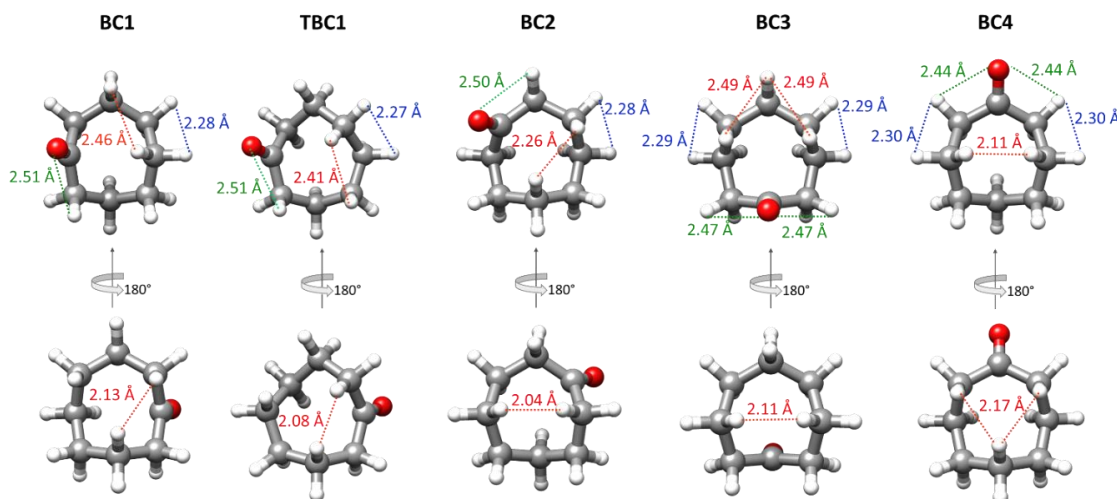


Figure 4.4. Intramolecular distances for the observed boat-chair and twisted boat-chair conformers **BC1**, **TBC1** and **BC2**, and the higher-energy boat-chair conformers **BC3** and **BC4** at MP2/6-311++G(d,p) level.

4.4. Conclusions

Three conformers of cyclooctanone, two boat chair and one twisted boat chair configurations, have been identified from the analysis of its high-resolution rotational spectrum in a supersonic jet, and their spectroscopic parameters have been determined to high accuracy. The experimental data obtained using different carrier gases demonstrates the strong preference of cyclooctanone to adopt the boat chair **BC1** conformation, which is about 40 times more abundant than the next conformation in the energy ordering, the twisted boat **TBC1** conformation. The least abundant conformer is a second boat-chair conformation (**BC2**). Our experimental results validate the conformations and energy ordering predicted by our computational calculations and are consistent with theoretical Gibbs free energies.

The experimental structure of the most abundant conformation of cyclooctanone has been determined, which, to our knowledge, is the first structure of an eight-membered ring determined by rotational spectroscopy. The insertion of a carbonyl group in place of a methylene group does not change the conformational preferences with respect to the eight-membered cycloalkane, but it introduces changes in the bond and dihedral angles that make cyclooctanone a “flatter” molecule than cyclooctane.

Three main types of non-bonded interactions are at play in cyclooctanone, namely attractive C–H \cdots O interactions, eclipsed configurations of hydrogen atoms that cause steric strain, and repulsive CH \cdots HC interactions across the ring. Our data shows that the strong preference of cyclooctanone to be in the boat chair configuration **BC1** is due to a reduction of the repulsive interactions for this configuration of the cycle. The energy ordering of cyclooctanone conformers is determined by the strength of the repulsive interactions and the number of eclipsed configurations around the ring.

The conformational and structural analysis presented in this work reveals the intramolecular forces responsible for conformational preferences, and shows the importance of repulsive interactions, which are likely to play a relevant role in other medium-sized cycles. Our results highlight the unique application of rotational spectroscopy to obtain accurate information on the behaviour of complex multiconformational systems. Further studies on the pseudorotation and inversion pathways of cyclooctanone will help understand conformational interconversion and internal dynamics. Structural investigations of larger cyclic ketones will yield information on the balance of intramolecular forces in more flexible and complex rings and help elucidate possible trends as the size of the ring increases. Accurate information on these interactions is of use for the design and control of reactions involving medium-sized cycles.^{59,60}

4.5. Bibliography

1. Chan, S. I., Zinn, J., Fernandez, J. & Gwinn, W. D. Trimethylene oxide. I. Microwave spectrum, dipole moment, and double minimum vibration. *The Journal of Chemical Physics* **33**, 1643–1655 (1960).
2. Harris, D. O., Harrington, H. W., Luntz, A. C. & Gwinn, W. D. Microwave spectrum, vibration-rotation interaction, and potential function for the ring-puckering vibration of trimethylene sulfide. *The Journal of Chemical Physics* **44**, 3467–3480 (1966).
3. Cotton, F. A. & Frenz, B. A. Conformations of cyclobutane. *Tetrahedron* **30**, 1587–1594 (1974).
4. Engerholm, G. G., Luntz, A. C., Gwinn, W. D. & Harris, D. O. Ring puckering in five-membered rings. II. The microwave spectrum, dipole moment, and barrier to pseudorotation in tetrahydrofuran. *The Journal of Chemical Physics* **50**, 2446–2457 (1969).
5. Ogata, T. & Kozima, K. Microwave Spectrum of Cyclohexene. *Bulletin of the Chemical Society of Japan* **42**, 1263–1265 (1969).
6. Ohnishi, Y. & Kozima, K. Microwave spectrum of cyclohexanone. *Bulletin of the Chemical Society of Japan* **41**, 1323–1325 (1968).
7. Laane, J. Origin of the ring-puckering potential energy function for four-membered rings and spiro compounds. A possibility for pseudorotation. *Journal of Physical Chemistry* **95**, 9246–9249 (1991).
8. Pitzer, K. S. & Donath, W. E. Conformations and Strain Energy of Cyclopentane and its Derivatives. *Journal of the American Chemical Society* **81**, 3213–3218 (1959).
9. Han, S. J. & Kang, Y. K. A pseudorotation model and ring-puckering of cyclopentane. *Journal of Molecular Structure: THEOCHEM* **362**, 243–255 (1996).
10. Kim, H. & Gwinn, W. D. Ring Puckering in Five-Membered Rings. III. The Microwave Spectrum, Dipole Moment, and Structure of Cyclopentanone. *The Journal of Chemical Physics* **51**, 1815–1819 (1969).
11. Geise, H. J., Buys, H. R. & Mijlhoff, F. C. Conformation of non-aromatic ring compounds. *Journal of Molecular Structure* **9**, 447–454 (1971).
12. Cremer, D. & Szabó, K. J. Conformational Behavior of Six-Membered Rings. in *Conformational Behavior of Six-Membered Rings* 59–135 (1995).
13. Díez, E., Esteban, A. L., Bermejo, F. J., Altona, C. & de Leeuw, F. A. A. M. Relationships between torsional angles and ring-puckering coordinates. Part II. *Journal of Molecular Structure* **125**, 49–65 (1984).
14. Tamagawa, K., Hilderbrandt, R. L. & Shen, Q. Molecular Structure of Cyclopentanone by Gas-Phase Electron Diffraction. *Journal of the American Chemical Society* **109**, 1380–1383 (1987).
15. Barton, H. R. The conformation of the steroid nucleus. *Experientia* **6**, 316–320 (1950).
16. Dommen, J., Brupbacher, T., Grassi, G. & Bauder, A. Microwave Spectra of Isotopic Species and Substitution Structure of Cyclohexane. *Journal of the American Chemical Society* **112**, 953–957 (1990).
17. Dillen, J. & Geise, H. J. The molecular structure of cyclohexanone determined by gas-phase electron diffraction, including microwave data. *Journal of Molecular Structure* **69**, 137–144 (1980).

18. Durig, J. R. *et al.* Microwave, Raman, and infrared spectra, structural parameters, conformational stability, and vibrational assignment of cyanocyclohexane. *Journal of Molecular Structure* **967**, 99–111 (2010).
19. Alonso, J. L. Microwave Spectrum of Cyclohexanone. *Journal of Molecular Structure* **73**, 63–69 (1981).
20. Dillen, J. & Geise, H. J. An Investigation of the Molecular Structure of Cycloheptanone By Gas Phase Electron Diffraction. *Journal of Molecular Structure* **72**, 247–255 (1981).
21. Jahn, M. K. *et al.* Pseudorotational Landscape of Seven-Membered Rings: The Most Stable Chair and Twist-Boat Conformers of ϵ -Caprolactone. *Chemistry - A European Journal* **20**, 14084–14089 (2014).
22. Prelog, V. Conformation and Reactivity of Medium-sized Ring Compounds. *Pure and Applied Chemistry* **6**, 545–560 (1963).
23. Rudman, R. & Post, B. Polymorphism of Crystalline Cyclooctanone and Cyclononanone. *Molecular Crystals* **3**, 325–337 (1968).
24. Groth, P. On the Crystal Structure of Cyclododecanone. *Acta Chemica Scandinavica* **33 A**, 203–205 (1979).
25. Anet, F. A. L., Cheng, A. K. & Wagner, J. J. Determination of conformational energy barriers in medium- and large-ring cycloalkanes by proton and carbon-13 nuclear magnetic resonance. *Journal of the American Chemical Society* **94**, 9250–9252 (1972).
26. Anet, F. A. L., Degen, P. J. & Krane, J. Dynamics of eight-membered rings. 1,3-Dioxocane and its gem-dimethyl derivatives. *Journal of the American Chemical Society* **98**, 2059–2066 (1976).
27. Anet, F. A. L. Dynamics of Eight-Membered Rings in the Cyclooctane Class. *Dynamic Chemistry* **45**, 169–220 (1974).
28. Rubin, B. H. *et al.* Conformation of a Saturated 13-Membered Ring. *Journal of the American Chemical Society* **106**, 2088–2092 (1984).
29. Dillen, J. & Geise, H. J. An Investigation of the Molecular Structure of Cycloheptanone By Gas Phase Electron Diffraction. *Journal of Molecular Structure* **72**, 247–255 (1981).
30. Brown, G. G. *et al.* A broadband Fourier transform microwave spectrometer based on chirped pulse excitation. *Review of Scientific Instruments* **79**, 1–13 (2008).
31. Narula, A. P. S. The search for new amber ingredients. *Chemistry and Biodiversity* **11**, 1629–1638 (2014).
32. Kraft, P. Design and Synthesis of Violet Odorants with Bicyclo [6.4.0] dodecene and Bicyclo [5.4.0] undecene Skeletons. *Synthesis* **4**, 695–703 (1999).
33. Aono, T. & Hesse, M. 62. Synthesis of 14-Membered Lactones from Cyclooctanone. *Helvetica Chimica Acta* **67**, 1448–1452 (1984).
34. Wani, M. C., Taylor, H. L., Wall, M. E., Coggon, P. & Mcphail, A. T. Plant Antitumor Agents. VI. The Isolation and Structure of Taxol, a Novel Antileukemic and Antitumor Agent from *Taxus brevifolia*. *Journal of the American Chemical Society* **93**, 2325–2327 (1971).
35. Appukkuttan, P., Dehaen, W. & Van Der Eycken, E. Microwave-assisted transition-metal-catalyzed synthesis of N-shifted and ring-expanded bufavine analogues. *Chemistry - A European Journal* **13**, 6452–6460 (2007).

36. Ferraz, H. M. C., Bombonato, F. I., Sano, M. K. & Longo, L. S. Natural occurrence, biological activities and synthesis of eight-, nine-, and eleven-membered ring lactones. *Quimica Nova* **31**, 885–900 (2008).
37. Allinger, N. L., Langley, C. H. & Lii, J.-H. Molecular Mechanics Calculations on Carbonyl Compounds. III. Cycloketones. *Journal of Computational Chemistry* **22**, 1451–1475 (2001).
38. Allinger, N. L., Chen, K., Rahman, M. & Pathiaseril, A. Molecular mechanics (MM3) calculations on aldehydes and ketones. *Journal of the American Chemical Society* **113**, 4505–4517 (1991).
39. Rozada, T. C. *et al.* The conformational analysis of 2-halocyclooctanones. *Spectrochimica Acta: Molecular and Biomolecular Spectroscopy* **137**, 176–184 (2015).
40. Rounds, T. C. & Strauss, H. L. Vibration, rotation spectra, and conformations of cyclooctanone. *The Journal of Chemical Physics* **69**, 268–276 (1978).
41. Frisch, M. J. *et al.* Gaussian09 Revision E.01, Gaussian Inc. Wallingford CT. *Gaussian 09 Revision E.01* (2010).
42. Loru, D., Bermúdez, M. A. & Sanz, M. E. Structure of fenchone by broadband rotational spectroscopy Structure of fenchone by broadband rotational spectroscopy. *The Journal of Chemical Physics* **145**, 074311–8 (2016).
43. Loru, D. *et al.* Conformational Flexibility of Limonene Oxide Studied By Microwave Spectroscopy. *ChemPhysChem* **18**, 268 (2017).
44. Rounds, T. C. & Strauss, H. L. Vibration, rotation spectra, and conformations of cyclooctanone. *The Journal of Chemical Physics* **69**, 268–276 (1978).
45. Watson, J. K. G. *Vibrational Spectra and Structure. Elsevier Amsterdam* **6**, 1–89 (1977).
46. Pickett, H. M. The fitting and prediction of vibration-rotation spectra with spin interactions. *Journal of Molecular Spectroscopy* **148**, 371–377 (1991).
47. Watson, J. K. G. Aspects of Quartic and Sextic Centrifugal Effects on Rotational Energy Levels. in *Vibrational Spectra and Structure* 1–89 (1977).
48. Ruoff, R. S., Klots, T. D., Emilsson, T. & Gutowsky, H. S. Relaxation of conformers and isomers in seeded supersonic jets of inert gases. *The Journal of Chemical Physics* **93**, 3142–3150 (1990).
49. Jung, M. Conformational Analysis of Cyclooctanone: Evidence from ¹³C Nuclear Magnetic Resonance. *Bulletin of the Korean Chemical Society* **12**, 224–227 (1991).
50. Florio, G. M., Christie, R. A., Jordan, K. D. & Zwier, T. S. Conformational preferences of jet-cooled melatonin: Probing trans- and cis-amide regions of the potential energy surface. *Journal of the American Chemical Society* **124**, 10236–10247 (2002).
51. Kraitchman, J. Determination of Molecular Structure from Microwave Spectroscopic Data. *American Journal of Physics* **21**, 17–24 (1953).
52. Kraft, P., Bajgrowicz, J. A., Denis, C. & Fra, G. Odds and Trends : Recent Developments in the Chemistry of Odorants. *Angewandte Chemie - International Edition* **39**, 2980–3010 (2000).
53. Kisiel, Z. PROSPE - Programs for ROTational SPEctroscopy. *Spectroscopy from space* 91–106 (2001).
54. Almenningenlc, A., Dorofeeva, O. v., Mastryukov, V. S. & Allinger, N. L. The molecular structure and conformation of Cyclooctane as determined by electron diffraction and molecular mechanics calculations. *The Journal of Physical Chemistry* **89**, 252–257 (1985).

55. Anet, F. A. L. Dynamics of Eight-Membered Rings in the Cyclooctane Class. *Dynamic Chemistry* **45**, 169–220 (1974).
56. Legon, A. C. Equilibrium Conformations of Four- and Five-Membered Cyclic Molecules in the Gas Phase: Determination and Classification. *Chemical Reviews* **80**, 231–262 (1980).
57. Tamagawa, K., Hilderbrandt, R. L. & Shen, Q. Molecular Structure of Cyclopentanone by Gas-Phase Electron Diffraction. *Journal of the American Chemical Society* **109**, 1380–1383 (1987).
58. Iijima, T. Zero-point Average Structure of a Molecule Containing Two Symmetric Internal Rotors. Acetone. *Bulletin of the Chemical Society of Japan* **45**, 3526–3530 (1972).
59. Clarke, P., Black, R. & Iqbal, M. Investigation of Transannulation Reactions Across a Cyclononene Ring. *Synlett* **2010**, 543–546 (2010).
60. Wang, N. *et al.* Direct Photocatalytic Synthesis of Medium-Sized Lactams through C-C Bond Cleavage. *Angewandte Chemie International Edition*, **57**, 14225–14229, (2018).



STRUCTURES OF THE COMPLEXES OF CYCLOOCTANONE WITH WATER

Chapter 5



5. STRUCTURES OF THE COMPLEXES OF CYCLOOCTANONE WITH WATER

5.1. Introduction

Cyclooctanone is an odorant commonly used in the synthesis of more complex odorants, such as amber- and violet-smelling compounds. Structurally cyclooctanone is an 8-membered ring ketone, for which we have previously reported the observation of three conformers in gas phase: boat-chair (BC1), twisted boat-chair (TBC1) and boat-chair (BC2), with BC1 significantly more abundant than the other two.¹ Cyclooctanone is easily released into the atmosphere, hence it can be classified as a volatile organic compound (VOC). In the atmosphere VOCs can interact with water and other compounds, producing secondary organic species with unknown reactivity and effects on the climate change.

Water could act as a catalyst or inhibitor in atmospheric reactions by forming non-covalent interactions with VOCs.²⁻⁵ Whilst hydration of aldehydes and ketones is known to be extensive in condensed phases, gas-phase hydration of carbonyl compounds has been overlooked in atmospheric models, as it is believed that the concentration of water in atmosphere is not high enough to favour these reactions. However, recent gas-phase studies on the hydration of methylglyoxal by infrared spectroscopy⁴ and acrolein-water complexes by rotational spectroscopy⁶ provide new evidence of aldehyde hydration in the gas phase. In both cases the reaction occurs via the formation of *geminal* diols, which are reactive species with two hydroxyl groups bound to the same carbon atom that could potentially be involved in atmospheric processes. In liquid phase *gem*-diols are unstable and tend to return quickly to the carbonyl form. However, there is insufficient evidence to understand their reactivity in gas phase. The only studies available up to date on carbonyl hydration in the gas phase involve aldehydes, which are more reactive compared to ketones.⁷

Using broadband chirped pulse Fourier transform microwave (CP-FTMW) spectroscopy, we have studied the complexes of cyclooctanone with water and identified two complexes of cyclooctanone-H₂O and two of cyclooctanone-(H₂O)₂. In addition to characterising their non-covalent interactions and determining their experimental structures, we provide the first evidence of *gem*-diol formation on hydration of a ketone in the gas phase. The formation of a geminal diol can have important implications for atmospheric processes and opens a possible new channel for the formation of secondary organic aerosol.

5.2. Methods

Theoretical

The complexes of cyclooctanone with one and two water molecules were predicted using the CREST software,¹⁰ with conformers **BC1**, **BC2**, **TBC1** and **CR** of cyclooctanone¹ as initial structures for the configurational search. The resulting isomers were optimised at B3LYP-D3BJ and MP2 levels of theory with the 6-311++G(d,p) basis set. The structures within 1000 cm⁻¹ monohydrates are presented in Table 5.1 and the dihydrates within 600 cm⁻¹ in Table 5.3. All isomers were confirmed to be local minima by performing harmonic vibrational calculations, and their zero-point relative energies were obtained. Dissociation energies using the counterpoise method,¹¹ including fragment relaxation terms,¹² were determined. Energy decomposition analysis with symmetry-adapted perturbation theory (SAPT)^{13,14} for the complexes with one water molecule was also performed (Table 5.2).

Experimental

The spectrum of cyclooctanone with water was collected using our CP-FTMW spectrometer at King's College London, which operates in the 2-8 GHz frequency range.^{8,9} Cyclooctanone (98%) is a crystalline solid at room temperature, with a melting point of 313 K. In order to increase its concentration in the gas phase, the sample was placed in a bespoke heated nozzle and heated to 347 K, which was found to be the optimal temperature after several tests. Water was added by placing it in a receptacle outside the vacuum chamber and passing neon over it at stagnation pressures of 5 bar. The mixture of cyclooctanone and water was conducted to the vacuum chamber, where it forms a supersonic jet after going through a 1 mm diameter nozzle. The molecular pulse duration in the experimental setup was 1000 μ s. The species in the supersonic jet were polarised with 4 chirped microwave pulses of 4 μ s length varying linearly in frequency from 2 to 8 GHz. After each excitation pulse, molecular relaxation signals (free inductions decays, FIDs) were collected for 20 μ s by our digital oscilloscope. The time domain spectrum was converted to the frequency domain using a fast Fourier-transform algorithm with a Kaiser-Bessel window. 1.4 million FIDs were coherently added to produce our final spectrum. The spectrum of cyclooctanone with ¹⁸O isotopically enriched water (1:1 mixture of H₂¹⁶O and H₂¹⁸O) was recorded to determine the experimental positions of the oxygen atoms in the complexes.

5.3. Results and Discussion

Theoretical results

5.3.1.1. Cyclooctanone-H₂O

The complexes where cyclooctanone adopts the BC1 conformation are energetically most favoured, being at least 600 cm⁻¹ lower in energy compared to the complexes with other conformations of the cycloketone. It indicates that upon complexation with water the conformational preference of cyclooctanone remains unchanged.

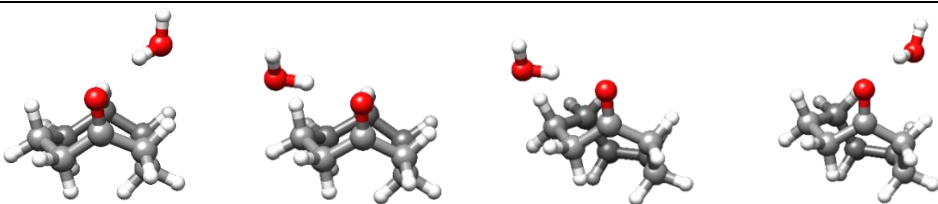
Comparing the results yielded by the two methods a few differences can be noted. Whilst the zero-point corrected energies agree that the global minimum is **BC1-1w-1**, differences in energy ordering are observed in the higher energy complexes, including the zero-point corrected relative energies.

For some isomers there are substantial discrepancies between the rotational constants predicted by each of the methods. For example, the agreement is good for **BC1-1w-2**, but not for isomer **BC1-1w-1**. The differences in the rotational constants for **BC1-1w-1** are related to a slight change in the structure: in the predicted MP2 configuration the water molecule is shifted closer to the centre of the cyclooctanone ring (Figure 5.1). A similar behaviour is observed for **BC2-1w-2** and **TBC1-1w-2**, where the displacement of the water molecule towards the centre of the ring changes the secondary interactions formed between the lone pairs of the water oxygen and the H-C groups of cyclooctanone. The differences between the rotational constantans and the dipole moments predicted by the two methods are particularly large in **TBC1-1w-2**. Finally, the **CR-1w** complexes, have the same spectroscopic parameters at B3LYP-D3BJ level of theory due to being enantiomers.

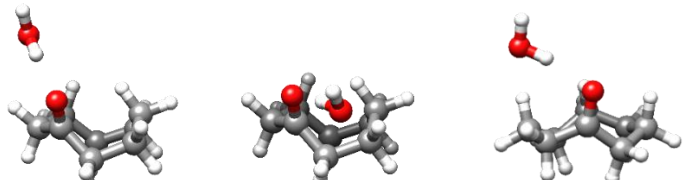
The energy decomposition analysis, based on SAPT calculations on both B3LYP-D3BJ and MP2 structures, show that contributions from the electrostatic interactions are about 4 times greater than dispersion forces for all isomers, due to the hydrogen bond formed between the water and the carbonyl group (Tables 5.2).

Table 5.1. Theoretical spectroscopic parameters and relative energies for the isomers of cyclooctanone-H₂O within 1000 cm⁻¹.

	BC1-1w-1		BC1-1w-2		TBC1-1w-1		TBC1-1w-2	
	B3LYP-D3BJ ^a	MP2	B3LYP-D3BJ	MP2	B3LYP-D3BJ	MP2	B3LYP-D3BJ	MP2
A ^b (MHz)	1409.3	1363.6	1763.9	1782.1	1879.0	1906.4	1507.0	1270.3
B (MHz)	1001.7	1062.2	891.3	887.3	856.6	850.0	881.6	1072.5
C (MHz)	842.3	900.9	719.3	720.6	668.2	668.8	728.3	963.6
μ_a (D)	-2.4	-1.8	2.9	2.6	3.0	2.7	3.0	1.2
μ_b (D)	0.3	0.2	0.6	0.6	0.7	0.7	0.4	0.2
μ_c (D)	-1.2	-1.0	-0.9	-0.8	-0.6	-0.4	0.9	1.0
ΔE^c (cm ⁻¹)	74.4	0.0	0.0	52.3	609.7	768.1	783.2	811.2
ΔE_0^d (cm ⁻¹)	0.0	0.0	47.4	26.8	558.8	684.3	680.2	722.1
D_e^e (kJ/mol)	32.5	22.8	33.4	23.6	34.3	23.8	32.3	21.8



	BC2-1w-2		BC2-1w-1		CR-1w-1 (12)	
	B3LYP-D3BJ	MP2	B3LYP-D3BJ	MP2	B3LYP-D3BJ	MP2
A ^b (MHz)	1496.1	1418.3	1825.0	1841.2	1574.5	1578.1
B (MHz)	960.4	1023.5	892.4	887.0	933.0	934.2
C (MHz)	803.4	867.7	689.1	690.4	769.0	785.9
μ_a (D)	2.3	1.8	2.9	2.7	2.4	2.2
μ_b (D)	0.3	0.2	0.7	0.7	0.1	0.2
μ_c (D)	-1.1	0.8	-0.6	-0.4	-1.2	-1.0
ΔE^c (cm ⁻¹)	838.2	752.1	696.3	727.3	786.9	906.8
ΔE_0^d (cm ⁻¹)	866.5	760.4	778.0	796.9	748.6	837.7
D_e^e (kJ/mol)	32.3	22.1	33.8	23.8	33.5	23.7



[a] B3LYP-D3BJ and MP2 with 6-311++G(d,p) basis set. [b] A, B, C are the rotational constants; μ_a , μ_b and μ_c are the electric dipole moment components. [c] Relative electronic energies. [d] Relative electronic energies including the zero-point correction [e] Binding energies from BSSE calculations.

Table 5.2. Binding energy decomposition analysis in kJ mol^{-1} for the complexes of cyclooctanone- (H_2O) on their MP2 and B3LYP-D3BJ geometries, using SAPT(0)/jun-cc-pDVZ calculations within Psi4.

	$\Delta E_{\text{electrostatic}}$		$\Delta E_{\text{exchange}}$		$\Delta E_{\text{induction}}$		$\Delta E_{\text{dispersion}}$		ΔE_{total}	
	MP2	B3LYP	MP2	B3LYP	MP2	B3LYP	MP2	B3LYP	MP2	B3LYP
BC1-1w-1	-46.5	-51.3	40.3	46.7	-12.8	-15.1	-12.8	-12.6	-31.8	-32.2
BC1-1w-2	-49.0	-53.1	42.1	49.0	-13.5	-15.8	-11.9	-12.8	-32.4	-32.7
BC2-1w-1	-49.5	-53.5	42.6	49.4	-13.8	-16.0	-12.1	-13.0	-32.8	-33.0
BC2-1w-2	-44.5	-50.3	38.9	45.4	-12.2	-14.7	-13.3	-12.4	-31.0	-32.0
CR-1w-1	-48.4	-52.6	41.4	48.3	-13.5	-15.7	-12.0	-12.9	-32.5	-32.8
CR-1w-2	-47.4	-52.5	40.2	48.3	-13.2	-15.7	-11.7	-12.8	-32.0	-32.8
TBC1-1w-1	-49.5	-53.7	42.3	49.3	-13.7	-15.9	-11.9	-12.9	-32.8	-33.3
TBC1-1w-2	-44.1	-51.8	37.8	46.8	-11.7	-15.2	-12.9	-11.5	-30.8	-31.9

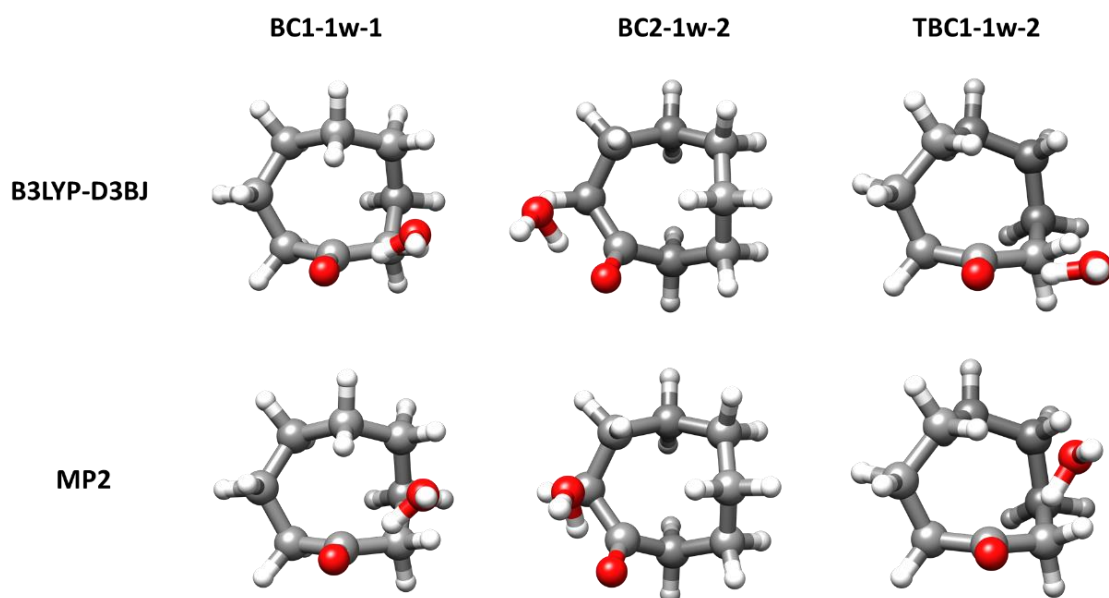


Figure 5.1. Top view of some cyclooctanone- H_2O structures from B3LYP-D3BJ and MP2 calculations.

5.3.1.2. Cyclooctanone-(H₂O)₂

The optimised complexes of cyclooctanone with two water molecules, predicted by CREST, also have the most energetically stable structures with cyclooctanone in the BC1 conformation (Table 5.3), which indicates that the increase in complexation order of cyclooctanone with water does not change cyclooctanone's conformational preferences. The global minimum in both MP2 and B3LYP-D3BJ, is isomer **2a**, where the water molecules are binding to the same lone pair of the carbonyl oxygen as in **BC1-1w-1**. The second water molecule binds to the first water molecule via hydrogen bonding, also forming secondary interactions between the lone pair on the oxygen and the H-C groups of the ring. Whilst water prefers to form a hydrogen bond chain arrangement, we also have predicted structures where water molecules bind to different lone pairs of the oxygen in the carbonyl group, forming a triangle as in **BC1-2w-13a** and **BC1-2w-11a** isomers, or being separated as in **BC1-2w-14a**. However, these isomers are not energetically favourable.

There is better agreement between the predicted structures by the two levels of theory in cyclooctanone-(H₂O)₂ than in cyclooctanone-H₂O, except for isomer **BC1-2w-8a**, where the second water molecule at MP2 level is predicted to be located closer to the centre of the ring. For the complexes with two water molecules.

Table 5.3. Theoretical spectroscopic parameters and relative energies for the isomers of cyclooctanone-(H₂O)₂ within 600 cm⁻¹.

	2a (BC1)		3a (BC1)		16a (BC1)		5a (BC1)	
	B3LYP-D3BJ ^a	MP2	B3LYP-D3BJ	MP2	B3LYP-D3BJ	MP2	B3LYP-D3BJ	MP2
A ^b (MHz)	1154.3	1163.9	1157.1	1157.1	1445.5	1445.3	1440.9	1446.1
B (MHz)	717.5	707.2	714.7	709.3	580.9	578.2	581.0	574.8
C (MHz)	581.8	575.0	578.3	577.9	522.8	521.9	508.6	503.9
μ _a (D)	2.0	1.6	1.6	1.1	1.7	1.4	2.6	2.2
μ _b (D)	0.0	0.2	0.2	0.4	0.9	0.9	0.1	0.0
μ _c (D)	-0.4	-0.2	-1.1	-1.1	-0.5	-0.3	0.0	0.1
ΔE ^c (cm ⁻¹)	0.0	0.0	112.1	103.8	143.8	199.9	142.8	201.9
ΔE ₀ ^d (cm ⁻¹)	0.0	0.0	69.1	51.4	145.3	152.8	120.7	153.0
D _e ^e (kJ/mol)	72.5	53.0	71.3	52.0	71.2	51.8	71.5	52.1

	1a (BC1)		7a (BC1)		4a (BC1)		6a (BC1)	
	B3LYP-D3BJ	MP2	B3LYP-D3BJ	MP2	B3LYP-D3BJ	MP2	B3LYP-D3BJ	MP2
A ^b (MHz)	1453.4	1460.7	1493.4	1490.0	1433.9	1458.4	1428.4	1471.6
B (MHz)	569.4	561.6	601.0	608.1	550.8	576.1	550.5	570.4
C (MHz)	513.5	512.7	521.8	526.3	497.3	533.2	490.6	529.6
μ _a (D)	2.7	2.4	-1.1	-0.8	-1.8	-0.7	-2.5	-1.2
μ _b (D)	0.4	0.4	0.1	0.3	0.4	0.6	-0.4	-1.0
μ _c (D)	0.0	0.2	1.0	0.9	0.2	0.3	-0.1	-0.4
ΔE ^c (cm ⁻¹)	87.6	155.8	371.7	222.9	315.2	303.6	408.9	320.1
ΔE ₀ ^d (cm ⁻¹)	129.9	166.8	358.2	167.2	287.5	230.2	334.7	239.0
D _e ^e (kJ/mol)	71.4	51.6	68.3	50.1	69.1	49.8	68.2	49.7

	8a (BC1)		10a (BC1)		2b (TBC1)		13a (BC1)	
	B3LYP-D3BJ	MP2	B3LYP-D3BJ	MP2	B3LYP-D3BJ	MP2	B3LYP-D3BJ	MP2
A ^b (MHz)	1279.3	1179.8	1176.7	1175.8	1091.4	1089.6	1054.3	1042.6
B (MHz)	631.0	712.4	706.1	707.6	738.5	738.2	762.4	783.8
C (MHz)	508.5	576.5	571.1	571.6	638.5	636.1	690.9	711.4
μ _a (D)	2.5	1.5	2.5	2.1	-1.2	-0.8	-3.1	-3.0
μ _b (D)	-1.0	-0.9	-1.0	-1.1	-0.2	-0.3	2.5	2.4
μ _c (D)	-1.4	-0.7	-1.4	-1.1	-0.2	-0.1	-2.4	-2.0
ΔE ^c (cm ⁻¹)	425.7	332.8	557.6	455.8	612.8	649.2	781.3	782.3
ΔE ₀ ^d (cm ⁻¹)	390.9	239.0	443.3	319.3	576.6	606.2	805.7	663.7
D _e ^e (kJ/mol)	67.7	49.5	66.2	48.6	64.9	54.5	63.3	43.3

[a] B3LYP-D3BJ and MP2 with 6-311++G(d,p) basis set. [b] A, B, C are the rotational constants; μ_a, μ_b and μ_c are the electric dipole moment components. [c] Relative electronic energies. [d] Relative electronic energies including the zero-point correction. [e] Binding energies from BSSE calculations.

Spectral assignment

5.3.1.3. Cyclooctanone-H₂O

The most intense lines in the spectrum of cyclooctanone-water belonged to the BC1 conformer of cyclooctanone.¹ Once these lines were removed, a pattern belonging to a less intense species was identified. The pattern corresponded to R-branch α -type transitions with $K_1 = 0, 1$. After an initial fit of a few transitions, a set of rotational constants was determined. More α -type as well as c -type transitions were measured and added to the fit. The final experimental rotational and centrifugal distortion constants are presented in the first column of Table 5.4. The Watson A-reduced Hamiltonian in the I' representation¹⁵ and Pickett's program^{16,17} were used in the fits. The measured frequencies are included in Appendix II.

The experimental rotational constants and observed relative intensities of α - and c -type transitions could match those predicted for **BC1-1w-1** and **BC2-1w-2**. However, the much higher relative energy predicted for **BC2-1w-2** points to **BC1-1w-1** (the theoretical global minimum) as the complex in our supersonic jet. Definite confirmation was obtained from the observation of all the ¹³C isotopologues in their natural abundance. The ¹⁸O isotopologues were observed by using a mixture of ¹⁸O-enriched and normal water. Surprisingly, we have also observed the spectrum of the ¹⁸O species corresponding to the carbonyl oxygen in cyclooctanone (see Section 5.5). The spectroscopic parameters of all isotopologues are collected in Table 5.5. Measured frequencies are presented in Appendix II, Tables S5.2–S5.11.

The second complex in the energy ordering, **BC1-1w-2**, was identified following the same procedure. **BC1-1w-2** is predicted to have a strong μ_α dipole moment component, hence the α -type lines were searched for and identified first. The relatively strong μ_c dipole moment (see Table 5.1) allowed observation of c -type lines. A total of 81 transitions from R- and Q-branches were observed and fit using the Watson A-reduced Hamiltonian in the I' representation¹⁵ and Pickett's program.¹⁶ The determined rotational and centrifugal distortion constants are collected in Table 5.4, second column. The measured frequencies are included in Table S5.12 of Appendix II. Observation of all ¹³C and ¹⁸O isotopologues at the predicted frequency shifts led to the unambiguous identification of this complex as **BC1-1w-2**. The experimental spectroscopic parameters of all observed isotopic species are presented in Table 5.5, and the measured frequencies in Tables S5.13–S5.22, Appendix II.

Higher energy complexes of cyclooctanone-H₂O, including the ones where cyclooctanone is in **TBC1** and **BC2** conformations, specifically **BC2-1w-1** and **TBC1-1w-1** which were predicted more favourable binding energies, were searched for in the spectrum, but they could not be assigned. This could be due to their low population in our supersonic jet, owing to the

significantly lower abundance of cyclooctanone in these configurations (about 12 and 525 times, respectively, lower than **BC1** in Ne as a carrier gas)¹ and by the higher relative energies of these complexes, which are at least 550 cm⁻¹ above the global minimum.

Table 5.4. Experimental spectroscopic constants of the observed isomers of cyclooctanone-water.

Parameters	BC1-H ₂ O		BC1-(H ₂ O) ₂	
	BC1-1w-1	BC1-1w-2	BC1-2w-2a	BC1-2w-5a
A ^a (MHz)	1366.8386(12) ^e	1778.97826(551)	1151.47283(582)	1433.9555(10)
B (MHz)	1025.83340(58)	873.07912(32)	697.99633(35)	575.553605(66)
C (MHz)	873.02639(56)	708.30424(41)	564.91587(37)	502.85461(24)
Δ _J (kHz)	1.139(21)	0.2355(90)	0.1767(48)	0.0907(21)
Δ _{JK} (kHz)	-2.906(35)	-0.095(13)	0.988(15)	0.3521(74)
Δ _K (kHz)	3.30(17)	0.988(37)	-0.78(12)	-
δ _J (kHz)	0.0363(21)	0.0098(20)	0.0121(24)	-
δ _K (kHz)	-	0.540(37)	0.569(25)	-
a/b/c ^b (D)	y/n/y	y/n/y	y/n/y	y/n/y
σ ^c (kHz)	4.8	7.1	4.7	4.5
N ^d	35	81	58	45

[a] A, B and C are the rotational constants. Δ_J, Δ_{JK}, Δ_K, δ_J and δ_K are the centrifugal distortion constants. [b] a, b and c are the type of transitions observed. [c] σ is the rms deviation of the fit. [d] N is the number of the fitted transitions. [e] Standard error in parentheses in units of the last digit.

5.3.1.4. Cyclooctanone-(H₂O)₂

The complexes of cyclooctanone with two water molecules, where cyclooctanone adopts the BC1 conformation, are significantly lower in energy than the rest (see Table 5.3). Hence, we started searching for them in our spectrum. All lower-energy isomers have sizable dipole moments along the *a* inertial axis. R-branch *a*-type line patterns were identified in the spectrum, and one species was assigned. The final fit, using the A-reduced Watson Hamiltonian in the I' representation,¹⁵ contains 47 *a*- and *c*-type transitions and yielded the rotational constants of the third column in Table 5.4. The measured frequencies are included in Appendix II.

The experimental rotational constants could be matched with the theoretical rotational constants for complexes **BC1-2w-2a** and **BC1-2w-3a**, where the arrangement of the water molecules is very similar. The only difference between the two predicted complexes is the orientation of the hydrogen atoms in the water molecules which are not part of the hydrogen bonding. This causes a slight energy difference and a larger difference in the μ_c dipole moment component, which helped with the identification of the assigned species. The assigned isomer showed mainly *a*-type spectrum with a strong intensity and a few *c*-type lines with approximately seven times lower intensity compared to the *a*-type, which is in better agreement with the predicted μ_a and μ_c dipole moments of the **BC1-2w-2a** complex. **BC1-2w-3a** is expected

to show *a*- and *c*-type spectra with similar intensities according to the MP2 predicted dipole moments, or *a*-type spectrum twice as intense compared to the *c*-type spectrum at B3LYP-D3BJ level. Other complexes with similar predicted rotational constants are **BC1-2w-8a** and **BC1-2w-10a**. These are much higher in energy and correspond to configurations where the water molecules bind to the other lone pair of the carbonyl oxygen. The assignment of our observed species to **BC1-2w-2a** was confirmed by the observations of the monosubstituted ^{13}C and ^{18}O isotopologues, including the ^{18}O corresponding to the carbonyl oxygen of cyclooctanone. The measured frequencies are included in Table S5.23. The experimental spectroscopic parameters of all observed isotopic species are presented in Table 5.5, and the measured frequencies in Tables S5.24–S5.34, Appendix II.

Using a similar approach, another isomer of cyclooctanone-(H_2O)₂, with predominantly *a*-type spectrum, was assigned. A few *c*-type transitions were also measured. Its experimental rotational constants (see fourth column of Table 5.4) are similar to those predicted for complexes **BC1-2w-1a**, **BC1-2w-16a** and **BC1-2w-5a**. The differences between the three complexes are the orientation of the non-bonding hydrogens in the water molecules. The fact that we could not observe *b*-type transitions allows us to discard **BC1-2w-16a**, with a sizable theoretical μ_b dipole moment of 0.9 D (Table 5.3). With our experimental data it is not possible to discriminate between **BC1-2w-1a** and **BC1-2w-5a**, although we tentatively assign our observed species to **BC1-2w-5a** since it is predicted to be slightly lower in energy by both theoretical methods and there is a slightly better agreement with the experimental rotational constants. The measured frequencies of the monosubstituted ^{13}C and ^{18}O isotopologues are included in Table S5.35. The experimental spectroscopic parameters of all observed isotopic species are presented in Table 5.5, and the measured frequencies in Tables S5.36–S5.46, Appendix II.

Table 5.5. Experimental spectroscopic parameters for all singly substituted ^{13}C and ^{18}O isotopic species of the water complexes of **BC1**.

BC1-1w-1	A^a (MHz)	B (MHz)	C (MHz)	σ^b (kHz)	N^c
$^{13}\text{C}_1$	1351.730(20) ^d	1025.4822(11)	866.6115(11)	6.7	10
$^{13}\text{C}_2$	1357.308(19)	1022.3081(11)	870.0362(10)	6.5	10
$^{13}\text{C}_3$	1363.400(15)	1015.51781(83)	866.65584(86)	6.4	11
$^{13}\text{C}_4$	1360.018(17)	1018.1061(11)	866.2339(12)	6.5	8
$^{13}\text{C}_5$	1356.9203(68)	1022.88733(41)	867.70985(43)	3.0	7
$^{13}\text{C}_6$	1361.6619(48)	1024.90360(58)	871.22396(57)	5.5	12
$^{18}\text{O}_7$	1348.98330(98)	1019.49614(34)	861.26116(35)	4.4	19
$^{13}\text{C}_8$	1353.028(13)	1021.17404(86)	870.37354(84)	5.1	8
$^{13}\text{C}_9$	1358.9177(97)	1020.33585(58)	872.25701(62)	4.3	10
$^{18}\text{O}_{10}$	1358.78082(50)	984.93777(22)	845.47419(24)	2.9	21
BC1-1w-2					
$^{13}\text{C}_1$	1776.854(52)	863.18511(89)	702.14275(78)	6.4	11
$^{13}\text{C}_2$	1765.626(26)	868.51283(75)	705.15658(65)	5.7	13
$^{13}\text{C}_3$	1756.309(32)	871.97260(87)	703.99941(76)	6.7	14
$^{13}\text{C}_4$	1762.599(25)	872.12225(74)	705.75516(65)	5.7	15
$^{13}\text{C}_5$	1770.146(18)	870.18290(50)	707.81121(43)	3.8	13
$^{13}\text{C}_6$	1772.808(33)	872.77043(81)	707.18568(72)	6.2	12
$^{18}\text{O}_7$	1754.5948(12)	866.94279(40)	702.02152(36)	5.4	25
$^{13}\text{C}_8$	1772.288(27)	865.96086(74)	703.05286(68)	5.9	14
$^{13}\text{C}_9$	1759.714(47)	871.88704(99)	704.56440(89)	7.6	12
$^{18}\text{O}_{10}$	1776.75883(70)	833.936232(13)	682.410557(28)	6.3	42
BC1-2w-2a					
$^{13}\text{C}_1$	1140.6978(87) ^d	697.93644(53)	562.27452(40)	5.4	14
$^{13}\text{C}_2$	1144.055(13)	695.99998(82)	563.43629(51)	6.1	12
$^{13}\text{C}_3$	1147.6805(11)	691.84557(48)	561.17383(49)	6.4	14
$^{13}\text{C}_4$	1148.488(13)	691.79313(45)	560.79547(48)	5.9	16
$^{13}\text{C}_5$	1146.309(11)	694.43578(50)	561.76922(50)	7.3	18
$^{13}\text{C}_6$	1147.1730(69)	697.53459(37)	564.05881(38)	4.3	14
$^{18}\text{O}_7$	1132.6442(66)	697.78346(25)	560.20857(25)	3.4	20
$^{13}\text{C}_8$	1141.850(14)	695.91627(61)	563.67886(45)	4.5	11
$^{13}\text{C}_9$	1146.0846(68)	695.88273(41)	564.86557(35)	4.0	13
$^{18}\text{O}_{10}$	1139.87404(31)	679.93382(13)	551.393886(14)	3.4	44
$^{18}\text{O}_{11}$	1141.81862(29)	679.50480(14)	550.61679(13)	3.4	43
BC1-2w-5a					
$^{13}\text{C}_1$	1432.824(52)	569.67561(68)	498.40369(68)	6.5	10
$^{13}\text{C}_2$	1424.206(50)	572.51492(56)	500.74531(55)	6.5	13
$^{13}\text{C}_3$	1418.457(57)	574.91369(82)	500.55689(81)	8.7	11
$^{13}\text{C}_4$	1426.299(60)	575.47057(73)	501.84013(74)	7.9	12
$^{13}\text{C}_5$	1429.776(60)	574.79591(66)	502.78323(57)	6.4	14
$^{13}\text{C}_6$	1429.067(66)	575.4797(10)	502.29030(87)	8.7	12
$^{18}\text{O}_7$	1409.301(29)	574.95678(40)	499.79099(41)	5.1	18
$^{13}\text{C}_8$	1430.314(40)	570.64627(49)	499.36085(50)	6.2	13
$^{13}\text{C}_9$	1422.777(53)	573.66133(72)	500.46046(61)	8.2	12
$^{18}\text{O}_{10}$	1417.688(16)	561.73600(22)	492.74634(21)	3.3	32
$^{18}\text{O}_{11}$	1420.3496(12)	557.47670(16)	488.72429(16)	2.6	30

[a] A , B and C are the rotational constants. Δ_i , Δ_{JK} , Δ_K , δ_i and δ_K centrifugal distortion constants were fixed to parent species values. [b] σ is the rms deviation of the fit. [c] N is the number of the fitted transitions. [d] Standard error in parentheses in units of the last digit.

Experimental structures

From the experimental rotational constants of the parent and isotopic species, we calculated the coordinates in the principal inertial axes of all heavy atoms of the four observed cyclooctanone-water complexes using Kraitchman's equations and their substitution structures r_s ¹⁸ (Table 5.8). The effective structures r_0 were determined from a least-squares fit of all the experimental moments of inertia for each complex (Table 5.6-7).¹⁹ Some of the structural parameters could not be floated, including those of the hydrogen atoms, and they were fixed to the theoretical values predicted by MP2/6-311++G(d,p).

There are several substitution C–C bond distances that are shorter or longer than the expected values of 1.54 Å for sp^3 hybridized carbon bonds. They can be attributed to the imaginary values of some of the substitution coordinates, which were set to zero, whilst others could be explained by large errors in the determined coordinates. For example, the **BC1-1w-1** complex has quite short or long values for the bond lengths where C_1 or C_9 are involved, which could be ascribed to the large errors of the c coordinate of C_1 and b coordinate of C_9 . Comparing the values of these bond lengths with the ones determined by r_0 method, they appear to be artifacts of the calculation method rather than real structural effects. There are also differences of more than 2° between the bond angles in the complex and those in bare cyclooctanone involving C_1 , C_9 and C_7 . The latter has a large error for its c coordinate. In the **BC1-1w-2** complex, similar effects are observed for the substitution bond lengths involving C_1 and C_5 , such as $r(C_2-C_1)$, $r(C_5-C_4)$, $r(C_6-C_5)$ and $r(C_8-C_1)$, which vary from 1.441(17) to 1.639(20) Å. These are likely due to the imaginary b coordinates of C_1 and C_5 atoms, which were set to zero.

The r_0 structural parameters for the monohydrates show more consistent values, and they agree well with those for the **BC1** conformer of bare cyclooctanone, indicating that the structure of the ring does not significantly change upon complexation (Table 5.6). Moreover, it shows a better agreement with the r_e equilibrium structure. One of the largest differences is noted for $r(C_5-C_4)$ of **BC1-1w-1**, with a value of 1.501(14) Å compared to 1.541(6) Å in BC1. Comparing the r_0 parameters of **BC1-1w-2** with the values for BC1, angle $\angle(O_7-C_6-C_9)$ is noted to be larger by over 1°. However, the determined value of 120.6(8)° is in agreement with r_e equilibrium structure of 120.8°. The same angle could not be determined in **BC1-1w-1**.

The r_s structures of the dehydrates also show abnormal bond lengths which could be linked to imaginary coordinates of carbons, or high errors in the coordinates (Table 5.7). **BC1-2w-2a** has a larger $r(C_2-C_1)$ bond length of 1.571(26) Å, which can be ascribed to the high error of c coordinate of C_1 . Moreover, the imaginary coordinate of C_9 translates in the bond angle $\angle(O_7-C_6-C_9)$ which is larger than value of the r_e structure and of the bare BC1 experimentally

determined parameter by 1° and 3° , respectively. Moreover $\angle(\text{O}_9\text{-C}_8\text{-C}_1)$ has been determined to have an abnormally small value compared to the r_0 , r_e and BC1 structures. The dihedral angles involving C_1 and C_9 differ by over 7° compared to BC1. The r_0 parameters show more consistency and better agreement with to the r_e and BC1 structures.

The large deviation in the r_s bond lengths $r(\text{C}_4\text{-C}_3)$, $r(\text{C}_5\text{-C}_4)$ and $r(\text{C}_6\text{-C}_5)$ of **BC1-2w-5a**, can be attributed to the high errors in the C_5 b coordinated and the imaginary coordinate c coordinate of C_4 . Some of the r_0 bond lengths such as $r(\text{C}_3\text{-C}_2)$ and $r(\text{C}_4\text{-C}_3)$ also show odd values of 1.449(16) and 1.625(65) Å, respectively.

With the addition of the second water molecule in the system, the $\text{C}=\text{O}\cdots\text{O}$ distances shorten from 2.841(7) Å to 2.792(12) Å for **BC1-2w-2a** and from and 2.871(6) Å to 2.745(40) Å for **BC1-2w-5a**, respectively. The water $\text{O}\cdots\text{O}$ in the dihydrates are 2.823(2) Å for **BC1-2w-2a** and 2.831(9) Å for **BC1-2w-5a**. These distances are shorter compared to the water dimer $\text{O}\cdots\text{O}$ of 2.98(4) Å.²⁰ This is an expected phenomenon due to the cooperative effect in the hydrogen bonding chain $\text{C}=\text{O}\cdots\text{H}-\text{O}\cdots\text{H}-\text{O}$. H-bond cooperativity originates from classical electrostatics and occurs as donor strength of a hydrogen-bond donor increases if the donor concurrently acts also as acceptor for a second hydrogen bond.²¹

Overlapping the experimental structures with the theoretical MP2 structures, which predicted the spectroscopic parameters closer to experimental values, in Figure 5.2. There is a very good agreement between them.

Table 5.6. Comparison of the bond lengths (in Å) and angles (in degrees) of the heavy atoms of complexes of BC1–H₂O determined experimentally with the experimental structural parameters of BC1 monomer.

	BC1-1w-1			BC1-1w-2			BC1
	r_s^a	r_o^b	r_e	r_s	r_o	r_e	r_o
$r(\text{C}_2\text{-C}_1)$	1.485(18)	1.537(17)	1.536	1.577(14)	1.540(12)	1.536	1.539(6)
$r(\text{C}_3\text{-C}_2)$	1.588(4)	1.551(18)	1.545	1.542(11)	1.543(11)	1.544	1.544(6)
$r(\text{C}_4\text{-C}_3)$	1.507(6)	1.545(18)	1.535	1.504(6)	1.534(14)	1.534	1.540(6)
$r(\text{C}_5\text{-C}_4)$	1.529(3)	1.501(14)	1.542	1.639(20)	1.564(11)	1.543	1.541(6)
$r(\text{C}_6\text{-C}_5)$	1.494(4)	-	1.517	1.441(17)	-	1.517	1.520(9) ^c
$r(\text{C}_6\text{-O}_7)$	1.240(8)	1.209(17)	1.228	1.235(9)	1.212(16)	1.228	1.215(9)
$r(\text{C}_9\text{-C}_6)$	1.473(17)	1.523(18)	1.514	1.487(5)	1.534(18)	1.515	1.520(9)
$r(\text{C}_9\text{-C}_8)$	1.591(16)	-	1.533	1.544(3)	1.538(12)	1.533	1.535(6)
$r(\text{C}_8\text{-C}_1)$	1.582(20)	1.555(14)	1.532	1.488(13)	1.526(10)	1.531	1.533(6)
$r(\text{O}_7\text{-O}_{10})$	2.862(5)	2.841(7)	2.857	2.871(3)	2.871(6)	2.863	-
$\angle(\text{C}_3\text{-C}_2\text{-C}_1)$	115.2(5)	-	115.0	116.0(4)	115.6(6)	114.7	115.2(3)
$\angle(\text{C}_4\text{-C}_3\text{-C}_2)$	114.9(2)	114.6(5)	114.6	115.3(4)	114.3(3)	114.5	114.8(2)
$\angle(\text{C}_5\text{-C}_4\text{-C}_3)$	116.1(2)	116.2(7)	115.7	117.1(3)	116.7(7)	115.8	115.7(2)
$\angle(\text{C}_6\text{-C}_5\text{-C}_4)$	111.9(2)	-	111.5	110.5(5)	-	112.2	111.8(4) ^c
$\angle(\text{O}_7\text{-C}_6\text{-C}_5)$	119.4(3)	-	119.5	119.3(4)	-	120.5	120.4(5) ^c
$\angle(\text{O}_7\text{-C}_6\text{-C}_9)$	120.0(4)	-	121.8	120.4(6)	120.6(8)	120.8	118.8(6) ^c
$\angle(\text{C}_9\text{-C}_6\text{-C}_5)$	120.6(3)	-	118.6	119.9(7)	-	118.7	120.7(8)
$\angle(\text{C}_8\text{-C}_9\text{-C}_6)$	114.0(2)	115.7(5)	114.9	115.3(2)	115.8(5)	115.2	115.6(3)
$\angle(\text{C}_9\text{-C}_8\text{-C}_1)$	112.5(4)	113.6(5)	113.9	114.8(5)	114.9(3)	114.0	114.5(4)
$\angle(\text{C}_8\text{-C}_1\text{-C}_2)$	115.4(2)	115.7(5)	115.5	115.6(2)	115.1(3)	115.5	116.0(2)
$\tau(\text{C}_4\text{C}_3\text{C}_2\text{C}_1)$	106.5(4)	-	105.6	102.9(8)	-	106.0	105.1(2)
$\tau(\text{C}_5\text{C}_4\text{C}_3\text{C}_2)$	-64.7(2)	-	-64.5	-61.3(9)	-	-64.0	-
$\tau(\text{C}_6\text{C}_5\text{C}_4\text{C}_3)$	65.6(2)	-	65.8	63.0(7)	-	65.4	-
$\tau(\text{O}_7\text{C}_6\text{C}_5\text{C}_4)$	75.5(6)	-	74.4	80.5(6)	-	75.6	-
$\tau(\text{C}_9\text{C}_8\text{C}_7\text{C}_6)$	-107.6(7)	-	-106.8	-106.4(7)	-	-105.9	-
$\tau(\text{C}_8\text{C}_9\text{C}_6\text{C}_5)$	44.4(9)	-	44.0	47.0(12)	-	43.0	-
$\tau(\text{C}_8\text{C}_9\text{C}_6\text{O}_7)$	-138.7(6)	-	-137.3	-139.9(6)	-	-138.5	-139.7(4)
$\tau(\text{C}_1\text{C}_8\text{C}_9\text{C}_6)$	67.1(9)	-	67.6	68.0(10)	-	67.8	67.4(10)
$\tau(\text{C}_2\text{C}_1\text{C}_8\text{C}_9)$	-58.2(7)	-	-59.5	-59.0(11)	-	-58.8	-57.4(5)
$\tau(\text{C}_3\text{C}_2\text{C}_1\text{C}_8)$	-51.1(5)	-	-52.0	-51.2(10)	-	-53.0	-53.6(5)

[a] The substitution structure has been determined from the atomic coordinates including Costain's error, and with signs taken from *ab initio* calculations. [b] Effective structure; non fitted parameters were fixed to the MP2/6-311++G(d,p) values. [c] Derived from the determined r_o structure, not fitted directly.

Table 5.7. Comparison of the bond lengths (in Å) and angles (in degrees) of the heavy atoms of complexes of BC1-(H₂O)₂ determined experimentally with the experimental structural parameters of BC1 monomer.

	BC1-2w-2a			BC1-2w-5a			BC1
	r_s^a	r_0^b	r_e	r_s	r_0	r_e	r_s^a
$r(C_2-C_1)$	1.571(26)	1.519(24)	1.535	1.569(7)	1.591(42)	1.536	1.539(6)
$r(C_3-C_2)$	1.558(2)	1.561(15)	1.545	1.548(8)	1.471(57)	1.545	1.544(6)
$r(C_4-C_3)$	1.520(4)	1.553(17)	1.534	1.449(16)	1.625(65)	1.534	1.540(6)
$r(C_5-C_4)$	1.539(4)	1.508(18)	1.542	1.642(48)	1.579(63)	1.542	1.541(6)
$r(C_6-C_5)$	1.532(5)	1.524(19)	1.516	1.433(39)	1.589(75)	1.513	1.520(9) ^b
$r(C_6-O_7)$	1.179(25)	1.224(19)	1.230	1.194(20)	1.142(64)	1.230	1.215(9)
$r(C_9-C_6)$	1.534(8)	-	1.512	1.553(30)	-	1.514	1.520(9)
$r(C_9-C_8)$	1.536(9)	1.542(26)	1.534	1.528(5)	1.560(47)	1.533	1.535(6)
$r(C_8-C_1)$	1.549(29)	1.550(23)	1.532	1.526(10)	-	1.531	1.533(6)
$r(O_7-O_{10})$	2.841(13)	2.792(12)	2.803	2.819(4)	2.745(40)	2.812	-
$r(O_{10}-O_{11})$	2.823(2)	2.831(9)	2.808	2.835(2)	2.811(34)	2.810	-
$\angle(C_3-C_2-C_1)$	118.9(7)	-	115.0	114.4(5)	113.1(24)	114.9	115.2(3)
$\angle(C_4-C_3-C_2)$	114.9(1)	114.8(6)	114.6	113.3(11)	116.1(18)	114.5	114.8(2)
$\angle(C_5-C_4-C_3)$	115.8(2)	115.2(5)	115.6	116.5(14)	114.0(28)	115.7	115.7(2)
$\angle(C_6-C_5-C_4)$	112.1(2)	114.2(8)	111.7	108.9(14)	109.4(20)	112.0	111.8(4)
$\angle(O_7-C_6-C_5)$	117.0(7)	-	119.1	125.3(24)	-	120.8	120.4(5)
$\angle(O_7-C_6-C_9)$	122.7(9)	-	121.9	117.4(12)	-	120.4	118.8(6)
$\angle(C_9-C_6-C_5)$	120.2(3)	-	118.9	117.2(14)	-	118.8	120.7(8)
$\angle(C_8-C_9-C_6)$	113.6(3)	-	115.2	116.2(5)	-	115.2	115.6(3)
$\angle(C_9-C_8-C_1)$	110.5(4)	112.8(7)	113.7	114.6(4)	-	114.0	114.5(4)
$\angle(C_8-C_1-C_2)$	111.8(3)	115.8(6)	115.3	116.4(2)	116.1(11)	115.6	116.0(2)
$\angle(O_7-O_{10}-O_{11})$	100.3(2)	100.1(2)	98.3	102.80(1)	104.8(7)	99.6	-
$\tau(C_4C_3C_2C_1)$	104.0(6)	-	105.8	106.0(19)	-	105.7	-
$\tau(C_5C_4C_3C_2)$	-64.3(2)	-	-64.2	-67.9(33)	-	-64.3	-
$\tau(C_6C_5C_4C_3)$	66.5(2)	-	66.2	71.8(32)	-	66.2	-
$\tau(O_7C_6C_5C_4)$	78.2(22)	-	75.6	76.6(23)	-	75.1	-
$\tau(C_9C_6C_5C_4)$	-104.5(4)	-	-106.2	-106.1(11)	-	-106.2	-
$\tau(C_8C_9C_6C_5)$	38.4(4)	-	42.1	42.1(19)	-	42.5	-
$\tau(C_8C_9C_6O_7)$	-144.5(23)	-	-139.7	-140.4(10)	-	-138.7	-139.7(4)
$\tau(C_1C_8C_9C_6)$	75.8(7)	-	68.7	68.1(9)	-	68.0	67.4(10)
$\tau(C_2C_1C_8C_9)$	-67.6(5)	-	-58.8	-56.4(9)	-	-58.3	-57.4(5)
$\tau(C_3C_2C_1C_8)$	-46.5(4)	-	-53.1	-53.3(8)	-	-53.1	-53.6(5)
$\tau(C_6O_7O_{10}O_{11})$	13.7(31)	-	12.3	12.5(9)	-	4.6	-

[a] The substitution structure has been determined from the atomic coordinates including Costain's error, and with signs taken from *ab initio* calculations. [b] Effective structure; non fitted parameters were fixed to the MP2/6-311++G(d,p) values. [c] Derived from the determined r_0 structure, not fitted directly.

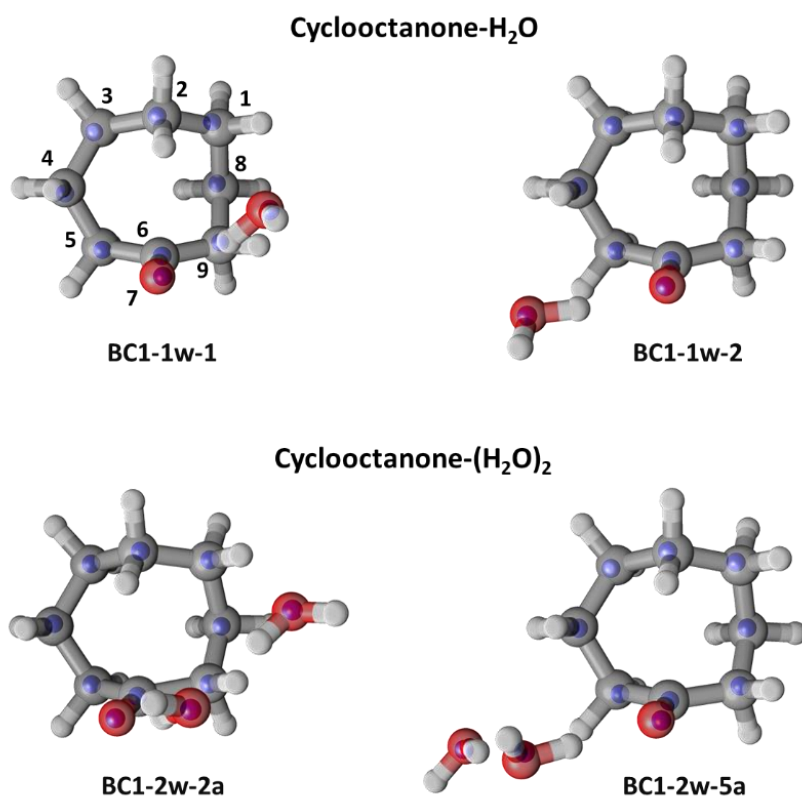


Figure 5.2. r_s structures for the assigned complexes of cyclooctanone-(H₂O)_{1,2}. The blue dots are the experimental r_s positions of the heavy atoms overlapped with the MP2 electronic structures.

Table 5.8. Substitution coordinates of the heavy atoms of water complexes of **BC1** in Å.

BC1-1w-1	a	b	c
C ₁	0.3946(39) ^a	-2.03577(75)	-0.093(17)
C ₂	0.7339(21)	-1.1982(13)	1.0860(14)
C ₃	2.03925(75)	-0.3070(50)	0.9282(16)
C ₄	1.78349(86)	1.1655(13)	0.7385(21)
C ₅	1.0544(14)	1.5615(10)	-0.5459(28)
C ₆	-0.3444(44)	1.0387(15)	-0.5770(26)
O ₇	-1.2148(12)	1.58860(95)	0.115(13)
C ₈	0.3417(44)	-1.2696(12)	-1.4759(10)
C ₉	-0.7082(21)	-0.074(20)	-1.4706(10)
O ₁₀	-3.04684(49)	-0.4139(36)	1.0225(15)
BC1-1w-2			
C ₁	2.50917(61)	0.000(12) ^b	0.6026(26)
C ₂	1.4264(11)	1.0716(14)	1.0102(15)
C ₃	0.8421(18)	1.9155(8)	-0.141(11)
C ₄	-0.5336(29)	1.5151(10)	-0.5970(26)
C ₅	-0.7094(21)	0.000(19) ^b	-1.1959(13)
C ₆	-0.4151(37)	-0.9798(16)	-0.1813(84)
O ₇	-1.2776(12)	-1.2590(12)	0.6579(22)
C ₈	2.12335(72)	-0.9142(17)	-0.5056(30)
C ₉	0.8540(18)	-1.75220(88)	-0.2423(64)
O ₁₀	-3.69017(41)	0.2670(56)	0.3484(43)
BC1-2w-2a			
C ₁	0.2423(72)	-2.03853(86)	-0.053(33)
C ₂	0.8864(23)	-1.2474(16)	1.1421(18)
C ₃	2.33893(79)	-0.7052(26)	0.9889(19)
C ₄	2.44121(80)	0.7895(25)	0.7351(27)
C ₅	1.8332(10)	1.2879(15)	-0.58829(32)
C ₆	0.3107(53)	1.1242(15)	-0.6217(27)
O ₇	-0.3271(48)	1.92106(82)	-0.032(50)
C ₈	0.4611(45)	-1.3173(16)	-1.4059(15)
C ₉	-0.3279(51)	0.0000(99) ^b	-1.4483(11)
O ₁₀	-3.02262(50)	1.3848(11)	0.6874(22)
O ₁₁	-3.12709(48)	-1.3975(11)	0.2214(68)
BC1-2w-5a			
C ₁	2.98319(54)	0.3138(52)	0.4298(38)
C ₂	1.79906(89)	0.9953(16)	1.2009(13)
C ₃	0.9306(18)	1.93830(85)	0.3332(50)
C ₄	-0.3649(45)	1.3800(12)	0.000(20) ^b
C ₅	-0.3676(44)	0.088(18)	-1.0128(16)
C ₆	0.135(13)	-1.0552(16)	-0.3093(55)
O ₇	-0.4757(32)	-1.69556(89)	0.4920(31)
C ₈	2.61765(60)	-0.4368(36)	-0.8479(19)
C ₉	1.5691(10)	-1.5330(11)	-0.6630(25)
O ₁₀	-3.09442(52)	-0.8863(18)	1.1499(14)
O ₁₁	-3.68731(45)	1.0200(17)	-0.8635(20)

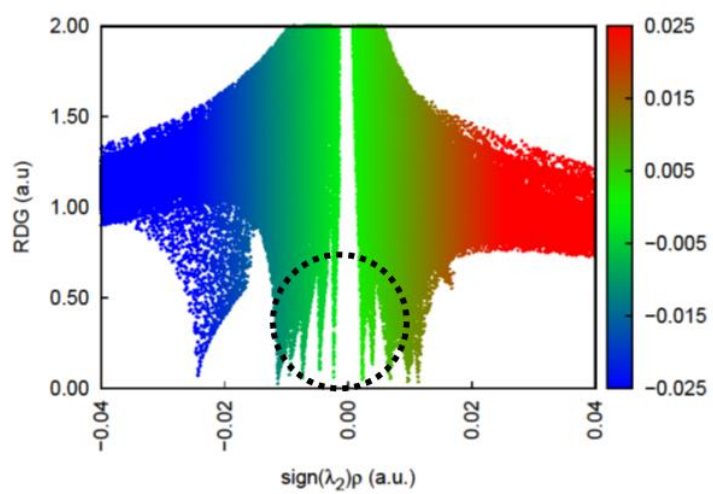
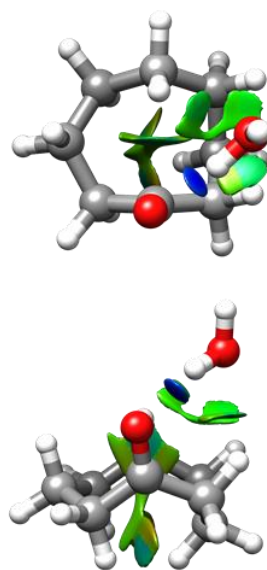
[a] Signs are taken from the theoretical calculations. Errors include Costain's errors. [b] Imaginary coordinate set to zero.

Non-covalent interactions and conformational abundances

The interactions involved in stabilizing the observed isomers of cyclooctanone-water were analysed and visualized using the non-covalent interaction (NCIs) method, which is based on the electron density and its derivatives.²² The NCI plots of the cyclooctanone-H₂O complexes (Figure 5.3) show the hydrogen bond between the carbonyl group and the water molecule as dark-blue disks, indicative of strong attractive interactions. The secondary interactions between the lone pairs of the oxygen in the water molecule and the hydrogens in the cyclooctanone ring are presented as green isosurfaces, indicative of weak attractive interactions. There are other green isosurfaces, with more yellow patches, in the centre of the ring showing slightly repulsive interactions between the H atoms pointing towards the centre of the ring. The reduced density gradient (RDG) are plotted with respect to electron density (Figure 5.3), and their spikes are associated with interaction critical points. Comparing the RDG maps of the two monohydrates we observe that isomer **BC1-1w-1** has two additional critical points close to zero, which indicate weak attractive interactions. This additional interactions seem to be contributing to the overall stabilisation of the complex and further to a higher relative abundance in the supersonic jet, with **BC1-1w-1** being 2.7 more abundant compared to **BC1-1w-2**. The relative abundances of the monohydrates also agree with the zero-point corrected relative energies, whilst not in agreement with binding energies which predict **BC1-1w-2** more energetically favourable.

The NCI plots of the cyclooctanone-(H₂O)₂ complexes (Figure 5.4) also show O-H...O hydrogen bonds involving the water molecules and carbonyl oxygen and secondary interactions between the oxygens of water and the hydrogens from the -CH₂ groups of cyclooctanone. A second strong interaction illustrated in dark blue represents the O-H...O-H hydrogen bonds between the two water molecules. The position of the first water molecule changes compared to the equivalent water molecules in monohydrates presumably to maximise intermolecular interactions. The RDG plots of the dihydrates do also differ, with that corresponding to the **BC1-2w-5a** isomer showing a cluster of spikes around zero. These additional van der Waals interactions are most likely stabilising this isomer and resulting in its higher abundance (1.3 times) with respect to **BC1-2w-2a**. The experimental relative abundances of the dehydrates are in disagreement with their relative and binding energies.

BC1-1w-1



BC1-1w-2

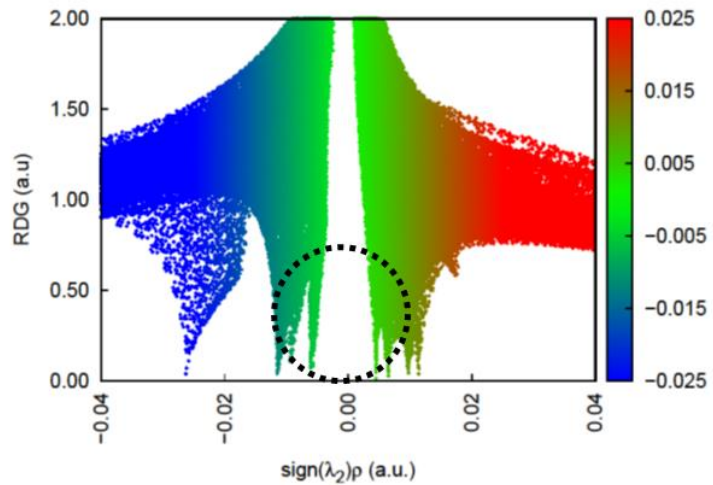
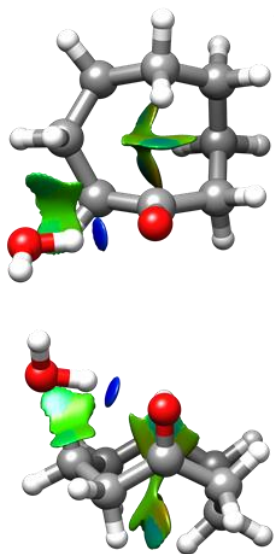
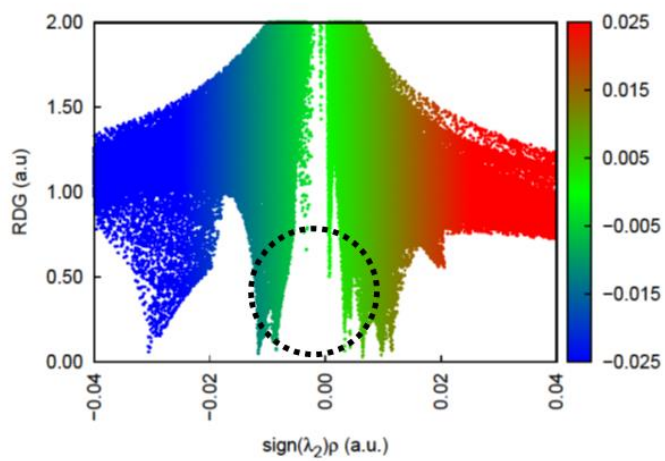
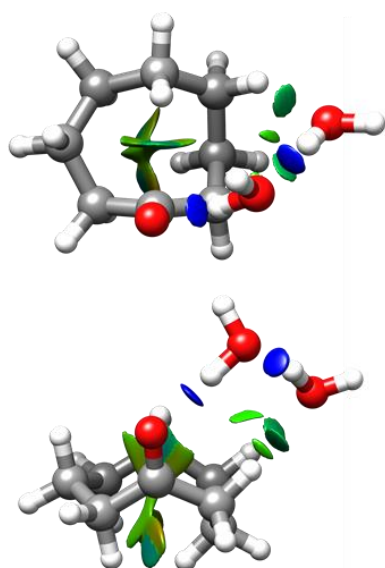


Figure 5.3. NCI and RDG plots of the observed isomers of BC1-1w.

BC1-2w-2a



BC1-2w-5a

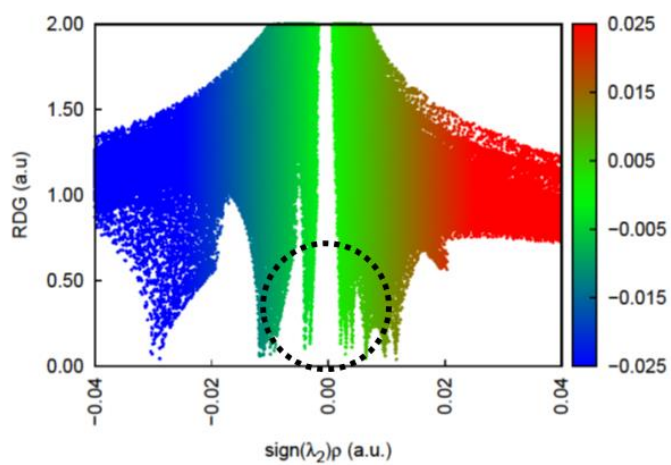
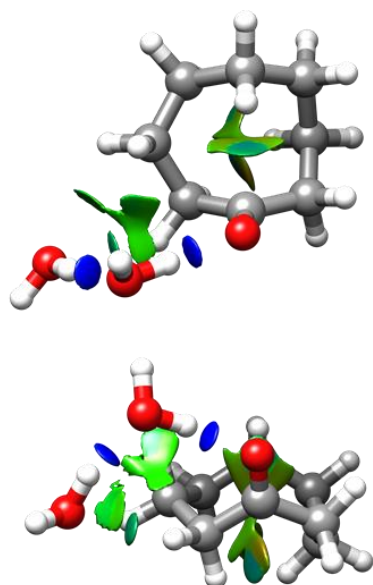


Figure 5.4. NCI plots of the observed isomers of BC1-2w.

Ketone hydration: Geminal-diol formation

The ^{18}O isotopologue corresponding to the substitution of the carbonyl oxygen is not observable in the H_2^{16}O spectrum of the complexes of cyclooctanone with one and two water molecules. It is only observed in the broadband spectrum recorded using enriched H_2^{18}O water (Figures 5.5 and 5.6).

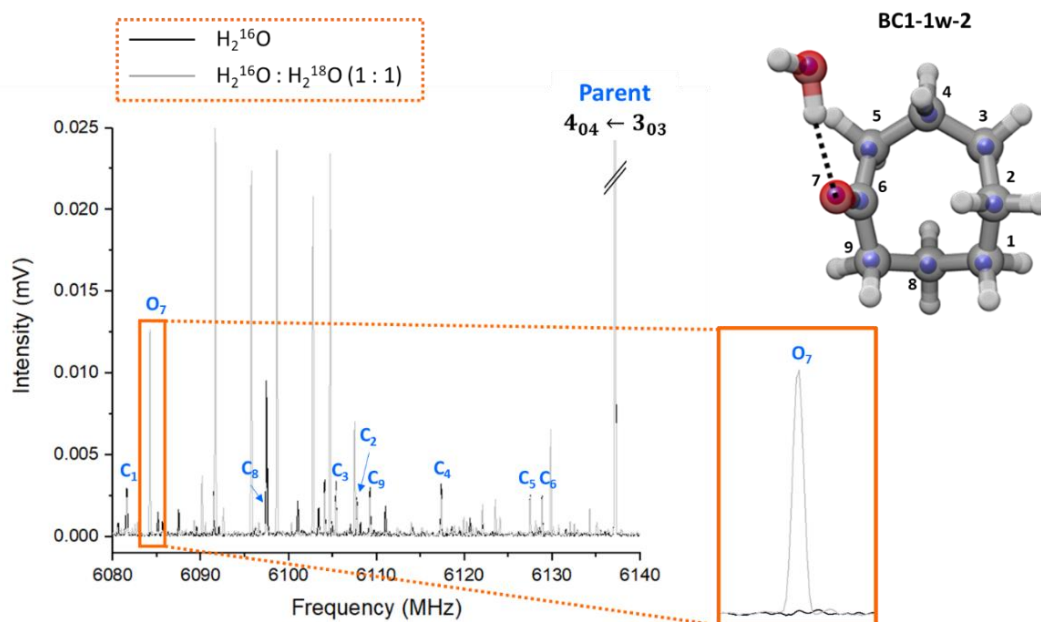


Figure 5.5. Overlapped spectra of normal water (black) and ^{18}O isotopically enriched water (grey) showing the presence of the $^{18}\text{O}=\text{C}$ species in the later for **BC1-1w-2** complex.

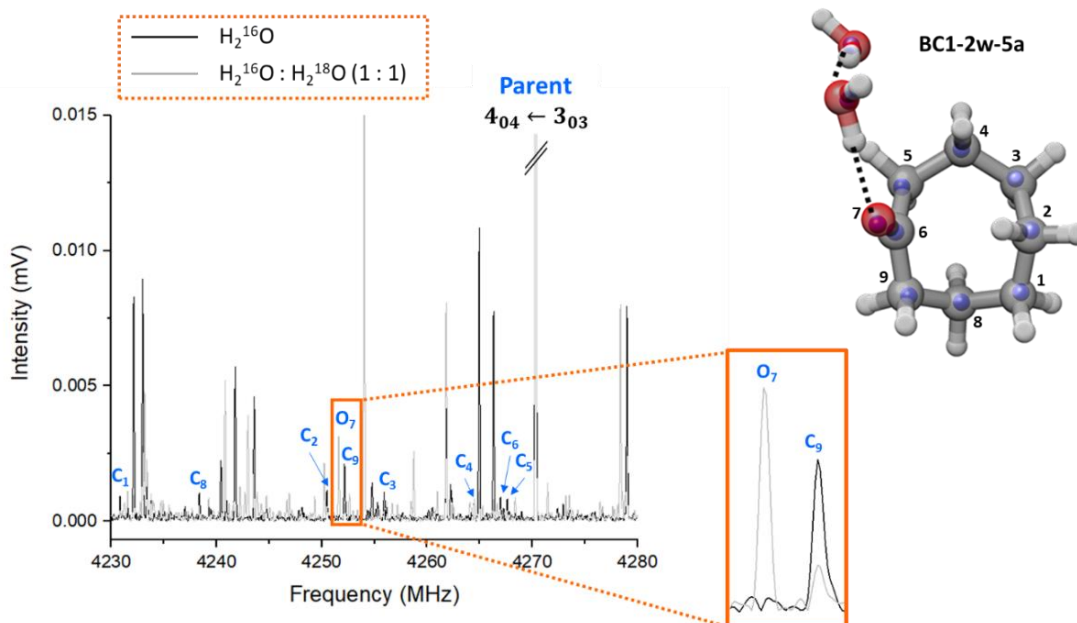


Figure 5.6. Overlapped spectra of normal water (black) and ^{18}O isotopically enriched water (red) showing the presence of the $^{18}\text{O}=\text{C}$ species in the later for **BC1-2w-5a** complex.

This indicates that an exchange reaction between ^{16}O and ^{18}O occurs in the supersonic jet. A possible mechanism for this exchange reaction is geminal diol formation, which is a reversible reaction that involves addition of water to a ketone or an aldehyde (Figure 5.7).⁴ The fact that the $^{18}\text{O}=\text{C}$ lines show a significantly larger intensity than those of the ^{13}C species indicates that the reaction occurs extensively. Whilst hydration of aldehydes and ketones is common in aqueous state, it is not considered favourable in water-restricted environments such as the gas phase due to limited water availability. In spite of this, there have been a few reported observations of *gem*-diol formation from hydration of aldehydes in the gas phase^{4,6,23} and in water-restricted conditions.²⁴

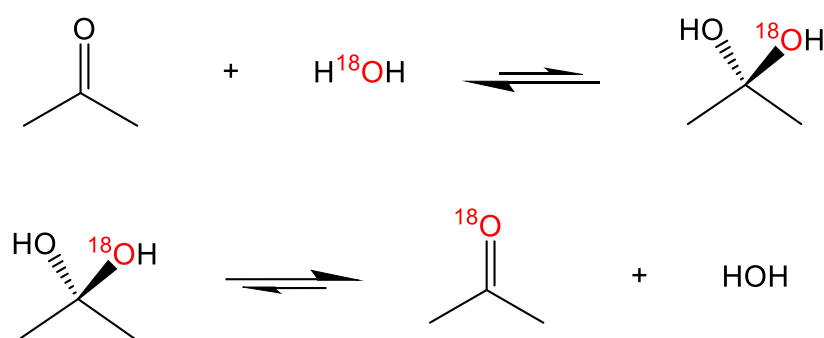


Figure 5.7. Reaction scheme of the ketone hydration via the *gem*-diol formation step.

To our knowledge, this work presents the first evidence of ketone hydration in the gas phase via *gem*-diol formation. *Gem*-diols are usually very unstable, and the reverse reaction is favoured (Figure 5.6). Nevertheless, we explored the potential energy landscape of the cycloocta-diol species using CREST. After optimising the obtained structures using B3LYP-D3BJ and MP2 methods twelve conformations were predicted within 1000 cm^{-1} (Table 5.9). Interestingly, the lowest in energy *gem*-diol has the ring shape of the **BC5** conformation, where the diol group is at a corner position. The equivalent ketone configuration, where the carbonyl occupies the same position could not be optimised as it returned the **TBC1** conformation. This can be explained by the angle of the corner angles, which being more acute does not prefer to be sp^2 hybridised. Nonetheless, in the *gem*-diol, due to the bulkiness of the $-\text{OH}$ groups a corner position is more favoured. Formation of the *gem*-diol in this configuration of the ring implies conformational interconversion. We searched for these species in the H_2^{16}O spectrum, but it could not be identified. This could be due to the low population of the *gem*-diol in the molecular jet, or to the low magnitude of its dipole moment components. Another explanation could be that the reaction rate is faster than our experimental timescale.

Table 5.9. B3LYP-D3BJ and MP2 spectroscopic parameters and relative energies for the gem-diol species within 1000 cm^{-1} . All calculations were performed with the 6-311++G(d,p) basis set.

	4 (BC5)		1 (BC5)		2 (BC3)		7 (TBC3)	
	B3LYP-D3BJ ^a	MP2	B3LYP-D3BJ	MP2	B3LYP-D3BJ	MP2	B3LYP-D3BJ	MP2
A^b (MHz)	1848.8	1855.2	1854.2	1862.9	1909.4	1915.2	1916.5	1942.0
B (MHz)	1115.5	1129.3	1110.0	1121.9	1062.3	1073.9	1050.1	1054.1
C (MHz)	850.3	859.3	854.3	862.8	868.3	878.7	834.8	842.2
μ_a (D)	0.5	0.5	0.5	0.4	-0.5	-0.4	0.5	0.4
μ_b (D)	0.0	0.0	0.1	0.1	0.0	0.1	-0.1	-0.1
μ_c (D)	-0.1	0.1	0.0	0.0	0.1	0.1	0.0	0.0
ΔE^c (cm^{-1})	0.0	0.0	6.0	52.0	85.7	100.4	541.1	580.8
ΔE_0^d (cm^{-1})	0.0	0.0	1.5	56.0	30.5	99.9	488.8	527.0
ΔG^e (cm^{-1})	0.0	0.0	10.8	69.4	40.6	119.6	428.4	462.9

	11 (TBC3)		9 (BC2)		12 (BC2)		3 (TBC2)	
	B3LYP-D3BJ	MP2	B3LYP-D3BJ	MP2	B3LYP-D3BJ	MP2	B3LYP-D3BJ	MP2
A (MHz)	1910.2	1934.9	1886.9	1898.1	1892.3	1904.8	1912.5	1996.6
B (MHz)	1054.3	1059.0	1121.9	1129.3	1121.2	1128.2	1036.9	1023.3
C (MHz)	831.3	838.8	885.8	893.5	882.1	889.1	812.2	822.0
μ_a (D)	0.6	-0.6	0.4	0.4	0.3	-0.3	0.5	-0.4
μ_b (D)	-0.1	-0.1	-0.2	-0.2	0.0	0.0	-0.1	0.0
μ_c (D)	0.1	0.1	0.0	-0.2	0.0	0.0	0.0	0.1
ΔE (cm^{-1})	586.0	603.7	672.8	840.6	718.1	855.1	730.8	1021.3
ΔE_0 (cm^{-1})	524.3	533.3	683.9	842.6	732.6	846.3	552.6	873.1
ΔG (cm^{-1})	449.9	455.0	726.2	853.5	775.6	846.3	183.0	673.3

	16 (BC5)		32 (BB2)		8 (BC1)		5 (BC1)	
	B3LYP-D3BJ	MP2	B3LYP-D3BJ	MP2	B3LYP-D3BJ	MP2	B3LYP-D3BJ	MP2
A (MHz)	1844.2	1849.5	1843.3	1855.7	1810.1	1824.2	1809.6	1823.8
B (MHz)	1115.1	1128.8	1138.5	1160.8	1153.4	1156.5	1152.9	1156.0
C (MHz)	856.1	864.8	889.6	911.5	908.2	912.8	910.3	915.8
μ_a (D)	0.7	-0.6	0.5	-0.5	0.3	-0.2	0.3	-0.3
μ_b (D)	1.6	-1.6	0.0	0.0	-0.1	-0.1	0.1	0.1
μ_c (D)	-1.8	1.8	0.1	0.1	0.0	0.0	0.1	0.1
ΔE (cm^{-1})	974.0	1026.5	957.0	1056.4	922.1	1139.8	936.4	1219.1
ΔE_0 (cm^{-1})	835.5	922.7	1050.0	1124.6	911.3	1122.0	921.1	1185.4
ΔG (cm^{-1})	705.2	836.2	997.3	1051.9	924.4	1104.0	939.1	1162.3

[a] B3LYP-D3BJ and MP2 with 6-311++G(d,p) basis set. [b] A , B , C are the rotational constants; μ_a , μ_b and μ_c are the electric dipole moment components. [c] Relative electronic energies. [d] Relative electronic energies including the zero-point correction. [e] Gibbs free energy.

5.4. Conclusions

Two complexes of cyclooctanone in the BC1 conformation with one water molecule and two with two water molecules have been identified in the broadband rotational spectrum. The experimental substitution and effective structures of the four complexes have been determined upon observation of all the ^{13}C and ^{18}O monosubstituted species. Observation of the $^{18}\text{O}=\text{C}$ monosubstituted species in the $\text{H}_2^{16}\text{O} : \text{H}_2^{18}\text{O}$ spectrum provides direct indication of a reversible water addition reaction, which occurs through geminal diol formation. To our knowledge, this is the first evidence of this process taking place in gas phase for ketones. Our results highlight the exceptional application of rotational spectroscopy in combination with theoretical calculations to obtain the structures of weakly bound complexes allowing the study of the intermolecular interactions. Moreover, in this investigation rotational spectroscopy has proved to be applicable in the study of the reactions and processes in gas phase.

5.5. Bibliography

1. Burevschi, E., Penã, I. & Sanz, M. E. Medium-sized rings: Conformational preferences in cyclooctanone driven by transannular repulsive interactions. *Physical Chemistry Chemical Physics* **21**, 4331–4338 (2019).
2. Vaida, V. Perspective: Water cluster mediated atmospheric chemistry. *Journal of Chemical Physics* **135**, 020901–08 (2011).
3. Jiang, X., Yang, Z. L., Liao, H. & Wiedinmyer, C. Sensitivity of biogenic secondary organic aerosols to future climate change at regional scales: An online coupled simulation. *Atmospheric Environment* **44**, 4891–4907 (2010).
4. Axson, J. L., Takahashi, K., de Haan, D. O. & Vaida, V. Gas-phase water-mediated equilibrium between methylglyoxal and its geminal diol. *Proceedings of the National Academy of Sciences* **107**, 6687–6692 (2010).
5. Schnitzler, E. G., Badran, C. & Jäger, W. Contrasting Effects of Water on the Barriers to Decarboxylation of Two Oxalic Acid Monohydrates: A Combined Rotational Spectroscopic and Ab Initio Study. *Journal of Physical Chemistry Letters* **7**, 1143–1147 (2016).
6. Li, W. *et al.* Atmospherically relevant acrolein-water complexes: Spectroscopic evidence of aldehyde hydration and oxygen atom exchange. *Physical Chemistry Chemical Physics* **21**, 23559–23566 (2019).
7. Carter, W. P. L. A detailed mechanism for the gas-phase atmospheric reactions of organic compounds. *Atmospheric Environment Part A, General Topics* **24**, 481–518 (1990).
8. Loru, D. *et al.* Conformational Flexibility of Limonene Oxide Studied by Microwave Spectroscopy. *ChemPhysChem* **18**, 274–280 (2017).
9. Loru, D., Bermúdez, M. A. & Sanz, M. E. Structure of fenchone by broadband rotational spectroscopy Structure of fenchone by broadband rotational spectroscopy. *The Journal of Chemical Physics* **145**, 074311–8 (2016).

10. Pracht, P., Bohle, F. & Grimme, S. Automated exploration of the low-energy chemical space with fast quantum chemical methods. *Physical Chemistry Chemical Physics* **22**, 7169–7192 (2020).
11. Boys, S. F. & Bernardi, F. The calculation of small molecular interactions by the differences of separate total energies. Some procedures with reduced errors. *Molecular Physics* **19**, 553–566 (1970).
12. Xantheas, S. S. On the importance of the fragment relaxation energy terms in the estimation of the Basis Set Superposition Error correction to the intermolecular interaction energy. *Journal of Chemical Physics* **104**, 8821–8824 (1996).
13. Jeziorski, B., Moszynski, R. & Szalewicz, K. Perturbation Theory Approach to Intermolecular Potential Energy Surfaces of van der Waals Complexes. *Chemical Reviews* **94**, 1887–1930 (1994).
14. Parrish, R. M. *et al.* Psi4 1.1: An Open-Source Electronic Structure Program Emphasizing Automation, Advanced Libraries, and Interoperability. *Journal of Chemical Theory and Computation* **13**, 3185–3197 (2017).
15. Watson, J. K. G. *Vibrational Spectra and Structure*. Elsevier Amsterdam **6**, 1–89 (1977).
16. Pickett, H. M. The fitting and prediction of vibration-rotation spectra with spin interactions. *Journal of Molecular Spectroscopy* **148**, 371–377 (1991).
17. Novick, S. E. A beginner's guide to Pickett's SPCAT/SPFIT. *Journal of Molecular Spectroscopy* **329**, 1–7 (2016).
18. Kraitchman, J. Determination of Molecular Structure from Microwave Spectroscopic Data. *American Journal of Physics* **21**, 17–24 (1953).
19. Kisiel, Z. PROSPE-Programs for Rotational spectroscopy. *Spectroscopy from space* 91–106 (2001).
20. Dyke, T. R. & Muentzer, J. S. Microwave spectrum and structure of hydrogen bonded water dimer. *The Journal of Chemical Physics* **60**, 2930–2931 (1974).
21. Karpfen, A. Cooperative Effects in Hydrogen Bonding. in *Advances in Chemical Physics* (eds. Prigogine, I. & Rice, S. A.) 469–510 (2002).
22. Johnson, E. R. *et al.* Revealing noncovalent interactions. *Journal of the American Chemical Society* **132**, 6498–6506 (2010).
23. Plath, K. L. *et al.* Gas-phase vibrational spectra of glyoxylic acid and its gem diol monohydrate. Implications for atmospheric chemistry. *Reaction Kinetics and Catalysis Letters* **96**, 209–224 (2009).
24. Maroń, M. K., Takahashi, K., Shoemaker, R. K. & Vaida, V. Hydration of pyruvic acid to its geminal-diol, 2,2-dihydroxypropanoic acid, in a water-restricted environment. *Chemical Physics Letters* **513**, 184–190 (2011).



CONFORMATIONAL INVESTIGATION OF CYCLODODECANONE

Chapter 6



6. CONFORMATIONAL INVESTIGATION OF CYCLODODECANONE

6.1. Introduction

Macrocycles are molecules containing twelve-membered or larger rings, used in drug discovery,¹ catalysis and materials.² Their stability, reactivity and physicochemical characteristics are related to their structural properties, specifically to the conformations they adopt and their intramolecular forces. However, investigation of their intrinsic conformational behaviour is particularly challenging because they are highly flexible, and present serious difficulties for their experimental analysis. The focus of many studies has been on small (up to 7 atoms) and medium (8 to 11 atoms) rings.³⁻⁸ The study of small cycloalkane rings C_nH_{n+2} with $n = 3-5$ reveal that torsional and angle strain determine their conformations. Due to ring constraints $\angle CCC$ angles are reduced to values below 109.5° , and in four and five-membered rings large amplitude motions, such as pseudorotation and ring-puckering, are common to minimise strain. Torsional and angle strain are basically removed in six-membered cyclohexane ($n = 6$), which adopts a chair conformation where bond and torsional angles are close to their optimal values for tetrahedral carbons, and all C–H bonds are staggered avoiding eclipsed interactions.⁹ Cycloheptane ($n = 7$) shows torsional strain due to eclipsing interactions between H atoms, similar to smaller rings, and also steric strain caused by transannular repulsive interactions, which are characteristic of medium-sized rings.¹⁰ It is therefore not strain-free and experiences pseudorotation.¹⁰⁻¹²

Unlike small rings, medium-sized rings have less angle and torsional strain, but they exhibit a high level of steric strain. This is often due to the unfavourable transannular interactions involving the hydrogen atoms pointing inside the ring. The decrease of angle and torsional strain and the increase in ring flexibility result in medium-sized cycloalkanes generally adopting more than one conformation. Structural studies on cyclooctane in gas phase revealed two conformations being present, a predominant boat-chair conformation and a crown conformation.¹³ Similarly, cyclononane¹⁴ and cyclodecane¹⁵ show a more favoured conformation and a few less abundant ones. The last member of the series, cycloundecane, has been found to present two conformations in solution at low temperature.¹⁶

In large cycloalkanes with 12 atoms and above, belonging to the macrocyclic class, there is a considerable reduction in strain. For cyclododecane, studies by electron diffraction,¹⁷ X-ray crystallography¹⁸ and NMR¹⁹ identified a square configuration, with three C–C bonds per side, as the predominant one. In this conformation the carbon chain adopts a structure similar to an aliphatic chain, with an *anti*-zigzag configuration and staggered hydrogens.¹⁸ Whilst there was evidence of other more distorted structures being present, they could not be identified.

Experimental investigations on larger cycloalkanes are considerably sparser. To our knowledge, there is only an X-ray structural determination of cyclotetradecane.²⁰

Elucidating the forces determining the conformational behaviour of 12-membered rings is the basis to understand the conformational features of larger macrocycles. Structural experimental techniques such as NMR, X-ray and electron diffraction are still limited in their capacity to distinguish between multiple conformations despite advances in their capabilities.^{21–23} In some cases, macrocycle derivatives have been investigated as substituents helped crystallisation or removed some of the conformational flexibility. The studies of derivatives are also important as modifications of the forces involved in modelling the conformational landscape shed light on their relative significance.^{24–29}

In this paper we apply broadband rotational spectroscopy to the conformational study of cyclododecanone, the smallest of the large-ring ketones. Cyclododecanone is used in the synthesis of complex natural compounds containing macrocycles in their structures, such as the anticancer reagent rospheillin,^{30,31} and in the synthesis of macrocycles used in musk fragrances, such as muscone, exaltolide and others.^{32–36} It has been studied in condensed phases by X-ray diffraction³⁷ and by low-temperature ¹³C NMR and ¹H NMR,²⁸ where it was found that it exists as one conformer that maintains the [3333] square configuration reported for cyclododecane. However, there are no previous studies of cyclododecanone in the gas phase, where its intrinsic conformational preferences, unaffected by intermolecular forces, can be revealed.

Rotational spectroscopy is arguably the most powerful structural technique for conformational identification because each conformation produces a distinct rotational spectral pattern reflective of its mass distribution and they can be unequivocally recognised. Broadband spectral collection, typically of several GHz, is essential for decoding the complex spectrum of multiconformational molecules.^{38–42} We have recently analysed the conformational behaviour of cyclooctanone, a medium-size cyclic ketone, using broadband rotational spectroscopy and quantum-chemistry calculations.⁴³ We identified three conformations: a strongly prevalent boat-chair, a twisted boat-chair and another boat-chair conformation.⁴³ The preferred conformation was analogous to that of the unsubstituted cycloalkane. The presence of transannular interactions was the driving force behind conformational behaviour.

Cyclododecanone is expected to have a richer conformational landscape than cyclooctanone due to its larger size. We have identified seven conformations of cyclododecanone, of which a square configuration is the most abundant, and characterised their non-covalent interactions. A combination of transannular interactions and eclipsed HCCH configurations determine the conformational stability of cyclododecanone.

6.2. Methods

Theoretical

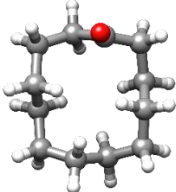
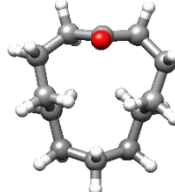
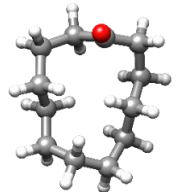
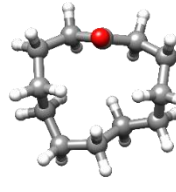
The potential energy surface of cyclododecanone was explored using the semiempirical method AM1 within the conformational search function implemented in the program HyperChem,⁴⁴ and the conformer sampling program CREST.⁴⁵ The first 200 conformations generated by HyperChem were optimised at the B3LYP-GD3BJ/6-311++G(d,p) level of theory, returning 16 distinct conformers within 1000 cm⁻¹. CREST generated 176 conformers, which were optimised using the same method. The structures predicted by both methods agree well, except for conformers 19, 27 and 74 that have been predicted only by HyperChem, and conformers 3 and 8 which have been predicted only by CREST. Together both methods have generated 18 distinct conformations within 1000 cm⁻¹. The resulting geometries have been further optimised at MP2 level of theory with 6-311++G(d,p) basis set, and their zero-point corrections were calculated for both methods to confirm that the predicted conformers are real minima and not saddle points. The predicted conformers within 850 cm⁻¹ are presented in Table 6.1. All of them have a sizable μ_c dipole moment component and are expected to show predominantly *c*-type spectrum.

Experimental

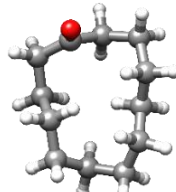
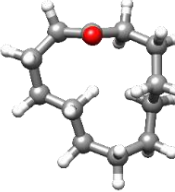
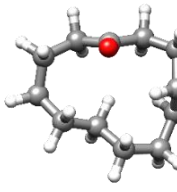
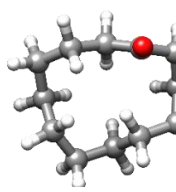
The broadband spectrum of cyclododecanone (Sigma-Aldrich, >99%) was recorded using our chirped-pulse Fourier transform microwave spectrometer at King's College London, which operates in the 2-8 GHz frequency range and has been previously described.⁴⁶ Cyclododecanone, heated at 417 K in our bespoke heating nozzle, was seeded in neon at 5 bar and conducted to the vacuum chamber, where the molecules expanded adiabatically forming a supersonic jet. The molecular pulse was polarized by four chirped microwave pulses of 4 μ s duration each. After each microwave pulse, the emission signal was collected as free induction decay (FID) for 20 μ s, amplified and stored in a fast oscilloscope in the time domain. A fast Fourier transform algorithm is used to convert the time domain spectrum to the frequency domain. The final spectrum has 1.5M FIDs.

Table 6.1. *Ab initio*^a spectroscopic parameters for the conformers cyclododecanone within 850 cm^{-1} .

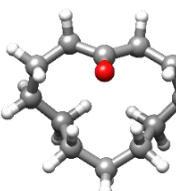
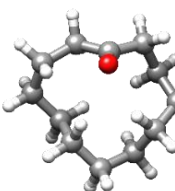
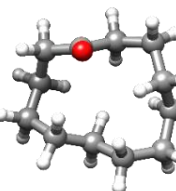
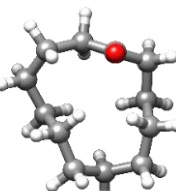
	1		9		7		13	
	B3LYP	MP2	B3LYP	MP2	B3LYP	MP2	B3LYP	MP2
A^b (MHz)	872.3	888.5	896.1	918.6	967.3	979.6	858.0	880.7
B (MHz)	691.1	693.2	693.2	697.0	632.2	641.2	740.9	741.3
C (MHz)	447.0	453.0	450.7	459.1	450.4	459.4	461.2	468.1
μ_a (D)	0.9	0.8	0.8	0.6	0.9	0.7	-0.2	-0.2
μ_b (D)	0.2	0.2	0.2	0.4	-0.6	-0.5	0.5	0.5
μ_c (D)	-2.6	-2.4	-2.3	-2.2	2.6	2.4	2.4	2.2
ΔE^c (cm^{-1})	0.0	0.0	469.1	516.4	461.6	401.9	583.8	574.0
ΔE_0^d (cm^{-1})	0.0	0.0	446.4	527.8	455.8	443.3	575.0	585.1
ΔG^e (cm^{-1})	0.0	0.0	269.7	566.5	537.7	579.2	521.7	649.4

	11		4		14		8	
	B3LYP	MP2	B3LYP	MP2	B3LYP	MP2	B3LYP	MP2
A (MHz)	988.5	1002.0	914.3	925.0	943.7	951.8	890.5	915.4
B (MHz)	630.1	635.2	673.7	680.3	682.2	687.6	678.6	675.0
C (MHz)	445.6	451.7	442.3	447.9	453.3	458.3	451.7	455.8
μ_a (D)	1.3	1.1	0.3	0.2	-0.1	-0.1	0.5	0.6
μ_b (D)	0.4	0.4	-0.3	-0.3	-0.3	-0.2	-1.1	-1.0
μ_c (D)	-2.5	-2.3	-2.4	-2.2	2.4	2.2	2.6	2.4
ΔE (cm^{-1})	495.3	452.6	645.6	604.9	698.0	726.3	823.8	962.2
ΔE_0 (cm^{-1})	590.6	508.3	592.1	572.0	611.2	673.8	780.7	956.5
ΔG (cm^{-1})	780.9	663.3	583.4	538.2	594.6	696.4	595.2	875.0

	74		3		19		10	
	B3LYP	MP2	B3LYP	MP2	B3LYP	MP2	B3LYP	MP2
A (MHz)	944.1	956.8	849.8	855.0	910.0	924.9	887.4	898.3
B (MHz)	699.1	699.7	746.4	753.1	694.6	699.7	700.6	706.9
C (MHz)	477.3	483.3	480.6	487.0	468.6	475.5	462.9	470.0
μ_a (D)	0.2	0.3	-0.1	-0.1	-0.6	-0.6	0.3	0.3
μ_b (D)	-1.1	-0.9	0.7	0.7	0.2	0.2	0.2	0.2
μ_c (D)	-2.1	-2.0	-2.5	-2.3	2.6	2.4	-2.6	-2.4
ΔE (cm^{-1})	851.1	1031.2	824.8	918.9	845.7	848.8	860.3	986.5
ΔE_0 (cm^{-1})	802.8	1005.2	816.2	960.4	843.0	879.9	858.4	1030.2
ΔG (cm^{-1})	802.8	1123.9	843.4	1003.0	848.0	885.8	894.6	1126.1

[a] B3LYP-D3BJ and MP2 with 6-311++G(d,p) basis set. [b] A , B , C are the rotational constants; μ_a , μ_b and μ_c are the electric dipole moment components. [c] Relative electronic energies. [d] Relative electronic energies including the zero-point correction. [e] Gibbs free energies at 417 K.

6.3. Results

Rotational spectrum

The broadband rotational spectrum of cyclododecanone showed a set of lines significantly more intense than all others. They were easily identified as *c*-type $J + 1 \leftarrow J$ transitions. From a preliminary fit of these transitions and subsequent prediction of the spectrum, *a*- and *b*-type lines belonging to the same species were observed with much lower intensity and measured. A total of 81 transitions (see Table S6.1) were fit to the semi-rigid rotor Watson Hamiltonian in the A reduction and III^I representation⁴⁷ using Pickett's program,⁴⁸ yielding the rotational and centrifugal distortion constants of column 1 in Table 6.2. Comparison with the theoretical rotational constants identify the observed species as conformer **1** of cyclododecanone. Due to the high intensity of the lines, the ¹³C isotopic species were also observed at the predicted frequency shifts with respect to the parent species and assigned. Their observed transitions were fit to the same Hamiltonian⁴⁷ as the lines from the parent species and the determined rotational constants are collected in Table 6.3. The ¹⁸O isotopologue was searched for, but it could not be observed, probably due to its lower natural abundance (0.2%) compared to the ¹³C (1.1%).

Removing the lines belonging to conformer **1** allowed for the observation of less intense lines, revealing the true density of the spectrum, and suggesting that more conformations were present. Using the automated spectral assignment of PGOPHER⁴⁹ in spectral searches, six additional conformations of cyclododecanone were assigned. All the conformations showed primarily *c*-type spectra, and their transitions were fit to the same Hamiltonian used for conformer **1** for oblate tops, and A reduction and I^r representation⁴⁷ for prolate tops. The resulting rotational and centrifugal distortion constants are shown in Table 6.2. The measured transitions are shown in Appendix III. The conformations can be identified as conformers **7**, **9**, **11**, **13**, **4**, and **14** from the close values of the theoretical and experimental rotational constants. Higher energy conformations have been searched for, but they were not observed in the spectrum, probably due to their low population in the molecular jet.

We have estimated the relative abundances of the observed conformers by comparing common *c*-type transitions, and considering that the relative abundance of a conformer is directly proportional to the intensity of its transitions and inversely proportional to the square of the corresponding dipole moment component. The values obtained are **1** : **7** : **13** : **11** : **4** : **14** : **9** = 77 : 4 : 3 : 2 : 2 : 2 : 1, respectively (Figure 6.1). Conformer **1** is significantly more abundant than the others, as expected from its spectral intensity. It is 19 times more abundant than the

second most abundant conformer. The other six conformers are much more similar in terms of abundances, with a range of 1-4 between them.

Table 6.2. Experimental spectroscopic parameters of the seven observed conformers of cyclododecanone.

Parameter	1	7	9	11
A^a (MHz)	865.65309(34) ^f	966.10552(37)	894.30343(70)	987.56296(46)
B (MHz)	700.47771(44)	638.54651(35)	677.77615(98)	634.23070(56)
C (MHz)	449.16998(30)	453.92116(42)	451.3106(34)	447.67064(45)
Δ_J (kHz)	0.140(13)	0.0295(51)	0.080(17)	0.0359(62)
Δ_{JK} (kHz)	-0.350(44)	-	-	-
Δ_K (kHz)	0.209(32)	-	-	-
δ_J (kHz)	-	-	-	0.0174(35)
δ_K (kHz)	0.213(34)	-	-	-
$a/b/c^b$ (D)	y/y/y	y/y/y	n/n/y	y/n/y
κ^c	0.21	-0.28	0.02	-0.31
σ^d (kHz)	6.0	6.6	5.4	6.8
N^e	81	49	15	42

	13	4	14
A (MHz)	868.61009(42)	915.21738(48)	942.67936(52)
B (MHz)	739.83405(53)	677.88681(41)	684.66240(45)
C (MHz)	463.7153(46)	444.28266(29)	454.18201(29)
Δ_J (kHz)	0.144(10)	-	-
Δ_{JK} (kHz)	0.275(30)	-	-
Δ_K (kHz)	-	-	-
δ_J (kHz)	-	-	-
δ_K (kHz)	-	-	-
$a/b/c$ (D)	n/n/y	n/n/y	n/n/y
κ	0.36	-0.01	-0.06
σ (kHz)	3.5	4.9	5.4
N	21	19	19

[a] A , B and C are the rotational constants. Δ_J , Δ_{JK} , Δ_K , δ_J and δ_K are the centrifugal distortion constants. [b] a , b and c are the type of transitions observed. [c] Ray's asymmetry parameter. [d] σ is the rms deviation of the fit. [e] N is the number of the fitted transitions. [f] Standard error in parentheses in units of the last digit.

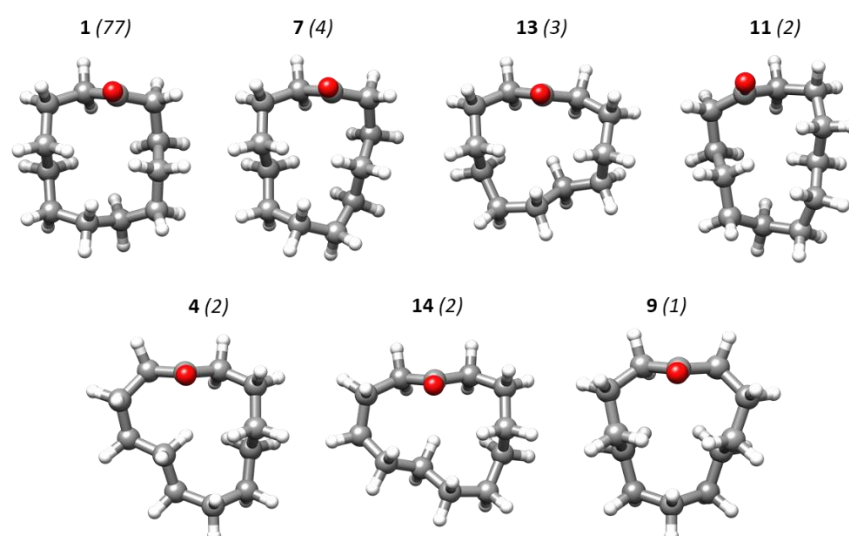


Figure 6.1. Relative conformational abundances (in parentheses) of the seven assigned conformers.

Table 6.3. Experimental spectroscopic parameters for all singly substituted ^{13}C isotopic species of conformer **1** of cyclododecanone.

Parameter	A^a (MHz)	B (MHz)	C (MHz)	σ^b (kHz)	N^c
$^{13}\text{C}_1$	864.87565(64) ^d	694.12690(55)	446.6421(49)	5.9	12
$^{13}\text{C}_2$	861.13713(76)	695.25470(67)	445.8176(57)	6.9	13
$^{13}\text{C}_3$	859.18804(63)	699.31518(53)	447.2121(49)	5.2	14
$^{13}\text{C}_4$	858.93690(56)	700.26334(50)	447.4247(51)	5.1	13
$^{13}\text{C}_5$	859.16111(84)	697.84248(66)	446.3483(71)	6.2	11
$^{13}\text{C}_6$	863.75146(64)	695.85305(52)	447.2802(45)	5.6	14
$^{13}\text{C}_7$	865.46173(57)	696.17589(47)	447.3416(44)	4.5	11
$^{13}\text{C}_8$	864.64181(61)	694.31584(51)	446.4740(44)	5.5	12
$^{13}\text{C}_9$	859.48586(73)	696.61114(75)	445.9533(66)	6.3	13
$^{13}\text{C}_{10}$	859.12065(92)	700.06064(63)	447.4062(64)	5.2	10
$^{13}\text{C}_{11}$	858.85598(61)	699.71291(54)	447.5046(52)	5.5	13
$^{13}\text{C}_{12}$	860.93999(63)	696.70630(54)	446.5240(49)	5.8	15

[a] A , B and C are the rotational constants. Δ_J , Δ_{JK} , Δ_K , δ_J and δ_K centrifugal distortion constants were fixed to parent species values. [b] σ is the rms deviation of the fit. [c] N is the number of the fitted transitions. [d] Standard error in parentheses in units of the last digit.

Table 6.4. Substitution coordinates of the heavy atoms of conformer **1** of cyclododecanone in Å.

	a	b	c
C_1	2.4947(14) ^a	-0.3931(91)	0.6193(57)
C_2	2.3021(17)	-1.7832(23)	-0.100(40)
C_3	0.9169(37)	-2.0230(17)	-0.5807(60)
C_4	-0.144(24)	-2.0919(17)	0.4476(81)
C_5	-1.6219(29)	-2.1208(23)	-0.105(46)
C_6	-2.0287(16)	-0.8018(41)	-0.8186(40)
C_7	-2.1138(15)	0.3760(87)	0.000(40) ^b
C_8	2.4986(13)	0.7512(44)	-0.3839(84)
C_9	1.9629(22)	2.0689(22)	0.198(23)
C_{10}	0.4537(93)	2.0585(21)	0.4678(94)
C_{11}	-0.4142(85)	2.0047(18)	-0.7860(47)
C_{12}	-1.9010(18)	1.7509(20)	-0.4690(75)

[a] The errors include Costain's error. [b] Imaginary coordinate set to zero.

The theoretical rotational constants predicted by B3LYP-D3BJ and MP2 agree well one with another, and are very close to the experimental values, with average deviations of 0.6% for B3LYP-D3BJ and 1.2% for MP2 (Table 6.5). Both methods predict conformer **1** as the global minimum, and an energy gap to the next conformer of approximately 450 cm^{-1} , which is consistent with experimental observations. The observed conformers are calculated to be those lower in energy by both theoretical methods, and although the energy ordering is not exactly the same, the differences in values are small.

Table 6.5. Benchmarking of the theoretical rotational constants against the experimental ($A_{calc} - A_{exp})/A_{exp} \times 100\%$.

		Exp.	B3LYP	% error	MP2	% error
1	A	865.6533	872.3	0.8%	888.5	2.6%
	B	700.4774	691.1	-1.3%	693.2	-1.0%
	C	449.1701	447.0	-0.5%	453.0	0.9%
7	A	966.1056	967.3	0.1%	979.6	1.4%
	B	638.5465	632.2	-1.0%	641.2	0.4%
	C	453.9216	450.4	-0.8%	459.4	1.2%
11	A	987.5630	988.5	0.1%	1002.0	1.5%
	B	634.2307	630.1	-0.7%	635.2	0.2%
	C	447.6706	445.6	-0.5%	451.7	0.9%
9	A	894.3034	896.1	0.2%	918.6	2.7%
	B	677.7762	693.2	2.3%	697.0	2.8%
	C	451.3106	450.7	-0.1%	459.1	1.7%
13	A	868.6112	858.0	-1.2%	880.8	1.4%
	B	739.8331	740.9	0.1%	741.3	0.2%
	C	463.7072	461.2	-0.5%	468.1	0.9%
4	A	915.2201	914.3	-0.1%	925.0	1.1%
	B	677.8858	673.7	-0.6%	680.3	0.4%
	C	444.2806	442.3	-0.4%	447.9	0.8%
14	A	942.6801	943.7	0.1%	951.8	1.0%
	B	684.6639	682.2	-0.4%	687.6	0.4%
	C	454.1837	453.3	-0.2%	458.3	0.9%

Experimental structure of conformer 1

The observation of the ^{13}C monosubstituted isotopic species has allowed the determination of the coordinates of the carbon atoms in the principal inertial axis system using Kraitchman's equations (Table 6.4), and the subsequent calculation of the substitution structure r_s ⁵⁰ of the carbon framework. The experimentally determined bond lengths (r), bond angles (\angle) and dihedral angles (τ) of cyclododecanone are shown in Table 6.6 and Figure 6.2.

There is quite a disparity in the values of the bond lengths determined by the r_s structure, which could be attributed to the small coordinates of some of the carbon atoms. The most obvious example is C_7 , whose c coordinate was fixed to zero as the Kraitchman calculation returns an imaginary value. The bond lengths involving C_7 are abnormally small considering that the average sp^3 C–C distance is 1.54 Å. The atoms C_2 , C_4 and C_5 also have small coordinates affected by large uncertainties, and this is reflected in the r_s values of the bond lengths in which they participate. The uncertainties in the coordinates also result in an unreasonably large value of 125.2(37)° for the bond angle $\angle\text{C}_{12}\text{C}_7\text{C}_6$. The other bond angles are mostly similar to those of the B3LYP-D3BJ equilibrium structure (Table 6.6). However, some of the dihedrals involving C_2 and C_7 display differences of up to 5° with r_e and r_0 values.

The r_0 structure was obtained from the fit of the 39 experimental moments of inertia to determine 11 bond lengths, 9 bond angles and 6 dihedral angles involving the carbon atoms. The structural parameters which were not floated were fixed to their B3LYP-D3BJ values. The r_0 bond lengths are close to the expected values for single C–C bonds, ranging between 1.54 - 1.52 Å. The bond angles roughly span 111°-115°, and they are similar to those determined for cyclooctanone.⁴³ The majority of the dihedral angles are close to those of 60°, 180° and -60°, reducing torsional strain. For comparison, cyclooctanone had two dihedral angles with values of 105.1(2)° and 139.7(4)°, indicative of higher torsional strain. There is a good agreement between the r_0 and the r_e structure.

The previously reported X-ray structural data on cyclododecanone shows atypical values for bond lengths and bond angles varying between 1.45-1.62 Å, and 108-119°,³⁷ respectively, which the authors attribute to problems with X-ray crystal structure refinement. Therefore, we are not comparing our data to their reported parameters. Cyclododecane has been shown by electron diffraction¹⁷ and X-ray crystallography¹⁸ to predominantly adopt a square conformation like that reported here for cyclododecanone. However, the above studies on cyclododecane only provide averaged structural parameters, which does not allow for a proper comparison with our data.

Table 6.6. Substitution and effective experimental bond lengths (Å), angles and dihedral angles (°) of conformer 1 of cyclododecanone, and B3LYP-D3BJ/6-311++G(d,p) equilibrium structural parameters of all observed conformers of cyclododecanone.

Conformer	1	1	1	7	13	11	4	14	9
Parameter	r_s^a	r_0^b	r_e	r_e	r_e	r_e	r_e	r_e	r_e
$r(C_2-C_1)$	1.577(20)	1.528(15)	1.537	1.541	1.538	1.541	1.542	1.532	1.540
$r(C_3-C_2)$	1.486(14)	1.524(9)	1.537	1.540	1.538	1.542	1.530	1.532	1.537
$r(C_4-C_3)$	1.479(19)	1.527(16)	1.533	1.533	1.537	1.539	1.527	1.539	1.532
$r(C_5-C_4)$	1.579(28)	1.541(14)	1.535	1.536	1.536	1.532	1.527	1.539	1.536
$r(C_6-C_5)$	1.554(22)	1.523(12)	1.533	1.535	1.535	1.543	1.540	1.534	1.534
$r(C_7-C_6)$	1.437(24)	1.526(10) ^c	1.525	1.525	1.525	1.520	1.529	1.526	1.524
$r(C_{12}-C_7)$	1.468(15)	1.526(10)	1.519	1.522	1.523	1.524	1.524	1.524	1.524
$r(C_{12}-C_{11})$	1.541(9)	1.537(13)	1.544	1.541	1.532	1.536	1.534	1.534	1.538
$r(C_{11}-C_{10})$	1.526(11)	1.533(14)	1.533	1.532	1.539	1.536	1.538	1.536	1.536
$r(C_{10}-C_9)$	1.533(10)	1.534(14)	1.537	1.531	1.541	1.532	1.534	1.538	1.531
$r(C_9-C_8)$	1.537(10)	1.527(10)	1.537	1.536	1.538	1.533	1.537	1.539	1.538
$r(C_8-C_1)$	1.522(10)	1.542(13)	1.541	1.540	1.533	1.535	1.542	1.540	1.540
$\angle(C_3-C_2-C_1)$	113.8(4)	114.3(2)	114.1	117.0	114.6	116.4	112.7	113.2	117.4
$\angle(C_4-C_3-C_2)$	116.8(17)	114.4(7)	113.9	114.3	113.9	117.1	116.3	114.7	114.0
$\angle(C_5-C_4-C_3)$	115.4(17)	114.5(8) ^c	114.5	114.6	114.8	114.1	112.7	116.5	114.6
$\angle(C_6-C_5-C_4)$	113.0(4)	113.5(2)	113.9	114.6	113.5	113.4	114.0	116.4	113.6
$\angle(C_7-C_6-C_5)$	116.7(20)	114.2(8) ^c	114.1	114.3	113.9	113.1	114.4	115.6	113.3
$\angle(C_{12}-C_7-C_6)$	125.2(27)	116.5(6) ^c	116.8	117.6	117.2	117.2	117.0	116.1	118.2
$\angle(C_{11}-C_{12}-C_7)$	111.1(2)	111.5(2)	111.6	112.7	114.3	114.5	115.4	115.4	112.7
$\angle(C_{12}-C_{11}-C_{10})$	112.7(5)	113.2(7)	113.5	113.0	116.2	114.1	114.7	114.2	114.1
$\angle(C_{11}-C_{10}-C_9)$	114.5(11)	113.8(10)	113.7	113.4	116.2	114.7	114.3	115.0	114.6
$\angle(C_{10}-C_9-C_8)$	113.8(3)	114.1(2)	114.1	114.0	115.9	113.1	115.1	114.1	114.2
$\angle(C_9-C_8-C_1)$	113.2(9)	114.1(8)	114.1	116.7	114.1	114.3	117.4	114.4	117.5
$\angle(C_8-C_1-C_2)$	111.2(14)	114.8(7)	113.9	116.5	114.2	116.6	116.1	114.6	116.7
$\tau(C_4C_3C_2C_1)$	-63.0(21)	-68.1(7) ^c	-68.1	-64.3	-61.7	84.0	177.1	172.8	-62.2
$\tau(C_5C_4C_3C_2)$	170.8(2)	171.4(3)	172.8	178.3	156.9	64.4	-176.4	-84.6	175.9
$\tau(C_6C_5C_4C_3)$	-66.0(23)	-68.6(10)	-66.1	-61.5	-64.4	-178.3	64.1	68.0	-64.4
$\tau(C_7C_6C_5C_4)$	-66.0(24)	-63.8(10) ^c	-65.1	-63.5	-59.3	60.4	-75.2	-87.2	-62.7
$\tau(C_{12}C_7C_6C_5)$	152.0(9)	153.8(3) ^c	151.8	150.6	152.5	70.2	134.3	162.4	146.2
$\tau(C_{11}C_{12}C_7C_6)$	-71.1(13)	-75.0(5) ^c	-75.2	-62.7	-159.8	-149.5	-159.6	-164.9	-138.1
$\tau(C_{10}C_{11}C_{12}C_7)$	-70.6(16)	-65.1(6) ^c	-65.1	-55.1	62.3	56.3	67.1	59.2	57.3
$\tau(C_{12}C_{11}C_{10}C_9)$	170.1(2)	170.1(2)	171.5	164.0	63.8	56.5	60.6	61.3	58.2
$\tau(C_{11}C_{10}C_9C_8)$	-68.1(13)	-69.1(4)	-68.3	-166.6	-86.5	-165.5	-173.8	-155.3	179.3
$\tau(C_{10}C_9C_8C_1)$	-70.3(14)	-68.8(8) ^c	-68.8	56.2	-68.9	164.6	62.3	55.1	62.9
$\tau(C_9C_8C_1C_2)$	150.2(4)	149.5(4)	148.0	59.5	173.2	-56.7	54.4	51.5	78.4
$\tau(C_8C_1C_2C_3)$	-74.0(21)	-68.2(3)	-69.0	-83.6	-59.6	-58.3	-85.9	-168.8	-72.4

[a] The substitution structure has been determined from the atomic coordinates including Costain's error, and with signs taken from the B3LYP-D3BJ calculated structure. [b] Effective structure; non fitted parameters were fixed to the B3LYP-D3BJ/6-311++G(d,p) values. [c] Derived from the determined r_0 structure, not fitted directly.

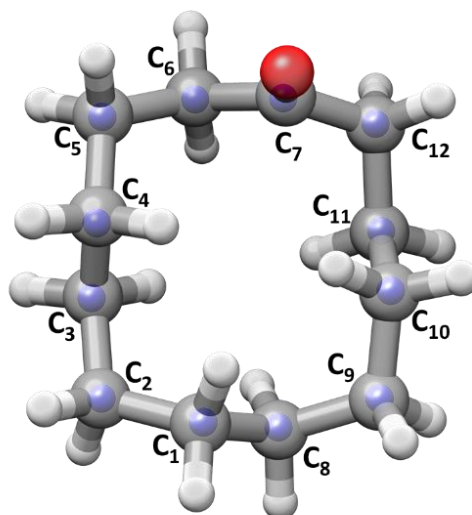


Figure 6.2. r_s structure (blue spheres indicating the position of the C atoms) overlapped with B3LYP-D3BJ/6-311++G(d,p) (grey framework), including atom labelling.

6.4. Discussion

The conformational landscape of cyclododecanone can be understood in terms of the various types of strain at play. Because cyclododecanone is a large ring, it is anticipated to have low torsional and angle strain. Normally angle strain does not contribute strongly to conformational energy differences.¹² Considering B3LYP-D3BJ cyclododecanone structures, which are expected to be very close to the experimental ones, \angle CCC bond angles are very similar among all the observed conformations, in the range 112-117°. Torsional strain is expected to introduce larger differences between conformations. However, CCCC angles are mostly close to the idealised angles of 60°, 180° and -60°. Marginally bigger differences from ideal angles are observed in the least abundant conformers, such as conformer **9** with torsional angles of -138.1° and 78.4°, and conformer **14** with angles of -155.3° and -168.8°.

Transannular interactions, or steric strain, occur in all conformations of cyclododecanone. These are due to the interactions of the H atoms directed to the interior of the ring. The majority of conformers have seven intra-annular H atoms, 3 on the same side of the ring as the carbonyl group and 4 on the other side. The exception is conformer **4**, with 6 intra-annular H atoms. These hydrogens are generally at distances shorter than the sum of the van der Waals radii of the hydrogen atoms (2.40 Å),^{51,52} giving rise to a varying number of transannular interactions (Figure 6.3). In addition, some of the conformers also show HCCH eclipsed configurations, at distances of 2.31-2.38 Å and dihedral angles of 32°- 49°. For comparison, eclipsed interactions occurred in all observed conformers of cyclooctanone at slightly shorter distances of 2.27-2.28 Å and

dihedral angles of 13° - 22° .⁴³ The effect of eclipsed configurations is therefore expected to be less relevant for cyclododecanone, but their combination with transannular interactions drives conformational stabilities. The strong preference for conformer **1** can be explained by its lack of eclipsed configurations and the fact that it shows 6 transannular interactions at distances ranging between 2.11 Å and 2.26 Å. Conformer **7**, the second in abundance, presents 7 transannular interactions with distances between 2.08 Å and 2.33 Å. All the other conformers present both transannular and eclipsed interactions (Figure 6.3). The least abundant conformer **9** shows the shortest transannular interaction by far (1.96 Å), out of 7 overall, and two eclipsed configurations.

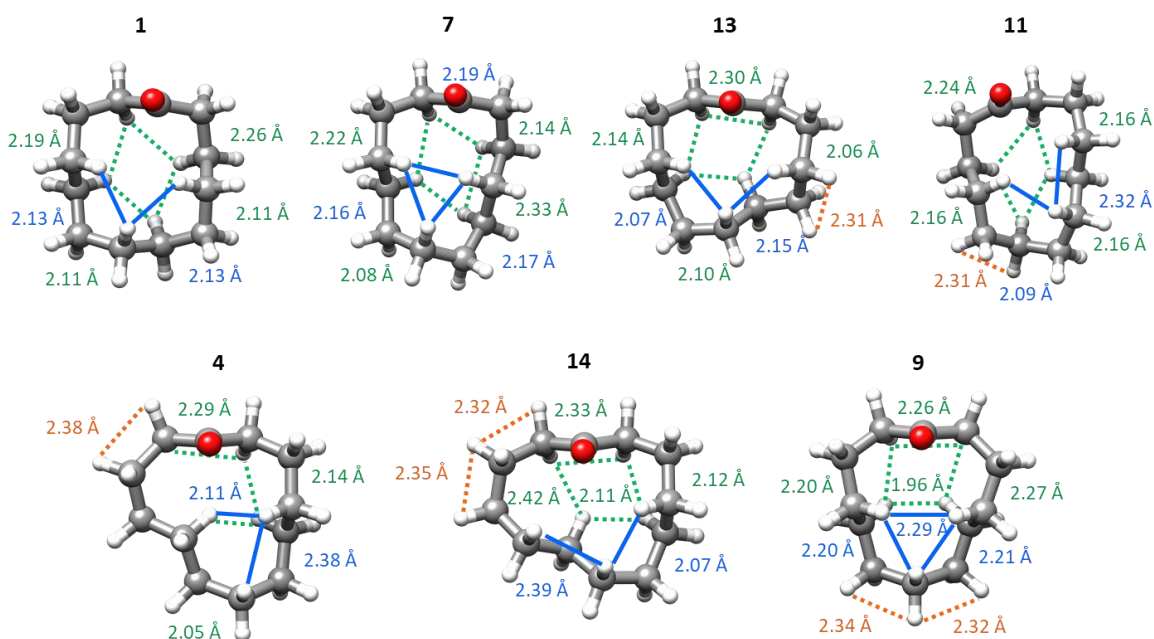


Figure 6.3. Intramolecular interactions in the observed conformers of cyclododecanone. All conformers show transannular interactions (blue on the side of the carbonyl group, green on the opposite side) and HCCH eclipsed interactions (in orange). In all the conformations the carbonyl bond is roughly perpendicular to the plane of the ring. This angle is reduced from that in cyclooctanone, where it was roughly around 120 degrees. This behaviour is consistent with expectations of angle changes in this angle in moving from smaller to larger rings. In small rings with 3-5 atoms the angle between the carbonyl group and the plane of the ring is around 180 degrees. As the size of the ring increases, the angle becomes more and more acute, until for very large rings the carbonyl bond could even point inside the ring, forming an angle of zero degrees. These different configurations respond to the smaller strain expected in large rings and the possibility of interactions of the carbonyl oxygen with the H atoms pointing towards the inside of the ring.

The conformational preferences in cyclododecanone are strongly biased to conformer **1**, that is 19 times more abundant than the second most abundant conformer. This strong preference for one conformation was also observed in cyclooctanone, but with a more marked predominance of the most abundant conformer, which was 44 times more abundant than the second one. In comparison with cyclooctanone, the number of lower-energy conformations is larger in cyclododecanone and the gap between the global minimum and the next conformer is smaller. Therefore, in cyclododecanone the population is spread over a larger number of structures decreasing the span of relative abundances. Further studies of even larger cycloketones will be able to ascertain whether there is a general trend where the dominance of one conformation decreases as the size of the ring increases.

Although there is less strain in cyclododecanone in comparison with cyclooctanone, the same intramolecular interactions control conformational preferences. Both cycloketones are even-membered cycles, which generally have received more attention than odd-membered ones, and have a higher number of theoretical and experimental investigations devoted to them. Odd-membered cycles are more difficult to synthesise and more reactive. Assessing their conformational behaviour in light of that of even-membered cycles will improve our understanding of their reactivity and physicochemical characteristics. In this respect, studies using rotational spectroscopy in the gas phase are invaluable to reveal the intrinsic forces mediating structural preferences.

6.5. Conclusions

Seven conformations of cyclododecanone have been unambiguously identified by broadband rotational spectroscopy. There is a strong preference for the macrocycle to adopt a conformation with a square configuration of the heavy atom framework featuring three C–C bonds per side. This conformer is 19 times more abundant than the second most abundant conformer and 77 times more abundant than the least abundant one. Minimisation of transannular interactions and, to a less extent, HCCH eclipsed configurations drives conformational preferences. Rotational spectroscopy is an ideal method to disclose the conformations of flexible molecules and get insight on the intramolecular forces at play.

6.6. Bibliography

1. Marsault, E. & Peterson, M. L. Macrocycles are great cycles: applications, opportunities, and challenges of synthetic macrocycles in drug discovery. *Journal of Medicinal Chemistry* **54**, 1961–2004 (2011).
2. Davis, F. & Higson, S. *Macrocycles: Construction, Chemistry and Nanotechnology Applications*. (John Wiley & Sons, 2011).
3. Skinner, H. A. Structure of Cyclopropane. *Nature* **160**, 902 (1947).
4. Harris, D. O., Harrington, H. W., Luntz, A. C. & Gwinn, W. D. Microwave spectrum, vibration-rotation interaction, and potential function for the ring-puckering vibration of Trimethylene Sulfide. *The Journal of Chemical Physics* **44**, 3467–3480 (1966).
5. Cotton, F. A. & Frenz, B. A. Conformations of Cyclobutane. *Tetrahedron* **30**, 1587–1594 (1974).
6. Harris, D. O. *et al.* Ring puckering in five-membered rings. I. General theory. *The Journal of Chemical Physics* **50**, 2438–2445 (1969).
7. Engerholm, G. G., Luntz, A. C., Gwinn, W. D. & Harris, D. O. Ring puckering in five-membered rings. II. The microwave spectrum, dipole moment, and barrier to pseudorotation in Tetrahydrofuran. *The Journal of Chemical Physics* **50**, 2446–2457 (1969).
8. Ogata, T. & Kozima, K. Microwave spectrum of Cyclohexene. *Bulletin of the Chemical Society of Japan* **42**, 1263–1265 (1969).
9. Lewis, J. S. *Encyclopedia of Physical Science and Technology (Third Edition)*. Academic Press (2003).
10. Rounds, T. C., Strauss, H. L., Bocian, D. F. & Pickett, H. M. Conformations of Cycloheptane. *Journal of the American Chemical Society* **97**, 687–695 (1975).
11. Bocian, D. F. & Strauss, H. L. Conformational structure and energy of Cycloheptane and some related oxepanes. *Journal of the American Chemical Society* **99**, 2876–2882 (1977).
12. Dragojlovic, V. Conformational analysis of cycloalkanes. *ChemTexts* **1**, 1–30 (2015).
13. Dorofeeva, O. v., Mastryukov, V. S., Allinger, N. L. & Almenningen, A. The molecular structure and conformation of cyclooctane as determined by electron diffraction and molecular mechanics calculations. *The Journal of Physical Chemistry* **89**, 252–257 (1985).
14. Anet, F. A. L. & Krane, J. The conformations of Cyclononane dynamic Nuclear Magnetic Resonance and force-field calculations. *Israel Journal of Chemistry* **20**, 72–83 (1980).
15. Pawar, D. M., Smith, S. v., Mark, H. L., Odom, R. M. & Noe, E. A. Conformational study of Cyclodecane and substituted cyclodecanes by dynamic NMR spectroscopy and computational methods. *Journal of the American Chemical Society* **120**, 10715–10720 (1998).
16. Pawar, D. M., Brown, J., Chen, K. H., Allinger, N. L. & Noe, E. A. Conformations of Cycloundecane. *Journal of Organic Chemistry* **71**, 6512–6515 (2006).
17. Atavin, E. G., Mastryukov, V. S., Allinger, N. L., Almenningen, A. & Seip, R. Molecular structure of Cyclododecane, C₁₂H₂₄, as determined by electron diffraction and molecular mechanics. *Journal of Molecular Structure* **212**, 87–95 (1989).
18. Dunitz, J. D. & Shearer, H. M. M. Die Strukturen der mittleren ringverbindungen III. Die struktur des cyclododecans. *Helvetica Chimica Acta* **43**, 18–35 (1960).

19. Anet, F. A. L. & Rawdah, T. N. Cyclododecane. Force-field calculations and NMR spectra of deuterated isotopomers. *Journal of the American Chemical Society* **100**, 7166–7171 (1978).
20. Groth, P., Nord, G., Woldbye, F., Watson, K. J. & Sandström, M. Crystal structure of Cyclotetradecane at -157 degrees C. *Acta Chemica Scandinavica* **30a**, 155–156 (1976).
21. Vajnštejn, B. K. Structure analysis by electron diffraction. *Il Nuovo Cimento Series 10* **3**, 773–797 (1956).
22. Thompson, A. L. & Watkin, D. J. X-ray crystallography and chirality: understanding the limitations. *Tetrahedron Asymmetry* **20**, 712–717 (2009).
23. Tormena, C. F. Conformational analysis of small molecules: NMR and quantum mechanics calculations. *Progress in Nuclear Magnetic Resonance Spectroscopy* **96**, 73–88 (2016).
24. Skibinski, M. *et al.* Alicyclic ring structure: conformational influence of the CF₂ group in cyclododecanes. *Angewandte Chemie* **123**, 10769–10772 (2011).
25. Groth, P. On the crystal conformations of cyclic oximes, (CH₂)_(n-1) CNOH with n = 10, ..., 14. *Acta Chemica Scandinavica* **33a**, 503–513 (1979).
26. Wang, M. A., Zhang, N., Lu, H. Z. & Wang, D. Q. Conformation of α,α,α' -trisubstituted Cyclododecanone. *Chinese Journal of Chemistry* **25**, 1196–1201 (2007).
27. Dehli, J. *et al.* Crystal structure of 2,12-dibromo-cyclododecanone. *Acta Chemica Scandinavica* **23**, 587–596 (1969).
28. Anet, F. A. L., Cheng, A. K. & Wagner, J. J. Determination of conformational energy barriers in medium- and large-ring cycloalkanes by ¹H and ¹³C Nuclear Magnetic Resonance. *Journal of the American Chemical Society* **94**, 9250–9252 (1972).
29. Rubin, B. H. *et al.* Conformation of a saturated 13-membered ring. *Journal of the American Chemical Society* **106**, 2088–2092 (1984).
30. Hayakawa, Y., Kawakami, K., Seto, H. & Furihata, K. Structure of a new antibiotic, Roseophilin. *Tetrahedron Letters* **33**, 2701–2704 (1992).
31. Boger, D. L. & Hong, J. Asymmetric total synthesis of ent-(-)-Roseophilin: assignment of absolute configuration. *Journal of the American Chemical Society* **123**, 8515–8519 (2001).
32. Zoorob, H. H., Elsherbini, M. S. & Hamama, W. S. Reactivity features of Cyclododecanone. *Arkivoc* **2011**, 429–495 (2011).
33. Bollbuck, B., Kraft, P. & Tochtermann, W. Nature-like odorants by stereoselective ring enlargement of Cyclohexanone and Cyclododecanone. *Tetrahedron* **52**, 4581–4592 (1996).
34. Scafato, P., Larocca, A. & Rosini, C. An alternative stereoselective synthesis of the macrocyclic fragrances (R)-12-Methyltridecanolide and (S)-Muscolide by means of an asymmetric catalytic conjugate addition/Baeyer-Villiger oxidation. *Tetrahedron Asymmetry* **17**, 2511–2515 (2006).
35. Nowicki, J. Claisen, Cope and related rearrangements in the synthesis of flavour and fragrance compounds. *Molecules* **5**, 1033–1050 (2000).
36. Dowd, P. & Choi, S. C. Homologation of large rings. *Tetrahedron* **48**, 4773–4792 (1992).
37. Groth, P. On the crystal structure of Cyclododecanone. *Acta Chemica Scandanavica* **33 A**, 203–205 (1979).

38. Obenchain, D. A. *et al.* Rotational spectrum of three conformers of 3,3-difluoropentane: construction of a 480 MHz bandwidth chirped-pulse Fourier-transform microwave spectrometer. *Journal of Molecular Spectroscopy* **261**, 35–40 (2010).
39. Powoski, R. A., Grubbs, G. S. & Cooke, S. A. A conformational study of Butyryl Chloride using chirped pulse Fourier transform microwave spectroscopy and quantum chemical calculations. *Journal of Molecular Structure* **963**, 106–110 (2010).
40. Peña, I., Sanz, M. E., Alonso, E. R. & Alonso, J. L. The multiple hydrogen-bonding networks of Polyol Ribitol. *Chemistry - A European Journal* **24**, 13408–13412 (2018).
41. Loru, D. *et al.* Conformational flexibility of Limonene Oxide studied by microwave spectroscopy. *ChemPhysChem* **18**, 274–280 (2017).
42. Shipman, S. T., Neill, J. L., Suenram, R. D., Muckle, M. T. & Pate, B. H. Structure determination of strawberry aldehyde by broadband microwave spectroscopy: Conformational stabilization by dispersive interactions. *Journal of Physical Chemistry Letters* **2**, 443–448 (2011).
43. Burevschi, E., Penã, I. & Sanz, M. E. Medium-sized rings: Conformational preferences in cyclooctanone driven by transannular repulsive interactions. *Physical Chemistry Chemical Physics* **21**, 4331–4338 (2019).
44. Froimowitz, M. HyperChem(TM): A software package for computational chemistry and molecular modeling. *BioTechniques* **14**, (1993).
45. Pracht, P., Bohle, F. & Grimme, S. Automated exploration of the low-energy chemical space with fast quantum chemical methods. *Physical Chemistry Chemical Physics* **22**, 7169–7192 (2020).
46. Loru, D., Bermúdez, M. A. & Sanz, M. E. Structure of fenchone by broadband rotational spectroscopy. *Journal of Chemical Physics* **145**, 07114311–8 (2016).
47. Watson, J. K. G. *Vibrational Spectra and Structure*. Elsevier Amsterdam **6**, 1–89 (1977).
48. Pickett, H. M. The fitting and prediction of vibration-rotation spectra with spin interactions. *Journal of Molecular Spectroscopy* **148**, 371–377 (1991).
49. Western, C. M. PGOPHER: A program for simulating rotational, vibrational and electronic spectra. *Journal of Quantitative Spectroscopy and Radiative Transfer* **186**, 221–242 (2017).
50. Kraitchman, J. Determination of Molecular Structure from Microwave Spectroscopic Data. *American Journal of Physics* **21**, 17–24 (1953).
51. Pauling, L. *The Nature of the Chemical Bond and the Structure of Molecules and Crystals: An Introduction to Modern Structural Chemistry*. (Cornell University Press, 1960).
52. Bondi, A. Van der Waals volumes and radii. *Journal of Physical Chemistry* **68**, 441–451 (1964).



THE RICH CONFORMATIONAL LANDSCAPE OF MUSCONE

Chapter 7



7. THE RICH CONFORMATIONAL LANDSCAPE OF MUSCONE

7.1. Introduction

Muscone is the one of the finest musks available. It was discovered in 1906 to be the active compound of the musk pod of the male musk deer.¹ Muscone, or 3-methyl-1-cyclopentadecanone ($C_{16}H_{30}O$), is a 15-membered ring ketone with a methyl substituent (Figure 7.1). It belongs to the macrocyclic class of musks and is chiral. The *R* enantiomer, which is muscone's natural form, has a stronger musk odour than the *S* enantiomer. Since (*R*)-muscone is the preferred one in perfume formulations, there have been numerous efforts to produce it synthetically over the years. The main challenges organic chemists had to overcome in muscone synthesis were building of the macrocycle and insertion of the stereoselective methyl group.²⁻⁵ Most of the routes known to date allow only low-scale synthesis, hence muscone remains expensive and is used only in exquisite perfume formulas.

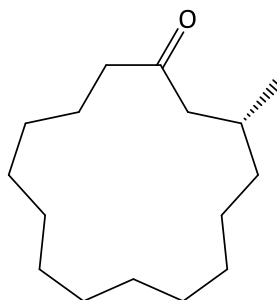


Figure 7.1. Molecular structure of (*R*)-muscone, 15-membered ring ketone.

Although muscone has been the subject of many synthetic studies^{3,4,6} as a key ingredient of perfumes, little is known about its structure. The large conformational flexibility of muscone and difficulties to crystallise it have prevented its structural determination. Attempts to gain some insight investigated muscone derivatives, to reduce the conformational flexibility of the ring and enable crystallisation. In 1982, Bernardinelli and Gerdil obtained the 2,4-dinitrophenyl hydrazine derivative of muscone (DNP-muscone) and analysed it by X-ray crystallography.⁷ They reported eight different ring conformations, which suggests a high degree of flexibility even in this more rigid derivative of muscone. Another structural study on muscone derivatives involved introducing one or two $-CF_2$ groups in various positions.⁸ The fluorinated carbon occupies a corner position and thus significantly reduces the flexibility of the macrocycle, making it possible to be analysed by X-ray crystallography. A total of nine fluorinated muscone derivatives were analysed, including three that included DNP as a substituent in addition to the $-CF_2$ groups.

The first structure-odour relationship study on muscone was conducted in 1975, where the effects of introducing a methylene bridge in the macrocycle, producing a bicyclic compound and introducing rigidity, were analysed.⁹ Most of the bicyclic derivatives of muscone have the musky smell altered by either reducing the muskiness or adding different notes. In the investigation of the structure-odour relationship of fluorinated muscone derivatives, only three structures preserved the musk scent.⁸ These studies only provided limited information on the olfactory properties of muscone. Further studies on the conformational preferences of unmodified muscone are essential to progress our understanding of the structure-odour relationship for this compound.

We present here the first conformational data on (*R*)-muscone using broadband rotational spectroscopy in combination with quantum mechanical calculations. In the case of muscone, rotational spectroscopy is superior to all the available structural techniques. Crystallization of muscone without structural modification has been unsuccessful due to its high degree of flexibility, while structural studies in the liquid phase would not resolve all the different possible conformations. We have identified 30 conformers of muscone, and their experimental abundances have been determined. The potential energy surface (PES) of muscone was mapped for the first time using various theoretical methods. The interplay between experiment and theory has been crucial to identify muscone conformations. An iterative process of prediction, experimental spectral assignment, and further predictions and spectral assignments has been followed. We have characterised the structural features of muscone conformers and their intramolecular interactions. The computational methods used to optimise the geometries of the predicted conformers have been benchmarked against experimental results.

7.2. Methods

Theoretical

Muscone (Figure 7.1) has many single bonds and therefore is expected to have a very rich conformational landscape. Exploring the full PES of macrocycles, such as muscone, is tremendously challenging. One of the concerns is the completeness of the search. Have we covered all the conformational space? Some of the initially predicted low-energy conformers of muscone could not be found in the spectrum, while some of the assigned species in the spectrum could not be matched with any of the theoretically predicted conformers. Therefore, we decided to use a multipronged approach, taking advantage of different packages and

computational methods, and applied them in an iterative manner, guided by our experimental results.

We ran 21 conformational searches in total, using different packages and computational methods. Initially, searches were carried out with HyperChem, using the molecular mechanics MM+ and semi-empirical Amber methods. Optimising the structures produced by these two conformational searches at B3LYP-D3BJ^{10,11}/6-311++G(d,p) level of theory, and further zero-point correcting their energies, 6 conformers within 520 cm⁻¹ were predicted. Further, we tested Maestro with three different force-fields: OPLS, OPLS3 and MMFFs, which predicted 11 more structures within the above energy range. Finally, CREST was used. The first conformational search with CREST returned thousands of conformers, of which the lowest 200 in energy were further optimised at B3LYP-D3BJ/6-311++G(d,p) level. The returned conformers matched our experimental results better, but we were not convinced the mapping was complete. Therefore, we conducted a second conformational search using a different starting structure, which predicted some new conformational minima different from the first search and a new global minimum. This was an indication that multiple conformational searches were necessary to appropriately map the PES of muscone. As a new global minimum was predicted, it was used in further conformational searches as a starting point. From each conformational search the lowest 100-200 configurations were optimised at B3LYP-D3BJ level of theory. Since CREST predicted more minima that could be identified experimentally, it was used further in the other conformational searches. A total of 16 conformational searches were run with CREST using different starting structures each time. With each conformational search fewer new minima were predicted, until the last search which did not return any new minima below 600 cm⁻¹. The 16 conformational searches performed with CREST also predicted all the low energy conformers generated by HyperChem and Maestro.

All conformational searches predicted a total of 88 distinct conformers within 500 cm⁻¹, optimised at B3LYP-D3BJ/6-311++G(d,p) level of theory. These structures were optimised further at the MP2¹²/6-311++G(d,p), wB97XD¹³/6-311++G(d,p) and B2PLYP-D3BJ¹⁴/def2TZVP levels of theory for benchmarking purposes. Their zero-point energies were calculated at the B3LYP-D3BJ and wB97XD levels with 6-311++G(d,p) basis set. The excessive computational cost prevented calculation of the zero-point energies at MP2 and B2PLYP levels. The results identified four conformers which were not real minima, but saddle points in the PES. The spectroscopic parameters, including the rotational constants and dipole moments, are presented in the *Spectral assignment* section below. The labelling for the conformers consists of a number and letter, the number indicates the order of that structure in the conformational search and the letter indicates each individual conformational search. The methyl rotation barrier of the methyl

group in position 2 from C=O group has been calculated for conformer **3f** at B3LYP-D3BJ/6-311++G(d,p) level, which is above 1000 cm^{-1} , indicating that no splitting of lines due to internal motion was expected to be observed in our spectrum.

Experimental

The rotational spectrum of muscone was measured in the 2-8 GHz frequency range using our CP-FTMW spectrometer at King's College London. The sample of muscone (99% purity, Firmenich) was used without any further purification. At room temperature muscone is an oily liquid with low vapour pressure (0.03 Pa at 20°C), hence heating was required in order to increase its concentration in gas phase. Muscone was placed in our bespoke heating nozzle and heated to a temperature of 437 K. Neon with a backing pressure of 5 bar was used to seed muscone into the vacuum chamber. Molecular pulses of $1000\ \mu\text{s}$ duration were followed by four microwave excitation pulses of $4\ \mu\text{s}$ length, spaced $30\ \mu\text{s}$. The chirped MW polarisation pulses were applied with a delay of $100\ \mu\text{s}$ with respect to the end of the molecular pulse. The subsequent free induction decays (FIDs) were recorded for $20\ \mu\text{s}$ using a digital oscilloscope, starting $2.5\ \mu\text{s}$ after the end of the excitation pulse. The FIDs were recorded in the time domain and then converted to the frequency domain through a Fast Fourier transform algorithm implemented in a python script. The final spectrum was obtained by averaging *ca.* 1M FIDs and is depicted in Figure 7.2.

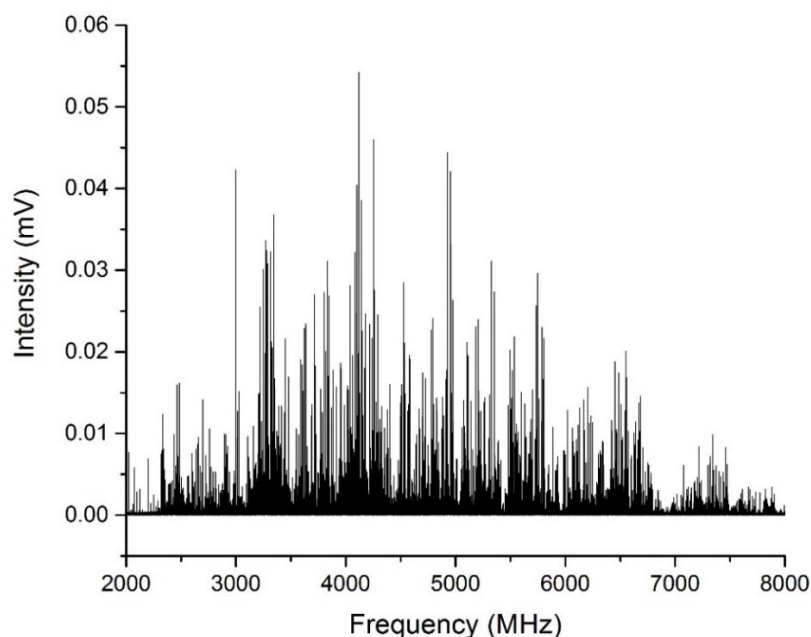


Figure 7.2. Broadband rotational spectrum of muscone collected in neon at 5 bar, temperature of 437 K, 1M FIDs.

7.3. Results

Spectral assignment

The huge conformational flexibility of muscone is apparent in its rotational spectrum, which is probably one of the densest ever recorded. Considering lines with a signal to noise ratio of 3:1, the average overall density of the rotational spectrum of muscone is 0.9 line/MHz. Almost one line per MHz in the frequency region of 2 to 8 GHz, that is, 6000 MHz.

The theoretical predictions (Tables 7.2-7.5, 7.7-7.10, 7.12-7.15, 7.17-7.20) yielded conformations with very similar rotational parameters, including rotational constants and dipole moments. Most of the low-energy conformers predominantly have a large *c*-type dipole moment and hence *c*-type spectra is expected to be dominant. Due to the density of the spectrum and the similarity between the predicted conformers, the assignment of the spectrum has been rather challenging.

Initially typical patterns of R-branch *c*-type transitions with sets of lines separated by approximately $A + B$ were searched for. Unfortunately, no species were assigned in this manner because, due to the high density of the spectrum, it was difficult to identify related transitions and very time consuming to check all the possibilities. Therefore, we decided to try automated assignment as implemented in the program PGOPHER.¹⁵ This is based on the AUTOFIT routine developed by Prof. Pate's group.¹⁶ After testing it in already assigned spectra, we run several searches considering the predicted rotational constants for the lower-energy conformers of muscone, and floating them by different amounts. Using this approach, we initially identified one rotamer in the spectrum. The lines belonging to this rotamer were cut from the spectrum to simplify it, but the density of lines at this point was making it still difficult to identify patterns. The next search in the spectrum, following the same procedure, resulted in the assignment of three rotamers with very similar sets of rotational constants, for which we only had one suitable structure predicted from calculations. This prompted us to perform further conformational searches. As new species were assigned in the spectrum, their lines were removed, and further spectral searches were carried out. After the success of CREST was established, we started an iterative procedure whereby we would identify new conformers in the rotational spectrum, and if they could not be matched to any of the theoretical structures, we would run more conformational searches using different low-energy structures as starting points. Mapping the PES starting from a different structure generally returned new lower-energy conformers, which in turn speeded up the spectral assignment by carrying out further guided searches in the rotational spectrum.

Following this procedure, a total of thirty species have been identified in the spectrum. Most of the assigned rotamers mainly have *c*-type spectra as expected from the theoretical predictions, although a few of them had predominantly *a*- and *b*-type spectra. Transitions up to $J = 10$ have been measured for conformers with *c*-type spectrum, and up to $J = 14$ for those with *a*- and *b*-type spectra. The assigned transitions for each conformer were fit to the Watson Hamiltonian in the A reduction and I^r (prolate tops) or III^l (oblate tops) representation¹⁷ using Pickett's SPFIT/SPCAT programs.^{18,19} The experimental rotational and centrifugal distortion constants are presented in Tables 7.1, 7.6, 7.11 and 7.16. The measured transitions of all rotamers are presented in Appendix IV.

The rotational constants of some of the assigned species are very much alike. In order to unambiguously assign the identified rotamers to predicted conformers, we decided to group all of them into smaller subgroups with similar characteristics.

Class I – oblate asymmetric tops (0.63 < κ < 0.83)

The first of these classes comprises rotamers with very close *A* and *B* rotational constants, with *A* – *B* differences between 20 and 40 MHz (Table 7.1). Their Ray's asymmetry parameter, $k = (2B - A - C)/(A - C)$, which is a measure of the degree of asymmetry of a molecule, have been calculated to be between 0.63-0.83. These rotamers are then oblate asymmetric tops near the oblate symmetric top limit. They could be assigned to conformers **3f**, **33I**, **37a** and **13f** in a relatively straightforward manner due to their distinctive sets of rotational constants, the values of the planar moment of inertia P_c (which provide a measure of the mass distribution along the *c* principal inertial axis, out of the *ab* inertial plane), and the type of observed transitions (which are related to the values of their dipole moment components along the *a*, *b* and *c* principal inertial axes). Considering the values of their rotational constants and Ray's parameters, they could be any of the 14 conformers of Table 7.2-5. Rotamers I and II only have *c*-type spectrum and a value of P_c of about 131 uÅ². Other conformers of Tables 7.2-7.5 are expected to present other types of spectrum since they have higher values of the predicted dipole moment components (such as **64a**, **13f** or **5e**), or have very different values of P_c . Final assignment of I and II to conformer **3f** and **33I**, respectively, was based on the relative differences of their rotational constants, with **33I** being consistently predicted by the three theoretical methods used to have higher values of *A* and *C* than **3f**. We can discriminate between III and IV from their P_c values. That of rotamer III is only compatible with those predicted for **13f**, **99g** and **5e**. **99g** was discarded as it is not expected to present *a* and *b* spectra, which was observed for rotamer III. The rotational constants and P_c value of rotamer III are better

agreement with those predicted for **13f** than **5e**. Moreover, **13f** is predicted to have lower relative energy. Therefore, predicted for **13f**, led us to assign this conformer as **13f**. Rotamer IV can only be matched with conformer **37a** considering its P_c value.

Conformer **3f** is closest to a symmetric top out of all the assigned species, with a κ value of 0.83. Hence it has clearly recognisable spectral patterns, associated with oblate tops close to the symmetry limit. Whilst these patterns were not obvious from the start due to the high density of the spectrum, once a few species were assigned and removed, they could be identified (Figure 7.3). Conformer **3f** has only c -type spectrum, and transitions with the same J values appear to be separated evenly from each other by approximately $A + B$, which for **3f** is *ca.* 820 MHz.

Table 7.1. Experimental spectroscopic parameters of the conformers of muscone belonging to class I.

Parameters	I – 3f	II – 33I	III – 13f	IV – 37a
A^a (MHz)	417.973081(21) ^g	442.41982(54)	429.06203(26)	422.99796(45)
B (MHz)	401.985035(21)	407.48400(56)	393.86122(27)	384.72199(47)
C (MHz)	229.2663(66)	238.3542(80)	228.01043(30)	217.49998(40)
Δ_J (kHz)	0.0194(27)	0.0167(25)	0.0056(17)	0.0177(18)
Δ_{JK} (kHz)	-0.045(11)	-	0.0359(36)	-
Δ_K (kHz)	0.0803(88)	0.0295(65)	-	0.0265(62)
δ_J (kHz)	0.01032(72)	-	0.01127(79)	0.0113(12)
δ_K (kHz)	-	0.0384(59)	-	-
κ^b	0.83	0.66	0.65	0.63
P_c^c (uÅ)	130.9976(635)	131.1317(712)	122.2680(031)	92.3973(047)
$a/b/c^d$ (D)	n/n/y	n/n/y	y/y/y	y/y/y
σ^e (kHz)	2.2	7.2	4.2	8.4
N^f	66	68	87	116

[a] A , B and C are the rotational constants. Δ_J , Δ_{JK} , Δ_K , δ_J and δ_K are the quartic centrifugal distortion constants [b] κ is Ray's asymmetry parameter [c] P_c planar moment [d] a , b and c are the type of transitions observed [e] σ is the rms deviation of the fit [f] N is the number of the fitted transitions [g] Standard error in parentheses in units of the last digit.

Table 7.2. B3LYP-D3BJ/6-311++G(d,p) theoretical spectroscopic parameters and relative energies of the conformers of muscone belonging to class I.

B3LYP-D3BJ	3f	64a	33l	13f	16t	99g	5e
A ^a (MHz)	415.5	458.5	443.2	428.6	431.8	420.9	411.9
B (MHz)	400.6	422.1	403.8	392.8	404.5	396.1	395.1
C (MHz)	227.6	249.1	237.1	228.1	229.4	225.1	224.8
P _c ^b (uÅ ²)	128.7	135.4	130.2	125.1	108.4	115.7	129.0
κ ^c	0.84	0.65	0.62	0.64	0.73	0.75	0.82
μ _a ^d (D)	-0.2	0.2	0.2	0.5	0.6	0.2	-0.6
μ _b (D)	-0.1	-1.7	-0.3	-0.6	0.4	0.0	-0.6
μ _c (D)	2.4	-1.8	2.3	2.3	2.2	-2.3	-2.3
ΔE ^e (cm ⁻¹)	0.0	29.3	63.6	225.5	137.3	265.2	310.3
ΔE ₀ ^f (cm ⁻¹)	0.0	141.3	169.0	186.8	267.1	271.7	346.6
ΔG ^{437K} _g (cm ⁻¹)	249.1	768.6	555.9	384.1	924.4	640.2	489.4
	135s	47h	37a	93s	40h	12c	88o
A (MHz)	431.2	421.0	424.4	423.3	428.5	427.1	421.3
B (MHz)	386.6	395.3	381.5	384.5	390.2	390.6	387.9
C (MHz)	222.3	224.4	216.9	221.6	232.2	231.8	220.9
P _c (uÅ ²)	102.9	113.4	92.8	113.8	149.1	148.4	107.3
κ	0.57	0.74	0.59	0.62	0.61	0.63	0.67
μ _a (D)	-0.3	0.3	-1.0	-2.4	-1.5	-0.5	2.0
μ _b (D)	-0.5	-2.6	1.3	-1.4	0.0	0.6	-0.8
μ _c (D)	2.3	-1.8	-2.0	-1.5	2.1	2.4	1.7
ΔE (cm ⁻¹)	386.1	325.9	371.4	330.4	377.5	469.7	484.0
ΔE ₀ (cm ⁻¹)	358.4	375.1	375.5	424.7	437.4	456.7	475.4
ΔG ^{437K} (cm ⁻¹)	549.3	283.1	481.5	578.3	724.0	489.4	591.3

[a] A, B, C are the rotational constants [b] P_c planar moment [c] κ is Ray's asymmetry parameter [d] μ_a, μ_b and μ_c are the electric dipole moment components [e] Relative electronic energies [f] Relative electronic energies including the zero-point correction [g] Gibbs energies calculated at 437 K.

Table 7.3. MP2/6-311++G(d,p) theoretical spectroscopic parameters and relative energies of the conformers of muscone belonging to class I.

MP2	3f	64a*	33l	13f	16t	99g	5e
A ^a (MHz)	432.5	463.8	446.6	434.0	438.3	422.9	418.9
B (MHz)	397.6	428.8	411.8	397.7	408.8	404.7	397.3
C (MHz)	233.6	253.4	241.3	231.7	232.8	228.8	227.0
P _c ^b (uÅ ²)	138.1	136.9	132.2	127.0	109.2	117.5	126.1
κ ^c	0.65	0.67	0.66	0.64	0.71	0.81	0.77
μ _a ^d (D)	-0.1	-0.2	0.1	-0.5	-0.5	-0.1	0.4
μ _b (D)	-0.1	-1.6	0.2	0.5	-0.4	-0.1	-0.7
μ _c (D)	-2.2	1.7	-2.1	2.1	-2.0	-2.1	-2.0
ΔE ^e (cm ⁻¹)	407.2	90.4	211.0	496.5	314.6	548.9	654.2
	135s	47h	37a	93s	40h	12c	88o
A (MHz)	439.6	429.3	420.6	432.0	430.3	435.0	428.0
B (MHz)	388.6	398.8	392.4	387.6	398.3	394.2	391.1
C (MHz)	225.3	227.5	219.4	225.2	236.0	235.5	223.9
P _c (uÅ ²)	103.5	111.5	93.0	114.8	150.9	148.9	107.9
κ	0.52	0.70	0.72	0.57	0.67	0.59	0.64
μ _a (D)	0.2	-0.3	-1.2	2.3	-1.4	-0.5	1.8
μ _b (D)	-0.5	2.4	0.9	-1.0	0.0	0.7	-0.8
μ _c (D)	2.1	-1.7	1.9	1.2	-2.0	-2.1	-1.6
ΔE (cm ⁻¹)	637.4	502.5	715.4	395.3	684.3	709.0	759.9

[a] A, B, C are the rotational constants [b] P_c planar moment [c] κ is Ray's asymmetry parameter [d] μ_a, μ_b and μ_c are the electric dipole moment components [e] Relative electronic energies.

Table 7.4. *wB97XD/6-311++G(d,p) theoretical spectroscopic parameters and relative energies of the conformers of muscone belonging to class I.*

wB97XD	3f	64a	33l	13f	16t	99g	5e
A^a (MHz)	423.0	460.6	445.8	428.1	435.0	424.8	419.5
B (MHz)	400.0	426.2	406.4	398.4	406.4	397.7	392.7
C (MHz)	230.6	251.5	238.6	230.2	230.8	226.6	226.1
P_c^b ($\text{u}\text{\AA}^2$)	133.3	136.8	129.5	126.8	107.8	115.1	128.2
κ^c	0.76	0.67	0.62	0.70	0.72	0.73	0.72
μ_a^d (D)	-0.2	0.2	-0.2	0.7	-0.6	0.2	-0.5
μ_b (D)	0.0	-1.7	-0.4	0.6	-0.4	0.0	-0.6
μ_c (D)	2.4	-1.8	-2.4	-2.3	2.2	-2.3	-2.3
ΔE^e (cm^{-1})	346.6	32.2	193.8	349.3	199.9	533.6	646.0
ΔE_0^f (cm^{-1})	169.0	158.2	22.8	207.4	261.4	334.3	604.4
ΔG^{437Kg} (cm^{-1})	222.5	762.5	0.0	364.8	859.9	548.7	603.1
	135s	47h	37a	93s	40h	12c	88o
A (MHz)	436.0	431.2	424.7	428.4	428.9	431.7	426.6
B (MHz)	386.3	394.1	384.9	386.9	394.2	391.5	388.8
C (MHz)	223.3	226.8	217.7	223.9	233.9	234.0	222.6
P_c ($\text{u}\text{\AA}^2$)	102.1	113.0	90.8	114.4	149.8	150.9	107.1
κ	0.53	0.64	0.62	0.59	0.64	0.59	0.63
μ_a (D)	-0.3	0.1	-1.2	-2.6	-1.5	-0.5	2.0
μ_b (D)	-0.6	-2.6	-1.2	-1.1	0.1	0.6	-0.9
μ_c (D)	2.3	-1.8	-2.0	1.3	2.2	2.4	1.6
ΔE (cm^{-1})	660.0	461.0	526.8	360.8	631.1	616.0	653.0
ΔE_0 (cm^{-1})	572.0	393.3	491.6	505.7	673.6	598.1	615.4
ΔG^{437K} (cm^{-1})	810.1	358.6	648.1	983.9	987.9	830.9	843.0

[a] A , B , C are the rotational constants [b] P_c planar moment [c] κ is Ray's asymmetry parameter [d] μ_a , μ_b and μ_c are the electric dipole moment components [e] Relative electronic energies [f] Relative electronic energies including the zero-point correction [g] Gibbs energies calculated at 431 K.

Table 7.5. *B2PLYP-D3BJ/def2TZVP theoretical spectroscopic parameters and relative energies of the conformers of muscone belonging to class I.*

B2PLYP-D3BJ	3f	64a	33l	13f	16t	99g	5e
A^a (MHz)	421.9	462.6	449.0	432.4	436.8	424.3	416.6
B (MHz)	403.3	427.0	408.1	397.1	408.1	401.3	398.7
C (MHz)	230.7	252.0	240.3	230.5	231.9	227.6	226.8
P_c^b ($\text{u}\text{\AA}^2$)	129.9	135.3	130.5	124.3	107.8	115.2	126.2
κ^c	0.81	0.66	0.61	0.65	0.72	0.77	0.81
μ_a^d (D)	0.1	-0.2	0.1	-0.5	0.5	-0.2	0.4
μ_b (D)	-0.1	-1.6	0.2	0.5	-0.4	0.0	0.8
μ_c (D)	-2.3	1.7	-2.2	2.2	-2.1	-2.2	-2.1
ΔE^e (cm^{-1})	101.5	37.6	127.2	308.2	185.9	311.9	386.2
	135s	47h	37a	93s	40h	12c	88o
A (MHz)	439.5	427.4	426.8	428.0	432.1	432.6	426.8
B (MHz)	387.1	398.2	386.4	388.6	394.8	394.3	390.7
C (MHz)	224.7	226.8	219.0	224.2	234.7	234.6	223.2
P_c ($\text{u}\text{\AA}^2$)	103.3	111.6	91.9	113.3	148.2	147.8	106.8
κ	0.51	0.71	0.61	0.61	0.62	0.61	0.65
μ_a (D)	0.2	-0.1	-0.9	-2.0	1.4	-0.5	1.7
μ_b (D)	0.5	2.4	1.2	-1.7	-0.2	-0.7	1.0
μ_c (D)	2.2	-1.7	1.9	-1.4	-2.0	-2.2	-1.6
ΔE (cm^{-1})	424.5	403.9	470.2	365.1	461.1	534.6	568.2

[a] A , B , C are the rotational constants [b] P_c planar moment [c] κ is Ray's asymmetry parameter [d] μ_a , μ_b and μ_c are the electric dipole moment components [e] Relative electronic energies.

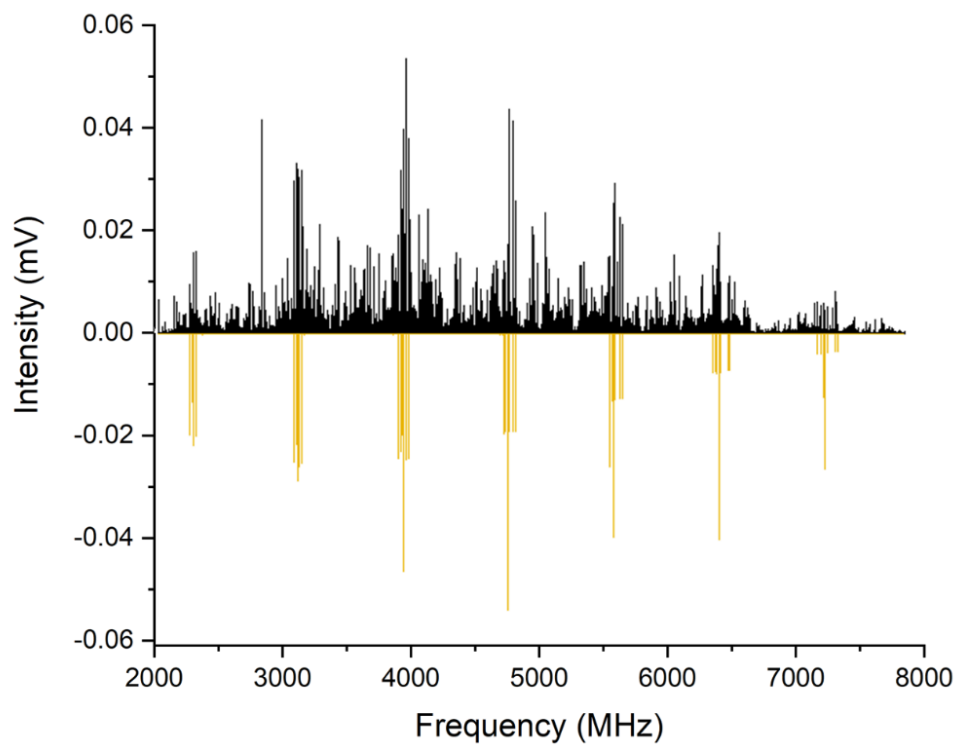


Figure 7.3. Overlay of experimental spectrum (upper trace) and predicted spectrum of **3f** conformer using the experimental parameters (lower trace).

Class II – prolate asymmetric tops ($-0.39 < \kappa < -0.26$)

A few of the assigned rotamers are prolate and more asymmetric, with κ values between -0.39 and -0.26 . This second class of rotamers all have their A constant above 500 MHz, and considerably lower B and C constants (Table 7.6). The firstly observed, rotamer IV, was assigned to conformer **8g** (Tables 7.7-10). This is the only conformer whose theoretical parameters are consistent with the experimental values of the rotational constants, P_c and the predominant b -type spectrum, which indicates that $\mu_b > \mu_c$. The other rotamers in this group have only c -type spectrum. They are assigned as **2f** and **31d**, which were consistently the best matches at the three levels of theory used considering their predicted rotational constants, dipole moments and values of P_c . They are also the candidates with lower relative energy. Other plausible matches were expected to show a - and b -type spectrum, such as **14l**, **28m**, and **9h**, or they lie at higher relative energies and they show a worse agreement with the experimental parameters, like **33j** and **34h**.

Table 7.6. Experimental spectroscopic parameters of the conformers of muscone belonging to class II.

Parameters	IV – 8g	V – 2f	VI – 31d
A^a (MHz)	534.96143(24) ^g	527.06881(61)	504.88046(30)
B (MHz)	340.49248(10)	311.25084(49)	323.10850(32)
C (MHz)	226.00002(16)	216.5939(11)	215.25731(77)
Δ_J (kHz)	0.0089(11)	0.0108(19)	0.0184(23)
Δ_{JK} (kHz)	-	-	-
Δ_K (kHz)	0.0466(47)	0.057(11)	-
δ_J (kHz)	0.00386(52)	-	0.00721(21)
δ_K (kHz)	0.0262(58)	0.0284(89)	-
κ^b	-0.26	-0.39	-0.26
P_c^c (uÅ)	96.3853(017)	124.6247(122)	108.6564(086)
$a/b/c^d$ (D)	n/y/y	n/n/y	n/n/y
σ^e (kHz)	5.9	7.6	6.5
N^f	106	67	58

[a] A , B and C are the rotational constants. Δ_J , Δ_{JK} , Δ_K , δ_J and δ_K are the quartic centrifugal distortion constants [b] κ is Ray's asymmetry parameter [c] P_c planar moment [d] a , b and c are the type of transitions observed [e] σ is the rms deviation of the fit [f] N is the number of the fitted transitions [g] Standard error in parentheses in units of the last digit.

Table 7.7. B3LYP-D3BJ/6-311++G(d,p) theoretical spectroscopic parameters and relative energies of the conformers of muscone belonging to class II.

B3LYP-D3BJ	2f	5h	8g	14l	57g	28m	9h	31d	21h
A ^a (MHz)	523.8	531.2	535.5	549.1	546.5	544.9	550.9	505.0	513.9
B (MHz)	310.6	358.1	338.3	348.3	345.6	313.5	301.2	320.2	341.4
C (MHz)	215.8	255.7	225.6	237.7	244.2	217.9	217.1	213.9	233.6
P _c ^b (uÅ ²)	125.0	193.1	98.7	122.6	158.8	110.1	133.7	108.2	150.1
κ ^c	-0.38	-0.26	-0.27	-0.29	-0.33	-0.42	-0.50	-0.27	-0.23
μ _a ^d (D)	0.3	-1.7	1.1	-1.1	0.9	0.5	0.5	0.1	-2.5
μ _b (D)	0.1	-1.3	2.1	1.2	0.6	0.6	0.7	0.0	-0.2
μ _c (D)	-2.4	1.5	-0.9	1.7	-2.1	-2.2	-2.3	2.3	-1.7
ΔE ^e (cm ⁻¹)	172.6	31.0	298.2	108.6	245.5	343.7	417.8	454.0	326.6
ΔE ₀ ^f (cm ⁻¹)	135.9	156.7	263.4	284.9	367.4	368.9	372.2	377.9	387.4
ΔG ^{437K} _g (cm ⁻¹)	246.9	708.7	448.6	958.4	857.5	799.3	276.8	543.6	655.4
	19o	33j	34h	94h	12e	9b	36g	23t	
A (MHz)	523.7	530.3	550.5	565.7	498.2	506.3	509.1	501.6	
B (MHz)	321.1	322.1	307.6	337.3	331.8	320.3	328.8	328.8	
C (MHz)	225.8	218.5	213.9	241.0	223.6	214.8	220.3	216.6	
P _c (uÅ ²)	150.4	104.5	99.2	147.3	138.7	111.6	117.8	105.7	
κ	-0.36	-0.34	-0.44	-0.41	-0.21	-0.28	-0.25	-0.21	
μ _a (D)	0.0	0.2	-0.3	1.2	-0.4	-0.7	0.1	0.3	
μ _b (D)	0.6	0.4	0.3	1.5	-1.1	-0.3	0.3	-0.9	
μ _c (D)	2.6	-2.4	-2.2	-1.5	-2.2	2.3	2.4	2.4	
ΔE (cm ⁻¹)	374.6	447.8	429.2	433.3	489.1	479.8	392.0	418.9	
ΔE ₀ (cm ⁻¹)	391.1	414.8	419.6	464.8	467.5	469.7	476.3	480.4	
ΔG ^{437K} (cm ⁻¹)	647.5	518.4	824.3	764.6	619.4	561.6	807.2	839.9	

[a] A, B, C are the rotational constants [b] P_c planar moment [c] κ is Ray's asymmetry parameter [d] μ_a, μ_b and μ_c are the electric dipole moment components [e] Relative electronic energies [f] Relative electronic energies including the zero-point correction [g] Gibbs energies calculated at 437 K.

Table 7.8. MP2/6-311++G(d,p) theoretical spectroscopic parameters and relative energies of the conformers of muscone belonging to class II.

MP2	2f	5h	8g	14l	57g	28m	9h	31d	21h
A ^a (MHz)	539.0	536.5	540.6	555.0	556.6	552.4	558.3	515.1	512.4
B (MHz)	310.6	363.9	342.4	352.9	348.7	316.5	303.3	321.8	346.9
C (MHz)	219.2	260.0	228.3	241.0	247.5	221.0	219.9	216.9	236.6
P _c ^b (uÅ ²)	129.6	193.5	98.6	122.8	157.7	112.4	136.6	110.8	153.6
κ ^c	-0.43	-0.25	-0.27	-0.29	-0.35	-0.42	-0.51	-0.30	-0.20
μ _a ^d (D)	0.2	-1.6	1.1	1.0	0.8	-0.4	0.5	0.1	-2.2
μ _b (D)	0.0	-1.2	-2.4	-1.1	0.6	0.5	-0.7	0.0	0.3
μ _c (D)	-2.2	-1.4	0.8	1.6	-1.9	-2.1	-2.1	-2.1	-1.6
ΔE ^e (cm ⁻¹)	615.6	0.0	498.4	195.0	267.4	576.6	865.5	815.8	568.3
	19o	33j	34h	94h	12e	9b	36g	23t	
A (MHz)	526.3	536.6	558.5	574.7	505.8	509.2	516.5	507.0	
B (MHz)	327.4	328.8	309.9	339.8	335.2	325.0	332.9	332.3	
C (MHz)	229.4	223.1	216.3	244.0	227.4	217.9	223.4	219.5	
P _c (uÅ ²)	150.4	106.8	99.6	147.7	142.2	114.1	117.2	107.6	
κ	-0.34	-0.33	-0.45	-0.42	-0.23	-0.26	-0.25	-0.22	
μ _a (D)	0.2	0.0	0.4	1.1	-0.4	0.8	0.0	-0.3	
μ _b (D)	-0.6	-0.5	0.2	-1.4	1.1	-0.2	-0.3	0.8	
μ _c (D)	2.4	-2.2	-2.1	1.4	-1.9	-2.1	-2.2	-2.2	
ΔE (cm ⁻¹)	655.7	770.1	784.6	511.6	701.9	841.2	760.7	779.3	

[a] A, B, C are the rotational constants [b] P_c planar moment [c] κ is Ray's asymmetry parameter [d] μ_a, μ_b and μ_c are the electric dipole moment components [e] Relative electronic energies.

Table 7.9. *wB97XD/6-311++G(d,p) theoretical spectroscopic parameters and relative energies of the conformers of muscone belonging to class II.*

wB97XD	2f	5h	8g	14l	57g	28m	9h	31d	21h
A ^a (MHz)	535.8	543.3	539.9	552.2	551.3	546.5	561.2	508.6	518.1
B (MHz)	309.8	360.6	339.5	351.2	346.2	316.4	300.4	322.0	344.1
C (MHz)	218.3	258.4	226.7	239.8	245.3	219.4	218.5	215.4	235.7
P _c ^b (uÅ ²)	129.7	187.9	97.7	123.4	158.1	109.3	135.0	108.5	150.0
κ ^c	-0.42	-0.28	-0.28	-0.29	-0.34	-0.41	-0.52	-0.27	-0.23
μ _a ^d (D)	0.3	-1.6	1.2	-1.1	0.8	0.5	0.6	0.1	-2.4
μ _b (D)	0.1	-1.3	2.1	1.2	0.5	0.6	0.8	-0.1	-0.2
μ _c (D)	-2.4	1.5	-0.9	1.8	-2.1	-2.3	-2.3	2.3	-1.7
ΔE ^e (cm ⁻¹)	470.6	0.0	641.2	141.5	135.9	397.5	633.8	699.7	432.0
ΔE ₀ ^f (cm ⁻¹)	271.3	142.9	442.7	217.7	173.8	307.0	519.3	595.7	459.6
ΔG ^{437K} _g (cm ⁻¹)	226.5	749.9	579.9	816.0	654.7	672.3	609.0	829.2	554.0
	19o	33j	34h	94h	12e	9b	36g	23t	
A (MHz)	533.0	535.8	554.6	571.0	505.0	517.5	515.0	510.8	
B (MHz)	321.2	326.6	308.7	338.5	331.6	317.3	330.1	327.8	
C (MHz)	227.8	222.8	214.9	243.9	225.8	215.5	221.9	217.8	
P _c (uÅ ²)	151.5	111.2	98.3	153.0	143.3	112.1	117.4	105.4	
κ	-0.39	-0.34	-0.45	-0.42	-0.24	-0.33	-0.26	-0.25	
μ _a (D)	0.1	0.0	-0.3	1.2	-0.3	-0.6	0.0	0.4	
μ _b (D)	0.6	0.4	0.3	1.5	-1.1	-0.6	0.3	0.9	
μ _c (D)	2.7	-2.4	-2.3	-1.6	-2.2	2.3	2.4	-2.4	
ΔE (cm ⁻¹)	370.3	665.0	552.3	562.3	732.2	775.9	564.7	539.3	
ΔE ₀ (cm ⁻¹)	415.7	498.2	456.7	475.4	605.1	564.0	558.5	425.6	
ΔG ^{437K} (cm ⁻¹)	877.2	604.0	807.0	684.5	706.7	399.7	869.8	631.4	

[a] A, B, C are the rotational constants [b] P_c planar moment [c] κ is Ray's asymmetry parameter [d] μ_a, μ_b and μ_c are the electric dipole moment components [e] Relative electronic energies [f] Relative electronic energies including the zero-point correction [g] Gibbs energies calculated at 437 K.

Table 7.10. *B2PLYP-D3BJ/def2TZVP theoretical spectroscopic parameters and relative energies of the conformers of muscone belonging to class II.*

B2PLYP-D3BJ	2f	5h	8g	14l	57g	28m	9h	31d	21h
A ^a (MHz)	533.1	536.8	541.1	553.5	553.5	550.5	558.4	511.4	516.6
B (MHz)	312.3	362.0	341.9	352.0	348.6	316.7	303.0	322.9	345.8
C (MHz)	218.5	258.4	227.7	240.0	246.7	220.4	219.1	216.3	236.3
P _c ^b (uÅ ²)	126.4	191.0	96.5	121.6	157.3	110.2	133.1	108.4	150.7
κ ^c	-0.40	-0.26	-0.27	-0.29	-0.34	-0.42	-0.51	-0.28	-0.22
μ _a ^d (D)	0.2	1.6	1.1	1.0	0.9	0.4	0.5	-0.1	-2.2
μ _b (D)	0.0	-1.3	-2.1	-1.2	0.7	0.5	0.7	-0.0	-0.2
μ _c (D)	-2.3	-1.4	0.8	1.7	-1.9	-2.1	-2.2	-2.2	-1.7
ΔE ^e (cm ⁻¹)	290.9	0.0	251.2	144.7	224.5	400.9	546.3	536.5	382.7
	19o	33j	34h	94h	12e	9b	36g	23t	
A (MHz)	527.5	535.7	556.4	570.8	503.8	511.2	514.5	506.1	
B (MHz)	325.7	327.1	310.2	340.6	335.0	323.7	332.3	332.4	
C (MHz)	228.5	222.0	215.9	243.4	226.3	217.1	222.6	219.1	
P _c (uÅ ²)	149.3	105.9	98.5	146.4	139.2	111.1	116.5	106.1	
κ	-0.35	-0.33	-0.45	-0.41	-0.22	-0.28	-0.25	-0.21	
μ _a (D)	0.1	-0.1	0.3	1.1	-0.4	0.7	0.0	-0.2	
μ _b (D)	-0.6	-0.5	-0.2	-1.5	-1.1	-0.2	0.3	-0.8	
μ _c (D)	-2.5	-2.3	-2.1	1.4	-2.0	-2.1	-2.2	-2.3	
ΔE (cm ⁻¹)	437.1	534.0	508.4	454.8	543.6	528.6	505.7	502.2	

[a] A, B, C are the rotational constants [b] P_c planar moment [c] κ is Ray's asymmetry parameter [d] μ_a, μ_b and μ_c are the electric dipole moment components [e] Relative electronic energies.

Class III – highly asymmetric tops ($-0.01 < \kappa < -0.16$)

The next class of rotamers is formed by those which are highly asymmetric, with κ values between -0.01 and -0.16 (Table 7.11). Rotamers VIII-X have values of the planar moment of inertia P_c ranging between $175.542(11)$ and $166.3064(29)$ $\text{u}\text{\AA}^2$, that are only consistent with the predicted conformers **1h**, **6j**, **19c** and **17f** (Tables 7.12-15). Rotamer IX displays *a*-, *b*- and *c*-type spectrum, and therefore it was identified as conformer **1h**, which is the only one of the possible conformers predicted to have sizable μ_a , μ_b and μ_c . The other two rotamers have very similar rotational constants. Rotamer X has a more intense *c*-type spectrum and lower value of P_c , and also displays *a*-type spectrum. Considering this, and the predictions by the different theoretical methods where **6j** is consistently predicted to have a lower P_c and a higher value of the *A* rotational constant, we have assigned rotamer X to **6j**, and rotamer VIII to **19c**. **19c** would be expected to also show *a*-type spectrum, but the slightly lower value of its predicted μ_a together with its lower spectral intensity explains its non-observation. **19c** has rotational constants closer to the experimental ones and it is predicted at lower energy than **17f**.

Rotamers XI-XIII have very similar experimental rotational constants but different values of P_c and types of observed spectrum. **2l** is the only predicted conformer with a suitable value of P_c and was identified as rotamer XI. Although it has a relatively low predicted value of μ_b , *b*-type transitions were observed due to its high intensity in the spectrum. Rotamer XII and XIV were assigned to **1f** and **4h**, respectively, considering their P_c values and the agreement with the predicted rotational constants at all levels of theory. There was a large difference in intensity in their spectra, with **1f** being quite intense and **4h** being one of the least intense conformers observed, and we believe that this is the reason for the observation of *a*- and *b*-type spectra for conformer **1f** but no *b*-type spectrum for conformer **4h**. The other possible conformers that could match experimental observations, **7g** and **53h**, are higher in energy and their theoretical constants deviate more from the experimental ones. Similar criteria were applied to assigned rotamer XIII to conformer **9i**. Its observed spectrum (*a*- and *c*-type) is consistent with this assignment. Rotamers XV and XVI have very similar constants and P_c values, and only showed *c*-type spectrum. Based on the relative values of their rotational constants we have identified them as **15k** and **13h**, respectively.

Table 7.11. Experimental spectroscopic parameters of the conformers of muscone belonging to class III.

Parameters	VIII – 19c	IX – 1h	X – 6j	XI – 2l	XII – 1f
A^a (MHz)	482.27103(20) ^f	499.47838(31)	489.39790(38)	471.14318(19)	474.77636(21)
B (MHz)	345.35633(25)	371.02959(25)	344.23166(28)	347.60450(20)	345.73768(24)
C (MHz)	233.9515(12)	248.26582(17)	233.08924(27)	227.37027(27)	224.85209(26)
Δ_J (kHz)	0.0207(18)	0.01257(95)	0.0254(22)	0.0220(11)	0.0162(13)
Δ_{JK} (kHz)	-	-	-0.0377(89)	-	-
Δ_K (kHz)	-	0.0534(63)	0.0510(78)	-	-
δ_J (kHz)	-	0.00445(54)	-	-	-
δ_K (kHz)	0.063(17)	0.0193(48)	0.0192(52)	0.0487(42)	0.0313(56)
κ^b	-0.10	-0.02	-0.13	-0.01	-0.03
P_c^c ($\mu\text{Å}$)	175.5417(111)	169.1379(018)	166.3064(029)	151.9213(028)	139.2959(028)
$a/b/c^d$ (D)	n/n/y	y/y/y	y/n/y	y/y/y	y/y/y
σ^e (kHz)	4.8	6.2	6.6	6.3	7.9
N^f	43	114	87	77	90
	XIII – 9i	XIV – 4h	XV – 15k	XVI – 13h	
A (MHz)	476.33288(33)	494.10670(41)	496.02393(34)	489.93126(38)	
B (MHz)	347.88807(13)	340.84062(40)	335.12693(34)	342.23400(32)	
C (MHz)	222.07612(15)	226.8686(14)	218.44425(97)	219.8352(11)	
Δ_J (kHz)	0.00517(75)	0.0268(25)	0.0180(31)	0.0165(31)	
Δ_{JK} (kHz)	0.0510(56)	-	-0.057(12)	-0.067(13)	
Δ_K (kHz)	-0.0269(80)	0.0659(65)	0.100(11)	0.117(12)	
δ_J (kHz)	-	0.0118(23)	-	0.0067(12)	
δ_K (kHz)	0.0234(36)	-0.108(14)	-	-	
κ	-0.01	-0.15	-0.16	-0.09	
P_c ($\mu\text{Å}$)	118.9914(018)	138.9639(139)	106.6726(104)	104.6686(116)	
$a/b/c^d$ (D)	y/n/y	n/n/y	n/n/y	n/n/y	
σ^e (kHz)	7.1	5.5	4.2	5.6	
N	144	53	47	78	

[a] A , B and C are the rotational constants. Δ_J , Δ_{JK} , Δ_K , δ_J and δ_K are the quartic centrifugal distortion constants [b] κ is Ray's asymmetry parameter [c] P_c planar moment [d] a , b and c are the type of transitions observed [e] σ is the rms deviation of the fit [f] N is the number of the fitted transitions [g] Standard error in parentheses in units of the last digit.

Table 7.12. B3LYP-D3BJ/6-311++G(d,p) theoretical spectroscopic parameters and relative energies of the conformers of muscone belonging to class III.

B3LYP-D3BJ	13h	9i	1f	1h	2l	6j	4h
A ^a (MHz)	492.1	475.6	474.5	500.2	470.5	488.7	492.1
B (MHz)	337.4	345.2	343.0	369.5	345.2	341.8	340.3
C (MHz)	217.6	220.9	223.7	249.1	226.4	232.3	226.7
P _c ^b (uÅ ²)	101.2	119.4	139.7	174.6	153.0	168.6	141.4
κ ^c	-0.13	-0.02	-0.05	-0.04	-0.03	-0.15	-0.14
μ _a ^d (D)	-0.4	0.8	-0.3	-1.4	-0.8	-0.9	-0.9
μ _b (D)	-0.1	-0.3	0.5	-1.0	0.4	0.1	0.1
μ _c (D)	-2.2	2.4	2.4	1.8	2.5	-2.5	3.3
ΔE ^e (cm ⁻¹)	176.5	67.8	143.3	52.1	191.9	170.3	251.5
ΔE ₀ ^f (cm ⁻¹)	92.8	101.8	135.0	167.2	206.3	217.7	288.8
ΔG ^{437K} _g (cm ⁻¹)	0.0	403.4	275.0	472.1	287.7	385.8	376.0
	1c	19c	15k	7g	17f	74h	53h
A (MHz)	502.0	482.0	492.0	498.9	507.6	507.5	495.3
B (MHz)	354.6	342.1	335.4	361.0	361.5	344.2	362.6
C (MHz)	230.5	232.9	217.8	235.5	246.0	225.3	236.7
P _c (uÅ ²)	119.7	177.9	106.8	133.5	169.6	110.5	139.5
κ	-0.09	-0.12	-0.14	-0.05	-0.12	-0.16	-0.03
μ _a (D)	0.7	-0.7	-0.5	0.2	-0.2	-0.7	0.9
μ _b (D)	-1.4	-0.3	-0.5	0.7	-0.8	-0.3	0.1
μ _c (D)	1.9	2.3	-2.2	2.2	-2.3	-2.1	-2.2
ΔE (cm ⁻¹)	237.0	359.9	381.1	413.3	352.6	436.5	360.5
ΔE ₀ (cm ⁻¹)	355.8	392.6	418.8	440.9	448.8	480.0	494.0
ΔG ^{437K} (cm ⁻¹)	719.9	628.1	673.1	942.9	608.8	899.8	899.8

[a] A, B, C are the rotational constants [b] P_c planar moment [c] κ is Ray's asymmetry parameter [d] μ_a, μ_b and μ_c are the electric dipole moment components [e] Relative electronic energies [f] Relative electronic energies including the zero-point correction [g] Gibbs energies calculated at 437 K.

Table 7.13. MP2/6-311++G(d,p) theoretical spectroscopic parameters and relative energies of the conformers of muscone belonging to class III.

MP2	13h	9i	1f	1h	2l	6j	4h
A ^a (MHz)	495.5	478.4	479.5	509.2	470.0	487.4	484.3
B (MHz)	344.8	353.5	347.8	372.8	353.3	351.7	353.3
C (MHz)	222.4	225.5	226.9	252.4	230.7	237.3	231.7
P _c ^b (uÅ ²)	106.6	122.4	139.9	172.9	157.5	172.1	146.4
κ ^c	-0.10	0.01	-0.04	-0.06	0.02	-0.09	-0.04
μ _a ^d (D)	0.4	-0.6	-0.4	1.4	-0.8	-0.9	0.9
μ _b (D)	-0.2	-0.1	0.5	-1.0	0.3	-0.2	0.0
μ _c (D)	-2.0	2.2	-2.2	1.6	-2.3	-2.2	-2.2
ΔE ^e (cm ⁻¹)	412.2	209.2	423.8	128.2	501.4	442.6	548.5
	1c	19c	15k	7g	17f	74h	53h
A (MHz)	508.6	484.7	503.5	505.8	521.9	511.6	501.7
B (MHz)	358.5	349.1	334.9	363.6	365.4	350.2	369.5
C (MHz)	233.8	236.8	220.1	238.7	250.9	228.4	240.9
P _c (uÅ ²)	120.9	178.1	108.3	135.9	168.6	109.1	138.6
κ	-0.09	-0.09	-0.19	-0.06	-0.15	-0.15	-0.01
μ _a (D)	-0.7	0.7	-0.5	0.2	-0.3	-0.6	1.0
μ _b (D)	-1.3	-0.3	0.4	0.6	-0.9	-0.4	0.3
μ _c (D)	1.8	2.1	-2.0	-2.0	-2.0	-1.9	-1.9
ΔE (cm ⁻¹)	445.5	438.6	771.3	683.6	450.9	731.6	443.5

[a] A, B, C are the rotational constants [b] P_c planar moment [c] κ is Ray's asymmetry parameter [d] μ_a, μ_b and μ_c are the electric dipole moment components [e] Relative electronic energies.

Table 7.14. *wB97XD/6-311++G(d,p)* theoretical spectroscopic parameters and relative energies of the conformers of muscone belonging to class III.

wB97XD	13h	9i	1f	1h	2l	6j	4h
A^a (MHz)	492.6	478.9	480.0	508.6	477.0	489.2	481.0
B (MHz)	343.6	347.4	342.8	369.7	343.9	345.6	352.0
C (MHz)	221.4	222.4	224.9	251.9	228.0	234.0	230.7
P_c^b ($\text{u}\text{\AA}^2$)	107.1	118.8	140.0	177.2	156.2	167.8	147.9
κ^c	-0.10	-0.03	-0.08	-0.08	-0.07	-0.13	-0.03
μ_a^d (D)	-0.4	0.9	-0.3	-1.4	-0.7	-0.9	0.8
μ_b (D)	-0.3	-0.3	-0.5	-1.1	0.4	0.0	-0.1
μ_c (D)	-2.2	2.4	-2.5	1.8	2.5	-2.5	2.4
ΔE^e (cm^{-1})	369.2	231.5	416.9	201.4	500.0	369.6	568.7
ΔE_0^f (cm^{-1})	207.6	43.5	347.0	175.6	292.6	276.1	485.9
ΔG^{437Kg} (cm^{-1})	251.7	169.9	369.4	265.3	175.6	344.6	312.3
	1c	19c	15k	7g	17f	74h	53h
A (MHz)	511.4	482.4	492.0	504.8	517.2	509.9	502.8
B (MHz)	353.9	346.7	335.4	361.4	359.5	347.1	363.4
C (MHz)	232.0	236.0	217.8	237.3	247.5	226.8	238.7
P_c ($\text{u}\text{\AA}^2$)	118.9	181.9	106.8	134.9	170.5	109.4	139.3
κ	-0.13	-0.10	-0.14	-0.07	-0.17	-0.14	-0.06
μ_a (D)	0.8	-0.7	-0.5	0.1	-0.1	-0.7	0.9
μ_b (D)	-1.5	-0.3	-0.5	0.6	0.7	-0.4	0.0
μ_c (D)	1.9	2.4	-2.2	2.2	2.4	-2.1	-2.2
ΔE (cm^{-1})	172.9	535.8	712.9	498.1	441.0	529.5	376.4
ΔE_0 (cm^{-1})	267.1	471.0	475.2	368.5	398.8	457.6	416.1
ΔG^{437K} (cm^{-1})	692.9	689.4	603.6	747.3	554.0	776.3	441.8

[a] A , B , C are the rotational constants [b] P_c planar moment [c] κ is Ray's asymmetry parameter [d] μ_a , μ_b and μ_c are the electric dipole moment components [e] Relative electronic energies [f] Relative electronic energies including the zero-point correction [g] Gibbs energies calculated at 437 K.

Table 7.15. *B2PLYP-D3BJ/6-311++G(d,p)* theoretical spectroscopic parameters and relative energies of the conformers of muscone belonging to class III.

B2PLYP-D3BJ	13h	9i	1f	1h	2l	6j	4h
A^a (MHz)	492.7	479.8	479.4	507.5	474.2	492.5	493.5
B (MHz)	344.9	349.9	346.7	372.5	349.7	346.6	346.0
C (MHz)	221.7	223.7	226.4	252.0	229.3	235.1	229.6
P_c^b ($\text{u}\text{\AA}^2$)	105.7	119.4	139.5	173.3	153.4	167.3	141.6
κ^c	-0.09	-0.01	-0.05	-0.06	-0.02	-0.13	-0.12
μ_a^d (D)	0.4	-0.7	-0.4	1.4	0.8	0.9	-0.9
μ_b (D)	0.3	-0.2	-0.5	-1.1	0.3	-0.2	0.0
μ_c (D)	-2.1	-2.3	-2.3	-1.7	-2.3	-2.3	-2.2
ΔE^e (cm^{-1})	228.1	100.0	198.6	63.4	255.1	245.7	318.2
	1c	19c	15k	7g	17f	74h	53h
A (MHz)	507.6	486.0	498.9	504.1	515.9	511.4	501.5
B (MHz)	357.8	347.0	337.2	364.1	364.7	348.6	366.9
C (MHz)	233.0	235.8	219.9	238.0	249.1	227.7	239.6
P_c ($\text{u}\text{\AA}^2$)	119.6	176.4	106.6	133.3	168.1	109.2	137.8
κ	-0.09	-0.11	-0.16	-0.05	-0.13	-0.15	-0.03
μ_a (D)	0.8	0.7	-0.5	-0.2	-0.2	-0.7	1.0
μ_b (D)	1.6	0.4	-0.5	0.6	-0.9	-0.4	0.2
μ_c (D)	1.8	2.2	-2.1	-2.1	-2.2	-2.0	-2.0
ΔE (cm^{-1})	291.9	389.8	486.5	476.3	397.2	521.2	353.8

[a] A , B , C are the rotational constants [b] P_c planar moment [c] κ is Ray's asymmetry parameter [d] μ_a , μ_b and μ_c are the electric dipole moment components [e] Relative electronic energies.

Class IV – oblate asymmetric tops ($0.11 < \kappa < 0.46$)

The final group of rotamers is also the largest, and it is formed by species that are oblate asymmetric tops with values of κ between 0.11 and 0.46 (Table 7.16). Identification of these species with specific conformers is quite challenging as many of them have very similar rotational constants. Therefore, we will discuss them in groups considering their κ values.

The first set comprises the rotamers that are closer to the oblate symmetric top limit, with values of κ between 0.42 and 0.31. Considering the theoretical κ , they could be conformers **7b**, **16g**, **18j**, **24g**, **3h**, **14r**, **7d**, **20o**, **3d**, **23h**, **24h**, **14k**, and **36i** (Tables 7.17-20). The theoretical constants of **20o** and **3d** differ too much from the experimental ones in light of our previous assignments, so we discarded them. **14r**, **7d**, **24h**, **14k** and **36i** have values of P_c that differ too much from the experimental ones, and were discarded too, which leaves us with **7b**, **16g**, **18j**, **24g**, **3h**, and **23h**. Rotamer XIX shows a -, b - and c -type spectrum of similar intensities, which, together with its rotational constants and P_c value, makes it easier to identify it as conformer **3h**. Rotamers XXI and XXII have very similar rotational constants and P_c values, but they can be distinguished by their observed spectrum. Rotamer XXI exhibits b - and c -type spectra while only c -type transitions were observed for rotamer XXII. They are thus assigned to conformers **24g** and **15h**, respectively. Rotamers XVII and XX only display c -type spectrum, while for XVIII a - and b -type lines have been observed, but overlapped, so it is not clear whether both type of spectra are present or only one of them. The best match for rotamer XVII, across all levels of theory, is conformer **7b**, although in this case a -type spectrum was expected to be observable due to the predicted μ_a of 1.1 D. It is possible that the low intensity of the spectrum prevented the observation of a -type transitions. The assignment for rotamers XVIII and XX is only tentative. Conformers **16g** and **18j** seem to be the best matches, respectively, although considering the type of spectra observed rotamer XVIII could also be **18j**. Another possible match for rotamer XX could be **23h**.

Among the next set of rotamers with κ between 0.29 and 0.11, rotamers XXIII and XXVII have values of P_c larger than $140 \text{ u}\text{\AA}^2$. They could correspond to **7d**, **42g**, **2g**, **36i**, **14h**. Of these, **7d** and **42g** are the best matches for XXX and XXIII, respectively, considering the relative values of the predicted rotational constants and P_c . Conformer **7d** was quite weak in the spectrum, which may have prevented observation of b -type spectrum, expected considering the predicted value of μ_b of 1.4 D.

Rotamers XXIV and XXIX have P_c values around $90 \text{ u}\text{\AA}^2$. These can only match the theoretical conformers **14g**, **43n** and **48p**. From the experimental values of the rotational constants, we can

assign XXIX to **14g** and XXVII to **43n**, which is consistent with their observed spectra. Both species have mainly *b*-type spectra and less intense *c*-type transitions.

Rotamer XXV and XXVIII are identified as **12i** and **21c**, respectively, considering its κ and P_c values, as well as the theoretical rotational constants and dipole moment components. Only *c*-type transitions have been observed for these two species. Rotamer XXVI, from its P_c value of $121.4980(91) \text{ u}\text{\AA}^2$ and those of the rotational constants, together with the observation of *a*- and *c*-type transitions, has been assigned as conformer **48b**. Similarly, rotamer XXX with a distinctively predominant *a*-type spectrum, and rotational constants, has been assigned to conformer **19h**. *C*-type spectrum is also observed for this conformer, but weaker than *a*-type spectrum, which agrees with the predicted μ_a and μ_c of 2.8 D and 1.6 D, respectively.

Table 7.16. Experimental spectroscopic parameters of the conformers of muscone belonging to class IV.

Parameters	XVII – 7b	XVIII – 16g/18j	XIX – 3h	XX – 18j/23h	XXI – 24g
A^a (MHz)	451.39949(54)	442.53507(31)	460.48839(32)	449.16935(47)	445.03918(36)
B (MHz)	390.81843(50)	379.57467(32)	387.68592(28)	377.16767(46)	367.38776(30)
C (MHz)	230.2492(38)	224.58831(48)	233.02348(17)	225.30668(23)	219.70670(33)
Δ_J (kHz)	0.01912(23)	0.0113(16)	0.0083(16)	0.0090(21)	0.0136(20)
Δ_{JK} (kHz)	-	-	0.0300(49)	-	-0.0200(89)
Δ_K (kHz)	0.0293(95)	0.0596(40)	-	0.0428(57)	0.0396(72)
δ_J (kHz)	-	0.00613(89)	0.00240(82)	0.0120(17)	0.00720(79)
δ_K (kHz)	0.0356(56)	-	0.0154(31)	-	-
κ^b	0.45	0.42	0.36	0.36	0.31
P_c^c (uÅ)	108.8953(363)	111.5989(050)	116.1366(020)	111.0009(030)	105.4702(037)
$a/b/c^d$ (D)	n/n/y	y/y/y	y/y/y	n/n/y	n/y/y
σ^e (kHz)	6.0	6.8	7.5	5.9	6.6
N^f	60	91	183	60	102
	XXII – 15h	XXIII – 7d	XXIV – 14g	XXV – 12i	XXVI – 48b
A (MHz)	447.74206(25)	472.07870(60)	469.93190(25)	463.47104(33)	441.33424(14)
B (MHz)	369.75054(30)	390.75968(58)	379.01237(23)	371.95084(36)	354.83861(20)
C (MHz)	221.4070(22)	242.9425(43)	226.71963(17)	226.7272(25)	217.23925(20)
Δ_J (kHz)	0.01400(18)	0.0576(54)	0.0091(10)	0.0161(21)	0.01414(85)
Δ_{JK} (kHz)	-	-	-	-	-
Δ_K (kHz)	-	0.079(10)	0.0187(40)	-	-
δ_J (kHz)	-	-0.0191(50)	0.00347(59)	-	0.00536(52)
δ_K (kHz)	0.0310(61)	0.123(21)	0.0227(37)	0.0648(80)	-
κ	0.31	0.29	0.25	0.23	0.23
P_c (uÅ)	106.480(23)	141.8114(369)	89.8741(019)	110.0647(246)	121.4980(91)
$a/b/c^d$ (D)	n/n/y	n/n/y	n/y/y	n/n/y	y/n/y
σ^e (kHz)	5.7	6.7	6.8	9.3	5.5
N	52	47	143	69	88
	XXVII – 42g	XXVIII – 21c	XXIX – 43n	XXX – 19h	
A (MHz)	447.68261(19)	450.21166(64)	479.51708(19)	466.35138(51)	
B (MHz)	360.48343(22)	356.54337(60)	373.79680(11)	357.31303(18)	
C (MHz)	225.3332(16)	217.2708(24)	227.89042(10)	220.85704(19)	
Δ_J (kHz)	0.0197(16)	0.0083(27)	0.00340(32)	0.00231(73)	
Δ_{JK} (kHz)	-	-	-	0.077(10)	
Δ_K (kHz)	-	0.0402(83)	0.0512(36)	-0.081(18)	
δ_J (kHz)	-	0.0106(22)	-	-	
δ_K (kHz)	0.0400(86)	-	-	0.0307(65)	
κ	0.22	0.20	0.16	0.11	
P_c (uÅ)	144.009(16)	106.972(26)	94.1541(011)	104.9057(24)	
$a/b/c^d$ (D)	n/n/y	n/n/y	n/y/y	y/n/y	
σ^e (kHz)	4.4	7.9	4.7	6.8	
N	50	62	106	91	

[a] A , B and C are the rotational constants. Δ_J , Δ_{JK} , Δ_K , δ_J and δ_K are the quartic centrifugal distortion constants [b] κ is Ray's asymmetry parameter [c] P_c planar moment [d] a , b and c are the type of transitions observed [e] σ is the rms deviation of the fit [f] N is the number of the fitted transitions [g] Standard error in parentheses in units of the last digit.

Table 7.17. B3LYP-D3BJ/6-311++G(d,p) theoretical spectroscopic parameters and relative energies of the conformers of muscone belonging to class IV.

B3LYP-D3BJ	7b	16g	12i	18j	24g	3h	14r	19h	7d	20o
A ^a (MHz)	448.9	439.9	461.6	447.0	442.8	460.4	469.9	466.5	468.8	470.2
B (MHz)	389.8	378.9	369.8	374.6	366.1	386.4	402.2	354.3	391.6	411.3
C (MHz)	229.2	223.8	224.9	224.3	218.8	232.9	243.5	219.7	242.9	250.9
P _c ^b (uÅ ²)	108.7	112.2	107.2	113.3	106.0	117.8	128.3	104.7	144.0	144.6
κ ^c	0.46	0.44	0.22	0.35	0.32	0.35	0.40	0.09	0.32	0.46
μ _a ^d (D)	1.1	-0.4	-0.4	0.8	0.0	1.1	0.4	2.8	-0.6	0.1
μ _b (D)	-0.8	0.4	0.4	-0.7	0.9	1.5	1.8	0.8	1.3	2.0
μ _c (D)	2.1	2.2	-2.3	2.2	-2.3	1.4	-1.6	1.6	1.9	1.6
ΔE ^e (cm ⁻¹)	8.1	218.4	173.9	253.7	161.3	210.4	196.3	215.5	130.3	43.5
ΔE ₀ ^f (cm ⁻¹)	175.6	198.8	209.2	221.2	244.1	246.0	285.1	291.2	296.7	298.9
ΔG ^{437K} _g (cm ⁻¹)	747.8	383.4	577.0	420.3	594.3	623.1	805.7	453.2	602.7	1028.2
	3d	23h	43n	42g	96h	24h	14g	15h	48p	8i
A (MHz)	428.7	448.6	479.7	446.8	476.2	457.0	467.4	448.2	454.7	471.4
B (MHz)	371.6	378.5	371.8	358.3	365.2	385.5	379.3	367.5	351.7	385.5
C (MHz)	219.0	226.9	227.4	225.0	230.4	246.8	226.3	220.9	213.2	235.9
P _c (uÅ ²)	115.6	117.2	95.2	147.7	125.8	184.6	90.2	107.5	89.0	120.4
κ	0.46	0.37	0.14	0.20	0.10	0.32	0.27	0.29	0.15	0.27
μ _a (D)	0.3	-0.3	0.6	0.7	1.4	-2.6	-0.2	-0.2	1.8	-1.1
μ _b (D)	-0.7	-0.5	2.4	0.2	0.0	-0.5	-2.0	-0.2	-0.5	1.5
μ _c (D)	2.4	2.3	-0.8	2.3	-2.4	-1.3	-1.4	2.3	-1.9	-1.5
ΔE (cm ⁻¹)	213.5	347.6	360.2	269.1	241.8	216.1	350.4	465.9	432.0	389.2
ΔE ₀ (cm ⁻¹)	341.5	346.6	348.3	356.0	370.0	372.9	395.1	401.9	406.5	408.9
ΔG ^{437K} (cm ⁻¹)	701.2	466.8	612.8	680.6	910.8	635.8	707.1	697.1	542.5	703.0
	2g	78h	21c	21j	8e	14k	36i	53i	48b	14h
A (MHz)	493.5	447.4	448.5	451.1	469.3	447.7	453.0	460.6	451.4	479.4
B (MHz)	380.5	362.5	354.7	357.5	368.4	389.8	380.8	372.2	362.7	385.2
C (MHz)	243.5	218.8	216.3	227.6	238.3	238.2	234.4	239.1	223.9	243.1
P _c (uÅ ²)	138.4	107.0	107.6	156.8	164.0	151.8	143.4	170.7	127.9	143.6
κ	0.10	0.26	0.19	0.16	0.13	0.45	0.34	0.20	0.22	0.20
μ _a (D)	1.0	0.9	-0.2	-0.4	-1.3	-0.5	-0.4	0.5	1.4	0.0
μ _b (D)	1.9	0.3	-0.4	-0.7	-1.5	-0.8	0.9	0.6	0.1	-1.2
μ _c (D)	-1.4	-2.3	2.4	2.3	2.2	-2.1	2.0	2.5	2.4	-2.2
ΔE (cm ⁻¹)	301.7	424.2	487.2	484.2	225.1	420.2	490.2	507.7	479.9	348.4
ΔE ₀ (cm ⁻¹)	425.8	426.4	451.5	454.5	466.8	473.4	475.2	478.0	481.1	499.7
ΔG ^{437K} (cm ⁻¹)	920.9	524.5	503.3	483.3	1125.0	633.2	537.5	449.0	732.8	890.4

[a] A, B, C are the rotational constants [b] P_c planar moment [c] κ is Ray's asymmetry parameter [d] μ_a, μ_b and μ_c are the electric dipole moment components [e] Relative electronic energies [f] Relative electronic energies including the zero-point correction [g] Gibbs energies calculated at 437 K.

Table 7.18. MP2/6-311++G(d,p) theoretical spectroscopic parameters and relative energies of the conformers of muscone belonging to class IV.

MP2	7b	16g	12i	18j	24g	3h	14r	19h	7d*	20o
A ^a (MHz)	453.2	450.1	465.2	445.2	448.0	469.3	477.1	470.9	472.8	479.7
B (MHz)	395.7	383.8	377.9	385.7	370.7	389.6	407.2	362.1	400.2	414.8
C (MHz)	232.6	228.1	229.4	228.8	221.8	237.5	246.9	223.5	247.7	256.0
P _c ^b (uÅ ²)	109.8	112.0	110.3	118.3	106.4	123.1	126.7	103.9	145.7	148.9
κ ^c	0.48	0.40	0.26	0.45	0.32	0.31	0.39	0.12	0.35	0.42
μ _a ^d (D)	1.1	0.5	-0.4	0.8	0.0	-1.2	-0.4	2.5	-0.5	-0.2
μ _b (D)	0.6	-0.4	0.4	0.6	0.7	1.4	-1.7	-0.9	-1.4	-1.8
μ _c (D)	-1.9	-2.0	-2.1	-2.0	2.1	-1.3	-1.5	1.5	-1.7	1.5
ΔE ^e (cm ⁻¹)	153.2	470.7	446.6	562.1	423.0	364.8	285.6	365.2	272.6	73.0
	3d	23h	43n	42g	96h	24h	14g	15h	48p	8i
A (MHz)	436.1	442.7	477.9	448.9	480.4	461.2	472.0	456.8	460.2	477.4
B (MHz)	374.4	392.9	380.1	364.5	373.4	392.4	386.2	369.4	354.7	390.9
C (MHz)	222.3	230.4	230.2	227.9	235.1	251.7	230.2	223.8	215.8	240.3
P _c (uÅ ²)	117.6	117.2	95.9	147.4	127.9	187.9	92.0	108.1	90.5	124.2
κ	0.42	0.53	0.21	0.24	0.13	0.34	0.29	0.25	0.14	0.27
μ _a (D)	0.2	-0.1	0.5	0.7	-1.2	-2.4	0.1	0.1	-1.6	-1.1
μ _b (D)	0.6	0.1	-2.2	-0.2	0.0	-0.4	-2.0	-0.1	0.4	1.4
μ _c (D)	-2.2	-2.1	0.8	2.1	-2.3	-1.3	1.2	-2.1	1.8	-1.4
ΔE (cm ⁻¹)	476.6	783.3	582.4	527.1	233.4	316.2	498.9	867.2	761.3	700.7
	2g	78h	21c	21j	8e	14k	36i	53i	48b	14h
A (MHz)	501.9	453.1	455.3	449.2	473.4	453.0	460.3	462.7	456.1	498.1
B (MHz)	383.5	368.7	357.6	368.6	375.6	397.3	386.8	381.5	369.2	386.3
C (MHz)	246.6	223.1	219.3	232.3	242.6	242.1	238.8	244.4	227.8	246.9
P _c (uÅ ²)	137.7	110.4	109.4	160.3	164.9	150.1	144.1	174.6	129.2	138.0
κ	0.07	0.27	0.17	0.26	0.15	0.47	0.34	0.26	0.24	0.11
μ _a (D)	-0.9	0.7	0.3	0.2	1.2	-0.5	-0.4	-0.5	1.1	-0.3
μ _b (D)	-1.8	0.2	0.3	-0.7	-1.4	0.9	-0.9	0.5	0.2	-1.5
μ _c (D)	-1.3	-2.2	-2.2	2.2	2.0	-1.8	-1.8	2.3	-2.3	-1.7
ΔE (cm ⁻¹)	319.3	722.5	823.2	748.7	210.7	518.6	737.7	665.5	699.9	392.0

[a] A, B, C are the rotational constants [b] P_c planar moment [c] κ is Ray's asymmetry parameter [d] μ_a, μ_b and μ_c are the electric dipole moment components [e] Relative electronic energies.

Table 7.19. *wB97XD/6-311++G(d,p)* theoretical spectroscopic parameters and relative energies of the conformers of muscone belonging to class IV.

wB97XD	7b	16g	12i	18j	24g	3h	14r	19h	7d	20o
A^a (MHz)	449.6	444.9	464.1	443.7	445.9	468.3	473.1	468.9	469.8	473.4
B (MHz)	393.4	382.3	373.4	381.3	368.5	385.8	404.6	359.0	400.6	414.3
C (MHz)	230.4	226.1	227.0	226.1	220.3	236.2	245.0	222.0	247.7	253.5
P_c^b ($\text{u}\text{\AA}^2$)	107.6	111.3	108.0	114.6	105.4	124.8	127.3	104.5	148.5	146.9
κ^c	0.49	0.43	0.23	0.43	0.31	0.29	0.40	0.11	0.38	0.46
μ_a^d (D)	1.3	-0.5	-0.4	1.0	0.0	1.3	0.4	2.7	-0.5	0.1
μ_b (D)	-0.7	-0.3	0.4	-0.7	0.9	1.3	1.8	0.9	1.4	2.0
μ_c (D)	2.1	-2.2	-2.3	2.2	-2.3	1.5	-1.6	1.6	1.9	1.6
ΔE^e (cm^{-1})	75.7	427.7	389.4	424.6	381.8	383.2	185.2	367.6	275.5	1.4
ΔE_0^f (cm^{-1})	0.0	208.5	282.0	323.5	444.9	309.9	312.8	378.6	451.0	282.5
ΔG^{437K} (cm^{-1})	225.4	124.9	512.7	434.3	812.9	661.5	907.1	582.3	823.5	1156.6
	3d	23h	43n	42g	96h	24h	14g	15h	48p	8i
A (MHz)	430.7	446.4	475.8	448.4	479.6	465.6	469.4	455.1	460.5	475.6
B (MHz)	374.3	384.0	378.4	361.1	367.6	385.1	383.6	367.1	351.6	387.9
C (MHz)	220.3	228.4	229.1	226.1	232.0	249.1	228.5	222.6	214.3	239.0
P_c ($\text{u}\text{\AA}^2$)	114.8	117.8	95.9	145.7	125.1	184.5	91.2	108.4	88.3	125.5
κ	0.46	0.43	0.21	0.21	0.10	0.26	0.29	0.24	0.12	0.26
μ_a (D)	0.3	-0.3	0.6	0.8	1.4	-2.7	-0.2	-0.2	1.9	-1.2
μ_b (D)	-0.7	-0.4	2.4	0.2	0.0	-0.5	-2.1	-0.2	-0.5	1.4
μ_c (D)	2.4	2.3	-0.9	2.4	-2.4	1.3	-1.4	2.4	-1.9	-1.6
ΔE (cm^{-1})	405.1	698.4	699.8	451.5	126.4	287.2	567.5	739.0	672.5	529.5
ΔE_0 (cm^{-1})	258.1	519.3	626.8	554.8	282.5	245.6	582.0	574.6	501.3	416.1
ΔG^{437K} (cm^{-1})	318.2	307.7	1006.9	993.6	900.7	224.3	925.5	900.5	324.6	474.1
	2g	78h	21c	21j	8e	14k	36i	53i	48b	14h
A (MHz)	502.5	450.2	455.5	452.1	471.5	444.4	461.5	467.2	456.1	484.5
B (MHz)	379.9	364.5	353.2	363.7	373.2	398.1	381.7	373.3	364.6	386.9
C (MHz)	245.7	220.1	217.4	231.7	240.7	241.2	236.2	241.6	226.1	245.5
P_c ($\text{u}\text{\AA}^2$)	139.6	106.5	107.9	163.1	163.2	155.7	139.7	171.9	129.5	145.4
κ	0.05	0.26	0.14	0.20	0.15	0.54	0.29	0.17	0.20	0.18
μ_a (D)	1.0	0.9	-0.2	-0.4	-1.4	-0.5	-0.4	0.7	1.4	-0.1
μ_b (D)	1.9	0.4	-0.6	-0.8	-1.5	-0.8	1.0	0.5	0.2	-1.4
μ_c (D)	-1.5	-2.3	2.4	2.4	2.2	-2.2	2.0	2.5	2.4	-2.1
ΔE (cm^{-1})	422.0	723.6	807.6	603.1	78.4	494.2	817.4	575.1	574.4	406.7
ΔE_0 (cm^{-1})	417.7	663.5	592.1	637.6	112.2	474.3	815.3	501.7	498.6	495.6
ΔG^{437K} (cm^{-1})	881.0	620.9	421.2	937.6	547.8	287.1	1203.2	441.8	742.3	847.4

[a] A , B , C are the rotational constants [b] P_c planar moment [c] κ is Ray's asymmetry parameter [d] μ_a , μ_b and μ_c are the electric dipole moment components [e] Relative electronic energies [f] Relative electronic energies including the zero-point correction [g] Gibbs energies calculated at 437 K.

Table 7.20. B2PLYP-D3BJ/def2TZVP theoretical spectroscopic parameters and relative energies of the conformers of muscone belonging to class IV.

B2PLYP-D3BJ	7b	16g	12i	18j	24g	3h	14r	19h	7d	20o
A ^a (MHz)	453.7	448.5	465.3	449.5	447.7	466.0	475.0	471.0	473.1	476.3
B (MHz)	393.7	381.7	375.0	379.9	369.4	389.9	406.1	358.7	397.7	414.8
C (MHz)	231.8	226.7	227.8	226.9	221.1	235.9	245.8	222.1	246.4	253.7
P _c ^b (uÅ ²)	108.6	110.8	107.8	113.5	105.6	119.1	126.4	103.4	144.1	143.9
κ ^c	0.46	0.40	0.24	0.37	0.31	0.34	0.40	0.10	0.33	0.45
μ _a ^d (D)	1.0	0.5	-0.4	0.8	0.1	-1.1	-0.4	2.6	-0.5	-0.1
μ _b (D)	0.8	0.4	0.4	0.6	0.8	1.5	-1.7	0.9	-0.4	-1.9
μ _c (D)	-2.0	-2.1	-2.2	-2.1	2.2	-1.4	-1.5	1.5	-1.7	1.5
ΔE ^e (cm ⁻¹)	48.1	278.1	240.5	344.6	233.5	225.3	234.2	301.6	166.2	46.9
	3d	23h	43n	42g	96h	24h	14g	15h	48p	8i
A (MHz)	433.7	447.9	483.8	450.2	480.4	459.8	471.7	453.8	458.8	475.7
B (MHz)	375.1	385.5	376.0	362.6	370.2	391.0	383.7	370.6	355.3	389.6
C (MHz)	221.5	229.4	229.6	227.3	233.4	249.9	228.7	223.2	215.5	238.5
P _c (uÅ ²)	115.5	118.0	93.9	146.5	125.8	184.5	89.6	106.7	89.2	120.2
κ	0.45	0.43	0.15	0.21	0.11	0.34	0.28	0.28	0.15	0.27
μ _a (D)	0.2	-0.2	0.6	-0.7	-1.3	-2.5	0.2	0.1	-1.7	-1.0
μ _b (D)	0.6	0.3	-2.3	-0.2	0.0	-0.5	-2.0	-0.2	-0.4	1.5
μ _c (D)	-2.3	-2.2	0.8	2.2	-2.3	-1.3	1.3	-2.2	1.8	-1.4
ΔE (cm ⁻¹)	310.5	490.0	322.8	342.6	273.5	260.3	360.8	532.4	519.1	474.9
	2g	78h	21c	21j	8e	14k	36i	53i	48b	14h
A (MHz)	499.7	452.2	453.8	453.0	473.3	452.6	457.4	464.4	455.8	490.6
B (MHz)	383.7	366.6	358.0	363.4	373.0	394.9	385.5	377.4	367.2	387.0
C (MHz)	245.9	221.5	218.7	230.3	241.2	240.8	237.3	242.5	226.6	245.8
P _c (uÅ ²)	136.4	107.4	107.4	156.1	163.7	148.9	143.1	171.5	127.7	139.9
κ	0.09	0.26	0.19	0.20	0.14	0.46	0.35	0.22	0.23	0.15
μ _a (D)	-0.9	0.8	0.3	0.3	1.1	-0.6	-0.4	-0.4	1.3	-0.1
μ _b (D)	1.8	0.3	-0.3	0.6	1.5	0.9	-0.9	-0.5	0.1	-1.4
μ _c (D)	-1.3	-2.2	-2.3	2.2	2.1	-1.9	-2.0	2.5	-2.3	-1.9
ΔE (cm ⁻¹)	290.4	510.5	555.1	534.4	268.9	420.3	539.7	564.7	580.6	395.9

[a] A, B, C are the rotational constants [b] P_c planar moment [c] κ is Ray's asymmetry parameter [d] μ_a, μ_b and μ_c are the electric dipole moment components [e] Relative electronic energies.

The relative abundances of the assigned conformers were calculated from the relative intensities of the observed transitions and the predicted dipole moments using the B3LYP-D3BJ values. The relative abundances are directly proportional to the intensity of the transitions and inversely proportional to the square of the corresponding dipole moment component. Since all the assigned species had c-type spectrum, the relative abundances were calculated from the intensities of the same c-type transitions observed for all 30 conformers. The most abundant conformers in the spectrum are **13h**, **3f**, and **9i**, which are approximately twelve times more abundant than the least abundant ones, **4h** and **19c**. Conformers **8g**, **2l** and **1f** have a relative abundance of 7 to 1 with respect to the least abundant. Conformers **24g**, **3h** and **2f**, of 6 to 1; **13f**, **43n**, and **6j** of 5 to 1; **33l**, **12i**, and **16g** of 4 to 1; **7b**, **1h**, **48b**, **18j**, **14g**, **37a** and **15h** of 3 to 1; **42g**, **7d**, **42g**, **15k**, **31d** and **19h** of 2 to 1.

7.4. Discussion

Theoretical methods and benchmarking

The theoretical rotational constants have been benchmarked with respect to the experimental ones for all methods (Table 7.21). We should note that ground-state rotational constants are compared with equilibrium theoretical constants, but this is standard practice in the field for large molecular systems such as muscone, for which anharmonic vibrational calculation are not practicable. The best performing method is B3LYP-D3BJ/6-311G++(d,p), with average deviations of 0.5 %, except for discrepancies in **13h** and **48b**. Rotational constants from MP2 deviate from experimental values by about 1.2%; this is the highest deviations among the four tested methods. The MP2 method, with a few exceptions, predicts the A rotational constant higher compared to the B3LYP-D3BJ method. wB97XD-D3BJ/6-311++G(d,p), which also includes empirical dispersion, showed very similar performance to B3LYP-D3BJ/6-311G++(d,p), with exception of conformers **12i**, **7d** and **4h**, where the discrepancies are higher than 2%. The 4th tested method, B2PLYP-D3BJ/def2TZVP, which is a double hybrid method, shows similar performance at predicting the rotational constants as wB97XD-D3BJ/6-311++G(d,p), being second best after B3LYP-D3BJ, but at much higher computational cost.

The experimental relative abundances can give us an indication of the conformational preference and energy stability. Hence, they can be used to evaluate the performance of the theoretical methods in predicting the energies. The most abundant conformers, **3f**, **13h** and **9i** are in good agreement with the zero-point corrected energies by B3LYP-D3BJ/6-311++G(d,p), all being within 100 cm⁻¹ with respect to the global minimum, **3f**. The least abundant conformers do not agree perfectly with the theoretical energies, as they are closer to each other in energy. Whilst the relative abundance is related to the Gibbs free energies, we do not observe a full agreement. The global minimum according to the Gibbs free energies is **13h**, which is one of the most abundant species in the spectrum, however the abundance of other species is not supported by the calculated Gibbs energies, with some of the assigned conformers having their relative Gibbs energies as high as 680 cm⁻¹. Nevertheless, some of the low energy predicted conformers, such as **64a**, **5h**, **20o**, **14l** and **16t**, which were expected to be present in the spectrum and could not be found, show high Gibbs free energies. This indicates that they are not thermodynamically stable at the experimental temperature of 437 K and hence explains their absence from the spectrum.

At wB97XD-D3BJ/6-311++G(d,p) level, for which zero-point corrections were determined and Gibbs energies calculated, the energy ordering is less consistent with the experimental

relative abundances. The global minimum by this method is predicted to be **7b**, whilst the most stable conformer by Gibbs is **33l**, which are not the most abundant species in the molecular jet.

The relative abundances are in further disagreement with MP2 results, where the energy ordering changes dramatically from B3LYP-D3BJ level. The global minimum by MP2 is **5h**, a conformer that could not be identified experimentally, although it is predicted to have a high Gibbs free energy by the other methods. It is followed by **20o** and **64a**, which weren't identified experimentally either. For the lower-energy conformers ordering changes dramatically compared to the predictions at B3LYP-D3BJ/6-311++G(d,p).

B2PLYP-D3BJ/def2TZVP predicts **5h**, **64a** and **20o**, which were not identified in the spectrum, as the lowest energy conformers, like MP2. The most abundant species is predicted to lay more than 100 cm^{-1} above the global minimum at this level. The performance of B2PLYP-D3BJ level of theory at predicting the energies is comparable to MP2.

Our results indicate that in highly flexible molecular systems, where the energy differences are small, commonly used computational methods do not agree on the energy ordering of the different conformers.

Table 7.21. Rotational constants of the assigned conformers predicted by B3LYP-D3BJ, MP2 and wB97XD levels of theory with 6-311++G(d,p), and B2PLYP-D3BJ with def2TZVP and the % errors calculated from experimental rotational constants as $(A_{THEOR} - A_{EXP})/A_{EXP}$.

		6-311++G(d,p)						def2TZVP	
		B3LYP-D3BJ		MP2		wB97XD		B2PLYP-D3BJ	
13h	A	492.1	0.44%	495.5	1.14%	492.6	0.54%	492.7	0.57%
	B	337.4	-1.41%	344.8	0.75%	343.6	0.40%	344.9	0.78%
	C	217.6	-1.02%	222.4	1.17%	221.4	0.71%	221.7	0.85%
3f	A	415.5	-0.59%	432.5	3.48%	423.0	1.20%	421.9	0.94%
	B	400.6	-0.34%	397.6	-1.09%	400.0	-0.49%	403.3	0.33%
	C	227.6	-0.73%	233.6	1.89%	230.6	0.58%	230.7	0.63%
9i	A	475.6	-0.15%	478.4	0.43%	478.9	0.54%	479.8	0.73%
	B	345.2	-0.77%	353.5	1.61%	347.4	-0.14%	349.9	0.58%
	C	220.9	-0.53%	225.5	1.54%	222.4	0.15%	223.7	0.73%
8g	A	535.5	0.10%	540.6	1.05%	539.9	0.92%	541.1	1.15%
	B	338.3	-0.64%	342.4	0.56%	339.5	-0.29%	341.9	0.41%
	C	225.6	-0.18%	228.3	1.02%	226.7	0.31%	227.7	0.75%
2l	A	470.5	-0.14%	470.0	-0.24%	477.0	1.24%	474.2	0.65%
	B	345.2	-0.69%	353.3	1.64%	343.9	-1.07%	349.7	0.60%
	C	226.4	-0.43%	230.7	1.46%	228.0	0.28%	229.3	0.85%
1f	A	474.5	-0.06%	479.5	0.99%	480.0	1.10%	479.4	0.97%
	B	343.0	-0.79%	347.8	0.60%	342.8	-0.85%	346.7	0.28%
	C	223.7	-0.51%	226.9	0.91%	224.9	0.02%	226.4	0.69%
24g	A	442.8	-0.50%	448.0	0.67%	445.9	0.19%	447.7	0.60%
	B	366.1	-0.35%	370.7	0.90%	368.5	0.30%	369.4	0.55%
	C	218.8	-0.41%	221.8	0.95%	220.3	0.27%	221.1	0.63%
3h	A	460.4	-0.02%	469.3	1.91%	468.3	1.70%	466.0	1.20%
	B	386.4	-0.33%	389.6	0.49%	385.8	-0.49%	389.9	0.57%
	C	232.9	-0.05%	237.5	1.92%	236.2	1.36%	235.9	1.23%
2f	A	523.8	-0.62%	539.0	2.26%	535.8	1.66%	533.1	1.14%
	B	310.6	-0.21%	310.6	-0.21%	309.8	-0.47%	312.3	0.34%
	C	215.8	-0.37%	219.2	1.20%	218.3	0.79%	218.5	0.88%
13f	A	428.6	-0.11%	434.0	1.15%	428.1	-0.22%	432.4	0.78%
	B	392.8	-0.27%	397.7	0.97%	398.4	1.15%	397.1	0.82%
	C	228.1	0.04%	231.7	1.62%	230.2	0.96%	230.5	1.09%
43n	A	479.7	0.04%	477.9	-0.34%	475.8	-0.78%	483.8	0.89%
	B	371.8	-0.53%	380.1	1.69%	378.4	1.23%	376.0	0.59%
	C	227.4	-0.22%	230.2	1.01%	229.1	0.53%	229.6	0.75%
6j	A	488.7	-0.14%	487.4	-0.41%	489.2	-0.04%	492.5	0.63%
	B	341.8	-0.71%	351.7	2.17%	345.6	0.40%	346.6	0.69%
	C	232.3	-0.34%	237.3	1.81%	234.0	0.39%	235.1	0.86%
33l	A	443.2	0.18%	446.6	0.94%	445.8	0.76%	449.0	1.49%
	B	403.8	-0.90%	411.8	1.06%	406.4	-0.27%	408.1	0.15%
	C	237.1	-0.53%	241.3	1.24%	238.6	0.10%	240.3	0.82%
12i	A	461.6	-0.40%	465.2	0.37%	444.9	-4.01%	465.3	0.39%
	B	369.8	-0.58%	377.9	1.60%	382.3	2.78%	375.0	0.82%
	C	224.9	-0.81%	229.4	1.18%	226.1	-0.28%	227.8	0.47%
16g	A	439.9	-0.60%	450.1	1.71%	445.2	0.60%	448.5	1.35%
	B	378.9	-0.18%	383.8	1.11%	381.9	0.61%	381.7	0.56%
	C	223.8	-0.35%	228.1	1.56%	226.1	0.67%	226.7	0.94%

Table 7.21 cont'd. Rotational constants of the assigned conformers predicted by B3LYP-D3BJ, MP2 and wB97XD levels of theory with 6-311++G(d,p), and B2PLYP-D3BJ with def2TZVP and the % errors calculated from experimental rotational constants as $(A_{THEOR} - A_{EXP})/A_{EXP}$.

		6-311++G(d,p)					def2TZVP			
		B3LYP-D3BJ		MP2		wB97XD		B2PLYP-D3BJ		
7b	A	448.9	-0.55%	453.2	0.40%	449.6	-0.40%	453.7	0.51%	
	B	389.8	-0.26%	395.7	1.25%	393.4	0.66%	393.7	0.74%	
	C	229.2	-0.46%	232.6	1.02%	230.4	0.07%	231.8	0.67%	
18j	A	447.0	-0.48%	445.2	-0.88%	443.7	-1.22%	449.5	0.07%	
	B	374.6	-0.68%	385.7	2.26%	381.3	1.10%	379.9	0.72%	
	C	224.3	-0.45%	228.8	1.55%	226.1	0.35%	226.9	0.71%	
48b	A	451.4	2.28%	456.1	3.35%	456.1	3.35%	455.8	3.28%	
	B	362.7	2.22%	369.2	4.05%	364.6	2.75%	367.2	3.48%	
	C	223.9	3.07%	227.8	4.86%	226.1	4.08%	226.6	4.31%	
1h	A	500.2	0.14%	509.2	1.95%	508.6	1.83%	507.5	1.61%	
	B	369.5	-0.41%	372.8	0.48%	369.7	-0.36%	372.5	0.40%	
	C	249.1	0.34%	252.4	1.67%	251.9	1.46%	252.0	1.50%	
14g	A	467.4	-0.54%	472	0.44%	469.4	-0.11%	471.7	0.38%	
	B	379.3	0.08%	386.2	1.90%	383.6	1.21%	383.7	1.24%	
	C	226.3	-0.19%	230.2	1.54%	228.5	0.79%	228.7	0.87%	
37a	A	424.4	0.33%	420.6	-0.57%	424.7	0.40%	426.8	0.90%	
	B	381.5	-0.84%	392.4	2.00%	384.9	0.05%	386.4	0.44%	
	C	216.9	-0.28%	219.4	0.87%	217.7	0.09%	219.0	0.69%	
15h	A	448.2	0.10%	456.8	2.02%	455.1	1.64%	453.8	1.35%	
	B	367.5	-0.61%	369.4	-0.09%	367.1	-0.72%	370.6	0.23%	
	C	220.9	-0.23%	223.8	1.08%	222.6	0.54%	223.2	0.81%	
7d	A	468.8	-0.69%	472.8	0.15%	469.8	-0.48%	473.1	0.22%	
	B	391.6	0.22%	400.2	2.42%	400.6	2.52%	397.7	1.78%	
	C	242.9	-0.02%	247.7	1.96%	247.7	1.96%	246.4	1.42%	
21c	A	448.5	-0.38%	455.3	1.13%	455.5	1.17%	453.8	0.80%	
	B	354.7	-0.52%	357.6	0.30%	353.2	-0.94%	358.0	0.41%	
	C	216.3	-0.45%	219.3	0.93%	217.4	0.06%	218.7	0.66%	
42g	A	446.8	-0.20%	448.9	0.27%	448.4	0.16%	450.2	0.56%	
	B	358.3	-0.61%	364.5	1.11%	361.1	0.17%	362.6	0.59%	
	C	225.0	-0.15%	227.9	1.14%	226.1	0.34%	227.3	0.87%	
15k	A	492.0	-0.81%	503.5	1.51%	492.0	-0.81%	498.9	0.58%	
	B	335.4	0.08%	334.9	-0.07%	335.4	0.08%	337.2	0.62%	
	C	217.8	-0.29%	220.1	0.76%	217.8	-0.29%	219.9	0.67%	
31d	A	505.0	0.02%	515.1	2.02%	508.6	0.74%	511.4	1.29%	
	B	320.2	-0.90%	321.8	-0.40%	322.0	-0.34%	322.9	-0.06%	
	C	213.9	-0.63%	216.9	0.76%	215.4	0.07%	216.3	0.48%	
19h	A	466.5	0.03%	470.9	0.98%	468.9	0.55%	471.0	1.00%	
	B	354.3	-0.84%	362.1	1.34%	359.0	0.47%	358.7	0.39%	
	C	219.7	-0.52%	223.5	1.20%	222.0	0.52%	222.1	0.56%	
4h	A	492.1	-0.41%	484.3	-1.98%	481.0	-2.65%	493.5	-0.12%	
	B	340.3	-0.16%	353.3	3.66%	352.0	3.27%	346.0	1.51%	
	C	226.7	-0.07%	231.7	2.13%	230.7	1.69%	229.6	1.20%	
19c	A	482.0	-0.06%	484.7	0.50%	482.4	0.03%	486.0	0.77%	
	B	342.1	-0.94%	349.1	1.08%	346.7	0.39%	347.0	0.48%	
	C	232.9	-0.45%	236.8	1.22%	236.0	0.88%	235.8	0.79%	

Conformational features in muscone

Because the average deviation between experimental and theoretical rotational constants were below 1% at the B3LYP-D3BJ level of theory, we can take these theoretical structures to be very close to the experimental ones. The identified conformations are presented in Figure 7.4 in decreasing order of their relative abundances, which is indicated in parentheses. At first glance the assigned conformations do not share obvious trends in either the ring shape or C=O and methyl moieties positioning and orientation. Generally, all the conformers are flat with the C=O group being perpendicular to the ring, with the exception conformers **8g**, **3h**, **43n**, **1h**, **7d**, where the C=O group is oriented towards the centre of the ring, and **19h**, where carbonyl forms an obtuse angle with the plane of the hydrocarbon ring. It is important to understand the behaviour of the C=O orientation, due to its proposed osmophoric role of inserting the odorant into the binding pocket of the receptor and forming stronger interactions with the amino acids residues.²⁰ Understanding the preferred orientation of the methyl group could reveal why the (*R*)-enantiomer of muscone has a stronger musk scent.²⁰ Most conformers have their methyl group in the second position clockwise from the carbonyl being perpendicular out of plane (Figure 7.4), except for **2l**, **6j**, **12i**, **1h** and the least abundant **19h**, **4h** and **19c** conformers, where it is in the second position anticlockwise. When the methyl group is anticlockwise from the C=O moiety, it generally points in the opposite direction of the hydrocarbon chain plane, with exception of **12i** where it is on the same side as C=O. In the configurations where the methyl group is to the right of C=O, different orientations are observed, including in plane (**13h**, **8g**, **1f**, **24g**, **3h**, **2f**, **43n**, **48p**, **14g**, **37a**, **7d**, **21c**, **15k**), out of plane on the same side as C=O (**3f**, **9i**, **13f**, **33l**, **7b**, **18j**, **15h**), on the opposite side of C=O (**16g**, **42g**), in corner positions (**13h**, **1f**, **2f**, **12i**, **16g**, **14g**, **42g**, **31d**) or on a straight side of the hydrocarbon framework (**3f**, **9i**, **8g**, **2l**, **13f**, **6j**, **33l**, **7b**, **18j**, **37a**, **15h**). Generally, in conformations where the methyl group is on the same side of the plane of the ring as the C=O group, the two moieties form weak attractive interactions. In the conformers where it is in corner positions, roughly on the plane of the ring or pointing to the opposite side of the plane of the ring from the carbonyl group, the methyl does not interact with any parts of the macrocycle.

Further similarities and differences between the identified conformers are in the shapes adopted by the macrocycle itself. The most abundant conformers (**13h**, **3f**, **9i**) adopt a distorted square shape. A similar ring configuration is preferred by low abundance conformers **24g**, **13f**, **33l**, **12i**, **16g**, **7b**, **18j**, **14g**, **37a**, **42g**, **15k**. Another preferred shape by a few conformers resembles a “heart”, where, viewed from the top, two “straight” sides of the macrocycle seemed to form a right angle, and the rest of the hydrocarbon chain appears “wavy”, with the zig-zag of the carbon chain occurring on the plane of the ring. Conformers **8g**, **2l**, **1f**, **3h**, **2f**, **43n**, **6j**, **15h** and

31d show this “heart” shape. Some more distorted ring shapes have been observed for the least abundant configurations, such as **1h**, **7d**, **21c**, **19h**, **4h** and **19c**.

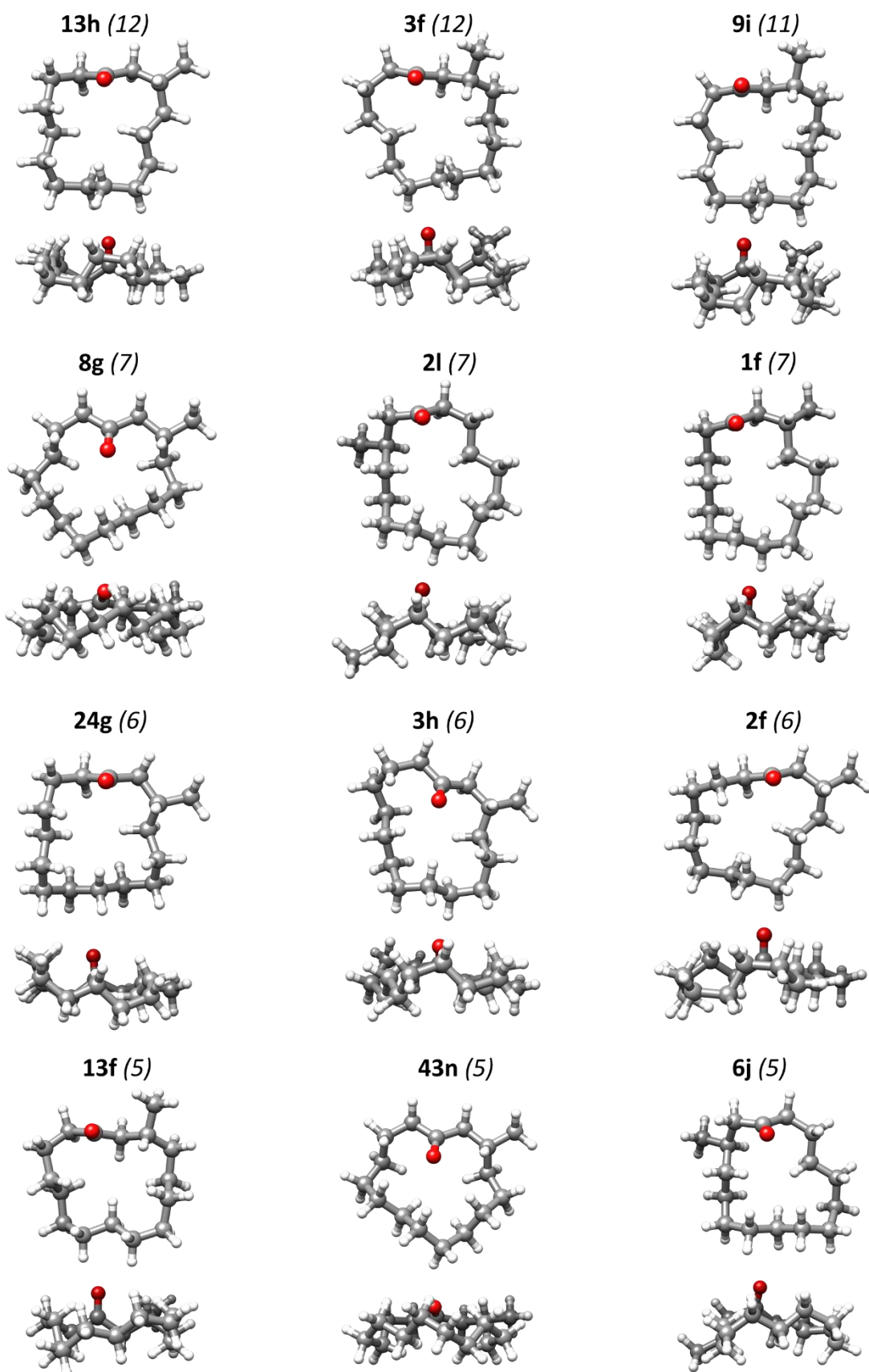


Figure 7.4. Top and side views of the assigned conformers of muscone in decreasing order of their conformational abundance. The relative conformational abundance ratio with respect to the least abundant conformer is indicated in parentheses.

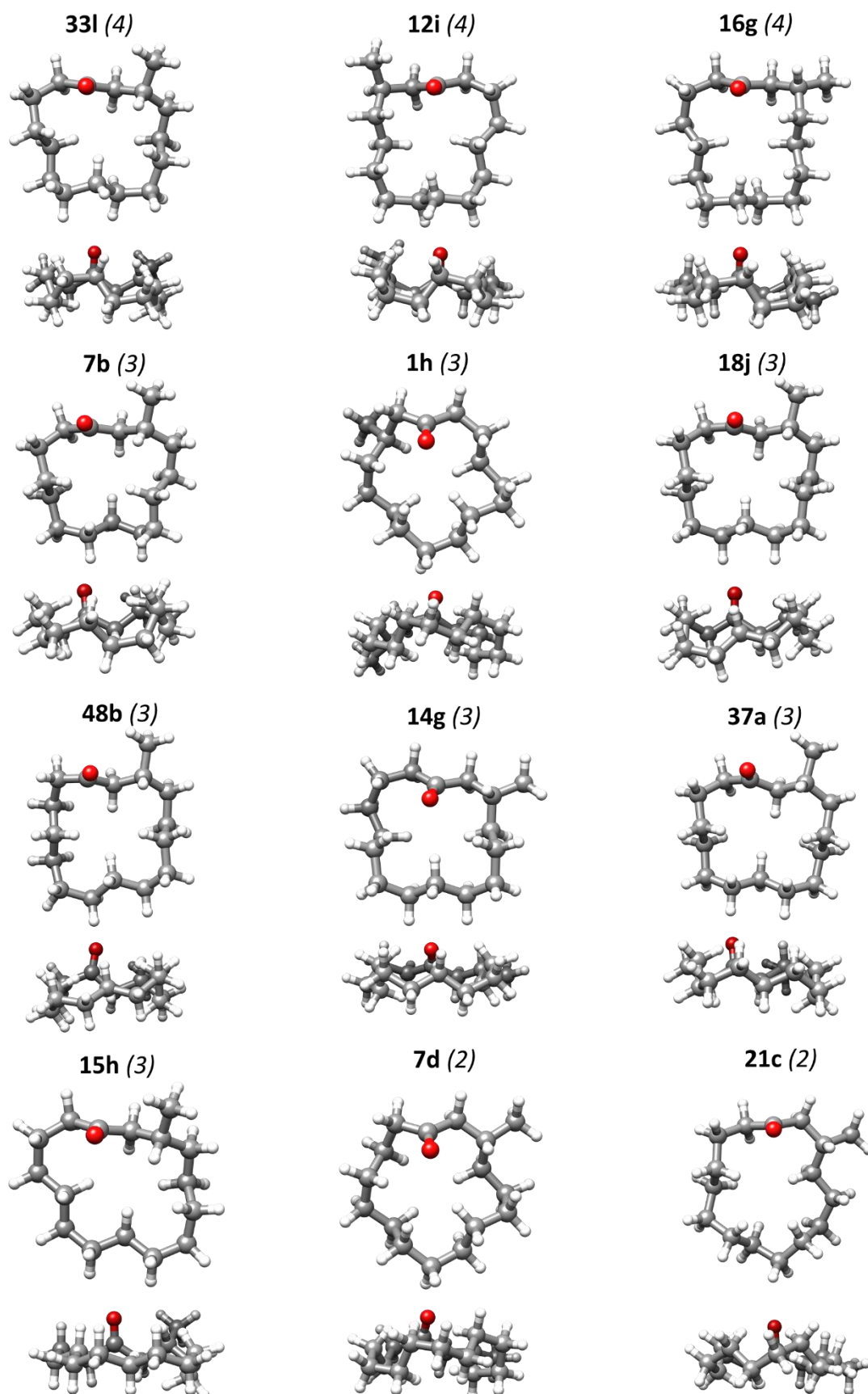


Figure 7.4 cont'd. Top and side views of the assigned conformers of muscone in decreasing order of their conformational abundance. The relative conformational abundance ratio with respect to the least abundant conformer is indicated in parentheses.

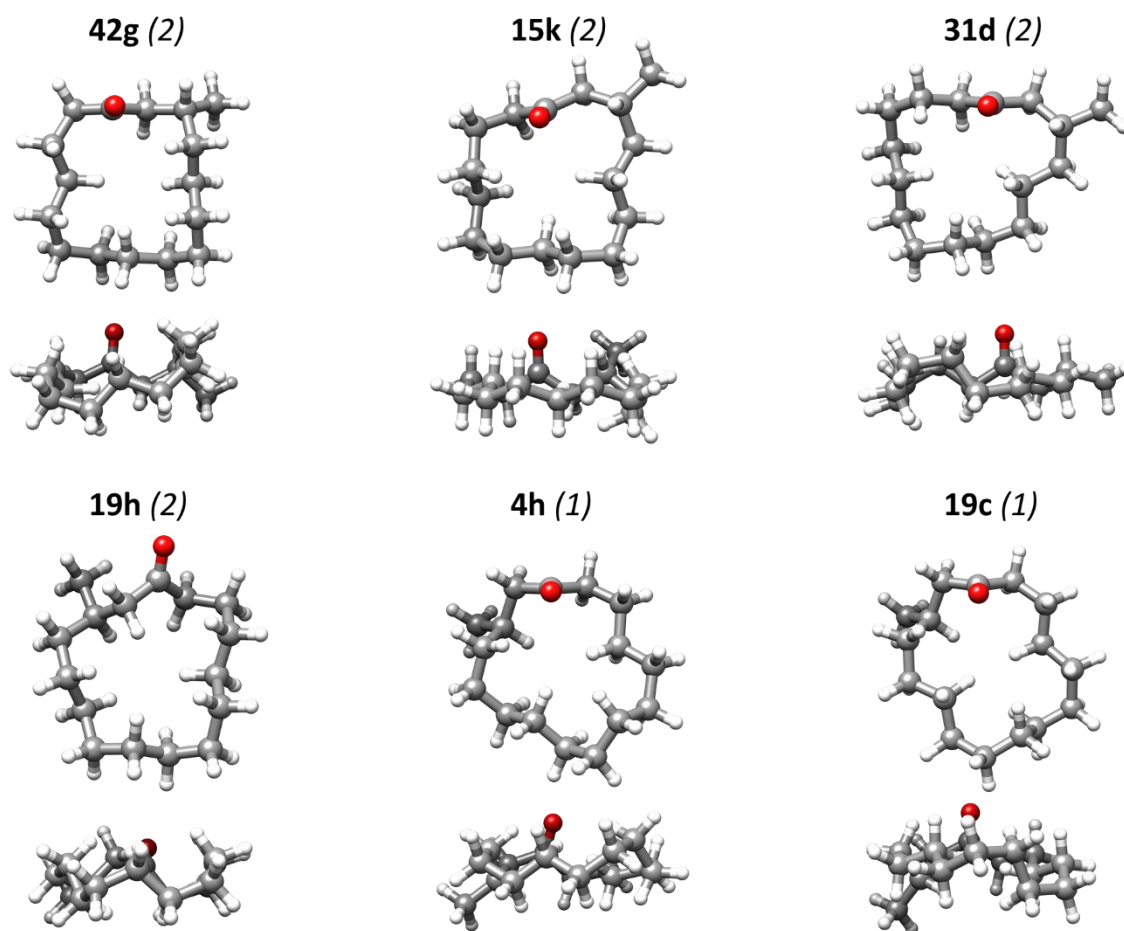


Figure 7.4 cont'd. Top and side views of the assigned conformers of muscone in decreasing order of their conformational abundance. The relative conformational abundance ratio with respect to the least abundant conformer is indicated in parentheses.

Non-covalent interactions

The intramolecular interactions taking place in the various conformers of muscone have been considered trying to rationalise the observed conformational abundances (Figure 7.5). All conformers show C–H \cdots O=C interactions involving the carbonyl group oxygen and neighbouring hydrogens, at distances of 2.49 – 2.53 Å. Conformers **19c** and **4h**, the least abundant conformers, have the carbonyl positioned on a shorter side losing two of C–H \cdots O=C interactions. This potentially is reflected in the low conformational abundance. In those conformers where the oxygen is pointing towards the centre of the ring, such as **8g**, **43n**, **1h**, **14g** and **7d**, there are weak attractive transannular interactions between the oxygen and the hydrogens across the ring.

The main differences between the most and the least abundant conformers lie in the 1,4-H \cdots H interactions and the transannular H \cdots H interactions across the ring. In the most abundant conformers, the intra-annular hydrogens are further apart and only conformer **13h** shows a H \cdots H interaction across the ring with a distance shorter than the sum of the van der Waals radii of hydrogens, 2.40 Å.^{21,22} The less abundant conformers display a larger number of transannular H \cdots H interactions, with the medium abundance conformers up showing up to two unfavourable interactions, and the least abundant ones three H \cdots H interactions, with distances as short as 2.05 Å (see **19c**, Figure 7.5). All conformers also show repulsive 1,4-H \cdots H interactions.^{21,22} However, there is no obvious relationship between these interactions and abundances of the conformers, as all conformers have a similar number of them with alike distances.

The intramolecular interactions involved in the observed conformers can be visualized by applying the non-covalent interactions (NCIs) method.²³ We have calculated the NCI plots for all assigned conformers (Figure 7.6). Strong attractive interactions are usually displayed in dark blue and repulsive interactions in red, with weak attractive interactions in green. The size of the macrocycle, 15-membered ring, is large enough for a flexible arrangement of the carbons in a way that strains are minimised. Most isosurfaces are coloured in green/yellow, which indicate weak attractive interactions/weak repulsive interactions, and they are associated with 1,4-H \cdots H interaction. These 1,4-H \cdots H interactions close a five-membered intramolecular ring and the strain associated to ring formation is reflected in the yellowish part of the isosurface. The two colours, green and yellow, appear where the distances between the H are shorter than the sum of their van der Waals radii. Given the similarities in the isosurfaces, the NCI and RDG plots do not offer enough detail to explain the higher preference of muscone for some conformers.

In summary, the stronger C–H···O=C interaction in more abundant conformers together with the fewer repulsive H···H interactions contribute to their higher stabilisation and higher abundance in the molecular jet.

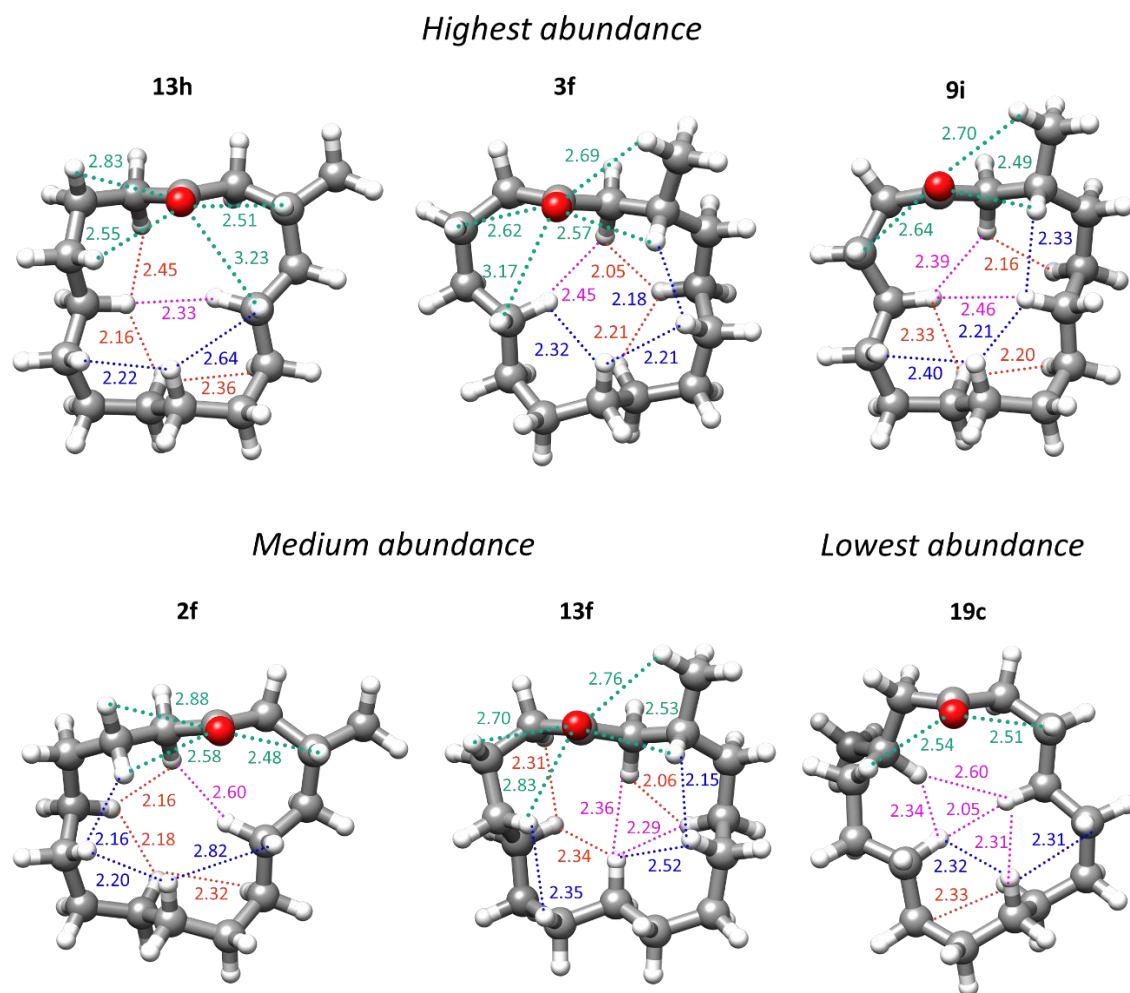


Figure 7.5. Intramolecular interactions in conformers of muscone with high, medium and low abundance, with C–H···O=C interactions depicted in green; 1,4-H···H interactions illustrated in orange (below the plane of the ring) and blue (above the plane of the ring); H···H interactions across the ring are shown in pink.

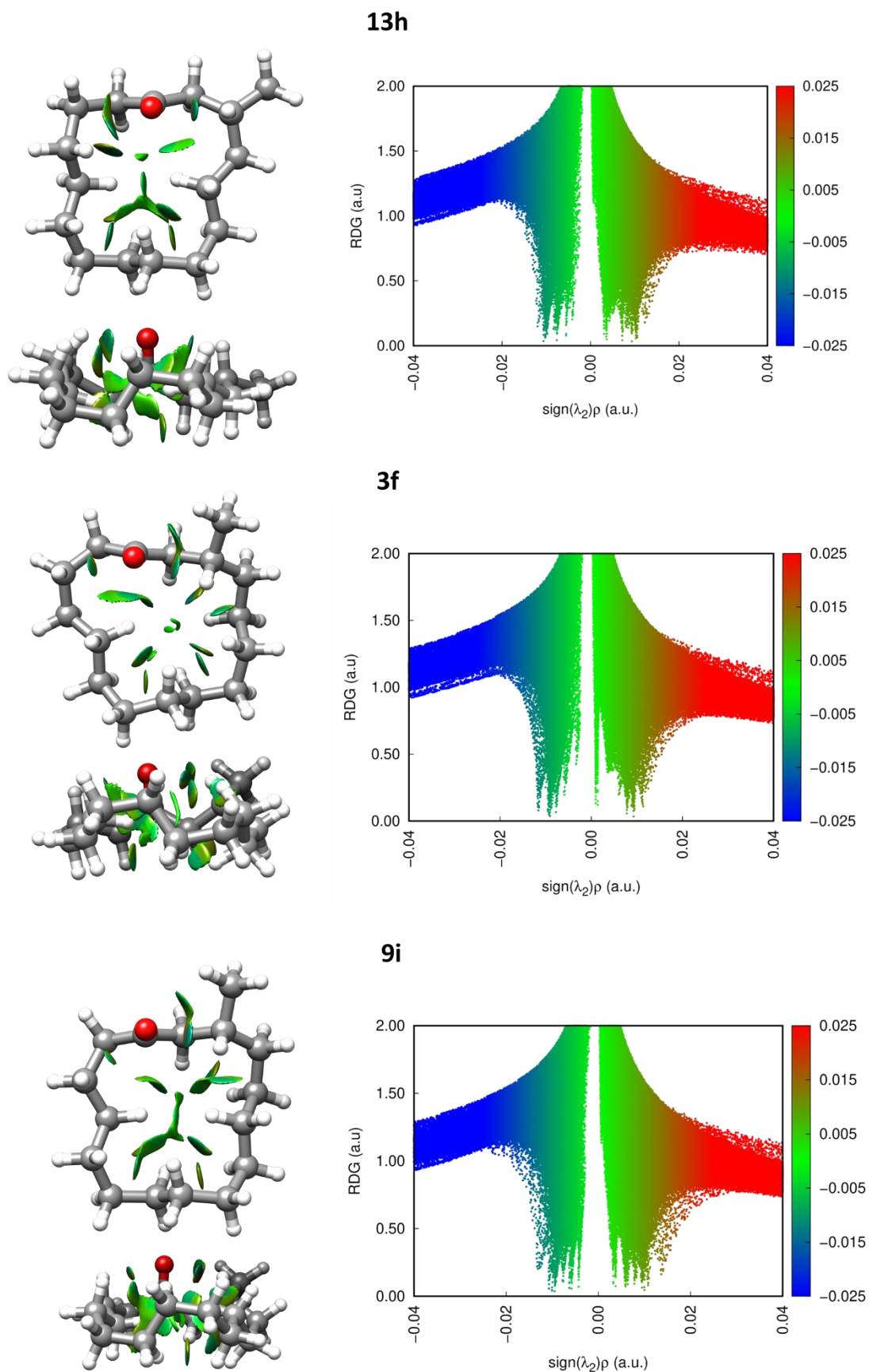


Figure 7.6. The NCI and RDG plots of all assigned conformers of muscone with top and side views. NCI plotted with 0.5 isosurfaces.

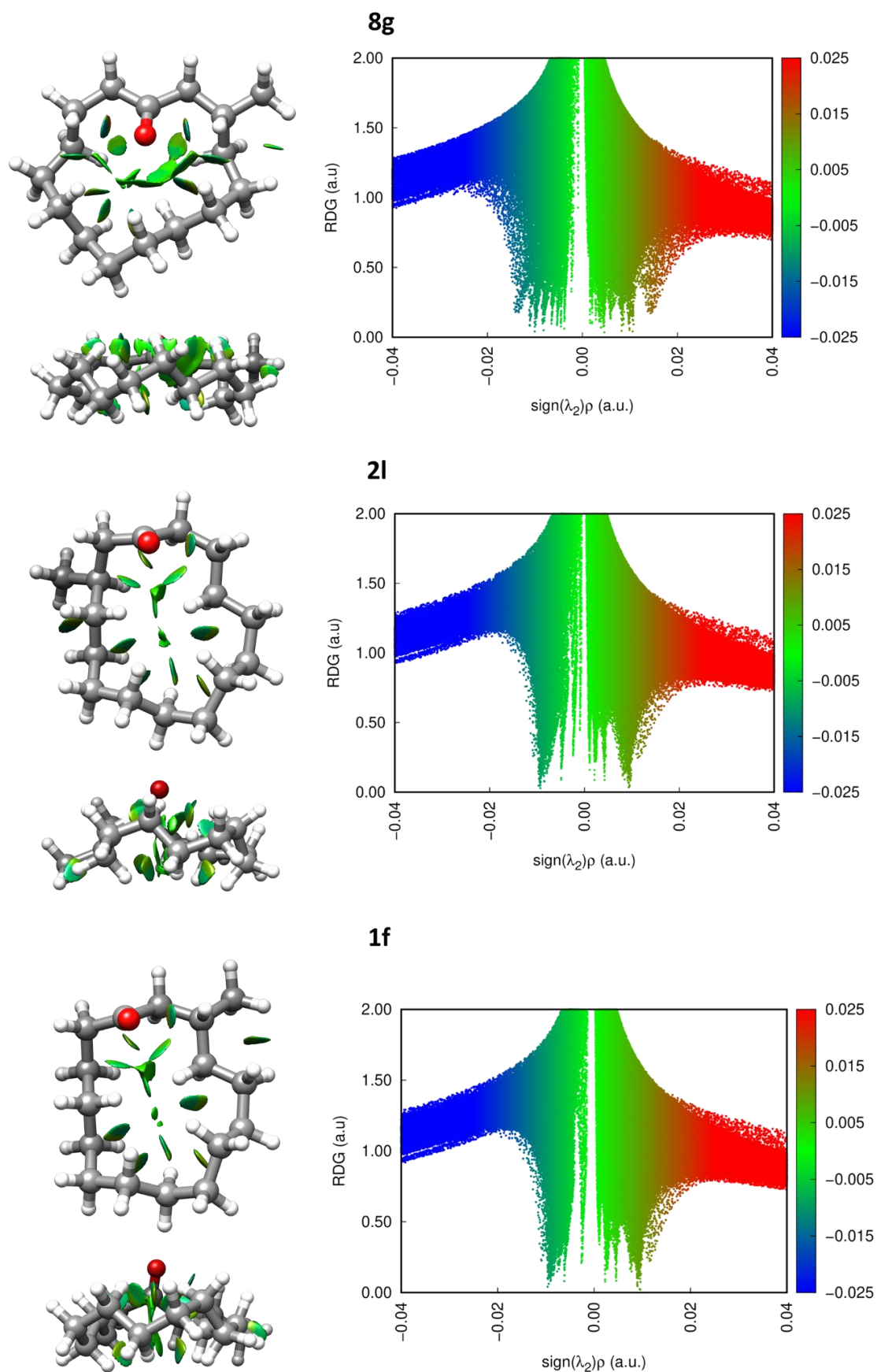


Figure 7.6 cont'd. The NCI and RDG plots of all assigned conformers of muscone with top and side views. NCI plotted with 0.5 isosurfaces.

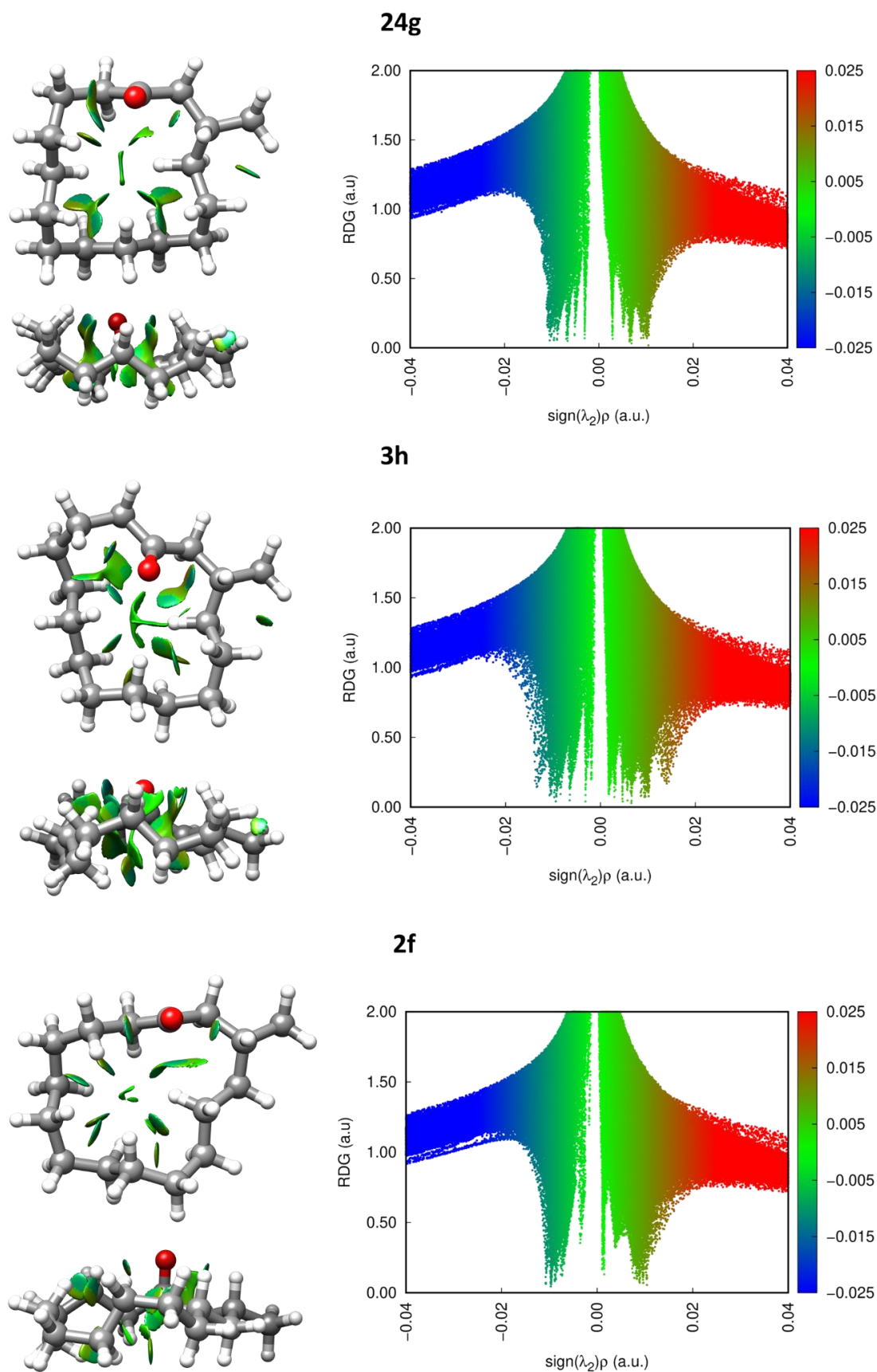


Figure 7.6 cont'd. The NCI and RDG plots of all assigned conformers of muscone with top and side views. NCI plotted with 0.5 isosurfaces.

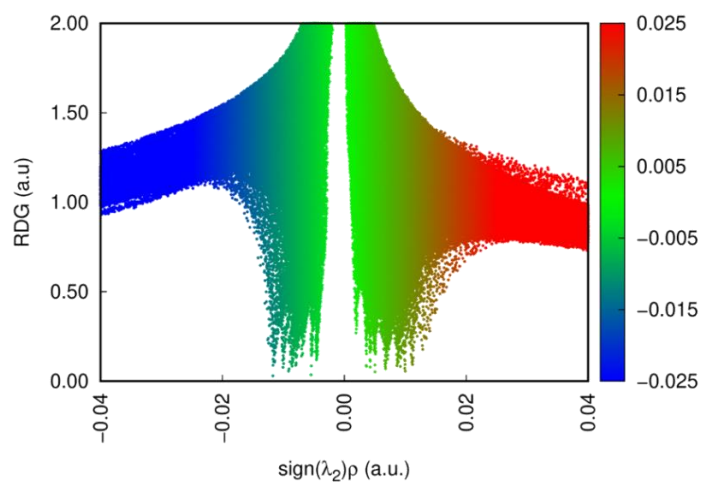
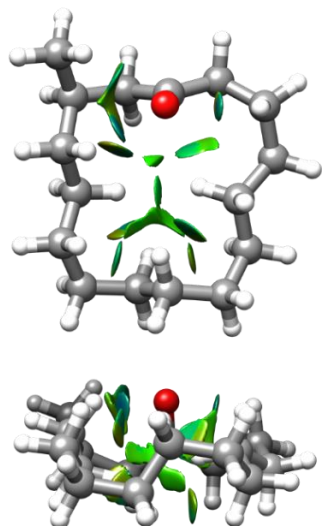
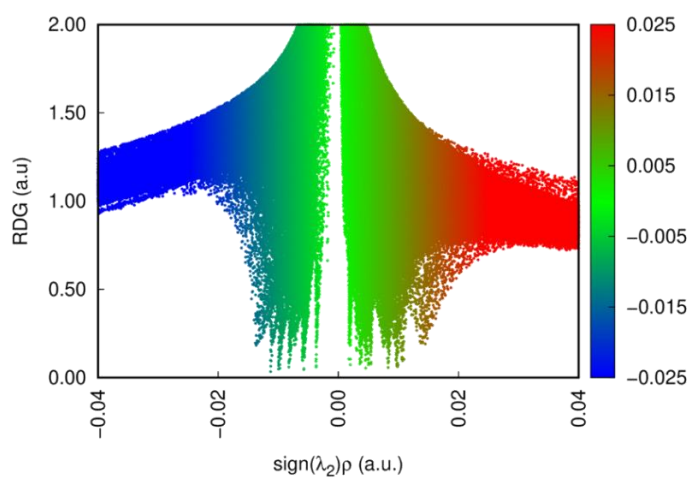
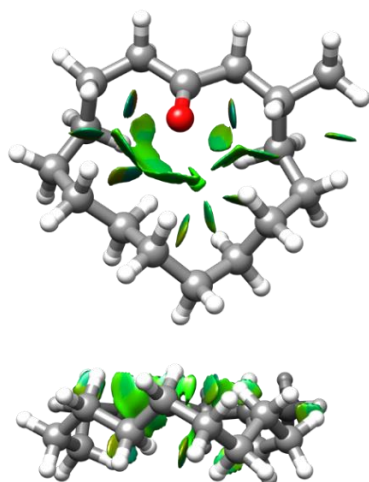
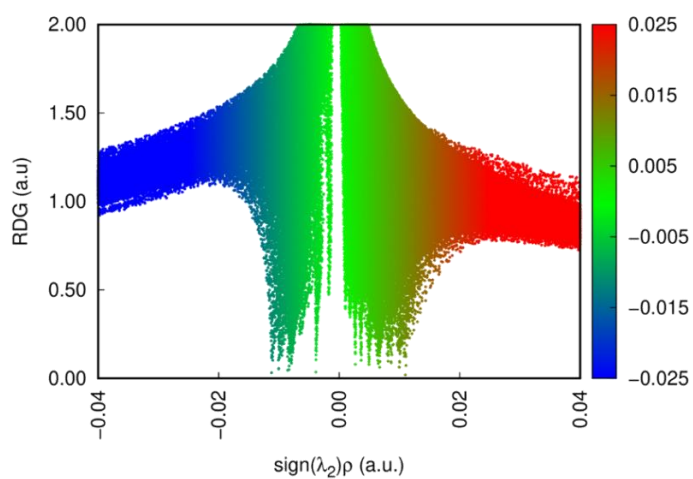
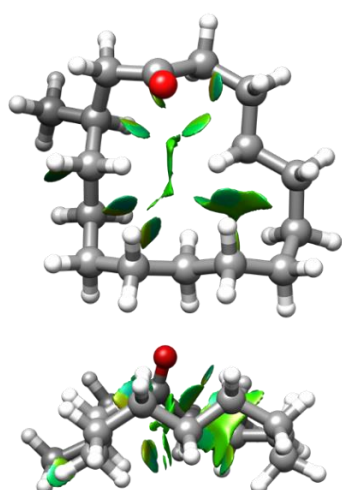
13f**43n****6j**

Figure 7.6 cont'd. The NCI and RDG plots of all assigned conformers of muscone with top and side views. NCI plotted with 0.5 isosurfaces.

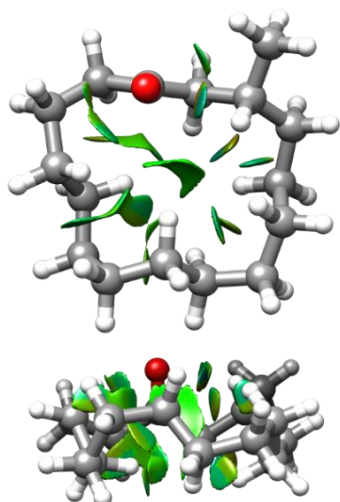
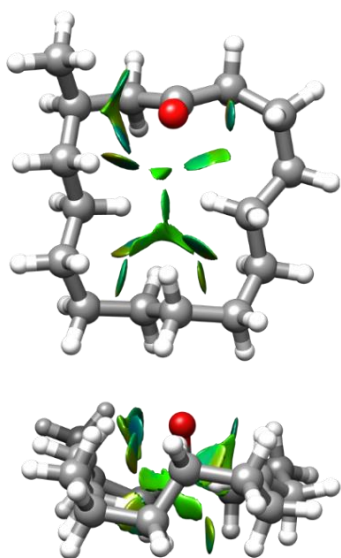
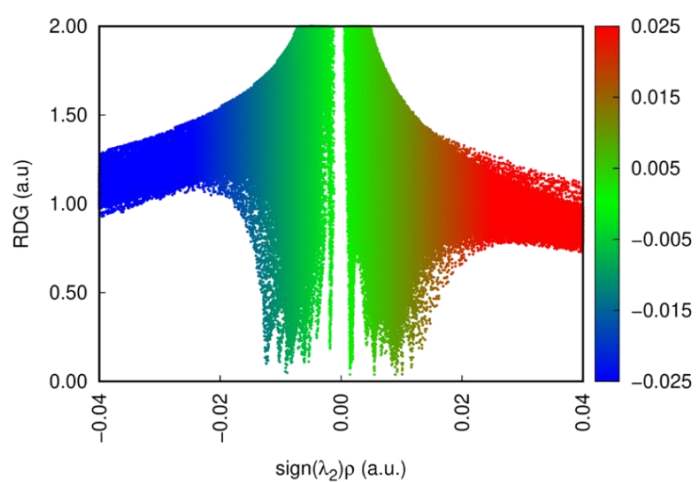
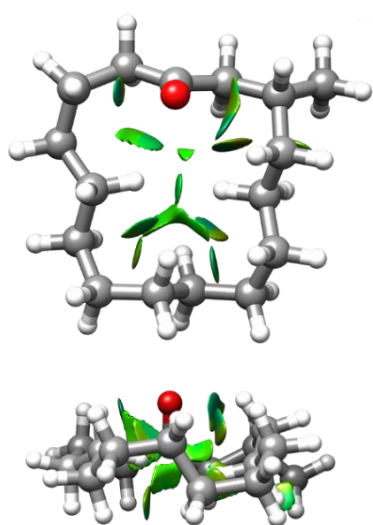
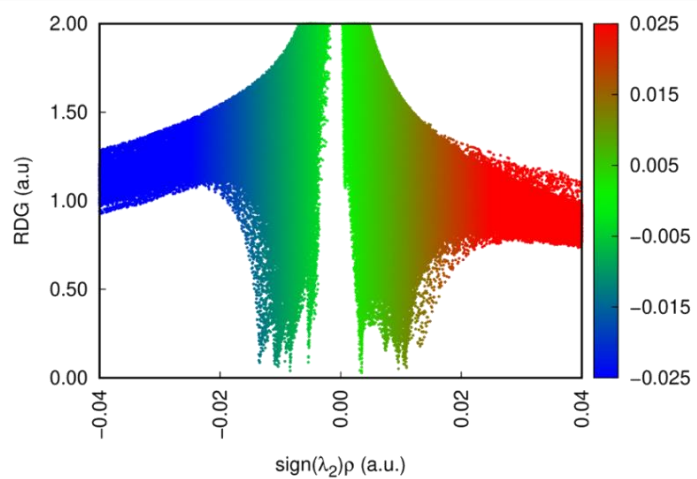
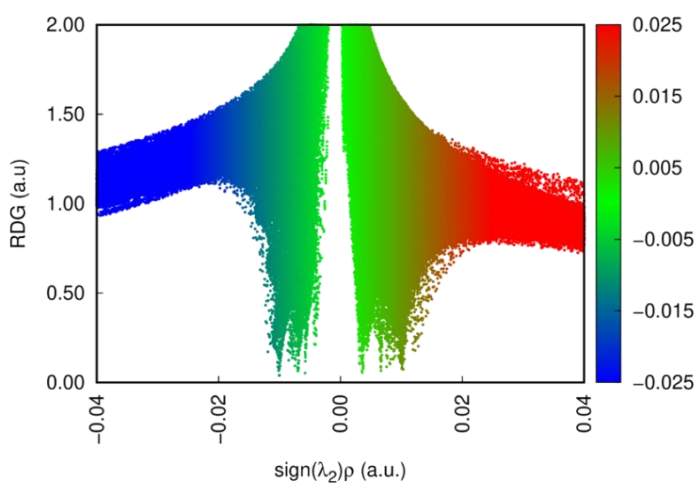
**33i****12i****16g**

Figure 7.6 cont'd. The NCI and RDG plots of all assigned conformers of muscone with top and side views. NCI plotted with 0.5 isosurfaces.

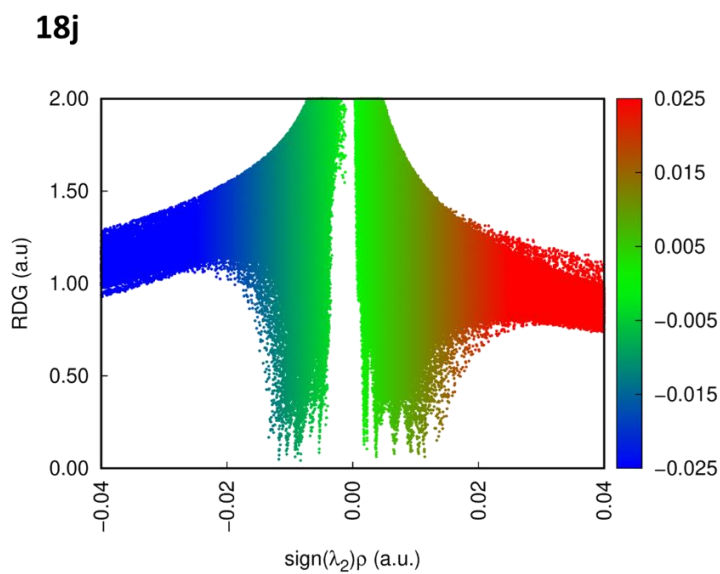
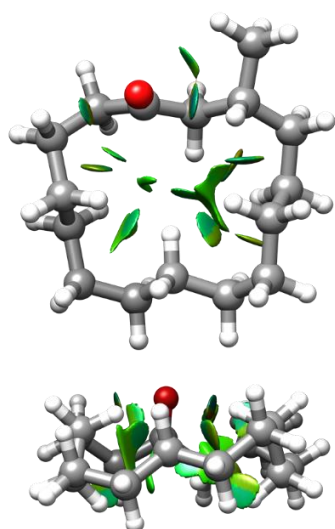
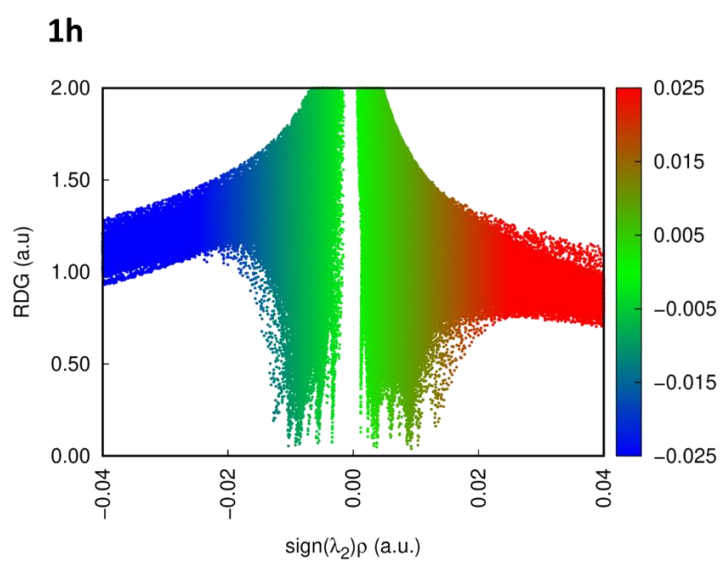
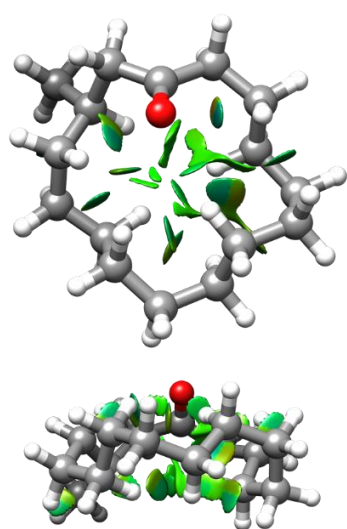
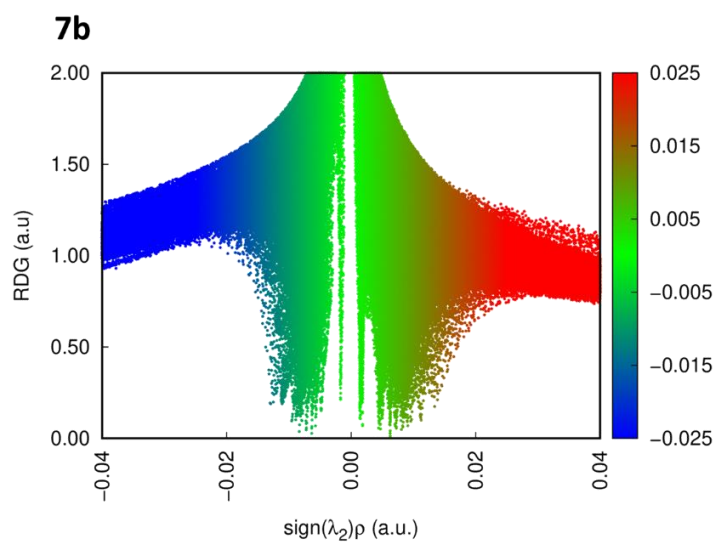
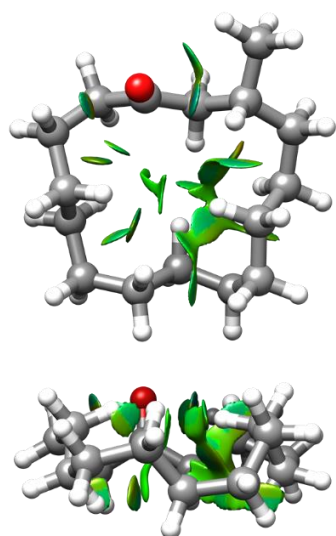


Figure 7.6 cont'd. The NCI and RDG plots of all assigned conformers of muscone with top and side views. NCI plotted with 0.5 isosurfaces.

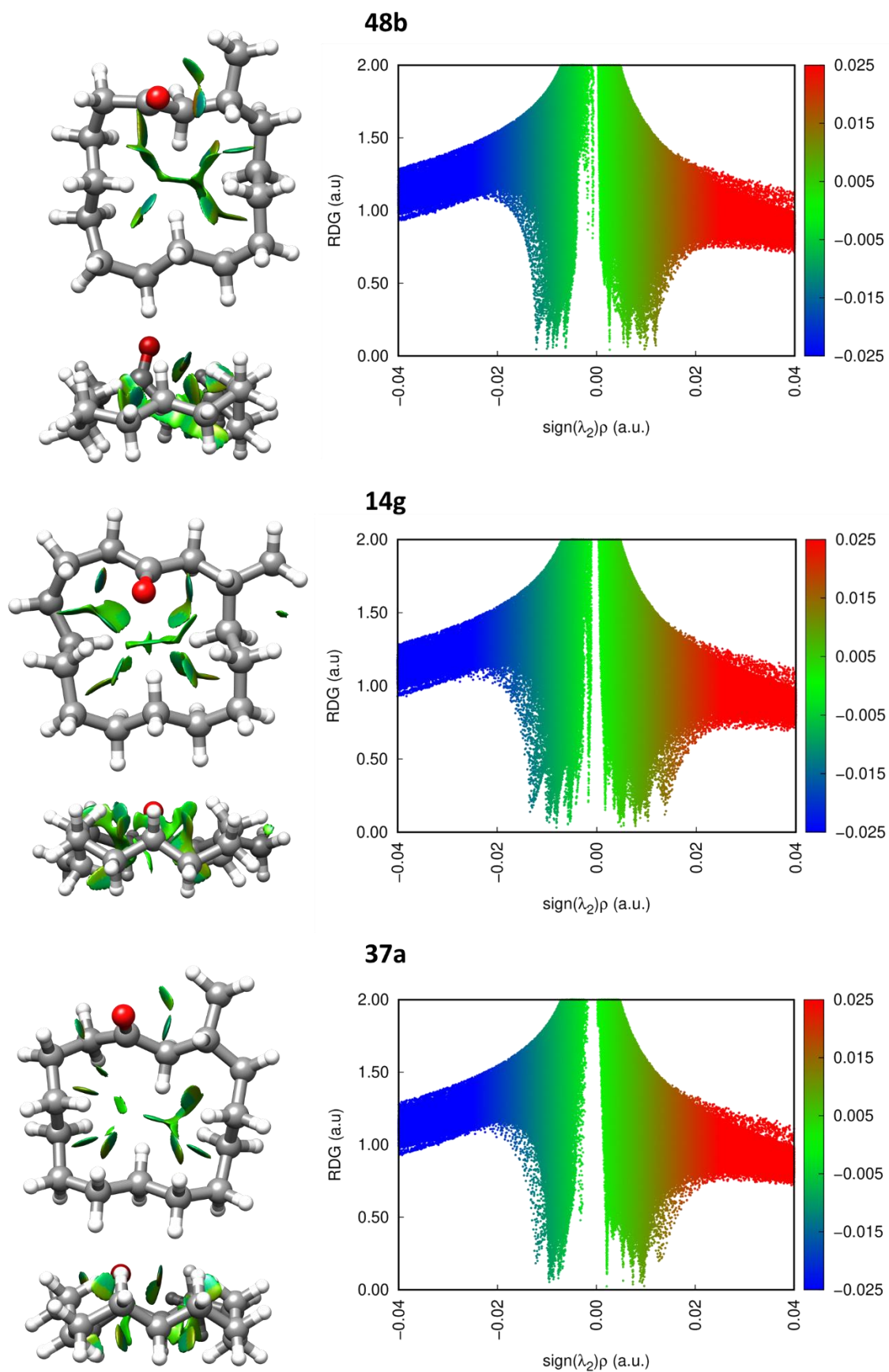


Figure 7.6 cont'd. The NCI and RDG plots of all assigned conformers of muscone with top and side views. NCI plotted with 0.5 isosurfaces.

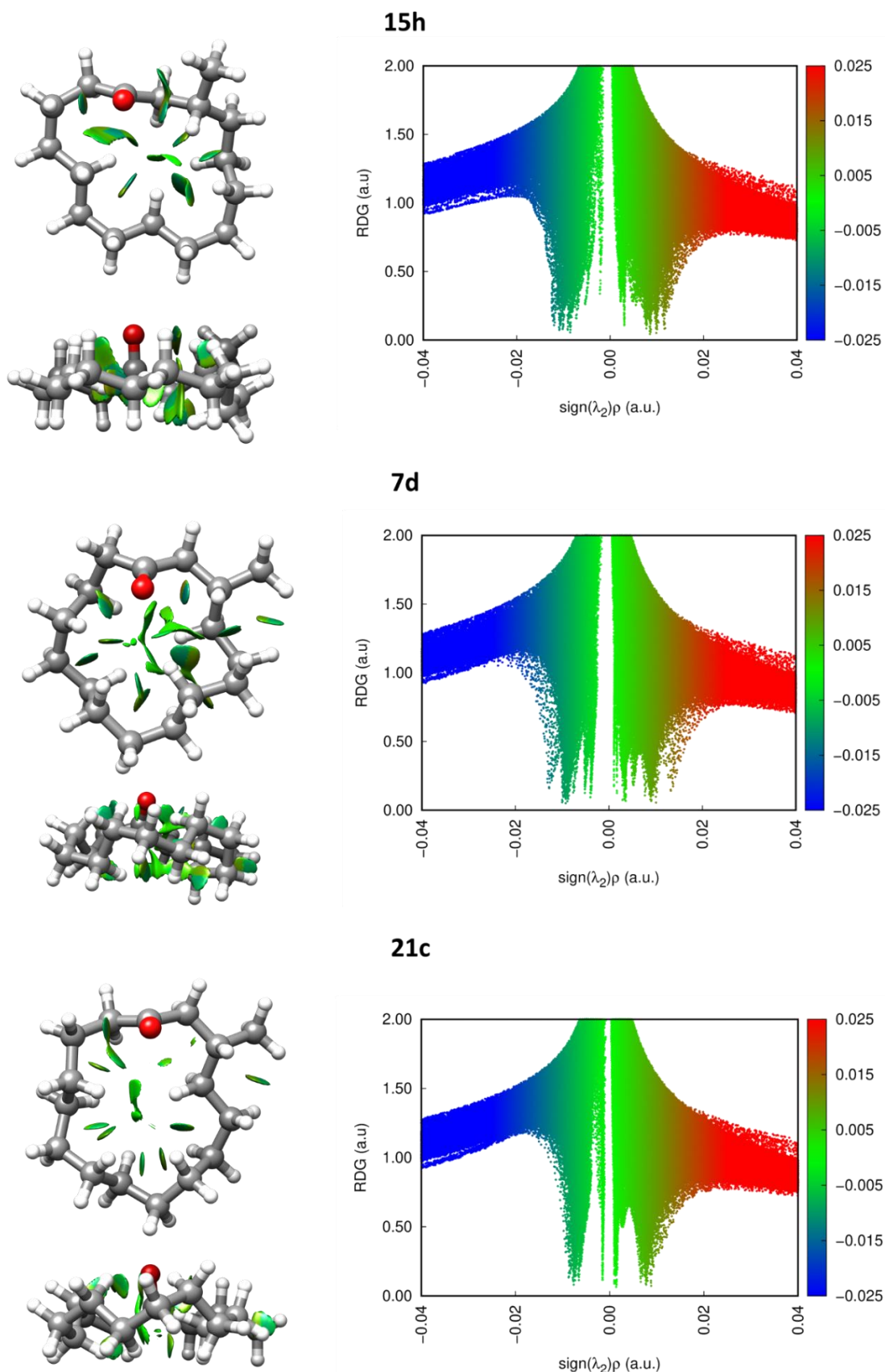


Figure 7.6 cont'd. The NCI and RDG plots of all assigned conformers of muscone with top and side views. NCI plotted with 0.5 isosurfaces.

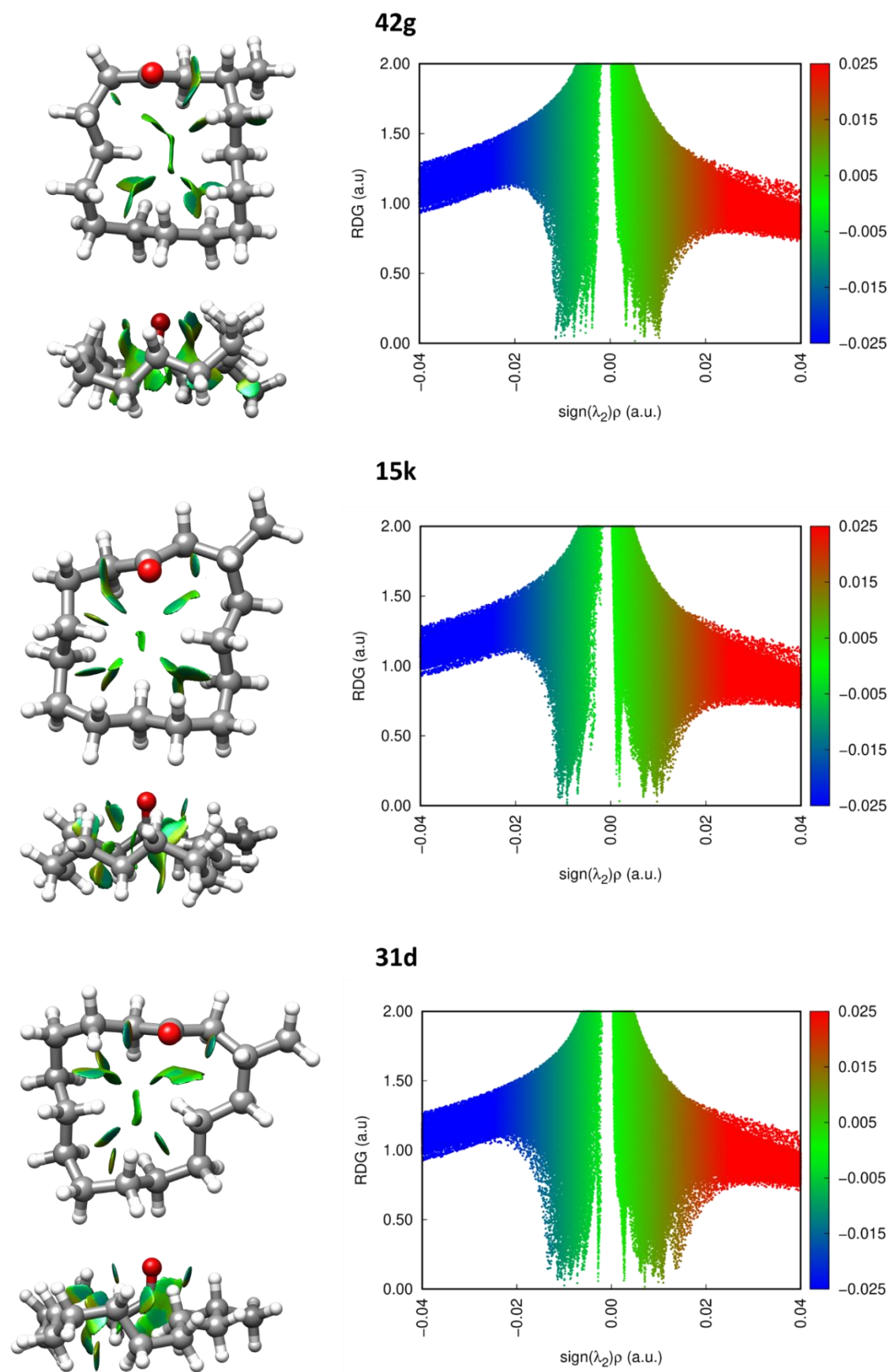


Figure 7.6 cont'd. The NCI and RDG plots of all assigned conformers of muscone with top and side views. NCI plotted with 0.5 isosurfaces.

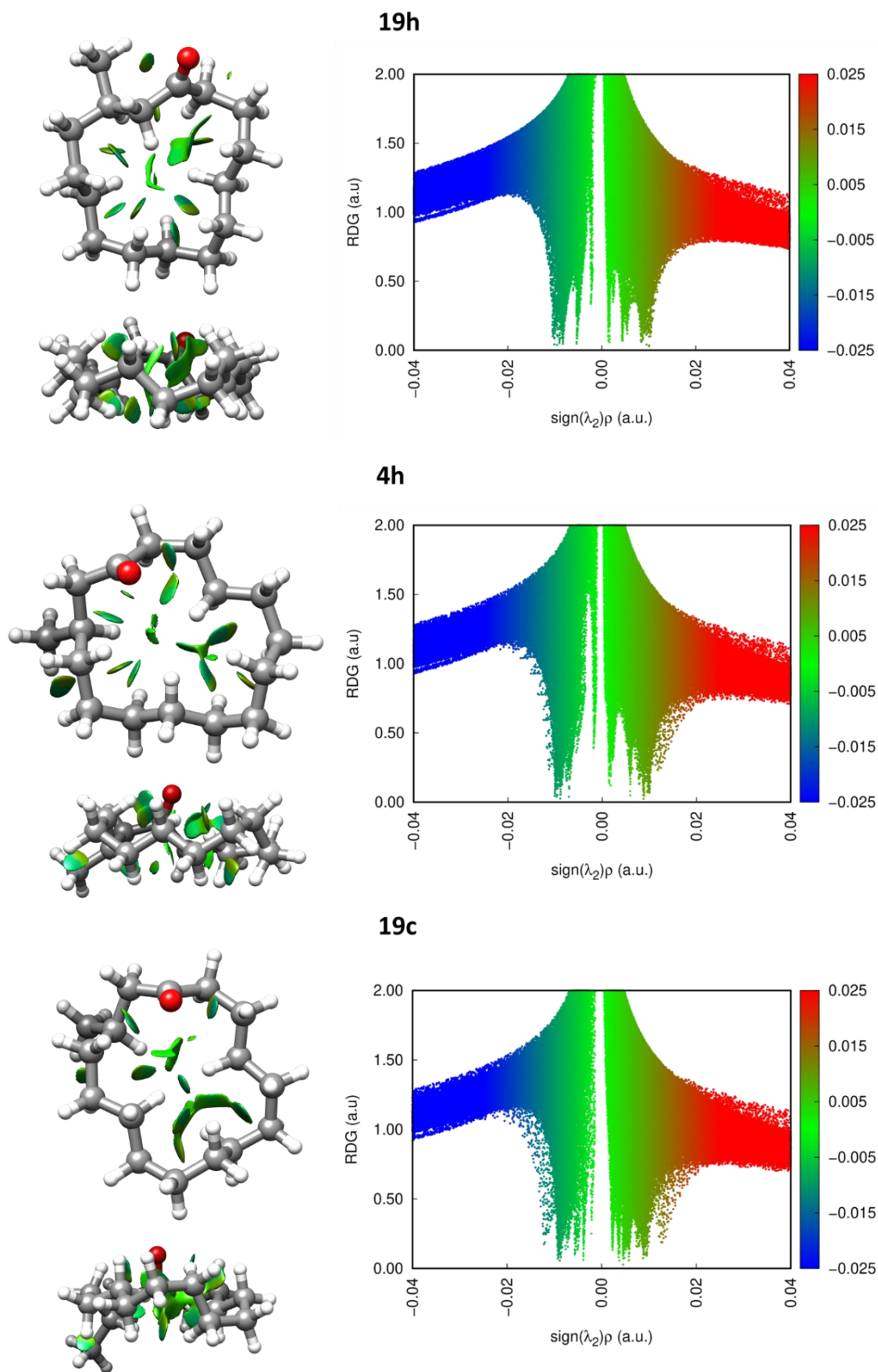


Figure 7.6 cont'd. The NCI and RDG plots of all assigned conformers of muscone with top and side views. NCI plotted with 0.5 isosurfaces.

7.5. Conclusions

Our results illustrate the large conformational space of muscone, one of the most exquisite odorants, with 30 conformations assigned in the broadband rotational spectrum. Comparing them we have identified common and distinct features to each of the conformers, which could be helpful in further studying and explaining the musk scent. Experimental observation of such vast number conformers is also useful for evaluation of the proposed musk olfactophore models. We have compared our most abundant conformations with olfactophore models below.

The first musk olfactophore model was developed in 1991 by Bersuker *et al.* by comparing 352 structure of musk odorants from the nitro-, polycyclic and macrocyclic classes. This model, with an accuracy of 54%, could predict musk scented odorants based on a few features. In order to smell musky an odorant had to have a pseudo-rectangular shape, with a shorter axis of 5-6 Å, compared to a longer axis of 6.2-7.2 Å. The second feature was the presence of a H-bonding acceptor such as -CO, -NO₂ or -CN groups along the shorter axis.²⁴⁻²⁶ Comparing our three most abundant conformers of muscone (Figure 7.7), **3f**, **13h** and **9i**, they fit well into this model, with all three conformers having their longer axes varying between 6.9 and 7.2 Å in length and the shorter axes between 5.7 and 6.2 Å. Conformer **3f** has a less rectangular and more square shape, which explains the smaller difference between the longer and shorter axes, and the relatively long shorter axis, outside the suggested range of 5-6 Å. The next most abundant conformers **1f**, **2l** and **8g**, do also fit well in the model, except for the longer axis of the **8g** conformer, that exceeds the proposed length due to the methyl group pointing away from the ring and the carbonyl moiety. Nevertheless, this model is very inaccurate, and more deviations are observed from the suggested dimensions in less abundant conformations of muscone.

In 1995, Kansey *et al.* evaluated and improved Bersuker's model to 65% accuracy by adding another hydrophobic moiety.²⁶ According to the newly suggested model the three hydrophobic moieties should be at 5.5, 6.5 and 8.0 Å distances from the H-bonding acceptor in order for a compound to have musky odour, similar to the positions of the methyl groups with respect to the oxygen in galaxolide.²⁶ Whilst these distances have been determined by also including macrocycles in the development of the model, such as pentadecane-15-lactone, none of the six most abundant conformations of muscone mentioned above satisfy the criterium of the hydrophobic moiety being at 8.0 Å from the carbonyl group (Figure 7.7). All the measured distances vary between 5.3 and 6.1 Å, with the exception of conformer **8g**. In conformer **8g** the carbonyl group points towards the centre of the cycle, making the distances between the H-bonding acceptor and the hydrophobic moieties shorter, ranging from 3.9 to 4.5 Å.

Due to the high potency of galaxolide as a musk odorant and its rigid structure, it became the structure of choice in further investigations of musk olfactophore model. Comparing all the four stereoisomers of galaxolide Kraft *et al.* determined in 2001 that the enantioselectivity of the methyl group in the 3rd position with respect to the oxygen is essential for the musk odour.^{20,26} Based on this additional feature a more complete musk olfactophore model was constructed, which presented the first potential interactions between a musk odorant and the binding pocket of the olfactory receptor. The model suggests that the H-bonding acceptor moiety has the role of an osmophore in the odorant, which is to insert the odorant in the binding pocket, hence forming stronger interactions with the pocket. The middle part of the odorant should be less bulky not to interfere with the insertion, whilst the spatial arrangement in the hydrophobic site is of less significance for the musky odour as it is situated just outside the binding pocket. Changing the chirality of the C7 in galaxolide reduced slightly the olfactory potential of the odorant.^{20,26} In the most abundant conformations of muscone, **3f**, **13h**, **9i**, **1f**, **2l** and **8g**, we cannot conclude a preferred position or orientation of the methyl group with respect to the carbonyl group, our H-bond acceptor. The orientation of the methyl group changes from being on the same side of the ring as C=O group where the two moieties form weak attractive interactions in conformers **3f** and **9i** to occupying a corner position in plane with the ring in **13h** to facing the other side of the ring in **1f** and **2l**.

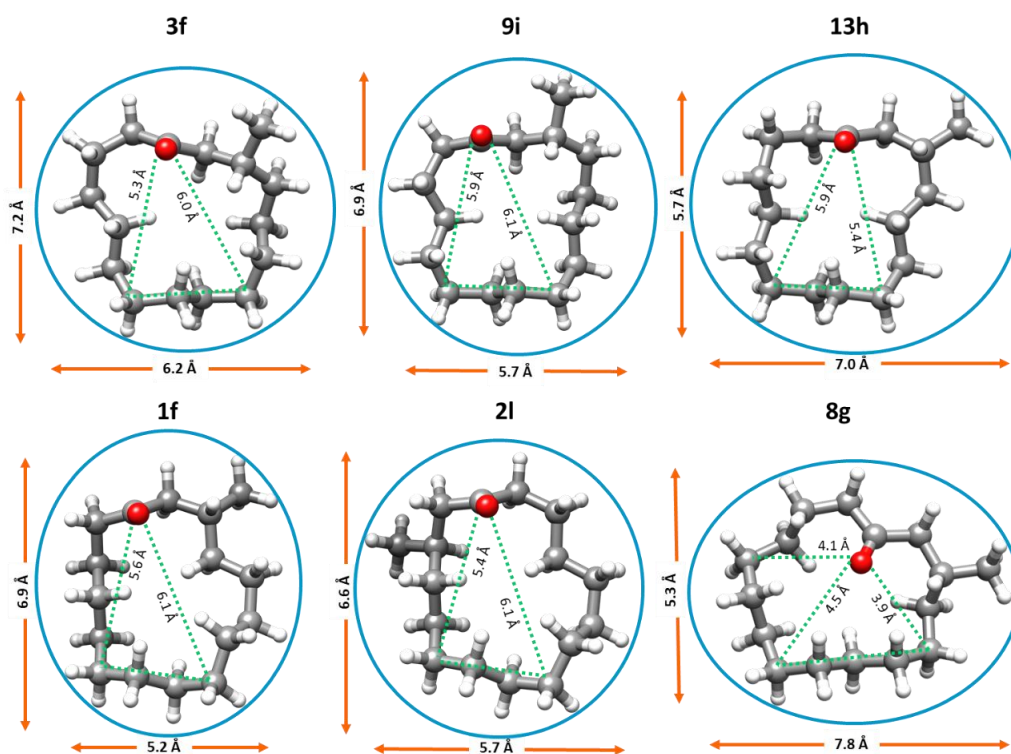


Figure 7.7. Comparison of the six most abundant conformations of muscone with Bersuiker's and Kansey's olfactophore models.

The most recent model developed by Zou *et al.* in 2012,²⁷ and further improved in 2016,²⁸ suggests that two hydrogen-bond acceptors separated by 6.96 Å and two aliphatic hydrophobes positioned at 7.51 Å are required for the musky scent. This model has been developed on alicyclic and cyclic musks comprising more than one hydrogen-bond acceptor. Muscone, with only one hydrogen-bond acceptor, could not be fully compared to it. Nevertheless, if we compare the distances for the hydrophobes, no agreement can be found. The variations in the conformations of muscone, including the shape of the ring, orientation of the methyl group and the carbonyl group, indicate that there is not a single preferred geometry. This most likely means that there is not a unique and rigid olfactophore that could describe the musk scent, especially given the structural diversity of these compounds.

The fact that the most abundant structures of muscone are so different supports the theory that olfaction is a more complex process than simply a lock-and-key interaction between an odorant and an olfactory receptor. The vibrational theory of olfaction, which was tested on muscone by Block *et al.* in 2015, has mostly been rejected as the possible mechanism of odorant recognition.²⁹ The study of muscone by broadband rotational spectroscopy not only has answered long-time challenging questions in relation to musk odorants, but also has shown the potential of the technique in the study of large conformationally flexible molecules, such as macrocyclic musks.

7.6. Bibliography

1. Sommer, C. The role of musk and musk compounds in the fragrance industry. *Handbook of Environmental Chemistry* **3**, 1–16 (2004).
2. Shen, J., Shi, Y. & Tian, W. Synthesis of (R)-(-)-muscone from (R)-5-bromo-4-methylpentanoate: A chiron approach. *Chinese Journal of Chemistry* **33**, 683–687 (2015).
3. Oppolzer, W. & Radinov, R. N. Synthesis of (R)-(-)-Muscone by an Asymmetrically Catalyzed Macrocyclization of an ω -Alkynal. *Journal of the American Chemical Society* **115**, 1593–1594 (1993).
4. Kamat, V. P., Hagiwara, H., Katsumi, T. & Hoshi, T. Ring Closing Metathesis Directed Synthesis of (R)-(+)-Muscone from (+)-Citronellal. **56**, 4397–4403 (2000).
5. Fujimoto, S., Yoshikawa, K., Itoh, M. & Kitahara, T. Synthesis of (R)- and (S)- Muscone. *Bioscience, Biotechnology and Biochemistry* **66**, 1389–1392 (2002).
6. Stork, G. & Macdonald, T. L. A Synthesis of d,l-Muscone from Cyclododecanone. *Journal of the American Chemical Society* **97**, 1264–1265 (1975).
7. Bernardinelli, G. & Gerdil, R. Structures cristallines et moléculaires des muscs macrocycliques') 111. La muscone et sa 2,4-dinitrophenylhydrazone. *Helvetica Chimica Acta* **4**, 1310–1317 (1982).

8. Callejo, R. *et al.* Fluorinated Musk Fragrances: The CF₂ Group as a Conformational Bias Influencing the Odour of Civetone and (R)-Muscone. *Chemistry - A European Journal* **22**, 8137–8151 (2016).
9. McAndrew, B. A. & Russell, S. W. Bicyclic analogues of exaltone (cyclopentadecanone) and muscone (3-methylcyclopentadecanone). *Journal of the Chemical Society, Perkin Transactions 1* **12**, 1172–1180 (1975).
10. Grimme, S., Antony, J., Ehrlich, S. & Krieg, H. A consistent and accurate ab initio parametrization of density functional dispersion correction (DFT-D) for the 94 elements H-Pu. *Journal of Chemical Physics* **132**, 154104 (2010).
11. Grimme, S., Ehrlich, S. & Goerigk, L. Effect of the damping function in dispersion corrected density functional theory. *Journal of Computational Chemistry* **32**, 1456–1465 (2011).
12. Møller, C. & Plesset, M. S. Note on an approximation treatment for many-electron systems. *Physical Review* **46**, 618–622 (1934).
13. Chai, J. da & Head-Gordon, M. Long-range corrected hybrid density functionals with damped atom-atom dispersion corrections. *Physical Chemistry Chemical Physics* **10**, 6615–6620 (2008).
14. Grimme, S. Semiempirical hybrid density functional with perturbative second-order correlation. *Journal of Chemical Physics* **124**, 034108 (2006).
15. Western, C. M. PGOPHER: A program for simulating rotational, vibrational and electronic spectra. *Journal of Quantitative Spectroscopy and Radiative Transfer* **186**, 221–242 (2017).
16. Seifert, N. A. *et al.* AUTOFIT, an automated fitting tool for broadband rotational spectra, and applications to 1-hexanal. *Journal of Molecular Spectroscopy* **312**, 13–21 (2015).
17. Watson, J. K. G. *Vibrational Spectra and Structure*. Elsevier Amsterdam **6**, 1–89 (1977).
18. Pickett, H. M. The fitting and prediction of vibration-rotation spectra with spin interactions. *Journal of Molecular Spectroscopy* **148**, 371–377 (1991).
19. Novick, S. E. A beginner's guide to Pickett's SPCAT/SPFIT. *Journal of Molecular Spectroscopy* **329**, 1–7 (2016).
20. Kraft, P. & Fráter, G. Enantioselectivity of the musk odor sensation. *Chirality* **13**, 388–394 (2001).
21. Pauling, L. *The Nature of the Chemical Bond and the Structure of Molecules and Crystals: An Introduction to Modern Structural Chemistry*. (Cornell University Press, 1960).
22. Bondi, A. Van der Waals volumes and radii. *Journal of Physical Chemistry* **68**, 441–451 (1964).
23. Johnson, E. R. *et al.* Revealing noncovalent interactions. *Journal of the American Chemical Society* **132**, 6498–6506 (2010).
24. Fráter, G., Bajgrowicz, J. A. & Kraft, P. Fragrance chemistry. *Tetrahedron* **54**, 7633–7703 (1998).
25. Bersuker, I., Dimoglo, A., Gorbachov, M. & Vlad, P. Origin of musk fragrance activity: the electron -topologic approach. *New Journal of Chemistry* **15**, 307–320 (1991).
26. Kraft, P. "Brain aided" musk design. *Chemistry and Biodiversity* **1**, 1957–1974 (2004).

27. Zou, Y. *et al.* Efficient macrocyclization by a novel oxy-oxonia-cope reaction: Synthesis and olfactory properties of new macrocyclic musks. *Chemistry - A European Journal* **18**, 7010–7015 (2012).
28. Liu, J. *et al.* Synthesis and Olfactory Properties of Silicon-Containing Analogs of Rosamusk, Romandolide, and Applelide: Insights into the Structural Parameters of Linear Alicyclic Musks. *European Journal of Organic Chemistry* **2016**, 976–982 (2016).
29. Vosshall, L. B. Laying a controversial smell theory to rest. *Proceedings of the National Academy of Sciences of the United States of America* **112**, 6525–6526 (2015).



**CIVETONE: THE
INFLUENCE OF A DOUBLE
BOND IN THE
CONFORMATIONS OF A
KETONE MACROCYCLE**

Chapter 8



8. CIVETONE: THE INFLUENCE OF A DOUBLE BOND IN THE CONFORMATIONS OF A KETONE MACROCYCLE

8.1. Introduction

Civetone (cycloheptadec-9-en-1-one) is 17-membered ring ketone with a double bond at position 9 (see Figure 8.1). It is a natural pheromone which was extracted from the male African civet for the first time.¹ The natural form of civetone is *cis*-civetone, although the non-natural isomer *trans*-civetone shares the same olfactory properties. In 1926 Ružička revealed civetone's structure and confirmed it by synthesis, demonstrating for the first time that macrocycles are stable and introducing the macrocyclic class of compounds.²⁻⁴ The olfactory properties of civetone, which can be described as musky, sweet, natural and animalistic, made it a desirable product for perfumers. However, because the African civet was protected for conservation and ethical reasons, civetone became scarce, which led to searching for synthetic alternatives.⁵⁻⁹ Whilst there are numerous ways to synthesise civetone, the available routes only work on low-scale synthesis and are not cost-efficient. Hence, structure-odour relationship in civetone has received attention along the years, with the aim of finding more optimal and affordable replacements.

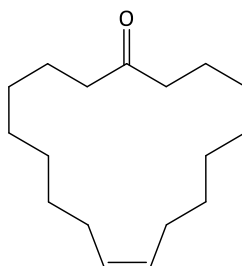


Figure 8.1. Molecular structure of civetone, *cis* double bond at position 9.

Civetone is a solid at room temperature, with a melting point of 31-32 °C. Nonetheless, its vast conformational flexibility due to the high number of single bonds in the ring has prevented its crystallisation and successful study by X-ray crystallography. No structural studies by other techniques are available either. Only civetone derivatives, where the insertion of bulky substituents on the ring allows crystallisation, have been reported.^{10,11}

In this chapter, we present the conformational investigation of natural *cis*-civetone using broadband rotational spectroscopy for the first time, without structural modifications or conformational constraints. We have identified 17 conformers of *cis*-civetone, estimated their relative abundances, and characterise the possible intramolecular interactions that drive conformational preferences.

8.2. Methods

Computational

Due to the large conformational flexibility of civetone several conformational searches were performed to map its potential energy surface (PES) in a thorough manner. A total of 8 searches using CREST¹² have been run using different structures as starting points, that were selected because they are low energy conformations quite different from each other. Optimizing the structures returned by CREST at B3LYP-D3BJ/6-311++G(d,p) level and further including zero-point corrections to their energies returned 35 conformers within 450 cm⁻¹. The final conformational search did not produce new conformations, indicating that the PES of civetone was appropriately mapped. The Gibbs free energies were also calculated. The predicted spectroscopic parameters of all species, including their rotational constants and dipole moments, and their energies, are presented in Table 8.1. The labelling for the conformers includes a number indicating the order of that structure in the conformational search and a letter signifying each conformational search. The structures marked with an asterisk have been used as starting structures in the conformational searches with CREST.

Experimental

The broadband rotational spectrum of civetone (Firmenich, >99%) was recorded using our CP-FTMW spectrometer at King's College London, which operates in the 2-8 GHz frequency range and has been previously described.^{13,14} Civetone was placed in our bespoke heating nozzle, heated to 437 K and seeded into the vacuum chamber using neon with a backing pressure of 5 bar. Molecular pulses of 1000 μ s duration were created. Once the supersonic jet is formed, the molecules were polarised by four microwave pulses of 4 μ s length, separated by 30 μ s. The chirped MW polarisation pulses were applied with a delay of 100 μ s with respect to the end of the molecular pulse. The molecular free induction decays (FIDs) were recorded for 20 μ s using a digital oscilloscope, starting 2.5 μ s after the end of the excitation pulse. The FIDs were recorded in the time domain and then converted to the frequency domain using a Fast Fourier transform algorithm. The final spectrum was recorded by accumulating *ca.* 2M FIDs.

Table 8.1. B3LYP-D3BJ/6-311++G(d,p) spectroscopic parameters of the conformers of civetone within 450 cm⁻¹.

B3LYP-D3BJ	8a*	1a*	6a*	12a*	6b*	20d*	20b	5a	12c	35b
A ^a (MHz)	470.0	482.7	519.1	545.5	555.0	501.7	420.4	561.3	507.7	484.3
B (MHz)	280.3	249.2	251.1	253.3	258.8	280.1	291.5	234.0	274.3	284.7
C (MHz)	192.3	178.6	187.6	189.5	198.6	202.2	187.0	178.9	202.0	201.2
P _c ^b (uÅ ²)	125.1	122.7	146.2	127.4	159.3	156.1	116.6	117.6	168.0	153.4
κ ^c	-0.37	-0.54	-0.62	-0.64	-0.66	-0.48	-0.10	-0.71	-0.53	-0.41
μ _a ^d (D)	1.9	0.2	-0.2	1.9	1.0	0.9	1.5	-0.3	-0.3	1.0
μ _b (D)	1.5	-0.2	-0.2	1.1	-1.3	0.6	-0.9	-0.7	-1.4	1.2
μ _c (D)	1.7	2.8	2.8	-1.6	2.3	2.3	-2.1	-2.6	-2.2	2.1
ΔE ^e (cm ⁻¹)	0.0	14.2	108.6	148.2	5.7	102.5	284.5	218.9	174.1	251.3
ΔE ₀ ^f (cm ⁻¹)	0.0	53.8	156.0	163.3	177.3	202.4	238.3	259.0	260.1	270.8
ΔG ^{437K} ^g (cm ⁻¹)	108.6	88.7	272.4	363.4	700.6	562.5	0.0	515.3	585.8	437.6
	4a	12d	3a	85a	2a	24c	67b	11a	7b	27b*
A (MHz)	439.5	538.5	480.4	365.0	461.7	387.2	401.9	478.3	517.4	405.4
B (MHz)	265.4	248.0	258.9	339.8	249.0	344.6	305.6	259.5	251.9	322.1
C (MHz)	179.6	188.4	182.7	188.4	174.5	207.5	187.7	185.1	185.4	210.0
P _c (uÅ ²)	120.1	146.9	118.9	94.7	114.0	168.1	109.4	136.9	128.6	165.6
κ	-0.34	-0.66	-0.49	0.71	-0.48	0.53	0.10	-0.49	-0.60	0.54
μ _a (D)	-0.4	-0.4	0.4	0.4	1.4	2.1	1.4	-0.8	0.6	1.1
μ _b (D)	-0.5	0.0	-0.5	3.1	-0.5	-1.3	-2.3	0.0	-0.1	-0.3
μ _c (D)	-2.7	2.8	-2.8	-0.5	-2.8	-1.8	-1.2	2.8	-2.8	2.4
ΔE (cm ⁻¹)	274.0	265.8	232.8	322.5	286.2	176.6	343.1	447.8	235.2	169.3
ΔE ₀ (cm ⁻¹)	275.7	277.0	294.5	303.1	303.8	332.5	334.3	336.9	341.5	343.7
ΔG ^{437K} (cm ⁻¹)	185.7	398.8	397.9	118.5	175.4	442.0	239.2	25.2	647.0	502.2
	17e	30a	10d	34a	14b	13a	34e	7a	38a	71a
A (MHz)	462.1	369.1	483.8	536.9	503.7	455.0	495.7	482.8	444.0	415.8
B (MHz)	280.4	343.4	248.7	247.1	254.6	267.0	298.5	257.7	315.4	306.8
C (MHz)	197.0	202.5	178.3	190.1	183.5	184.3	209.0	186.3	210.3	192.0
P _c (uÅ ²)	165.3	172.6	121.1	164.0	117.1	130.7	147.3	147.6	168.7	115.3
κ	-0.37	0.69	-0.54	-0.67	-0.56	-0.39	-0.38	-0.52	-0.10	0.03
μ _a (D)	0.6	-1.4	-1.5	-0.8	0.7	0.8	2.1	1.4	2.1	2.5
μ _b (D)	0.7	-1.4	0.3	-0.6	1.0	1.2	-1.6	-0.4	-1.9	-1.6
μ _c (D)	-2.6	-2.1	-2.7	2.6	2.5	-2.3	1.2	2.0	-1.0	1.0
ΔE (cm ⁻¹)	259.2	265.2	333.4	391.7	433.0	394.5	286.0	377.9	309.7	497.6
ΔE ₀ (cm ⁻¹)	343.9	372.4	406.5	408.7	412.0	412.4	422.5	422.9	424.5	433.0
ΔG ^{437K} (cm ⁻¹)	334.0	440.5	522.8	515.3	523.9	485.0	1036.1	482.4	555.1	139.4
	5b	9a	8b	49f	50f					
A (MHz)	505.7	451.3	483.4	476.7	383.6					
B (MHz)	243.9	268.1	257.7	260.4	352.5					
C (MHz)	178.0	188.1	183.8	184.8	206.8					
P _c (uÅ ²)	116.1	159.1	128.5	133.1	153.7					
κ	-0.60	-0.39	-0.51	-0.48	0.65					
μ _a (D)	0.1	2.7	-0.3	0.3	-2.0					
μ _b (D)	-0.3	0.0	-0.2	0.3	-2.2					
μ _c (D)	-2.8	1.3	2.9	2.7	1.0					
ΔE (cm ⁻¹)	463.4	405.9	347.4	498.2	359.4					
ΔE ₀ (cm ⁻¹)	442.5	442.9	444.0	447.1	447.5					
ΔG ^{437K} (cm ⁻¹)	393.5	325.0	661.9	408.2	328.8					

[a] A, B, C are the rotational constants [b] P_c planar moment along the c inertial axis [c] Ray's asymmetry parameter [d] μ_a, μ_b and μ_c are the electric dipole moment components [e] Relative electronic energies [f] Relative electronic energies including the zero-point correction. [g] Relative Gibbs free energies at 437 K.

Table 8.2. *wB97XD/6-311++G(d,p)* spectroscopic parameters of the conformers of civetone within 450 cm^{-1} .

wB97XD	6b	8a	6a	1a	12d	12a	5a	12c	7b	20d
A^a (MHz)	568.8	475.2	536.1	498.2	558.0	573.3	571.9	517.6	539.4	508.1
B (MHz)	258.8	282.4	249.7	247.3	246.3	249.2	234.1	274.1	249.7	281.8
C (MHz)	200.3	194.9	189.0	179.4	189.7	191.1	179.9	203.9	186.8	205.1
P_c^b ($\text{u}\text{\AA}^2$)	159.1	130.0	146.3	120.5	146.7	132.5	116.6	170.8	127.7	162.0
κ^c	-0.68	-0.38	-0.65	-0.57	-0.69	-0.70	-0.72	-0.55	-0.64	-0.49
μ_a^d (D)	-1.0	-1.9	0.1	-0.1	0.5	1.7	0.2	-0.3	-0.8	0.8
μ_b (D)	1.2	-1.5	0.2	0.1	0.0	-0.9	0.6	-1.3	-0.1	0.6
μ_c (D)	2.3	1.7	2.8	2.8	2.8	1.8	-2.7	-2.3	2.8	2.4
ΔE^e (cm^{-1})	0.0	199.2	153.5	217.5	298.7	317.2	275.1	294.1	276.7	179.9
ΔE_0^f (cm^{-1})	0.0	70.9	97.9	156.3	159.8	163.1	196.2	201.3	221.2	229.1
ΔG^{437Kg} (cm^{-1})	543.6	366.5	466.2	311.7	523.7	469.2	476.3	513.4	582.9	738.8
	3a	27b	20b	24c	5b	2a	34a	7a	14b	17e
A (MHz)	502.9	413.7	439.5	396.3	518.8	476.7	554.6	501.3	512.9	481.6
B (MHz)	255.8	320.7	287.8	347.5	243.0	247.3	247.3	255.7	253.9	275.5
C (MHz)	184.4	211.7	190.3	214.1	179.2	175.5	193.1	188.3	184.3	197.5
P_c ($\text{u}\text{\AA}^2$)	120.0	205.1	125.1	184.5	116.8	112.0	168.8	150.3	116.8	162.5
κ	-0.55	0.08	-0.22	0.46	-0.62	-0.52	-0.70	-0.57	-0.58	-0.45
μ_a (D)	-0.5	-1.0	1.5	2.1	-0.2	-1.5	-0.7	1.6	-0.6	-0.4
μ_b (D)	-0.6	0.4	-0.8	-1.1	-0.4	-0.6	-0.8	0.4	-0.9	-0.6
μ_c (D)	2.8	2.5	-2.3	-1.9	2.8	2.8	2.5	-1.9	2.5	-2.7
ΔE (cm^{-1})	317.6	404.5	585.7	309.7	504.1	439.5	416.7	490.8	544.4	421.3
ΔE_0 (cm^{-1})	255.0	288.4	289.3	289.3	297.6	309.7	330.7	354.0	355.8	374.9
ΔG^{437K} (cm^{-1})	557.0	400.8	0.0	403.4	364.1	366.3	732.6	473.0	536.2	440.9
	35b	9a	49f	11a	10d	8b	38a	4a	30a	34e
A (MHz)	491.9	467.4	496.9	505.3	495.1	490.6	456.2	449.6	371.8	501.2
B (MHz)	284.2	266.3	255.9	256.7	247.9	258.1	313.9	264.9	345.5	299.7
C (MHz)	202.5	190.7	185.6	188.6	179.1	184.9	212.7	181.2	204.3	210.5
P_c ($\text{u}\text{\AA}^2$)	155.0	164.5	134.5	144.6	118.8	127.5	170.9	121.4	174.2	146.9
κ	-0.44	-0.45	-0.55	-0.57	-0.56	-0.52	-0.17	-0.38	0.69	-0.39
μ_a (D)	0.9	2.8	-0.1	-0.8	-1.6	-0.3	-2.1	0.4	1.3	-2.1
μ_b (D)	1.1	0.0	-0.4	0.2	-0.3	-0.2	-1.9	-0.5	1.5	-1.5
μ_c (D)	2.2	1.2	2.7	2.7	2.6	2.9	1.0	2.7	-2.2	-1.2
ΔE (cm^{-1})	441.9	500.3	641.3	584.8	440.9	487.8	598.5	564.6	514.8	424.7
ΔE_0 (cm^{-1})	379.9	397.2	405.1	411.3	418.3	437.2	454.3	463.7	471.9	488.3
ΔG^{437K} (cm^{-1})	719.4	398.8	221.4	458.5	693.5	712.4	1244.6	518.8	403.0	1269.9
	13a	50f	67b	85a	71a					
A (MHz)	464.0	394.2	404.6	367.5	420.9					
B (MHz)	265.9	350.2	306.7	341.9	306.7					
C (MHz)	185.1	210.6	188.7	189.9	193.3					
P_c ($\text{u}\text{\AA}^2$)	129.8	162.7	109.3	96.0	117.0					
κ	-0.42	0.52	0.09	0.71	0.00					
μ_a (D)	0.7	2.3	1.4	1.3	2.5					
μ_b (D)	1.2	-1.7	-2.3	2.9	-1.7					
μ_c (D)	-2.3	-1.2	-1.3	-0.6	1.0					
ΔE (cm^{-1})	587.1	587.4	736.7	826.5	927.3					
ΔE_0 (cm^{-1})	496.0	530.9	602.5	647.7	736.1					
ΔG^{437K} (cm^{-1})	673.8	603.3	694.0	473.2	568.4					

[a] A , B , C are the rotational constants [b] P_c planar moment along the c inertial axis [c] Ray's asymmetry parameter [d] μ_a , μ_b and μ_c are the electric dipole moment components [e] Relative electronic energies [f] Relative electronic energies including the zero-point correction. [g] Relative Gibbs free energies at 437 K.

Table 8.3. MP2/6-311++G(d,p) spectroscopic parameters of the conformers of civetone within 450 cm⁻¹.

MP2	24c	27b	8a	6b	34e	6a	1a	30a	20d	50f
A ^a (MHz)	395.2	395.3	472.7	559.8	507.1	523.6	484.6	372.6	505.8	391.8
B (MHz)	350.7	350.7	284.7	261.3	300.2	254.4	252.9	351.1	283.1	355.2
C (MHz)	213.6	213.6	194.7	200.7	211.8	190.3	180.9	206.9	190.1	210.6
P _c ^b (uÅ ²)	176.9	176.8	124.3	159.4	147.0	148.0	123.8	176.6	62.9	156.5
κ ^c	0.51	0.51	-0.35	-0.66	-0.40	-0.62	-0.53	0.74	-0.41	0.60
μ _a ^d (D)	1.9	-1.9	-1.8	1.0	-1.9	0.3	-0.3	1.3	-0.8	-1.8
μ _b (D)	-1.4	-0.4	1.4	1.3	-1.5	-0.3	-0.3	-1.3	0.6	-2.2
μ _c (D)	1.7	1.7	1.5	-2.1	-1.0	-2.5	-2.6	1.9	-2.2	0.9
ΔE ^e (cm ⁻¹)	0.0	0.0	96.9	101.9	129.5	150.5	177.5	205.2	207.5	220.4
	3a	38a	12d	7b	17e	12c	12a	8b	35b	10d
A (MHz)	485.0	450.3	542.7	523.0	461.4	513.8	556.3	481.6	485.3	483.7
B (MHz)	262.4	318.5	251.3	255.0	288.2	277.5	254.3	263.1	291.9	252.8
C (MHz)	185.4	212.5	191.2	188.1	201.4	205.8	191.5	186.3	207.3	180.6
P _c (uÅ ²)	121.1	165.4	149.5	130.7	169.8	174.6	128.4	128.8	167.4	122.8
κ	-0.49	-0.11	-0.66	-0.60	-0.33	-0.53	-0.66	-0.48	-0.39	-0.52
μ _a (D)	-0.2	1.9	-0.3	-0.5	-0.7	-0.3	1.8	0.0	0.9	-1.3
μ _b (D)	0.5	1.9	0.0	-0.1	-0.8	1.3	1.0	-0.3	1.1	0.4
μ _c (D)	-2.6	0.8	-2.6	-2.6	-2.4	2.0	-1.5	-2.7	1.9	-2.5
ΔE (cm ⁻¹)	234.5	260.1	279.9	290.2	291.4	300.8	318.5	351.1	392.0	401.4
	13a	5a	20b	34a	67b	2a	4a	7a	11a	9a
A (MHz)	458.2	565.3	429.0	541.1	406.0	464.9	443.9	487.3	485.9	453.9
B (MHz)	270.9	236.8	294.1	250.8	308.2	252.0	269.0	260.8	263.9	273.5
C (MHz)	186.8	180.9	190.1	193.3	189.8	176.6	182.4	188.9	189.4	192.3
P _c (uÅ ²)	131.5	117.3	119.0	167.3	110.9	115.4	123.3	149.8	143.4	166.6
κ	-0.38	-0.71	-0.13	-0.67	0.10	-0.48	-0.34	-0.52	-0.50	-0.38
μ _a (D)	0.9	-0.4	1.5	0.6	-1.3	1.2	-0.5	1.2	-0.5	-2.5
μ _b (D)	1.1	-0.7	-0.9	0.6	-2.1	-0.5	-0.5	-0.4	0.1	0.0
μ _c (D)	-2.1	-2.4	-1.9	2.4	-1.2	-2.7	-2.5	-1.9	2.6	1.2
ΔE (cm ⁻¹)	417.3	444.0	449.5	450.7	458.7	472.7	485.5	496.8	516.0	530.8
	85a	49f	14b	5b	71a					
A (MHz)	371.0	480.9	509.6	507.1	420.1					
B (MHz)	342.8	264.4	257.5	247.4	312.9					
C (MHz)	191.8	187.8	186.0	180.3	195.4					
P _c (uÅ ²)	100.8	135.6	118.6	118.2	115.9					
κ	0.69	-0.48	-0.56	-0.59	0.05					
μ _a (D)	0.9	-0.4	0.7	0.0	-2.4					
μ _b (D)	-2.8	0.2	-1.0	0.3	1.4					
μ _c (D)	0.5	-2.4	-2.2	-2.6	0.8					
ΔE (cm ⁻¹)	542.8	558.6	601.5	628.6	754.6					

[a] A, B, C are the rotational constants [b] P_c planar moment along the c inertial axis [c] Ray's asymmetry parameter [d] μ_a, μ_b and μ_c are the electric dipole moment components [e] Relative electronic energies.

8.3. Spectral assignment

Similar to muscone, the rotational spectrum of civetone is very dense, which makes it challenging to identify patterns belonging to individual species. Nonetheless, a set of lines in the spectrum appeared more intense than the others (Figure 8.2). After a few fitting attempts using Pickett's program SPFIT,^{15,16} they were identified as *c*-type $J + 1 \leftarrow J$ transitions. Following an initial assignment and further predictions of additional transitions, a total of 102 transitions were measured and fit to the semi-rigid rotor Watson Hamiltonian in the A reduction and I' representation,¹⁷ using Pickett's program.¹⁶ Once the transitions belonging to this conformation were removed, many lines of similar intensity remained.

The theoretical predictions (Tables 8.1-8.3) indicated that most of the lower energy conformers have a predominant *c*-type dipole moment. Since the values of the rotational constants for some conformers were quite similar, we used the automated spectral fitting routine of the program PGOPHER¹⁸ for assignment. Once a possible assignment of a species was confirmed through fitting and measuring further transitions, its lines were removed from the spectrum to facilitate further searches.

Following this iterative procedure, sixteen additional conformations of civetone were identified. Most of the assigned rotamers have mainly *c*-type spectrum, although a few of them had predominantly *a*- and *b*-type spectra. Only two rotamers show no *c*-type spectrum. Transitions up to $J = 15$ have been measured for conformers with *c*-type spectrum, and up to $J = 18$ for those with *a*- and *b*-type spectra. The assigned transitions for each conformer were fit to the Watson Hamiltonian in the A reduction and I' (prolate tops) or III' (oblate tops) representation¹⁷ using Pickett's SPFIT/SPCAT programs.¹⁵ The experimental rotational and centrifugal distortion constants are presented in Table 8.4. The measured transitions of all rotamers are presented in Appendix V.

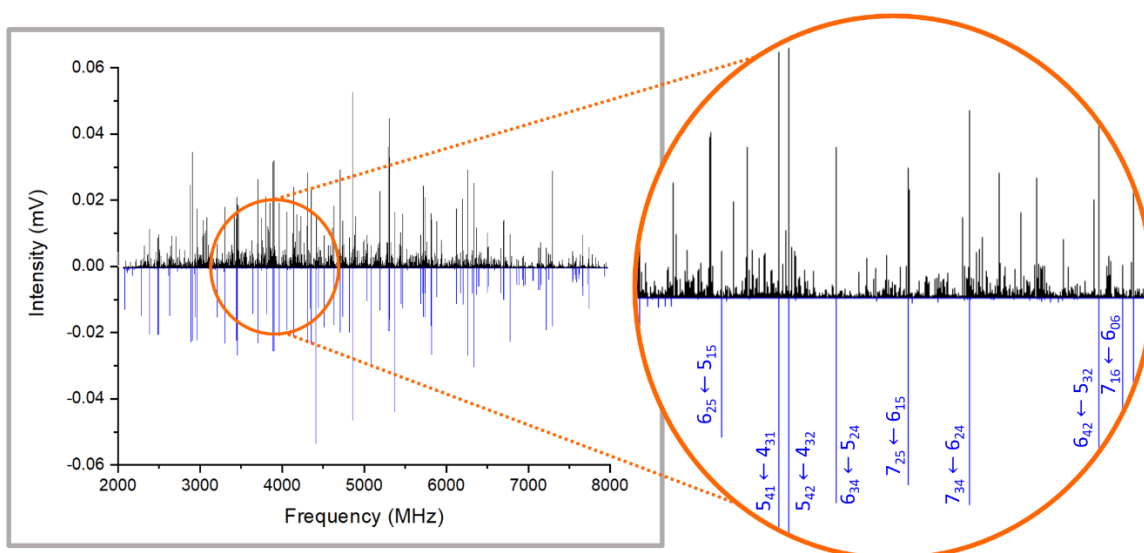


Figure 8.2. Experimental rotational spectrum of civetone (top trace, black) overlaid with the predicted spectrum of **1a** (low trace, blue) using its experimental parameters. The region 3800-4400 MHz has been enlarged to show the assignment.

Table 8.4. Experimental spectroscopic parameters of the observed rotamers of civetone.

	I – 5a	II – 6b	III – 12a	IV – 6a	V – 11a
A^a (MHz)	550.44076(41) ^g	543.33603(46)	535.77757(32)	509.02450(28)	487.20776(31)
B (MHz)	237.44267(32)	261.82656(47)	256.27025(19)	254.64257(22)	256.57711(21)
C (MHz)	179.67046(58)	198.62715(40)	189.41146(13)	188.08970(31)	186.26639(18)
Δ_J (kHz)	0.0108(16)	0.0086(27)	0.00628(65)	0.00515(12)	0.056(12)
Δ_{JK} (kHz)	-	-	-	0.0625(36)	0.0232(49)
Δ_K (kHz)	0.0655(73)	0.0615(92)	0.0729(73)	-	0.0301(52)
δ_J (kHz)	0.00328(89)	-	0.00257(32)	-	-
δ_K (kHz)	-	-	0.0295(80)	0.0391(67)	0.0175(50)
$a/b/c^b$ (D)	n/n/y	y/y/y	y/y/y	n/n/y	y/n/y
κ^c	-0.69	-0.63	-0.61	-0.59	-0.53
P_c^d ($\text{u}\text{\AA}^2$)	116.9	158.0	123.6	145.3	146.9
σ^e (kHz)	5.5	7.9	6.7	4.6	6.1
N^f	56	49	147	79	99
	VI – 10d	VII – 1a	VIII – 2a	IX – 3a	X – 20d
A (MHz)	474.61271(50)	474.49470(18)	458.59019(23)	472.17061(33)	493.17073(56)
B (MHz)	246.34171(43)	253.43748(13)	251.83169(12)	263.72769(25)	283.45660(48)
C (MHz)	173.45856(75)	179.61100(26)	175.42503(15)	183.93753(63)	202.36429(72)
Δ_J (kHz)	0.0067(17)	0.00783(50)	0.01033(49)	-0.00593(113)	0.0145(28)
Δ_{JK} (kHz)	-	0.0145(27)	-	-	0.0335(84)
Δ_K (kHz)	0.0583(72)	0.0393(38)	0.0385(32)	-0.0803(47)	-
δ_J (kHz)	-	-	-	-0.00223(85)	-
δ_K (kHz)	-	0.0332(22)	0.0476(44)	-0.0340(80)	-
$a/b/c$ (D)	n/n/y	n/n/y	y/n/y	n/n/y	n/n/y
κ	-0.52	-0.50	-0.46	-0.45	-0.44
P_c ($\text{u}\text{\AA}^2$)	101.4	122.7	114.0	119.5	155.1
σ (kHz)	6.7	3.2	6.2	5.6	7.9
N	57	102	108	89	49
	XI – 8a	XII – 4a	XIII – 20b	XIV – 67b	XV – 50f
A (MHz)	463.03763(17)	437.28440(28)	417.42565(30)	401.60779(26)	387.1395(41)
B (MHz)	283.888605(98)	268.79973(23)	294.77808(22)	307.29197(18)	350.8112(38)
C (MHz)	191.927069(75)	180.82629(45)	187.30184(19)	187.52384(12)	205.77135(30)
Δ_J (kHz)	0.00570(41)	0.0128(12)	0.0097(80)	0.01028(94)	0.00599(62)
Δ_{JK} (kHz)	0.0325(21)	0.0235(44)	-	0.0204(53)	-
Δ_K (kHz)	-	-	0.0469(49)	0.0252(53)	-
δ_J (kHz)	0.00180(20)	-	0.00452(48)	0.00398(46)	-
δ_K (kHz)	0.0217(20)	-	-0.0202(45)	0.0302(24)	-
$a/b/c$ (D)	y/y/y	n/n/y	y/n/y	y/y/y	y/y/n
κ	-0.32	-0.31	-0.07	0.12	0.61
P_c ($\text{u}\text{\AA}^2$)	119.2	120.5	113.5	104.0	145.0
σ (kHz)	6.0	4.6	6.8	6.6	9.2
N	308	59	110	228	97
	XVI – 30a	XVII – 85a			
A (MHz)	369.38116(26)	360.62514(14)			
B (MHz)	347.06836(25)	344.33975(13)			
C (MHz)	202.99427(27)	188.269401(98)			
Δ_J (kHz)	0.0311(15)	0.03562(79)			
Δ_{JK} (kHz)	0.0255(24)	-0.0441(27)			
Δ_K (kHz)	-	0.0098(20)			
δ_J (kHz)	-	-			
δ_K (kHz)	0.2784(21)	-0.233(13)			
$a/b/c$ (D)	y/y/y	n/y/n			
κ	0.73	0.81			
P_c ($\text{u}\text{\AA}^2$)	167.5	92.4			
σ (kHz)	6.6	5.4			
N	104	192			

[a] A , B and C are the rotational constants. Δ_J , Δ_{JK} , Δ_K , δ_J and δ_K are the quartic centrifugal distortion constants [b] a , b and c are the type of transitions observed [c] Ray's asymmetry parameter [d] Experimental P_c planar moment [e] σ is the rms deviation of the fit [f] N is the number of the fitted transitions [g] Standard error in parentheses in units of the last digit.

Considering the values of the experimental spectroscopic constants, we can group the observed species in several classes. We have a few rotamers, I-IV, that have high A rotational constants, with values over 500 MHz and Ray's asymmetry parameters closer to the prolate limit, between -0.69 and -0.59. Their assignment to theoretical structures was relatively straightforward. The most prolate rotamer in this class, rotamer I, was identified as conformer **5a**. This is the only conformer for which theoretical rotational constants, dipole moment components, κ , and P_c are consistent with the experimental ones. Rotamers II and III both have similar rotational constants and show *a*-, *b*- and *c*-type spectra, but they differ in their P_c values. This, and the difference in the intensity ratios of their *a*- and *c*-type transitions, allows their identification as **6b** and **12a**, respectively. **12a** has *a*- and *c*-type spectra of comparable intensity, while in **6b** *c*-type transitions are more intense than *a*-type transitions. Rotamer IV matches the rotational constants, κ , and P_c values of conformer **6a**. The assignment is confirmed by the observation of only *c*-type spectrum, consistent with the predicted dipole moments components. Conformer **7b**, with similar rotational constants, lies at higher relative energy and has a consistently lower P_c predicted by all theoretical methods.

A second class of rotamers comprises those prolate tops with κ between -0.53 and -0.31, and values of the rotational constant A between 430 and 500 MHz. The majority of the observed and predicted species of civetone fall in this category. The first rotamer in this class, rotamer V, has been assigned to conformer **11a**, based on the agreement with the rotational constants and the intensity ratio of its observed transitions. The assigned *a*-type transitions are approximately 10 times less intense than the *c*-type lines, in agreement with the predicted dipole moments of **11a**. Conformers **7a** and **8b** are also possible matches, however according to their predicted dipole moments **7a** would be expected to show a much stronger *a*-type spectrum, whilst **8b** would not be showing any *a*-type spectrum. The predicted P_c of **11a** at wB97XD and MP2 levels agree better with the experimental value for this rotamer, compared to the B3LYP-D3BJ value. **3a**, other possible match, has much lower values of P_c .

Rotamer VI was assigned as **10d**, as this conformation matched best the experimental constants. However, conformer **10d** is expected to show *a*-type spectrum and only *c*-type spectrum has been observed for this rotamer, which potentially could not be observed due to the low abundance and hence low intensity of this rotamer in the spectrum. The experimental value of P_c is also lower than the predicted one. Therefore, this is a tentative assignment. Rotamer VII has similar rotational constants, P_c and type of spectrum observed to rotamer IX. They can be assigned to **1a** and **3a**, respectively, based on the relative values of the predicted rotational constants, consistent among all theoretical methods. Rotamer X has been identified

as conformer **2a**, as it is the only one consistent with the observation of *a*- and *c*-type spectrum and the experimental P_c value.

Rotamers X-XII have a higher *B* rotational constant between 268 and 284 MHz. They can be discriminated by their rotational constants, P_c values, and type of spectrum. On this basis, rotamer X, XI and XII, can be identified as conformers **20d**, **8a** and **4a**, respectively. Rotamer X only shows *c*-type spectrum, which rules out conformers such **29f** and **45a** as they would predominantly show *a*-type transitions. **35b** could be a possible match for rotamer X, but it was discarded as it is consistently predicted to lie at higher energy. For rotamer XI, the observed *a*-, *b*- and *c*-type transitions were of comparable intensities indicating very similar dipole moment components, specific only to **8a**. Other predicted conformations with similar rotational constants are **17e**, **28a**, **64b**, **52f**, and **16a** but their P_c values are further away from the experimental one and their spectra will have a different ratio of intensities for the three types of transitions observed. Rotamer XII has a lower *A* rotational constant, and there are no other possible matches among the predicted conformers than **4a**.

Rotamers XIII and XIV are very asymmetric, with an asymmetry parameter close to zero. Their distinct rotational constants made their identification straightforward as **20b** and **67b**. Their assignment is supported by the agreement between predicted dipole moments and observed spectra. Conformer **20b** showed *a*- and *c*-type spectrum, with *c*-type being predominant. Conformer **67b** showed *a*-, *b*- and *c*-type spectra, with *b*-type being slightly more intense than the other two. There is also good agreement between predicted and experimental P_c values.

The final class of rotamers are those close to the oblate limit, with asymmetry parameters between 0.61 and 0.81. Three rotamers fall in this group, and all have *A*-*B* differences below 25 MHz. Rotamers XV could be assigned to **24c** or **50f**, considering its rotational constants. However, the experimental P_c value is lower than those predicted for these conformers, and we have only observed overlapped *a*- and *b*-type spectrum for this species. We have tentatively assigned it to **50f**, even if this conformer is predicted to lie at higher energy, as it has a closer P_c value to experiment and a lower predicted μ_c , which agrees better with our observations. Rotamer XVI is identified as **30a**, based on its rotational constants, P_c value, and the agreement between the observed spectrum and the predictions of the dipole moment components.

The assignment of rotamer XVII, the most oblate asymmetric top, to conformer **85a** clear due to the distinct set of rotational constants, P_c value, and the intense *b*-type spectrum, in agreement with the predicted μ_b dipole moment of 3.1 D.

The relative abundances of the assigned conformations have been calculated from common observed *c*-type transitions and their predicted μ_c dipole moments (Figure 8.3). Relative abundances of **85a** and **24c** have been estimated by measuring their corresponding *b*-type and *a*-type transitions with respect to conformer **8a**, for which all three *a*-, *b*- and *c*-type spectra have been observed.

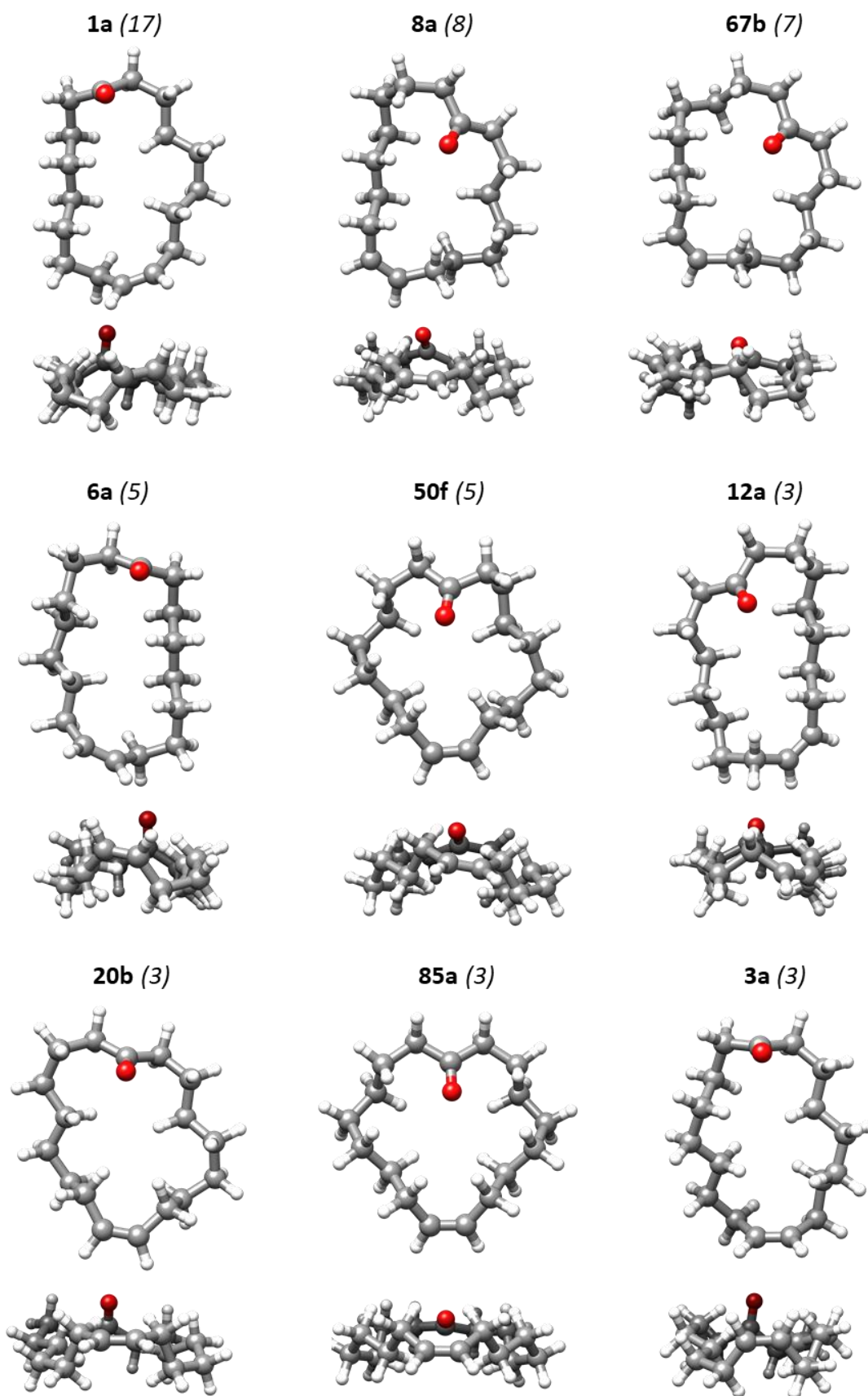


Figure 8.3. Top and side views of the identified conformations of civetone optimised at the B3LP-D3B/6-311++G(d,p) level of theory, in decreasing order of relative conformational abundance (in parentheses).

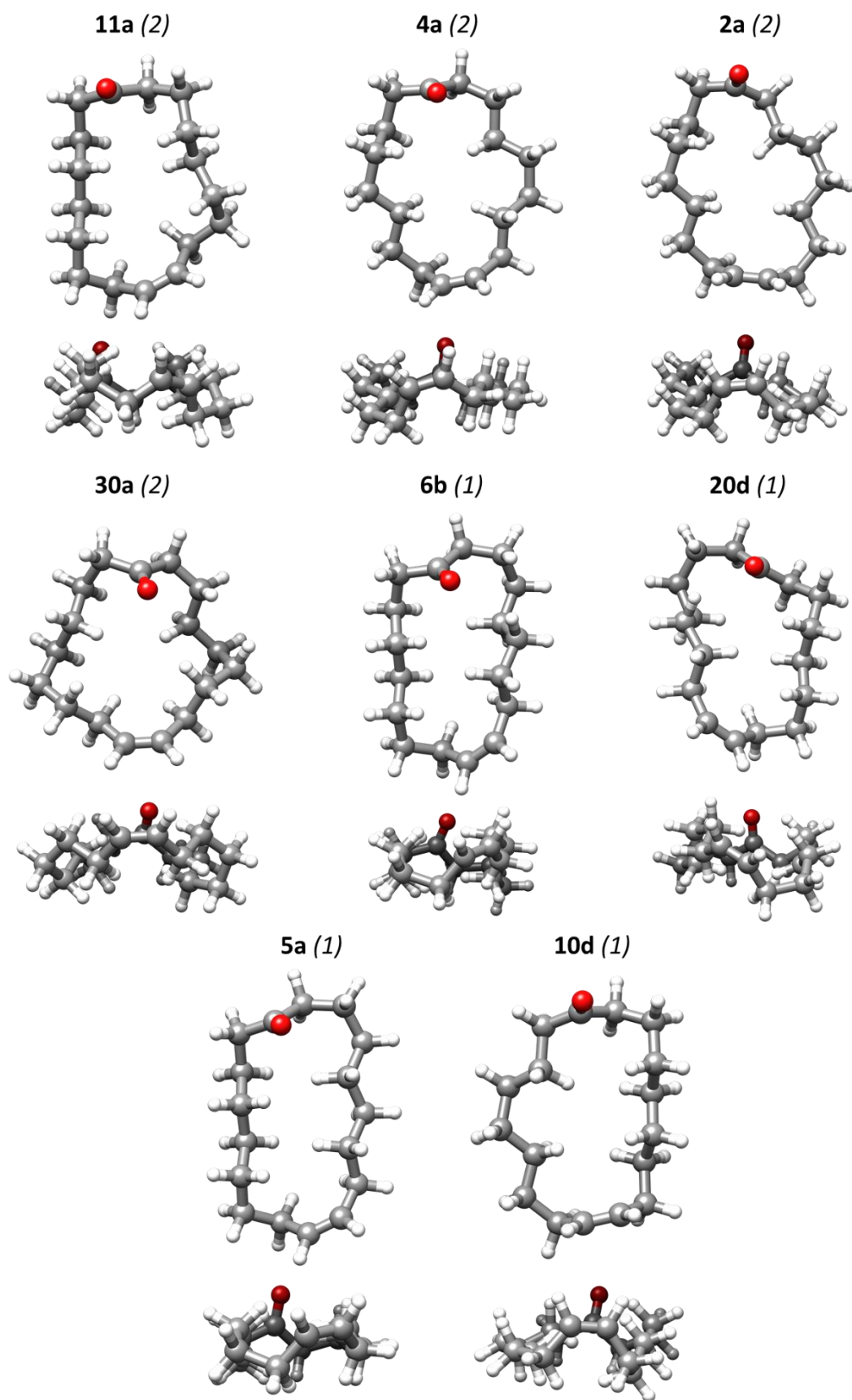


Figure 8.3 cont'd. Top and side views of the identified conformations of civetone optimised at the B3LP-D3B/6-311++G(d,p) level of theory, in decreasing order of relative conformational abundance (in parentheses).

8.4. Discussion

Theoretical benchmarking

The performance of three theoretical methods B3LYP-D3BJ, MP2 and wB97XD, all in combination with the 6-311++G(d,p) basis set has been benchmarked against experimental data.

The deviations between theoretical and experimental values of the rotational constants have been calculated as: $(A_{THEOR} - A_{EXP})/A_{EXP}$ (Table 8.5). The B3LYP-D3LYP percentage differences are the lowest with an average deviation of 1.0 %, with A rotational constants showing the largest differences and C rotational constants the smallest. The most significant deviations have been noted for C constants of **10d** and A constant of **6b**, with values of 2.8% and 2.2% respectively. The predicted rotational constants by wB96XD show much larger differences, up to 7.0% for the A constant of **12a**, and an overall deviation of 2.0% from the experimental rotational constants. MP2 performed slightly better than wB97XD, with an average deviation of 1.2%. Some of the largest discrepancies were noted for conformers **12a**, **24c**, **10d** and **6b**, which are higher than 3%. Therefore B3LYP-D3BJ is the method that better reproduces the experimental rotational constants.

Comparing the energy ordering predicted by the different methods, there are significant discrepancies. At B3LYP-D3BJ level the lowest-energy conformers are **8a** followed by **1a**, which are two of the most abundant ones. At wB97XD level, these two conformers are predicted to be 4th and 5th in order, with **6b**, **6a**, **20d**. as the most energetically favourable. The assigned 17 conformations at B3LYP level are predicted to be some of the lowest in energy, all within an energy window of 410 cm⁻¹ (zero-point corrected). The only conformations within this energy limit that have not been observed are **12c**, **35b**, **12d**, **7b**, **27b** and **17e**, which could be related to conformational relaxation.^{19,20} At wB97XD level of theory the assigned species are scattered in energies, with some of the assigned conformations, such as **67b** and **85a**, predicted to be higher than 700 cm⁻¹ with respect to the global minimum **6b**. At MP2 level of theory the global minimum is **24c**, and the assigned conformations are distributed up to 550 cm⁻¹ in energy.

Our results suggest that in highly flexible molecular systems, where the energy differences between the conformers are small, the computational methods used do not agree on the energy ordering. Of the methods employed, B3LYP-D3BJ/6-311++G(d,p) is the one that yields predictions closer to experimental observations.

Table 8.5. Experimental and predicted rotational constants by B3YP-D3BJ, wB97XD and MP2, including deviation from the experiment; calculated as $(A_{THEOR} - A_{EXP})/A_{EXP} \times 100\%$.

Conformer		B3YP-D3BJ		wB97XD		MP2	
8a	A	470.0	1.50%	475.2	2.63%	472.7	2.09%
	B	280.3	-1.26%	282.4	-0.52%	284.7	0.29%
	C	192.3	0.19%	194.9	1.55%	194.7	1.44%
1a	A	482.7	1.73%	498.2	5.00%	484.6	2.13%
	B	249.2	-1.67%	247.3	-2.42%	252.9	-0.21%
	C	178.6	-0.56%	179.4	-0.12%	180.9	0.72%
4a	A	439.5	0.51%	449.6	2.82%	443.9	1.51%
	B	265.4	-1.26%	264.9	-1.45%	269.0	0.07%
	C	179.6	-0.68%	181.2	0.21%	182.4	0.87%
6a	A	519.1	1.98%	536.1	5.32%	523.6	2.86%
	B	251.1	-1.39%	249.7	-1.94%	254.4	-0.10%
	C	187.6	-0.26%	189.0	0.48%	190.3	1.18%
12a	A	545.5	1.82%	573.3	7.01%	556.3	3.84%
	B	253.3	-1.16%	249.2	-2.76%	254.3	-0.77%
	C	189.5	0.05%	191.1	0.89%	191.5	1.10%
5a	A	561.3	1.97%	571.9	3.90%	565.3	2.70%
	B	234.0	-1.45%	234.1	-1.41%	236.8	-0.27%
	C	178.9	-0.43%	179.9	0.13%	180.9	0.68%
2a	A	461.7	0.68%	476.7	3.95%	464.9	1.38%
	B	249.0	-1.12%	247.3	-1.80%	252.0	0.07%
	C	174.5	-0.53%	175.5	0.04%	176.6	0.67%
3a	A	480.4	1.74%	502.9	6.51%	485.0	2.72%
	B	258.9	-1.83%	255.8	-3.01%	262.4	-0.50%
	C	182.7	-0.67%	184.4	0.25%	185.4	0.80%
20d	A	501.7	1.73%	508.1	3.02%	505.8	2.56%
	B	280.1	-1.19%	281.8	-0.59%	283.1	-0.13%
	C	202.2	0.06%	205.1	1.50%	190.1	-5.92%
11a	A	478.3	-1.83%	505.3	3.71%	485.9	-0.27%
	B	259.5	1.14%	256.7	0.05%	263.9	2.85%
	C	185.1	-0.63%	188.6	1.25%	189.4	1.68%
20b	A	420.4	0.71%	439.5	5.29%	429.0	2.77%
	B	291.5	-1.11%	287.8	-2.37%	294.1	-0.23%
	C	187.0	-0.16%	190.3	1.60%	190.1	1.49%
85a	A	365.0	1.21%	367.5	1.91%	371.0	2.88%
	B	339.8	-1.32%	341.9	-0.71%	342.8	-0.45%
	C	188.4	0.07%	189.9	0.87%	191.8	1.88%
67b	A	401.9	0.07%	404.6	0.75%	406.0	1.09%
	B	305.6	-0.55%	306.7	-0.19%	308.2	0.30%
	C	187.7	0.09%	188.7	0.63%	189.8	1.21%
30a	A	369.1	-0.08%	371.8	0.66%	372.6	0.87%
	B	343.4	-1.06%	345.5	-0.45%	351.1	1.16%
	C	202.5	-0.25%	204.3	0.63%	206.9	1.91%
50f	A	383.6	-0.91%	394.2	1.82%	391.8	1.20%
	B	352.5	0.48%	350.2	-0.17%	355.2	1.25%
	C	206.8	0.50%	210.6	2.35%	210.6	2.35%
10d	A	483.8	1.94%	495.1	4.32%	483.7	1.91%
	B	248.7	0.96%	247.9	0.63%	252.8	2.62%
	C	178.3	2.79%	179.1	3.25%	180.6	4.12%
6b	A	555.0	2.15%	568.8	4.69%	559.8	3.03%
	B	258.8	-1.16%	258.8	-1.16%	261.3	-0.20%
	C	198.6	-0.01%	200.3	0.84%	200.7	1.04%

Identified conformations of civetone

Civetone, with seventeen observed conformations, shows a less rich conformational landscape than muscone. This could be attributed to the double bond, which introduces some rigidity in the macrocycle. The double bond is located opposite the carbonyl group in all conformers and it is probably responsible for the overall preference for an elliptical shape in civetone.

Unlike muscone, civetone shows a strong preference for one conformation, **1a**, which is 17 times more abundant than the least abundant conformations **6b**, **20d**, **5a** and **10d** (Figure 8.3). **1a** has an elliptical shape with the carbonyl group and the double bond located in the shorter sides of the ellipsis. The C=O group in this configuration is perpendicular to the ring.

The second most abundant conformation is **8a**, with a conformational abundance of 8 to 1 compared to the least abundant ones. Structurally, it has a similar elliptical shape of the ring as the preferred conformation **1a**, but the position of the carbonyl group and double bond have changed, and they are no longer on the shorter sides of the ellipsis. The double bond occupies a corner position opposite to the carbonyl group and with the H atoms pointing to the opposite side of the plane of the ring. The carbonyl moiety is pointing towards the center of the ring forming an angle much more acute with the plane of the ring than the *ca.* 90° angle of **1a** (Figure 8.4). The third most abundant conformation is **67b**, with a relative abundance of 7 to 1. Here the macrocycle changes to a broader shape. The carbonyl group is in a very similar configuration as in **8a**, with the oxygen pointing towards the centre. The double bond is also in a similar configuration as in **8a**, opposite to the carbonyl group and with the H atoms pointing to the opposite side of the ring plane to the carbonyl oxygen.

The low-abundance conformers, **6b**, **11a**, **5a** and **10d** have very similar structures as the most abundant conformation **1a**, displaying an elliptical shape of the macrocycle, a carbonyl group perpendicular to the plane of the ring, and the H of the double bond on the same side of the plane as the carbonyl group.

Some of the experimentally detected conformers have more distorted structures than the most abundant ones, such as **20b**, **3a**, **4a**, **2a** and **30a**, but also symmetrical structures have been observed such as **85a** and less symmetrical **50f** where oxygen in carbonyl is oriented inwards the ring.

Non-covalent interactions

Considering the intramolecular interactions in the most abundant conformer of civetone, **1a**, it displays C=O \cdots H–C interactions with neighbouring hydrogens, at distances of 2.55 – 2.67 Å (Figure 8.4). Additionally, 1,4-H \cdots H interactions occur between the hydrogens in the plane above and below the cycle, as well as H \cdots H interactions across the ring. Two 1,4-H \cdots H interactions take place at distances shorter than the sum of the van der Waals radii of the H atoms^{21,22} and are expected to contribute to steric strain.

In conformers **8a** and **67b**, due to the position of the carbonyl group pointing into the ring, additional C=O \cdots H–C interactions are established with the hydrogens in the ring in comparison with conformer **1a**. However, **8a** and **67b** have a higher number of transannular C–H \cdots H–C and 1,4-H \cdots H interactions with respect to conformer **1a**, at distances varying between 2.11 – 2.40 Å, which may explain their lower abundance.

Considering the intramolecular interactions in the least abundant conformers **3a**, **5a**, **10d** (Figure 8.4), more transannular C–H \cdots H–C interactions are present compared to the higher-abundance species. These could lead to destabilisation of these conformers and explain their lower abundance. The C=O \cdots H–C interactions in this configurations are similar to **1a**.

The non-covalent interactions (NCIs) method was employed to visualise the intramolecular interactions involved in stabilizing the observed conformers.²⁵ We have calculated the NCI plots for all assigned conformers (Figure 8.5). The isosurfaces of all are coloured in green, which indicate weak attractive interactions. The larger green isosurfaces occur due to the transannular C–H \cdots H–C and 1,4-H \cdots H interactions, whilst large surfaces are also detected for C=O \cdots H–C interactions, specifically where the C=O group points towards the center of the ring. These include **8a**, **6a**, **12a**, **11a** configurations. The broader shaped conformers such as **67b**, **50f**, **20b**, **85a**, show larger green isosurfaces due to further transannular interactions between the oxygen oriented towards the center of the ring interacting with inner hydrogens, but also some smaller areas are located in the corners, where weak attractive interactions between the hydrogens occur.

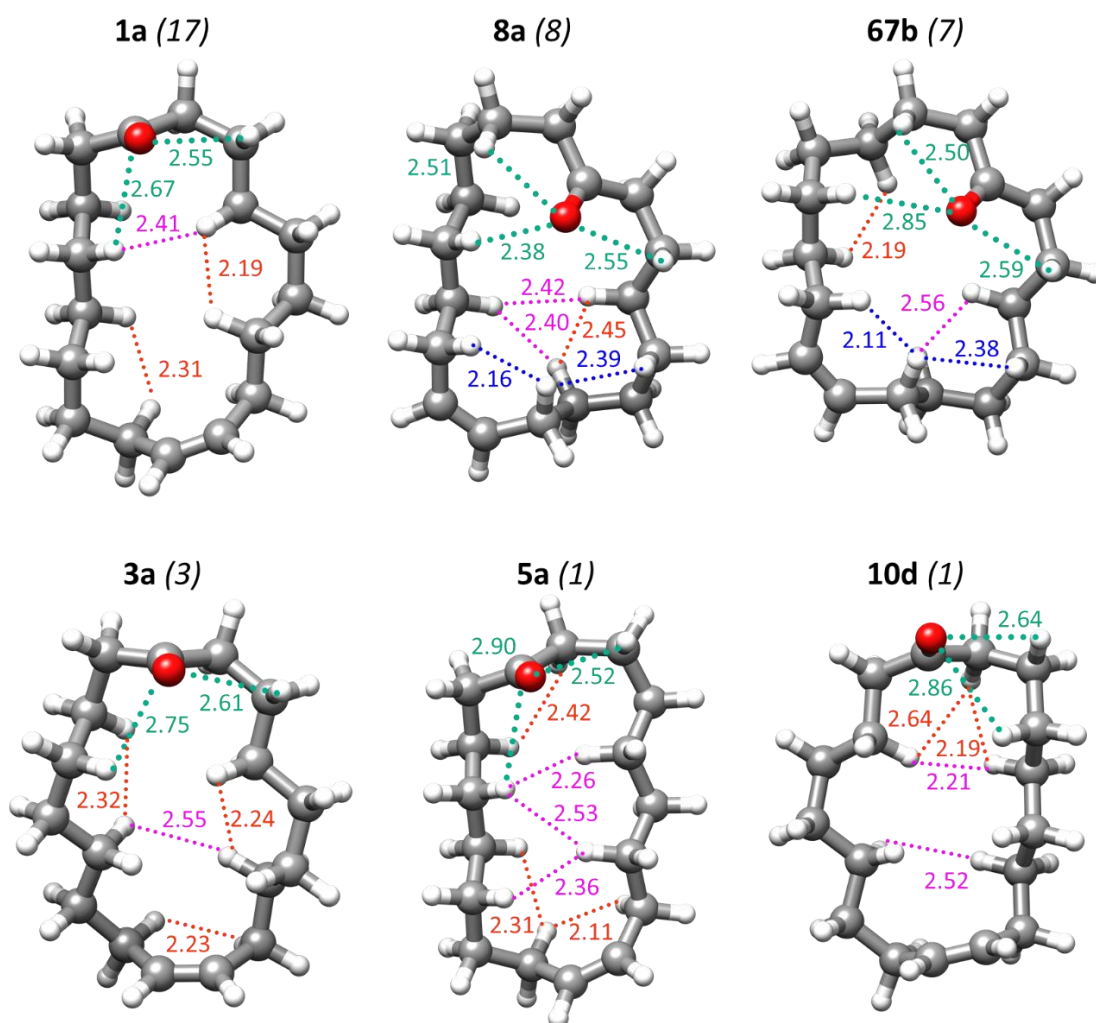


Figure 8.4. Intramolecular interactions in conformers of civetone with different abundances from high to low (indicated in parentheses), with C-H...O=C interactions depicted in green; 1,4-H...H interactions illustrated in orange (below the plane of the ring) and blue (above the plane of the ring); H...H interactions across the ring are shown in pink.

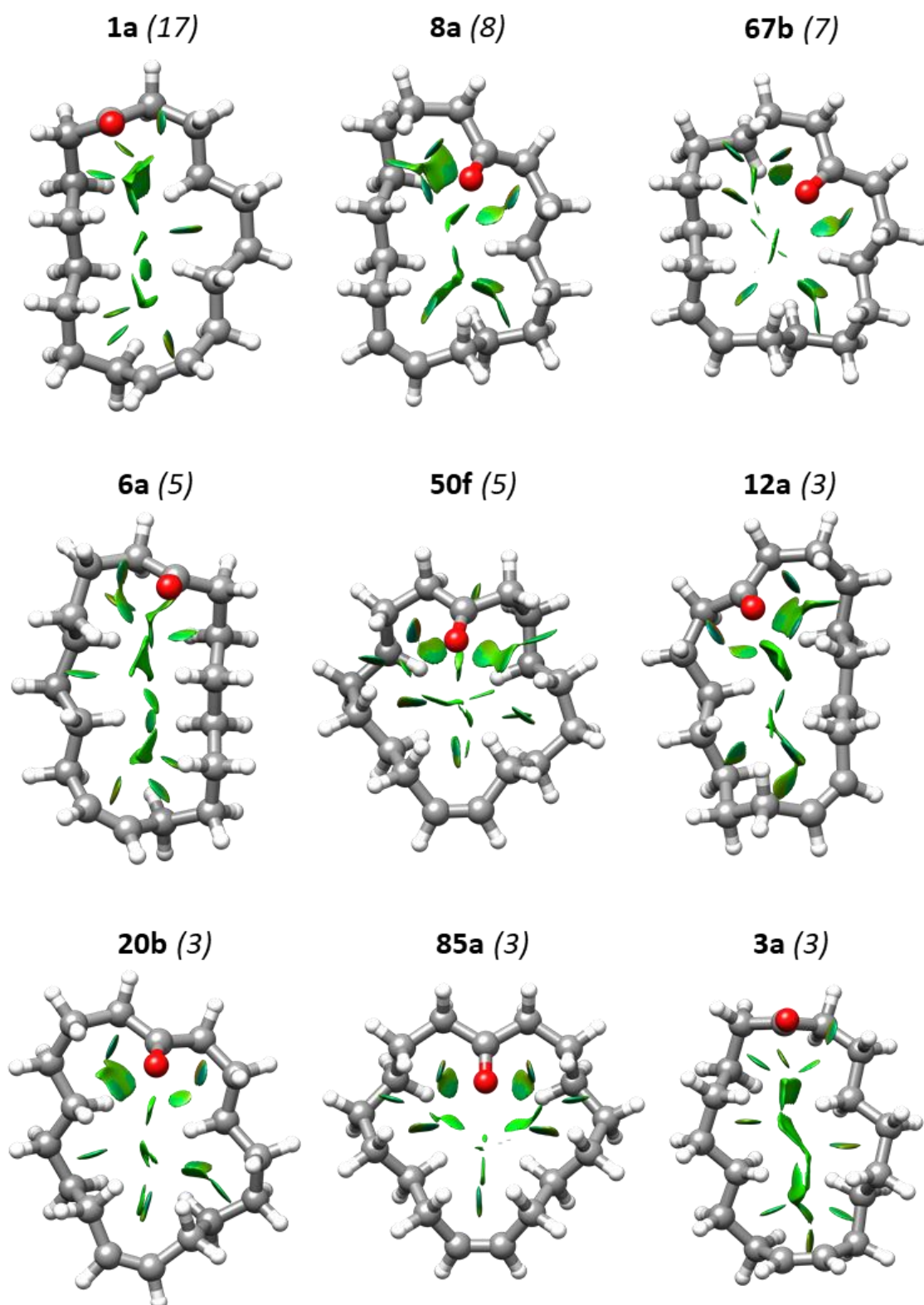


Figure 8.5. NCI plots of the 17 identified conformations of civetone plotted on the B3LYP-D3BJ/6-311++G(d,p) structures.

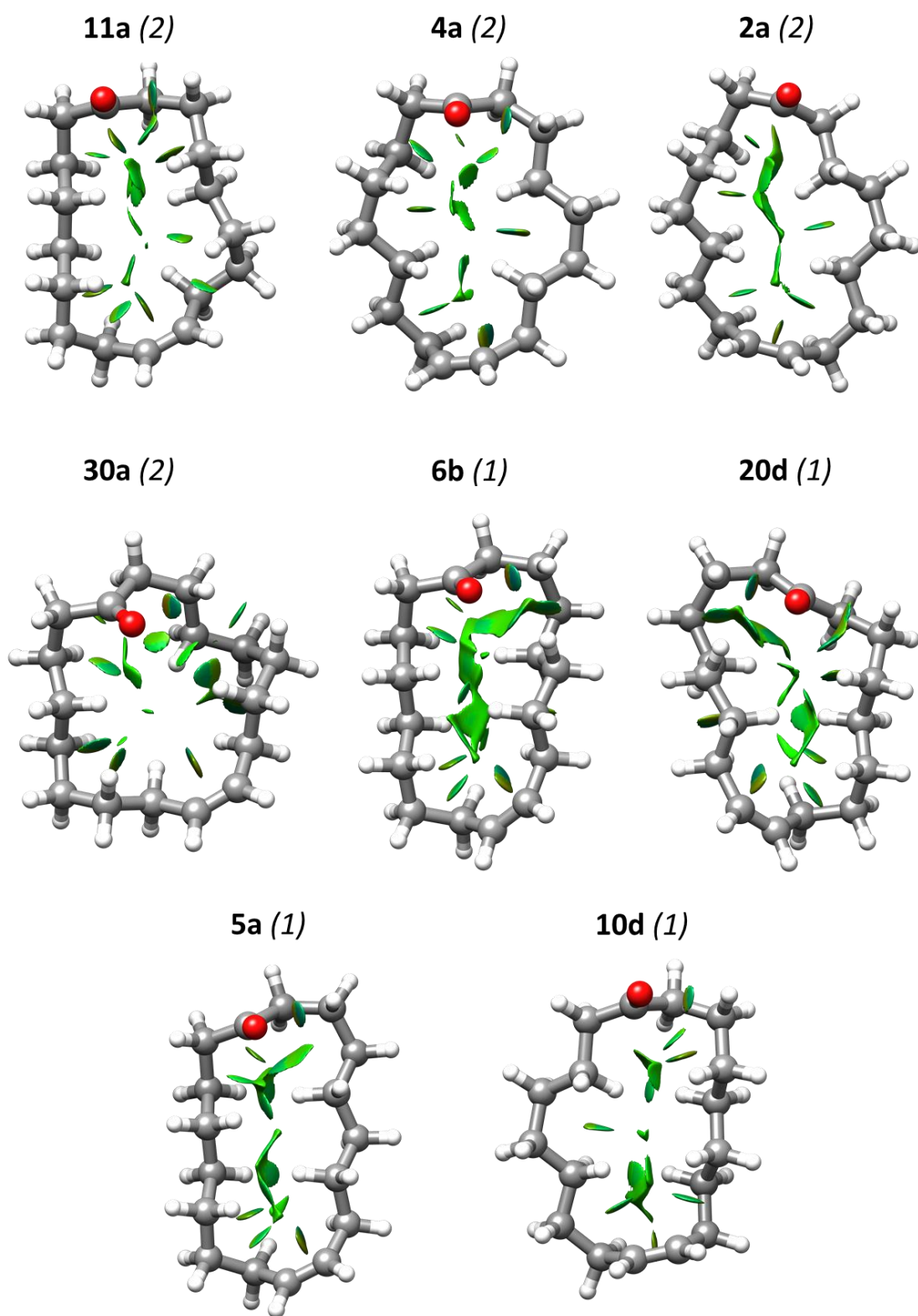


Figure 8.5 cont'd. NCI plots of the 17 identified conformations of civetone plotted on the B3LYP-D3BJ/6-311++G(d,p) structures.

Civetone within Bersuker's and Kansy's olfactophore models

The three most abundant conformations of civetone, **1a**, **8a** and **67b** have been compared with the two earlier olfactophore models: Bersuker's²⁶ and Kansy's,²⁷ as these are the only ones suggesting only one hydrogen-bond acceptor (HBA), Figure 8.3. Bersuker's model states that the vertical axis of the odorant should be 6.2-7.2 Å, and the horizontal one 5-6 Å, and that the hydrogen bond acceptor should be located at the end of the longer (vertical) axis in order for the compound to smell musky. None of the three most abundant conformers of civetone satisfy these three rules. **1a** and **8a** have a longer vertical axis, whilst **8a** and **67b** do not have the HBA at the end of the vertical axis.

According to Kansy's model²⁷ there should be three hydrophobic moieties at 5.5, 6.5 and 8.0 Å distances from the HBA. These dimensions are not noted in any of the three most abundant species (Figure 8.6). Lack of agreement between our findings in civetone with the suggested olfactophore models indicates their implausibility. The results revealed in the conformational study of civetone, together with the results for muscone, which also does not fit in the models (Chapter 7), call for further investigations using more up to date structural and conformational data on musks.

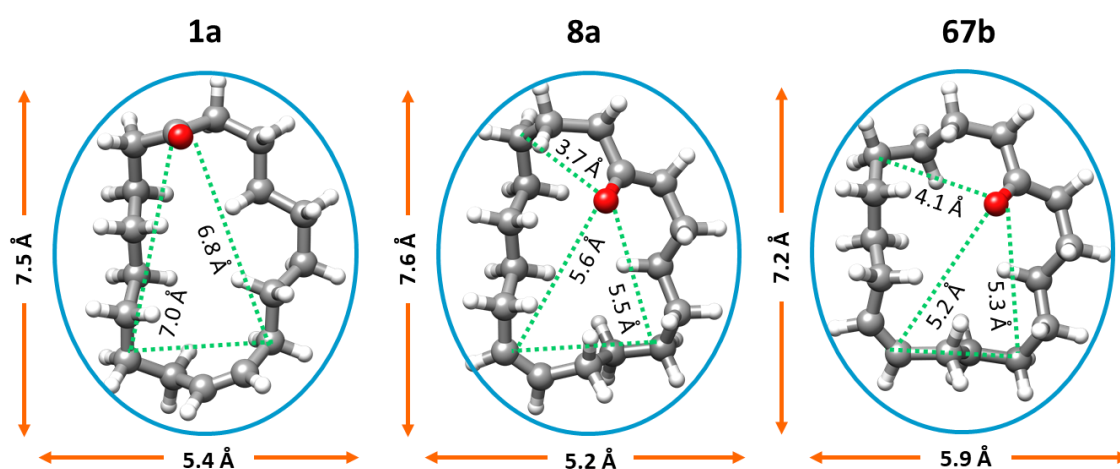


Figure 8.6. Comparison of **1a**, **8a** and **67b** with Bersuker's and Kansy's models. The blue frame indicates the elliptical shape suggested by both models. The orange axes are the vertical and horizontal axes measurements. The green dotted lines are the intramolecular distances between the C=O and the hydrophobic moieties.

8.5. Conclusions

Seventeen conformations of civetone have been observed in the broadband rotational spectrum, showing rich conformational landscape of this macrocyclic musk. The double bond introduces constraints in the arrangement of the ring and leads to a single conformation being favoured. The lower number of observed conformations in comparison with muscone also suggests that the double bond reduces the conformational flexibility of the macrocycle. Three computational methods have been evaluated against our experimental results. The B3LYP-D3BJ/6-311++G(d,p) level of theory performs is the best performing one at predicting the spectroscopic parameters of civetone.

The three most abundant conformations of civetone have been considered in the context of the Bersuiker's²⁶ and Kansy's²⁷ olfactophore models. No agreement between the molecular features of civetone conformers and those proposed to be conducive to musk smell have been found. This highlights that the existing olfactophore models are not accurate enough. Our experimental data could help understand the molecular requirements associated to musk smell and help develop improved olfactophore models.

8.6. Bibliography

1. Sack, E. Study of civet. *Chemiker Zeitung* (1915).
2. Ruzicka, L. Zur Kenntnis des Kohlenstoffringes VIII. Weitere Beiträge zur Konstitution des Muscons. *Helvetica Chimica Acta* **9**, 1008–1017 (1926).
3. Ruzicka, L. Zur Kenntnis des Kohlenstoffringes I. Über die Konstitution des Zibetons. *Helvetica Chimica Acta* **9**, 230–248 (1926).
4. Sommer, C. The role of musk and musk compounds in the fragrance industry. *Handbook of Environmental Chemistry* **3**, 1–16 (2004).
5. Winnik, M. A. Cyclization and the Conformation of Hydrocarbon Chains. *Chemical Reviews* **81**, 491–524 (1981).
6. Choo, Y. M., Ooi, K. E. & Ooi, I. H. Synthesis of civetone from palm oil products. *Journal of the American Oil Chemists' Society* **71**, 911–913 (1994).
7. Hamasaki, R., Funakoshi, S., Misaki, T. & Tanabe, Y. A highly efficient synthesis of civetone. *Tetrahedron* **56**, 7423–7425 (2000).
8. Tsuji, J. & Hashiguchi, S. Application of olefin metathesis to organic synthesis. Syntheses of civetone and macrolides. *Tetrahedron Letters* **21**, 2955–2958 (1980).
9. Fu, A. Ring closing alkyne metathesis : stereoselective synthesis of civetone. **606**, 75–78 (2000).

10. Bernardinelli, G. & Gerdil, R. Structures cristallines et moléculaires des muscs macrocycliques. I. La cis-civettone et les variétés polymorphes α et β de sa 2,4-dinitrophénylhydrazone. *Helvetica Chimica Acta* **65**, 558–572 (1982).
11. Bernardinelli, G. & Gerdil, R. Structures cristallines et moléculaires des muscs macrocycliques. II. La trans-civettone et sa 2,4-dinitrophénylhydrazone. *Helvetica Chimica Acta* **65**, 730–738 (1982).
12. Pracht, P., Bohle, F. & Grimme, S. Automated exploration of the low-energy chemical space with fast quantum chemical methods. *Physical Chemistry Chemical Physics* **22**, 7169–7192 (2020).
13. Loru, D., Bermúdez, M. A. & Sanz, M. E. Structure of fenchone by broadband rotational spectroscopy. *Journal of Chemical Physics* **145**, 07114311–8 (2016).
14. Loru, D., Peña, I. & Sanz, M. E. Ethanol dimer: Observation of three new conformers by broadband rotational spectroscopy. *Journal of Molecular Spectroscopy* **335**, 93–101 (2017).
15. Pickett, H. M. The fitting and prediction of vibration-rotation spectra with spin interactions. *Journal of Molecular Spectroscopy* **148**, 371–377 (1991).
16. Novick, S. E. A beginner's guide to Pickett's SPCAT/SPFIT. *Journal of Molecular Spectroscopy* **329**, 1–7 (2016).
17. Watson, J. K. G. Vibrational Spectra and Structure. *Elsevier Amsterdam* **6**, 1–89 (1977).
18. Western, C. M. PGOPHER: A program for simulating rotational, vibrational and electronic spectra. *Journal of Quantitative Spectroscopy and Radiative Transfer* **186**, 221–242 (2017).
19. Ruoff, R. S., Klots, T. D., Emilsson, T. & Gutowsky, H. S. Relaxation of conformers and isomers in seeded supersonic jets of inert gases. *The Journal of Chemical Physics* **93**, 3142–3150 (1990).
20. Zwier, T. S. Laser spectroscopy of jet-cooled biomolecules and their water-containing clusters: Water bridges and molecular conformation. *Journal of Physical Chemistry A* **105**, 8827–8839 (2001).
21. Pauling, L. *The Nature of the Chemical Bond and the Structure of Molecules and Crystals: An Introduction to Modern Structural Chemistry*. (Cornell University Press, 1960).
22. Bondi, A. Van der Waals volumes and radii. *Journal of Physical Chemistry* **68**, 441–451 (1964).
23. Kraft, P. & Fráter, G. Enantioselectivity of the musk odor sensation. *Chirality* **13**, 388–394 (2001).
24. Liu, M. T., Na, M., Li, Y., Biscoe, M. R. & Ryan, K. Conformational Sensing by a Mammalian Olfactory Receptor. *Chemistry - A European Journal* **26**, 11462–11469 (2020).
25. Johnson, E. R. *et al.* Revealing noncovalent interactions. *Journal of the American Chemical Society* **132**, 6498–6506 (2010).
26. Bersuker, I., Dimoglo, A., Gorbachov, M. & Vlad, P. Origin of musk fragrance activity: the electron -topologic approach. *New Journal of Chemistry* **15**, 307–320 (1991).
27. Kraft, P. "Brain aided" musk design. *Chemistry and Biodiversity* **1**, 1957–1974 (2004).



THE PREFERRED CONFORMATIONS OF THE MACROCYCLIC LACTONE EXALTOLIDE

Chapter 9



9. THE PREFERRED CONFORMATIONS OF THE MACROCYCLIC LACTONE EXALTOLIDE

9.1. Introduction

Exaltolide, also known as cyclopentadecanolide, is a macrocyclic lactone occurring in small amounts in angelica root and the prototypical macrocyclic musk of plant origin. Nowadays, it is produced synthetically and widely used in perfumery, for its delicate animal, musky and sweet odour. Moreover, the strong fixative properties of this musk makes it a popular choice in different creations.

Exaltolide was isolated for the first time as the musk smelling compound from angelica root oil in 1927.¹ One year later Stoll and Ružička reproduced it synthetically and confirmed its structure as a macrocyclic lactone, naming it exaltolide.² Macrocyclic lactones generally have less complex synthesis compared to macrocyclic ketones, therefore exaltolide has received considerable attention over the years from the synthetic point of view.³⁻⁷ One of the most common synthesis route for exaltolide is by ring expansion of cyclotetradecanone,³ or from smaller rings such as cyclododecanone.⁸ Another synthesis route is the depolymerization of polyesters of 15-hydroxypentadecanoic acid.⁹

Similar to the other macrocyclic musks, exaltolide has not been studied structurally or conformationally. Exaltolide has been chosen to be investigated as a part of this thesis in order to analyse a 16-membered ring, between the sizes of muscone (15-membered ring) and civetone (17-membered ring), and compare the behaviour of the macrocycle with a functional change from ketone to lactone (Figure 9.1).

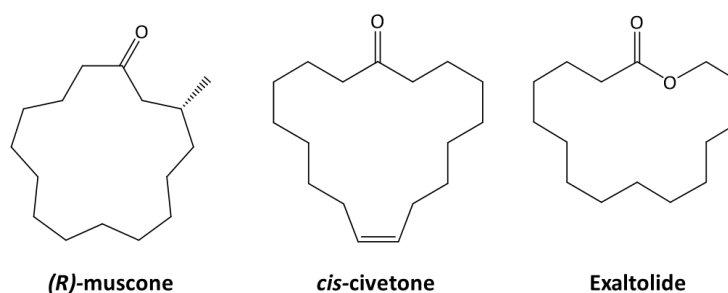


Figure 9.1. Structures of (R)-muscone, cis-civetone and exaltolide studied in this thesis.

We have employed broadband rotational spectroscopy in combination with quantum mechanical calculations to investigate the conformational landscape of exaltolide. The analysis of its rotational spectrum revealed nine conformers. Their conformational abundances have been estimated from the intensities of their spectra, and the identified conformers have been compared with those of the other two macrocycles presented in this thesis.

9.2. Methods

Theoretical

The potential energy surface (PES) of exaltolide was explored using the conformer sampling program Conformer – Rotamer Ensemble Sampling Tool (CREST).¹⁰ A total of ten conformational searches using CREST¹⁰ have been run using different structures as a starting point. The structures returned by CREST were optimized at B3LYP-D3BJ/6-311++G(d,p) level and their energies further corrected including their zero-point energies, to yield 30 conformers within 450 cm^{-1} . The final conformational search did not produce new conformations, indicating that the PES of exaltolide was appropriately mapped. The predicted spectroscopic parameters of all 30 species, including their rotational constants, dipole moment components, and their energies, are presented in Table 9.1. The labelling for the conformers comprises a number indicating the order of that structure in the conformational search and a letter signifying each conformational search. The structures marked with an asterisk (*) have been used as starting structures in the conformational searches with CREST. The obtained conformations of exaltolide have also been optimized at MP2 and wB97XD levels of theory with the 6-311++G(d,p) basis set, for benchmarking purposes. The zero-point energies at wB97XD level have been calculated, and the resulting spectroscopic parameters are presented in Tables 9.2-9.3.

Experimental

The broadband spectrum of exaltolide (Scientific Laboratory Supplies Ltd, $\geq 99\%$) was recorded using our CP-FTMW spectrometer at King's, which operates in the 2-8 GHz frequency range. Exaltolide, heated at 450 K in a bespoke nozzle, was seeded in neon at 5 bar and conducted to the vacuum chamber where the molecules expand adiabatically forming a supersonic jet. The molecular pulse was polarized by four chirped microwave pulses of 4 μs duration each. After each microwave pulse, the emission signal was collected as free induction decay (FID) for 20 μs into the oscilloscope. The final spectrum was obtained from adding up about 2.8 M FIDs. The time domain spectrum was converted to frequency domain using a fast Fourier transform algorithm.

Table 9.1. Spectroscopic parameters of the conformers of civetone within 450 cm^{-1} predicted at the B3LYP-D3BJ/6-311++G(d,p) level of theory.

B3LYP-D3BJ	2b*	6c*	21d*	49a*	53a*	3c*	7b*	3b*	1a	4e
A ^a (MHz)	438.2	417.0	429.2	414.4	434.5	523.8	513.5	543.1	501.9	602.1
B (MHz)	364.5	380.5	372.4	387.8	363.4	355.8	346.6	303.6	314.0	280.4
C (MHz)	219.1	216.5	217.8	222.2	226.7	239.8	232.8	211.0	210.0	209.8
P _c ^b (uÅ ²)	116.6	102.9	107.1	124.2	162.3	138.9	135.7	100.0	104.9	116.4
κ ^c	0.33	0.64	0.46	0.72	0.32	-0.18	-0.19	-0.44	-0.29	-0.64
μ _a ^d (D)	-1.0	-1.4	1.0	-0.9	-0.9	-1.2	-0.6	-1.4	1.3	-1.3
μ _b (D)	0.3	-0.2	0.7	0.3	0.7	-0.3	0.2	-0.1	0.4	0.4
μ _c (D)	1.3	-1.3	-1.4	-1.5	1.9	1.0	-1.4	1.2	1.4	1.6
ΔE ^e (cm ⁻¹)	0.0	113.8	186.7	161.0	151.5	40.5	117.3	254.5	326.3	300.4
ΔE ₀ ^f (cm ⁻¹)	0.0	25.5	62.3	67.4	78.1	82.5	83.0	184.1	230.0	237.0
ΔG ^{450K} _B (cm ⁻¹)	327.7	52.2	0.0	56.6	132.8	498.9	283.1	65.2	132.8	334.3
	4a	4b	37b*	13a	71e	60a	37a	6b	1c	69a
A (MHz)	497.7	488.2	436.7	473.1	508.5	414.3	459.0	449.2	552.4	514.9
B (MHz)	330.6	319.1	393.7	391.5	312.8	375.4	347.4	346.2	317.9	306.1
C (MHz)	217.4	207.5	231.6	249.7	215.5	217.3	219.1	212.3	227.7	206.1
P _c (uÅ ²)	109.7	91.7	129.4	167.6	132.2	120.2	124.6	102.2	142.6	90.2
κ	-0.19	-0.20	0.58	0.27	-0.34	0.61	0.07	0.13	-0.44	-0.35
μ _a (D)	-0.2	-0.2	1.1	-1.2	-1.4	0.2	-0.9	-0.7	0.5	2.1
μ _b (D)	-0.7	0.7	-0.5	-0.4	-0.8	0.9	0.4	0.7	-0.2	-0.1
μ _c (D)	1.5	1.5	1.3	-1.1	1.7	1.6	-1.5	1.5	1.6	-1.2
ΔE (cm ⁻¹)	260.3	383.6	238.3	277.1	477.3	495.2	418.3	429.5	365.5	487.1
ΔE ₀ (cm ⁻¹)	238.1	270.8	297.8	307.9	324.4	349.4	356.2	371.4	373.1	385.0
ΔG ^{450K} (cm ⁻¹)	397.0	217.1	720.3	475.8	167.2	199.1	605.3	354.0	527.8	481.5
	9a	7a	18a	26h	18d	7g	10c	42d	12b	29c
A (MHz)	473.2	469.4	482.5	471.1	494.3	425.4	475.0	435.7	471.8	438.1
B (MHz)	332.2	369.0	385.2	377.9	315.9	403.2	344.9	396.3	349.5	362.5
C (MHz)	212.6	232.4	241.9	238.8	210.1	233.3	221.6	234.4	224.0	218.4
P _c (uÅ ²)	106.1	135.8	135.1	146.9	108.4	137.6	124.3	139.6	130.5	116.9
κ	-0.08	0.15	0.19	0.20	-0.26	0.77	-0.03	0.61	0.01	0.31
μ _a (D)	-0.1	-0.6	-0.2	0.8	1.4	0.5	-0.1	0.8	-0.8	2.3
μ _b (D)	-0.6	-0.4	0.9	0.4	0.2	0.9	0.4	0.5	0.6	0.1
μ _c (D)	1.4	-1.3	-1.0	1.2	-1.6	1.4	-1.4	-1.3	1.5	-0.9
ΔE (cm ⁻¹)	459.3	365.2	354.8	388.2	493.2	371.5	479.0	424.8	466.3	490.7
ΔE ₀ (cm ⁻¹)	389.8	391.3	393.7	395.9	400.3	414.4	414.8	421.8	436.3	452.6
ΔG ^{450K} (cm ⁻¹)	388.3	710.0	634.1	621.3	429.7	527.2	646.6	659.1	373.5	259.0

[a] A, B, C are the rotational constants. [b] P_c planar moment along the c inertial axis. [c] Ray's asymmetry parameter [d] μ_a, μ_b and μ_c are the electric dipole moment components. [e] Relative electronic energies. [f] Relative electronic energies including the zero-point correction. [g] Relative Gibbs free energies at 450 K.

Table 9.2. Spectroscopic parameters of the conformers of civetone within 450 cm^{-1} predicted at the MP2/6-311++G(d,p) level of theory.

MP2	53a	2b	6c	3c	21d	37b	49a	7b	18a	13a
A^a (MHz)	440.7	447.1	430.2	533.4	436.2	442.1	416.5	518.3	492.2	465.0
B (MHz)	369.9	368.3	380.3	361.7	379.3	401.8	394.7	352.5	389.6	404.4
C (MHz)	231.3	223.2	219.9	242.5	222.2	236.4	225.0	236.7	245.7	254.5
P_c^b ($\text{u}\text{\AA}^2$)	164.0	119.1	102.7	130.3	108.3	131.6	123.8	136.8	133.5	175.4
κ^c	0.32	0.30	0.53	-0.18	0.47	0.61	0.77	-0.18	0.17	0.42
μ_a^d (D)	0.7	0.9	-1.2	-1.2	1.0	1.0	-0.8	-0.7	-0.1	-1.1
μ_b (D)	0.6	-0.3	0.3	-0.4	0.5	0.4	0.3	0.2	-0.9	0.3
μ_c (D)	-1.7	1.1	1.2	0.7	1.3	-1.2	-1.4	-1.2	0.9	-1.1
ΔE^e (cm^{-1})	0.0	29.4	51.6	81.1	87.8	100.1	143.3	150.6	183.0	276.8
	7g	26h	3b	4e	69a	10c	42d	12b	71e	4a
A (MHz)	434.6	485.0	561.0	618.2	518.9	478.6	444.1	477.6	515.1	504.3
B (MHz)	405.8	379.8	305.3	282.7	312.3	350.7	402.5	356.7	318.1	335.9
C (MHz)	236.7	242.9	215.2	213.5	210.1	224.7	239.7	228.4	219.6	220.8
P_c ($\text{u}\text{\AA}^2$)	136.6	146.0	103.9	119.0	93.4	123.9	142.6	131.1	134.3	108.9
κ	0.71	0.13	-0.48	-0.66	-0.34	-0.01	0.59	0.03	-0.33	-0.19
μ_a (D)	0.3	0.8	1.2	1.1	1.8	0.2	-0.7	0.5	-1.1	0.1
μ_b (D)	0.8	-0.5	-0.1	0.4	-0.1	-0.4	-0.4	0.6	0.7	0.6
μ_c (D)	-1.3	-0.9	-1.1	-1.5	-1.1	-1.3	-1.2	-1.3	-1.6	-1.3
ΔE (cm^{-1})	282.9	312.8	327.0	364.8	369.1	382.1	414.9	447.7	453.7	463.1
	37a	29c	18d	60a	1a	6b	7a	1c	4b	9a
A (MHz)	465.0	441.6	501.0	411.9	517.2	456.9	475.2	558.5	493.7	476.8
B (MHz)	351.6	368.4	321.3	384.2	315.5	352.3	374.5	321.1	322.5	339.4
C (MHz)	222.4	220.9	214.5	219.5	214.1	216.7	235.7	231.2	210.0	215.8
P_c ($\text{u}\text{\AA}^2$)	125.9	114.2	112.8	120.0	109.2	104.2	134.4	146.4	92.1	103.5
κ	0.07	0.34	-0.25	0.71	-0.33	0.13	0.16	-0.45	-0.21	-0.05
μ_a (D)	0.8	-2.1	1.1	0.0	-1.1	0.4	0.7	-0.5	0.1	0.3
μ_b (D)	-0.4	0.0	0.2	0.9	0.4	0.6	0.2	-0.2	0.6	-0.6
μ_c (D)	-1.3	-0.8	-1.5	-1.5	-1.2	-1.3	-1.1	-1.5	-1.3	-1.2
ΔE (cm^{-1})	467.9	474.2	486.2	503.4	509.3	512.3	513.1	549.4	673.2	729.6

[a] A , B , C are the rotational constants. [b] P_c planar moment along the c inertial axis. [c] Ray's asymmetry parameter [d] μ_a , μ_b and μ_c are the electric dipole moment components. [e] Relative electronic energies.

Table 9.3. Spectroscopic parameters of the conformers of civetone within 450 cm^{-1} predicted at the wB97XD/6-311++G(d,p) level of theory.

wB97XD	6c	3c	7b	2b	37b	21d	4a	49a	53a	4e
A^a (MHz)	423.2	532.2	520.2	442.6	439.9	430.2	507.6	416.5	439.1	634.9
B (MHz)	380.8	358.6	348.1	366.8	397.2	378.3	331.6	391.0	364.9	278.5
C (MHz)	218.2	241.7	235.1	221.0	233.7	220.1	219.4	223.8	228.2	212.5
P_c^b ($\text{u}\text{\AA}^2$)	102.6	134.0	136.8	116.4	129.3	107.3	108.1	123.9	160.6	116.2
κ^c	0.59	-0.20	-0.21	0.32	0.59	0.51	-0.22	0.74	0.30	-0.69
μ_a^d (D)	1.4	-1.3	0.6	1.0	1.1	0.9	0.0	0.9	0.9	1.4
μ_b (D)	-0.1	0.5	-0.2	0.3	0.6	-0.8	-0.6	-0.4	-0.7	0.4
μ_c (D)	1.4	-0.9	-1.4	-1.3	-1.4	1.5	1.5	-1.5	1.9	-1.6
ΔE^e (cm^{-1})	176.4	0.0	34.3	24.1	148.0	212.9	201.0	210.8	179.1	167.8
ΔE_0^f (cm^{-1})	0.0	10.5	17.1	24.4	164.4	165.5	183.7	186.8	190.1	210.7
$\Delta G^{450\text{K}}^g$ (cm^{-1})	0.0	375.5	435.2	497.1	627.7	340.0	525.9	366.3	394.0	820.8
	13a	42d	3b	18a	26h	7g	71e	1c	1a	4b
A (MHz)	472.6	441.4	574.7	491.3	490.1	435.9	521.7	563.4	524.8	500.4
B (MHz)	396.7	398.9	299.7	386.5	373.7	398.0	313.0	317.0	309.2	319.1
C (MHz)	252.4	237.0	214.2	244.3	241.3	234.3	217.9	230.3	211.7	209.5
P_c ($\text{u}\text{\AA}^2$)	170.5	139.7	103.1	133.8	144.6	136.1	132.0	148.4	105.1	90.7
κ	0.31	0.58	-0.53	0.15	0.06	0.62	-0.37	-0.48	-0.38	-0.25
μ_a (D)	-1.1	-0.8	1.4	0.2	0.9	-0.9	1.4	-0.4	1.4	-0.1
μ_b (D)	0.3	0.5	0.2	1.0	-0.5	0.8	0.8	-0.2	0.3	-0.6
μ_c (D)	1.2	1.4	1.2	1.0	-1.1	1.4	1.8	-1.7	1.3	-1.5
ΔE (cm^{-1})	241.4	353.4	284.5	200.5	301.6	289.9	541.6	385.3	464.2	442.2
ΔE_0 (cm^{-1})	213.5	247.7	266.2	277.0	304.0	310.3	331.6	363.9	364.5	367.4
$\Delta G^{450\text{K}}$ (cm^{-1})	491.8	384.7	450.6	804.6	661.1	499.5	235.3	597.4	266.7	614.7
	12b	29c	10c	69a	18d	37a	7a	6b	60a	9a
A (MHz)	480.8	440.9	478.6	519.5	502.7	462.2	475.7	458.1	416.7	481.1
B (MHz)	349.5	367.3	348.1	308.1	316.9	349.4	369.6	347.1	378.2	332.9
C (MHz)	226.1	220.8	223.5	207.7	211.9	220.6	234.1	214.7	218.9	214.5
P_c ($\text{u}\text{\AA}^2$)	131.0	116.7	123.3	90.0	107.5	124.5	135.5	102.7	120.2	106.2
κ	-0.03	0.33	-0.02	-0.36	-0.28	0.07	0.12	0.09	0.61	-0.11
μ_a (D)	0.8	2.3	-0.2	2.1	-1.4	0.9	-0.6	-0.6	-0.1	-0.1
μ_b (D)	0.6	0.1	-0.4	-0.1	0.2	-0.4	0.3	-0.7	-0.9	0.6
μ_c (D)	-1.5	-0.9	1.5	-1.2	1.6	-1.5	1.3	-1.5	1.6	-1.5
ΔE (cm^{-1})	425.3	379.6	418.0	385.9	543.1	542.1	419.5	521.2	551.2	585.0
ΔE_0 (cm^{-1})	383.4	424.7	426.2	429.1	430.2	438.9	449.7	467.9	473.6	487.5
$\Delta G^{450\text{K}}$ (cm^{-1})	466.2	427.8	840.8	830.1	477.8	751.7	765.1	601.6	599.6	512.0

[a] A , B , C are the rotational constants. [b] P_c planar moment along the c inertial axis. [c] Ray's asymmetry parameter [d] μ_a , μ_b and μ_c are the electric dipole moment components. [e] Relative electronic energies. [f] Relative electronic energies including the zero-point correction. [g] Relative Gibbs free energies at 450 K.

9.3. Results and discussion

Rotational spectrum

The rotational spectrum of exaltolide is dense and hence difficult to observe patterns arising from individual rotamers. Therefore, the automated assignment within the program PGOPHER¹¹ was used for the spectral analysis. Guided by the predicted rotational parameters, a first rotamer, showing α - and c -type transitions, was assigned in the spectrum. A total of 137 transitions were measured and fit to the semi-rigid rotor Hamiltonian of Watson in the A reduction and III^I representation,¹² using Pickett's program.¹³ Once measured, the transitions belonging to this conformation were removed to simplify the spectrum. The theoretical predictions (Tables 9.1-9.3) indicated that the low energy conformers have a predominant c -type dipole moment, whilst some species also present strong α -type dipole moment components. Using the automated method and focusing on α - and c -type transitions resulted in the identification and assignment of other eight rotamers in the spectrum, which were fit to the same reduction and representation for oblate rotamer as the first rotamer, whilst the prolate rotamers were fit to I^r representation (Table 9.4). The measured transitions are presented in Appendix VI.

The observed conformers of exaltolide can be divided into two main groups, corresponding to oblate and prolate asymmetric tops. Rotamers I and II, from the oblate group, have very similar rotational constants, but they can be discriminated from their very different P_c values and observed spectrum. Rotamer I shows similarly intense α - and c -type spectra while rotamer II displays intense c -type spectrum and lower intensity α -type. This led to the identification of rotamer I as **2b** and rotamer II as **53a**, which is also in agreement with their P_c values. Conformer **29c** could also match the experimental constants of rotamers I and II, but was discarded as it would predominantly have α -type spectrum.

Rotamer III is very close to the oblate limit, with a κ asymmetry parameter of 0.75. This, together with its rotational constants and P_c value, matches it to conformer **49a**. Conformer **7g** is also predicted to have a high κ asymmetry parameter closer to the oblate limit, but it lies at higher energy and the agreement between experimental and theoretical parameters is worse. Rotamer IV is also close to the oblate limit with a κ value of 0.66, and exhibits α - and c -type transitions of similar intensity. It has been assigned to conformer **6c** from the comparison of experimental and theoretical rotational constants, P_c value and dipole moment components. The final oblate rotamer observed in the spectrum, rotamer V, has a κ value of 0.49. It displays α - and c -type spectra with similar intensities, with c -type slightly more intense, which together with the agreement between the experimental and theoretical rotational constants led to its

assignment as conformer **21d**. The experimental P_c of 106.7981(20) $\mu\text{Å}$ also agrees with the theoretical values at all levels of theory.

The second group of rotamers are prolate asymmetric tops, with negative values of κ . Rotamers VI-VIII have their κ asymmetry parameters between -0.21 and -0.16, quite a distinct set of rotational constants and P_c values that allow their identification as **4b** (rotamer VI), **4a** (rotamer VII) and **7b** (rotamer VIII).

Rotamer IX is slightly closer to the prolate limit, with a κ of -0.46, and has both a - and c -type spectra with similar intensities. Its rotational constants and P_c value match those of conformer **3b**. The predicted μ_a and μ_c of 1.4 and 1.2 D, respectively, of conformer **3b** also support the assignment.

Table 9.4. Experimental spectroscopic parameters of the observed conformers of exaltolide.

	I - 2b	II - 53a	III - 49a	IV - 6c	V - 21d
A^a (MHz)	440.48679(20) ^g	437.61271(20)	414.93798(31)	417.99242(32)	430.23407(19)
B (MHz)	366.92610(18)	364.42327(21)	390.46830(33)	384.31125(27)	375.93251(20)
C (MHz)	220.63260(17)	227.67061(22)	222.862(12)	218.11613(17)	219.21551(17)
Δ_J (kHz)	0.0234(12)	0.02484(132)	0.0214(30)	0.0596(19)	0.0347(12)
Δ_{JK} (kHz)	-0.0200(13)	-0.02192(159)	0.073(15)	-0.1785(94)	-0.0325(137)
Δ_K (kHz)	-	-	-	0.1211(78)	-
δ_J (kHz)	-	-	-	-0.0039(12)	-
δ_K (kHz)	-0.0416(51)	-0.0478(70)	-0.715(77)	0.367(33)	-0.1006(74)
P_c^b ($\mu\text{Å}$)	117.0298(22)	160.9317(27)	122.2311(115)	103.5357(21)	106.7981(20)
κ^c	0.33	0.30	0.75	0.66	0.49
$a/b/c^d$ (D)	y/n/y	y/n/y	n/n/y	y/n/y	y/n/y
σ^e (kHz)	7.1	6.8	6.4	6.2	6.1
N^f	131	104	63	137	114
	VI - 4b	VII - 4a	VIII - 7b	IX - 3b	
A^a (MHz)	492.43142(31)	499.81442(31)	511.99091(30)	539.04191(38)	
B (MHz)	321.44465(29)	334.42234(41)	350.20549(45)	307.65446(24)	
C (MHz)	209.13039(53)	219.3716(12)	233.2615(14)	212.53520(20)	
Δ_J (kHz)	0.0101(17)	0.0248(24)	0.0222(28)	0.0105(12)	
Δ_{JK} (kHz)	0.0404(46)	-	-	0.0297(79)	
Δ_K (kHz)	-	-	-	0.104(11)	
δ_J (kHz)	-	-	-	0.00439(62)	
δ_K (kHz)	-	-	0.047(16)	0.0535(80)	
P_c^b ($\mu\text{Å}$)	90.9655(63)	109.2878(23)	131.8008(29)	101.1870(27)	
κ^c	-0.21	-0.18	-0.16	-0.42	
$a/b/c^d$ (D)	n/n/y	n/n/y	n/n/y	y/n/y	
σ^e (kHz)	4.7	6.4	6.0	6.6	
N^f	57	35	33	95	

[a] A , B and C are the rotational constants. Δ_J , Δ_{JK} , Δ_K , δ_J and δ_K are the quartic centrifugal distortion constants. [b] Experimental P_c planar moment. [c] Ray's asymmetry parameter. [d] a , b and c are the type of transitions observed. [e] σ is the rms deviation of the fit. [f] N is the number of the fitted transitions. [g] Standard error in parentheses in units of the last digit.

Conformational abundance and structural comparison

The relative abundances of the experimentally observed species (see Fig. 9.2) were calculated using common observed *c*-type transitions and the square of their predicted dipole moments from B3LYP-D3BJ calculations. The estimated relative abundances of the assigned conformers **6c** : **2b** : **49a** : **21d** : **53a** : **4b** : **7b** : **3b** : **4a** in the molecular jet is 4.2 : 2.3 : 2.0 : 1.6 : 1.6 : 1.2 : 1.1 : 1.1 : 1.0, respectively. There are no large differences in abundance between the conformers of exaltolide. The most abundant species is about 4 times more abundant than the least abundant. Exaltolide has a clear preference for oblate conformers: the five more abundant conformers are the five oblate ones.

The most abundant conformer is **6c**. Structurally this conformation adopts a trapezium-like shape with the ester moiety located in the middle of the longer side, with 5 bonds. It has the C=O group perpendicular to the rest of the ring, and it is relatively planar. The second most abundant conformer, with approximately half the abundance of **6c**, is **2b**. This conformer adopts a square configuration [4444], with each side formed of four bonds between the heavy atoms. In this structure the C=O group is also perpendicular to the plane of the molecule. **49a** is just slightly less abundant than **2b**, and has a very similar structure to the most abundant **6c**. The main difference is the ester group, that in **49a** has the CO group closer to the shorter side of the trapezium (with three C–C bonds) while in **6c** has the ethyl oxygen closer to the shorter side of the ring. This change re-accommodates all the carbons in the ring giving rise to **6c** and **49a** being almost specular images of each other, except for the arrangement of the lactone group, that faces opposite sides of the ring considering the same configuration of the carbon framework for **6c** and **49a**.

Conformer **21d**, with a relative conformational abundance slightly lower than **4a**, has a much more distorted structure. It is also a trapezium, but the lactone group, although still in the longer side, is now opposite the shorter side. This introduces some more strain in the cycle, and forces the carbonyl group to point out of the ring and the intra-annular hydrogens to come closer to each other. Conformer **53a** has the same relative abundance as **21d**, although structurally it is comparable to **2b**. It has the same square configuration [4444], but it differs in the position of the ester moiety, which now has the carbonyl group rather than the ethyl oxygen adjacent to a corner atom. Comparing **2b** and **53a** considering the side view, **2b** is more symmetrical having the CO group in the centre, while in **53a** is shifted to one side.

The four prolate conformations of exaltolide are very similar in abundance, ranging from 1.2-1.0. Their structures seem to be more elongated, and rectangular or having a distorted heart shape. In all conformers the carbon chains that form the sides of the ring adopt a zig-zag

configuration, but while in the oblate conformers the zig-zag happens above and below the plane of the ring, in three of the prolate conformers the zig-zag takes place mostly on the plane of the ring. This results in a different orientation of the hydrogen atoms, causing the hydrogens pointing inside the ring to be at shorter distances from each other, which would explain the lower abundance.

Conformers **4b** and **4a** have very similar structures. The main difference is the configuration of the lactone moiety and the arrangement of the carbon atoms opposite to it. In **4a**, some of the hydrogens are at shorter distances, which may result in its lower abundance (see section 9.3.3). Conformer **7b** has an elliptical shape and is the only conformer with the carbonyl group oriented towards the ring center. Conformer **3b** has the hydrocarbon ring arranged in a rectangular shape and the carbonyl group pointing out of the ring forming an obtuse angle with the plane of the ring.

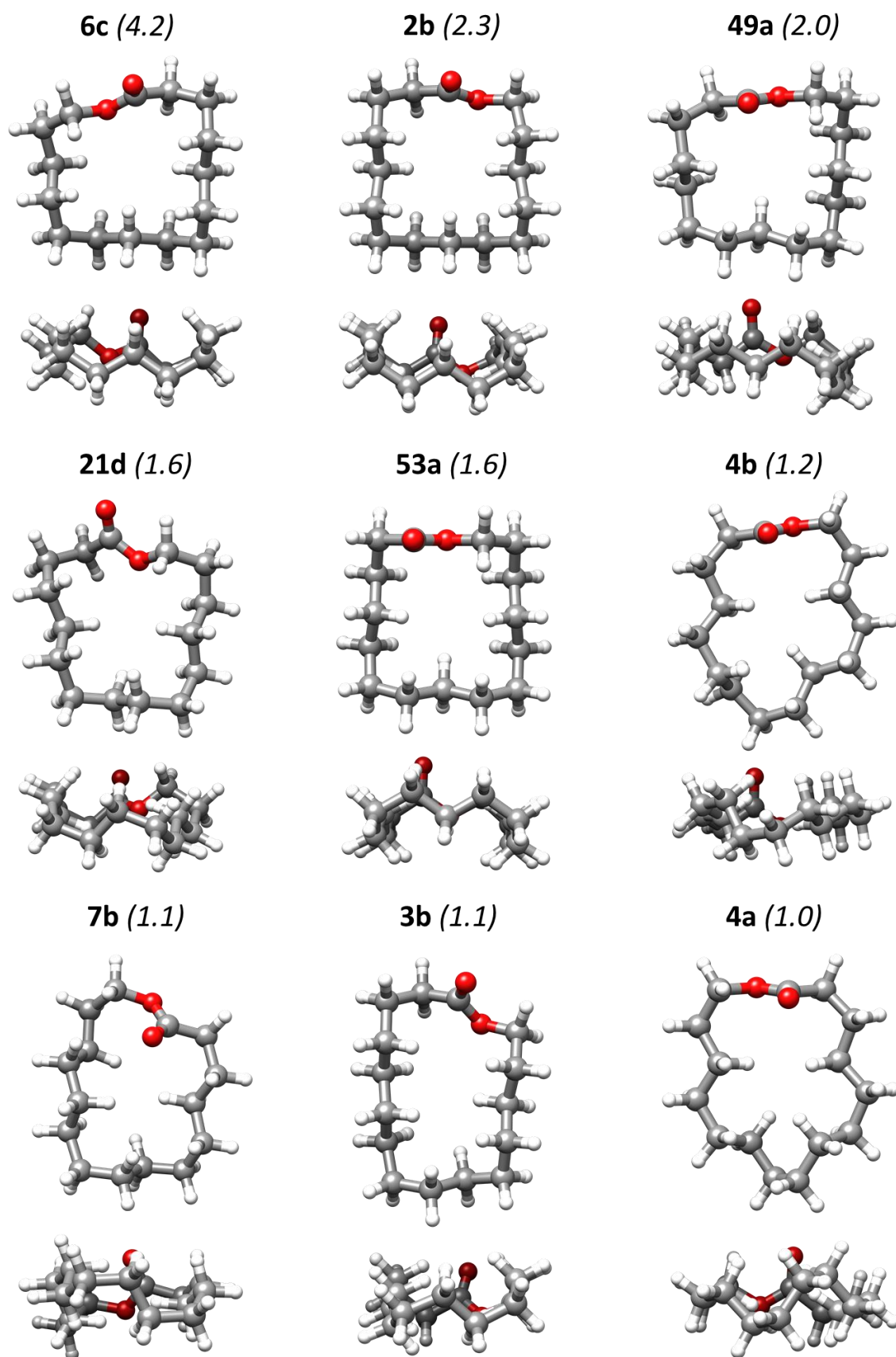


Figure 9.2. Top and side views of the assigned conformers of exaltolide in decreasing order of conformational abundance (indicated in brackets).

Non-covalent interactions

To visualise the intramolecular interactions involved in stabilizing the observed conformers, we have employed the non-covalent interactions (NCIs) method.¹⁴ The calculated NCI plots for all nine assigned conformers are presented in Figure 9.3.

Examining the conformations, there are clear differences between the interactions in the oblate and the prolate ones (Figure 9.4, Tables 9.5-6). In all of them there are C–H \cdots O=C interactions involving the carbonyl and the ethyl oxygens. The stronger CH \cdots O interaction involves the carbonyl oxygen and the hydrogens of the –CH₂ group bonded to the ethyl oxygen. This interaction is longer in the oblate conformers (2.43 Å - 2.59 Å) than in the prolate ones (2.26 Å - 2.30 Å), and in oblate conformers (except **2b**) is bifurcated. These interactions close a five-membered ring and the strain associated to it is reflected in the red area of the NCI isosurface (Figure 9.3). Weaker C–H \cdots O=C take place in all conformers in a similar manner, involving the other lone pair of the carbonyl oxygen, but at much longer distances (2.63 Å - 2.79 Å). All conformers also show a C–H \cdots O interaction involving the ethyl oxygen with one or two of the intra-annular hydrogens at distances typically between 2.59 Å and 2.69 Å.

In addition to the stronger C–H \cdots O=C interaction, the main difference between oblate and prolate conformers lie in the 1,4-H \cdots H interactions between the H pointing inside the ring, and the transannular H \cdots H interactions across the ring. In oblate conformers the intra-annular hydrogens are far apart and there are no interactions between hydrogens across the ring. All prolate conformers display transannular H \cdots H interactions, with the shortest ones being at 2.33 Å (**4a**), 2.39 Å (**7b**) and 2.47 Å (**4b**). **3b**, being the prolate conformer with a more similar arrangement of the zig-zag carbon chain to the oblate conformers, shows longer transannular H \cdots H interactions, with the shortest one of 2.64 Å. All conformers show repulsive 1,4-H \cdots H interactions where the Hs are at distances shorter than the sum of their van der Waals radii, which is 2.40 Å.^{15,16} However, while these interactions have H \cdots H distances between 2.19 Å and 2.34 Å in oblate conformers, they are generally shorter in prolate conformers.

In summary, the stronger C–H \cdots O=C interaction in prolate conformers partially compensates the stronger repulsive H \cdots H interactions, which makes them just slightly less abundant than the oblate conformers.

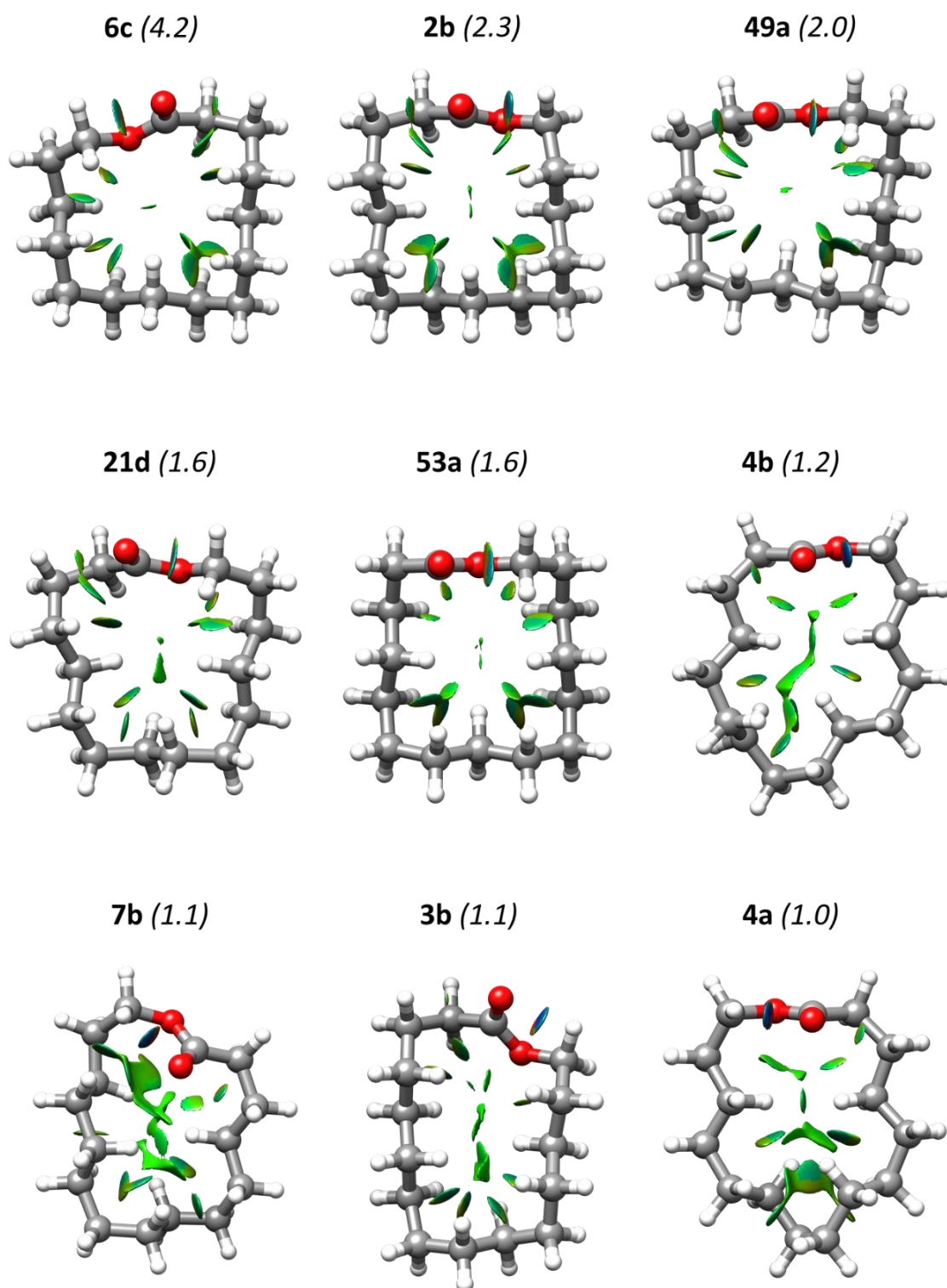


Figure 9.3. The NCI plots of the nine assigned conformers of exaltolide in their decreasing order of conformational abundance.

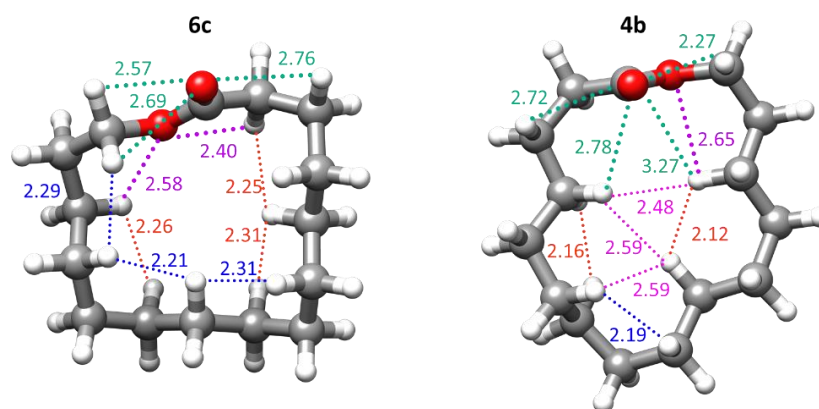


Figure 9.4. Intramolecular interactions in oblate (**6c**) and prolate (**4b**) conformers of exaltolide, with C–H···O=C interactions depicted in green; C–H···O in purple; 1,4-H···H interactions are separated by four carbons and illustrated in orange (below the plane of the ring) and blue (above the plane of the ring); H···H interactions across the ring are shown in pink.

Table 9.5. Intramolecular distances in the oblate conformers of exaltolide.

	6c	2b	49a	21d	53a
Carbonyl	2.57	2.43	2.66	2.66	2.57
C–H···O=C	2.76 (2.69)	2.72 (2.75)	2.79 (2.71)	2.79 (2.67)	2.66
Ethyl	2.58	2.59	2.62	2.65	2.68
C–H···O	2.40	2.59	2.62	2.65	2.69
1,4-H···H	2.26	2.28	2.20	2.34	2.20
below the ring	2.30	2.26	2.31	2.24	2.19
	2.25	2.24	2.27	2.25	
1,4-H···H	2.21	2.24	2.28	2.27	2.25
above the ring	2.29	2.23	2.24	2.21	2.24
	2.31		2.23	2.35	2.27
H···H across		3.08		2.91	3.06

Table 9.6. Intramolecular distances in the prolate conformers of exaltolide.

	4b	7b	3b	4a
Carbonyl	2.26	2.29	2.30	2.26
C–H···O=C	2.72 (2.78) (3.27)	2.63 (2.75) (2.87)	2.78 (2.90)	2.68 (2.82) (3.15)
Ethyl	2.65	2.65	2.69	2.69
C–H···O	2.65	2.65	2.69	2.69
1,4-H···H	2.16	2.39	2.20	2.18
below the ring	2.12	2.17 2.24	2.11 2.18	2.28
1,4-H···H	2.19	2.19	2.11	2.09
above the ring		2.17 2.26	2.16 2.16	2.35
H···H across	2.47	2.42	2.64	2.33
	2.58	2.39	2.74	2.47
	2.58		2.88	2.49
				2.29

Benchmarking of theoretical methods

We have benchmarked the performance of three theoretical methods B3LYP-D3BJ, MP2 and wB97XD with the 6-311++G(d,p) basis set at predicting the rotational parameters and energies of exaltolide.

Considering the rotational constants, deviations between theoretical and experimental values have been calculated as $(A_{\text{calc}} - A_{\text{exp}})/A_{\text{exp}}$ (Table 9.7). The overall deviations are 0.33% for B3LYP-D3BJ, 0.65% for MP2 and 0.84% for wB97XD. The higher deviation in wB97XD is affected by the predictions for conformer **3b**, where the *A* constant is predicted 6.6% away. Excluding this anomaly, it can be concluded that B3LYP-D3BJ is the best performing method, followed by wB97XD and then by MP2. This with the caveat that we are comparing equilibrium rotational constants with ground-state experimental ones. Unfortunately, the computational cost to calculate theoretical ground-state rotational constants for this large molecule is prohibitive at the moment.

Comparing the energy ordering from one level of theory to another (including zero-point corrections), significant discrepancies are noted. At B3LYP-D3BJ level the conformers that are lowest in energy are **2b**, followed by **6c**. At MP2 level, conformers **2b** and **6c** are predicted to be 2nd and 3rd in order, respectively, whilst the global minimum is predicted to be **53a**. At wB97XD level of theory, the global minimum is **6c**, followed by **3c**, which has not been identified experimentally. 3rd and 4th in order of energy are **7b** and **2b**, and conformer **53a** in 9th.

The assigned nine conformations at B3LYP-D3BJ are predicted to be some of the lowest in energy, all within an energy window of 270 cm⁻¹. The only conformations within this energy limit at this level of theory that have not been observed are **3c**, **1a** and **4e**. It is possible that the reason for not observing these conformers is that they relax in the supersonic expansion to lower-energy conformers.^{17,18} The five most abundant conformers, **6c**, **2b**, **49a**, **21d** and **53a** are predicted at B3LYP-D3BJ level to be within 100 cm⁻¹ (ZPE). This is in agreement with their close relative abundances. The Gibbs free energies predict the most favoured conformer to be **21d** and thus do not agree with the experimentally determined relative conformational abundances.

At wB97XD level of theory the observed species are also predicted to be at low energies, within 200 cm⁻¹ (considering zero-point corrected values), except for conformer **4b**, which is predicted to be 367 cm⁻¹ above the global minimum. Gibbs free energies are not in agreement with experimental observations either, and are generally higher than those predicted by B3LYP-D3BJ. At MP2 level of theory six of assigned conformers are predicted to be low in energy, within 150 cm⁻¹, whilst conformers **3b**, **4a** and **4b** are predicted to lie at higher energies. **4b** is consistently predicted to lie at the highest energy of the observed conformers.

The disagreement between relative abundances from Gibbs free energies and the experimentally determined ones could be related to the effects of conformational relaxation,^{17,18} or it may be due to the levels of theory used not being adequate to reproduce experimental observations. Further investigations on the possible relaxation pathways between exaltolide conformations, and applying different theoretical methods to describe exaltolide can shed more light on this.

Table 9.7. Theoretical rotational constants and the % deviation from experiment by B3LYP-D3BJ, MP2 and wB97XD levels of theory with 6-311++G(d,p) basis set.

		6-311++G(d,p)					
		B3LYP-D3BJ		MP2		wB97XD	
2b	A ^a	438.2	-0.5%	447.1	1.5%	442.6	0.5%
	B	364.5	-0.7%	368.3	0.4%	366.8	0.0%
	C	219.1	-0.7%	223.2	1.2%	221.0	0.2%
53a	A	434.5	-0.7%	440.7	0.7%	439.1	0.3%
	B	363.4	-0.3%	369.9	1.5%	364.9	0.1%
	C	226.7	-0.4%	231.3	1.6%	228.2	0.2%
49a	A	414.4	-0.1%	416.5	0.4%	416.5	0.4%
	B	387.8	-0.7%	394.7	1.1%	391.0	0.1%
	C	222.2	-0.3%	225.0	1.0%	223.8	0.4%
6c	A	417.0	-0.2%	430.2	2.9%	423.2	1.2%
	B	380.5	-1.0%	380.3	-1.0%	380.8	-0.9%
	C	216.5	-0.7%	219.9	0.8%	218.2	0.0%
21d	A	429.2	-0.2%	436.2	1.4%	430.2	0.0%
	B	372.4	-0.9%	379.3	0.9%	378.3	0.6%
	C	217.8	-0.6%	222.2	1.4%	220.1	0.4%
4b	A	488.2	-0.9%	493.7	0.3%	500.4	1.6%
	B	319.1	-0.7%	322.5	0.3%	319.1	-0.7%
	C	207.5	-0.8%	210.0	0.4%	209.5	0.2%
4a	A	497.7	-0.4%	504.3	0.9%	507.6	1.6%
	B	330.6	-1.1%	335.9	0.4%	331.6	-0.8%
	C	217.4	-0.9%	220.8	0.7%	219.4	0.0%
7b	A	513.5	0.3%	518.3	1.2%	520.2	1.6%
	B	346.6	-1.0%	352.5	0.7%	348.1	-0.6%
	C	232.8	-0.2%	236.7	1.5%	235.1	0.8%
3b	A	543.1	0.8%	561.0	4.1%	574.7	6.6%
	B	303.6	-1.3%	305.3	-0.8%	299.7	-2.6%
	C	211.0	-0.7%	215.2	1.3%	214.2	0.8%

[a] A, B, and C are the rotational constants. [b] Deviation from the experiment; calculated as $(A_{\text{calc}} - A_{\text{exp}}) / A_{\text{exp}} \times 100\%$.

Comparison with the other muscone and civetone macrocycle ketone

Comparing the most abundant conformations of the three cycles (Figure 9.5), clear similarities and unique differences can be observed. Among the similarities, we can cite the tendency of all macrocycles to present relatively flat configurations of the carbon framework while allowing a zig-zag arrangement to minimise strain. Most of the conformers observed for all macrocycles have the carbonyl groups perpendicular to the plane of the ring, with the exception of one civetone conformer. Exaltolide and muscone do not show a significantly stronger preference for one conformation, which could be due to the fact that both are composed of only saturated bonds (with the exception of the carbonyl group). Civetone has a double bond in its structure that introduces more constraints and may be the reason behind its stronger preference for one conformation.

The general shapes adopted by the macrocycles are different, with civetone preferring an elliptical or rectangular shape and exaltolide a square or trapezium-like configuration, while muscone can be described as a distorted square. The different shapes could be related to the size of the ring. Muscone and civetone are odd-membered rings, while exaltolide is an even-membered one. In the case of civetone, this is modulated by the presence of a double bond.

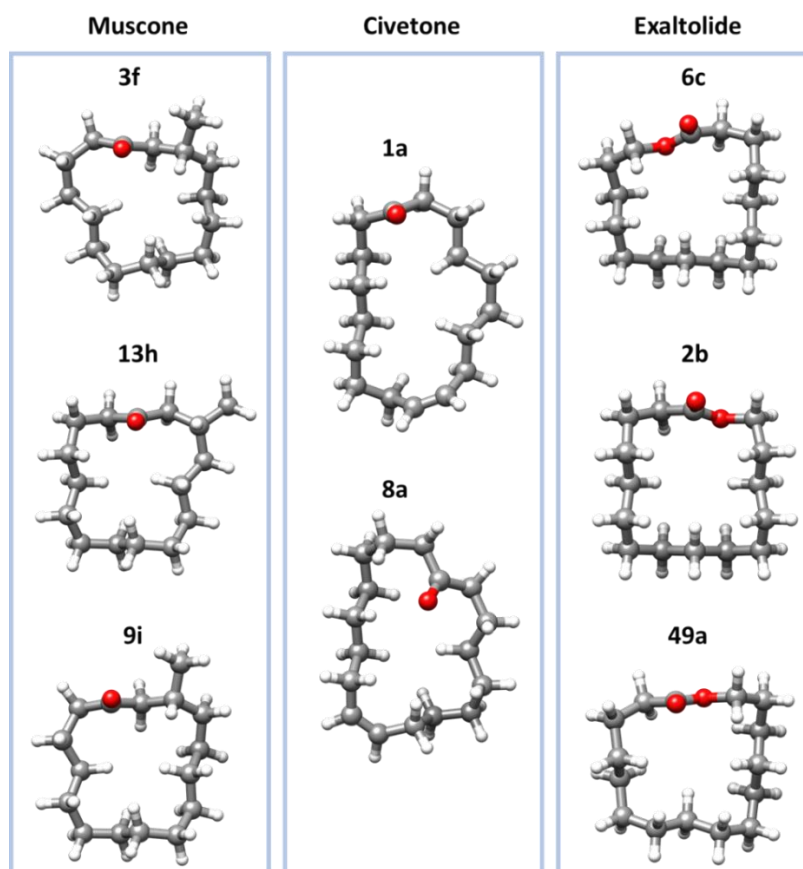


Figure 9.5. The most abundant conformations of muscone, civetone and exaltolide.

9.4. Conclusions

Nine conformations of exaltolide have been observed in its broadband rotational spectrum, which shows the rich conformational landscape of this macrocyclic musk of plant origin. The conformers can be divided into oblate and prolate tops, where the oblate ones are more abundant. There are no huge differences in conformational abundance, differently to what was observed for the smaller cycloketones studied here. This seems to confirm the trend that, as the size of the ring increases, the predominance of one conformation decreases. Further comparisons with other macrocyclic cycloketones will be determinant to establish this trend.

Three computational methods have been evaluated against our experimental results. The B3LYP-D3BJ/6-311++G(d,p) level of theory performs best at predicting the spectroscopic rotational constants of exaltolide, and the predicted energies seem to be in better agreement with the experimental abundances.

The most abundant conformers of exaltolide adopt more organised ‘squared’ and ‘trapezium-shaped’ structures in comparison with those of their muscone and civetone. This data, together with that of the other musks studied here, could help advance our understanding of the interactions of musks with olfactory receptors, and help improve the musk olfactophore model. Additional studies of other macrocyclic musks are necessary to understand the effects of substituting ketone by lactone and changing the size of the macrocycle at the molecular level.

9.5. Bibliography

1. Kerschbaum, M. Über Lactone mit großen Ringen - die Träger des vegetabilischen Moschus-Duftes. *Berichte der deutschen chemischen Gesellschaft (A and B Series)* **60**, 902–909 (1927).
2. Sommer, C. The role of musk and musk compounds in the fragrance industry. *Handbook of Environmental Chemistry* **3**, 1–16 (2004).
3. Williams, A. S. The synthesis of macrocyclic musks. *Synthesis* 1707–1723 (1999).
4. Ravi, S., Padmanabhan, D. & Mamdapur, V. R. Macrocyclic musk compounds: Synthetic approaches to key intermediates for exaltolide, exaltone and dilactones. *Journal of the Indian Institute of Science* **81**, 299–312 (2001).
5. Subramanian, G. B. v., Mehrotra, A. & Mehrotra, K. ChemInform Abstract: A Synthesis of exaltolide from threo-aleuritic acid. *Chemischer Informationsdienst* **16**, 379–380 (1985).
6. Dhekne, V. v., Ghatge, B. B., Nayak, U. G., Chakravarti, K. K. & Bhattacharyya, S. C. 452. Macrocyclic musk compounds. Part I. New syntheses of exaltolide, exaltone, and dihydrocivetone. *Journal of the Chemical Society (Resumed)* 2348–2352 (1962).

7. Sato, T., Kawara, T., Kokubu, Y. & Fujisawa, T. A Simple Method for the Synthesis of Exaltolide. *Bulletin of the Chemical Society of Japan* **54**, 945–946 (1981).
8. Bollbuck, B., Kraft, P. & Tochtermann, W. Nature-like odorants by stereoselective ring enlargement of Cyclohexanone and Cyclododecanone. *Tetrahedron* **52**, 4581–4592 (1996).
9. Antczak, U., Góra, J., Antczak, T. & Galas, E. Enzymatic lactonization of 15-hydroxypentadecanoic and 16-hydroxyhexadecanoic acids to macrocyclic lactones. *Enzyme and Microbial Technology* **13**, 589–593 (1991).
10. Pracht, P., Bohle, F. & Grimme, S. Automated exploration of the low-energy chemical space with fast quantum chemical methods. *Physical Chemistry Chemical Physics* **22**, 7169–7192 (2020).
11. Western, C. M. PGOPHER: A program for simulating rotational, vibrational and electronic spectra. *Journal of Quantitative Spectroscopy and Radiative Transfer* **186**, 221–242 (2017).
12. Watson, J. K. G. *Vibrational Spectra and Structure*. Elsevier Amsterdam **6**, 1–89 (1977).
13. Novick, S. E. A beginner's guide to Pickett's SPCAT/SPFIT. *Journal of Molecular Spectroscopy* **329**, 1–7 (2016).
14. Johnson, E. R. *et al.* Revealing noncovalent interactions. *Journal of the American Chemical Society* **132**, 6498–6506 (2010).
15. Pauling, L. *The Nature of the Chemical Bond and the Structure of Molecules and Crystals: An Introduction to Modern Structural Chemistry*. (Cornell University Press, 1960).
16. Bondi, A. Van der Waals volumes and radii. *Journal of Physical Chemistry* **68**, 441–451 (1964).
17. Ruoff, R. S., Klots, T. D., Emilsson, T. & Gutowsky, H. S. Relaxation of conformers and isomers in seeded supersonic jets of inert gases. *The Journal of Chemical Physics* **93**, 3142–3150 (1990).
18. Zwier, T. S. Laser spectroscopy of jet-cooled biomolecules and their water-containing clusters: Water bridges and molecular conformation. *Journal of Physical Chemistry A* **105**, 8827–8839 (2001).



**EXPERIMENTALLY
OBSERVED HORSESHOE
CONFIGURATIONS OF THE
ALICYCLIC MUSK
ROMANDOLIDE**

Chapter 10



10. EXPERIMENTALLY OBSERVED HORSESHOE CONFIGURATIONS OF THE ALICYCLIC MUSK ROMANDOLIDE

10.1. Introduction

Alicyclic musks represent a class of commercially important musks, also known as 4th generation musks. They were introduced in 1975 with the discovery of cyclomusk, which is a derivative of cyclopentene with a strawberry-like musk odour.¹ Fifteen years later, a new addition to this family of musks followed with the discovery of helvetolide. It was discovered by Giersch and Schulte-Elte at Firmenich and its fragrance can be described as fruity and pear-like.¹ In 2000, romandolide was discovered by Alvin Williams by replacing the *gem*-dimethyl moiety of helvetolide with a carbonyl group, which preserved the muskiness of the compound. The olfactive description of romandolide says that it is a very delicate musk, with less fruity and more ambrette-like notes than Helvetolide.²

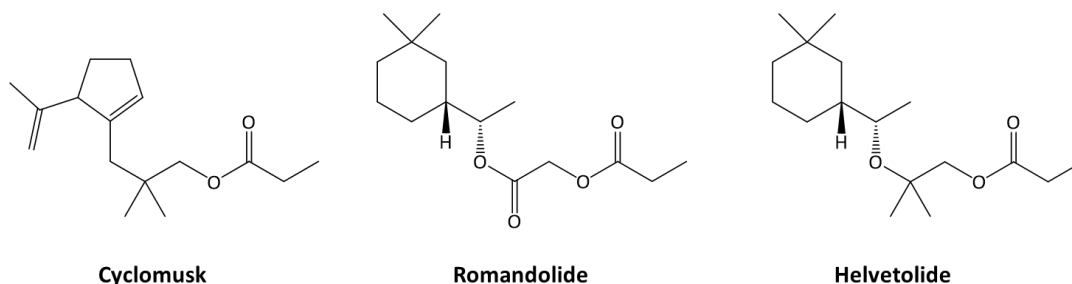


Figure 10.1. Structures of cyclomusk, romandolide and helvetolide from the alicyclic family of musks.

The olfactory properties of alicyclic musks have been explained by the horseshoe conformation they were predicted to adopt by folding, mimicking in this way the macrocyclic musks and potentially binding to the same odorant receptors.³ This hypothesis was tested by Kraft *et al.*, who developed a common olfactophore model for macrocyclic and linear musks, describing the structural features in both classes that are responsible for the musk odour.⁴ The model had a correlation of 54%. Kraft *et al.* further tested their olfactophore on sila-analogs of alicyclic musks, including romandolide, improving the olfactophore model correlation to 80.5%. The study concluded with the hypothesis that macrocyclic and alicyclic musks potentially address the same olfactory receptors, given the similarity between their conformational space.²

There is no structural or conformational information on romandolide, and in general on this class of musks. This could be linked to their rich conformational landscape resulting from the large flexibility of their aliphatic tails due to large number of single bonds, preventing their

crystallisation. The lowest energy conformer of romandolide were predicted using semiempirical methods to develop olfactophore models. These methods are known to yield unreliable energy orderings of flexible molecules. Nevertheless, they predicted that alicyclic musks fold upon themselves, adopting horseshoe conformations. Potentially these conformations may have similarities to those of macrocyclic musks and bind the same odorant receptors.

We have employed broadband rotational spectroscopy in combination with theoretical methods to investigate the conformational landscape of romandolide. We have identified experimentally six conformations and their relative abundances have been estimated. All the conformers observed display horseshoe conformations where the alicyclic tail interacts with the cyclohexane rings through weak attractive interactions. The data we are reporting here should be taken as a basis to describe the interactions of romandolide with the residues of olfactory receptors and is important to re-evaluate the proposed olfactophore models.

10.2. Methods

Theoretical

The potential energy surface of romandolide was explored using the conformer sampling program Conformer – Rotamer Ensemble Sampling Tool (CREST).⁵ The first conformational search generated a total of 314 conformations. All conformers have been optimised at B3LYP-GD3BJ level of theory with 6-311++G(d,p) basis set. Other six conformational searches using CREST with different starting structures have been used to confirm that the full potential surface was mapped, and the lower-energy 150 structures of each search were optimised at B3LYP-GD3BJ/6-311++G(d,p). A total of 40 distinct conformers were returned within 1000 cm⁻¹. Of these, the 20 conformers predicted to lie at lower energy have also been optimised using MP2 and B2PLYP with the 6-311++G(d,p) basis set, and the B3LYP-GD3BJ level of theory with the def2-TZPV and def2-QZVP basis sets, in order to benchmark the different theoretical methods. All these 20 conformers were confirmed to be local minima by performing harmonic vibrational calculations, and their zero-point relative energies were obtained at B3LYP-GD3BJ level with 6-311++G(d,p) and def2-TZVP basis sets. The zero-point energies at the other three levels of theory were not calculated due to computational cost. Tables 10.1-10.5 show the theoretical spectroscopic parameters predicted by the five theoretical methods. The rotation barriers of all 4 methyl groups of conformer **2** have been calculated at B3LYP-D3BJ/6-311++G(d,p) level. They are all predicted to be higher than 800 cm⁻¹ (Figure 10.2), and therefore no splitting of lines due to methyl internal rotation was expected to be observed in our rotational spectrum.

Experimental

The broadband spectrum of romandolide (Firmenich, $\geq 80\%$) was recorded using our CP-FTMW spectrometer at King's, which operates in the 2-8 GHz frequency range. Romanolide, heated at 431 K in a bespoke nozzle, was seeded in neon at 5 bar and conducted to the vacuum chamber where the molecules expand adiabatically forming a supersonic jet. The molecular pulse was polarized by four chirped microwave pulses of 4 μs duration each. After each microwave pulse, the emission signal was collected as free induction decay (FID) for 20 μs into the oscilloscope. The final spectrum was obtained from adding up 1300k FIDs. The time domain spectrum was converted to the frequency domain using a fast Fourier transform algorithm. The spectrum obtained was incredibly dense, with 0.6 lines/MHz with a signal to noise ratio of 3 : 1.

Table 10.1. B3LYP-D3BJ/6-311++G(d,p) spectroscopic rotational parameters, relative raw and ZPC energies for romandolide conformations within 700 cm^{-1} .

B3LYP-D3BJ/ 6-311++G(d,p)	2	63	30	3	49	9	50	48	89	59
A^a (MHz)	450.1	444.7	435.0	468.2	473.3	467.9	510.7	499.6	457.0	504.9
B (MHz)	310.7	282.4	300.7	283.4	280.5	302.6	257.2	247.3	247.8	252.6
C (MHz)	228.1	225.5	205.6	218.3	237.9	247.5	210.2	181.7	202.5	197.6
κ^b	-0.26	-0.48	-0.17	-0.48	-0.64	-0.50	-0.69	-0.59	-0.64	-0.64
μ_a^c (D)	-1.4	-0.5	0.9	1.7	-0.1	0.1	0.7	0.1	-2.2	-0.9
μ_b (D)	-1.1	0.5	0.9	-2.1	0.4	-1.7	-1.3	-1.1	2.2	-1.7
μ_c (D)	2.2	-2.9	-2.9	1.6	-3.1	-2.3	-2.6	-0.8	0.1	-2.6
ΔE^d (cm^{-1})	0.0	145.4	156.6	284.3	184.2	270.9	373.3	367.9	566.2	521.0
ΔE_0^e (cm^{-1})	0.0	151.4	175.8	313.8	345.0	362.6	410.0	449.0	449.0	499.7
ΔG^f (cm^{-1})	495.8	479.8	669.0	912.1	826.5	815.6	882.3	831.4	371.8	655.1
	6	13	51	58	15	5	122	42	83	16
A (MHz)	561.7	445.5	523.9	462.9	525.6	560.8	485.0	481.6	611.0	510.3
B (MHz)	205.0	297.1	237.2	263.2	235.7	187.7	283.6	281.8	217.5	253.4
C (MHz)	172.6	226.4	208.2	209.4	185.4	160.7	225.3	220.5	200.5	206.7
κ	-0.83	-0.35	-0.82	-0.58	-0.70	-0.87	-0.55	-0.53	-0.92	-0.69
μ_a (D)	-0.3	0.2	-2.4	-0.4	0.1	-0.1	-2.4	-1.2	-1.0	2.3
μ_b (D)	-0.8	-1.7	2.4	0.6	-1.3	1.4	-1.6	-1.6	1.5	-2.2
μ_c (D)	1.0	-2.5	0.3	-3.1	-0.5	-0.4	1.3	-2.2	-2.3	-1.3
ΔE (cm^{-1})	544.2	441.2	513.8	556.7	561.9	613.7	563.9	471.3	541.1	608.4
ΔE_0 (cm^{-1})	519.1	562.7	573.5	581.4	617.4	629.5	646.1	669.0	718.1	733.7
ΔG (cm^{-1})	611.5	972.9	696.6	0.0	713.5	468.4	1280.0	1354.8	1325.6	1047.3

[a] A , B , C are the rotational constants. [b] Ray's asymmetry parameter. [c] μ_a , μ_b and μ_c are the electric dipole moment components. [d] Relative electronic energies. [e] Relative electronic energies including the zero-point correction. [f] Gibbs energies calculated at 431 K.

Table 10.2. B3LYP-D3BJ/def2-TZVP spectroscopic rotational parameters, relative raw and ZPC energies for romandolide conformations within 700 cm⁻¹.

B3LYP-D3BJ/ def2-TZVP	2	63	30	3	49	48	9	50	6	89
A ^a (MHz)	450.8	445.9	436.4	469.0	474.2	502.8	468.8	513.7	568.7	461.4
B (MHz)	310.1	282.1	300.8	283.1	280.6	246.5	302.0	256.7	202.9	243.9
C (MHz)	227.5	225.8	205.4	218.0	238.6	181.7	246.9	210.4	171.6	201.5
κ ^b	-0.26	-0.49	-0.17	-0.48	-0.64	-0.60	-0.50	-0.69	-0.84	-0.67
μ _a ^c (D)	-1.3	-0.6	0.8	-2.3	-0.3	0.0	-0.1	-0.8	-0.2	2.1
μ _b (D)	1.1	0.5	0.9	1.5	0.4	-1.1	1.7	1.3	0.9	2.2
μ _c (D)	2.2	-2.9	-2.9	-1.4	-3.1	-0.8	-2.2	-2.6	-1.0	0.1
ΔE ^d (cm ⁻¹)	0.0	129.0	139.8	267.4	164.4	291.6	271.0	350.8	475.6	536.1
ΔE ₀ ^e (cm ⁻¹)	0.0	133.0	154.1	275.4	319.6	367.0	369.6	383.9	440.3	543.6
ΔG ^f (cm ⁻¹)	86.5	65.4	259.9	412.4	340.8	374.4	393.1	465.7	122.5	0.0
	59	15	51	5	13	58	42	122	83	16
A (MHz)	505.9	527.3	524.7	565.3	446.7	459.6	482.5	485.6	613.0	512.3
B (MHz)	252.8	236.1	237.4	187.0	296.8	265.4	281.5	283.2	217.6	253.2
C (MHz)	197.8	185.6	207.8	160.5	226.5	206.7	220.0	224.9	200.5	206.7
κ	-0.64	-0.70	-0.81	-0.87	-0.36	-0.54	-0.53	-0.55	-0.92	-0.70
μ _a (D)	-0.8	0.0	2.3	-0.1	0.0	0.4	1.3	2.3	1.1	-2.2
μ _b (D)	-1.6	-1.3	2.4	1.4	1.6	0.7	1.6	1.6	-1.5	2.2
μ _c (D)	-2.6	-0.5	-0.2	-0.4	-2.4	-3.0	-2.2	1.3	-2.3	-1.3
ΔE (cm ⁻¹)	514.9	471.8	477.8	542.8	454.3	555.0	444.0	586.7	513.0	569.7
ΔE ₀ (cm ⁻¹)	482.4	534.4	539.2	543.6	571.5	584.7	637.1	656.0	683.0	691.1
ΔG (cm ⁻¹)	214.9	316.3	230.2	138.9	554.4	905.6	626.2	797.8	863.9	626.6

[a] A, B, C are the rotational constants. [b] Ray's asymmetry parameter. [c] μ_a, μ_b and μ_c are the electric dipole moment components. [d] Relative electronic energies. [e] Relative electronic energies including the zero-point correction. [f] Gibbs energies calculated at 431 K.

Table 10.3. B3LYP-D3BJ/def2-QZVP spectroscopic rotational parameters and relative raw energies for romandolide conformations within 700 cm⁻¹.

B3LYP-D3BJ/ def2-QZVP	2	30	63/58 ^e	49	3	9	48	50	42	13
A ^a (MHz)	451.3	437.1	445.6	474.2	469.0	468.9	503.5	514.2	482.3	446.1
B (MHz)	310.2	301.8	282.3	280.6	283.5	301.5	245.7	256.8	281.7	297.0
C (MHz)	227.7	205.3	225.0	237.5	218.1	246.5	181.4	210.5	220.0	226.1
κ ^b	-0.26	-0.17	-0.48	-0.64	-0.48	-0.51	-0.60	-0.70	-0.53	-0.36
μ _a ^c (D)	-1.4	0.9	-0.6	-0.2	-2.4	0.0	0.0	-0.7	1.4	0.1
μ _b (D)	1.1	0.9	0.5	0.4	1.5	1.7	-1.1	1.3	1.6	1.7
μ _c (D)	2.2	-2.9	-2.9	-3.1	-1.4	-2.3	-0.8	-2.6	-2.2	-2.5
ΔE ^d (cm ⁻¹)	0.0	129.5	139.1	181.0	283.3	300.8	301.4	341.8	440.7	77.6
	51	6	15	83	59	5	89	16	122	
A (MHz)	534.2	570.6	528.3	615.2	506.9	566.7	459.7	512.0	485.7	
B (MHz)	237.8	201.9	234.7	217.6	252.1	186.1	245.8	253.5	283.7	
C (MHz)	207.8	171.1	184.9	200.5	197.4	160.0	201.7	206.6	225.2	
κ	-0.82	-0.85	-0.71	-0.92	-0.65	-0.87	-0.66	-0.69	-0.55	
μ _a (D)	2.3	-0.2	0.1	1.0	-0.8	-0.1	2.1	-2.2	2.3	
μ _b (D)	2.4	0.9	-1.3	1.5	-1.7	1.4	2.2	2.2	1.6	
μ _c (D)	-0.2	-1.0	-0.5	2.3	-2.6	-0.4	0.1	1.3	1.3	
ΔE (cm ⁻¹)	479.2	482.1	485.3	506.0	507.4	524.5	543.8	584.4	599.1	

[a] A, B, C are the rotational constants. [b] Ray's asymmetry parameter. [c] μ_a, μ_b and μ_c are the electric dipole moment components. [d] Relative electronic energies. [e] Conformer 58 converged to 63.

Table 10.4. MP2/6-311++G(d,p) spectroscopic rotational parameters and relative raw energies for romandolide conformations within 700 cm^{-1} .

MP2/ 6-311++G(d,p)	2	49	9	50	63	30	3	13	83	48
A^a (MHz)	454.2	485.9	478.6	523.3	457.1	445.7	482.1	459.0	611.4	505.8
B (MHz)	315.9	279.9	304.2	261.9	282.0	302.7	283.8	297.1	225.3	251.3
C (MHz)	236.7	246.9	252.2	218.0	232.5	208.0	221.4	231.6	208.5	184.6
κ^b	-0.27	-0.72	-0.54	-0.71	-0.56	-0.20	-0.52	-0.42	-0.92	-0.58
μ_a^c (D)	-0.7	0.5	-0.2	-0.9	0.6	-0.9	2.1	-0.2	1.2	-0.1
μ_b (D)	-1.1	0.0	1.6	-1.1	-0.3	-0.7	-1.4	-1.4	1.4	-1.0
μ_c (D)	2.3	-2.9	-2.1	2.3	2.7	2.6	1.3	-2.3	-2.1	0.7
ΔE^d (cm^{-1})	0.0	129.9	143.5	147.2	176.6	191.6	271.4	351.8	398.3	433.9
	51	5	42	15	58	122	59	6	16	89
A (MHz)	543.4	500.0	491.5	522.0	463.6	497.2	514.7	543.4	524.8	478.2
B (MHz)	234.9	253.1	283.5	249.8	270.8	281.5	261.5	222.1	254.5	241.3
C (MHz)	211.1	197.0	222.6	193.5	207.5	226.0	205.7	183.1	209.1	206.5
κ	-0.86	-0.63	-0.55	-0.66	-0.51	-0.59	-0.64	-0.78	-0.71	-0.74
μ_a (D)	-2.1	0.6	-1.5	-0.1	0.1	-2.0	1.1	-0.1	2.0	-2.0
μ_b (D)	-2.3	-0.4	-1.5	-1.2	0.9	-1.6	-1.5	-0.7	-2.1	-2.1
μ_c (D)	0.3	-0.8	1.9	-0.3	2.8	-1.2	-2.3	0.8	1.2	0.0
ΔE (cm^{-1})	452.2	473.7	483.3	484.4	532.0	532.1	560.2	606.3	608.9	617.5

[a] A , B , C are the rotational constants. [b] Ray's asymmetry parameter. [c] μ_a , μ_b and μ_c are the electric dipole moment components. [d] Relative electronic energies.

Table 10.5. B2PLYP-D3BJ/6-311++G(d,p) spectroscopic rotational parameters and relative raw energies for romandolide conformations within 700 cm^{-1} .

B2PLYP-D3BJ/ 6-311++G(d,p)	2	49	63	30	9	3	50	13	48	42
A^a (MHz)	453.2	478.3	449.6	440.0	471.9	474.2	515.4	449.5	500.3	486.5
B (MHz)	313.7	282.2	284.0	303.0	305.9	285.3	260.7	300.3	252.1	282.7
C (MHz)	231.3	243.6	229.8	207.4	251.0	220.7	214.6	229.8	184.3	221.6
κ^b	-0.26	-0.67	-0.51	-0.18	-0.50	-0.49	-0.69	-0.36	-0.57	-0.54
μ_a^c (D)	-1.2	0.3	0.6	-0.9	0.0	2.3	-0.8	0.0	-0.1	-1.5
μ_b (D)	-1.1	0.2	-0.4	0.8	-1.7	-1.4	-1.3	1.6	-1.0	-1.6
μ_c (D)	2.2	-3.1	2.9	2.8	-2.2	1.3	-2.5	2.4	-0.8	2.1
ΔE^d (cm^{-1})	0.0	147.1	175.8	189.0	201.8	296.4	338.4	420.0	456.4	494.0
	51	83	122	59	58	15	16	89	6	5
A (MHz)	532.1	614.5	490.1	509.0	469.0	518.2	517.7	462.1	546.1	501.5
B (MHz)	237.8	220.3	284.8	259.0	264.2	248.5	255.2	251.6	216.9	243.6
C (MHz)	210.3	203.6	227.2	202.9	214.9	192.2	208.3	206.6	179.6	191.6
κ	-0.83	-0.92	-0.56	-0.63	-0.61	-0.65	-0.70	-0.65	-0.80	-0.66
μ_a (D)	-2.3	1.0	-2.3	-1.0	-0.5	-0.1	-2.1	-2.2	-0.1	0.6
μ_b (D)	-2.4	1.5	-1.6	-1.6	0.5	-1.2	2.2	-2.1	-0.8	-0.5
μ_c (D)	0.3	-2.3	-1.3	2.5	3.0	-0.4	-1.2	-0.1	-0.9	-0.9
ΔE (cm^{-1})	521.7	532.6	559.7	574.7	589.6	594.4	641.5	655.1	658.9	684.1

[a] A , B , C are the rotational constants. [b] Ray's asymmetry parameter. [c] μ_a , μ_b and μ_c are the electric dipole moment components. [d] Relative electronic energies.

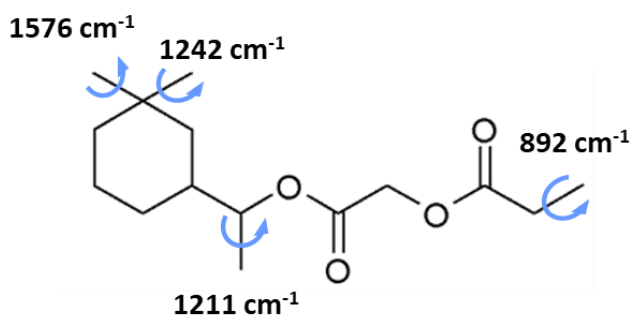


Figure 10.2. Methyl internal rotation barrier heights of the four methyl groups calculated for conformer **2** of romandolide at the B3LYP-D3BJ/6-311++G(d,p) level of theory.

10.3. Results

Rotational spectrum

The rotational spectrum of romandolide is very dense. However, a close look into the spectrum allowed for identification of distinct patterns such as the ones depicted in Figure 10.3.a., where doublets of lines came closer together with the increase in frequency. After a few fitting attempts using Pickett's program SPFIT,^{6,7} a set of these transitions were identified as *c*-type $J + 1 \leftarrow J$ transitions. This rotamer also gave rise to *a*- and *b*-type spectra, with patterns as presented in Figure 10.3.b. A total of 243 transitions were measured and fit to the semi-rigid rotor Watson Hamiltonian in the A reduction and I' representation,⁸ using Pickett's program.⁷ The resulting rotational constants have been compared to our theoretical results and identified this species as conformer **2**. Once assigned, the transitions belonging to this conformation were removed from the spectrum to ease further assignments.

Most of the low-energy conformers have predominantly *c*-type dipole moment, with some species showing also strong *a*- and *b*-type dipole moments components (Tables 10.1-10.5). Using the automated fitting routine of the program PGOPHER,⁹ and focusing on *c*-type transitions, five more rotamers were assigned. Their experimental spectroscopic parameters were determined by fitting to the same Hamiltonian as indicated above and are presented in Table 10.6. The measured transitions of all rotamers are included in Appendix VII.

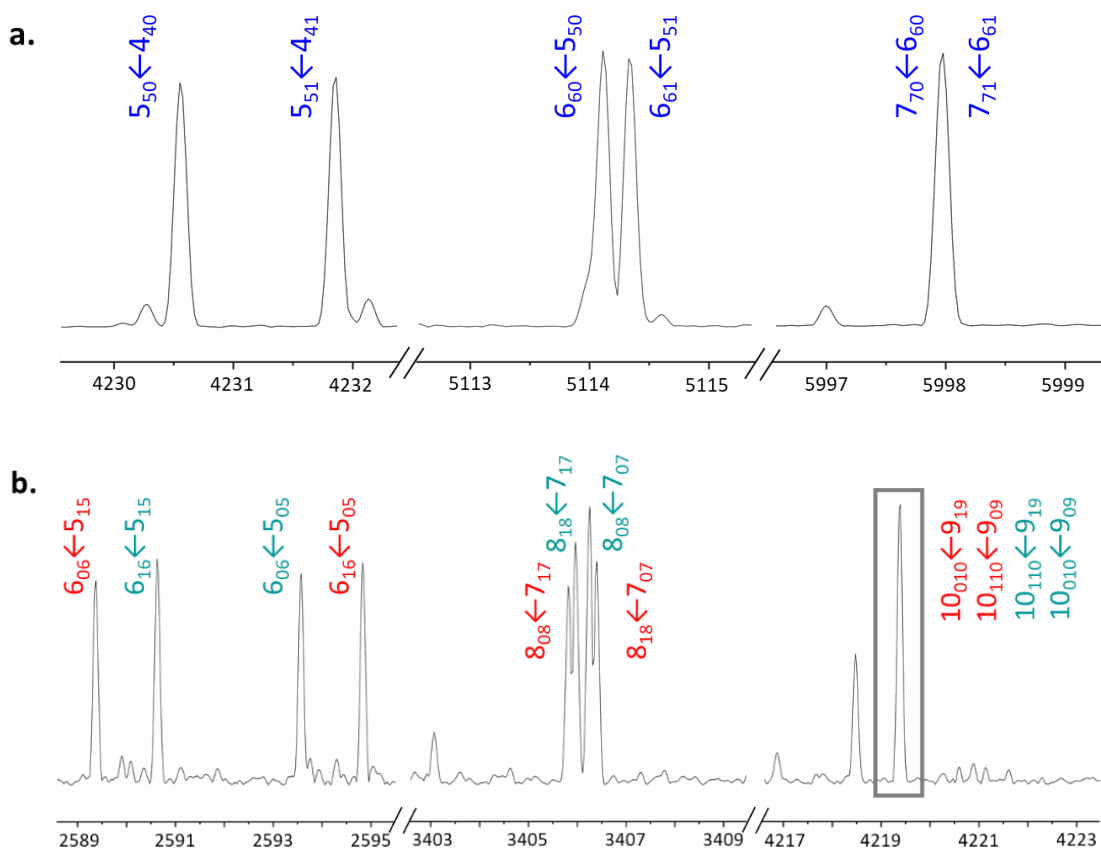


Figure 10.3. **a.** Segments of the spectrum with *c*-type transitions of conformer **30**. **b.** Segments of the spectrum with *a*- and *b*-type transitions of conformer **30**.

All the assigned rotamers have a negative κ asymmetry parameter, hence they are prolate asymmetric tops. The first four rotamers have a κ asymmetry parameters of -0.31, -0.21, -0.49 and -0.41. They all have the *A* rotational constant between 440 and 470 MHz, and the *B* constant between 280 and 305 MHz. The assignment of the first rotamer to conformer **2** was relatively straightforward, supported by the agreement between the rotational constants, and the intensity of the observed *a*-, *b*- and *c*-type spectra, in line with the predicted μ_a , μ_b and μ_c , and expected low relative energy. The second assigned rotamer, which is the most asymmetric of the seven species, has been identified as conformer **30**. The agreement between experimental and theoretical constants was excellent, and also the predominantly *c*-type spectrum is supported by the predicted μ_c dipole moment of 2.9 D. The *a*- and *b*-type spectra were assigned with a significantly lower intensity, which agrees with the respective dipole moments of 0.9 D. The 3rd rotamer was identified as conformer **3** based on the agreement between experimental and theoretically predicted parameters, and the observation of *a*- *b*- and *c*-type spectra with similar intensities, which is in agreement with the predicted dipole moments and rules out its assignment to conformer **63**. The 4th rotamer could be best matched to conformer **9**, considering

its rotational constants and the observation of *b*- and *c*-type spectra. This is a tentative assignment due to the large difference between the experimental and theoretical *A* rotational constant (>6%). The observed transitions for this rotamer were *b*- and *c*-type, with a relative intensity ratio of 2 to 3, respectively, which agrees with the predicted dipole moments μ_b and μ_c of 1.7 and 2.3 D. It could also be assigned to conformer **13**, but in this case the *C* rotational constant is predicted to differ more than 10% from the experimental one.

The final three assigned rotamers in the spectrum have an asymmetry parameter κ closer to a symmetric prolate top. The three rotamers have *A* constant above 500 MHz and a *B*-*C* difference lower than 50 MHz. The first rotamer in this group has been identified as conformer **48**, from the agreement of experimental rotational constants with the theoretical ones. The rotamer had *b*-type spectrum with a slightly less intense *c*-type transitions, observed in the spectrum with a ratio of 4 to 3, respectively, which is consistent with predicted dipole moments μ_b and μ_c of 1.1 and 0.8 D, respectively. The second rotamer was assigned to conformer **50**, also from the comparison of rotational constants, type of observed spectrum and dipole moment components. Conformer **16** is predicted to have similar rotational constants, but it was ruled out as it is expected to show *a*-type spectrum, which was not observed for this rotamer. Moreover conformer **16** is much higher in energy. Attempts to assign conformers **49** and **63**, which are also predicted to be energetically favourable, were not successful. This could be due to conformational relaxation of these species to lower energy ones.^{10,11} The assigned conformers are all within 500 cm⁻¹ with respect to the global minimum at all levels of theory.

Table 10.6. Experimental spectroscopic constants of the observed conformers of romandolide.

Parameter	2	30	3
A (MHz) ^a	452.90770(11) ^f	441.64023(15)	469.34965(30)
B (MHz)	303.024038(72)	298.085155(81)	281.39025(19)
C (MHz)	223.685528(49)	203.455152(64)	216.87717(10)
Δ_J (kHz)	0.01949(33)	0.01276(29)	0.0190(66)
Δ_{JK} (kHz)	-0.0130(19)	0.0106(16)	0.0304(53)
Δ_K (kHz)	0.0355(20)	-	0.0218(56)
δ_J (kHz)	0.00466(17)	0.00396(13)	0.00506(37)
δ_K (kHz)	-0.0191(13)	0.0198(12)	-
κ^b	-0.31	-0.21	-0.49
$a/b/c$ (D) ^c	y/y/y	y/y/y	y/y/y
σ (kHz) ^d	3.6	6.1	7.7
N ^e	243	347	203
	9	48	50
A (MHz)	439.63253(15)	509.80486(34)	522.65835(36)
B (MHz)	304.44470(19)	239.67492(18)	253.35048(17)
C (MHz)	247.48663(20)	179.23361(12)	210.39057(18)
Δ_J (kHz)	0.02686(67)	0.03512(52)	0.02456(59)
Δ_{JK} (kHz)	-	-0.0965(32)	-0.0366(40)
Δ_K (kHz)	-	0.1082(50)	0.0812(57)
δ_J (kHz)	0.00294(37)	0.01168(24)	0.0546(29)
δ_K (kHz)	-	0.0453(54)	-
κ	-0.41	-0.63	-0.72
$a/b/c$ (D)	n/y/y	n/y/y	n/y/y
σ (kHz)	8.4	8.9	7.3
N	120	183	129

[a] A, B and C are the rotational constants. Δ_J , Δ_{JK} , Δ_K , δ_J and δ_K are the quartic centrifugal distortion constants; [b] κ is the asymmetry parameter; [c] a, b and c are the type of transitions observed; [d] σ is the rms deviation of the fit; [e] N is the number of the fitted transitions; [f] Standard error in parentheses in units of the last digit.

Theoretical results

Most of the low energy conformations of romandolide are predicted to adopt folded configurations with the alicyclic tail bending above, below or around the cyclohexane moiety (Figures 10.4-10.8). Extended configurations, where the aliphatic tail is either perpendicular to or in line with the cyclohexane ring, have also been found in the potential energy surface. However, they are more uncommon and tend to lie at higher energies than folded structures. Out of the 20 lower-energy conformations, 7 have the aliphatic tail above the ring (Figure 10.4), 5 have the aliphatic tail below the ring (Figure 10.5), 3 have their aliphatic tail around the cyclohexane on the same side as the dimethyl moiety (Figure 10.6), and 3 have the aliphatic tail around the cyclohexane on the opposite side to the dimethyl groups (Figure 10.7). Only two extended configurations have been predicted within our chosen energy limit of 730 cm⁻¹ at B3LYP-D3BJ/6-311+G(d,p) (Figure 10.8).

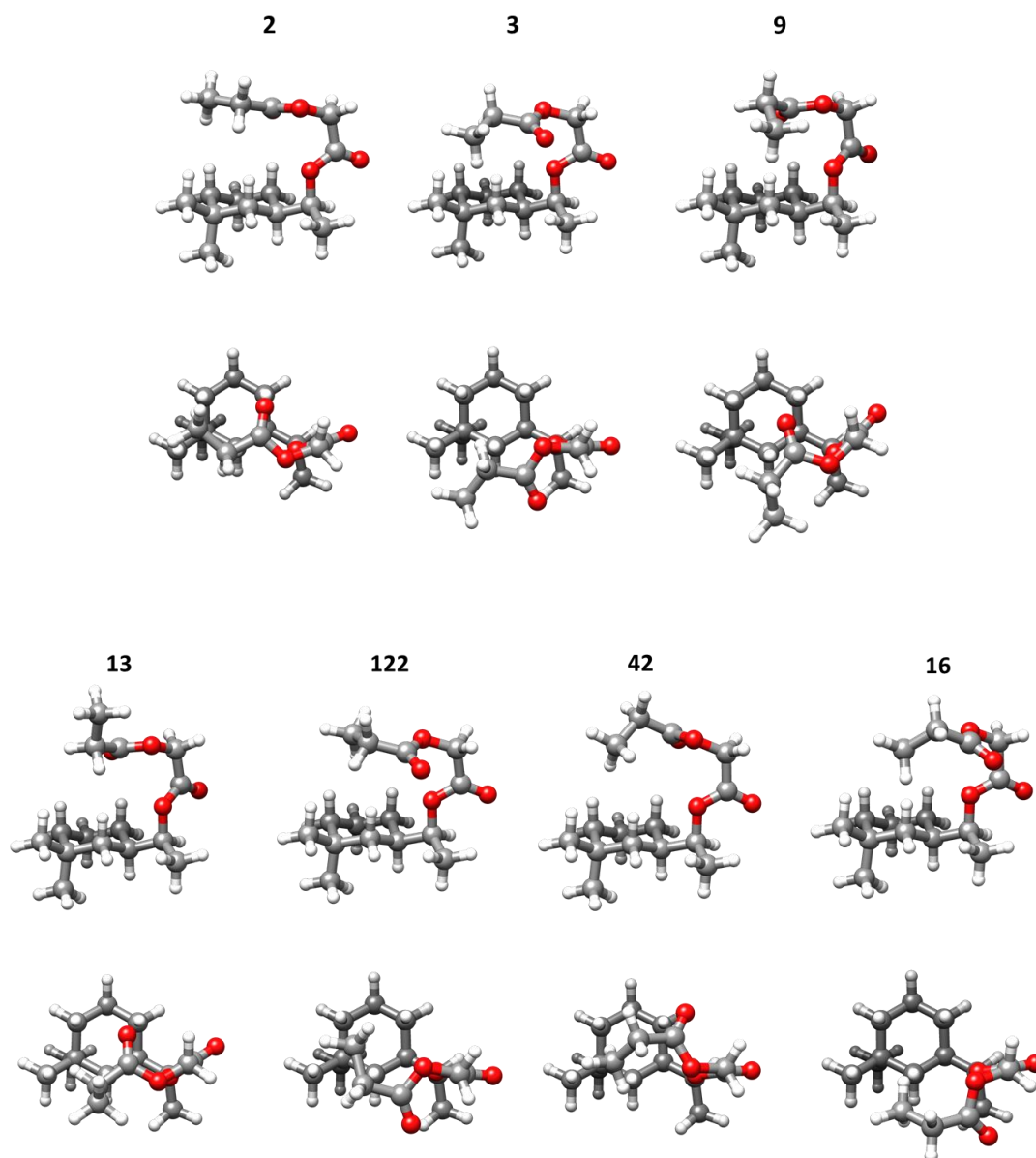


Figure 10.4. Conformations of romandolide with aliphatic tails **above** the cyclohexane ring optimised at B3LYP-D3BJ/6-311++G(d,p), with side and top views.

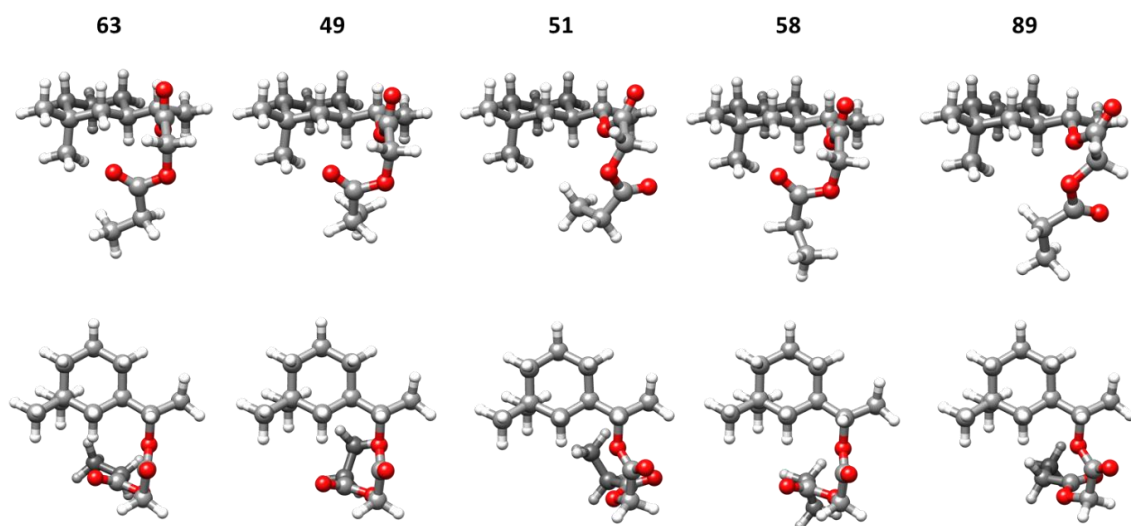


Figure 10.5. Conformations of romandolide with aliphatic tails **below** the cyclohexane ring optimised at B3LYP-D3BJ/6-311++G(d,p), with side and top views.

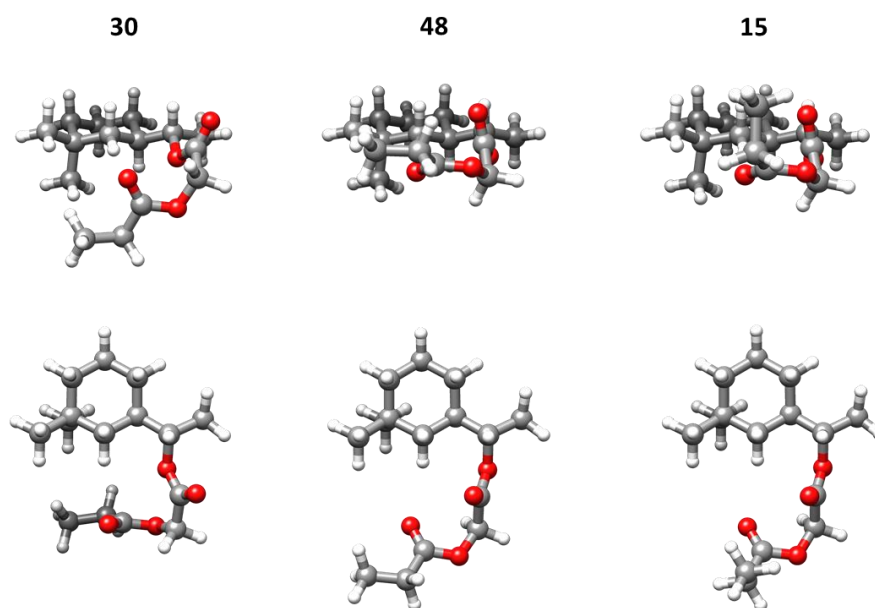


Figure 10.6. Conformations of romandolide with aliphatic tails **around (front)** the cyclohexane ring optimised at B3LYP-D3BJ/6-311++G(d,p), with side and top views.

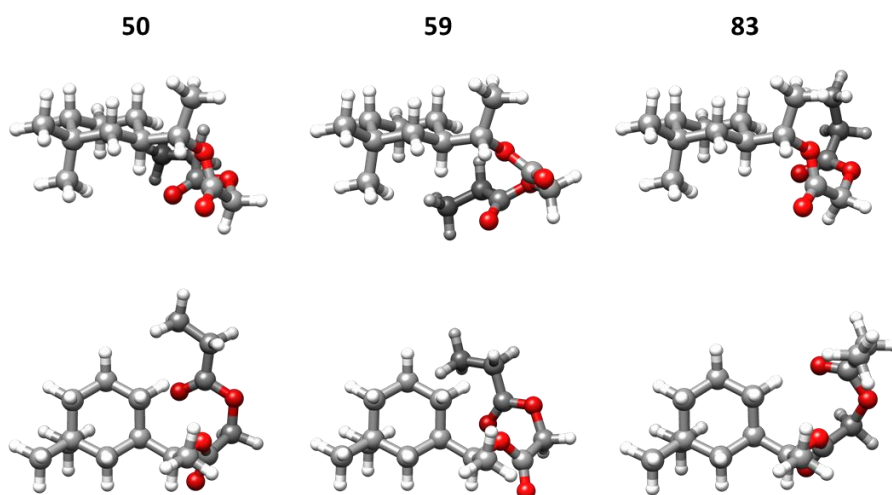


Figure 10.7. Conformations of romandolide with aliphatic tails **around (back)** the cyclohexane ring optimised at B3LYP-D3BJ/6-311++G(d,p) within 600 cm^{-1} , with side and top views.

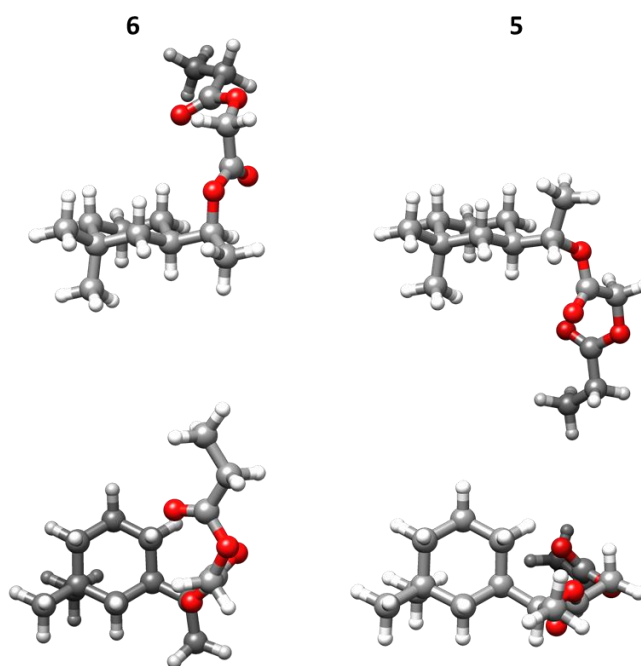


Figure 10.8. Conformations of romandolide with aliphatic tails **away** from the cyclohexane ring predicted by B3LYP-D3BJ/6-311++G(d,p), with side and top views.

10.4. Discussion

Conformational preferences and intramolecular interactions

The relative abundances of experimentally determined species were calculated using common observed *c*-type transitions and the square of their predicted dipole moments. From the calculations it was determined that the ratio of the assigned conformers **48** : **30** : **2** : **50** : **3** : **9** in the molecular jet was 17 : 7 : 6 : 2 : 1 : 1, respectively. The most abundant conformer **48** has the aliphatic chain around the cyclohexane ring forming interactions with the C–H groups of the cyclohexane ring and dimethyl moiety. The 2nd most abundant species is conformer **30**, which also has the alicyclic chain around the cyclohexane ring in a similar arrangement to conformer **48**. Comparing the structures of **48** and **30**, in conformer **48** the aliphatic tail is almost levelled with the cyclohexane plane, whilst in conformer **30** it is slightly below the plane.

Conformer **2** was estimated to be 3rd most abundant in the molecular jet with a relative abundance of 6 to 1 with respect to the least abundant conformers **3** and **9**. Nonetheless, all three structures **2**, **3** and **9** are similar by having the aliphatic tail located above the cyclohexane ring. The higher abundance of conformer **2** seems to be associated with a more favourable folding of the tail, which appears to sit on top of the ring potentially forming further interactions with the hydrogens of cyclohexane. In conformers **3** and **9** the tail is slightly displaced towards the side of the cyclohexane, resulting in a decrease in stability. Conformer **50** has a relative abundance of 2 to 1 with respect to conformers **3** and **9**. It is the only assigned conformer where the aliphatic tail is arranged around the cyclohexane on the side opposite to the dimethyl group. Interaction of aliphatic tail with the dimethyl moiety seems to have a considerable effect to stabilise conformers **30** and **48**, compared to conformer **50** where these contacts are lacking.

The relative abundance results do not agree with the energy ordering predicted by the theoretical methods. Furthermore, the Gibbs energies at B3LYP-D3BJ/6-311++G(d,p) and B3LYP-D3BJ/def2TZVP are not in agreement with the experimental relative abundances of the observed conformers. The most thermodynamically favoured conformers according to Gibbs predictions are **58** at B3LYP-D3BJ/6-311++G(d,p) and **89** at B3LYP-D3BJ/def2TZVP, which have not been observed experimentally. Both **58** and **89** have the aliphatic tail below and further away from the cyclohexane moiety. The disagreements between experimental and theoretically expected abundances could be explained by conformational relaxation of higher energy conformers to lower energy configurations.^{10,11} Investigation of conformational interconversion pathways is out of the scope of this work, and it can be very complex given the high flexibility in the aliphatic tail.

To visualise the intramolecular interactions involved in stabilizing the observed conformers, we have employed the non-covalent interactions (NCIs) method.¹² The calculated NCI and RDG plots for all six assigned conformers are presented in Figure 10.9. On first look, the predominant colour in the isosurfaces is green, which indicates weak attractive interactions between the aliphatic tails and the cyclohexane group. Interestingly, both the hydrogens and the oxygens in the aliphatic tail form weak attractive interactions with the H–C groups in cyclohexane. There are also attractive intramolecular interactions within the aliphatic tail in all conformers, and repulsive interactions between H atoms in the tail and those in cyclohexane. The intricate network established by all these interactions drives the stability of the conformations.

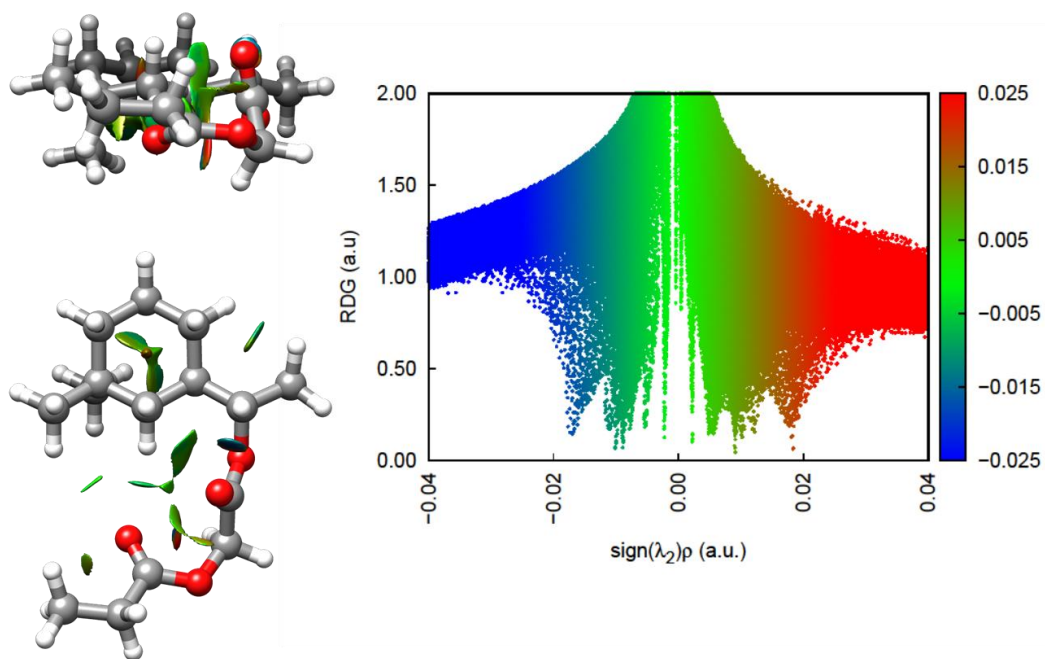
All conformers display two CH \cdots O=C interactions within the aliphatic tail, closing a five-membered intramolecular ring. These interactions are displayed as blue/red isosurfaces, indicating the stabilising attractive interactions (blue) and the strain due to the formation of the ring (red). All conformers except conformer **9** also display a weaker attractive interaction between the carbonyl oxygen O₄ (labelled in Figure 10.10) and a H atom of the tail's terminal methyl group (Figure 10.11). Conformer **9** shows a weak attractive interaction between ethyl oxygen O₃ and a H atom of the tail's terminal methyl group. In addition, all conformers except **48** show an interaction between the ethyl oxygens that seem to have attractive and strain components like the CH \cdots O=C interactions, given their blue/red isosurfaces.

Considering the interactions between the aliphatic tail and the hydrogens of cyclohexane, all conformers show an attractive interaction between the ethyl oxygen O₁ and one (conformers **48**, **30**, **50**) or two (conformers **2**, **3**, **9**) of the hydrogens of cyclohexane. These interactions also display attractive/strain features. In addition to these, there are weak attractive interactions between the hydrogens of cyclohexane and the hydrogens of the aliphatic tail. The latter involve Hs of the terminal ethyl group and/or the carbonyl oxygens. Finally, repulsive interactions where H atoms are closer than the sum of their van der Waals radii (2.40 Å)^{13,14}, occur in all conformers between the tail's methyl group in alpha to cyclohexane and a nearby H atom. These repulsive interactions are at distances of 2.22 Å - 2.32 Å.

Conformer **48** is the only conformer where both carbonyl oxygens form contacts with the H–C groups in cyclohexane, with distances of 2.53, 2.96 and 3.14 Å. Moreover, the carbonyl closer to the end of the tail has a more favourable orientation of the oxygen lone pairs to interact with the hydrogens of cyclohexane than in conformer **30**. This could explain the higher abundance of conformer **48** with respect to conformer **30**, since the other interactions are very similar. In conformers **2**, **3** and **9** there is an additional H-H interaction involving one of the H of the tail's terminal methyl group, and in conformer **50** involving the tail's methyl group in alpha and a second H of cyclohexane. This additional interaction could explain the slightly lower

abundance of **2** with respect to **30**. In conformers **50** and **3** the oxygens of the tail are not involved in attractive interactions with cyclohexane, which may be the reason for their lower abundance. Conformer **9** does have O₄-cyclohexane interactions, but the tail seems to bend over itself which may not be an optimal configuration.

Conformer 48



Conformer 30

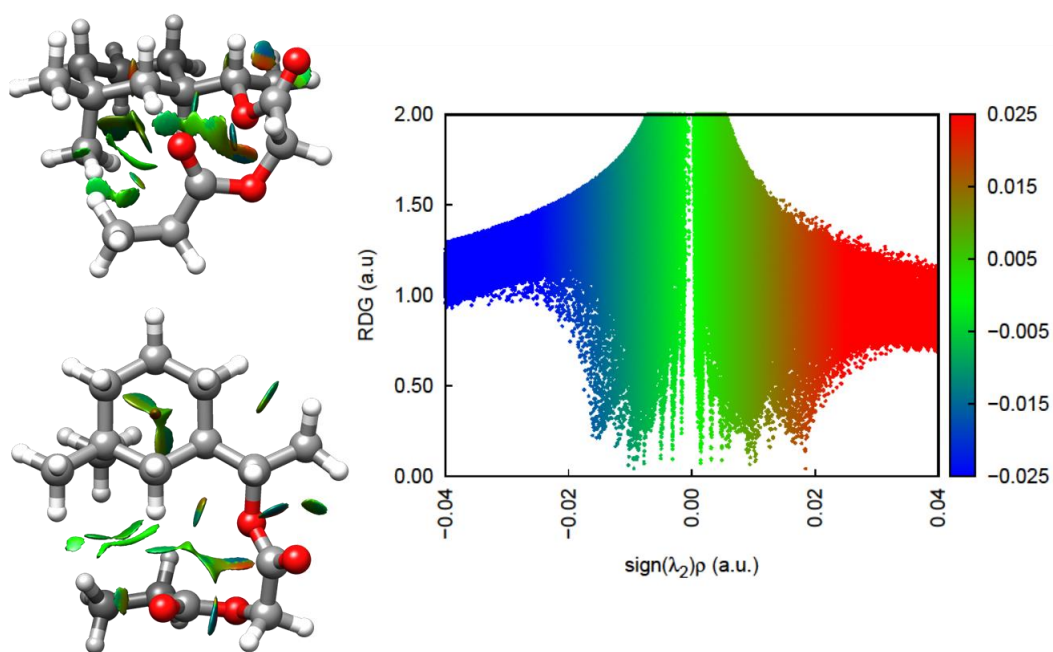


Figure 10.9. Non-covalent interactions analysis, NCI and RDG plots, of the six identified conformers of romandolide.

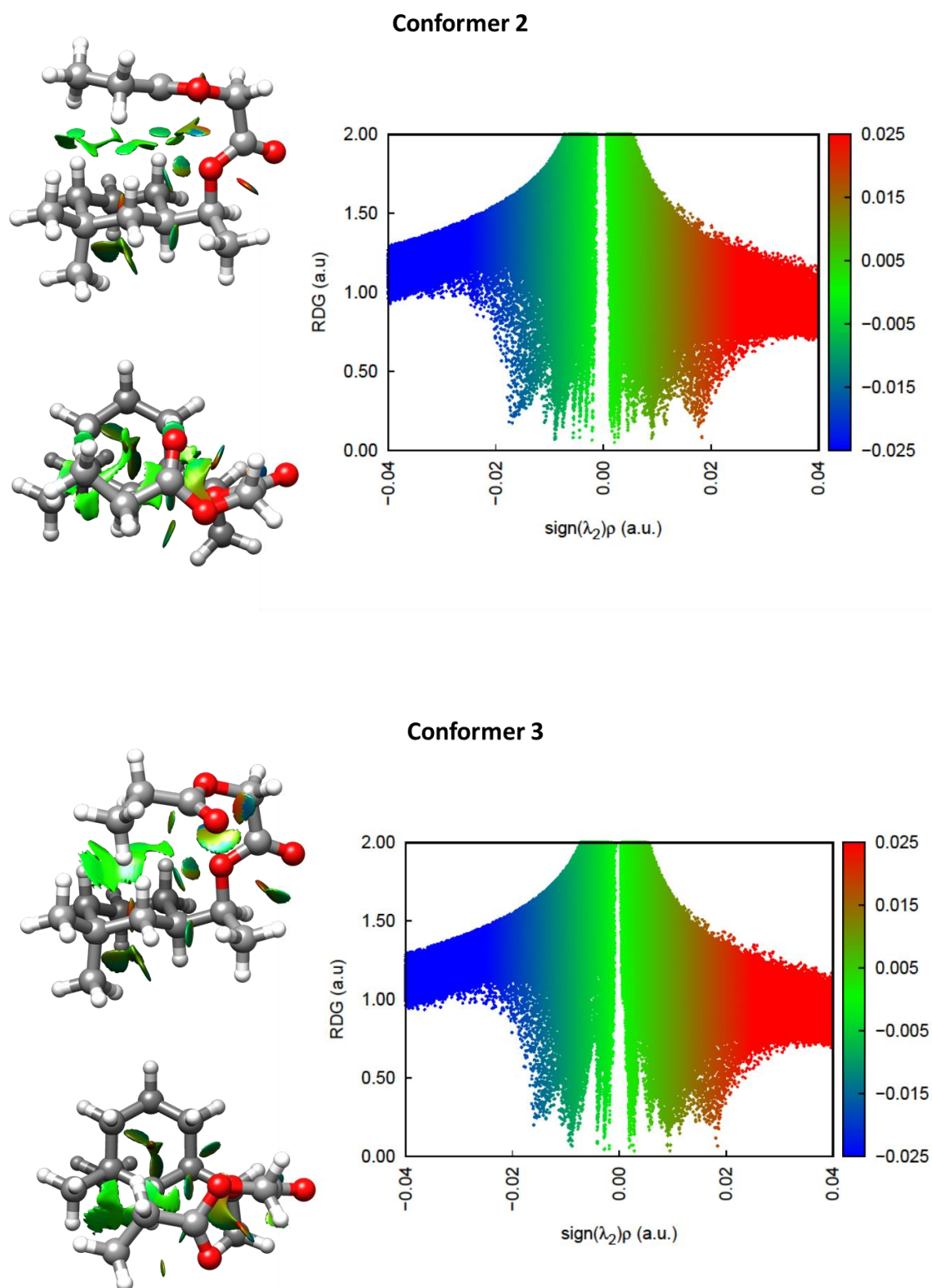
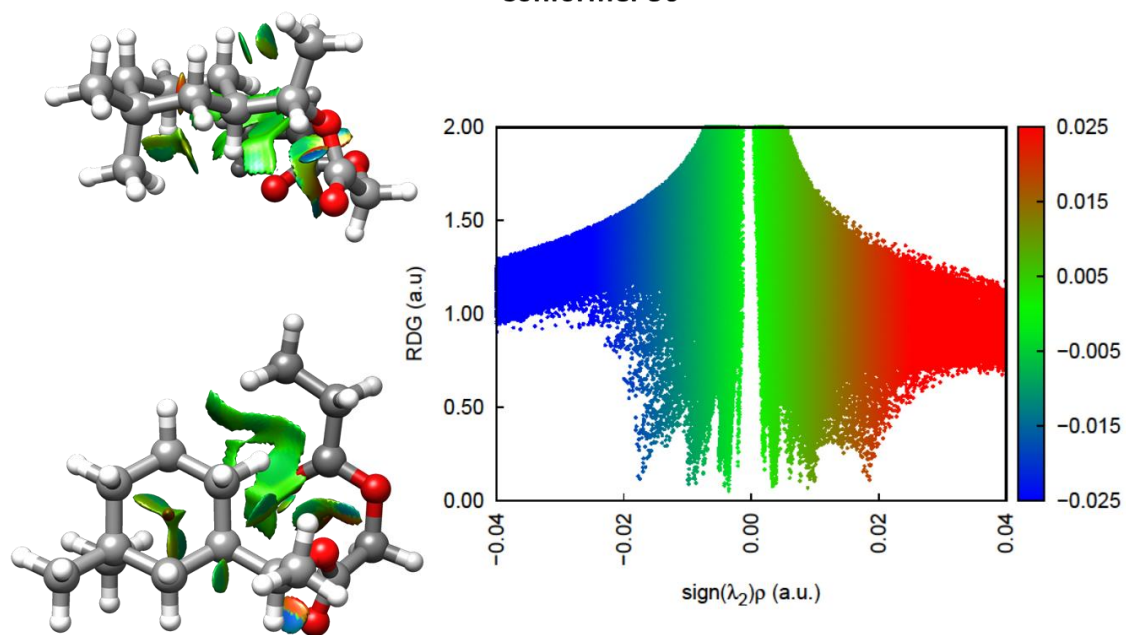


Figure 10.9 cont'd. Non-covalent interactions analysis, NCI and RDG plots, of the six identified conformers of romandolide.

Conformer 50



Conformer 9

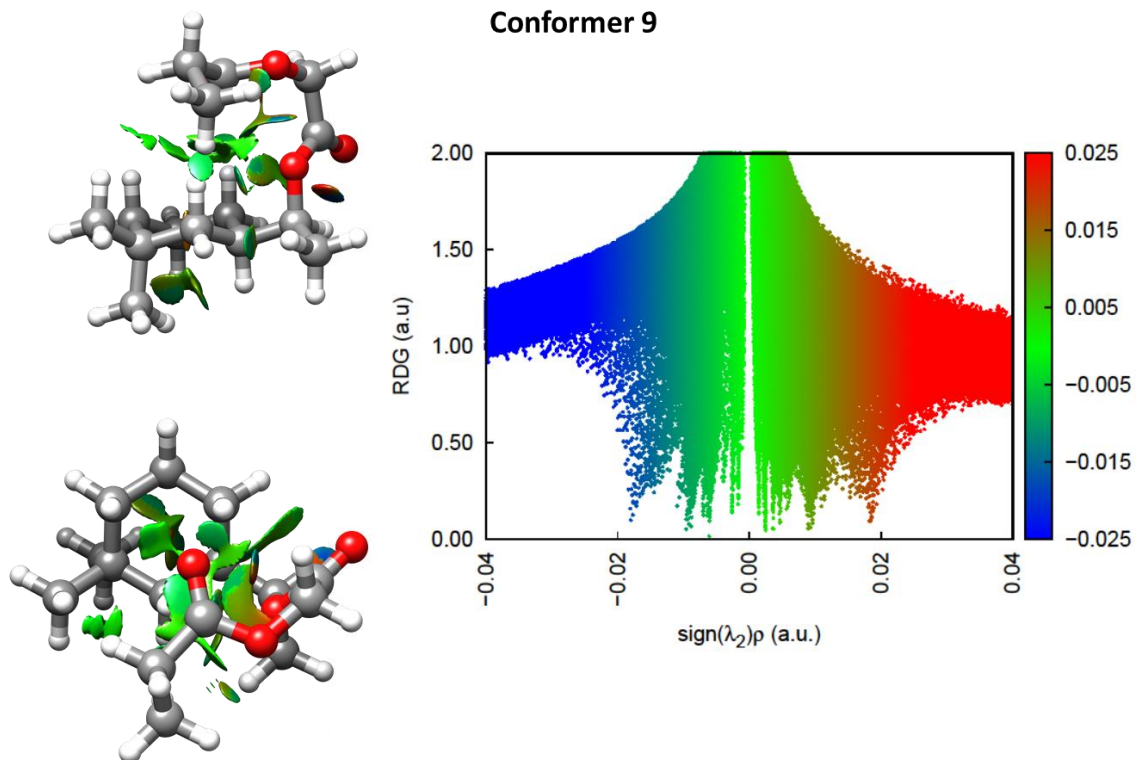


Figure 10.9 cont'd. Non-covalent interactions analysis, NCI and RDG plots, of the six identified conformers of romandolide.

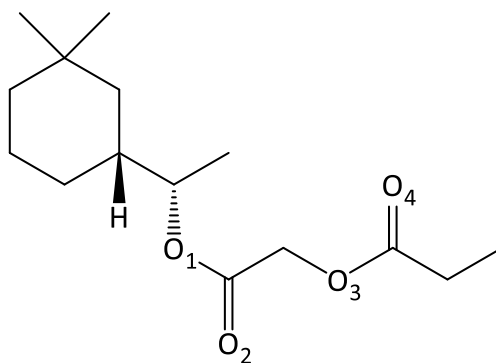


Figure 10.10. Oxygen labels in the structure of romandolide.

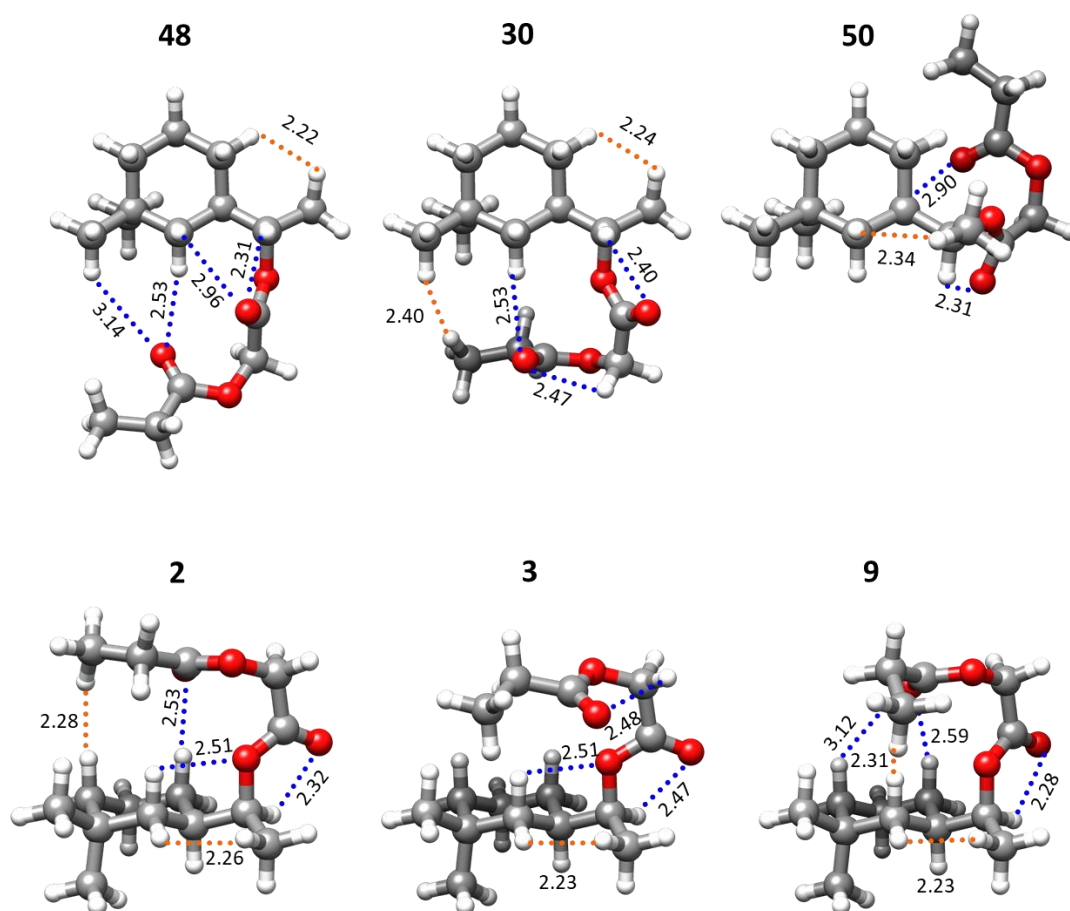


Figure 10.11. Intramolecular interactions in the assigned conformers of romandolide. The interactions in blue represent weak attractive interactions between O...H-C groups and their distances in Å, and the distances in orange are the H...H interactions, measured on the B3LYP-D3BJ structures.

Benchmarking of computational methods

To our knowledge, there are no theoretical studies on alicyclic musks using density functional theory and/or ab initio calculations, and no information on their performance. We have carried out a series of calculations using different levels of theory and basis sets and benchmarked them by comparing their predicted rotational constants against the experimental values.

Comparing the results from the three methods used with the same basis set (Table 10.7), the overall deviations of the predicted rotational constants from the experimental ones are 1.5% for B3LYP-D3BJ, 1.8% for MP2 and 1.6% for B2PLYP-D3BJ. It can be concluded that B3LYP-GD3BJ is the best performing method, followed by B2PLYP-D3BJ. The MP2 theoretical predictions are the furthest from experimental values, with higher deviations for *B* and *C* constants. B3LYP-GD3BJ not only provide the best accuracy, but also outperformed MP2 and B2PLYP-D3BJ in computational cost.

Once the best method was determined, we benchmarked its performance with two other basis sets, def2TZVP and def2QZVP (Table 10.8). Def2TZPV and def2QZVP performed overall slightly better compared to 6-311++G(d,p), with B3LYP-GD3BJ/def2TZPV offering the best combination of computational speed and accuracy.

The energy ordering of the assigned conformers changes slightly from one level of theory to another. Nevertheless, all methods predicted conformer **2** as the global minimum, followed by conformer **30** in all B3LYP-GD3BJ and B2PLYP-GD3BJ calculations, and conformer **9** in MP2 predictions. The highest in energy consistently being conformer **48** and **50**. These findings are in disagreement with our experimental estimations of their experimental relative abundances.

Table 10.7. Theoretical rotational constants and the % deviation from experiment by B3LYP-D3BJ, MP2 and B2PLYP-D3BJ levels of theory with 6-311++G(d,p) basis set.

Conformer	Parameter	6-311++G(d,p)					
		B3LYP-D3BJ		MP2		B2PLYP-D3BJ	
2	A ^a	450.1	-0.6% ^b	454.2	0.3%	453.2	0.1%
	B	310.7	2.5%	315.9	4.2%	313.7	3.5%
	C	228.1	2.0%	236.7	5.8%	231.3	3.4%
30	A	435.0	-1.5%	445.7	0.9%	440.0	-0.4%
	B	300.7	0.9%	302.7	1.5%	303.0	1.6%
	C	205.6	1.1%	208.0	2.2%	207.4	1.9%
3	A	468.2	-0.2%	482.1	2.7%	474.2	1.0%
	B	283.4	0.7%	283.8	0.9%	285.3	1.4%
	C	218.3	0.7%	221.4	2.1%	220.7	1.8%
9	A	467.9	6.4%	478.6	8.9%	471.9	7.3%
	B	302.6	-0.6%	304.2	-0.1%	305.9	0.5%
	C	247.5	0.0%	252.2	1.9%	251.0	1.4%
48	A	499.6	-2.0%	505.8	-0.8%	500.3	-1.9%
	B	247.3	3.2%	251.3	4.9%	252.1	5.2%
	C	181.7	1.4%	184.6	3.0%	184.3	2.8%
0	A	510.7	-2.3%	523.3	0.1%	515.4	-1.4%
	B	257.2	1.5%	261.9	3.4%	260.7	2.9%
	C	210.2	-0.1%	218.0	3.6%	214.6	2.0%

[a] A, B, and C are the rotational constants. [b] Deviation from the experiment; calculated as $(A_{\text{calc}} - A_{\text{exp}}) / A_{\text{exp}} \times 100\%$.

Table 10.8. Theoretical rotational constants and the % deviation from experiment by B3LYP-D3BJ with 6-311++G(d,p), def2TZVP and def2QZVP basis sets.

Conformer	Parameter	B3LYP-D3BJ					
		6-311++G(d,p)		def2TZVP		def2QZVP	
2	A ^a	450.1	-0.6% ^b	450.8	-0.5%	451.3	-0.4%
	B	310.7	2.5%	310.1	2.3%	310.2	2.4%
	C	228.1	2.0%	227.5	1.7%	227.7	1.8%
30	A	435.0	-1.5%	436.4	-1.2%	437.1	-1.0%
	B	300.7	0.9%	300.8	0.9%	301.8	1.3%
	C	205.6	1.1%	205.4	1.0%	205.3	0.9%
3	A	468.2	-0.2%	469.0	-0.1%	469.0	-0.1%
	B	283.4	0.7%	283.1	0.6%	283.5	0.7%
	C	218.3	0.7%	218.0	0.5%	218.1	0.6%
9	A	467.9	6.4%	468.8	6.6%	468.9	6.7%
	B	302.6	-0.6%	302.0	-0.8%	301.5	-1.0%
	C	247.5	0.0%	246.9	-0.2%	246.5	-0.4%
48	A	499.6	-2.0%	502.8	-1.4%	503.5	-1.2%
	B	247.3	3.2%	246.5	2.8%	245.7	2.5%
	C	181.7	1.4%	181.7	1.4%	181.4	1.2%
50	A	510.7	-2.3%	513.7	-1.7%	514.2	-1.6%
	B	257.2	1.5%	256.7	1.3%	256.8	1.4%
	C	210.2	-0.1%	210.4	0.0%	210.5	0.1%

[a] A, B, and C are the rotational constants. [b] Deviation from the experiment; calculated as $(A_{\text{calc}} - A_{\text{exp}}) / A_{\text{exp}} \times 100\%$.

Comparison with macrocycles

In our molecular jet we have only assigned folded conformations of romandolide. Having analysed the macrocycles muscone, civetone and exaltolide, we can compare the most abundant conformers of romandolide with those of the macrocyclic musks (Figure 10.10) and determine whether there are any similarities. Firstly, all structures, except civetone **8a**, have the carbonyl group perpendicular to the plane of the rest of the molecule. This suggests that this configuration may play a role in the binding process to the musk olfactory receptor. The two most abundant conformers of romandolide, **48** and **30**, have the aliphatic tail on, or close to, the plane of cyclohexane, resembling the planar arrangement of macrocycles. Further, the methyl groups in romandolide **48** and **30** are in plane with the rest of the molecule and point away, which is similar to muscone, specifically with the orientation of methyl group in muscone **13h**.

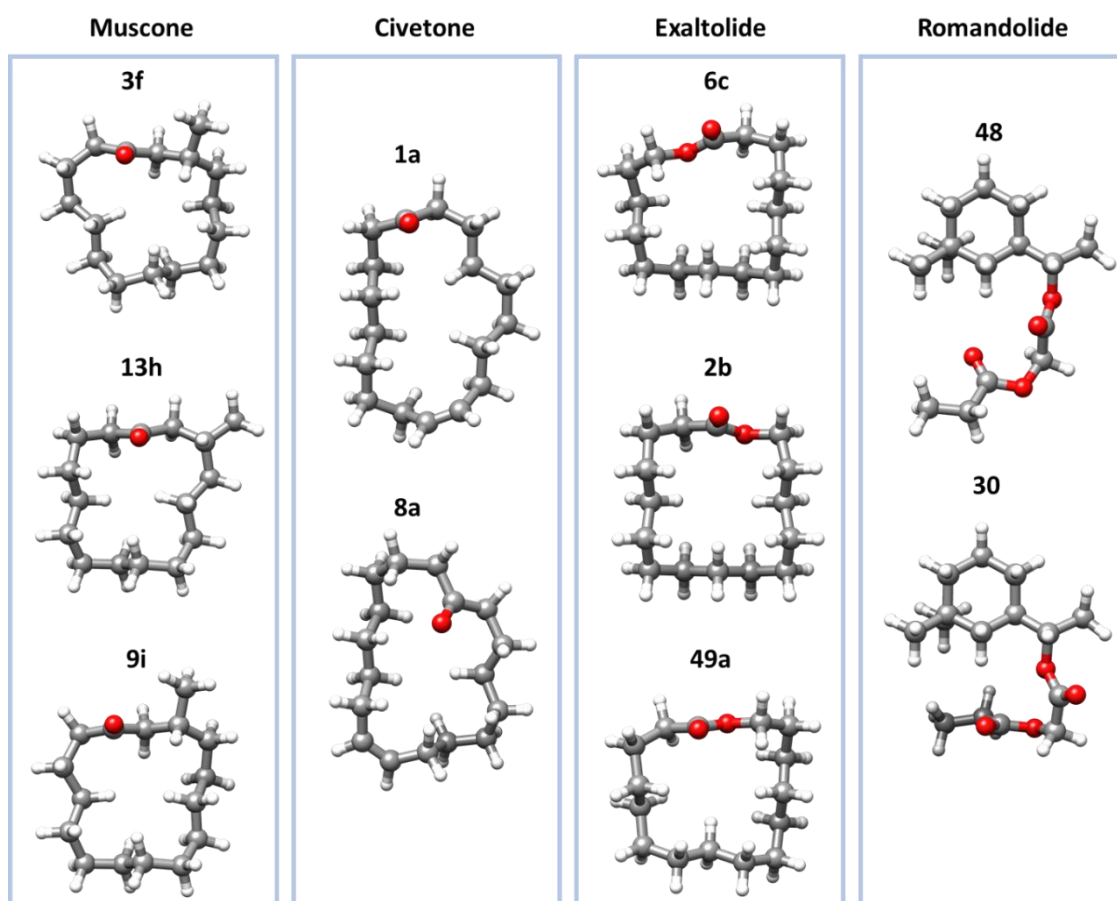


Figure 10.12. The most abundant conformations of muscone, civetone, exaltolide and romandolide.

Kraft's olfactophore model

The olfactophore model suggested by Kraft *et al.* is mainly based on silicon containing analogues of alicyclic musks and provides a correlation of 84%.² It consists of two hydrogen-bond acceptors (HBA) at a distance of 6.96 Å from one another and two aliphatic hydrophobes situated at a distance of 7.51 Å from one another, with one of the hydrophobes right in front of one of the hydrogen-bond acceptors at a distance of only 0.91 Å. None of the observed conformations of romandolide fit in this olfactophore model, as all HBA are situated at closer distances than 6.96 Å proposed in the model.

Only one structure of unmodified romandolide was included in the development of the model, and it was obtained theoretically. This configuration of romandolide is different from the experimental ones identified here, as it is not folded and has the aliphatic tail away from the cyclohexane moiety. Moreover, the structures included in the development of the olfactophore have been optimised at B3LYP/6-31G(d) level of theory, which from our previous experience does not perform well with large systems where dispersion forces are involved.^{15,16} Another drawback of the olfactophore model is that it only included one conformation of each alicyclic musk. We have learned from our investigation that romandolide has a high degree of flexibility, implying that more than one conformation could take part in the olfaction process.¹⁷

The inclusion of experimental evidence, such as the conformations of romandolide presented in this chapter, could lead to an improved olfactophore model.

10.5. Conclusions

The conformations of the commercial alicyclic musk romandolide have been characterised for the first time using broadband rotational spectroscopy in combination with quantum chemistry calculations. Six conformers have been unambiguously identified, corresponding to folded configurations. All identified conformations of romandolide adopt a horseshoe shape, with the most abundant conformer being 17 times more abundant than the least abundant ones. Romandolide shows a strong preference for the conformations where the aliphatic tail is arranged around the cyclohexane moiety, adopting similar configurations to the macrocyclic musks muscone (Chapter 7), civetone (Chapter 8) and exaltolide (Chapter 9). The conformational preference of romandolide is influenced by a balance of different weak attractive interactions and repulsive H···H contacts. Several density functional theory and *ab initio* methods have been benchmarked against our experimental data. Our results show that the functional B3LYP including Grimme's D3BJ dispersion performs best for molecular systems like romandolide.

Further theoretical investigation comparing the most favoured conformations of the macrocyclic and the alicyclic musks presented in this thesis could elucidate whether the two classes are activating the same olfactory receptors.

10.6. Bibliography

1. Eh, M. New Alicyclic Musks: The Fourth Generation of Musk Odorants. *Chemistry and Biodiversity* **1**, 1975–1984 (2004).
2. Liu, J. *et al.* Synthesis and Olfactory Properties of Silicon-Containing Analogs of Rosamusks, Romandolide, and Applelide: Insights into the Structural Parameters of Linear Alicyclic Musks. *European Journal of Organic Chemistry* **2016**, 976–982 (2016).
3. Kraft, P. “Brain aided” musk design. *Chemistry and Biodiversity* **1**, 1957–1974 (2004).
4. Zou, Y. *et al.* Efficient macrocyclization by a novel oxy-oxonia-cope reaction: Synthesis and olfactory properties of new macrocyclic musks. *Chemistry - A European Journal* **18**, 7010–7015 (2012).
5. Pracht, P., Bohle, F. & Grimme, S. Automated exploration of the low-energy chemical space with fast quantum chemical methods. *Physical Chemistry Chemical Physics* **22**, 7169–7192 (2020).
6. Pickett, H. M. The fitting and prediction of vibration-rotation spectra with spin interactions. *Journal of Molecular Spectroscopy* **148**, 371–377 (1991).
7. Novick, S. E. A beginner’s guide to Pickett’s SPCAT/SPFIT. *Journal of Molecular Spectroscopy* **329**, 1–7 (2016).
8. Watson, J. K. G. *Vibrational Spectra and Structure*. Elsevier Amsterdam **6**, 1–89 (1977).
9. Western, C. M. PGOPHER: A program for simulating rotational, vibrational and electronic spectra. *Journal of Quantitative Spectroscopy and Radiative Transfer* **186**, 221–242 (2017).
10. Ruoff, R. S., Klots, T. D., Emilsson, T. & Gutowsky, H. S. Relaxation of conformers and isomers in seeded supersonic jets of inert gases. *The Journal of Chemical Physics* **93**, 3142–3150 (1990).
11. Zwier, T. S. Laser spectroscopy of jet-cooled biomolecules and their water-containing clusters: Water bridges and molecular conformation. *Journal of Physical Chemistry A* **105**, 8827–8839 (2001).
12. Johnson, E. R. *et al.* Revealing noncovalent interactions. *Journal of the American Chemical Society* **132**, 6498–6506 (2010).
13. Pauling, L. *The Nature of the Chemical Bond and the Structure of Molecules and Crystals: An Introduction to Modern Structural Chemistry*. (Cornell University Press, 1960).
14. Bondi, A. Van der Waals volumes and radii. *Journal of Physical Chemistry* **68**, 441–451 (1964).
15. Burevschi, E., Alonso, E. R. & Sanz, M. E. Binding Site Switch by Dispersion Interactions: Rotational Signatures of Fenchone–Phenol and Fenchone–Benzene Complexes. *Chemistry - A European Journal* **26**, 11327–11333 (2020).

16. Loru, D., Vigorito, A., Santos, A. F. M., Tang, J. & Sanz, M. E. The axial/equatorial conformational landscape and intramolecular dispersion: New insights from the rotational spectra of monoterpenoids. *Physical Chemistry Chemical Physics* **21**, 26111–26116 (2019).
17. Liu, M. T., Na, M., Li, Y., Biscoe, M. R. & Ryan, K. Conformational Sensing by a Mammalian Olfactory Receptor. *Chemistry - A European Journal* **26**, 11462–11469 (2020).



CONFORMATIONAL INVESTIGATION OF AN ALICYCLIC MUSK: HELVETOLOLIDE

Chapter 11



11. CONFORMATIONAL INVESTIGATION OF AN ALICYCLIC MUSK: HELVETOLIDE

11.1. Introduction

Helvetolide is a member of the alicyclic musk class. It was discovered in 1990 by Giersch and Schulte-Elte at Firmenich and its fragrance is described as fruity and pear-like.¹⁻³ It is structurally related to romandolide, discussed in Chapter 10 of this thesis. The difference between the two musk compounds lies in the functionality on the aliphatic tail, where helvetolide contains a *gem*-dimethyl group instead of the carbonyl group in romandolide (Figure 11.1). Both odorants are widely applied in perfume oil formulas.

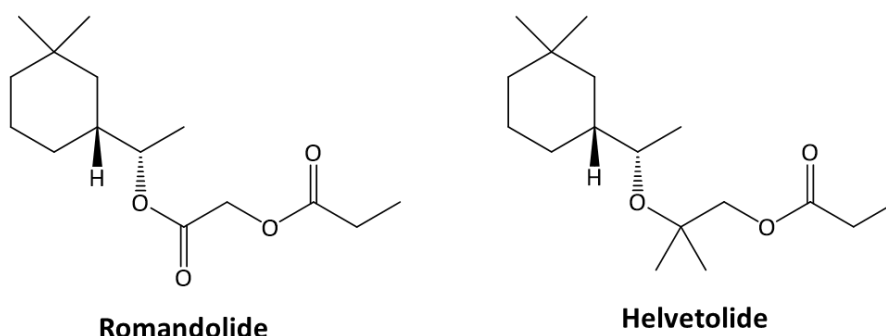


Figure 11.2. Molecular structures of romandolide and helvetolide.

Helvetolide, similar to romandolide, has not been studied structurally or conformationally due to the large flexibility of the aliphatic tail, which results in a rich conformational landscape preventing its crystallisation. Only one study on the structure-odour relationship of helvetolide is available up to date, where Kraft *et al.* have substituted certain parts of the odorant with different functional groups and measured the musk potency of the analogues.⁴ Interestingly, it was discovered that moving the position of the ester group in the tail led to loss of musky character, confirming its osmophoric role, which is to bind to the olfactory receptor (OR). Moreover, substituting the ethyl oxygen closer to the cyclohexane ring by a $-\text{CH}_2$ group also contributed to total loss of muskiness. This indicates that electronegativity of this site in the tail plays an important role in the odorant's binding to the OR.⁴

In this work, we have employed broadband rotational spectroscopy in combination with theoretical methods to investigate the conformational landscape of helvetolide. We have identified experimentally six conformations and their relative abundances have been estimated. All the conformers observed display a horseshoe configuration where the alicyclic tail interacts with the cyclohexane ring through weak attractive interactions.

11.2. Methods

Theoretical

The potential energy surface of helvetolide was explored using molecular mechanics, with the MMFFs force field and an energy limit of 25 kJ/mol. The conformational search returned a total of 575 conformations. All conformers were optimised at B3LYP-D3BJ level of theory with the 6-311++G(d,p) basis set. A total of 190 distinct conformers were returned within 1000 cm⁻¹. We performed harmonic vibrational calculations on the conformers within 500 cm⁻¹ using B3LYP-D3BJ/6-311++G(d,p) and confirmed that they were local minima. Their zero-point relative energies and Gibbs free energies at the temperature at which the experiment was conducted were obtained and are shown in Table 11.1. For benchmarking purposes these conformers have been optimized at MP2/6-311++G(d,p) level (Table 11.2). The zero-point energies at MP2 level of theory were not calculated due to the high computational cost. The rotation barriers of all six methyl groups for the conformer predicted to be the global minimum by B3LYP-D3BJ have been calculated at the same level of theory. They are all predicted to be higher than 750 cm⁻¹ (Figure 11.2), and therefore no splitting of lines due to methyl internal rotation was expected to be observed in our rotational spectrum.

Experimental

The broadband spectrum of helvetolide (Firmenich, ≥80%) was recorded using our CP-FTMW spectrometer at King's, which operates in the 2-8 GHz frequency range.^{5,6} Helvetolide was heated at 447 K in a bespoke nozzle, was seeded in neon at 5 bar, and conducted to the vacuum chamber where the molecules expand adiabatically forming a supersonic jet. The molecular pulse was polarized by four chirped microwave pulses of 4 μs duration each. After each microwave pulse, the emission signal was collected as free induction decay (FID) for 20 μs into the oscilloscope. The final spectrum was obtained from adding up 2.3M FIDs. The time domain spectrum was converted to the frequency domain using a fast Fourier transform algorithm. The spectrum obtained was very dense, with 0.5 lines/MHz with a signal to noise ratio of 3 : 1.

Table 11.1. B3LYP-D3BJ/6-311++G(d,p) spectroscopic rotational parameters, relative raw and ZPC energies for helvetolide conformations within 500 cm⁻¹.

B3LYP-D3BJ	1	2	37	171	34	12	15	19	21	62
A ^a (MHz)	374.7	391.2	404.2	411.6	415.2	358.5	452.7	336.5	390.5	430.7
B (MHz)	279.4	280.4	282.5	264.3	265.8	281.1	254.9	308.2	250.3	238.5
C (MHz)	195.8	198.2	208.4	202.9	207.5	210.0	207.1	185.4	180.5	186.4
κ ^b	-0.07	-0.15	-0.24	-0.41	-0.44	-0.04	-0.61	0.63	-0.34	-0.57
μ _a ^c (D)	0.6	-1.1	-1.2	-1.3	1.1	0.8	-1.5	-0.4	-1.0	-1.1
μ _b (D)	0.1	0.3	-1.4	-1.9	0.6	-0.6	0.0	-1.1	0.5	1.6
μ _c (D)	-2.0	0.4	2.2	-1.5	-0.6	2.1	0.5	-0.6	-0.4	2.1
ΔE ^d (cm ⁻¹)	0.0	5.6	115.6	320.3	259.6	308.4	145.6	208.6	302.7	367.5
ΔE ₀ ^e (cm ⁻¹)	0.0	30.5	144.0	304.2	314.7	318.0	318.5	323.3	333.2	347.6
ΔG ^f (cm ⁻¹)	101.2	144.0	376.2	238.3	246.3	444.0	728.2	819.7	230.9	376.6
	27	53	6	75	81	281	18	36	16	92
A ^a (MHz)	405.0	395.4	385.4	428.6	377.5	409.9	399.6	426.1	384.0	411.2
B (MHz)	269.6	233.2	269.7	241.0	271.2	277.5	235.6	246.5	266.9	210.7
C (MHz)	210.3	173.1	198.9	189.6	194.1	207.8	179.2	192.9	195.8	183.6
κ ^b	-0.39	-0.46	-0.24	-0.57	-0.16	-0.31	-0.49	-0.54	-0.24	-0.76
μ _a ^c (D)	0.8	-1.4	0.9	-1.6	0.8	-1.6	0.9	-1.2	0.7	0.7
μ _b (D)	0.3	0.1	0.2	0.5	-1.4	-1.5	0.8	0.5	0.6	0.7
μ _c (D)	-2.1	0.4	-2.1	0.3	2.2	-1.1	2.1	-0.7	-0.7	1.1
ΔE ^d (cm ⁻¹)	324.5	411.5	329.9	317.1	371.3	354.7	491.0	345.5	390.9	539.1
ΔE ₀ ^e (cm ⁻¹)	357.5	370.0	386.9	387.4	392.2	395.1	460.7	476.5	490.3	514.7
ΔG ^f (cm ⁻¹)	422.5	0.0	334.7	236.2	486.6	778.7	380.3	459.1	380.3	162.2

[a] A, B, C are the rotational constants [b] Ray's asymmetry parameter [c] μ_a, μ_b and μ_c are the electric dipole moment components. [d] Relative electronic energies. [e] Relative electronic energies including the zero-point correction. [f] Gibbs free energies calculated at 447 K.

Table 11.2. MP2/6-311++G(d,p) spectroscopic rotational parameters, relative raw and ZPC energies for helvetolide conformations within 500 cm⁻¹.

MP2	2	1	37	15	171	6	34	12	36	16
A ^a (MHz)	388.4	369.8	413.3	456.6	423.0	383.4	406.6	358.4	428.5	383.6
B (MHz)	285.5	286.0	281.5	258.2	267.1	275.3	270.3	285.0	253.9	270.3
C (MHz)	200.4	197.2	211.1	209.9	206.9	200.6	209.3	209.0	197.5	198.0
κ ^b	-0.09	0.03	-0.30	-0.61	-0.44	-0.18	-0.38	0.02	-0.51	-0.22
μ _a ^c (D)	-0.8	-0.4	-1.1	1.4	1.3	-0.7	0.7	0.8	1.0	0.5
μ _b (D)	0.2	0.3	-1.4	0.0	-1.7	0.4	-0.5	-0.5	0.6	-0.5
μ _c (D)	0.3	1.8	1.9	0.3	1.4	1.9	0.6	-2.0	0.6	0.6
ΔE ^d (cm ⁻¹)	0.0	54.6	165.2	171.9	222.5	250.2	298.1	304.3	331.8	335.2
	75	27	19	62	281	21	53	81	18	92
A ^a (MHz)	431.0	407.0	339.8	439.9	415.2	398.4	403.9	390.5	402.2	418.3
B (MHz)	244.2	274.0	308.4	240.5	278.7	251.4	236.3	269.5	239.0	213.2
C (MHz)	193.2	214.3	185.2	190.5	209.5	183.1	176.4	200.6	181.5	187.0
κ ^b	-0.57	-0.38	0.59	-0.60	-0.33	-0.37	-0.47	-0.27	-0.48	-0.77
μ _a ^c (D)	1.4	-0.7	0.2	1.1	-1.6	0.8	1.2	0.6	-0.9	0.5
μ _b (D)	0.4	-0.6	-1.0	-1.5	-1.4	0.7	0.0	-1.4	-0.7	0.8
μ _c (D)	-0.3	1.9	0.4	1.8	-1.0	0.4	-0.5	1.9	2.0	0.9
ΔE ^d (cm ⁻¹)	343.4	360.5	372.5	397.2	410.4	420.6	490.2	492.0	586.0	751.1

[a] A, B, C are the rotational constants [b] Ray's asymmetry parameter [c] μ_a, μ_b and μ_c are the electric dipole moment components. [d] Relative electronic energies.

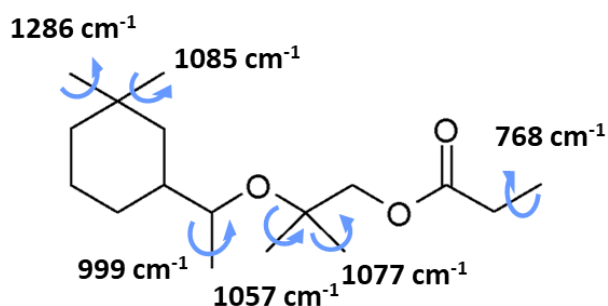


Figure 11.2. Methyl rotation barrier heights of the six methyl groups of conformer **1** of helvetolide at the B3LYP-D3BJ/6-311++G(d,p) level of theory.

11.3. Results

Theoretical results

Most of the low energy conformations of helvetolide are predicted to adopt folded configurations with the alicyclic tail bending below, above or around the cyclohexane moiety (Figures 11.3-11.6). Extended configurations, where the aliphatic tail is either perpendicular to or in line with the cyclohexane ring, have also been found in the potential energy surface but they lie at higher energies than the folded structures. Only one low-energy conformation within 500 cm⁻¹ has the aliphatic tail not forming interactions with cyclohexane ring (Figure 11.6). Helvetolide prefers to adopt folded configurations where the aliphatic tail is below the cyclohexane, with ten out of 20 low-energy conformations showing this arrangement (Figure 11.3). Four have the aliphatic tail above the ring (Figure 11.4), three have their aliphatic tail around the cyclohexane on the same side as the dimethyl moiety (Figure 11.5), and two have the aliphatic tail around the cyclohexane on the opposite side to the dimethyl groups (Figure 11.6).

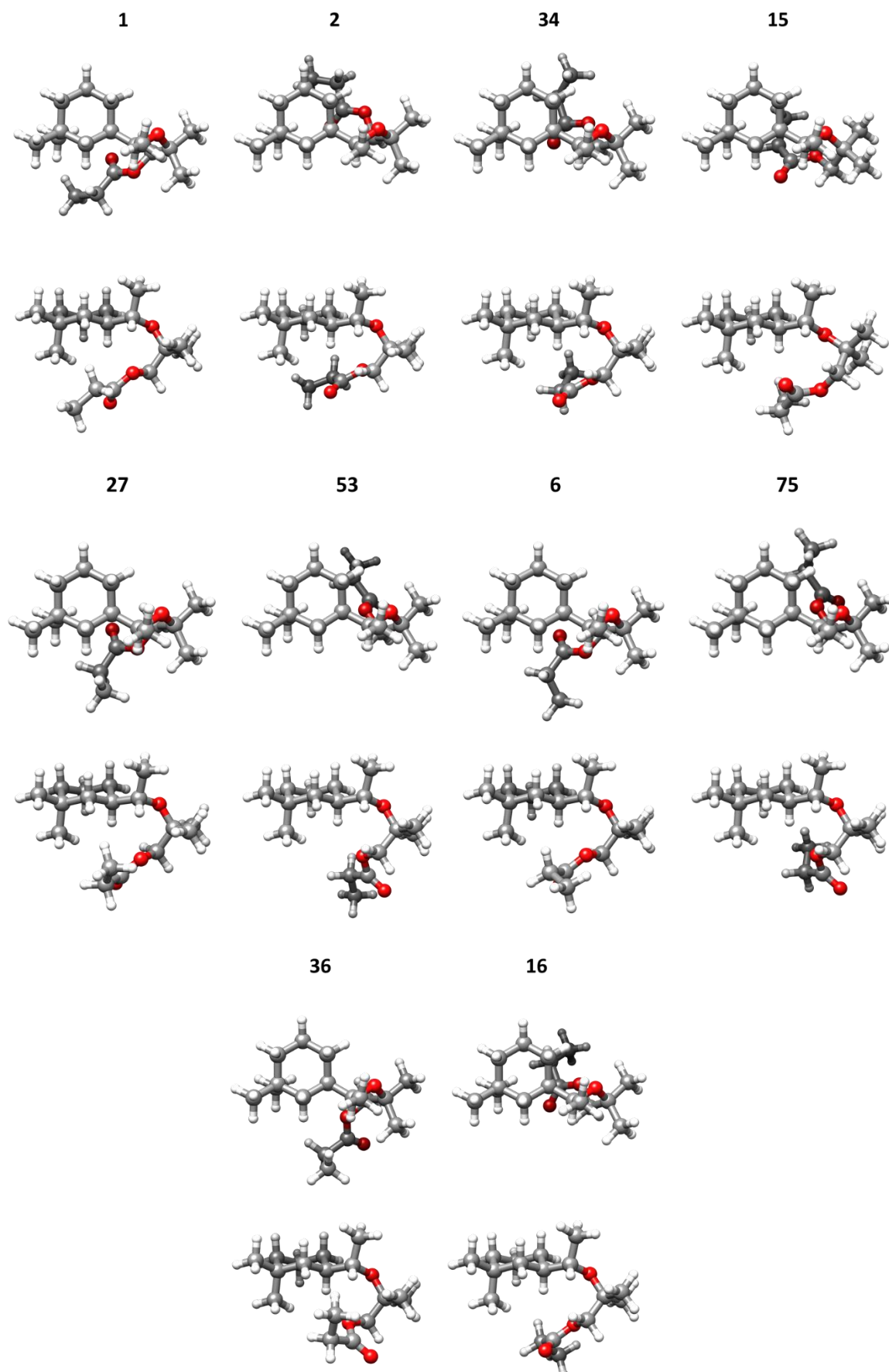


Figure 11.3. Top and side views of the conformations of helvetolide with aliphatic tails **below** the cyclohexane ring optimised at B3LYP-D3BJ/6-311++G(d,p) level.

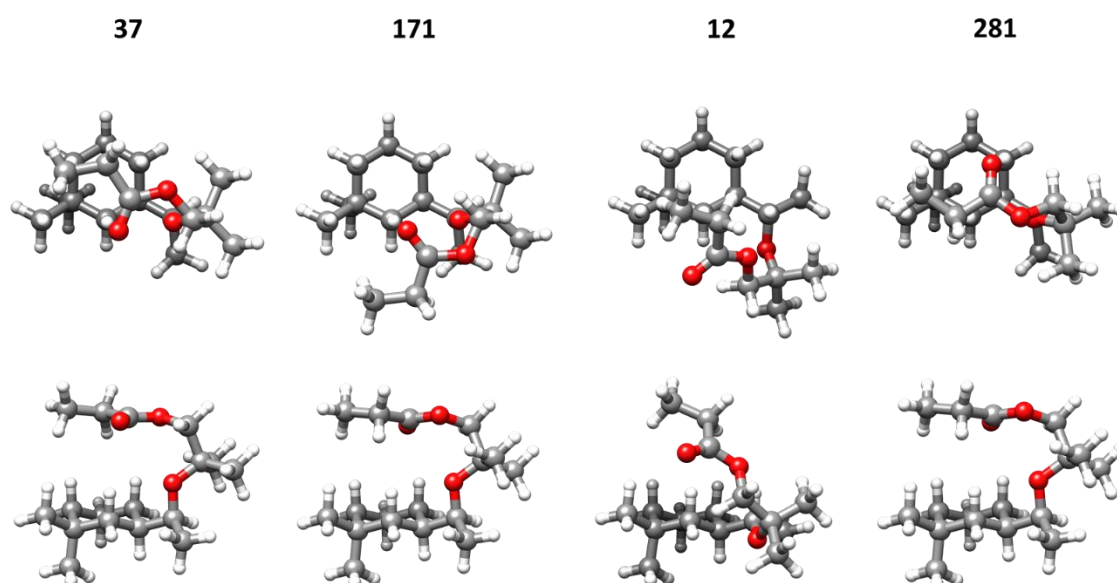


Figure 11.4. Top and side views of the conformations of helvetolide with aliphatic tails **above** the cyclohexane ring optimised at B3LYP-D3BJ/6-311++G(d,p) level.

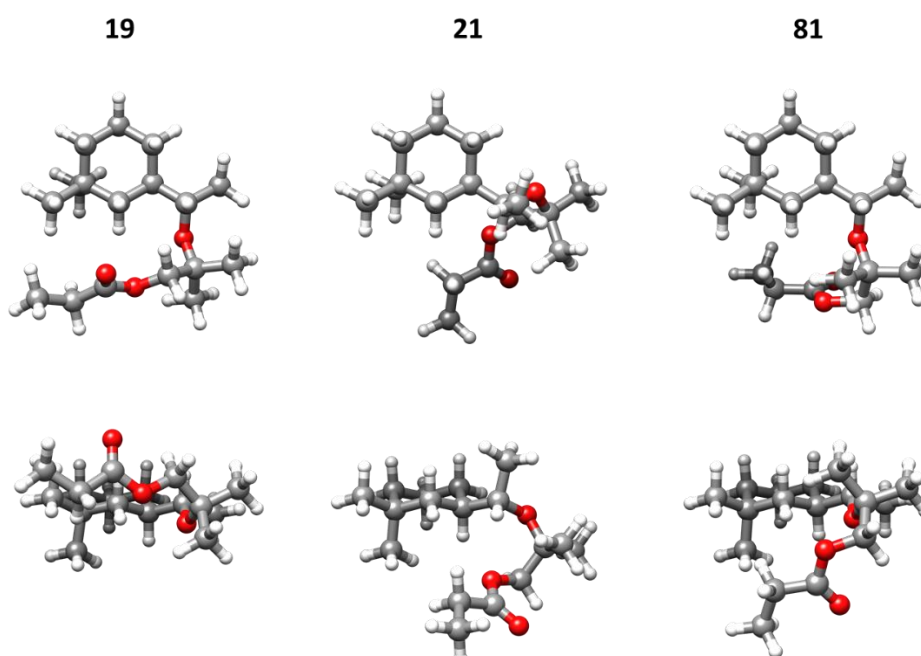


Figure 11.5. Top and side views of the conformations of helvetolide with aliphatic tails **around** the cyclohexane ring on the same side as the dimethyl groups optimised at B3LYP-D3BJ/6-311++G(d,p) level.

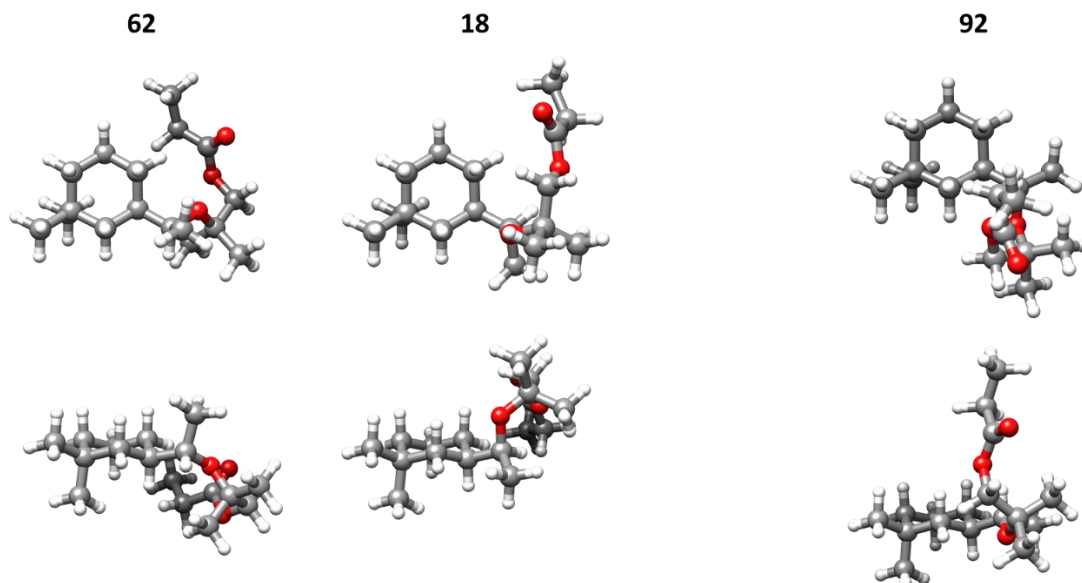


Figure 11.6. Top and side views of the conformations of helvetolide with aliphatic tails **around** the cyclohexane ring on the opposite side to the dimethyl groups and one conformation with the tail **away** from the cyclohexane ring optimised at B3LYP-D3BJ/6-311++G(d,p).

Spectral assignment

Most of the predicted low-energy conformers of helvetolide are highly asymmetric with a κ asymmetry parameter close to zero, which, together with the high spectral density, makes patterns belonging to individual species difficult to identify. Therefore, the automated fitting method implemented in PGOPHER^{7,8} was used for spectral assignment. Guided by the theoretical predictions, six rotamers were assigned in the spectrum of helvetolide. Their experimental spectroscopic parameters were determined by fitting the observed transitions to the semi-rigid rotor Watson Hamiltonian in the A reduction and I' representation,⁹ using Pickett's program.^{10,11} All measured transitions are included in Appendix VIII.

The first assigned rotamer **I** has a κ asymmetry parameter very close to zero, -0.01 . Experimentally it has shown mainly *c*-type spectrum and the assigned lines are some of the most intense. Its assignment to conformer **1**, the global minimum at B3LYP level and 2nd in the energy order at MP2 level, was straightforward, based on the agreement between the rotational constants, predicted dipole moments and the intensity of the spectrum. For this rotamer, also *a*- and *b*-type transitions with $K_{-1} = 0, 1, 2$ with much lower intensity compared to *c*-type transitions have been observed. These transitions appeared overlapped in the spectrum.

Conformer **2** was predicted to have very similar rotational constants, however it was discarded as a possible assignment because it is expected to show predominantly *a*-type transitions from its predicted dipole moment components (Tables 11.1 and 11.2).

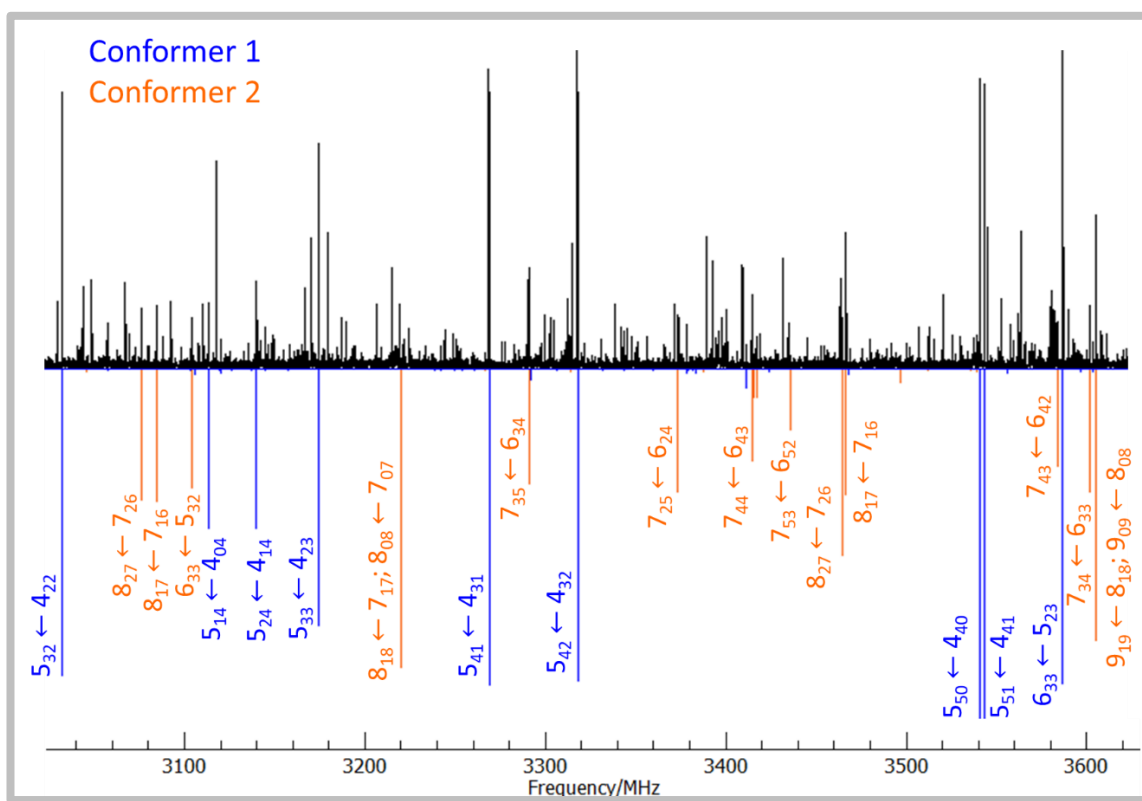


Figure 11.7. Experimental broadband rotational spectrum between 3000-3650 MHz (black, upper trace), and simulated spectrum (lower trace) of conformers **1** (blue) and **2** (orange) using their experimental rotational constants.

The assignment of rotamer **II**, another highly asymmetric species, to conformer **2**, was supported by the agreement between the rotational constants, and the intensity of the observed *a*-, *b*- and *c*-type spectra, in line with the predicted μ_a , μ_b and μ_c . Whilst the rotational constants of this rotamer are similar to conformer **1**, observation of *a*-type spectrum with higher intensity than *b*- and *c*-type spectra allows its unambiguous assignment to conformer **2**. Figure 11.7 shows a segment of the spectrum between 3000-3650 MHz, and the assigned *a*- and *c*-type transitions of conformers **2** and **1**, respectively.

Rotamer **III**, which is an asymmetric top closer to the prolate limit with a κ value of -0.2 , was identified as conformer **37** based on the agreement between experimental and theoretically predicted parameters, and the observation of *c*-type spectrum with higher intensity compared to *a*- and *b*-type spectra. This is in agreement with the predicted dipole moments and rules out

its assignment to conformer **281**, which has similar theoretical rotational constants but is expected to show predominantly *a*- and *b*-type transitions. It is also predicted higher in energy.

Rotamer **IV** is identified as conformer **34**, from the observation of *a*-type spectrum slightly higher in intensity than the similarly intense *b*- and *c*-type spectra, in agreement with the predicted dipole moments. The experimental κ asymmetry parameter of this rotamer is -0.42 , which is consistent with the predicted κ asymmetry parameters at both B3LYP and MP2 level of theory, further supporting the assignment. Conformer **34** is the most prolate conformer of helvetolide identified in the spectrum.

Rotamer **V** is another highly asymmetric top, and is identified as conformer **12**, supported by the agreement between the experimental and theoretical rotational constants and the predicted dipole moments vs. observed spectral intensity. *A*-, *b*- and *c*-type transitions were observed for this rotamer, with *c*-type transitions being more intense. There are no other predicted conformations with similar parameters, hence the assignment of this rotamer to **12** was unambiguous. The final observed rotamer in the spectrum, rotamer **VI**, has a positive κ asymmetry parameter of 0.55 , unlike the other five rotamers. It is the only observed species that is an oblate rotor. It has been identified as conformer **19** due to its distinct set of theoretical rotational constants. Conformer **19** is the only predicted conformation with a similar value of κ . Moreover, observation of *b*-type spectrum agrees well with the predicted dipole moment components. The experimental parameters of this rotamer were determined by fitting the observed transitions to the semi-rigid rotor Watson Hamiltonian in the A reduction and III^I representation,⁹ using Pickett's program.¹⁰

No other low-energy conformers could be identified in the spectrum despite repeated searches for them. Their non-observation could be because they relax to other conformers lower in energy, by collisions in the supersonic jet,^{12,13} or because they are not sufficiently populated in our supersonic jet.

Table 11.3. Experimental spectroscopic constants of the observed conformers of helvetolide.

Parameter	I - 1	II - 2	III - 37
A (MHz) ^a	367.60101(17)	372.05486(24)	401.07575(21)
B (MHz)	279.76859(14)	278.93852(12)	277.67751(11)
C (MHz)	193.35639(13)	194.037882(95)	206.265207(80)
Δ_J (kHz)	0.00914(44)	0.00812(36)	0.01103(35)
Δ_{JK} (kHz)	0.0165(22)	0.0455(25)	0.0324(19)
Δ_K (kHz)	0.0082(23)	0.0172(41)	-
δ_J (kHz)	0.00199(23)	0.001505(17)	0.00314(19)
δ_K (kHz)	0.0178(17)	0.0226(16)	-
κ^b	-0.01	-0.05	-0.27
$a/b/c$ (D) ^c	y/y/y	y/y/y	y/y/y
σ (kHz) ^d	5.0	8.1	7.1
N^e	143	307	276
	IV - 34	V - 12	VI - 19
A (MHz)	411.89131(26)	370.07099(51)	339.35(29)
B (MHz)	261.56831(20)	281.35888(42)	303.39(223)
C (MHz)	200.539137(11)	208.51201(15)	183.58701(16)
Δ_J (kHz)	0.01843(77)	0.0127(13)	0.00370(16)
Δ_{JK} (kHz)	0.0542(40)	0.0222(60)	-
Δ_K (kHz)	-0.0386(43)	-	-
δ_J (kHz)	0.00360(38)	0.00234(66)	-
δ_K (kHz)	0.0290(36)	-	-
κ	-0.42	-0.10	0.55
$a/b/c$ (D)	y/y/y	y/y/y	n/y/n
σ (kHz)	8.7	7.9	5.3
N	260	100	54

[a] A , B and C are the rotational constants. Δ_J , Δ_{JK} , Δ_K , δ_J and δ_K are the quartic centrifugal distortion constants; [b] κ is the asymmetry parameter; [c] a , b and c are the type of transitions observed; [d] σ is the rms deviation of the fit; [e] N is the number of the fitted transitions; [f] Standard error in parentheses in units of the last digit.

11.4. Discussion

Benchmarking of computational methods

The performance of the B3LYP-D3BJ and MP2 methods using the 6-311++G(d,p) basis set at predicting the rotational constants was benchmarked against experimental data. B3LYP-D3BJ performed slightly better, with an average deviation of 1.1% from the experimental values, whilst MP2 showed a 1.4% deviation. The largest discrepancies at B3LYP/6-311++G(d,p) level are noted for the A constant of conformer **2**, C constant of **34** and A constant of **12**, with discrepancies of 5.1%, 3.5% and -3.1%, respectively. MP2 shows similar differences for the same rotational constants, and also slightly larger deviations than B3LYP-D3BJ for the rotational constants of conformer **37**. These average deviations are slightly larger than the ones observed for romandolide.

Table 11.4. Theoretical rotational constants and the % deviation from experiment by B3LYP-D3BJ and MP2 with 6-311++G(d,p) basis set.

		B3LYP-D3BJ		MP2	
1	A ^a	374.7	1.9% ^b	369.8	0.6%
	B	279.4	-0.1%	286.0	2.2%
	C	195.8	1.3%	197.2	2.0%
2	A	391.2	5.1%	388.4	4.4%
	B	280.4	0.5%	285.5	2.4%
	C	198.2	2.1%	200.4	3.3%
37	A	404.2	0.8%	413.3	3.0%
	B	282.5	1.7%	281.5	1.4%
	C	208.4	1.0%	211.1	2.3%
34	A	415.2	0.8%	406.6	-1.3%
	B	265.8	1.6%	270.3	3.3%
	C	207.5	3.5%	209.3	4.4%
12	A	358.5	-3.1%	358.4	-3.2%
	B	281.1	-0.1%	285.0	1.3%
	C	210.0	0.7%	209.0	0.2%
19	A	336.5	-0.7%	339.8	0.3%
	B	308.2	1.5%	308.4	1.5%
	C	185.4	1.0%	185.2	0.9%

[a] A, B, and C are the rotational constants. [b] Deviation from the experiment; calculated as $(A_{\text{calc}} - A_{\text{exp}})/A_{\text{exp}} \times 100\%$.

Conformational preferences and intramolecular interactions

The relative abundances of the experimentally observed species were calculated using common *a* and *b*-type transitions and the square of their predicted dipole moments as $\mu_a^2 + \mu_b^2$, as most of the *a*- and *b*-type transitions with $K_{-1} = 0, 1, 2$ appear overlapped in the spectrum.¹⁴ The ratio of the assigned conformers **34** : **2** : **1** : **37** : **12** : **19** in the molecular jet was estimated to be 2.7 : 2.6 : 1.6 : 1.2 : 1.0 : 1.0, respectively. The relative abundances are quite close to each other. Compared to romandolide, helvetolide does not show a strong preference for a single conformation.

The most abundant conformer **34** has the aliphatic chain below the cyclohexane ring forming interactions with the $-\text{CH}_2$ groups of cyclohexane (Figure 11.9). The 2nd most abundant species, with very similar relative abundance to conformer **34**, is conformer **2**, which also has the alicyclic chain below the cyclohexane ring in a similar arrangement to conformer **34**. The main differences are that in conformer **2** the aliphatic tail appears to be closer to the center of the cyclohexane ring than in conformer **34**, and the terminal ethyl group is rotated 120° compared to its position in conformer **34**. The 3rd most abundant conformer **1** also has the aliphatic tail below the cyclohexane ring, but displaced to be closer to the dimethyl moiety. The fact the three most abundant conformers have their tail below the cyclohexane potentially implies that this configuration is related to the olfactory properties of this musk odorant.

The next most abundant conformers are **37** and **12** with a relative abundance of 1.6 : 1.2, respectively. Both conformers have their aliphatic tail above the ring, but the aliphatic tail is displaced towards the dimethyl moiety in conformer **12** (see Figure 11.9). Conformer **19** was present in the molecular jet with the same relative abundance as conformer **12**, and has the aliphatic tail around the cyclohexane ring. This conformation is unique among the identified ones and comparable to those of the most abundant conformers **48** and **30** of romandolide.

The experimentally determined relative abundances of the six conformers do not agree with the energy ordering predicted by the theoretical methods. Furthermore, the Gibbs energies at B3LYP-D3BJ/6-311++G(d,p) do not correspond to the experimental relative abundances of the observed conformers. The most thermodynamically stable conformer according to Gibbs predictions at B3LYP-D3BJ/6-311++G(d,p) is **53**, which was not observed experimentally. The disagreement between experimental and theoretically expected abundances could be related to conformational relaxation of higher energy conformers to lower energy configurations.^{12,13} However, the conformational flexibility of helvetolide makes investigation of relaxation pathways a very challenging task, out of the scope of this thesis.

We have looked at the intramolecular interactions established in the conformations of helvetolide to get an insight on the forces that determine conformational preferences. In the discussion below, we use the labelling for the oxygens indicated in Fig. 11.8. We have indicated the relevant interactions in Fig. 11.9. We have employed the NCI method, which analyses the electron density and its derivatives, to visualise the intramolecular interactions.¹⁵ The calculated NCI plots for all six identified conformers are presented in Figure 11.10.

On first look, the predominant colour in the isosurfaces is green, which indicates weak attractive interactions between the aliphatic tails and the cyclohexane group. Interestingly, both the hydrogens and the oxygens in the aliphatic tail form weak attractive interactions with the hydrogens in cyclohexane and in the methyl groups. There are also attractive intramolecular interactions within the aliphatic tail in all conformers, and repulsive interactions between H atoms in the tail and those in cyclohexane.

All conformers display CH \cdots O=C interactions within the aliphatic tail, closing a five-membered intramolecular ring. These interactions are depicted as “almond”-shaped isosurfaces coloured half blue and half red in the NCI plots, indicating the stabilising attractive interactions (blue) and the strain due to the formation of the ring (red). Additional interactions within the tail are formed between the hydrogens of the methyl group closer to cyclohexane and the ones of the dimethyl group of conformers **37**, **12** and **19**, depicted in orange in Figure 11.9. Their distances are below the sum of van der Waals hydrogen radii of 2.4 Å,^{16,17} and in the NCI plots

they can be seen again as “almond”-shaped isosurfaces coloured in green/yellow, where yellow indicates steric strain. In addition, weak attractive interactions are formed in conformers **1** and **12** between the ethyl oxygen O₂ (see Figure 11.8 for labelling) and the hydrogens in the tail, including the dimethyl group ones. These interactions are indicated in blue in Figure 11.9 and their isosurfaces are coloured in light blue.

Further weak attractive interactions are formed between the carbonyl oxygen O₃ and the H atoms of the cyclohexane and the dimethyl group (in blue in Figure 11.9). The more abundant conformers **34**, **2** and **1** show more than one of these interactions, and they are slightly shorter. Conformer **1** shows slightly weaker interactions, longer than 3.0 Å, which may be the reason for its lower abundancy. In the least abundant conformers **37** and **12** only one of these interactions occur, whilst **19** has two CH \cdots O=C interactions but they are above 3.0 Å. The least abundant conformers also show H \cdots H interactions between the terminal methyl hydrogens in the tail and the dimethyl moiety in the cyclohexane, depicted in orange in Figure 11.9.

Finally, H \cdots H repulsive interactions where the H atoms are closer than the sum of their van der Waals radii (2.40 Å)^{16,17} occur in all conformers between the first methyl group in the tail from cyclohexane with the nearby H atoms in the cyclohexane. These repulsive interactions are at distances of 2.16 - 2.23 Å.

In summary, the intricate network established by all these interactions drives the stability of the conformations.

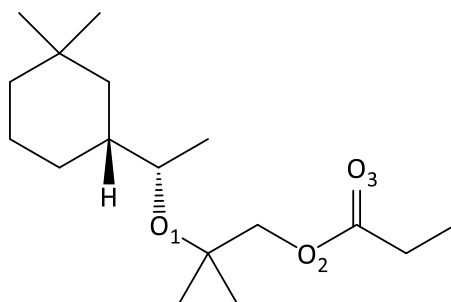


Figure 11.8. Oxygen labels in the structure of helvetolide.

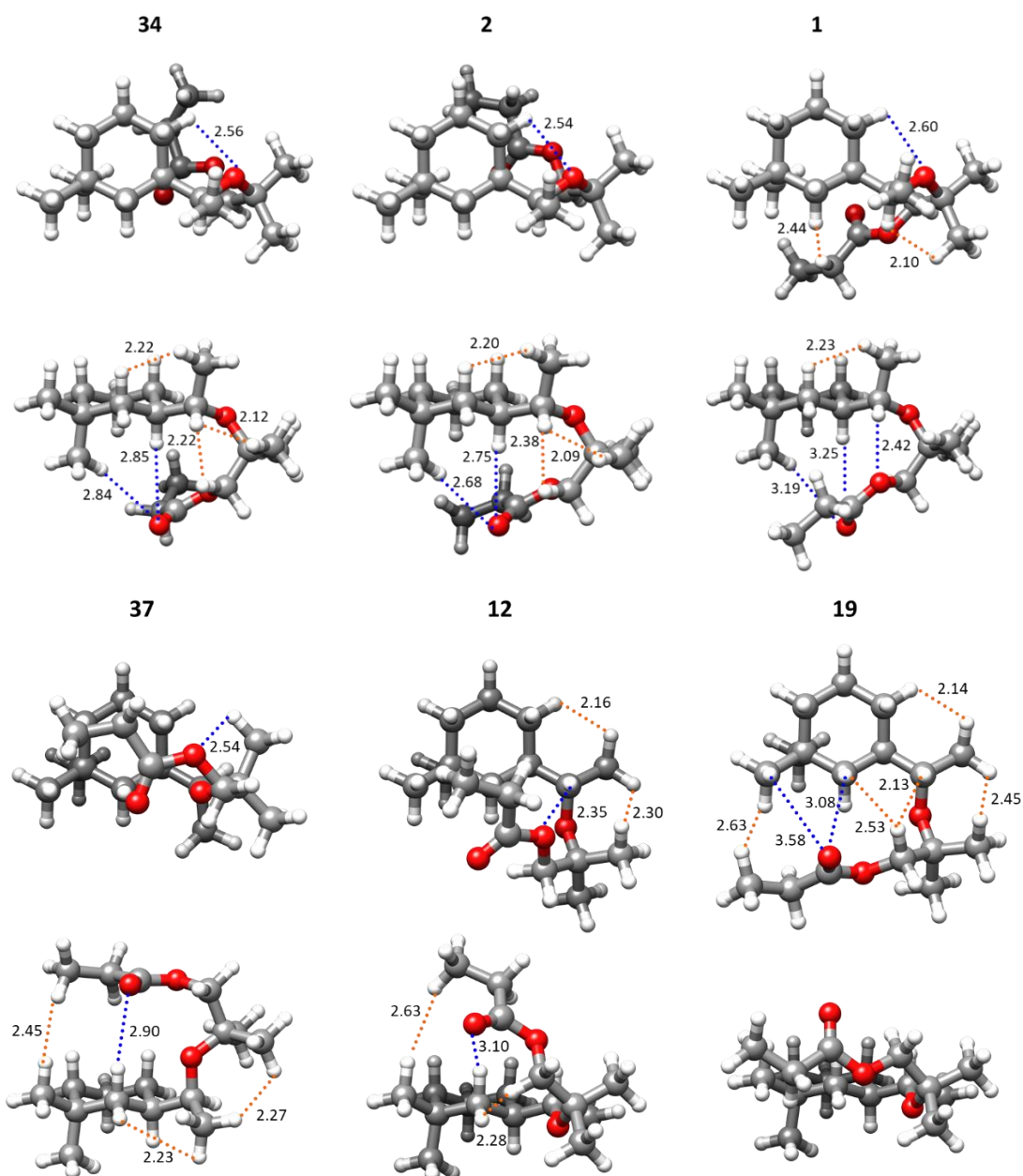


Figure 11.9. Intramolecular interactions (B3LYP-D3BJ distances in Å) in the observed conformers of helvetolide. Those in blue represent C-H...O attractive interactions, and those in orange represent H...H interactions.

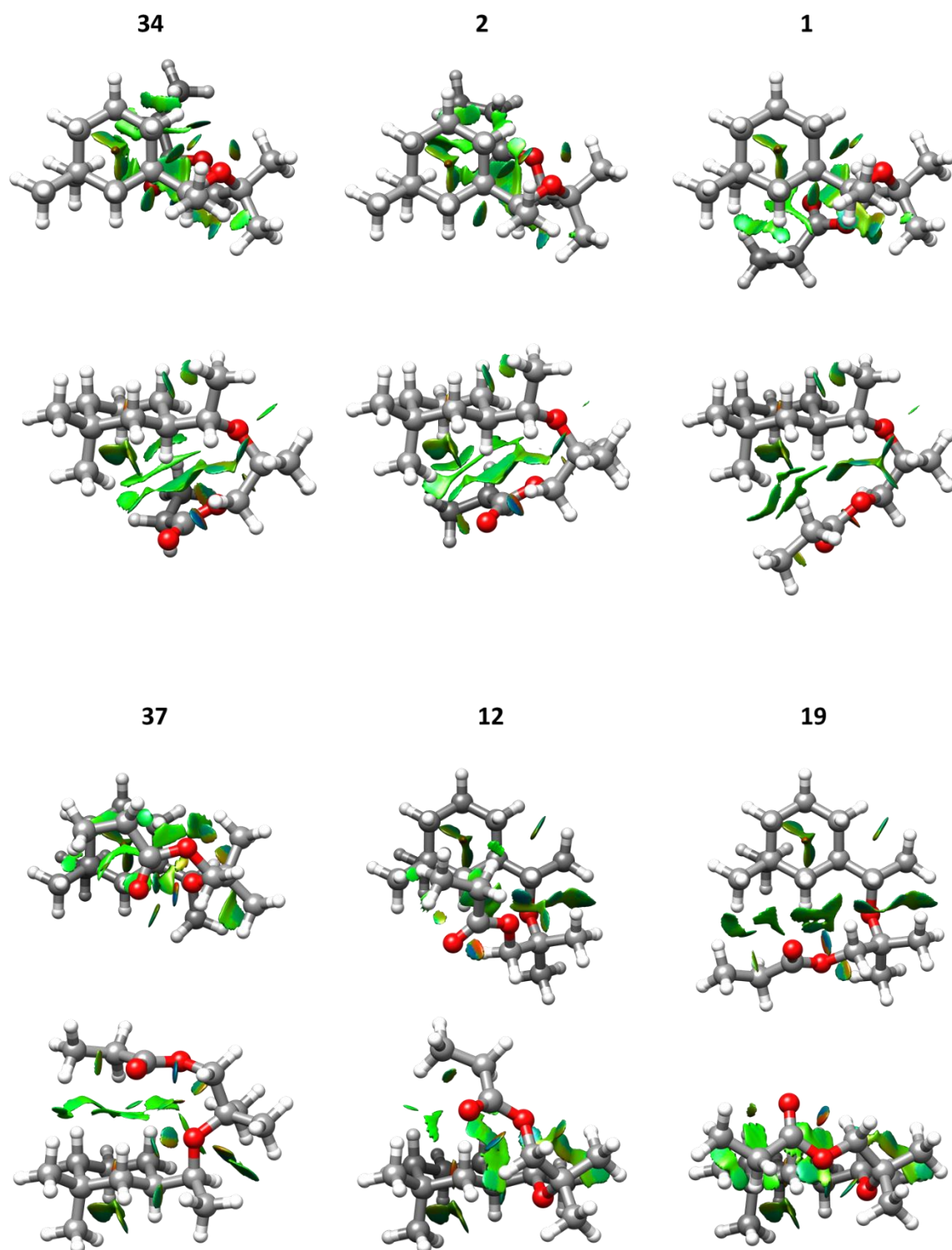


Figure 11.10. Non-covalent interactions (NCI) analysis of the six observed conformers of helvetolide.

Comparison with romandolide and macrocycles

Comparing the assigned conformations of helvetolide with the ones identified for romandolide, several similarities and differences can be observed. Firstly, helvetolide, unlike romandolide, does not show a strong preference for one conformation, and the abundance is relatively evenly distributed over a few conformations. Helvetolide shows a slight preference for conformers where the aliphatic tail is below the cyclohexane moiety. In romandolide the most favoured configurations, **48** and **30**, have the tail around the cyclohexane ring (Figure 11.11). This shows how the substitution of a carbonyl group by a dimethyl group, in going from romandolide to helvetolide, changes the preferred configuration of the aliphatic tail.

Hence, the conformers preferred by romandolide are closer to the macrocyclic musk conformers in terms of planarity. In helvetolide this feature is not as obvious, as only one of the six identified conformers, conformer **19**, has the tail and the cyclohexane moiety arranged in a plane. Conformer **37** of helvetolide is very similar to conformers **2**, **3** and **9** in romandolide, which are the least abundant. Changing the perspective of the most abundant conformers of helvetolide, the carbonyl group in the aliphatic tail shows similarities with the other macrocyclic musks potentially confirming the validity of the osmophoric role of this moiety.

Our results from the romandolide and helvetolide investigations give rise to further questions on the similarity between alicyclic and macrocyclic musks, and whether they could indeed activate the same olfactory receptor. More experimental work on other macrocyclic and alicyclic musks is needed in order to address these questions.

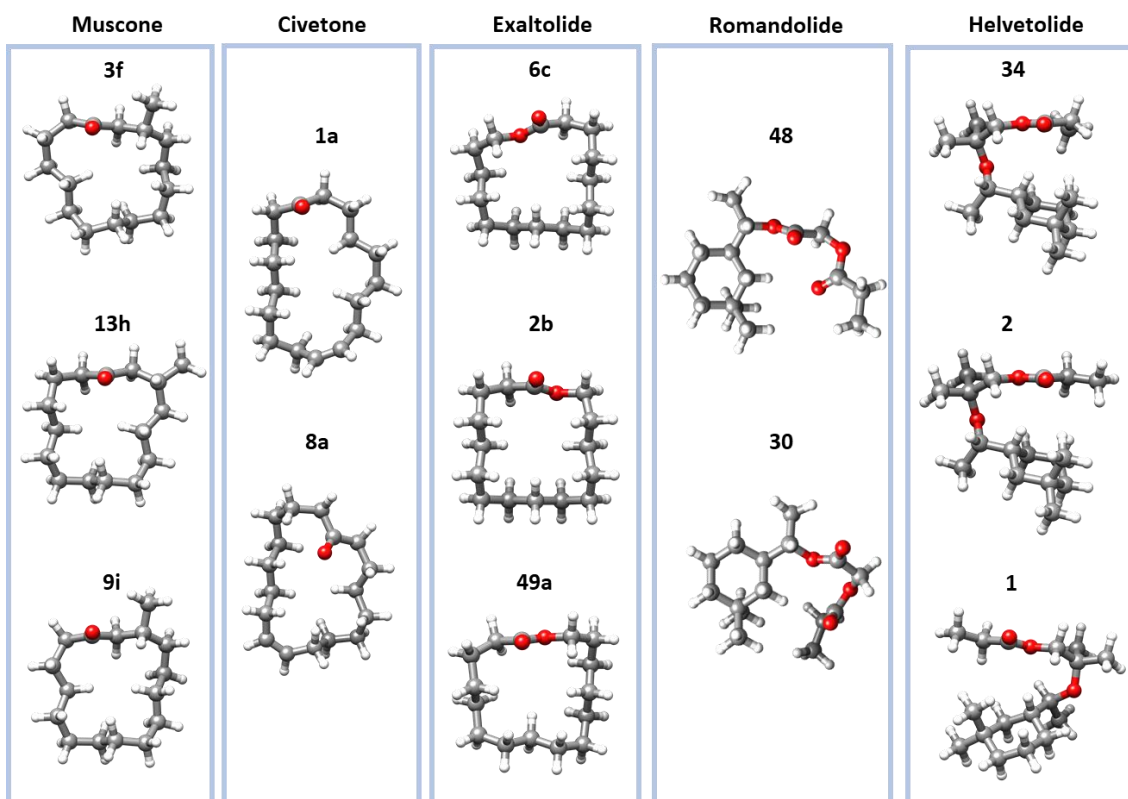


Figure 11.11. The most abundant conformations of muscone, civetone, exaltolide, romandolide and helvetolide.

11.5. Conclusions

The conformational landscape of the synthetic alicyclic musk helvetolide has been characterised for the first time using broadband rotational spectroscopy in combination with quantum chemistry calculations. Six conformers have been unambiguously identified, corresponding to folded configurations. All identified conformations of helvetolide adopt a horseshoe shape, with helvetolide showing a slight preference for conformations where the aliphatic tail is below the cyclohexane moiety.

Compared to the other alicyclic musk investigated, romandolide (see Chapter 10), helvetolide exhibits a larger flexibility, with a larger number of conformations predicted at low energy, and different preferred configurations of the aliphatic tail. This is a consequence of substituting a carbonyl group by a dimethyl group.

The results of this investigation should contribute to advance our understanding of the structure-odour relationship in the alicyclic musk family and inspire further conformational studies of other alicyclic musks. Investigation of other alicyclic musks could help understand whether the way in which the aliphatic tail folds has a significance in the odorant-receptor binding. Moreover, comparing other alicyclic musks with the macrocyclic musks presented in

this thesis could offer information on whether the two classes activate the same olfactory receptors.

11.6. Bibliography

1. Eh, M. New Alicyclic Musks: The Fourth Generation of Musk Odorants. *Chemistry and Biodiversity* **1**, 1975–1984 (2004).
2. Kraft, P. “Brain aided” musk design. *Chemistry and Biodiversity* **1**, 1957–1974 (2004).
3. Kraft, P. & Eichenberger, W. Synthesis and Odor of Aliphatic Musks: Discovery of a New Class of Odorants. *European Journal of Organic Chemistry* **2**, 354–365 (2004).
4. Nguyen, K., Sutter, P. & Kraft, P. Search for New Linear Musks Devoid of a 2,2-Dimethyl-1,4-dioxabutane Unit: Synthesis and Olfactory Properties of 5-Substituted (3E)-Hex-3-enoates on the Way to Carba-Helvetolide and Carba-Serenolide. *Synthesis (Germany)* **49**, 2443–2460 (2017).
5. Loru, D., Bermúdez, M. A. & Sanz, M. E. Structure of fenchone by broadband rotational spectroscopy. *Journal of Chemical Physics* **145**, 07114311–8 (2016).
6. Loru, D., Peña, I. & Sanz, M. E. Ethanol dimer: Observation of three new conformers by broadband rotational spectroscopy. *Journal of Molecular Spectroscopy* **335**, 93–101 (2017).
7. Western, C. M. PGOPHER: A program for simulating rotational, vibrational and electronic spectra. *Journal of Quantitative Spectroscopy and Radiative Transfer* **186**, 221–242 (2017).
8. Western, C. M. & Billinghurst, B. E. Automatic assignment and fitting of spectra with PGOPHER. *Physical Chemistry Chemical Physics* **19**, 10222–10226 (2017).
9. Watson, J. K. G. *Vibrational Spectra and Structure*. Elsevier Amsterdam **6**, 1–89 (1977).
10. Novick, S. E. A beginner’s guide to Pickett’s SPCAT/SPFIT. *Journal of Molecular Spectroscopy* **329**, 1–7 (2016).
11. Pickett, H. M. The fitting and prediction of vibration-rotation spectra with spin interactions. *Journal of Molecular Spectroscopy* **148**, 371–377 (1991).
12. Ruoff, R. S., Klots, T. D., Emilsson, T. & Gutowsky, H. S. Relaxation of conformers and isomers in seeded supersonic jets of inert gases. *The Journal of Chemical Physics* **93**, 3142–3150 (1990).
13. Zwier, T. S. Laser spectroscopy of jet-cooled biomolecules and their water-containing clusters: Water bridges and molecular conformation. *Journal of Physical Chemistry A* **105**, 8827–8839 (2001).
14. Watson, J. K. G. Asymptotic energy levels of a rigid asymmetric top. *Molecular Physics* **105**, 679–688 (2007).
15. Johnson, E. R. *et al.* Revealing noncovalent interactions. *Journal of the American Chemical Society* **132**, 6498–6506 (2010).
16. Pauling, L. *The Nature of the Chemical Bond and the Structure of Molecules and Crystals: An Introduction to Modern Structural Chemistry*. (Cornell University Press, 1960).

17. Bondi, A. Van der Waals volumes and radii. *Journal of Physical Chemistry* **68**, 441–451 (1964).



CONCLUSIONS AND PERSPECTIVES

Chapter 12



12. CONCLUSIONS AND PERSPECTIVES

In this thesis the conformational landscapes of two cycloketones, the complexes of one of them with water, and several musk odorants from the macrocyclic and alicyclic classes have been investigated using broadband rotational spectroscopy in combination with quantum-chemistry calculations. Several conformations for each species have been characterised and the interactions driving their conformational preferences have been identified. Conclusions from each of the systems investigated are specified at the end of each chapter. Besides, some general conclusions can be drawn from the global comparison of the target species.

From the investigation of the cyclic ketones, the conformational preferences change dramatically with the increase of the size of the ring from medium-sized to the large rings. In medium-sized rings one conformation is much more favoured, whilst in large rings (12 members and above) the population is distributed among several conformers. In large rings there is a higher number of lower-energy conformations and the gap between the global minimum and the next conformer is energy is smaller. In medium rings conformational preferences are mainly driven by minimisation of HCCH eclipsed and H \cdots H interactions across the ring to, in turn, minimise strain. In larger rings, there is less torsional and angle strain. The main interactions determining conformational preferences are still H \cdots H transannular interactions. However, HCCH eclipsed interactions have a smaller influence as the ring becomes larger and are replaced by 1,4-H \cdots H interactions. H \cdots H interactions across the ring are still taking place in larger rings, with their number increasing for the less abundant conformations.

The three macrocyclic musks, muscone, civetone and exaltolide mostly adopt relatively flat configurations of the carbon chain, with the carbonyl groups perpendicular to the ring. The preferred shapes of the rings change from one odorant to another and is mainly related to the presence of functional groups (carbonyl vs lactone, double bond presence vs fully saturated chain) and whether they are odd or even membered rings. The conformational similarities between the macrocyclic musks suggest that they could be activating the same olfactory receptors. The variety and huge number of conformations observed for this class of musks, as well as the population spread among them point to the validity of the theory of multiconformational activation of olfactory receptors, recently proposed.

The conformational preferences of the alicyclic musks, romandolide and helvetolide, are very similar, with all the conformers adopting folded or “horseshoe”-shaped structures. These conformations are stabilised by weak attractive interactions between the aliphatic tails and the cyclohexane moieties and resemble the conformational space of the macrocyclic class. The similarities in conformational space between the two musk classes further suggest that they

interact in the same way with musk olfactory receptors. These results should open interest for further work, including additional structural comparisons between the two classes in order to confirm this hypothesis.

Benchmarking of different computational methods has been performed for all species studied in this thesis. For most molecular systems the B3LYP-D3BJ level of theory performed better at predicting the rotational constants, especially where weak interactions are predominant, and consistently outperformed MP2, wB97XD and B2PLYP, with the advantage of having a lower computational cost. This has the caveat that we are comparing the ground-state experimental parameters to theoretical equilibrium ones, although it is usual practice in the field given the computational costs of performing anharmonic vibrational calculations for the large molecular systems investigated.

Our investigation provides the first experimental conformational and theoretical data on some of the most successful musk odorants, which could help further advance our knowledge and understanding of their structure-odour relationship and the interactions with the olfactory receptors. The olfactophore models developed up to date are not accurate enough being based mainly on theoretical data and structurally modified or rigid musks. The conformations of macrocyclic and alicyclic musks presented in this thesis could be further utilised in developing a new and more accurate and detailed olfactophore model. Moreover, the data could be useful in evaluating the proposed musk olfactory receptors OR5AN1 and OR1A1.

We have shown the capabilities of chirped-pulse Fourier transform rotational spectroscopy to characterise very complex conformational landscape of large molecules, in combination with theoretical calculations. Further investigations of macrocyclic and alicyclic musks should be undertaken to help shed more light on the interactions of musk odorants with musk olfactory receptors, and improvement of the olfactophore model. The results presented in this thesis should inspire further work on ketones of atmospheric interest and their interaction with water in gas phase, where formation of *gem*-diols could have implications in the reactivity of these compounds.



APPENDICES

The Rich Conformational Landscape of Musks and
their Precursors Revealed by Broadband Rotational
Spectroscopy



1. APPENDIX I

Table S4.1. Measured frequencies and residuals (in MHz) for the rotational transitions of the parent species of cyclooctanone BC1.

J'	K'_{-1}	K'_{+1}	J''	K''_{-1}	K''_{+1}	V _{obs}	V _{obs} - V _{calc}
4	4	1	4	3	1	2197.7575	0.0010
5	3	2	5	3	3	2199.6797	0.0003
6	5	2	6	4	2	2283.9775	0.0059
2	2	0	2	1	2	2595.0648	0.0194
4	2	2	4	2	3	2628.2886	0.0003
3	3	0	3	2	2	2809.7264	-0.0026
1	0	1	0	0	0	2845.3742	-0.0015
3	1	2	3	1	3	2928.8730	0.0033
1	1	1	0	0	0	3071.9416	0.0031
5	5	1	5	4	1	3149.7381	-0.0013
4	4	0	4	3	2	3206.0952	-0.0034
7	4	3	7	4	4	3289.0077	0.0024
7	6	2	7	5	2	3312.1505	-0.0013
4	3	2	4	1	3	3412.1423	0.0014
1	1	0	0	0	0	3592.5791	-0.0049
5	5	0	5	4	2	3766.7681	-0.0017
6	3	3	6	3	4	3788.8203	0.0006
6	6	1	6	5	1	4115.2158	-0.0024
5	2	3	5	2	4	4118.1711	-0.0008
5	4	1	5	3	3	4175.7158	0.0001
4	1	3	4	1	4	4288.8620	-0.0015
6	5	1	6	4	3	4292.2434	-0.0015
5	3	3	5	1	4	4379.1883	0.0010
8	7	2	8	6	2	4388.7380	0.0010
6	6	0	6	5	2	4445.5722	0.0001
2	0	2	1	1	0	4590.1200	0.0050
7	6	1	7	5	3	4637.1492	-0.0003
8	4	4	8	4	5	5000.3328	-0.0017
7	7	1	7	6	1	5040.7774	0.0032
2	0	2	1	1	1	5110.7477	-0.0128
2	1	2	1	1	1	5170.1082	0.0052
8	7	1	8	6	3	5174.6072	0.0034
7	7	0	7	6	2	5197.9806	-0.0042
7	3	4	7	3	5	5319.8702	0.0006
3	1	3	2	2	1	5333.1963	-0.0054
2	0	2	1	0	1	5337.3236	0.0004
2	1	2	1	0	1	5396.6701	0.0043
9	8	2	9	7	2	5428.9533	-0.0002
6	2	4	6	2	5	5490.0626	-0.0018
6	3	4	6	1	5	5551.2456	0.0010
8	6	2	8	5	4	5568.9579	0.0008
5	1	4	5	1	5	5572.1771	-0.0001
9	7	2	9	6	4	5640.8480	0.0011
7	5	2	7	4	4	5754.0101	-0.0013
9	8	1	9	7	3	5846.0310	-0.0054
8	8	1	8	7	1	5922.5425	-0.0074
8	8	0	8	7	2	5991.1218	0.0000
3	0	3	2	1	1	6002.7627	-0.0033
6	4	2	6	3	4	6122.0547	-0.0040
2	1	1	1	1	0	6211.3935	0.0019
9	4	5	9	4	6	6521.4145	-0.0026
8	3	5	8	3	6	6685.6046	-0.0014
4	1	4	3	2	2	6716.2328	0.0007
9	9	1	9	8	1	6776.1366	0.0076
7	2	5	7	2	6	6776.8091	-0.0036

7	3	5	7	1	6	6788.3516	-0.0008
6	1	5	6	1	6	6828.8018	0.0000
2	2	1	1	1	0	6891.0769	-0.0038
2	1	1	1	0	1	6958.6001	0.0002
4	0	4	3	1	2	6988.8503	-0.0009
2	2	0	1	1	0	7244.5029	0.0001
2	2	1	1	1	1	7411.7277	0.0014
3	0	3	2	1	2	7564.7025	0.0024
3	1	3	2	1	2	7574.8279	0.0029
3	0	3	2	0	2	7624.0441	0.0015
3	1	3	2	0	2	7634.1697	0.0022
10	4	6	10	4	7	7875.4128	0.0059
5	1	5	4	2	3	7890.3753	0.0011
5	0	5	4	1	3	7958.0775	-0.0011

Table S4.2. Measured frequencies and residuals (in MHz) for the rotational transitions of the $^{13}\text{C}_1$ isotopologue of cyclooctanone BC1.

J'	K'_{-1}	K'_{+1}	J''	K''_{-1}	K''_{+1}	ν_{obs}	$\nu_{\text{obs}} - \nu_{\text{calc}}$
1	0	1	0	0	0	2814.2090	-0.0062
1	1	0	0	0	0	3566.8421	-0.0008
2	1	2	1	1	1	5116.3318	0.0016
2	0	2	1	0	1	5290.0114	0.0034
2	1	1	1	1	0	6140.5224	0.0004
2	1	1	1	0	1	6893.1520	0.0023
2	2	0	1	1	0	7200.5290	-0.0015
3	1	3	2	1	2	7501.4046	-0.0046
3	0	3	2	0	2	7556.0982	0.0028

Table S4.3. Measured frequencies and residuals (in MHz) for the rotational transitions of the $^{13}\text{C}_2$ isotopologue of cyclooctanone BC1.

J'	K'_{-1}	K'_{+1}	J''	K''_{-1}	K''_{+1}	ν_{obs}	$\nu_{\text{obs}} - \nu_{\text{calc}}$
1	0	1	0	0	0	2822.6069	-0.0001
1	1	0	0	0	0	3569.0798	-0.0034
2	1	2	1	1	1	5134.8736	0.0002
2	0	2	1	0	1	5306.1333	-0.0004
2	1	1	1	1	0	6155.5451	-0.0008
2	1	1	1	0	1	6902.0236	0.0016
2	2	0	1	1	0	7203.0375	0.0008
3	1	3	2	1	2	7528.9720	0.0004
3	0	3	2	0	2	7582.1907	-0.0001

Table S4.4. Measured frequencies and residuals (in MHz) for the rotational transitions of the $^{13}\text{C}_3$ isotopologue of cyclooctanone BC1.

J'	K'_{-1}	K'_{+1}	J''	K''_{-1}	K''_{+1}	ν_{obs}	$\nu_{\text{obs}} - \nu_{\text{calc}}$
1	0	1	0	0	0	2826.7172	-0.0058
1	1	0	0	0	0	3567.2742	-0.0038
2	1	2	1	1	1	5130.9911	0.0000
2	0	2	1	0	1	5293.8069	-0.0007
2	1	1	1	1	0	6175.8914	-0.0006
2	1	1	1	0	1	6916.4509	0.0039
2	2	0	1	1	0	7189.8336	-0.0013
2	2	1	1	1	1	7352.6555	0.0009
3	1	3	2	1	2	7513.2113	0.0010
3	0	3	2	0	2	7559.3924	0.0007

Table S4.5. Measured frequencies and residuals (in MHz) for the rotational transitions of the $^{13}\text{C}_4$ isotopologue of cyclooctanone BC1.

J'	K'_{-1}	K'_{+1}	J''	K''_{-1}	K''_{+1}	ν_{obs}	$\nu_{\text{obs}} - \nu_{\text{calc}}$
1	0	1	0	0	0	2834.5673	-0.0085
1	1	0	0	0	0	3565.1608	-0.0064
2	1	2	1	1	1	5139.4307	0.0013
2	0	2	1	0	1	5293.1576	-0.0005
2	1	1	1	1	0	6198.8651	0.0001
2	1	1	1	0	1	6929.4604	0.0040
2	2	0	1	1	0	7177.4700	-0.0002
2	2	1	1	1	1	7331.2031	0.0010
3	1	3	2	1	2	7518.0276	0.0014
3	0	3	2	0	2	7558.0205	-0.0002

Table S4.6. Measured frequencies and residuals (in MHz) for the rotational transitions of the $^{13}\text{C}_5$ isotopologue of cyclooctanone BC1.

J'	K'_{-1}	K'_{+1}	J''	K''_{-1}	K''_{+1}	ν_{obs}	$\nu_{\text{obs}} - \nu_{\text{calc}}$
1	0	1	0	0	0	2827.9108	-0.0092
1	1	0	0	0	0	3570.5360	-0.0018
2	1	2	1	1	1	5141.8547	0.0021
2	0	2	1	0	1	5309.5621	-0.0006
2	1	1	1	1	0	6169.8180	-0.0007
2	1	1	1	0	1	6912.4403	0.0038
2	2	0	1	1	0	7201.9901	-0.0010
2	2	1	1	1	1	7369.7046	0.0002
3	1	3	2	1	2	7535.9815	0.0014
3	0	3	2	0	2	7586.3131	-0.0003

Table S4.7. Measured frequencies and residuals (in MHz) for the rotational transitions of the $^{13}\text{C}_6$ isotopologue of cyclooctanone BC1.

J'	K'_{-1}	K'_{+1}	J''	K''_{-1}	K''_{+1}	V_{obs}	$V_{\text{obs}} - V_{\text{calc}}$
1	0	1	0	0	0	2831.0670	-0.0020
2	1	2	1	1	1	5146.0876	0.0003
2	0	2	1	0	1	5317.3364	0.0000
2	1	1	1	1	0	6178.1788	-0.0009
3	0	3	2	0	2	7595.4359	-0.0011
3	1	3	2	1	2	7542.9578	0.0015
1	1	0	0	0	0	3582.1519	-0.0071
2	1	1	1	0	1	6929.2728	0.0031
2	2	1	1	1	1	7399.3569	0.0012
2	2	0	1	1	0	7228.1038	0.0003

Table S4.8. Measured frequencies and residuals (in MHz) for the rotational transitions of the $^{13}\text{C}_8$ isotopologue of cyclooctanone BC1.

J'	K'_{-1}	K'_{+1}	J''	K''_{-1}	K''_{+1}	V_{obs}	$V_{\text{obs}} - V_{\text{calc}}$
1	0	1	0	0	0	2829.5957	-0.0041
1	1	0	0	0	0	3565.4285	-0.0068
2	1	2	1	1	1	5138.7917	-0.0010
2	0	2	1	0	1	5299.9788	0.0015
2	1	1	1	1	0	6179.5981	0.0003
2	1	1	1	0	1	6915.4364	0.0031
2	2	0	1	1	0	7185.1084	-0.0012
2	2	1	1	1	1	7346.2995	0.0020
3	1	3	2	1	2	7525.1693	0.0012
3	0	3	2	0	2	7570.5441	-0.0007

Table S4.9. Measured frequencies and residuals (in MHz) for the rotational transitions of the $^{13}\text{C}_9$ isotopologue of cyclooctanone BC1.

J'	K'_{-1}	K'_{+1}	J''	K''_{-1}	K''_{+1}	V_{obs}	$V_{\text{obs}} - V_{\text{calc}}$
1	0	1	0	0	0	2835.1755	-0.0016
2	1	2	1	1	1	5143.8826	0.0009
2	0	2	1	0	1	5301.9008	-0.0003
2	1	1	1	1	0	6196.8170	-0.0010
2	1	1	1	0	1	6932.1391	0.0012
2	2	0	1	1	0	7191.8170	-0.0003
2	2	1	1	1	1	7349.8398	-0.0001
3	1	3	2	1	2	7528.3191	0.0011
3	0	3	2	0	2	7571.1345	-0.0009

Table S4.10. Measured frequencies and residuals (in MHz) for the rotational transitions of the $^{13}\text{O}_7$ isotopologue of cyclooctanone BC1.

J'	K'_{-1}	K'_{+1}	J''	K''_{-1}	K''_{+1}	ν_{obs}	$\nu_{\text{obs}} - \nu_{\text{calc}}$
1	0	1	0	0	0	2767.9788	0.0134
1	1	0	0	0	0	3521.9482	-0.0057
2	1	2	1	1	1	5048.5763	-0.0015
2	0	2	1	0	1	5232.0860	-0.0012
2	1	1	1	1	0	6023.2717	-0.0035
2	1	1	1	0	1	6777.2639	0.0002
2	2	0	1	1	0	7127.0337	0.0046
2	2	1	1	1	1	7310.5400	-0.0017
3	1	3	2	1	2	7416.6214	0.0005
3	0	3	2	0	2	7482.5757	-0.0010

Table S4.11. Measured frequencies and residuals (in MHz) for the rotational transitions of cyclooctanone TBC1.

J'	K'_{-1}	K'_{+1}	J''	K''_{-1}	K''_{+1}	ν_{obs}	$\nu_{\text{obs}} - \nu_{\text{calc}}$
4	2	2	4	2	3	2594.8198	-0.0065
1	0	1	0	0	0	2724.7589	-0.0063
7	4	3	7	4	4	2792.1636	-0.0064
3	1	2	3	1	3	3105.5121	-0.0006
4	4	1	4	3	1	3328.0771	0.0015
3	3	0	3	2	2	3410.1156	0.0016
1	1	0	0	0	0	3617.1094	-0.0042
6	3	3	6	3	4	3631.1505	-0.0013
4	4	0	4	3	2	4110.4209	-0.0032
4	3	2	4	1	3	4123.5168	-0.0069
2	0	2	1	1	0	4244.2377	-0.0045
5	2	3	5	2	4	4283.3386	-0.0024
4	1	3	4	1	4	4673.0759	0.0020
8	4	4	8	4	5	4726.6660	0.0012
2	0	2	1	1	1	4784.7981	0.0089
2	1	2	1	1	1	4908.9797	0.0000
5	3	3	5	1	4	4974.8132	0.0044
5	5	0	5	4	2	5016.1214	0.0001
2	0	2	1	0	1	5136.5888	-0.0019
2	1	2	1	0	1	5260.7903	0.0091
7	3	4	7	3	5	5478.1190	0.0108
3	0	3	2	1	1	5550.1844	-0.0112
6	2	4	6	2	5	5930.6433	-0.0021
2	1	1	1	1	0	5990.0618	-0.0023
5	1	4	5	1	5	6149.2532	0.0019
6	3	4	6	1	5	6162.8940	0.0046
9	4	5	9	4	6	6688.0565	0.0020
2	1	1	1	0	1	6882.4112	-0.0013
3	0	3	2	1	2	7171.8366	0.0097
8	3	5	8	3	6	7179.6412	-0.0059
3	1	3	2	1	2	7201.3659	0.0068
3	0	3	2	0	2	7296.0254	0.0080
3	1	3	2	0	2	7325.5343	-0.0154
2	2	0	1	1	0	7358.3881	0.0002
7	2	5	7	2	6	7436.6744	-0.0030
6	1	5	6	1	6	7566.6001	-0.0003
2	2	1	1	1	1	7586.0130	0.0002

Table S4.12. Measured frequencies and residuals (in MHz) for the rotational transitions of cyclooctanone BC2.

J'	K'_{-1}	K'_{+1}	J''	K''_{-1}	K''_{+1}	ν_{obs}	$\nu_{\text{obs}} - \nu_{\text{calc}}$
1	0	1	0	0	0	2753.8306	0.0036
3	1	2	3	1	3	3022.2846	-0.0029
3	2	2	3	0	3	3706.0092	-0.0007
4	2	3	4	0	4	4851.3487	0.0001
2	1	2	1	1	1	4984.7597	-0.0003
2	0	2	1	0	1	5223.2149	-0.0021
2	1	2	1	0	1	5373.1467	-0.0014
2	1	1	1	1	0	6030.5536	0.0007
3	1	3	2	1	2	7328.8701	-0.0138
3	0	3	2	0	2	7439.2517	-0.0137
3	1	3	2	0	2	7478.8012	-0.0137
2	2	0	1	1	0	7480.1497	-0.0068
2	2	1	1	1	1	7718.6153	0.0018

2. APPENDIX II

Table S5.1. Measured frequencies and residuals (in MHz) for the rotational transitions of the parent species of BC1-1w-1 complex.

J'	K'_{-1}	K'_{+1}	J''	K''_{-1}	K''_{+1}	V _{obs}	V _{obs} -V _{calc}
5	2	4	5	0	5	2508.8242	0.0006
5	3	3	5	1	4	2748.5275	0.0037
6	1	5	6	1	6	2760.4541	0.0005
4	3	2	4	1	3	2798.8433	0.0055
6	3	4	6	1	5	2837.4451	-0.0094
6	2	5	6	0	6	2966.5683	-0.0001
7	1	6	7	1	7	3375.6429	-0.0038
7	2	6	7	0	7	3472.0450	-0.0011
2	1	2	1	1	1	3644.8862	-0.0027
2	0	2	1	0	1	3756.7315	-0.0016
2	1	1	1	1	0	3950.5023	0.0017
8	1	7	8	1	8	3962.1635	-0.0121
8	2	7	8	0	8	4003.5489	0.0191
2	1	1	1	0	1	4444.3227	0.0076
9	2	8	9	0	9	4547.5808	-0.0014
3	1	2	2	2	0	4831.6352	0.0041
2	2	0	1	1	0	5014.4665	-0.0037
2	2	1	1	1	1	5126.3257	-0.0012
3	1	3	2	1	2	5444.3493	-0.0001
4	1	4	3	2	2	5491.1267	-0.0003
3	0	3	2	0	2	5548.9205	-0.0020
3	2	2	2	2	1	5696.5233	-0.0028
3	2	1	2	2	0	5844.0611	0.0011
3	1	2	2	1	1	5895.6005	-0.0002
3	1	2	2	0	2	6583.1833	0.0006
4	1	3	3	2	1	6782.7849	0.0042
3	2	1	2	1	1	6908.0281	-0.0015
3	2	2	2	1	2	7177.9650	0.0009
4	1	4	3	1	3	7224.7420	0.0003
4	0	4	3	0	3	7292.2725	-0.0007
4	2	3	3	2	2	7562.8209	0.0017
4	3	2	3	3	1	7660.1813	0.0001
4	3	1	3	3	0	7700.9189	-0.0039
4	1	3	3	1	2	7795.2088	-0.0009
4	2	2	3	2	1	7864.6612	-0.0005

Table S5.2. Measured frequencies and residuals (in MHz) for the rotational transitions of the ¹³C₁ isotopologue of BC1-1w-1.

J'	K'_{-1}	K'_{+1}	J''	K''_{-1}	K''_{+1}	V _{obs}	V _{obs} -V _{calc}
2	0	2	1	0	1	3738.7530	-0.0068
2	1	1	1	1	0	3943.0333	0.0011
3	1	3	2	1	2	5412.6096	-0.0065
3	0	3	2	0	2	5514.6313	-0.0075
3	2	2	2	2	1	5676.2325	0.0046
3	1	2	2	1	1	5880.6994	-0.0076
4	1	4	3	1	3	7179.5199	-0.0035
4	0	4	3	0	3	7241.9788	0.0074
4	2	3	3	2	2	7532.1636	0.0127
4	2	2	3	2	1	7856.9471	-0.0011

Table S5.3. Measured frequencies and residuals (in MHz) for the rotational transitions of the $^{13}\text{C}_2$ isotopologue of BC1-1w-1.

J'	K'_{-1}	K'_{+1}	J''	K''_{-1}	K''_{+1}	V _{obs}	V _{obs} -V _{calc}
2	1	2	1	1	1	3632.4044	0.0113
2	0	2	1	0	1	3743.3853	-0.0054
2	1	1	1	1	0	3936.9390	0.0045
3	1	3	2	1	2	5425.4623	0.0083
3	0	3	2	0	2	5528.5542	-0.0057
3	1	2	2	1	1	5874.9638	0.0058
4	1	4	3	1	3	7199.4055	-0.0072
4	0	4	3	0	3	7265.3971	-0.0006
4	2	3	3	2	2	7536.5007	0.0030
4	2	2	3	2	1	7839.1139	-0.0068

Table S5.4. Measured frequencies and residuals (in MHz) for the rotational transitions of the $^{13}\text{C}_3$ isotopologue of BC1-1w-1.

J'	K'_{-1}	K'_{+1}	J''	K''_{-1}	K''_{+1}	V _{obs}	V _{obs} -V _{calc}
2	1	2	1	1	1	3615.4573	-0.0044
2	0	2	1	0	1	3725.8304	-0.0032
2	1	1	1	1	0	3913.1860	0.0027
3	1	3	2	1	2	5401.5376	0.0136
3	0	3	2	0	2	5506.8763	0.0032
3	2	2	2	2	1	5646.4707	0.0030
3	1	2	2	1	1	5841.6301	-0.0009
4	1	4	3	1	3	7169.3228	-0.0129
4	0	4	3	0	3	7239.3597	0.0044
4	1	3	3	1	2	7727.7971	-0.0040
4	2	2	3	2	1	7786.2218	0.0008

Table S5.5. Measured frequencies and residuals (in MHz) for the rotational transitions of the $^{13}\text{C}_4$ isotopologue of BC1-1w-1.

J'	K'_{-1}	K'_{+1}	J''	K''_{-1}	K''_{+1}	V _{obs}	V _{obs} -V _{calc}
2	0	2	1	0	1	3728.2151	-0.0069
3	1	3	2	1	2	5402.4724	-0.0017
3	0	3	2	0	2	5507.0763	-0.0079
3	2	2	2	2	1	5652.9768	0.0102
3	2	1	2	2	0	5798.7743	-0.0050
3	1	2	2	1	1	5851.0732	0.0072
4	0	4	3	0	3	7237.2112	0.0056
4	1	3	3	1	2	7736.7913	-0.0043

Table S5.6. Measured frequencies and residuals (in MHz) for the rotational transitions of the $^{13}\text{C}_5$ isotopologue of BC1-1w-1.

J'	K'_{-1}	K'_{+1}	J''	K''_{-1}	K''_{+1}	V _{obs}	V _{obs} -V _{calc}
3	1	3	2	1	2	5415.0465	-0.0039
3	0	3	2	0	2	5518.4033	-0.0053
3	1	2	2	1	1	5872.8652	0.0003
4	1	4	3	1	3	7184.4912	0.0036
4	0	4	3	0	3	7249.7211	0.0021
4	1	3	3	1	2	7761.4703	0.0011
4	2	2	3	2	1	7839.5312	-0.0002

Table S5.7. Measured frequencies and residuals (in MHz) for the rotational transitions of the $^{13}\text{C}_6$ isotopologue of BC1-1w-1.

J'	K'_{-1}	K'_{+1}	J''	K''_{-1}	K''_{+1}	V _{obs}	V _{obs} -V _{calc}
2	1	2	1	1	1	3638.5446	-0.0072
2	0	2	1	0	1	3750.4567	0.0092
2	1	1	1	0	1	4436.3445	-0.0046
3	1	3	2	1	2	5434.4102	-0.0034
3	0	3	2	0	2	5538.1657	0.0021
3	2	2	2	2	1	5688.3215	-0.0080
3	2	1	2	2	0	5838.4215	-0.0040
3	1	2	2	1	1	5888.0326	0.0068
4	1	4	3	1	3	7210.9665	-0.0024
4	2	3	3	2	2	7551.2301	0.0069
4	1	3	3	1	2	7783.5407	0.0030
4	2	2	3	2	1	7857.1565	-0.0013

Table S5.8. Measured frequencies and residuals (in MHz) for the rotational transitions of the $^{18}\text{O}_7$ isotopologue of BC1-1w-1.

J'	K'_{-1}	K'_{+1}	J''	K''_{-1}	K''_{+1}	V _{obs}	V _{obs} -V _{calc}
2	1	2	1	1	1	3603.2484	-0.0077
2	0	2	1	0	1	3716.7426	-0.0026
2	1	1	1	1	0	3919.7221	-0.0014
2	2	0	1	1	0	4952.9241	0.0034
2	2	1	1	1	1	5066.4216	-0.0008
3	1	3	2	1	2	5379.9010	-0.0019
3	0	3	2	0	2	5482.6281	-0.0034
3	2	2	2	2	1	5642.2137	-0.0050
3	2	1	2	2	0	5801.7358	-0.0002
3	1	2	2	1	1	5846.3069	0.0004
3	1	2	2	0	2	6537.0054	-0.0034
4	1	4	3	1	3	7136.3186	0.0079
4	0	4	3	0	3	7199.7662	0.0010
4	2	3	3	2	2	7487.3392	-0.0037
4	3	2	3	3	1	7592.9400	0.0035
4	3	1	3	3	0	7639.8016	0.0063
4	1	3	3	1	2	7722.3707	-0.0023
4	2	2	3	2	1	7809.0513	0.0019

Table S5.9. Measured frequencies and residuals (in MHz) for the rotational transitions of the $^{13}\text{C}_8$ isotopologue of BC1-1w-1.

J'	K'_{-1}	K'_{+1}	J''	K''_{-1}	K''_{+1}	V _{obs}	V _{obs} -V _{calc}
2	0	2	1	0	1	3742.1972	-0.0053
2	1	1	1	1	0	3933.8785	0.0072
3	0	3	2	0	2	5527.6253	-0.0010
3	2	1	2	2	0	5821.4747	0.0023
4	1	4	3	1	3	7199.8128	0.0200
4	0	4	3	0	3	7265.1804	0.0055
4	2	3	3	2	2	7533.6380	0.0102
4	1	3	3	1	2	7761.9165	-0.0088

Table S5.10. Measured frequencies and residuals (in MHz) for the rotational transitions of the $^{13}\text{C}_9$ isotopologue of BC1-1w-1.

J'	K'_{-1}	K'_{+1}	J''	K''_{-1}	K''_{+1}	V_{obs}	$V_{\text{obs}}-V_{\text{calc}}$
2	0	2	1	0	1	3746.2090	-0.0035
3	1	3	2	1	2	5433.7298	-0.0013
3	0	3	2	0	2	5536.8839	-0.0072
3	2	2	2	2	1	5677.7345	0.0092
3	2	1	2	2	0	5818.4862	-0.0037
3	1	2	2	1	1	5871.2881	-0.0007
4	1	4	3	1	3	7212.0717	0.0033
4	2	3	3	2	2	7539.3652	-0.0008
4	1	3	3	1	2	7766.3352	0.0028
4	2	2	3	2	1	7828.7920	-0.0008

Table S5.11. Measured frequencies and residuals (in MHz) for the rotational transitions of the $^{18}\text{O}_{10}$ isotopologue of BC1-1w-1.

J'	K'_{-1}	K'_{+1}	J''	K''_{-1}	K''_{+1}	V_{obs}	$V_{\text{obs}}-V_{\text{calc}}$
2	1	2	1	1	1	3521.3346	-0.0021
2	0	2	1	0	1	3628.4871	-0.0026
2	1	1	1	1	0	3800.2624	0.0009
2	1	1	1	0	1	4313.5677	-0.0028
2	2	0	1	1	0	4954.0964	0.0039
2	2	1	1	1	1	5061.2555	-0.0026
3	1	3	2	1	2	5263.6366	-0.0010
3	0	3	2	0	2	5371.9241	0.0002
3	2	2	2	2	1	5491.1833	0.0007
3	2	1	2	2	0	5610.3726	0.0010
3	1	2	2	1	1	5677.1935	0.0014
3	1	2	2	0	2	6362.2744	0.0015
4	1	3	3	2	1	6432.7594	0.0011
3	2	1	2	1	1	6764.2020	-0.0006
4	1	4	3	1	3	6989.8041	-0.0017
4	0	4	3	0	3	7067.8938	0.0034
4	2	3	3	2	2	7295.9891	-0.0042
4	3	2	3	3	1	7374.2281	0.0067
4	3	1	3	3	0	7402.0880	-0.0061
4	1	3	3	1	2	7519.7712	0.0024
4	2	2	3	2	1	7548.8622	-0.0014

Table S5.12. Measured frequencies and residuals (in MHz) for the rotational transitions of the parent species of BC1-1w-2 complex.

J'	K' ₋₁	K' ₊₁	J''	K'' ₋₁	K'' ₊₁	V _{obs}	V _{obs} -V _{calc}
4	2	3	4	1	3	2184.8452	-0.0093
5	1	4	5	1	5	2427.7271	0.0128
5	2	3	5	1	4	2462.0655	0.0073
4	2	2	4	1	3	2473.5575	-0.0028
3	2	2	3	1	2	2484.2314	-0.0092
1	1	1	0	0	0	2487.2887	0.0067
3	2	1	3	1	2	2584.7082	0.0042
6	2	4	6	1	5	2596.1925	0.0070
1	1	0	0	0	0	2652.0504	-0.0044
7	2	5	7	1	6	2909.4702	0.0031
2	1	2	1	1	1	2997.9850	-0.0026
2	0	2	1	0	1	3142.2593	-0.0033
8	3	6	8	2	6	3177.6994	0.0146
2	1	1	1	1	0	3327.5334	0.0008
6	1	5	6	1	6	3332.6745	-0.0168
3	2	2	3	1	3	3471.2657	-0.0006
7	3	5	7	2	5	3691.3219	0.0028
4	2	3	4	1	4	3821.4252	0.0103
3	0	3	2	1	2	3902.5391	0.0044
2	1	2	1	0	1	3903.8872	0.0003
2	2	1	2	0	2	3973.6299	0.0002
7	3	4	7	2	5	3993.6035	0.0065
4	1	3	3	2	1	4024.1483	-0.0107
3	2	2	3	0	3	4053.5996	0.0013
4	1	3	3	2	2	4124.6137	-0.0087
6	3	4	6	2	4	4133.0798	-0.0103
4	2	3	4	0	4	4225.9460	-0.0021
6	3	3	6	2	4	4260.5214	-0.0046
7	1	6	7	1	7	4310.8999	0.0012
2	1	1	1	0	1	4398.2061	0.0014
5	3	3	5	2	3	4479.3536	0.0025
3	1	3	2	1	2	4484.8649	-0.0018
5	2	4	5	0	5	4519.9818	-0.0066
5	3	2	5	2	3	4523.2215	0.0162
3	0	3	2	0	2	4664.1583	-0.0008
4	3	2	4	2	2	4717.3730	-0.0035
3	2	2	2	2	1	4744.1217	-0.0059
3	2	1	2	2	0	4824.0920	-0.0019
3	3	1	3	2	1	4853.0062	-0.0056
6	2	5	6	0	6	4943.4089	-0.0230
3	1	2	2	1	1	4977.5748	0.0002
3	1	3	2	0	2	5246.4874	-0.0036
8	1	7	8	1	8	5315.9815	0.0129
4	0	4	3	1	3	5554.7974	0.0023
5	1	4	4	2	2	5737.9504	-0.0008
4	1	4	3	1	3	5959.3283	0.0000
5	1	4	4	2	3	6026.6635	0.0066
2	2	1	1	1	0	6045.2288	0.0086
2	2	0	1	1	0	6065.7179	0.0006
4	0	4	3	0	3	6137.1274	0.0003
2	2	1	1	1	1	6209.9956	0.0027
2	2	0	1	1	1	6230.4958	0.0058
3	1	2	2	0	2	6233.5216	0.0049
8	4	5	8	3	5	6308.0205	-0.0060
4	2	3	3	2	2	6309.4754	-0.0016
4	3	2	3	3	1	6362.0840	0.0000
4	3	1	3	3	0	6371.6343	-0.0013
4	2	2	3	2	1	6497.7200	0.0007
4	1	4	3	0	3	6541.6560	-0.0043
8	3	6	8	1	7	6600.3248	0.0094

7	3	5	7	1	6	6600.7686	-0.0177
4	1	3	3	1	2	6608.8626	-0.0005
6	3	4	6	1	5	6729.2872	0.0116
6	4	3	6	3	3	6743.0804	-0.0030
5	4	2	5	3	2	6831.6052	0.0078
4	4	1	4	3	1	6873.9805	-0.0015
5	3	3	5	1	4	6941.3960	-0.0133
5	0	5	4	1	4	7162.7628	0.0112
4	3	2	4	1	3	7190.9347	-0.0021
6	1	5	5	2	3	7311.6552	-0.0062
5	1	5	4	1	4	7420.3642	0.0067
3	2	2	2	1	1	7461.8113	-0.0039
3	2	1	2	1	1	7562.2768	-0.0018
5	0	5	4	0	4	7567.2902	0.0053
5	1	5	4	0	4	7824.8924	0.0016
5	2	4	4	2	3	7861.3225	-0.0026
5	4	2	4	4	1	7952.2990	0.0055
5	4	1	4	4	0	7953.1185	-0.0058
3	2	2	2	1	2	7956.1390	0.0060
5	3	3	4	3	2	7961.9820	-0.0020
5	3	2	4	3	1	7994.6755	-0.0026

Table S5.13. Measured frequencies and residuals (in MHz) for the rotational transitions of the $^{13}\text{C}_1$ isotopologue of BC1-1w-2.

J'	K'_{-1}	K'_{+1}	J''	K''_{-1}	K''_{+1}	V_{obs}	$V_{\text{obs}}-V_{\text{calc}}$
2	0	2	1	0	1	3111.1693	-0.0106
2	1	1	1	1	0	3291.6920	0.0036
3	1	3	2	1	2	4442.8858	-0.0032
3	0	3	2	0	2	4619.8962	-0.0070
3	2	2	2	2	1	4695.9507	-0.0097
3	1	2	2	1	1	4924.5291	0.0056
4	1	4	3	1	3	5904.2976	-0.0030
4	0	4	3	0	3	6081.5886	-0.0003
4	2	3	3	2	2	6246.0612	0.0007
4	1	3	3	1	2	6539.6421	0.0029
5	1	5	4	1	4	7352.8007	0.0112

Table S5.14. Measured frequencies and residuals (in MHz) for the rotational transitions of the $^{13}\text{C}_2$ isotopologue of BC1-1w-2.

J'	K'_{-1}	K'_{+1}	J''	K''_{-1}	K''_{+1}	V_{obs}	$V_{\text{obs}}-V_{\text{calc}}$
2	1	2	1	1	1	2983.9740	-0.0039
3	1	3	2	1	2	4463.9409	-0.0042
3	0	3	2	0	2	4641.6264	-0.0034
3	2	1	2	2	0	4800.3326	-0.0054
3	1	2	2	1	1	4952.4018	-0.0056
4	1	4	3	1	3	5931.5874	-0.0048
4	0	4	3	0	3	6107.7367	0.0020
4	2	3	3	2	2	6278.7393	-0.0029
4	2	2	3	2	1	6465.5346	0.0137
4	1	3	3	1	2	6575.5105	-0.0048
5	1	5	4	1	4	7385.9144	-0.0007
5	0	5	4	0	4	7531.4140	0.0085
5	2	4	4	2	3	7823.1038	0.0024

Table S5.15. Measured frequencies and residuals (in MHz) for the rotational transitions of the $^{13}\text{C}_3$ isotopologue of BC1-1w-2.

J'	K'_{-1}	K'_{+1}	J''	K''_{-1}	K''_{+1}	V _{obs}	V _{obs} -V _{calc}
2	1	2	1	1	1	2983.9740	0.0078
2	0	2	1	0	1	3130.1970	-0.0090
2	1	1	1	1	0	3319.9132	0.0056
3	1	3	2	1	2	4463.1261	-0.0069
3	0	3	2	0	2	4643.2772	-0.0019
3	2	1	2	2	0	4812.5154	0.0110
3	1	2	2	1	1	4965.2728	0.0037
4	1	4	3	1	3	5929.2499	-0.0023
4	0	4	3	0	3	6105.3787	-0.0072
4	2	3	3	2	2	6286.8562	-0.0064
4	1	3	3	1	2	6590.5982	-0.0030
5	1	5	4	1	4	7381.3903	0.0022
5	0	5	4	0	4	7524.2410	0.0120
5	2	4	4	2	3	7831.5317	-0.0043

Table S5.16. Measured frequencies and residuals (in MHz) for the rotational transitions of the $^{13}\text{C}_4$ isotopologue of BC1-1w-2.

J'	K'_{-1}	K'_{+1}	J''	K''_{-1}	K''_{+1}	V _{obs}	V _{obs} -V _{calc}
2	1	2	1	1	1	2989.3784	-0.0047
2	0	2	1	0	1	3134.5413	-0.0025
3	1	3	2	1	2	4471.5523	-0.0066
3	0	3	2	0	2	4650.9790	-0.0048
3	2	2	2	2	1	4733.6249	0.0158
3	2	1	2	2	0	4816.2237	-0.0084
3	1	2	2	1	1	4968.9480	0.0021
4	1	4	3	1	3	5940.9591	-0.0004
4	0	4	3	0	3	6117.3472	-0.0037
4	2	3	3	2	2	6294.8967	-0.0011
4	2	2	3	2	1	6488.8839	0.0013
4	1	3	3	1	2	6596.2917	0.0004
5	1	5	4	1	4	7396.6269	0.0075
5	0	5	4	0	4	7540.7105	0.0009
5	2	4	4	2	3	7842.2285	-0.0017

Table S5.17. Measured frequencies and residuals (in MHz) for the rotational transitions of the $^{13}\text{C}_5$ isotopologue of BC1-1w-2.

J'	K'_{-1}	K'_{+1}	J''	K''_{-1}	K''_{+1}	V _{obs}	V _{obs} -V _{calc}
2	1	2	1	1	1	2993.6036	-0.0082
2	0	2	1	0	1	3135.9254	-0.0054
3	1	3	2	1	2	4478.5619	-0.0009
3	0	3	2	0	2	4655.7054	-0.0024
3	1	2	2	1	1	4964.1087	0.0011
4	1	4	3	1	3	5951.3524	0.0053
4	0	4	3	0	3	6127.4729	0.0012
4	2	3	3	2	2	6296.2749	0.0057
4	2	2	3	2	1	6480.6128	-0.0001
4	1	3	3	1	2	6591.5466	0.0011
5	1	5	4	1	4	7410.9491	0.0011
5	0	5	4	0	4	7556.9950	-0.0005
5	2	4	4	2	3	7845.3652	-0.0045

Table S5.18. Measured frequencies and residuals (in MHz) for the rotational transitions of the $^{13}\text{C}_6$ isotopologue of BC1-1w-2.

J'	K'_{-1}	K'_{+1}	J''	K''_{-1}	K''_{+1}	V _{obs}	V _{obs} -V _{calc}
2	0	2	1	0	1	3139.0782	-0.0148
3	1	3	2	1	2	4479.1862	-0.0043
3	0	3	2	0	2	4658.6856	-0.0045
3	2	2	2	2	1	4739.8553	0.0101
3	1	2	2	1	1	4974.2869	0.0012
4	1	4	3	1	3	5951.4755	-0.0038
4	0	4	3	0	3	6128.8350	0.0030
4	2	3	3	2	2	6303.5261	0.0059
4	2	2	3	2	1	6494.3431	-0.0009
4	1	3	3	1	2	6604.0051	-0.0009
5	1	5	4	1	4	7410.1991	0.0052
5	2	4	4	2	3	7853.4877	-0.0035

Table S5.19. Measured frequencies and residuals (in MHz) for the rotational transitions of the $^{18}\text{O}_7$ isotopologue of BC1-1w-2.

J'	K'_{-1}	K'_{+1}	J''	K''_{-1}	K''_{+1}	V _{obs}	V _{obs} -V _{calc}
1	1	0	0	0	0	2621.5354	0.0008
2	1	2	1	1	1	2972.9976	-0.0045
2	0	2	1	0	1	3117.0083	0.0021
2	1	1	1	1	0	3302.8462	0.0074
2	1	1	1	0	1	4355.4006	-0.0100
3	1	3	2	1	2	4447.1509	-0.0040
3	0	3	2	0	2	4625.3485	-0.0027
3	2	2	2	2	1	4706.8767	0.0085
3	2	1	2	2	0	4788.3890	0.0060
3	1	2	2	1	1	4940.2374	0.0022
4	1	4	3	1	3	5908.6912	-0.0014
2	2	0	1	1	0	5986.7031	0.0016
4	0	4	3	0	3	6084.1908	-0.0044
2	2	1	1	1	1	6130.7114	0.0051
3	1	2	2	0	2	6178.6308	-0.0087
4	2	2	3	2	1	6450.9612	0.0023
4	1	3	3	1	2	6558.4280	0.0002
5	1	5	4	1	4	7356.6518	0.0064
5	0	5	4	0	4	7500.3524	-0.0038
5	2	4	4	2	3	7798.3027	-0.0016

Table S5.20. Measured frequencies and residuals (in MHz) for the rotational transitions of the $^{13}\text{C}_8$ isotopologue of BC1-1w-2.

J'	K'_{-1}	K'_{+1}	J''	K''_{-1}	K''_{+1}	V _{obs}	V _{obs} -V _{calc}
2	0	2	1	0	1	3117.9707	-0.0015
2	1	1	1	1	0	3300.9318	0.0060
3	1	3	2	1	2	4450.8222	0.0059
3	0	3	2	0	2	4628.7642	0.0019
3	2	1	2	2	0	4785.2599	-0.0115
3	1	2	2	1	1	4937.9805	0.0048
4	1	4	3	1	3	5914.3425	-0.0010
4	0	4	3	0	3	6091.4710	-0.0038
4	2	3	3	2	2	6260.3460	-0.0037
4	2	2	3	2	1	6444.7791	0.0096
4	1	3	3	1	2	6556.7191	-0.0005
5	1	5	4	1	4	7364.6701	0.0016
5	0	5	4	0	4	7511.7899	0.0057
5	2	4	4	2	3	7800.4618	-0.0102

Table S5.21. Measured frequencies and residuals (in MHz) for the rotational transitions of the $^{13}\text{C}_9$ isotopologue of BC1-1w-2.

J'	K'_{-1}	K'_{+1}	J''	K''_{-1}	K''_{+1}	V _{obs}	V _{obs} -V _{calc}
2	0	2	1	0	1	3131.3981	-0.0034
2	1	1	1	1	0	3320.2323	0.0164
3	1	3	2	1	2	4465.6753	-0.0064
3	0	3	2	0	2	4645.6053	-0.0027
3	2	1	2	2	0	4813.0597	0.0076
3	1	2	2	1	1	4965.8979	-0.0002
4	1	4	3	1	3	5932.8541	-0.0070
4	0	4	3	0	3	6109.2457	0.0077
4	2	3	3	2	2	6288.9589	-0.0072
4	1	3	3	1	2	6591.7883	-0.0074
5	1	5	4	1	4	7386.1723	0.0092
5	2	4	4	2	3	7834.4548	-0.0023

Table S5.22. Measured frequencies and residuals (in MHz) for the rotational transitions of the $^{18}\text{O}_{10}$ isotopologue of BC1-1w-2.

J'	K'_{-1}	K'_{+1}	J''	K''_{-1}	K''_{+1}	ν_{obs}	$\nu_{\text{obs}} - \nu_{\text{calc}}$
1	1	1	0	0	0	2459.1539	-0.0149
1	1	0	0	0	0	2610.6947	0.0025
2	1	2	1	1	1	2881.1590	-0.0042
2	0	2	1	0	1	3015.8474	-0.0034
2	1	1	1	1	0	3184.2114	0.0018
3	0	3	2	1	2	3674.8668	-0.0084
2	1	2	1	0	1	3823.9861	0.0000
3	1	3	2	1	2	4311.7349	-0.0016
3	0	3	2	0	2	4483.0094	-0.0012
3	2	2	2	2	1	4549.0204	0.0032
3	2	1	2	2	0	4615.0218	0.0002
3	1	2	2	1	1	4765.1266	-0.0005
3	1	3	2	0	2	5119.8645	-0.0074
4	0	4	3	1	3	5271.3069	0.0068
5	1	4	4	2	2	5300.3726	-0.0016
4	1	4	3	1	3	5731.8648	0.0003
4	0	4	3	0	3	5908.1612	-0.0002
2	2	1	1	1	0	6012.6849	0.0170
2	2	0	1	1	0	6029.5010	-0.0022
2	2	0	1	1	0	6029.5010	-0.0022
4	2	3	3	2	2	6052.1942	-0.0045
4	3	2	3	3	1	6095.7491	-0.0032
4	3	1	3	3	0	6102.7556	-0.0055
2	2	1	1	1	1	6164.1909	-0.0004
2	2	1	1	1	1	6164.1909	-0.0004
4	2	2	3	2	1	6209.2937	-0.0022
4	1	3	3	1	2	6330.9447	0.0000
4	1	4	3	0	3	6368.7179	-0.0079
5	0	5	4	1	4	6833.0586	0.0099
6	1	5	5	2	3	6853.2539	0.0020
5	1	5	4	1	4	7140.4246	0.0117
5	0	5	4	0	4	7293.6199	0.0068
3	2	1	2	1	1	7460.3103	-0.0049
5	2	4	4	2	3	7544.2544	-0.0024
5	1	5	4	0	4	7600.9823	0.0050
5	4	2	4	4	1	7618.9836	-0.0110
5	4	1	4	4	0	7619.5228	-0.0150
5	3	3	4	3	2	7628.1544	-0.0078
5	3	2	4	3	1	7652.2595	-0.0062
5	2	3	4	2	2	7831.7151	-0.0016
3	2	2	2	1	2	7832.0454	0.0001
5	1	4	4	1	3	7873.9083	-0.0052

Table S5.23. Measured frequencies and residuals (in MHz) for the rotational transitions of the parent species of BC1-2w-2a complex.

J'	K' ₋₁	K' ₊₁	J''	K'' ₋₁	K'' ₊₁	V _{obs}	V _{obs} -V _{calc}
2	1	2	1	1	1	2392.7120	-0.0235
2	0	2	1	0	1	2500.5824	-0.0003
2	1	1	1	1	0	2658.8923	-0.0015
2	1	1	1	0	1	3245.4508	0.0039
3	1	3	2	1	2	3574.5796	0.0038
3	0	3	2	0	2	3693.2505	0.0032
3	2	2	2	2	1	3788.6926	-0.0012
3	2	1	2	2	0	3884.1627	-0.0006
3	1	2	2	1	1	3970.7554	0.0009
2	2	0	1	1	0	4044.5512	0.0032
2	2	1	1	1	1	4152.3981	0.0061
4	1	4	3	1	3	4742.8412	0.0023
4	0	4	3	0	3	4839.9886	0.0049
4	2	3	3	2	2	5031.7774	0.0027
4	3	2	3	3	1	5094.1409	0.0064
4	3	1	3	3	0	5112.0191	-0.0006
4	2	2	3	2	1	5243.0870	-0.0005
4	1	3	3	1	2	5257.2636	0.0013
3	2	1	2	1	1	5269.8060	-0.0116
3	2	1	2	1	1	5269.8060	-0.0116
3	2	2	2	1	2	5548.3510	0.0007
5	1	5	4	1	4	5898.1537	0.0023
5	0	5	4	0	4	5961.2674	0.0027
5	2	4	4	2	3	6258.5437	-0.0013
4	1	3	3	0	3	6279.6296	-0.0039
5	4	2	4	4	1	6370.2078	0.0043
5	4	1	4	4	0	6372.6106	-0.0017
5	3	3	4	3	2	6373.9817	-0.0018
3	3	0	2	2	0	6381.1011	0.0041
3	3	1	2	2	1	6403.2737	-0.0028
5	3	2	4	3	1	6433.2286	-0.0003
5	1	4	4	1	3	6504.2581	0.0017
4	2	2	3	1	2	6542.1546	0.0040
5	2	3	4	2	2	6609.3408	-0.0012
4	2	3	3	1	3	7005.5524	0.0031
6	1	6	5	1	5	7043.1698	-0.0037
6	0	6	5	0	5	7078.0521	0.0000
6	2	5	5	2	4	7466.5003	-0.0016
4	3	1	3	2	1	7608.9524	-0.0010
6	3	4	5	3	3	7648.1195	-0.0008
6	4	3	5	4	2	7659.7128	-0.0013
6	4	2	5	4	1	7670.2407	-0.0012
6	1	5	5	1	4	7699.1476	0.0007
4	3	2	3	2	2	7708.7170	-0.0002
6	3	3	5	3	2	7790.3162	-0.0002
5	2	3	4	1	3	7894.2351	0.0048
6	2	4	5	2	3	7955.2363	-0.0004

Table S5.24. Measured frequencies and residuals (in MHz) for the rotational transitions of the $^{13}\text{C}_1$ isotopologue of BC1-2w-2a.

J'	K'_{-1}	K'_{+1}	J''	K''_{-1}	K''_{+1}	V _{obs}	V _{obs} -V _{calc}
3	1	3	2	1	2	3561.8104	0.0011
3	0	3	2	0	2	3680.0562	-0.0072
3	1	2	2	1	1	3965.4273	-0.0009
4	1	4	3	1	3	4724.7007	0.0054
4	0	4	3	0	3	4819.4619	0.0013
4	2	3	3	2	2	5019.8283	0.0088
4	2	2	3	2	1	5240.8045	-0.0040
4	1	3	3	1	2	5247.7211	0.0018
5	0	5	4	0	4	5934.3139	0.0102
5	1	4	4	1	3	6487.8476	-0.0032
6	1	6	5	1	5	7013.4139	-0.0040
6	0	6	5	0	5	7045.7782	-0.0095
6	2	5	5	2	4	7444.1496	0.0028
6	1	5	5	1	4	7673.1762	-0.0006

Table S5.25. Measured frequencies and residuals (in MHz) for the rotational transitions of the $^{13}\text{C}_2$ isotopologue of BC1-2w-2a.

J'	K'_{-1}	K'_{+1}	J''	K''_{-1}	K''_{+1}	V _{obs}	V _{obs} -V _{calc}
3	1	3	2	1	2	3564.8964	0.0081
3	0	3	2	0	2	3682.6010	0.0000
3	1	2	2	1	1	3959.4798	-0.0024
4	1	4	3	1	3	4729.8903	0.0017
4	0	4	3	0	3	4825.8655	-0.0026
4	1	3	3	1	2	5242.0640	-0.0014
5	1	5	4	1	4	5881.9738	0.0104
5	0	5	4	0	4	5944.0257	-0.0037
5	2	4	4	2	3	6240.9950	-0.0026
5	1	4	4	1	3	6484.9404	-0.0056
6	0	6	5	0	5	7057.9322	-0.0103
6	1	5	5	1	4	7675.6164	0.0101

Table S5.26. Measured frequencies and residuals (in MHz) for the rotational transitions of the $^{13}\text{C}_3$ isotopologue of BC1-2w-2a.

J'	K'_{-1}	K'_{+1}	J''	K''_{-1}	K''_{+1}	V _{obs}	V _{obs} -V _{calc}
3	0	3	2	0	2	3666.9639	-0.0039
3	1	2	2	1	1	3938.1549	-0.0080
4	1	4	3	1	3	4709.5550	-0.0016
4	0	4	3	0	3	4807.1838	-0.0078
4	2	3	3	2	2	4992.9592	0.0055
4	1	3	3	1	2	5215.3479	-0.0046
5	1	5	4	1	4	5857.4275	-0.0014
5	0	5	4	0	4	5921.7271	0.0119
5	1	4	4	1	3	6454.6956	-0.0094
5	2	3	4	2	2	6552.2461	0.0053
6	1	6	5	1	5	6995.1499	-0.0018
6	2	5	5	2	4	7411.1991	-0.0044
6	1	5	5	1	4	7643.8199	0.0090
6	2	4	5	2	3	7888.2714	0.0035

Table S5.27. Measured frequencies and residuals (in MHz) for the rotational transitions of the $^{13}\text{C}_4$ isotopologue of BC1-2w-2a.

J'	K'_{-1}	K'_{+1}	J''	K''_{-1}	K''_{+1}	ν_{obs}	$\nu_{\text{obs}} - \nu_{\text{calc}}$
3	1	3	2	1	2	3547.2180	0.0031
3	0	3	2	0	2	3665.3999	-0.0029
3	1	2	2	1	1	3937.3001	-0.0074
4	1	4	3	1	3	4707.0508	-0.0101
4	0	4	3	0	3	4804.8836	0.0025
4	2	3	3	2	2	4991.1865	0.0136
4	2	2	3	2	1	5196.3248	0.0074
4	1	3	3	1	2	5214.0978	-0.0032
5	1	5	4	1	4	5854.2228	-0.0044
5	0	5	4	0	4	5918.6202	0.0070
5	2	4	4	2	3	6208.8595	0.0027
5	1	4	4	1	3	6452.9366	-0.0017
5	2	3	4	2	2	6550.8616	-0.0022
6	1	6	5	1	5	6991.2158	-0.0038
6	2	5	5	2	4	7408.3025	0.0030
6	2	4	5	2	3	7886.6249	-0.0035

Table S5.28. Measured frequencies and residuals (in MHz) for the rotational transitions of the $^{13}\text{C}_5$ isotopologue of BC1-2w-2a.

J'	K'_{-1}	K'_{+1}	J''	K''_{-1}	K''_{+1}	ν_{obs}	$\nu_{\text{obs}} - \nu_{\text{calc}}$
3	1	3	2	1	2	3555.1211	0.0037
3	0	3	2	0	2	3673.4030	0.0092
3	1	2	2	1	1	3950.0596	0.0010
4	1	4	3	1	3	4716.9464	-0.0130
4	0	4	3	0	3	4813.7577	-0.0039
4	2	3	3	2	2	5005.0088	0.0086
4	2	2	3	2	1	5215.7006	-0.0076
4	1	3	3	1	2	5229.7616	-0.0064
5	1	5	4	1	4	5865.8995	0.0109
5	0	5	4	0	4	5928.7535	-0.0110
5	2	4	4	2	3	6225.1557	-0.0066
5	1	4	4	1	3	6470.0715	0.0027
5	2	3	4	2	2	6574.9400	0.0096
6	1	6	5	1	5	7004.5545	-0.0042
6	0	6	5	0	5	7039.3067	0.0090
6	2	5	5	2	4	7426.5639	0.0007
6	1	5	5	1	4	7658.4113	0.0013
6	2	4	5	2	3	7913.8302	-0.0035

Table S5.29. Measured frequencies and residuals (in MHz) for the rotational transitions of the $^{13}\text{C}_6$ isotopologue of BC1-2w-2a.

J'	K'_{-1}	K'_{+1}	J''	K''_{-1}	K''_{+1}	V _{obs}	V _{obs} -V _{calc}
3	1	3	2	1	2	3569.8550	0.0029
3	0	3	2	0	0	3688.1673	-0.0021
3	1	2	2	1	1	3967.1466	0.0034
4	1	4	3	1	1	4736.2942	-0.0020
4	0	4	3	0	0	4832.6173	0.0055
4	2	2	3	2	2	5239.6377	-0.0036
4	1	3	3	1	1	5251.9005	0.0059
5	1	5	4	1	1	5889.7158	-0.0003
5	0	5	4	0	0	5951.8777	-0.0026
5	2	4	4	2	2	6251.2478	0.0102
5	1	4	4	1	1	6496.5308	0.0018
5	2	3	4	2	2	6604.7441	-0.0019
6	2	5	5	2	2	7457.2231	0.0025
6	1	5	5	1	1	7688.4481	-0.0059

Table S5.30. Measured frequencies and residuals (in MHz) for the rotational transitions of the $^{18}\text{O}_7$ isotopologue of BC1-2w-2a.

J'	K'_{-1}	K'_{+1}	J''	K''_{-1}	K''_{+1}	V _{obs}	V _{obs} -V _{calc}
2	1	2	1	1	1	2378.4060	0.0038
2	0	2	1	0	1	2488.1759	-0.0033
2	1	1	1	1	0	2653.5432	-0.0035
3	1	3	2	1	2	3551.6762	0.0017
3	0	3	2	0	2	3669.5187	-0.0022
3	1	2	2	1	1	3960.7939	0.0024
4	1	4	3	1	3	4710.3297	-0.0006
4	0	4	3	0	3	4803.2448	-0.0035
4	2	3	3	2	2	5010.0570	0.0010
4	2	2	3	2	1	5238.3419	-0.0040
4	1	3	3	1	2	5239.6414	0.0072
5	1	5	4	1	4	5855.3917	0.0048
5	0	5	4	0	4	5913.1675	-0.0002
5	2	4	4	2	3	6228.2954	0.0047
5	1	4	4	1	3	6474.2694	-0.0026
5	2	3	4	2	2	6601.9702	-0.0018
6	1	6	5	1	5	6989.9872	-0.0004
6	0	6	5	0	5	7020.5529	-0.0057
6	2	5	5	2	4	7426.1176	0.0033
6	2	4	5	2	3	7940.1960	-0.0013

Table S5.31. Measured frequencies and residuals (in MHz) for the rotational transitions of the $^{13}\text{C}_8$ isotopologue of BC1-2w-2a.

J'	K'_{-1}	K'_{+1}	J''	K''_{-1}	K''_{+1}	ν_{obs}	$\nu_{\text{obs}} - \nu_{\text{calc}}$
3	1	3	2	1	2	3565.8640	0.0001
3	0	3	2	0	2	3683.1428	-0.0046
3	1	2	2	1	1	3959.4798	0.0054
4	1	4	3	1	3	4731.2153	0.0029
4	0	4	3	0	3	4826.7307	-0.0045
4	1	3	3	1	2	5242.0640	0.0052
5	1	5	4	1	4	5883.6596	-0.0007
5	0	5	4	0	4	5945.3552	0.0053
5	2	4	4	2	3	6241.8131	-0.0090
5	1	4	4	1	3	6484.9404	-0.0018
6	0	6	5	0	5	7059.7931	0.0022

Table S5.32. Measured frequencies and residuals (in MHz) for the rotational transitions of the $^{13}\text{C}_9$ isotopologue of BC1-2w-2a.

J'	K'_{-1}	K'_{+1}	J''	K''_{-1}	K''_{+1}	ν_{obs}	$\nu_{\text{obs}} - \nu_{\text{calc}}$
3	1	3	2	1	2	3571.4938	-0.0069
3	0	3	2	0	2	3688.8410	0.0034
3	1	2	2	1	1	3961.5687	-0.0088
4	1	4	3	1	3	4739.2245	0.0012
4	0	4	3	0	3	4835.6711	0.0041
4	2	3	3	2	2	5023.5691	0.0018
4	2	2	3	2	1	5230.5556	0.0020
4	1	3	3	1	2	5245.9212	0.0039
5	1	5	4	1	4	5894.2225	0.0026
5	0	5	4	0	4	5957.1754	-0.0039
5	2	4	4	2	3	6248.9789	-0.0019
5	1	4	4	1	3	6491.7038	0.0014
6	1	5	5	1	4	7686.5148	-0.0011

Table S5.33. Measured frequencies and residuals (in MHz) for the rotational transitions of the $^{18}\text{O}_{10}$ isotopologue of BC1-2w-2a.

J'	K'_{-1}	K'_{+1}	J''	K''_{-1}	K''_{+1}	V _{obs}	V _{obs} -V _{calc}
2	1	2	1	1	1	2334.1094	0.0009
2	0	2	1	0	1	2439.2744	0.0016
2	1	1	1	1	0	2591.1848	0.0018
3	1	3	2	1	2	3487.6668	0.0021
3	0	3	2	0	2	3605.1543	-0.0005
3	2	2	2	2	1	3693.9449	0.0046
3	2	1	2	2	0	3782.7511	0.0016
3	1	2	2	1	1	3870.5661	0.0017
2	2	1	1	1	1	4099.5435	0.0070
4	1	4	3	1	3	4628.4628	0.0014
4	0	4	3	0	3	4726.9071	-0.0006
4	2	3	3	2	2	4906.9074	-0.0004
4	3	2	3	3	1	4964.9180	-0.0004
4	3	1	3	3	0	4980.8143	-0.0004
4	2	2	3	2	1	5105.0069	0.0011
4	1	3	3	1	2	5126.7103	0.0007
3	2	1	2	1	1	5185.9335	-0.0088
3	2	2	2	1	2	5459.3650	-0.0032
5	1	5	4	1	4	5756.8976	-0.0005
5	0	5	4	0	4	5822.6540	0.0003
5	2	4	4	2	3	6104.7260	0.0010
4	1	3	3	0	3	6132.5088	0.0017
5	4	2	4	4	1	6208.1741	-0.0035
5	4	1	4	4	0	6210.2195	-0.0068
5	3	3	4	3	2	6212.5393	-0.0010
5	3	2	4	3	1	6265.4500	-0.0016
3	3	0	2	2	0	6307.7971	0.0044
3	3	1	2	2	1	6328.4581	-0.0009
5	1	4	4	1	3	6346.6422	0.0016
5	2	3	4	2	2	6436.5756	0.0029
6	1	6	5	1	5	6875.3071	-0.0026
4	2	3	3	1	3	6878.6154	0.0040
6	0	6	5	0	5	6912.6759	0.0001
6	2	5	5	2	4	7284.9572	0.0027
6	3	4	5	3	3	7455.3691	-0.0010
6	4	3	5	4	2	7464.3520	-0.0043
6	4	2	5	4	1	7473.3283	-0.0048
6	1	5	5	1	4	7518.1465	0.0073
6	3	3	5	3	2	7583.5249	0.0016
4	3	2	3	2	2	7599.4356	-0.0016
5	2	3	4	1	3	7730.2394	-0.0074
6	2	4	5	2	3	7751.1188	0.0053

Table S5.34. Measured frequencies and residuals (in MHz) for the rotational transitions of the $^{18}\text{O}_{11}$ isotopologue of BC1-2w-2a.

J'	K'_{-1}	K'_{+1}	J''	K''_{-1}	K''_{+1}	V_{obs}	$V_{\text{obs}}-V_{\text{calc}}$
2	1	2	1	1	1	2331.3494	0.0012
2	0	2	1	0	1	2436.8461	-0.0003
2	1	1	1	1	0	2589.1186	-0.0003
3	1	3	2	1	2	3483.5141	0.0000
3	0	3	2	0	2	3601.4630	-0.0015
3	2	2	2	2	1	3690.3151	-0.0069
3	2	1	2	2	0	3779.2037	0.0006
3	1	2	2	1	1	3867.4621	-0.0002
2	2	0	1	1	0	3999.4447	-0.0017
2	2	1	1	1	1	4104.9506	0.0097
4	1	4	3	1	3	4622.9034	-0.0004
4	0	4	3	0	3	4721.8470	-0.0019
4	2	3	3	2	2	4902.0718	-0.0011
4	3	2	3	3	1	4960.1360	0.0050
4	3	1	3	3	0	4976.0080	0.0041
4	2	2	3	2	1	5100.4040	-0.0023
4	1	3	3	1	2	5122.5659	-0.0018
3	2	1	2	1	1	5189.5275	-0.0031
5	1	5	4	1	4	5749.9057	-0.0025
5	0	5	4	0	4	5816.0867	-0.0006
5	2	4	4	2	3	6098.6617	-0.0007
4	1	3	3	0	3	6132.0376	0.0004
5	4	2	4	4	1	6202.1856	0.0064
5	4	1	4	4	0	6204.2244	0.0040
5	3	3	4	3	2	6206.5891	0.0023
3	3	0	2	2	0	6316.9083	0.0045
3	3	1	2	2	1	6337.5906	0.0020
5	1	4	4	1	3	6341.4545	-0.0023
4	2	2	3	1	2	6422.4708	-0.0038
5	2	3	4	2	2	6431.0493	-0.0042
6	1	6	5	1	5	6866.8575	0.0008
6	0	6	5	0	5	6904.5157	0.0001
6	2	5	5	2	4	7277.6441	-0.0018
6	3	4	5	3	3	7448.2729	0.0000
6	4	3	5	4	2	7457.1826	0.0052
6	4	2	5	4	1	7466.1302	0.0078
6	1	5	5	1	4	7511.8764	-0.0029
4	3	1	3	2	1	7513.7007	-0.0039
6	3	3	5	3	2	7576.3214	-0.0014
4	3	2	3	2	2	7607.3961	-0.0015
5	2	3	4	1	3	7730.9579	-0.0025
6	2	4	5	2	3	7744.7553	-0.0051
7	1	7	6	1	6	7976.7878	0.0014

Table S5.35. Measured frequencies and residuals (in MHz) for the rotational transitions of the parent species of BC1-2w-5a complex.

J'	K'_{-1}	K'_{+1}	J''	K''_{-1}	K''_{+1}	V _{obs}	V _{obs} -V _{calc}
2	0	2	1	0	1	2152.3842	-0.0047
2	1	1	1	1	0	2229.5157	0.0046
3	1	3	2	1	2	3123.4773	-0.0009
3	0	3	2	0	2	3217.6225	-0.0017
3	2	2	2	2	1	3235.2169	0.0105
3	2	1	2	2	0	3252.7907	-0.0063
3	1	2	2	1	1	3341.4074	0.0009
4	1	4	3	1	3	4159.8417	-0.0022
4	0	4	3	0	3	4270.3164	-0.0009
4	2	3	3	2	2	4310.1545	0.0007
4	3	2	3	3	1	4321.9492	0.0000
4	3	1	3	3	0	4322.9528	-0.0061
4	2	2	3	2	1	4353.4389	-0.0019
4	1	3	3	1	2	4449.6302	0.0011
2	2	0	1	1	0	4809.1292	-0.0059
5	1	5	4	1	4	5192.5728	-0.0036
5	0	5	4	0	4	5308.0590	-0.0004
5	2	4	4	2	3	5382.1550	0.0029
5	4	1	4	4	0	5401.8024	-0.0091
5	3	3	4	3	2	5405.4787	0.0014
5	3	2	4	3	1	5408.9920	-0.0013
5	2	3	4	2	2	5466.0411	-0.0048
5	1	4	4	1	3	5552.5559	0.0006
4	1	3	3	0	3	5581.6293	-0.0057
6	1	6	5	1	5	6221.3116	-0.0041
6	0	6	5	0	5	6330.8285	-0.0031
6	2	5	5	2	4	6450.4995	0.0050
6	5	1	5	5	0	6481.3498	0.0027
6	4	3	5	4	2	6485.2857	-0.0019
6	4	2	5	4	1	6485.4879	0.0092
6	3	4	5	3	3	6490.2072	0.0006
6	3	3	5	3	2	6499.4926	-0.0028
6	2	4	5	2	3	6589.8401	-0.0026
6	1	5	5	1	4	6648.2220	0.0026
4	2	2	3	1	2	6844.4620	0.0068
5	1	4	4	0	4	6863.8740	0.0011
7	1	7	6	1	6	7245.9891	0.0026
7	0	7	6	0	6	7341.2977	-0.0039
7	2	6	6	2	5	7514.5277	0.0100
7	6	2	6	6	1	7560.9671	0.0011
7	5	2	6	5	1	7564.3433	-0.0036
7	3	5	6	3	4	7575.6561	0.0025
7	3	4	6	3	3	7596.2236	-0.0032
7	2	5	6	2	4	7721.3060	-0.0089
7	1	6	6	1	5	7734.3006	0.0027

Table S5.36. Measured frequencies and residuals (in MHz) for the rotational transitions of the $^{13}\text{C}_1$ isotopologue of BC1-2w-5a.

J'	K'_{-1}	K'_{+1}	J''	K''_{-1}	K''_{+1}	V_{obs}	$V_{\text{obs}}-V_{\text{calc}}$
3	1	2	2	1	1	3308.3959	-0.0086
4	1	4	3	1	3	4121.7280	-0.0046
4	0	4	3	0	3	4230.8245	-0.0027
4	2	3	3	2	2	4268.9904	0.0035
4	1	3	3	1	2	4405.8700	-0.0073
5	0	5	4	0	4	5259.8393	-0.0054
5	1	4	4	1	3	5498.3015	0.0018
6	1	6	5	1	5	6164.8586	-0.0048
6	0	6	5	0	5	6274.2962	0.0123
6	2	4	5	2	3	6523.3218	0.0072

Table S5.37. Measured frequencies and residuals (in MHz) for the rotational transitions of the $^{13}\text{C}_2$ isotopologue of BC1-2w-5a.

J'	K'_{-1}	K'_{+1}	J''	K''_{-1}	K''_{+1}	V_{obs}	$V_{\text{obs}}-V_{\text{calc}}$
3	0	3	2	0	2	3202.4890	0.0015
3	1	2	2	1	1	3324.6139	-0.0053
4	1	4	3	1	3	4141.2573	0.0019
4	0	4	3	0	3	4250.4781	0.0029
4	2	3	3	2	2	4289.6265	0.0040
4	1	3	3	1	2	4427.3472	0.0007
5	1	5	4	1	4	5169.4734	0.0112
5	1	4	4	1	3	5524.8714	-0.0007
6	1	6	5	1	5	6193.7272	-0.0118
6	0	6	5	0	5	6302.2768	0.0112
6	2	5	5	2	4	6419.9490	-0.0054
7	0	7	6	0	6	7308.6025	-0.0088
7	1	6	6	1	5	7696.2654	0.0003

Table S5.38. Measured frequencies and residuals (in MHz) for the rotational transitions of the $^{13}\text{C}_3$ isotopologue of BC1-2w-5a.

J'	K'_{-1}	K'_{+1}	J''	K''_{-1}	K''_{+1}	V_{obs}	$V_{\text{obs}}-V_{\text{calc}}$
3	1	3	2	1	2	3112.0081	-0.0057
3	0	3	2	0	2	3207.7117	-0.0062
4	1	4	3	1	3	4144.2619	-0.0113
4	0	4	3	0	3	4255.9212	-0.0093
4	2	2	3	2	1	4344.0940	-0.0167
5	2	4	4	2	3	5366.8515	0.0028
5	1	4	4	1	3	5540.6118	0.0054
6	1	6	5	1	5	6196.9622	0.0145
6	0	6	5	0	5	6305.5429	0.0008
6	2	4	5	2	3	6578.6178	0.0042
6	1	5	5	1	4	6632.8424	-0.0001

Table S5.39. Measured frequencies and residuals (in MHz) for the rotational transitions of the $^{13}\text{C}_4$ isotopologue of BC1-2w-5a.

J'	K'_{-1}	K'_{+1}	J''	K''_{-1}	K''_{+1}	V _{obs}	V _{obs} -V _{calc}
3	0	3	2	0	2	3213.7268	-0.0124
3	1	2	2	1	1	3339.4222	0.0100
4	1	4	3	1	3	4153.3150	-0.0020
4	0	4	3	0	3	4264.4886	-0.0090
4	2	3	3	2	2	4305.6397	-0.0070
4	2	2	3	2	1	4350.3587	-0.0042
5	2	4	4	2	3	5376.3407	0.0097
5	1	4	4	1	3	5548.6481	0.0114
6	0	6	5	0	5	6320.0701	-0.0019
6	1	5	5	1	4	6642.9478	-0.0094
7	1	7	6	1	6	7233.5987	0.0045
7	0	7	6	0	6	7327.8991	0.0038

Table S5.40. Measured frequencies and residuals (in MHz) for the rotational transitions of the $^{13}\text{C}_5$ isotopologue of BC1-2w-5a.

J'	K'_{-1}	K'_{+1}	J''	K''_{-1}	K''_{+1}	V _{obs}	V _{obs} -V _{calc}
3	1	3	2	1	2	3122.0629	0.0035
3	0	3	2	0	2	3215.3780	-0.0153
3	1	2	2	1	1	3337.9365	0.0044
4	1	4	3	1	3	4158.0292	0.0089
4	0	4	3	0	3	4267.6200	-0.0051
4	2	3	3	2	2	4306.8884	0.0004
4	1	3	3	1	2	4445.0739	-0.0074
5	1	5	4	1	4	5190.3942	-0.0030
5	0	5	4	0	4	5305.0998	0.0006
5	2	4	4	2	3	5378.1579	0.0073
5	1	4	4	1	3	5547.0152	0.0014
6	1	6	5	1	5	6218.8247	-0.0071
6	0	6	5	0	5	6327.7693	0.0042
6	2	5	5	2	4	6445.8138	0.0036

Table S5.41. Measured frequencies and residuals (in MHz) for the rotational transitions of the $^{13}\text{C}_6$ isotopologue of BC1-2w-5a.

J'	K'_{-1}	K'_{+1}	J''	K''_{-1}	K''_{+1}	V _{obs}	V _{obs} -V _{calc}
3	0	3	2	0	2	3215.3781	-0.0051
3	1	2	2	1	1	3340.1722	-0.0010
4	1	4	3	1	3	4156.1697	0.0103
4	0	4	3	0	3	4266.9758	-0.0013
4	1	3	3	1	2	4447.8648	-0.0117
5	1	5	4	1	4	5187.8472	-0.0012
5	0	5	4	0	4	5303.3896	-0.0102
5	2	4	4	2	3	5378.7816	0.0041
6	1	6	5	1	5	6215.4705	-0.0157
6	2	5	5	2	4	6446.3093	0.0140
6	2	4	5	2	3	6587.9332	0.0023
7	0	7	6	0	6	7333.7016	0.0088

Table S5.42. Measured frequencies and residuals (in MHz) for the rotational transitions of the $^{18}\text{O}_7$ isotopologue of BC1-2w-5a.

J'	K'_{-1}	K'_{+1}	J''	K''_{-1}	K''_{+1}	V _{obs}	V _{obs} -V _{calc}
3	1	3	2	1	2	3108.5421	0.0005
3	0	3	2	0	2	3204.9642	0.0099
3	1	2	2	1	1	3333.8397	-0.0030
4	1	4	3	1	3	4139.4929	0.0034
4	0	4	3	0	3	4251.6089	-0.0008
4	2	3	3	2	2	4295.1757	-0.0024
4	2	2	3	2	1	4342.5370	0.0073
4	1	3	3	1	2	4438.9753	-0.0025
5	1	5	4	1	4	5166.5008	-0.0026
5	0	5	4	0	4	5282.1981	-0.0011
5	2	4	4	2	3	5362.9063	0.0077
5	2	3	4	2	2	5454.3391	-0.0012
5	1	4	4	1	3	5538.2336	-0.0102
6	1	6	5	1	5	6189.2276	-0.0027
6	0	6	5	0	5	6297.1083	-0.0019
6	2	5	5	2	4	6426.6135	-0.0026
6	2	4	5	2	3	6577.6752	-0.0030

Table S5.43. Measured frequencies and residuals (in MHz) for the rotational transitions of the $^{13}\text{C}_8$ isotopologue of BC1-2w-5a.

J'	K'_{-1}	K'_{+1}	J''	K''_{-1}	K''_{+1}	V _{obs}	V _{obs} -V _{calc}
3	0	3	2	0	2	3193.1163	0.0123
3	1	2	2	1	1	3314.1823	-0.0139
4	0	4	3	0	3	4238.3698	0.0008
4	2	2	3	2	1	4318.3165	0.0011
4	1	3	3	1	2	4413.5728	-0.0026
5	0	5	4	0	4	5269.1660	-0.0070
5	2	4	4	2	3	5340.5325	0.0020
5	1	4	4	1	3	5507.8829	0.0035
6	1	6	5	1	5	6176.2735	-0.0058
6	2	4	5	2	3	6535.2700	-0.0010
6	1	5	5	1	4	6595.2426	0.0046
7	1	7	6	1	6	7193.8471	0.0042

Table S5.44. Measured frequencies and residuals (in MHz) for the rotational transitions of the $^{13}\text{C}_9$ isotopologue of BC1-2w-5a.

J'	K'_{-1}	K'_{+1}	J''	K''_{-1}	K''_{+1}	V _{obs}	V _{obs} -V _{calc}
3	0	3	2	0	2	3204.3338	-0.0101
4	1	4	3	1	3	4141.5027	0.0021
4	0	4	3	0	3	4252.1556	-0.0029
4	2	3	3	2	2	4292.9331	0.0083
5	1	5	4	1	4	5169.4734	-0.0177
5	1	4	4	1	3	5531.8347	0.0014
6	1	6	5	1	5	6193.4296	0.0132
6	2	5	5	2	4	6424.3082	0.0101
6	2	4	5	2	3	6566.5464	-0.0017
6	1	5	5	1	4	6622.9439	-0.0050
7	1	7	6	1	6	7213.2092	-0.0038

Table S5.45. Measured frequencies and residuals (in MHz) for the rotational transitions of the $^{18}\text{O}_{10}$ isotopologue of BC1-2w-5a.

J'	K'_{-1}	K'_{+1}	J''	K''_{-1}	K''_{+1}	ν_{obs}	$\nu_{\text{obs}} - \nu_{\text{calc}}$
3	1	3	2	1	2	3033.0624	-0.0008
3	0	3	2	0	2	3122.8909	-0.0005
3	2	2	2	2	1	3138.5853	-0.0002
3	2	1	2	2	0	3154.2839	-0.0021
3	1	2	2	1	1	3239.1779	0.0004
4	1	4	3	1	3	4039.7866	-0.0019
4	0	4	3	0	3	4146.0711	-0.0009
4	2	3	3	2	2	4181.7013	0.0023
4	3	1	3	3	0	4193.0914	0.0009
4	2	2	3	2	1	4220.3998	-0.0005
4	1	3	3	1	2	4313.9460	-0.0014
5	1	5	4	1	4	5043.2333	-0.0002
5	0	5	4	0	4	5155.6726	0.0018
5	2	4	4	2	3	5222.1797	-0.0009
5	3	2	4	3	1	5246.0256	0.0011
5	2	3	4	2	2	5297.4275	-0.0017
5	1	4	4	1	3	5384.0330	-0.0016
6	1	6	5	1	5	6043.0432	-0.0008
6	1	6	5	1	5	6043.0432	-0.0008
6	0	6	5	0	5	6151.3551	-0.0004
6	3	4	5	3	3	6295.0299	-0.0018
6	3	3	5	3	2	6302.8575	0.0001
6	2	4	5	2	3	6385.0073	0.0014
7	1	7	6	1	6	7039.1119	-0.0012
7	0	7	6	0	6	7135.1665	0.0041
7	2	6	6	2	5	7292.7479	0.0001
7	3	5	6	3	4	7347.7496	0.0014
7	2	5	6	2	4	7480.3497	0.0029
7	1	6	6	1	5	7503.0049	-0.0021

Table S5.46. Measured frequencies and residuals (in MHz) for the rotational transitions of the $^{18}\text{O}_{11}$ isotopologue of BC1-2w-5a.

J'	K'_{-1}	K'_{+1}	J''	K''_{-1}	K''_{+1}	V _{obs}	V _{obs} -V _{calc}
3	1	3	2	1	2	3057.5172	0.0002
3	0	3	2	0	2	3147.5081	0.0000
3	2	2	2	2	1	3163.4253	-0.0040
3	2	1	2	2	0	3179.3507	-0.0061
3	1	2	2	1	1	3264.3391	0.0000
4	1	4	3	1	3	4072.3343	-0.0002
4	0	4	3	0	3	4178.6484	-0.0009
4	2	3	3	2	2	4214.7790	-0.0002
4	3	2	3	3	1	4225.4761	0.0052
4	3	1	3	3	0	4226.3415	-0.0006
4	2	2	3	2	1	4254.0277	-0.0003
4	1	3	3	1	2	4347.4189	-0.0012
5	1	5	4	1	4	5083.8318	0.0005
5	0	5	4	0	4	5196.0549	-0.0009
5	2	4	4	2	3	5263.4500	-0.0092
5	3	3	4	3	2	5284.6318	-0.0014
5	3	2	4	3	1	5287.6690	0.0006
5	2	3	4	2	2	5339.7277	-0.0001
5	1	4	4	1	3	5425.7394	-0.0026
6	1	6	5	1	5	6091.6539	-0.0002
6	0	6	5	0	5	6199.4499	0.0001
6	2	5	5	2	4	6308.8264	-0.0005
6	3	4	5	3	3	6344.9445	0.0035
6	3	3	5	3	2	6352.9654	-0.0012
6	2	4	5	2	3	6436.0237	-0.0001
7	1	7	6	1	6	7095.7008	-0.0011
7	0	7	6	0	6	7190.9654	0.0014
7	2	6	6	2	5	7350.2762	0.0005
7	3	5	6	3	4	7405.9902	0.0009
7	2	5	6	2	4	7540.0249	0.0016
7	1	6	6	1	5	7560.8194	0.0014

3. APPENDIX III

Table S6.1. Measured frequencies and residuals (in MHz) for the rotational transitions of the parent species of conformer 1.

J'	K'_{-1}	K'_{+1}	J''	K''_{-1}	K''_{+1}	V_{obs}	$V_{\text{obs}}-V_{\text{calc}}$
2	1	2	1	1	1	2047.9862	0.0000
2	0	2	1	0	1	2154.4526	-0.0066
2	1	1	1	1	0	2550.6091	0.0129
2	1	1	1	0	1	2967.0800	-0.0005
3	0	3	2	1	2	2982.8671	0.0055
3	1	3	2	1	2	2996.9284	0.0000
3	0	3	2	0	2	3041.5672	-0.0002
3	1	3	2	0	2	3055.6345	0.0003
2	2	0	1	1	0	3190.9575	-0.0057
2	2	1	1	1	1	3297.4298	-0.0069
3	1	2	2	1	1	3687.4884	0.0017
3	2	1	2	2	0	3856.3025	0.0006
4	0	4	3	1	3	3909.3566	-0.0041
4	1	4	3	1	3	3912.1279	-0.0006
4	0	4	3	0	3	3923.4270	-0.0005
4	1	4	3	0	3	3926.1921	-0.0032
4	1	3	3	2	2	4385.8828	0.0149
4	2	3	3	2	2	4476.1959	0.0005
3	2	1	2	1	1	4496.6700	0.0012
4	1	3	3	1	2	4642.8506	-0.0001
4	2	3	3	1	2	4733.1649	-0.0132
4	3	2	3	3	1	4782.4227	0.0065
5	0	5	4	1	4	4814.0629	0.0086
5	1	5	4	1	4	4814.5413	-0.0035
5	0	5	4	0	4	4816.8190	-0.0031
5	1	5	4	0	4	4817.3097	-0.0029
3	3	1	2	2	0	4833.3003	-0.0002
3	3	0	2	2	0	4896.6443	-0.0106
3	3	1	2	2	1	4978.1331	0.0006
3	3	0	2	2	1	5041.4823	-0.0046
4	2	2	3	2	1	5128.4440	-0.0016
5	1	4	4	2	3	5412.5518	0.0047
5	2	4	4	2	3	5436.0977	-0.0020
5	1	4	4	1	3	5502.8757	0.0012
5	2	4	4	1	3	5526.4325	0.0053
5	2	3	4	3	2	5591.5003	-0.0215
6	1	6	5	1	5	5713.6228	-0.0051
6	0	6	5	0	5	5714.0253	-0.0116
4	3	2	3	2	1	5759.4119	-0.0029
5	3	3	4	3	2	5896.3194	-0.0015
4	2	2	3	1	2	5937.6256	-0.0021
5	4	2	4	4	1	6060.3312	0.0056
4	3	1	3	2	1	6097.2585	-0.0008
4	1	3	3	0	3	6101.3953	0.0039
4	2	3	3	1	3	6177.6549	0.0029
5	2	3	4	2	2	6222.4889	-0.0021
4	3	2	3	2	2	6311.6153	0.0012
6	1	5	5	2	4	6350.6128	-0.0035
6	2	5	5	2	4	6355.7823	-0.0023
6	1	5	5	1	4	6374.1669	-0.0020
6	2	5	5	1	4	6379.3422	0.0050
5	3	3	4	2	2	6527.2989	0.0088
7	0	7	6	0	6	6612.0976	-0.0158
7	0	7	6	1	6	6612.0976	0.0657
4	4	1	3	3	0	6618.3448	-0.0002
4	4	0	3	3	0	6641.2434	0.0008

Appendix III

4	4	1	3	3	1	6681.6995	0.0001
4	4	0	3	3	1	6704.6007	0.0037
6	2	4	5	3	3	6819.7880	0.0055
6	3	4	5	3	3	6925.7809	-0.0015
6	2	4	5	2	3	7124.5692	-0.0124
6	3	4	5	2	3	7230.5949	0.0134
6	4	3	5	4	2	7252.3311	0.0056
7	2	6	6	2	5	7259.4120	0.0024
7	1	6	6	1	5	7263.5559	-0.0005
7	2	6	6	1	5	7264.5808	0.0029
6	5	2	5	5	1	7300.2319	0.0050
5	3	2	4	2	2	7425.9071	-0.0070
8	1	8	7	1	7	7510.3538	-0.0078
8	0	8	7	0	7	7510.3538	-0.0187
8	1	8	7	0	7	7510.3538	-0.0207
8	0	8	7	1	7	7510.3538	-0.0058
5	2	3	4	1	3	7517.2633	-0.0047
5	1	4	4	0	4	7680.8438	0.0054
5	2	4	4	1	4	7701.6282	0.0050
5	3	3	4	2	3	7731.7384	-0.0013
5	4	1	4	3	1	7789.6585	-0.0027
7	3	5	6	3	4	7885.0229	-0.0008
5	4	2	4	3	2	7959.6108	0.0020
7	2	5	6	2	4	7962.1564	-0.0028
7	3	5	6	2	4	7991.0215	-0.0022

Table S6.2. Measured frequencies and residuals (in MHz) for the rotational transitions of the $^{13}\text{C}_1$ isotopologue of conformer 1.

J'	K'_{-1}	K'_{+1}	J''	K''_{-1}	K''_{+1}	V _{obs}	V _{obs} -V _{calc}
3	2	1	2	1	1	4470.5727	0.0073
3	3	0	2	2	0	4886.8864	-0.0059
3	3	1	2	2	1	4967.1840	-0.0006
4	2	2	3	1	2	5894.6243	0.0075
4	3	1	3	2	1	6070.4794	0.0074
4	3	2	3	2	2	6286.4521	0.0067
4	4	0	3	3	0	6630.9947	-0.0023
4	4	1	3	3	1	6669.4630	0.0019
5	3	2	4	2	2	7378.4794	-0.0105
5	2	3	4	1	3	7459.4194	-0.0048
5	4	1	4	3	1	7766.6218	-0.0046
5	4	2	4	3	2	7932.7193	0.0025

Table S6.3. Measured frequencies and residuals (in MHz) for the rotational transitions of the $^{13}\text{C}_2$ isotopologue of conformer 1.

J'	K'_{-1}	K'_{+1}	J''	K''_{-1}	K''_{+1}	V _{obs}	V _{obs} -V _{calc}
3	2	1	2	1	1	4467.0738	-0.0014
3	3	0	2	2	0	4869.4408	-0.0056
3	3	1	2	2	1	4950.3413	-0.0006
4	3	1	3	2	1	6059.2971	-0.0050
4	1	3	3	0	3	6060.0375	0.0073
4	2	3	3	1	3	6137.8253	0.0171
4	4	0	3	3	0	6605.2172	0.0012
4	4	1	3	3	1	6645.0397	0.0006
5	3	2	4	2	2	7375.8864	-0.0030
5	2	3	4	1	3	7464.4933	-0.0076
5	3	3	4	2	3	7682.4172	-0.0005
5	4	1	4	3	1	7744.0833	0.0077
5	4	2	4	3	2	7912.4822	-0.0090

Table S6.4. Measured frequencies and residuals (in MHz) for the rotational transitions of the $^{13}\text{C}_3$ isotopologue of conformer 1.

J'	K'_{-1}	K'_{+1}	J''	K''_{-1}	K''_{+1}	V _{obs}	V _{obs} -V _{calc}
2	2	0	1	1	0	3172.4206	-0.0022
3	2	1	2	1	1	4478.8613	-0.0078
3	3	0	2	2	0	4863.9617	0.0057
3	3	1	2	2	1	4945.5705	-0.0059
4	2	2	3	1	2	5920.1820	-0.0071
4	3	1	3	2	1	6067.1539	0.0049
4	1	3	3	0	3	6081.0965	0.0029
4	2	3	3	1	3	6151.4691	0.0083
4	3	2	3	2	2	6278.4075	0.0081
4	4	1	3	3	1	6636.2535	-0.0051
5	3	2	4	2	2	7399.7829	-0.0008
5	3	3	4	2	3	7697.4208	-0.0009
5	4	1	4	3	1	7743.1686	-0.0020
5	4	2	4	3	2	7914.3196	-0.0002

Table S6.5. Measured frequencies and residuals (in MHz) for the rotational transitions of the $^{13}\text{C}_4$ isotopologue of conformer 1.

J'	K'_{-1}	K'_{+1}	J''	K''_{-1}	K''_{+1}	V _{obs}	V _{obs} -V _{calc}
3	2	1	2	1	1	4482.0418	0.0039
3	3	0	2	2	0	4863.6382	0.0072
3	3	1	2	2	1	4945.4462	0.0025
4	2	2	3	1	2	5926.0976	-0.0041
4	3	1	3	2	1	6069.7769	0.0075
4	2	3	3	1	3	6155.3042	-0.0065
4	3	2	3	2	2	6280.5171	0.0038
4	4	0	3	3	0	6593.5687	-0.0012
4	4	1	3	3	1	6635.5846	-0.0016
5	3	2	4	2	2	7405.9726	-0.0018
5	2	4	4	1	4	7675.9080	0.0073
5	4	1	4	3	1	7744.2274	-0.0041
5	4	2	4	3	2	7916.0184	-0.0080

Table S6.6. Measured frequencies and residuals (in MHz) for the rotational transitions of the $^{13}\text{C}_5$ isotopologue of conformer 1.

J'	K'_{-1}	K'_{+1}	J''	K''_{-1}	K''_{+1}	V _{obs}	V _{obs} -V _{calc}
3	2	1	2	1	1	4473.0510	0.0137
3	3	0	2	2	0	4862.2706	-0.0026
3	3	1	2	2	1	4943.7396	-0.0007
4	2	2	3	1	2	5910.5047	-0.0053
4	3	1	3	2	1	6061.2276	-0.0023
4	3	2	3	2	2	6273.1947	0.0111
4	4	0	3	3	0	6593.2107	0.0005
5	3	2	4	2	2	7389.0269	0.0007
5	3	3	4	2	3	7688.8439	-0.0072
5	4	1	4	3	1	7738.3317	-0.0035
5	4	2	4	3	2	7908.8884	0.0006

Table S6.7. Measured frequencies and residuals (in MHz) for the rotational transitions of the $^{13}\text{C}_6$ isotopologue of conformer 1.

J'	K'_{-1}	K'_{+1}	J''	K''_{-1}	K''_{+1}	V _{obs}	V _{obs} -V _{calc}
3	2	1	2	1	1	4473.0510	0.0137
3	3	0	2	2	0	4862.2706	-0.0026
3	3	1	2	2	1	4943.7396	-0.0007
4	2	2	3	1	2	5910.5047	-0.0053
4	3	1	3	2	1	6061.2276	-0.0023
4	3	2	3	2	2	6273.1947	0.0111
4	4	0	3	3	0	6593.2107	0.0005
5	3	2	4	2	2	7389.0269	0.0007
5	3	3	4	2	3	7688.8439	-0.0072
5	4	1	4	3	1	7738.3317	-0.0035
5	4	2	4	3	2	7908.8884	0.0006
3	2	1	2	1	1	4473.0510	0.0137
3	3	0	2	2	0	4862.2706	-0.0026
3	3	1	2	2	1	4943.7396	-0.0007

Table S6.8. Measured frequencies and residuals (in MHz) for the rotational transitions of the $^{13}\text{C}_7$ isotopologue of conformer 1.

J'	K'_{-1}	K'_{+1}	J''	K''_{-1}	K''_{+1}	ν_{obs}	$\nu_{\text{obs}} - \nu_{\text{calc}}$
3	2	1	2	1	1	4479.6446	0.0110
3	3	0	2	2	0	4891.5926	0.0047
3	3	1	2	2	1	4972.3154	0.0010
4	2	2	3	1	2	5909.0484	-0.0031
4	3	1	3	2	1	6080.2986	0.0032
4	2	3	3	1	3	6155.9684	0.0026
4	3	2	3	2	2	6296.0461	0.0006
4	4	1	3	3	1	6675.6513	-0.0034
5	3	2	4	2	2	7394.6437	-0.0047
5	3	3	4	2	3	7706.2133	-0.0009
5	4	1	4	3	1	7776.0255	-0.0043

Table S6.9. Measured frequencies and residuals (in MHz) for the rotational transitions of the $^{13}\text{C}_8$ isotopologue of conformer 1.

J'	K'_{-1}	K'_{+1}	J''	K''_{-1}	K''_{+1}	ν_{obs}	$\nu_{\text{obs}} - \nu_{\text{calc}}$
3	2	1	2	1	1	4470.7763	0.0052
3	3	0	2	2	0	4885.8461	0.0041
3	3	1	2	2	1	4966.2500	0.0000
4	2	2	3	1	2	5895.5499	-0.0027
4	1	3	3	0	3	6060.8839	0.0129
4	3	1	3	2	1	6070.0972	-0.0036
4	3	2	3	2	2	6285.9983	0.0005
4	4	0	3	3	0	6629.3987	0.0004
4	4	1	3	3	1	6668.0277	-0.0028
5	3	2	4	2	2	7379.1316	0.0034
5	2	3	4	1	3	7460.9559	-0.0101
5	4	1	4	3	1	7765.3418	-0.0027

Table S6.10. Measured frequencies and residuals (in MHz) for the rotational transitions of the $^{13}\text{C}_9$ isotopologue of conformer 1.

J'	K'_{-1}	K'_{+1}	J''	K''_{-1}	K''_{+1}	ν_{obs}	$\nu_{\text{obs}} - \nu_{\text{calc}}$
2	2	0	1	1	0	3169.6056	-0.0129
3	2	1	2	1	1	4468.9290	0.0073
3	2	2	2	1	2	4668.2718	-0.0121
3	3	0	2	2	0	4862.6614	-0.0051
3	3	1	2	2	1	4943.9062	0.0020
4	2	2	3	1	2	5902.8770	0.0017
4	3	1	3	2	1	6057.8209	-0.0030
4	3	2	3	2	2	6270.4340	0.0027
4	4	0	3	3	0	6594.5753	0.0071
4	4	1	3	3	1	6635.2487	0.0025
5	3	3	4	2	3	7683.1577	0.0035
5	4	1	4	3	1	7736.9114	0.0026
5	4	2	4	3	2	7906.6513	-0.0051

Table S6.11. Measured frequencies and residuals (in MHz) for the rotational transitions of the $^{13}\text{C}_{10}$ isotopologue of conformer 1.

J'	K'_{-1}	K'_{+1}	J''	K''_{-1}	K''_{+1}	V _{obs}	V _{obs} -V _{calc}
2	2	0	1	1	0	3173.2110	-0.0051
3	2	1	2	1	1	4481.6301	0.0051
3	3	0	2	2	0	4864.3305	-0.0011
3	3	1	2	2	1	4946.1007	0.0016
4	2	2	3	1	2	5925.0395	0.0053
4	3	1	3	2	1	6069.7076	-0.0090
4	2	3	3	1	3	6154.9048	0.0027
4	3	2	3	2	2	6280.6435	-0.0038
5	3	2	4	2	2	7404.9953	-0.0052
5	4	1	4	3	1	7744.8660	0.0077

Table S6.12. Measured frequencies and residuals (in MHz) for the rotational transitions of the $^{13}\text{C}_{11}$ isotopologue of conformer 1.

J'	K'_{-1}	K'_{+1}	J''	K''_{-1}	K''_{+1}	V _{obs}	V _{obs} -V _{calc}
3	3	0	2	2	0	4862.8183	0.0059
3	3	1	2	2	1	4944.4437	-0.0020
4	2	2	3	1	2	5922.2546	0.0024
4	3	1	3	2	1	6067.4833	-0.0084
4	1	3	3	0	3	6082.7368	0.0009
4	2	3	3	1	3	6152.3226	0.0101
4	3	2	3	2	2	6278.2861	-0.0096
4	4	0	3	3	0	6592.7185	0.0049
4	4	1	3	3	1	6634.4679	-0.0048
5	3	2	4	2	2	7401.7854	-0.0014
5	3	3	4	2	3	7698.2759	-0.0016
5	4	1	4	3	1	7742.3892	0.0052
5	4	2	4	3	2	7913.6761	-0.0010

Table S6.13. Measured frequencies and residuals (in MHz) for the rotational transitions of the $^{13}\text{C}_{12}$ isotopologue of conformer 1.

J'	K'_{-1}	K'_{+1}	J''	K''_{-1}	K''_{+1}	V _{obs}	V _{obs} -V _{calc}
2	2	0	1	1	0	3173.6023	-0.0053
3	2	1	2	1	1	4472.3197	0.0011
3	3	0	2	2	0	4869.9388	-0.0043
3	3	1	2	2	1	4951.0496	-0.0040
4	2	2	3	1	2	5905.6526	0.0020
4	3	1	3	2	1	6064.1002	0.0030
4	1	3	3	0	3	6068.5634	-0.0048
4	3	2	3	2	2	6277.3674	0.0040
4	4	0	3	3	0	6605.0041	-0.0035
4	4	1	3	3	1	6645.3194	0.0002
5	3	2	4	2	2	7385.7537	-0.0137
5	2	3	4	1	3	7476.9315	0.0014
5	3	3	4	2	3	7689.9191	0.0136
5	4	1	4	3	1	7747.1270	0.0028
5	4	2	4	3	2	7916.3410	0.0016

Table S6.14. Measured frequencies and residuals (in MHz) for the rotational transitions of the parent species of conformer 7.

J'	K'_{-1}	K'_{+1}	J''	K''_{-1}	K''_{+1}	V _{obs}	V _{obs} -V _{calc}
3	0	3	2	1	2	2871.2892	0.0151
2	1	1	1	0	1	2881.7420	-0.0021
3	1	3	2	1	2	2968.0578	-0.0044
3	0	3	2	0	2	3073.0396	0.0050
2	2	0	1	1	0	3411.0624	-0.0013
3	1	2	2	1	1	3509.4802	-0.0062
2	2	1	1	1	1	3536.8548	-0.0073
4	0	4	3	1	3	3872.5035	-0.0052
4	1	4	3	1	3	3911.1105	0.0018
4	0	4	3	0	3	3969.2944	-0.0025
3	1	2	2	0	2	4265.1235	0.0005
4	2	3	3	2	2	4322.9323	-0.0109
3	2	1	2	1	1	4523.2695	0.0005
4	1	3	3	1	2	4580.5476	-0.0037
3	2	2	2	1	2	4813.9433	-0.0096
5	0	5	4	1	4	4822.4448	-0.0013
5	1	5	4	1	4	4836.2002	0.0070
5	1	5	4	0	4	4874.7855	-0.0077
5	2	4	4	2	3	5332.7728	0.0099
3	3	1	2	2	0	5350.3424	0.0115
3	3	0	2	2	0	5362.7865	0.0037
3	3	1	2	2	1	5409.1642	0.0064
5	1	4	4	1	3	5555.6809	0.0020
4	2	2	3	1	2	5735.1231	-0.0020
6	0	6	5	1	5	5746.6377	-0.0021
6	1	6	5	1	5	5751.2032	-0.0034
6	0	6	5	0	5	5760.3900	0.0031
4	1	3	3	0	3	5772.6360	-0.0037
5	2	3	4	2	2	5917.5364	0.0045
4	2	3	3	1	3	6168.8366	0.0027
6	1	5	5	2	4	6182.2575	0.0155
6	2	5	5	2	4	6306.9305	0.0049
4	3	1	3	2	1	6409.4431	-0.0004
6	1	5	5	1	4	6452.3062	-0.0022
6	2	5	5	1	4	6576.9814	-0.0106
4	3	2	3	2	2	6591.1270	0.0021
7	0	7	6	1	6	6660.1861	0.0075
7	1	7	6	1	6	6661.6125	-0.0144
7	0	7	6	0	6	6664.7527	0.0074
5	2	3	4	1	3	7072.0972	-0.0084
4	4	1	3	3	0	7311.0447	0.0114
4	4	0	3	3	0	7313.2001	-0.0003
4	4	1	3	3	1	7323.4857	0.0005
4	4	0	3	3	1	7325.6459	-0.0064
7	1	6	6	1	5	7325.8971	-0.0024
5	1	4	4	0	4	7359.0263	0.0046
5	3	2	4	2	2	7460.6345	-0.0046
5	2	4	4	1	4	7590.4880	-0.0001
5	3	3	4	2	3	7837.4134	-0.0053

Table S6.15. Measured frequencies and residuals (in MHz) for the rotational transitions of conformer 9.

J'	K' ₋₁	K' ₊₁	J''	K'' ₋₁	K'' ₊₁	V _{obs}	V _{obs} -V _{calc}
4	1	3	3	0	3	5996.7302	-0.0032
5	1	4	4	0	4	7588.5744	0.0109
3	2	1	2	1	1	4474.7078	0.0037
4	2	2	3	1	2	5834.9445	-0.0058
5	2	3	4	1	3	7342.0322	-0.0010
4	2	3	3	1	3	6153.2563	-0.0069
3	3	0	2	2	0	5021.9413	0.0120
4	3	1	3	2	1	6146.8083	0.0003
5	3	2	4	2	2	7364.0171	0.0017
3	3	1	2	2	1	5093.0474	0.0014
4	3	2	3	2	2	6368.4064	0.0011
5	3	3	4	2	3	7726.2372	-0.0020
4	4	0	3	3	0	6829.9276	-0.0004
4	4	1	3	3	1	6856.3795	-0.0079
5	4	1	4	3	1	7939.6690	-0.0017

Table S6.16. Measured frequencies and residuals (in MHz) for the rotational transitions of conformer 11.

J'	K'_{-1}	K'_{+1}	J''	K''_{-1}	K''_{+1}	V_{obs}	$V_{\text{obs}}-V_{\text{calc}}$
2	1	1	1	0	1	2890.2417	-0.0115
3	1	3	2	1	2	2934.5141	-0.0033
3	0	3	2	0	2	3046.6988	-0.0013
2	2	0	1	1	0	3467.0124	0.0029
3	1	2	2	1	1	3482.8249	-0.0042
2	2	1	1	1	1	3596.9191	0.0007
4	1	4	3	1	3	3867.2873	0.0040
4	0	4	3	0	3	3932.3399	0.0104
3	1	2	2	0	2	4265.9482	0.0165
4	2	3	3	2	2	4282.5243	0.0077
4	3	2	3	3	1	4414.7782	-0.0152
4	1	3	3	1	2	4549.9694	0.0030
3	2	1	2	1	1	4561.3469	-0.0018
5	1	5	4	1	4	4781.6424	0.0073
5	0	5	4	0	4	4810.7006	-0.0038
3	2	2	2	1	2	4865.3736	-0.0028
5	2	4	4	2	3	5284.6017	-0.0166
3	3	0	2	2	0	5464.8201	0.0002
3	3	1	2	2	1	5510.1069	0.0006
5	3	3	4	3	2	5515.6536	-0.0026
5	1	4	4	1	3	5523.8147	0.0054
6	1	6	5	1	5	5685.2294	-0.0023
6	0	6	5	0	5	5696.4427	0.0043
4	2	2	3	1	2	5754.4262	-0.0012
4	1	3	3	0	3	5769.1964	-0.0016
5	2	3	4	2	2	5869.0471	0.0053
4	2	3	3	1	3	6213.3795	0.0038
6	2	5	5	2	4	6251.3523	-0.0038
6	1	5	5	1	4	6415.0664	-0.0010
4	3	1	3	2	1	6498.4613	-0.0001
7	1	7	6	1	6	6583.6962	-0.0006
7	0	7	6	0	6	6587.6612	-0.0021
4	3	2	3	2	2	6679.1979	-0.0017
6	4	2	5	4	1	6725.7164	-0.0159
6	2	4	5	2	3	6986.9207	0.0070
5	2	3	4	1	3	7073.5034	0.0007
7	2	6	6	2	5	7188.2262	-0.0022
7	1	6	6	1	5	7275.9865	0.0119
5	1	4	4	0	4	7360.6878	0.0100
4	4	0	3	3	0	7458.1250	-0.0034
4	4	1	3	3	1	7467.6121	-0.0053
8	1	8	7	1	7	7480.0657	-0.0017
5	3	2	4	2	2	7528.5444	0.0050
5	3	3	4	2	3	7912.3359	-0.0032

Table S6.17. Measured frequencies and residuals (in MHz) for the rotational transitions of conformer 13.

J'	K' ₋₁	K' ₊₁	J''	K'' ₋₁	K'' ₊₁	V _{obs}	V _{obs} -V _{calc}
2	1	1	1	0	1	3088.1067	0.0034
2	2	0	1	1	0	3252.4771	-0.0059
2	2	1	1	1	1	3345.6626	-0.0059
3	2	1	2	1	1	4658.4603	0.0025
3	1	2	2	0	2	4697.8200	0.0056
3	2	2	2	1	2	4825.3180	-0.0073
3	3	0	2	2	0	4952.8270	0.0007
3	3	1	2	2	1	5038.3542	-0.0023
4	2	2	3	1	2	6203.2278	-0.0039
4	3	1	3	2	1	6268.6642	-0.0027
4	1	3	3	0	3	6341.2806	-0.0024
4	2	3	3	1	3	6377.7866	0.0057
4	3	2	3	2	2	6461.9631	-0.0050
4	4	0	3	3	0	6693.4340	0.0045
4	4	1	3	3	1	6747.2680	-0.0013
5	3	2	4	2	2	7727.3472	-0.0133
5	2	3	4	1	3	7859.1029	-0.0117
5	4	1	4	3	1	7937.9156	-0.0041
5	1	4	4	0	4	7956.2172	0.0134
5	2	4	4	1	4	7963.6123	0.0007
5	3	3	4	2	3	7971.6436	-0.0095

Table S6.18. Measured frequencies and residuals (in MHz) for the rotational transitions of conformer 4.

J'	K' ₋₁	K' ₊₁	J''	K'' ₋₁	K'' ₊₁	V _{obs}	V _{obs} -V _{calc}
2	1	1	1	0	1	2948.8703	-0.0065
2	2	1	1	1	1	3423.5417	-0.0056
3	1	2	2	0	2	4436.8711	-0.0018
3	2	1	2	1	1	4519.2404	0.0035
3	2	2	2	1	2	4779.3145	-0.0035
3	3	0	2	2	0	5121.7544	-0.0088
3	3	1	2	2	1	5194.1657	-0.0092
4	2	2	3	1	2	5873.2444	0.0026
4	1	3	3	0	3	6038.0664	0.0072
4	2	3	3	1	3	6220.8158	-0.0004
4	3	1	3	2	1	6232.1137	-0.0046
4	3	2	3	2	2	6463.7185	-0.0075
4	4	0	3	3	0	6973.0222	-0.0246
4	4	1	3	3	1	6998.6729	-0.0295
5	2	3	4	1	3	7380.7334	-0.0019
5	3	2	4	2	2	7431.1968	-0.0042
5	1	4	4	0	4	7651.9888	-0.0024
5	2	4	4	1	4	7723.3725	0.0063
5	3	3	4	2	3	7818.6259	-0.0073

Table S6.19. Measured frequencies and residuals (in MHz) for the rotational transitions of conformer 14.

J'	K'_{-1}	K'_{+1}	J''	K''_{-1}	K''_{+1}	V _{obs}	V _{obs} -V _{calc}
2	1	1	1	0	1	2996.6621	-0.0045
2	2	0	1	1	0	3382.2550	-0.0010
2	2	1	1	1	1	3512.7079	0.0074
3	1	2	2	0	2	4497.5074	-0.0034
3	2	1	2	1	1	4607.7336	0.0050
3	2	2	2	1	2	4882.0376	0.0123
3	3	0	2	2	0	5266.5454	0.0056
3	3	1	2	2	1	5336.2165	0.0042
4	2	2	3	1	2	5964.0293	-0.0003
4	1	3	3	0	3	6119.9328	0.0039
4	2	3	3	1	3	6338.4500	0.0011
4	3	1	3	2	1	6382.7769	0.0056
4	3	2	3	2	2	6614.8154	0.0000
4	4	0	3	3	0	7173.5053	-0.0071
4	4	1	3	3	1	7196.3145	-0.0046
5	2	3	4	1	3	7474.1683	0.0025
5	3	2	4	2	2	7574.8089	-0.0043
5	1	4	4	0	4	7767.3184	-0.0024
5	3	3	4	2	3	7977.7700	-0.0099

4. APPENDIX IV

Table S7.1. Measured frequencies and residuals (in MHz) for the rotational transitions of the conformer **3f** of muscone.

J'	K'_{-1}	K'_{+1}	J''	K''_{-1}	K''_{+1}	V _{obs}	V _{obs} -V _{calc}
3	2	1	2	1	1	2436.5726	-0.0022
3	1	2	2	0	2	2455.6594	-0.0056
3	3	0	2	2	0	2464.0769	-0.0003
3	3	1	2	2	1	2484.4952	0.0012
4	3	1	3	2	1	3250.1019	-0.0028
4	2	2	3	1	2	3270.3265	-0.0001
4	1	3	3	0	3	3277.5763	0.0044
4	2	3	3	1	3	3277.8378	0.0025
4	3	2	3	2	2	3280.6523	0.0010
4	4	0	3	3	0	3290.1479	0.0008
4	4	1	3	3	1	3313.7935	0.0019
5	4	1	4	3	1	4064.9181	0.0015
5	3	2	4	2	2	4082.2303	0.0041
5	2	3	4	1	3	4095.6618	0.0002
5	3	3	4	2	3	4096.5785	0.0006
5	1	4	4	0	4	4097.4249	0.0071
5	2	4	4	1	4	4097.4249	-0.0050
5	4	2	4	3	2	4102.1309	0.0003
5	5	0	4	4	0	4119.6841	0.0000
5	5	1	4	4	1	4143.9378	0.0008
6	5	1	5	4	1	4881.4946	-0.0010
6	4	2	5	3	2	4891.6782	0.0001
6	3	3	5	2	3	4912.6391	-0.0004
6	4	3	5	3	3	4915.0523	-0.0034
6	2	4	5	1	4	4916.1163	0.0253
6	3	4	5	2	4	4916.1163	-0.0291
6	5	2	5	4	2	4924.4769	0.0003
6	6	0	5	5	0	4952.5630	0.0012
6	6	1	5	5	1	4974.9935	-0.0079
7	6	1	6	5	1	5700.4156	0.0000
7	4	3	6	3	3	5728.0650	0.0009
7	3	4	6	2	4	5734.2882	0.0013
7	4	4	6	3	4	5734.4656	-0.0014
7	2	5	6	1	5	5735.9117	0.0009
7	3	5	6	2	5	5735.9117	-0.0017
7	6	2	6	5	2	5747.8440	0.0004
7	7	0	6	6	0	5788.0157	0.0007
7	7	1	6	6	1	5806.9880	0.0027
8	6	2	7	5	2	6507.4576	-0.0001
8	7	1	7	6	1	6522.3027	0.0007
8	5	3	7	4	3	6541.4448	0.0005
8	5	4	7	4	4	6552.3650	-0.0009
8	3	5	7	2	5	6554.4213	0.0036
8	4	5	7	3	5	6554.4213	-0.0068
8	2	6	7	1	6	6555.6258	0.0013
8	3	6	7	2	6	6555.6258	0.0012
8	1	7	7	0	7	6556.3410	0.0013
8	2	7	7	1	7	6556.3410	0.0013
8	7	2	7	6	2	6572.3620	-0.0033
8	8	0	7	7	0	6624.9663	-0.0027
8	8	1	7	7	1	6639.8262	-0.0014
9	8	1	8	7	1	7347.7251	-0.0012
9	6	3	8	5	3	7352.3463	-0.0010
9	5	4	8	4	4	7368.6770	-0.0022
9	6	4	8	5	4	7369.8449	0.0014
9	7	3	8	6	3	7370.4959	0.0041

Appendix IV

9	4	5	8	3	5	7372.5706	0.0195
9	5	5	8	4	5	7372.5706	-0.0139
9	3	6	8	2	6	7374.2800	0.0000
9	4	6	8	3	6	7374.2800	-0.0005
9	2	7	8	1	7	7375.2977	0.0021
9	3	7	8	2	7	7375.2977	0.0021
9	1	8	8	0	8	7375.9513	-0.0021
9	2	8	8	1	8	7375.9513	-0.0021
9	9	0	8	8	0	7462.4742	-0.0022
9	9	1	8	8	1	7473.4218	-0.0001

Table S7.2. Measured frequencies and residuals (in MHz) for the rotational transitions of the conformer **33I** of muscone.

J'	K'_{-1}	K'_{+1}	J''	K''_{-1}	K''_{+1}	V _{obs}	V _{obs} - V _{calc}
3	2	1	2	1	1	2500.5957	0.0012
3	1	2	2	0	2	2530.8177	0.0054
3	3	0	2	2	0	2568.6025	-0.0021
3	3	1	2	2	1	2604.9713	0.0006
4	3	1	3	2	1	3340.8725	0.0002
4	2	2	3	1	2	3359.5205	-0.0025
4	1	3	3	0	3	3388.4800	0.0047
4	2	3	3	1	3	3391.0105	-0.0108
4	3	2	3	2	2	3403.4180	0.0014
4	4	0	3	3	0	3443.5293	-0.0027
4	4	1	3	3	1	3478.0672	0.0009
5	3	2	4	2	2	4182.8516	0.0017
5	4	1	4	3	1	4188.1653	-0.0006
5	2	3	4	1	3	4228.1166	-0.0008
5	3	3	4	2	3	4236.7754	-0.0033
5	1	4	4	0	4	4238.4558	0.0045
5	2	4	4	1	4	4238.6969	-0.0035
5	4	2	4	3	2	4260.3152	0.0006
5	5	0	4	4	0	4327.2164	-0.0005
5	5	1	4	4	1	4354.1744	-0.0004
6	4	2	5	3	2	5006.5541	-0.0007
6	5	1	5	4	1	5045.3048	-0.0024
6	3	3	5	2	3	5060.9803	-0.0093
6	2	4	5	1	4	5082.0721	-0.0008
6	4	3	5	3	3	5082.8780	0.0079
6	3	4	5	2	4	5083.1759	-0.0008
6	1	5	5	0	5	5087.1138	0.0072
6	2	5	5	1	5	5087.1138	-0.0134
6	5	2	5	4	2	5121.0322	0.0025
6	6	0	5	5	0	5214.9751	0.0008
6	6	1	5	5	1	5233.0105	0.0015
7	5	2	6	4	2	5835.6329	-0.0018
7	4	3	6	3	3	5885.5982	-0.0019
7	6	1	6	5	1	5914.4509	0.0074
7	3	4	6	2	4	5922.7806	-0.0018
7	4	4	6	3	4	5926.3687	0.0005
7	5	3	6	4	3	5930.4500	-0.0008
7	2	5	6	1	5	5931.7636	-0.0069
7	3	5	6	2	5	5931.8876	0.0051
7	6	2	6	5	2	5985.9720	0.0013
7	7	0	6	6	0	6103.2073	0.0009
7	7	1	6	6	1	6114.0174	0.0053
8	6	2	7	5	2	6673.3271	-0.0021
8	5	3	7	4	3	6703.0720	0.0176
8	4	4	7	3	4	6759.2008	-0.0056
8	5	4	7	4	4	6768.6673	-0.0014
8	3	5	7	2	5	6774.8203	-0.0045
8	4	5	7	3	5	6775.2610	-0.0045
8	2	6	7	1	6	6780.6722	0.0373
8	3	6	7	2	6	6780.6722	0.0274
8	1	7	7	0	7	6783.9135	-0.0029
8	2	7	7	1	7	6783.9135	-0.0030
8	7	1	7	6	1	6795.1993	0.0011
8	7	2	7	6	2	6855.2426	0.0042
8	8	0	7	7	0	6990.5448	-0.0023
8	8	1	7	7	1	6996.5350	-0.0225
9	6	3	8	5	3	7517.9219	-0.0001
9	7	2	8	6	2	7522.0434	-0.0123
9	5	4	8	4	4	7589.5144	-0.0067
9	6	4	8	5	4	7610.8185	-0.0047

Appendix IV

9	4	5	8	3	5	7615.8194	0.0152
9	5	5	8	4	5	7617.2015	-0.0007
9	2	7	8	1	7	7629.2502	-0.0131
9	3	7	8	2	7	7629.2502	-0.0139
9	8	1	8	7	1	7683.8855	0.0064
9	8	2	8	7	2	7728.5832	-0.0010
9	9	0	8	8	0	7876.9194	0.0011
9	9	1	8	8	1	7880.1058	0.0084

Table S7.3. Measured frequencies and residuals (in MHz) for the rotational transitions of the conformer **13f** of muscone.

J'	K'_{-1}	K'_{+1}	J''	K''_{-1}	K''_{+1}	V _{obs}	V _{obs} - V _{calc}
3	2	1	2	1	1	2419.3687	0.0002
3	1	2	2	0	2	2449.2846	-0.0038
3	3	0	2	2	0	2488.2450	0.0001
3	3	1	2	2	1	2524.5143	-0.0010
6	0	6	5	1	5	2918.7704	0.0109
6	1	6	5	1	5	2918.7704	0.0107
6	0	6	5	0	5	2918.7704	0.0086
6	1	6	5	0	5	2918.7704	0.0084
4	3	1	3	2	1	3232.8158	-0.0018
4	2	2	3	1	2	3250.5127	-0.0011
4	1	3	3	0	3	3280.1532	-0.0009
4	2	3	3	1	3	3282.8531	0.0063
4	3	2	3	2	2	3295.6169	-0.0019
4	4	0	3	3	0	3336.8288	0.0055
4	4	1	3	3	1	3370.9258	-0.0007
7	1	7	6	1	6	3374.7884	0.0074
7	0	7	6	1	6	3374.7884	0.0074
7	0	7	6	0	6	3374.7884	0.0072
7	1	7	6	0	6	3374.7884	0.0072
8	1	8	7	1	7	3830.8052	-0.0019
8	0	8	7	1	7	3830.8052	-0.0019
8	0	8	7	0	7	3830.8052	-0.0019
8	1	8	7	0	7	3830.8052	-0.0019
5	3	2	4	2	2	4046.5014	-0.0019
5	4	1	4	3	1	4053.5566	-0.0014
5	2	3	4	1	3	4092.4056	-0.0009
5	3	3	4	2	3	4101.5495	-0.0041
5	1	4	4	0	4	4103.1846	0.0083
5	2	4	4	1	4	4103.4434	-0.0031
5	4	2	4	3	2	4125.7591	-0.0027
5	5	0	4	4	0	4194.1297	0.0019
5	5	1	4	4	1	4220.4150	0.0055
9	1	9	8	1	8	4286.8284	-0.0091
9	0	9	8	1	8	4286.8284	-0.0091
9	0	9	8	0	8	4286.8284	-0.0091
9	1	9	8	0	8	4286.8284	-0.0091
6	4	2	5	3	2	4843.2335	0.0011
6	5	1	5	4	1	4884.5094	-0.0020
6	3	3	5	2	3	4897.6223	-0.0038
6	2	4	5	1	4	4919.5868	0.0000
6	4	3	5	3	3	4920.6613	-0.0053
6	3	4	5	2	4	4920.7861	0.0031
6	5	2	5	4	2	4959.8349	0.0007
6	6	0	5	5	0	5055.3084	0.0003
6	6	1	5	5	1	5072.6461	-0.0015
7	5	2	6	4	2	5645.7225	-0.0100
7	4	3	6	3	3	5694.3894	-0.0025
7	6	1	6	5	1	5727.7722	-0.0066
7	3	4	6	2	4	5732.9450	0.0007
7	4	4	6	3	4	5736.8341	0.0090
7	5	3	6	4	3	5741.3886	-0.0006
7	2	5	6	1	5	5742.3122	-0.0078
7	3	5	6	2	5	5742.4502	0.0057
7	1	6	6	0	6	5746.2214	0.0021
7	2	6	6	1	6	5746.2214	0.0004
7	6	2	6	5	2	5798.2379	-0.0024
7	7	0	6	6	0	5916.8046	-0.0014
7	7	1	6	6	1	5927.0544	0.0002
8	6	2	7	5	2	6457.2421	-0.0021
8	5	3	7	4	3	6484.1276	-0.0006

Appendix IV

8	4	4	7	3	4	6541.7910	0.0014
8	5	4	7	4	4	6552.0151	0.0076
8	3	5	7	2	5	6558.1562	0.0039
8	4	5	7	3	5	6558.6411	-0.0007
8	2	6	7	1	6	6564.1764	0.0060
8	3	6	7	2	6	6564.1764	-0.0052
8	6	3	7	5	3	6564.9441	-0.0015
8	1	7	7	0	7	6567.5559	0.0001
8	2	7	7	1	7	6567.5559	0.0000
8	7	1	7	6	1	6582.6903	-0.0070
8	7	2	7	6	2	6641.0515	-0.0053
8	8	0	7	7	0	6777.3629	0.0054
8	8	1	7	7	1	6782.9858	0.0018
9	6	3	8	5	3	7271.8177	0.0064
9	7	2	8	6	2	7280.2273	-0.0023
9	5	4	8	4	4	7344.2109	-0.0032
9	6	4	8	5	4	7367.1372	0.0055
9	5	5	8	4	5	7373.3614	-0.0009
9	2	7	8	1	7	7385.7741	0.0024
9	3	7	8	2	7	7385.7741	0.0015
9	1	8	8	0	8	7388.8608	0.0041
9	2	8	8	1	8	7388.8608	0.0041
9	7	3	8	6	3	7392.3781	-0.0033
9	8	1	8	7	1	7445.2137	-0.0022
9	8	2	8	7	2	7487.9981	0.0029
9	9	0	8	8	0	7636.9477	0.0035
9	9	1	8	8	1	7639.8789	-0.0045

Table S7.4. Measured frequencies and residuals (in MHz) for the rotational transitions of the conformer **37a** of muscone.

J'	K'_{-1}	K'_{+1}	J''	K''_{-1}	K''_{+1}	V _{obs}	V _{obs} - V _{calc}
3	2	1	2	1	1	2369.7226	-0.0006
3	2	3	2	1	2	2394.7891	0.0308
3	1	2	2	0	2	2400.6029	-0.0056
3	3	0	2	2	0	2445.6965	-0.0075
3	3	1	2	2	1	2483.9897	0.0056
6	1	6	5	1	5	2795.4057	0.0074
6	0	6	5	0	5	2795.4057	0.0043
6	1	6	5	0	5	2795.4057	0.0041
6	0	6	5	1	5	2795.4057	0.0076
4	3	1	3	2	1	3167.8571	-0.0010
4	2	2	3	1	2	3183.7123	-0.0018
4	1	3	3	0	3	3217.3244	-0.0099
4	2	3	3	1	3	3220.6895	0.0078
7	1	7	6	1	6	3230.3978	0.0053
7	0	7	6	0	6	3230.3978	0.0051
7	1	7	6	0	6	3230.3978	0.0051
7	0	7	6	1	6	3230.3978	0.0053
4	3	2	3	2	2	3235.4510	0.0025
4	4	0	3	3	0	3282.6521	0.0031
4	4	1	3	3	1	3317.6154	0.0012
7	1	6	6	1	5	3601.3218	-0.0351
7	2	6	6	2	5	3601.3218	-0.0021
7	1	6	6	2	5	3601.3218	0.0008
7	2	6	6	1	5	3601.3218	-0.0380
8	1	8	7	1	7	3665.3972	0.0076
8	0	8	7	0	7	3665.3972	0.0076
8	1	8	7	0	7	3665.3972	0.0076
8	0	8	7	1	7	3665.3972	0.0076
5	3	2	4	2	2	3961.7699	-0.0075
5	4	1	4	3	1	3974.6229	-0.0071
5	2	3	4	1	3	4012.3924	0.0011
5	3	3	4	2	3	4023.7086	-0.0013
5	1	4	4	0	4	4025.2405	-0.0144
5	2	4	4	1	4	4025.5990	-0.0158
8	1	7	7	1	6	4036.2637	-0.0010
8	2	7	7	2	6	4036.2637	0.0016
8	1	7	7	2	6	4036.2637	0.0019
8	2	7	7	1	6	4036.2637	-0.0013
5	4	2	4	3	2	4051.5549	-0.0026
9	1	9	8	1	8	4100.3941	0.0050
9	0	9	8	0	8	4100.3941	0.0050
9	1	9	8	0	8	4100.3941	0.0050
9	0	9	8	1	8	4100.3941	0.0050
5	5	0	4	4	0	4128.7158	-0.0030
5	5	1	4	4	1	4154.6916	0.0045
9	1	8	8	1	7	4471.2245	0.0051
9	2	8	8	2	7	4471.2245	0.0053
9	1	8	8	2	7	4471.2245	0.0053
9	2	8	8	1	7	4471.2245	0.0051
10	1	10	9	1	9	4535.3947	0.0042
10	0	10	9	0	9	4535.3947	0.0042
10	1	10	9	0	9	4535.3947	0.0042
10	0	10	9	1	9	4535.3947	0.0042
6	4	2	5	3	2	4741.7675	0.0008
6	5	1	5	4	1	4793.3970	-0.0071
6	3	3	5	2	3	4799.1540	0.0018
6	2	4	5	1	4	4825.3083	0.0025
6	3	4	5	2	4	4826.8975	0.0017
6	4	3	5	3	3	4827.4137	0.0054
6	1	5	5	0	5	4831.5246	0.0269

6	2	5	5	1	5	4831.5246	-0.0058
6	5	2	5	4	2	4872.1955	0.0012
11	1	11	10	1	10	4970.3866	-0.0068
11	0	11	10	0	10	4970.3866	-0.0068
11	1	11	10	0	10	4970.3866	-0.0068
11	0	11	10	1	10	4970.3866	-0.0068
6	6	0	5	5	0	4978.2978	-0.0035
6	6	1	5	5	1	4994.7677	-0.0019
11	1	10	10	1	9	5341.1784	0.0044
11	2	10	10	2	9	5341.1784	0.0044
11	1	10	10	2	9	5341.1784	0.0044
11	2	10	10	1	9	5341.1784	0.0044
12	1	12	11	1	11	5405.3892	-0.0086
12	0	12	11	0	11	5405.3892	-0.0086
12	1	12	11	0	11	5405.3892	-0.0086
12	0	12	11	1	11	5405.3892	-0.0086
7	5	2	6	4	2	5529.1017	-0.0045
7	4	3	6	3	3	5576.4148	-0.0040
7	3	4	6	2	4	5621.6442	-0.0001
7	6	1	6	5	1	5626.1824	0.0008
7	4	4	6	3	4	5626.7811	0.0001
7	2	5	6	1	5	5632.8868	-0.0062
7	5	3	6	4	3	5633.2070	0.0021
7	6	2	6	5	2	5697.7582	-0.0085
12	1	11	11	1	10	5776.1612	-0.0009
12	2	11	11	2	10	5776.1612	-0.0009
12	1	11	11	2	10	5776.1612	-0.0009
12	2	11	11	1	10	5776.1612	-0.0009
7	7	0	6	6	0	5827.7919	0.0101
7	7	1	6	6	1	5837.1417	-0.0056
8	6	2	7	5	2	6327.2668	-0.0006
8	4	4	7	3	4	6412.4415	0.0004
8	3	5	7	2	5	6432.3051	0.0098
8	4	5	7	3	5	6432.9982	0.0072
8	2	6	7	1	6	6439.3857	0.0060
8	3	6	7	2	6	6439.3857	-0.0112
8	6	3	7	5	3	6442.5036	0.0056
8	1	7	7	0	7	6443.3318	0.0065
8	2	7	7	1	7	6443.3318	0.0063
8	7	1	7	6	1	6471.2687	-0.0011
8	7	2	7	6	2	6528.2706	-0.0005
8	8	0	7	7	0	6676.1178	-0.0054
8	8	1	7	7	1	6681.0717	-0.0084
9	6	3	8	5	3	7116.7815	-0.0089
9	5	4	8	4	4	7195.4248	-0.0022
9	6	4	8	5	4	7225.2063	0.0081
9	4	5	8	3	5	7229.0779	0.0198
9	5	5	8	4	5	7231.2549	0.0010
9	4	6	8	3	6	7239.9369	-0.0267
9	2	7	8	1	7	7245.5652	0.0028
9	3	7	8	2	7	7245.5652	0.0013
9	1	8	8	0	8	7249.1754	0.0203
9	2	8	8	1	8	7249.1754	0.0203
9	7	3	8	6	3	7256.4156	-0.0107
9	8	1	8	7	1	7323.3193	-0.0001
9	9	0	8	8	0	7523.4748	0.0101

Table S7.5. Measured frequencies and residuals (in MHz) for the rotational transitions of the conformer **8g** of muscone.

J'	K'_{-1}	K'_{+1}	J''	K''_{-1}	K''_{+1}	V _{obs}	V _{obs} - V _{calc}
5	0	5	4	1	4	2434.8332	0.0076
3	2	1	2	1	1	2450.3158	-0.0085
5	1	5	4	0	4	2463.5684	0.0017
5	1	4	4	2	3	2598.1646	0.0044
4	2	3	3	1	2	2676.4914	0.0038
6	0	6	5	1	5	2895.9070	0.0018
6	1	6	5	0	5	2905.6974	0.0022
3	3	1	2	2	0	2941.0735	0.0012
3	3	0	2	2	0	2949.3283	-0.0011
6	2	4	5	3	3	2957.7875	-0.0097
3	3	1	2	2	1	2978.7236	0.0017
3	3	0	2	2	1	2986.9815	0.0025
5	2	4	4	1	3	3033.4842	0.0004
4	2	2	3	1	2	3094.5935	-0.0022
6	1	5	5	2	4	3173.0783	0.0007
7	0	7	6	1	6	3350.9829	0.0010
7	1	7	6	0	6	3354.1140	0.0008
6	2	5	5	1	4	3392.3773	0.0041
4	3	2	3	2	1	3434.6090	0.0020
4	3	1	3	2	1	3488.3868	-0.0005
4	3	2	3	2	2	3602.0469	-0.0014
4	3	1	3	2	2	3655.8275	-0.0010
7	1	6	6	2	5	3687.6111	-0.0116
7	2	5	6	3	4	3699.6405	-0.0018
7	2	6	6	1	5	3782.2996	-0.0004
8	0	8	7	1	7	3803.9170	-0.0076
8	1	8	7	0	7	3804.8865	0.0024
5	2	3	4	1	3	3816.5932	0.0086
5	3	3	4	2	2	3847.5112	0.0011
4	4	1	3	3	0	4029.1150	0.0008
4	4	0	3	3	0	4030.5962	-0.0064
5	3	2	4	2	2	4033.6746	-0.0002
4	4	1	3	3	1	4037.3716	0.0002
4	4	0	3	3	1	4038.8613	0.0016
8	1	7	7	2	6	4166.6519	0.0022
6	3	4	5	2	3	4190.9717	0.0034
8	2	7	7	1	6	4203.2007	0.0017
9	0	9	8	1	8	4256.1872	0.0123
9	1	9	8	0	8	4256.4494	-0.0106
5	3	3	4	2	3	4265.6044	-0.0137
5	3	2	4	2	3	4451.7818	-0.0010
7	3	5	6	2	4	4492.5423	-0.0001
5	4	2	4	3	1	4576.1157	0.0007
5	4	1	4	3	1	4588.8926	-0.0070
9	1	8	8	2	7	4628.9141	-0.0046
5	4	2	4	3	2	4629.8995	0.0043
9	2	8	8	1	7	4642.0037	0.0087
5	4	1	4	3	2	4642.6794	-0.0004
10	0	10	9	1	9	4708.2472	0.0281
10	1	10	9	0	9	4708.2472	-0.0546
6	4	3	5	3	2	5057.6882	-0.0037
10	1	9	9	2	8	5084.3439	0.0000
10	2	9	9	1	8	5088.7800	0.0020
5	5	1	4	4	0	5103.3193	0.0037
5	5	0	4	4	0	5103.5651	0.0077
5	5	1	4	4	1	5104.7988	-0.0052
5	5	0	4	4	1	5105.0468	0.0011
6	4	2	5	3	2	5116.3137	0.0106
9	3	7	8	2	6	5132.1114	-0.0012
6	4	3	5	3	3	5243.8551	-0.0016

Appendix IV

6	4	2	5	3	3	5302.4710	0.0031
7	3	4	6	2	4	5322.8310	-0.0129
10	2	8	9	3	7	5430.0303	-0.0011
7	4	4	6	3	3	5446.8903	0.0028
10	3	8	9	2	7	5519.0684	0.0017
11	1	10	10	2	9	5537.2766	0.0047
11	2	10	10	1	9	5538.7149	-0.0016
12	0	12	11	1	11	5612.1907	0.0026
12	1	12	11	0	11	5612.1907	-0.0040
7	4	3	6	3	3	5631.6971	0.0169
6	5	2	5	4	1	5673.7236	0.0006
6	5	1	5	4	2	5689.0737	0.0006
7	2	6	6	1	6	5739.4732	-0.0077
8	4	5	7	3	4	5750.8863	-0.0052
11	2	9	10	3	8	5905.1491	-0.0011
11	3	9	10	2	8	5939.9067	-0.0002
12	1	11	11	2	10	5989.3983	0.0134
12	2	11	11	1	10	5989.8397	-0.0015
9	4	6	8	3	5	6000.8278	0.0043
13	0	13	12	1	12	6064.1655	-0.0024
13	1	13	12	0	12	6064.1655	-0.0043
8	3	5	7	2	5	6107.5202	0.0109
6	6	1	5	5	0	6174.0628	-0.0035
6	6	0	5	5	1	6174.3599	0.0150
8	4	4	7	3	4	6189.2380	0.0006
7	5	3	6	4	2	6216.0146	-0.0027
7	5	2	6	4	3	6289.1307	-0.0033
14	0	14	13	1	13	6516.1589	0.0084
14	1	14	13	0	13	6516.1589	0.0079
11	4	8	10	3	7	6519.5800	-0.0032
8	4	5	7	3	5	6581.1940	0.0010
8	5	4	7	4	3	6693.9697	-0.0045
7	6	2	6	5	1	6750.9355	0.0013
7	6	1	6	5	2	6753.9677	0.0036
8	5	3	7	4	4	6935.9113	0.0019
9	5	5	8	4	4	7072.9265	-0.0081
7	7	1	6	6	0	7244.1269	-0.0138
8	6	3	7	5	2	7318.2631	0.0006
8	6	2	7	5	3	7335.8686	-0.0025
10	5	6	9	4	5	7350.0380	-0.0125
16	0	16	15	1	15	7420.1197	-0.0031
16	1	16	15	0	15	7420.1197	-0.0032
8	7	2	7	6	1	7822.6384	0.0085
8	7	1	7	6	2	7823.1741	0.0015
9	6	4	8	5	3	7858.5496	0.0071
9	6	3	8	5	4	7930.1624	-0.0070

Table S7.6. Measured frequencies and residuals (in MHz) for the rotational transitions of the conformer **2f** of muscone.

J'	K'_{-1}	K'_{+1}	J''	K''_{-1}	K''_{+1}	V _{obs}	V _{obs} - V _{calc}
3	2	1	2	1	1	2346.0838	-0.0008
3	2	2	2	1	2	2514.9536	-0.0032
4	1	3	3	0	3	2880.5851	0.0023
3	3	0	2	2	0	2892.5832	0.0014
3	3	1	2	2	1	2913.2323	-0.0109
4	2	2	3	1	2	2915.7373	0.0019
4	2	3	3	1	3	3179.0462	0.0178
4	3	1	3	2	1	3394.3304	0.0017
4	3	2	3	2	2	3480.7199	0.0005
5	2	3	4	1	3	3548.1896	-0.0031
5	1	4	4	0	4	3679.7443	0.0010
5	2	4	4	1	4	3880.7167	-0.0032
5	3	2	4	2	2	3883.6533	-0.0007
4	4	0	3	3	0	3955.4555	-0.0147
4	4	1	3	3	1	3959.1493	0.0011
5	3	3	4	2	3	4079.0351	-0.0004
6	2	4	5	1	4	4254.2800	-0.0014
6	3	3	5	2	3	4398.9443	0.0000
5	4	1	4	3	1	4479.0531	0.0015
6	1	5	5	0	5	4499.0435	0.0066
6	2	5	5	1	5	4612.8489	-0.0114
6	3	4	5	2	4	4714.1482	0.0018
6	4	2	5	3	2	4978.6386	0.0000
5	5	0	4	4	0	5011.3563	0.0003
5	5	1	4	4	1	5011.8866	0.0017
7	2	5	6	1	5	5034.8440	-0.0009
6	4	3	5	3	3	5058.4261	0.0025
7	1	6	6	0	6	5310.4622	0.0028
7	2	6	6	1	6	5366.3618	0.0001
7	3	5	6	2	5	5387.6996	0.0005
7	4	3	6	3	3	5451.0505	-0.0015
6	5	1	5	4	1	5544.2662	0.0012
6	5	2	5	4	2	5548.7351	-0.0013
7	4	4	6	3	4	5636.5712	0.0013
8	2	6	7	1	6	5864.4389	-0.0044
8	4	4	7	3	4	5922.4331	0.0015
6	6	0	5	5	0	6065.8119	0.0336
6	6	1	5	5	1	6065.8119	-0.0346
7	5	2	6	4	2	6067.3466	0.0016
7	5	3	6	4	3	6087.7216	0.0028
8	3	6	7	2	6	6096.7491	0.0023
8	1	7	7	0	7	6107.8835	-0.0008
8	2	7	7	1	7	6132.7259	0.0017
8	4	5	7	3	5	6245.8162	-0.0054
9	3	6	8	2	6	6372.1531	-0.0077
9	4	5	8	3	5	6437.4992	0.0020
8	5	3	7	4	3	6568.9035	-0.0015
7	6	1	6	5	1	6600.9736	0.0015
7	6	2	6	5	2	6601.6872	0.0002
8	5	4	7	4	4	6633.7493	0.0014
9	3	7	8	2	7	6834.4994	0.0016
9	4	6	8	3	6	6891.9076	0.0099
10	4	6	9	3	6	7030.1224	-0.0102
9	5	4	8	4	4	7038.3858	-0.0056
7	7	0	6	6	0	7119.9523	-0.0005
7	7	1	6	6	1	7119.9523	-0.0088
8	6	2	7	5	2	7132.6259	-0.0019
8	6	3	7	5	3	7136.6488	0.0029
10	3	7	9	2	7	7189.8229	0.0024
9	5	5	8	4	5	7195.0043	0.0054

Appendix IV

10	5	5	9	4	5	7484.4386	-0.0037
10	3	8	9	2	8	7592.3510	0.0026
9	6	3	8	5	3	7655.6246	0.0117
8	7	2	7	6	2	7655.8292	-0.0025
9	6	4	8	5	4	7671.5190	-0.0002
10	1	9	9	0	9	7677.6408	-0.0031
10	2	9	9	1	9	7681.7220	0.0025

Table S7.7. Measured frequencies and residuals (in MHz) for the rotational transitions of the conformer **31d** of muscone.

J'	K' ₋₁	K' ₊₁	J''	K'' ₋₁	K'' ₊₁	V _{obs}	V _{obs} - V _{calc}
3	2	1	2	1	1	2318.8449	-0.0052
3	2	2	2	1	2	2483.9897	0.0251
3	3	0	2	2	0	2785.3659	0.0040
3	3	1	2	2	1	2813.1570	0.0022
4	2	2	3	1	2	2931.0975	-0.0011
4	1	3	3	0	3	2962.2935	-0.0027
4	2	3	3	1	3	3175.1866	0.0118
4	3	1	3	2	1	3298.0636	0.0044
4	3	2	3	2	2	3405.2797	-0.0004
5	2	3	4	1	3	3616.5616	-0.0095
5	1	4	4	0	4	3784.1275	0.0037
4	4	0	3	3	0	3805.8324	0.0055
4	4	1	3	3	1	3812.2769	0.0066
5	3	2	4	2	2	3817.1980	-0.0034
5	2	4	4	1	4	3904.5032	-0.0057
5	3	3	4	2	3	4035.3668	-0.0020
5	4	1	4	3	1	4336.3904	-0.0067
5	4	2	4	3	2	4375.3625	0.0031
6	2	4	5	1	4	4383.5265	-0.0094
6	3	3	5	2	3	4390.1368	-0.0064
6	2	5	5	1	5	4661.2285	0.0001
6	3	4	5	2	4	4707.7145	0.0005
5	5	0	4	4	0	4818.4816	0.0066
6	4	2	5	3	2	4837.9240	0.0009
6	4	3	5	3	3	4958.7941	-0.0018
7	3	4	6	2	4	5043.7111	0.0066
7	2	5	6	1	5	5212.5583	0.0076
7	4	3	6	3	3	5328.8586	0.0017
6	5	1	5	4	1	5362.7062	-0.0014
6	5	2	5	4	2	5372.4938	0.0059
7	3	5	6	2	5	5420.3377	-0.0077
7	2	6	6	1	6	5434.1536	-0.0010
7	4	4	6	3	4	5574.0742	-0.0008
8	3	5	7	2	5	5788.8829	-0.0044
6	6	0	5	5	0	5828.8446	0.0036
6	6	1	5	5	1	5829.0369	-0.0017
8	4	4	7	3	4	5860.5369	-0.0040
7	5	2	6	4	2	5889.3278	-0.0045
7	5	3	6	4	3	5931.4673	-0.0004
8	2	6	7	1	6	6056.2266	0.0123
8	3	6	7	2	6	6165.5939	0.0104
8	1	7	7	0	7	6206.7749	0.0016
8	4	5	7	3	5	6229.0920	0.0070
7	6	1	6	5	1	6377.4244	-0.0015
7	6	2	6	5	2	6379.4530	0.0030
8	5	3	7	4	3	6384.1810	-0.0019
9	4	5	8	3	5	6474.5432	0.0071
8	5	4	7	4	4	6505.7374	-0.0024
9	3	6	8	2	6	6614.9473	-0.0079
9	5	4	8	4	4	6854.5309	0.0117
8	6	2	7	5	2	6919.0128	0.0083
8	6	3	7	5	3	6929.9523	-0.0239
9	5	5	8	4	5	7106.9609	-0.0126
8	7	1	7	6	1	7388.5271	-0.0002
9	6	3	8	5	3	7443.1065	0.0074
9	6	4	8	5	4	7484.0647	-0.0010
8	8	0	7	7	0	7848.5192	-0.0049
8	8	1	7	7	1	7848.5192	-0.0094

Table S7.8. Measured frequencies and residuals (in MHz) for the rotational transitions of the conformer **19c** of muscone.

J'	K' ₋₁	K' ₊₁	J''	K'' ₋₁	K'' ₊₁	V _{obs}	V _{obs} - V _{calc}
3	2	1	2	1	1	2341.8591	0.0080
3	3	0	2	2	0	2692.7811	-0.0104
3	3	1	2	2	1	2725.5073	0.0011
4	2	2	3	1	2	3020.5276	-0.0050
4	3	1	3	2	1	3256.5985	-0.0018
4	3	2	3	2	2	3369.6763	0.0001
4	4	0	3	3	0	3668.1302	0.0045
4	4	1	3	3	1	3678.0273	-0.0117
5	2	3	4	1	3	3774.3086	-0.0033
5	3	2	4	2	2	3850.8813	0.0014
5	2	4	4	1	4	3983.8982	-0.0043
5	4	1	4	3	1	4237.1390	-0.0007
5	4	2	4	3	2	4292.3522	0.0031
6	3	3	5	2	3	4514.9691	-0.0028
6	2	4	5	1	4	4599.3058	0.0038
5	5	0	4	4	0	4636.7510	0.0026
5	5	1	4	4	1	4639.1190	0.0004
6	4	3	5	3	3	4933.9072	-0.0051
6	5	1	5	4	1	5221.2906	-0.0015
6	5	2	5	4	2	5239.7214	0.0012
7	3	4	6	2	4	5264.3963	-0.0003
7	4	3	6	3	3	5358.5568	-0.0004
7	3	5	6	2	5	5542.0911	-0.0015
6	6	0	5	5	0	5602.3717	0.0005
6	6	1	5	5	1	5602.8745	0.0005
7	4	4	6	3	4	5613.0866	-0.0001
7	5	2	6	4	2	5780.5933	0.0044
7	5	3	6	4	3	5852.5581	-0.0056
8	4	4	7	3	4	6005.7936	0.0038
7	6	1	6	5	1	6194.0079	0.0070
7	6	2	6	5	2	6198.9715	0.0085
8	2	6	7	1	6	6289.6394	0.0041
8	5	3	7	4	3	6314.0153	0.0077
8	4	5	7	3	5	6333.2902	-0.0015
8	5	4	7	4	4	6490.0428	0.0016
7	7	0	6	6	0	6567.2349	0.0555
7	7	1	6	6	1	6567.2349	-0.0438
8	6	2	7	5	2	6772.7819	-0.0032
8	6	3	7	5	3	6798.0569	0.0028
9	4	6	8	3	6	7089.8730	-0.0020
9	6	3	8	5	3	7323.3193	-0.0095
8	8	0	7	7	0	7531.7906	0.0018
8	8	1	7	7	1	7531.7906	-0.0169

Table S7.9. Measured frequencies and residuals (in MHz) for the rotational transitions of the conformer **1h** of muscone.

J'	K'_{-1}	K'_{+1}	J''	K''_{-1}	K''_{+1}	V _{obs}	V _{obs} - V _{calc}
3	1	2	2	0	2	2424.3081	0.0065
4	2	3	3	2	2	2431.7905	0.0182
4	1	3	3	1	2	2557.4493	0.0015
3	2	2	2	1	2	2611.5221	0.0006
5	0	5	4	1	4	2655.1685	0.0024
5	1	5	4	1	4	2656.6222	-0.0031
5	0	5	4	0	4	2660.9864	-0.0004
5	1	5	4	0	4	2662.4516	0.0056
4	2	2	3	2	1	2734.2058	0.0043
3	3	0	2	2	0	2798.7372	-0.0019
3	3	1	2	2	1	2836.5192	-0.0057
5	1	4	4	2	3	2928.8675	0.0068
5	2	4	4	2	3	2975.4080	-0.0052
5	1	4	4	1	3	3051.5730	-0.0058
5	2	4	4	1	3	3098.1314	0.0001
6	0	6	5	1	5	3154.2129	-0.0026
6	0	6	5	0	5	3155.6667	-0.0080
6	1	6	5	0	5	3156.0122	-0.0049
5	3	3	4	3	2	3172.5217	0.0106
4	2	2	3	1	2	3211.3793	0.0002
4	1	3	3	0	3	3297.1557	-0.0044
5	2	3	4	2	2	3377.9077	-0.0020
4	2	3	3	1	3	3399.0513	0.0072
4	3	1	3	2	1	3409.9933	-0.0007
6	1	5	5	2	4	3480.2721	0.0010
6	2	5	5	2	4	3494.9516	-0.0021
6	1	5	5	1	4	3526.8160	-0.0076
4	3	2	3	2	2	3532.3668	0.0010
6	2	5	5	1	4	3541.4914	-0.0148
7	0	7	6	1	6	3651.3770	0.0509
7	1	7	6	1	6	3651.3770	-0.0260
7	0	7	6	0	6	3651.6754	0.0069
6	3	4	5	3	3	3759.6572	-0.0054
4	4	0	3	3	0	3808.8282	0.0000
4	4	1	3	3	1	3821.8992	-0.0005
6	4	3	5	4	2	3869.3383	0.0074
6	2	4	5	2	3	3937.8426	-0.0016
7	1	6	6	2	5	3996.2262	0.0036
7	2	6	6	2	5	4000.3514	-0.0036
7	2	6	6	1	5	4015.0435	0.0059
5	2	3	4	1	3	4031.8348	-0.0061
5	3	2	4	2	2	4066.0774	0.0013
5	2	4	4	1	4	4219.3610	0.0084
5	3	3	4	2	3	4273.1022	-0.0024
7	3	5	6	3	4	4312.8088	-0.0153
5	4	1	4	3	1	4416.9105	0.0018
7	2	5	6	2	4	4423.2877	-0.0026
5	4	2	4	3	2	4485.7100	0.0078
9	0	9	8	1	8	4644.4852	0.0008
9	1	9	8	1	8	4644.4852	-0.0027
9	0	9	8	0	8	4644.4852	-0.0159
9	1	9	8	0	8	4644.4852	-0.0194
6	3	3	5	2	3	4802.1497	-0.0013
5	5	0	4	4	0	4812.8765	0.0006
5	5	1	4	4	1	4816.4132	-0.0059
8	3	6	7	3	5	4838.2200	0.0037
8	2	6	7	2	5	4887.8465	0.0025
6	2	4	5	1	4	4918.0964	-0.0099
6	4	2	5	3	2	5012.9116	-0.0014
6	3	4	5	2	4	5057.3524	-0.0017

6	2	5	5	1	5	5057.6882	0.0073
8	4	5	7	4	4	5095.3626	-0.0012
10	0	10	9	1	9	5140.9917	-0.0035
10	1	10	9	1	9	5140.9917	-0.0042
10	0	10	9	0	9	5140.9917	-0.0071
10	1	10	9	0	9	5140.9917	-0.0078
6	4	3	5	3	3	5182.5223	0.0004
9	3	7	8	3	6	5346.3463	-0.0082
9	2	7	8	2	6	5364.2203	-0.0057
6	5	1	5	4	1	5437.1254	0.0013
6	5	2	5	4	2	5463.6696	0.0018
10	2	9	9	2	8	5493.0553	0.0122
10	1	9	9	1	8	5493.2503	0.0035
7	3	4	6	2	4	5629.9107	-0.0007
11	0	11	10	1	10	5637.5199	0.0135
11	1	11	10	1	10	5637.5199	0.0134
11	0	11	10	0	10	5637.5199	0.0128
11	1	11	10	0	10	5637.5199	0.0126
9	4	6	8	4	5	5655.2686	-0.0074
7	4	3	6	3	3	5655.8094	0.0022
6	6	0	5	5	0	5813.3542	-0.0009
6	6	1	5	5	1	5814.1969	-0.0069
7	2	5	6	1	5	5814.5720	-0.0010
10	3	8	9	3	7	5846.2971	-0.0017
10	2	8	9	2	7	5851.9422	0.0190
7	3	5	6	2	5	5875.2257	0.0012
7	2	6	6	1	6	5903.4816	0.0035
7	4	4	6	3	4	5921.9732	0.0052
7	5	2	6	4	2	6031.7479	-0.0007
7	5	3	6	4	3	6128.2478	-0.0010
12	0	12	11	1	11	6134.0083	-0.0117
12	1	12	11	1	11	6134.0083	-0.0118
12	0	12	11	0	11	6134.0083	-0.0119
12	1	12	11	0	11	6134.0083	-0.0119
7	6	1	6	5	1	6446.9579	0.0018
7	6	2	6	5	2	6455.1137	-0.0012
8	3	5	7	2	5	6529.3283	-0.0001
8	5	3	7	4	3	6612.4917	-0.0015
13	0	13	12	1	12	6630.5340	-0.0014
13	1	13	12	1	12	6630.5340	-0.0014
13	0	13	12	0	12	6630.5340	-0.0014
13	1	13	12	0	12	6630.5340	-0.0015
8	2	6	7	1	6	6691.5110	-0.0007
8	4	5	7	3	5	6704.5058	-0.0019
8	3	6	7	2	6	6713.0703	-0.0155
8	2	7	7	1	7	6751.6116	0.0047
7	7	0	6	6	0	6812.7092	0.0004
8	6	3	7	5	3	7101.8865	-0.0009
9	4	5	8	3	5	7221.8427	0.0000
9	5	4	8	4	4	7242.6435	0.0065
8	7	1	7	6	1	7449.8233	-0.0008
8	7	2	7	6	2	7452.0320	0.0051
9	3	7	8	2	7	7559.9087	0.0002
9	5	5	8	4	5	7562.5564	0.0049

Table S7.10. Measured frequencies and residuals (in MHz) for the rotational transitions of the conformer **6j** of muscone.

J'	K' ₋₁	K' ₊₁	J''	K'' ₋₁	K'' ₊₁	V _{obs}	V _{obs} - V _{calc}
3	1	2	2	0	2	2274.4601	-0.0138
3	2	1	2	1	1	2354.6093	0.0068
4	1	3	3	1	2	2406.3061	-0.0006
3	3	0	2	2	0	2727.2940	-0.0040
3	3	1	2	2	1	2759.2451	-0.0004
5	2	4	4	2	3	2790.6668	-0.0047
6	1	6	5	1	5	2965.1938	-0.0018
6	0	6	5	0	5	2967.3316	-0.0027
4	2	2	3	1	2	3027.0667	-0.0032
4	1	3	3	0	3	3092.2034	0.0063
4	2	3	3	1	3	3233.1437	0.0031
4	3	1	3	2	1	3286.4962	0.0003
4	3	2	3	2	2	3399.5060	0.0011
7	1	7	6	1	6	3432.0003	0.0176
7	0	7	6	0	6	3432.5816	0.0049
4	4	0	3	3	0	3717.0167	0.0015
4	4	1	3	3	1	3726.2165	0.0005
7	2	6	6	2	5	3764.2153	0.0057
5	2	3	4	1	3	3774.7709	-0.0023
7	1	6	6	1	5	3783.3551	-0.0108
5	3	2	4	2	2	3871.7660	-0.0019
8	1	8	7	1	7	3898.2894	0.0098
8	0	8	7	0	7	3898.4440	0.0076
5	1	4	4	0	4	3932.9665	-0.0070
5	2	4	4	1	4	3999.7572	-0.0026
5	3	3	4	2	3	4080.1987	-0.0077
5	4	1	4	3	1	4284.3085	-0.0008
5	4	2	4	3	2	4336.5194	0.0039
9	1	9	8	1	8	4364.4412	-0.0034
9	0	9	8	0	8	4364.4412	-0.0434
6	3	3	5	2	3	4524.9288	-0.0039
6	2	4	5	1	4	4597.0208	-0.0031
5	5	0	4	4	0	4699.6648	-0.0008
5	5	1	4	4	1	4701.7626	0.0006
6	1	5	5	0	5	4762.4020	0.0085
6	2	5	5	1	5	4788.0422	0.0049
6	3	4	5	2	4	4802.9348	-0.0004
6	4	2	5	3	2	4827.9774	-0.0007
6	4	3	5	3	3	4972.8734	-0.0022
7	3	4	6	2	4	5263.4426	-0.0037
6	5	1	5	4	1	5282.4509	-0.0003
6	5	2	5	4	2	5298.9446	-0.0009
7	4	3	6	3	3	5389.4664	0.0001
7	2	5	6	1	5	5453.3532	-0.0044
7	3	5	6	2	5	5561.8936	-0.0070
7	1	6	6	0	6	5578.4323	0.0072
7	2	6	6	1	6	5587.0566	0.0054
7	4	4	6	3	4	5646.1036	0.0000
6	6	1	5	5	1	5679.8585	0.0019
7	5	2	6	4	2	5841.1721	0.0007
7	5	3	6	4	3	5907.0869	-0.0030
8	4	4	7	3	4	6020.5354	-0.0016
8	3	5	7	2	5	6086.9830	-0.0016
7	6	1	6	5	1	6268.7627	0.0068
7	6	2	6	5	2	6272.9785	-0.0011
8	2	6	7	1	6	6299.7623	0.0025
8	3	6	7	2	6	6346.1534	0.0030
8	4	5	7	3	5	6360.6575	-0.0025
8	5	3	7	4	3	6370.8563	0.0067
8	1	7	7	0	7	6387.5987	-0.0032

Appendix IV

8	2	7	7	1	7	6390.2662	-0.0023
8	5	4	7	4	4	6538.1465	-0.0011
7	7	0	6	6	0	6658.4861	0.0315
7	7	1	6	6	1	6658.4861	-0.0485
9	4	5	8	3	5	6745.6515	-0.0002
8	6	2	7	5	2	6846.5506	-0.0006
8	6	3	7	5	3	6868.3772	-0.0001
9	3	6	8	2	6	6957.0152	-0.0048
9	4	6	8	3	6	7113.1675	0.0120
9	3	7	8	2	7	7144.3836	0.0002
9	1	8	8	0	8	7193.9724	0.0056
9	2	8	8	1	8	7194.7403	-0.0039
9	5	5	8	4	5	7203.8467	0.0044
8	7	1	7	6	1	7249.8653	-0.0014
8	7	2	7	6	2	7250.8212	-0.0045
9	6	3	8	5	3	7397.9125	0.0025
9	6	4	8	5	4	7472.9223	0.0075
10	5	5	9	4	5	7516.5404	0.0181
10	4	6	9	3	6	7566.4851	0.0027
8	8	0	7	7	0	7637.3094	0.0097
8	8	1	7	7	1	7637.3094	-0.0047
10	3	7	9	2	7	7821.5868	-0.0044
9	7	2	8	6	2	7836.2803	-0.0003
9	7	3	8	6	3	7842.2862	0.0112
10	4	7	9	3	7	7894.0191	0.0023
10	5	6	9	4	6	7910.5094	-0.0116
10	6	4	9	5	4	7915.6229	-0.0223

Table S7.11. Measured frequencies and residuals (in MHz) for the rotational transitions of the conformer **2I** of muscone.

J'	K' ₋₁	K' ₊₁	J''	K'' ₋₁	K'' ₊₁	V _{obs}	V _{obs} - V _{calc}
3	2	1	2	1	1	2321.3182	-0.0024
3	3	0	2	2	0	2635.1904	0.0011
3	3	1	2	2	1	2672.3632	0.0031
6	1	6	5	1	5	2899.4242	0.0079
6	0	6	5	0	5	2900.4478	0.0050
4	2	2	3	1	2	3014.9582	-0.0030
4	1	3	3	0	3	3099.4925	-0.0112
4	2	3	3	1	3	3195.7240	-0.0019
4	3	1	3	2	1	3203.3866	-0.0015
4	3	2	3	2	2	3322.8501	0.0006
7	1	7	6	1	6	3354.4139	-0.0216
7	0	7	6	1	6	3354.4139	0.0469
7	0	7	6	0	6	3354.6804	0.0040
7	1	7	6	0	6	3354.6804	-0.0646
4	4	0	3	3	0	3588.2732	0.0019
5	2	3	4	1	3	3787.7643	-0.0046
5	3	2	4	2	2	3816.5932	0.0060
5	1	4	4	0	4	3928.9843	0.0046
5	2	4	4	1	4	3966.8976	0.0003
5	3	3	4	2	3	4017.2870	-0.0006
5	4	1	4	3	1	4152.3633	0.0019
5	4	2	4	3	2	4220.5556	-0.0009
6	3	3	5	2	3	4508.3089	-0.0039
5	5	1	4	4	1	4539.2006	0.0000
6	2	4	5	1	4	4623.4324	-0.0040
6	4	2	5	3	2	4706.0294	0.0010
6	1	5	5	0	5	4743.1380	0.0029
6	3	4	5	2	4	4754.0507	-0.0022
6	2	5	5	1	5	4755.2736	-0.0005
6	4	3	5	3	3	4872.4281	0.0013
6	5	1	5	4	1	5115.3360	0.0008
6	5	2	5	4	2	5142.0823	0.0022
7	3	4	6	2	4	5289.4102	0.0089
7	4	3	6	3	3	5307.5146	0.0010
7	2	5	6	1	5	5467.2119	-0.0048
6	6	0	5	5	0	5479.4407	-0.0034
6	6	1	5	5	1	5480.3129	-0.0020
7	3	5	6	2	5	5523.1999	-0.0002
7	1	6	6	0	6	5547.2584	0.0203
7	2	6	6	1	6	5550.6636	-0.0074
7	4	4	6	3	4	5566.1091	-0.0008
7	5	2	6	4	2	5666.0202	0.0000
7	5	3	6	4	3	5762.3702	0.0015
8	4	4	7	3	4	5996.9951	-0.0024
7	6	1	6	5	1	6068.4849	0.0009
7	6	2	6	5	2	6076.8265	-0.0013
8	3	5	7	2	5	6138.3705	-0.0046
8	5	3	7	4	3	6205.1530	0.0040
8	2	6	7	1	6	6291.7157	0.0058
8	4	5	7	3	5	6301.6868	0.0018
8	3	6	7	2	6	6311.3255	-0.0008
8	1	7	7	0	7	6347.3144	-0.0044
8	2	7	7	1	7	6348.2317	0.0169
8	5	4	7	4	4	6414.0650	0.0045
7	7	0	6	6	0	6422.1456	-0.0064
7	7	1	6	6	1	6422.3420	-0.0065
8	6	2	7	5	2	6639.1089	0.0033
8	6	3	7	5	3	6679.4060	0.0034
9	4	5	8	3	5	6785.3383	-0.0040
9	5	4	8	4	4	6795.4724	0.0048

Appendix IV

8	7	1	7	6	1	7014.7361	-0.0084
8	7	2	7	6	2	7017.0238	-0.0051
9	4	6	8	3	6	7070.4038	-0.0007
9	2	7	8	1	7	7101.7442	0.0005
9	5	5	8	4	5	7106.9609	-0.0038
9	3	7	8	2	7	7107.7942	-0.0066
9	6	3	8	5	3	7176.5767	0.0090
9	6	4	8	5	4	7299.1207	0.0075
10	5	5	9	4	5	7482.4101	-0.0039
9	7	2	8	6	2	7598.6265	-0.0021
9	7	3	8	6	3	7612.2450	-0.0008
10	6	4	9	5	4	7701.6433	-0.0002
10	3	7	9	2	7	7831.7661	-0.0021
10	5	6	9	4	6	7841.9628	0.0029
10	4	7	9	3	7	7859.3835	0.0007
10	2	8	9	1	8	7905.1839	-0.0008
10	3	8	9	2	8	7906.9006	-0.0031

Table S7.12. Measured frequencies and residuals (in MHz) for the rotational transitions of the conformer **1f** of muscone.

J'	K' ₋₁	K' ₊₁	J''	K'' ₋₁	K'' ₊₁	V _{obs}	V _{obs} -V _{calc}
3	1	2	2	0	2	2272.1902	-0.0025
3	2	1	2	1	1	2322.2598	0.0003
3	3	0	2	2	0	2650.8904	0.0027
3	3	1	2	2	1	2687.9135	0.0063
6	0	6	5	1	5	2871.3973	0.0004
6	0	6	5	0	5	2872.9521	0.0081
6	1	6	5	0	5	2873.3029	-0.0092
4	2	2	3	1	2	3009.8742	0.0014
4	1	3	3	0	3	3093.6547	-0.0090
4	2	3	3	1	3	3198.0548	-0.0025
4	3	1	3	2	1	3212.3646	0.0021
7	0	7	6	1	6	3321.6850	-0.0277
7	1	7	6	1	6	3321.8088	0.0124
7	1	7	6	0	6	3322.1822	0.0176
4	3	2	3	2	2	3333.2637	0.0029
4	4	0	3	3	0	3611.5278	0.0035
4	4	1	3	3	1	3624.1273	0.0035
8	1	8	7	1	7	3771.5386	0.0009
8	0	8	7	1	7	3771.5386	0.0193
8	0	8	7	0	7	3771.5386	-0.0644
8	1	8	7	0	7	3771.5386	-0.0829
5	2	3	4	1	3	3777.6117	0.0001
5	3	2	4	2	2	3816.7263	-0.0013
5	1	4	4	0	4	3924.9336	0.0043
5	2	4	4	1	4	3967.3299	0.0018
5	3	3	4	2	3	4022.8467	0.0014
5	4	1	4	3	1	4170.9812	0.0026
9	1	9	8	1	8	4221.2426	0.0265
9	0	9	8	1	8	4221.2426	0.0304
9	0	9	8	0	8	4221.2426	0.0120
9	1	9	8	0	8	4221.2426	0.0080
5	4	2	4	3	2	4237.7982	0.0026
6	3	3	5	2	3	4499.6309	0.0022
5	5	0	4	4	0	4566.0308	0.0021
5	5	1	4	4	1	4569.3931	0.0016
6	2	4	5	1	4	4611.8695	0.0015
6	4	2	5	3	2	4717.0318	0.0035
6	1	5	5	0	5	4740.8683	0.0045
6	2	5	5	1	5	4754.8397	-0.0010
6	3	4	5	2	4	4755.5913	0.0064
6	4	3	5	3	3	4883.6455	0.0034
6	5	1	5	4	1	5141.6002	-0.0010
6	5	2	5	4	2	5166.9279	0.0049
7	3	4	6	2	4	5273.2444	-0.0061
7	4	3	6	3	3	5307.0971	0.0082
7	2	5	6	1	5	5458.3234	0.0016
6	6	0	5	5	0	5517.0463	-0.0034
6	6	1	5	5	1	5517.8387	-0.0046
7	3	5	6	2	5	5522.0379	0.0043
7	1	6	6	0	6	5545.9826	0.0033
7	2	6	6	1	6	5550.0311	-0.0132
7	4	4	6	3	4	5571.3812	0.0040
7	5	2	6	4	2	5688.0812	0.0052
7	5	3	6	4	3	5781.0427	0.0003
8	4	4	7	3	4	5984.4800	-0.0017
7	6	1	6	5	1	6101.6466	-0.0026
7	6	2	6	5	2	6109.3036	-0.0021
8	3	5	7	2	5	6119.8969	-0.0032
8	5	3	7	4	3	6218.7190	0.0037
8	2	6	7	1	6	6285.8030	0.0012

8	4	5	7	3	5	6301.8814	0.0027
8	3	6	7	2	6	6308.8486	0.0072
8	2	7	7	1	7	6347.7101	0.0070
8	5	4	7	4	4	6425.7867	0.0067
7	7	0	6	6	0	6466.9910	-0.0061
7	7	1	6	6	1	6467.1535	-0.0178
8	6	2	7	5	2	6668.7438	-0.0002
8	6	3	7	5	3	6706.1875	-0.0054
9	4	5	8	3	5	6762.5138	-0.0046
9	5	4	8	4	4	6794.7960	0.0030
9	3	6	8	2	6	6981.4900	-0.0070
8	7	1	7	6	1	7054.9252	-0.0072
8	7	2	7	6	2	7056.9539	-0.0141
9	4	6	8	3	6	7067.0860	-0.0148
9	3	7	8	2	7	7104.9620	-0.0025
9	5	5	8	4	5	7111.6037	-0.0084
9	6	3	8	5	3	7202.5846	0.0104
9	6	4	8	5	4	7319.0914	0.0049
8	8	0	7	7	0	7416.6874	0.0282
8	8	1	7	7	1	7416.6874	-0.0082
10	5	5	9	4	5	7465.9619	0.0002
10	4	6	9	3	6	7620.6169	-0.0039
9	7	2	8	6	2	7634.7536	-0.0011
9	7	3	8	6	3	7646.9939	-0.0015
10	6	4	9	5	4	7718.3299	0.0026
10	3	7	9	2	7	7821.2593	0.0055
10	5	6	9	4	6	7840.4572	0.0057
10	4	7	9	3	7	7854.3081	0.0056
10	2	8	9	1	8	7902.0634	0.0060
10	3	8	9	2	8	7904.1896	-0.0064

Table S7.13. Measured frequencies and residuals (in MHz) for the rotational transitions of the conformer **9i** of muscone.

J'	K'_{-1}	K'_{+1}	J''	K''_{-1}	K''_{+1}	V _{obs}	V _{obs} - V _{calc}
3	1	2	2	0	2	2287.0193	0.0020
3	2	1	2	1	1	2332.1126	0.0008
4	1	3	3	1	2	2358.9521	-0.0061
5	1	5	4	1	4	2398.0484	-0.0025
5	0	5	4	0	4	2402.2236	-0.0032
5	2	3	4	3	1	2458.4182	-0.0033
3	2	2	2	1	2	2472.6469	-0.0135
4	2	2	3	2	1	2543.7882	0.0032
3	3	0	2	2	0	2658.3002	-0.0036
3	3	1	2	2	1	2697.2556	-0.0023
5	2	4	4	2	3	2724.0231	0.0014
5	1	4	4	1	3	2799.0931	-0.0024
6	1	6	5	1	5	2843.5473	-0.0008
6	0	6	5	0	5	2844.5966	-0.0017
5	3	3	4	3	2	2927.7460	0.0093
6	2	4	5	3	2	2945.4039	-0.0054
4	2	2	3	1	2	3026.6415	0.0019
4	1	3	3	0	3	3115.2832	0.0045
5	2	3	4	2	2	3136.2282	0.0015
5	3	2	4	3	1	3154.5551	-0.0028
7	2	5	6	3	3	3188.0832	0.0067
6	2	5	5	2	4	3190.9009	-0.0054
4	2	3	3	1	3	3214.6814	0.0062
4	3	1	3	2	1	3221.5894	-0.0008
7	1	7	6	1	6	3287.9910	-0.0014
7	0	7	6	0	6	3288.2339	-0.0038
4	3	2	3	2	2	3346.4430	0.0005
4	4	0	3	3	0	3622.2204	-0.0024
4	4	1	3	3	1	3635.9681	-0.0018
6	2	4	5	2	3	3641.5411	-0.0046
7	2	6	6	2	5	3643.6465	0.0039
7	1	6	6	1	5	3653.6173	0.0044
6	4	2	5	4	1	3702.7918	-0.0086
8	0	8	7	0	7	3732.2312	0.0000
5	2	3	4	1	3	3803.9170	0.0089
6	3	3	5	3	2	3829.2335	0.0022
5	3	2	4	2	2	3832.3643	0.0012
5	1	4	4	0	4	3950.7234	0.0031
7	3	5	6	3	4	3963.9411	0.0066
5	2	4	4	1	4	3989.6912	0.0019
5	3	3	4	2	3	4041.6057	0.0007
7	2	5	6	2	4	4071.8998	0.0013
8	2	7	7	2	6	4090.2835	-0.0012
8	1	7	7	1	6	4093.1195	0.0032
7	4	4	6	4	3	4157.9188	-0.0117
9	1	9	8	1	8	4176.3418	0.0327
9	0	9	8	0	8	4176.3418	0.0210
5	4	1	4	3	1	4180.8406	-0.0013
7	5	2	6	5	1	4247.3055	-0.0123
5	4	2	4	3	2	4252.4978	-0.0015
7	3	4	6	3	3	4427.8834	-0.0070
7	4	3	6	4	2	4428.2127	0.0141
8	3	6	7	3	5	4436.2933	-0.0174
8	2	6	7	2	5	4483.6535	0.0049
6	3	3	5	2	3	4525.3649	-0.0028
9	2	8	8	2	7	4534.8888	0.0016
9	1	8	8	1	7	4535.6128	-0.0139
5	5	0	4	4	0	4580.1979	-0.0030
5	5	1	4	4	1	4583.9962	-0.0019
10	1	10	9	1	9	4620.4393	0.0031

10	0	10	9	0	9	4620.4393	0.0007
6	2	4	5	1	4	4646.3630	0.0047
6	4	2	5	3	2	4729.0933	0.0089
6	1	5	5	0	5	4770.1360	0.0054
6	3	4	5	2	4	4780.9546	0.0034
6	2	5	5	1	5	4782.5488	0.0041
8	5	4	7	5	3	4808.7105	0.0117
6	4	3	5	3	3	4903.2811	-0.0061
9	2	7	8	2	6	4908.2250	0.0100
8	3	5	7	3	4	4928.4223	0.0082
8	5	3	7	5	2	4961.3972	-0.0020
10	2	9	9	2	8	4978.9551	-0.0034
10	1	9	9	1	8	4979.1446	0.0039
11	1	11	10	1	10	5064.5688	0.0031
11	0	11	10	0	10	5064.5688	0.0026
8	4	4	7	4	3	5119.1190	0.0053
6	5	1	5	4	1	5155.0911	-0.0063
6	5	2	5	4	2	5183.3632	0.0009
9	4	6	8	4	5	5209.0307	0.0056
7	3	4	6	2	4	5311.7147	0.0024
7	4	3	6	3	3	5328.0504	-0.0014
10	2	8	9	2	7	5343.9498	-0.0082
9	3	6	8	3	5	5348.6634	0.0020
9	5	5	8	5	4	5396.1585	0.0003
11	2	10	10	2	9	5422.9276	-0.0163
11	1	10	10	1	9	5422.9276	-0.0593
7	2	5	6	1	5	5496.6220	0.0024
12	1	12	11	1	11	5508.6972	-0.0006
12	0	12	11	0	11	5508.6972	-0.0007
6	6	0	5	5	0	5534.4938	-0.0021
6	6	1	5	5	1	5535.4183	-0.0039
7	3	5	6	2	5	5553.9814	0.0020
7	1	6	6	0	6	5579.1521	0.0069
7	2	6	6	1	6	5582.6449	0.0057
7	4	4	6	3	4	5597.8513	0.0016
7	5	2	6	4	2	5699.5732	-0.0415
9	4	5	8	4	4	5722.8337	-0.0014
10	3	7	9	3	6	5749.4026	0.0002
11	3	9	10	3	8	5783.2473	-0.0053
7	5	3	6	4	3	5801.1048	-0.0012
13	1	13	12	1	12	5952.8339	0.0027
13	0	13	12	0	12	5952.8339	0.0026
8	4	4	7	3	4	6019.2712	-0.0039
7	6	1	6	5	1	6119.1996	-0.0026
7	6	2	6	5	2	6128.0663	-0.0006
8	3	5	7	2	5	6168.2299	0.0020
8	5	3	7	4	3	6232.8119	-0.0033
13	2	12	12	2	11	6310.9949	0.0153
13	1	12	12	1	11	6310.9949	0.0132
8	2	6	7	1	6	6326.6578	0.0025
8	4	5	7	3	5	6336.1318	0.0030
8	3	6	7	2	6	6346.6565	0.0091
8	1	7	7	0	7	6384.0303	0.0066
8	2	7	7	1	7	6384.9379	0.0063
8	5	4	7	4	4	6451.8774	0.0030
7	7	0	6	6	0	6487.6040	-0.0020
7	7	1	6	6	1	6487.8142	-0.0018
8	6	2	7	5	2	6684.4600	0.0002
8	6	3	7	5	3	6727.1816	0.0037
14	2	13	13	2	12	6755.0407	0.0038
14	1	13	13	1	12	6755.0407	0.0033
9	4	5	8	3	5	6813.6959	-0.0002
9	5	4	8	4	4	6820.5854	-0.0157
9	3	6	8	2	6	7033.2286	-0.0121
8	7	1	7	6	1	7076.0703	-0.0027

Appendix IV

8	7	2	7	6	2	7078.5108	-0.0012
9	4	6	8	3	6	7108.8398	-0.0034
9	2	7	8	1	7	7141.7577	0.0037
9	5	5	8	4	5	7145.8178	-0.0012
9	3	7	8	2	7	7147.9006	0.0039
9	1	8	8	0	8	7187.3976	-0.0216
9	2	8	8	1	8	7187.6524	0.0102
9	6	3	8	5	3	7215.0439	-0.0007
9	6	4	8	5	4	7344.4382	0.0001
10	5	5	9	4	5	7509.8054	-0.0052
9	7	2	8	6	2	7655.3290	0.0163
9	7	3	8	6	3	7669.8336	0.0040
10	4	6	9	3	6	7683.6231	-0.0057
10	6	4	9	5	4	7733.7155	-0.0030
10	3	7	9	2	7	7874.4236	-0.0046
10	5	6	9	4	6	7883.6801	0.0029
10	4	7	9	3	7	7902.4752	-0.0040
10	3	8	9	2	8	7951.8176	-0.0026
10	6	5	9	5	5	7994.5014	0.0047

Table S7.14. Measured frequencies and residuals (in MHz) for the rotational transitions of the conformer **4h** of muscone.

J'	K' ₋₁	K' ₊₁	J''	K'' ₋₁	K'' ₊₁	V _{obs}	V _{obs} - V _{calc}
6	1	5	5	0	5	4751.2779	0.0076
7	1	6	6	0	6	5567.6221	-0.0012
5	2	4	4	1	4	3994.5007	-0.0028
6	2	5	5	1	5	4780.2286	0.0092
3	2	1	2	1	1	2352.0588	-0.0057
4	2	2	3	1	2	3015.3126	0.0095
5	2	3	4	1	3	3755.7960	-0.0069
6	2	4	5	1	4	4574.2765	-0.0092
3	3	0	2	2	0	2745.7645	0.0006
4	3	1	3	2	1	3293.6721	-0.0016
5	3	2	4	2	2	3866.1204	-0.0051
6	3	3	5	2	3	4507.1669	-0.0061
7	3	4	6	2	4	5235.7345	-0.0051
8	3	5	7	2	5	6053.3101	0.0008
9	3	6	8	2	6	6923.5432	0.0096
3	3	1	2	2	1	2778.1677	-0.0019
4	3	2	3	2	2	3409.5418	-0.0016
6	3	4	5	2	4	4798.3953	0.0011
7	3	5	6	2	5	5552.3727	0.0127
9	3	7	8	2	7	7129.3729	-0.0150
4	4	0	3	3	0	3745.2313	0.0032
5	4	1	4	3	1	4302.8178	0.0012
6	4	2	5	3	2	4834.9740	0.0019
7	4	3	6	3	3	5381.8388	0.0006
8	4	4	7	3	4	5997.6286	-0.0022
9	4	5	8	3	5	6709.4696	-0.0019
4	4	1	3	3	1	3754.3363	0.0011
5	4	2	4	3	2	4354.9272	-0.0006
6	4	3	5	3	3	4981.6669	-0.0046
7	4	4	6	3	4	5645.8592	0.0109
8	4	5	7	3	5	6352.5286	0.0033
9	4	6	8	3	6	7098.8484	0.0032
5	5	0	4	4	0	4737.2776	-0.0013
6	5	1	5	4	1	5310.6954	-0.0005
7	5	2	6	4	2	5860.0510	0.0012
8	5	3	7	4	3	6378.4027	0.0042
5	5	1	4	4	1	4739.3073	0.0010
6	5	2	5	4	2	5326.7353	0.0021
7	5	3	6	4	3	5924.8003	-0.0001
8	5	4	7	4	4	6545.5324	0.0046
9	5	5	8	4	5	7201.0994	-0.0080
6	6	0	5	5	0	5726.4217	-0.0027
7	6	1	6	5	1	6306.2816	-0.0068
9	6	3	8	5	3	7417.3926	0.0056
6	6	1	5	5	1	5726.8181	-0.0075
8	6	3	7	5	3	6895.7696	-0.0059
7	7	0	6	6	0	6714.8772	0.0443
7	7	1	6	6	1	6714.8772	-0.0298
8	7	1	7	6	1	7296.7168	-0.0033
8	7	2	7	6	2	7297.6115	0.0019
9	7	3	8	6	3	7879.3426	-0.0025
8	8	0	7	7	0	7703.0714	0.0090
8	8	1	7	7	1	7703.0714	-0.0040

Table S7.15. Measured frequencies and residuals (in MHz) for the rotational transitions of the conformer **15k** of muscone.

J'	K'_{-1}	K'_{+1}	J''	K''_{-1}	K''_{+1}	V_{obs}	$V_{\text{obs}} - V_{\text{calc}}$
4	1	3	3	0	3	3047.0776	-0.0062
5	1	4	4	0	4	3883.9080	-0.0106
3	2	1	2	1	1	2334.5982	0.0014
4	2	2	3	1	2	2984.1379	-0.0001
5	2	3	4	1	3	3712.8616	0.0004
6	2	4	5	1	4	4522.6970	0.0052
4	2	3	3	1	3	3210.3028	0.0043
5	2	4	4	1	4	3964.3823	0.0055
6	2	5	5	1	5	4742.6477	0.0078
3	3	0	2	2	0	2748.0410	0.0017
4	3	1	3	2	1	3280.3284	0.0065
5	3	2	4	2	2	3835.7692	-0.0007
6	3	3	5	2	3	4460.4636	0.0019
7	3	4	6	2	4	5174.7087	-0.0007
8	3	5	7	2	5	5981.5214	-0.0009
3	3	1	2	2	1	2780.8893	-0.0052
4	3	2	3	2	2	3398.8719	-0.0010
5	3	3	4	2	3	4059.1117	-0.0035
6	3	4	5	2	4	4763.9741	0.0079
7	3	5	6	2	5	5508.1946	0.0003
8	3	6	7	2	6	6280.8710	0.0027
4	4	0	3	3	0	3751.6500	0.0000
5	4	1	4	3	1	4295.0256	0.0000
6	4	2	5	3	2	4811.4064	-0.0004
7	4	3	6	3	3	5339.7200	-0.0025
8	4	4	7	3	4	5936.2920	-0.0050
9	4	5	8	3	5	6630.7505	0.0015
4	4	1	3	3	1	3760.6898	-0.0003
5	4	2	4	3	2	4347.1118	-0.0058
7	4	4	6	3	4	5610.4830	-0.0042
8	4	5	7	3	5	6304.7518	-0.0051
5	5	0	4	4	0	4747.5410	0.0002
7	5	2	6	4	2	5842.4831	-0.0054
8	5	3	7	4	3	6345.3110	0.0067
6	5	2	5	4	2	5322.7195	0.0026
7	5	3	6	4	3	5906.3000	-0.0029
8	5	4	7	4	4	6512.3557	0.0003
6	6	0	5	5	0	5740.5092	-0.0038
7	6	1	6	5	1	6306.3910	-0.0027
6	6	1	5	5	1	5740.9000	0.0042
9	6	4	8	5	4	7460.6765	0.0004
7	7	0	6	6	0	6732.8029	0.0390
7	7	1	6	6	1	6732.8029	-0.0303
8	7	1	7	6	1	7300.6137	-0.0032
8	7	2	7	6	2	7301.4583	0.0070
8	8	0	7	7	0	7724.8483	0.0026
8	8	1	7	7	1	7724.8483	-0.0094

Table S7.16. Measured frequencies and residuals (in MHz) for the rotational transitions of the conformer **13h** of muscone.

J'	K' ₋₁	K' ₊₁	J''	K'' ₋₁	K'' ₊₁	V _{obs}	V _{obs} - V _{calc}
3	1	2	2	0	2	2271.2681	0.0065
3	2	1	2	1	1	2343.3823	-0.0028
3	2	2	2	1	2	2496.4852	-0.0096
3	3	0	2	2	0	2721.7252	0.0011
3	3	1	2	2	1	2757.8880	0.0024
4	2	2	3	1	2	3015.9133	0.0002
4	1	3	3	0	3	3094.2146	0.0009
4	2	3	3	1	3	3228.1896	-0.0107
4	3	1	3	2	1	3267.7063	0.0011
4	3	2	3	2	2	3391.8078	0.0017
4	4	0	3	3	0	3713.3790	0.0015
4	4	1	3	3	1	3724.5051	0.0017
5	2	3	4	1	3	3770.8162	-0.0009
5	3	2	4	2	2	3848.5455	-0.0007
5	1	4	4	0	4	3936.1079	0.0015
5	2	4	4	1	4	3995.9436	-0.0001
5	3	3	4	2	3	4070.4603	0.0026
5	4	1	4	3	1	4264.0975	0.0008
5	4	2	4	3	2	4325.6918	-0.0023
6	3	3	5	2	3	4506.5757	-0.0008
6	2	4	5	1	4	4602.6959	0.0034
5	5	0	4	4	0	4697.7917	0.0037
5	5	1	4	4	1	4700.4897	0.0028
6	1	5	5	0	5	4763.7164	-0.0014
6	2	5	5	1	5	4785.3696	-0.0005
6	4	2	5	3	2	4792.9770	0.0009
6	3	4	5	2	4	4794.5052	0.0007
6	4	3	5	3	3	4957.1907	0.0019
7	3	4	6	2	4	5258.2232	0.0028
6	5	1	5	4	1	5265.5418	0.0006
6	5	2	5	4	2	5286.4441	-0.0001
7	4	3	6	3	3	5351.7198	0.0021
7	2	5	6	1	5	5461.6893	0.0015
7	3	5	6	2	5	5556.2847	-0.0012
7	1	6	6	0	6	5578.0278	0.0044
7	2	6	6	1	6	5584.9063	-0.0007
7	4	4	6	3	4	5630.2166	0.0251
6	6	0	5	5	0	5678.8651	0.0009
6	6	1	5	5	1	5679.4488	0.0040
7	5	2	6	4	2	5805.2315	-0.0009
7	5	3	6	4	3	5886.2730	-0.0018
8	4	4	7	3	4	5992.9569	0.0021
7	6	1	6	5	1	6254.5752	-0.0131
7	6	2	6	5	2	6260.2968	-0.0058
8	2	6	7	1	6	6305.1594	0.0062
8	5	3	7	4	3	6317.7766	0.0012
8	3	6	7	2	6	6343.0173	-0.0022
8	4	5	7	3	5	6348.0914	-0.0077
8	1	7	7	0	7	6386.0850	-0.0131
8	2	7	7	1	7	6388.0947	-0.0179
8	5	4	7	4	4	6513.7062	0.0003
7	7	0	6	6	0	6659.0054	-0.0108
7	7	1	6	6	1	6659.1434	0.0110
9	4	5	8	3	5	6738.0476	0.0034
8	6	2	7	5	2	6815.7574	0.0034
8	6	3	7	5	3	6844.7140	-0.0014
9	5	4	8	4	4	6854.7492	-0.0066
9	3	6	8	2	6	6972.3930	-0.0006
9	4	6	8	3	6	7105.3855	-0.0056
9	3	7	8	2	7	7142.6140	0.0040

Appendix IV

9	5	5	8	4	5	7180.9512	-0.0008
9	1	8	8	0	8	7191.7458	0.0057
9	2	8	8	1	8	7192.2953	-0.0013
8	7	1	7	6	1	7237.4275	-0.0018
8	7	2	7	6	2	7238.8088	-0.0015
9	6	3	8	5	3	7345.3864	0.0007
9	6	4	8	5	4	7441.4894	-0.0044
10	5	5	9	4	5	7477.2700	-0.0053
10	4	6	9	3	6	7581.0874	0.0009
8	8	0	7	7	0	7638.9471	0.0119
8	8	1	7	7	1	7638.9471	-0.0103
9	7	2	8	6	2	7809.4158	0.0043
9	7	3	8	6	3	7817.9267	0.0013
10	3	7	9	2	7	7832.9971	-0.0028
10	6	4	9	5	4	7842.9559	0.0047
10	4	7	9	3	7	7890.3723	0.0009
10	5	6	9	4	6	7893.1421	0.0020
10	1	9	9	0	9	7996.4348	0.0084

Table S7.17. Measured frequencies and residuals (in MHz) for the rotational transitions of the conformer **7b** of muscone.

J'	K'_{-1}	K'_{+1}	J''	K''_{-1}	K''_{+1}	V _{obs}	V _{obs} - V _{calc}
3	2	1	2	1	1	2445.9360	0.0021
3	1	2	2	0	2	2474.4713	0.0042
3	3	0	2	2	0	2578.8322	-0.0018
3	3	1	2	2	1	2625.5371	-0.0011
4	2	2	3	1	2	3269.5496	0.0039
4	3	1	3	2	1	3283.0785	-0.0005
4	1	3	3	0	3	3333.4793	-0.0105
4	2	3	3	1	3	3345.8101	-0.0110
4	3	2	3	2	2	3380.0265	0.0003
4	4	0	3	3	0	3479.6079	-0.0016
4	4	1	3	3	1	3513.0676	-0.0010
5	3	2	4	2	2	4067.5115	0.0023
5	2	3	4	1	3	4140.9409	0.0054
5	4	1	4	3	1	4143.3813	-0.0077
5	1	4	4	0	4	4177.6955	0.0069
5	3	3	4	2	3	4180.4776	-0.0081
5	4	2	4	3	2	4242.3888	0.0017
5	5	0	4	4	0	4388.0298	0.0013
5	5	1	4	4	1	4406.7060	-0.0013
6	4	2	5	3	2	4881.1401	-0.0010
6	3	3	5	2	3	4930.2954	0.0033
6	2	4	5	1	4	4998.9125	0.0007
6	3	4	5	2	4	5007.8415	0.0017
6	4	3	5	3	3	5019.8291	0.0008
6	5	1	5	4	1	5030.9973	-0.0143
6	5	2	5	4	2	5114.6914	0.0007
6	6	0	5	5	0	5295.7631	0.0042
6	6	1	5	5	1	5304.6605	0.0046
7	4	3	6	3	3	5710.9068	0.0057
7	5	2	6	4	2	5718.2327	-0.0030
7	3	4	6	2	4	5807.6017	0.0042
7	4	4	6	3	4	5835.0151	0.0028
7	2	5	6	1	5	5842.9416	0.0038
7	3	5	6	2	5	5844.5008	-0.0028
7	1	6	6	0	6	5854.8334	0.0154
7	2	6	6	1	6	5854.8334	-0.0219
7	5	3	6	4	3	5867.1801	0.0114
7	6	1	6	5	1	5938.9446	0.0078
7	6	2	6	5	2	5996.6057	0.0023
7	7	0	6	6	0	6201.3026	0.0040
8	5	3	7	4	3	6499.8083	0.0004
8	6	2	7	5	2	6584.6729	-0.0073
8	3	5	7	2	5	6662.7865	0.0005
8	5	4	7	4	4	6664.3186	0.0018
8	2	6	7	1	6	6682.6944	0.0041
8	3	6	7	2	6	6682.9300	0.0031
8	1	7	7	0	7	6692.5416	0.0015
8	2	7	7	1	7	6692.5416	-0.0029
8	6	3	7	5	3	6724.8198	-0.0078
8	7	1	7	6	1	6853.2972	-0.0137
8	7	2	7	6	2	6886.5427	-0.0035
9	6	3	8	5	3	7310.3996	-0.0013
9	5	4	8	4	4	7373.0097	-0.0097
9	7	2	8	6	2	7480.8603	0.0212
9	5	5	8	4	5	7490.8533	-0.0057
9	6	4	8	5	4	7499.3805	-0.0007
9	1	8	8	0	8	7530.1502	-0.0002
9	2	8	8	1	8	7530.1502	-0.0007
9	7	3	8	6	3	7593.7339	0.0053
9	8	1	8	7	1	7765.4305	-0.0067

Table S7.18. Measured frequencies and residuals (in MHz) for the rotational transitions of the conformer **16g** of muscone.

J'	K' ₋₁	K' ₊₁	J''	K'' ₋₁	K'' ₊₁	V _{obs}	V _{obs} - V _{calc}
3	2	1	2	1	1	2383.1950	-0.0024
3	1	2	2	0	2	2409.2984	-0.0011
3	3	0	2	2	0	2523.3479	-0.0038
3	3	1	2	2	1	2569.5614	-0.0023
4	2	2	3	1	2	3181.7557	0.0016
4	3	1	3	2	1	3202.0528	0.0027
4	1	3	3	0	3	3248.8946	-0.0002
4	2	3	3	1	3	3263.3201	0.0097
4	3	2	3	2	2	3300.7630	-0.0016
7	1	7	6	1	6	3328.0674	-0.0007
7	0	7	6	1	6	3328.0674	-0.0002
7	0	7	6	0	6	3328.0674	-0.0047
7	1	7	6	0	6	3328.0674	-0.0052
4	4	0	3	3	0	3407.7676	-0.0033
4	4	1	3	3	1	3439.4667	-0.0036
8	1	8	7	1	7	3777.2316	-0.0016
8	0	8	7	1	7	3777.2316	-0.0015
8	0	8	7	0	7	3777.2316	-0.0020
8	1	8	7	0	7	3777.2316	-0.0020
5	3	2	4	2	2	3959.3149	0.0058
5	2	3	4	1	3	4032.0917	0.0007
5	4	1	4	3	1	4046.6569	-0.0017
5	1	4	4	0	4	4073.4025	-0.0264
5	2	4	4	1	4	4076.0177	-0.0043
5	3	3	4	2	3	4077.7630	0.0027
5	4	2	4	3	2	4145.0499	-0.0005
9	1	9	8	1	8	4226.3967	-0.0050
9	0	9	8	1	8	4226.3967	-0.0049
9	0	9	8	0	8	4226.3967	-0.0050
9	1	9	8	0	8	4226.3967	-0.0050
5	5	0	4	4	0	4298.8539	-0.0059
5	5	1	4	4	1	4315.7365	-0.0033
10	1	10	9	1	9	4675.5976	0.0248
10	0	10	9	0	9	4675.5976	0.0248
10	1	10	9	0	9	4675.5976	0.0248
10	0	10	9	1	9	4675.5976	0.0248
6	4	2	5	3	2	4755.1159	0.0033
6	3	3	5	2	3	4796.5815	0.0022
6	2	4	5	1	4	4871.8035	0.0043
6	3	4	5	2	4	4882.8716	0.0061
6	1	5	5	0	5	4892.2438	0.0089
6	4	3	5	3	3	4897.8148	-0.0021
6	5	1	5	4	1	4920.2125	-0.0016
6	5	2	5	4	2	5000.0655	-0.0022
11	1	11	10	1	10	5124.7355	-0.0102
11	0	11	10	0	10	5124.7355	-0.0102
11	1	11	10	0	10	5124.7355	-0.0102
11	0	11	10	1	10	5124.7355	-0.0102
6	6	0	5	5	0	5188.6395	-0.0044
6	6	1	5	5	1	5196.3255	-0.0026
7	4	3	6	3	3	5554.8055	0.0017
12	1	12	11	1	11	5573.9147	-0.0051
12	0	12	11	0	11	5573.9147	-0.0051
12	1	12	11	0	11	5573.9147	-0.0051
12	0	12	11	1	11	5573.9147	-0.0051
7	5	2	6	4	2	5577.3396	0.0016
7	3	4	6	2	4	5655.6812	0.0003
7	2	5	6	1	5	5696.3718	0.0040
7	3	5	6	2	5	5698.4454	0.0041
7	1	6	6	0	6	5709.7104	-0.0026

Appendix IV

7	2	6	6	1	6	5709.7524	-0.0135
7	5	3	6	4	3	5727.0221	0.0014
7	6	1	6	5	1	5812.9519	-0.0036
7	6	2	6	5	2	5865.1933	-0.0016
7	7	0	6	6	0	6076.1805	0.0125
7	7	1	6	6	1	6079.3542	-0.0011
8	5	3	7	4	3	6325.5100	0.0020
8	4	4	7	3	4	6420.1439	0.0004
8	6	2	7	5	2	6431.8154	0.0016
8	3	5	7	2	5	6493.1707	0.0048
8	5	4	7	4	4	6498.6966	0.0034
8	4	5	7	3	5	6500.9974	-0.0028
8	2	6	7	1	6	6515.9062	0.0050
8	1	7	7	0	7	6526.8575	0.0048
8	2	7	7	1	7	6526.8575	-0.0019
8	6	3	7	5	3	6567.6602	-0.0016
8	7	1	7	6	1	6709.9314	0.0037
8	7	2	7	6	2	6738.4726	0.0030
8	8	0	7	7	0	6962.3166	-0.0048
8	8	1	7	7	1	6963.5765	0.0084
9	6	3	8	5	3	7121.8374	-0.0091
9	5	4	8	4	4	7168.6484	-0.0158
9	4	5	8	3	5	7278.4180	-0.0036
9	5	5	8	4	5	7301.7224	0.0097
9	6	4	8	5	4	7315.2599	-0.0066
9	7	2	8	6	2	7316.4779	0.0026
9	3	6	8	2	6	7317.6719	0.0095
9	7	3	8	6	3	7420.3925	0.0092
9	8	1	8	7	1	7603.5940	0.0030
9	9	0	8	8	0	7847.8221	0.0012
9	9	1	8	8	1	7848.2769	-0.0126

Table S7.19. Measured frequencies and residuals (in MHz) for the rotational transitions of the conformer **3h** of muscone.

J'	K'_{-1}	K'_{+1}	J''	K''_{-1}	K''_{+1}	V _{obs}	V _{obs} - V _{calc}
4	2	3	3	2	2	2394.2497	0.0001
3	2	1	2	1	1	2450.3158	-0.0004
4	1	3	3	1	2	2462.3950	-0.0029
3	1	2	2	0	2	2472.0232	0.0007
4	2	3	3	1	2	2487.0130	-0.0025
3	2	2	2	1	2	2544.5274	0.0068
3	3	1	2	2	0	2562.8963	-0.0035
4	3	2	3	3	1	2605.8537	-0.0052
3	3	0	2	2	0	2617.0170	-0.0012
3	3	1	2	2	1	2665.0271	-0.0004
4	2	2	3	2	1	2799.3797	-0.0024
5	1	4	4	2	3	2880.9109	0.0014
5	2	4	4	2	3	2885.7386	-0.0062
5	1	4	4	1	3	2905.5254	-0.0016
5	2	4	4	1	3	2910.3647	0.0024
6	1	6	5	1	5	2983.9257	0.0263
6	0	6	5	0	5	2983.9257	-0.0393
6	1	6	5	0	5	2983.9257	-0.0489
6	0	6	5	1	5	2983.9257	0.0358
4	3	2	3	2	1	3038.9735	-0.0038
5	2	3	4	3	2	3097.3471	-0.0040
5	3	3	4	3	2	3186.3534	-0.0025
4	2	2	3	1	2	3261.9302	-0.0003
4	3	1	3	2	1	3299.8283	-0.0032
5	4	2	4	4	1	3321.3235	-0.0114
4	1	3	3	0	3	3339.9469	-0.0011
6	1	5	5	2	4	3357.5672	0.0001
6	2	5	5	2	4	3358.3739	0.0007
4	2	3	3	1	3	3360.8746	0.0039
6	1	5	5	1	4	3362.4008	-0.0016
6	2	5	5	1	4	3363.2111	0.0027
4	3	2	3	2	2	3408.7596	-0.0003
5	3	3	4	2	2	3425.9499	-0.0012
7	1	7	6	1	6	3449.9479	0.0054
7	0	7	6	0	6	3449.9479	-0.0030
7	1	7	6	0	6	3449.9479	-0.0041
7	0	7	6	1	6	3449.9479	0.0066
4	4	1	3	3	0	3516.0003	0.0031
4	4	0	3	3	0	3540.0776	0.0030
4	4	1	3	3	1	3570.1145	-0.0011
4	4	0	3	3	1	3594.1925	-0.0005
6	3	4	5	3	3	3710.3587	0.0030
6	2	4	5	2	3	3776.5286	-0.0233
6	3	4	5	2	3	3799.3629	0.0024
7	1	6	6	2	5	3825.3866	0.0075
7	2	6	6	1	5	3826.3004	-0.0063
8	1	8	7	1	7	3915.9742	0.0010
8	0	8	7	0	7	3915.9742	0.0000
8	1	8	7	0	7	3915.9742	-0.0002
8	0	8	7	1	7	3915.9742	0.0011
6	4	3	5	4	2	3949.9817	0.0072
5	4	2	4	3	1	4024.7322	-0.0052
5	3	2	4	2	2	4062.7560	0.0205
5	2	3	4	1	3	4136.4775	-0.0014
5	1	4	4	0	4	4191.8503	0.0009
7	2	5	6	3	4	4192.2671	0.0015
5	2	4	4	1	4	4196.1334	0.0034
7	3	5	6	3	4	4196.9052	-0.0053
5	3	3	4	2	3	4200.8648	-0.0014
7	2	5	6	2	4	4215.0832	0.0090

7	3	5	6	2	4	4219.7183	-0.0008
5	4	2	4	3	2	4285.5941	0.0026
8	1	7	7	2	6	4291.5379	0.0056
8	2	7	7	2	6	4291.5379	-0.0115
8	1	7	7	1	6	4291.6808	0.0270
8	2	7	7	1	6	4291.6808	0.0099
9	1	9	8	1	8	4382.0063	-0.0002
9	0	9	8	0	8	4382.0063	-0.0003
9	1	9	8	0	8	4382.0063	-0.0003
9	0	9	8	1	8	4382.0063	-0.0002
6	4	3	5	3	2	4412.4319	0.0061
7	3	4	6	4	3	4441.1515	0.0043
5	5	0	4	4	0	4467.9940	-0.0012
5	5	1	4	4	1	4482.5099	-0.0014
7	4	4	6	4	3	4516.8038	0.0141
8	2	6	7	3	5	4666.8448	0.0036
8	3	6	7	3	5	4667.6652	0.0005
8	2	6	7	2	5	4671.4929	0.0068
8	3	6	7	2	5	4672.3160	0.0063
7	4	4	6	3	3	4742.0161	0.0053
9	1	8	8	2	7	4757.4903	0.0150
9	2	8	8	1	7	4757.4903	-0.0044
9	1	8	8	1	7	4757.4903	-0.0021
9	2	8	8	2	7	4757.4903	0.0127
10	1	10	9	1	9	4848.0424	0.0002
10	0	10	9	0	9	4848.0424	0.0002
10	1	10	9	0	9	4848.0424	0.0002
10	0	10	9	1	9	4848.0424	0.0002
6	4	2	5	3	2	4889.2263	0.0012
6	3	3	5	2	3	4912.9874	-0.0063
6	2	4	5	1	4	5007.5043	0.0005
8	3	5	7	4	4	5010.1119	0.0116
6	3	4	5	2	4	5025.4735	-0.0037
6	4	3	5	3	3	5049.2132	0.0031
6	5	1	5	4	1	5099.6213	0.0006
8	4	5	7	3	4	5104.6422	0.0060
9	2	7	8	3	6	5133.9509	0.0070
9	2	7	8	2	6	5134.7372	-0.0303
9	3	7	8	2	6	5134.8898	-0.0106
6	5	2	5	4	2	5175.6733	0.0021
10	1	9	9	2	8	5223.4349	0.0078
10	2	9	9	1	8	5223.4349	0.0052
10	1	9	9	1	8	5223.4349	0.0055
10	2	9	9	2	8	5223.4349	0.0075
11	1	11	10	1	10	5314.0823	0.0032
11	0	11	10	0	10	5314.0823	0.0032
11	1	11	10	0	10	5314.0823	0.0032
11	0	11	10	1	10	5314.0823	0.0032
6	6	0	5	5	0	5393.4539	0.0015
6	6	1	5	5	1	5399.4742	-0.0033
9	3	6	8	4	5	5505.5379	-0.0005
9	4	6	8	4	5	5509.4554	-0.0135
9	4	6	8	3	5	5528.3622	0.0000
10	3	8	9	3	7	5599.7527	0.0003
10	2	8	9	3	7	5599.7527	0.0204
11	1	10	10	2	9	5689.4078	0.0038
11	2	10	10	1	9	5689.4078	0.0035
11	1	10	10	1	9	5689.4078	0.0036
11	2	10	10	2	9	5689.4078	0.0038
7	4	3	6	3	3	5690.1779	0.0003
7	5	2	6	4	2	5751.1589	0.0037
12	1	12	11	1	11	5780.1240	0.0076
12	0	12	11	0	11	5780.1240	0.0076
12	1	12	11	0	11	5780.1240	0.0076
12	0	12	11	1	11	5780.1240	0.0076

7	3	4	6	2	4	5802.8136	0.0035
7	4	4	6	3	4	5855.6480	0.0040
7	2	5	6	1	5	5860.1740	-0.0016
7	3	5	6	2	5	5864.0152	0.0007
7	1	6	6	0	6	5878.2812	-0.0022
7	2	6	6	1	6	5878.3894	-0.0059
7	5	3	6	4	3	5910.0921	-0.0007
10	3	7	9	4	6	5977.1588	-0.0008
7	6	1	6	5	1	6032.9551	0.0039
11	3	9	10	2	8	6065.4522	-0.0090
11	2	9	10	3	8	6065.4522	0.0140
11	2	9	10	2	8	6065.4522	-0.0061
11	3	9	10	3	8	6065.4522	0.0111
7	6	2	6	5	2	6077.5343	0.0021
13	1	13	12	1	12	6246.1373	-0.0162
13	0	13	12	0	12	6246.1373	-0.0162
13	1	13	12	0	12	6246.1373	-0.0162
13	0	13	12	1	12	6246.1373	-0.0162
7	7	0	6	6	0	6316.5062	-0.0013
7	7	1	6	6	1	6318.7988	0.0026
8	5	3	7	4	3	6490.4415	-0.0019
12	3	10	11	2	9	6531.2004	-0.0275
12	2	10	11	3	9	6531.2004	-0.0242
12	2	10	11	2	9	6531.2004	-0.0271
12	3	10	11	3	9	6531.2004	-0.0246
8	4	4	7	3	4	6574.3207	-0.0022
13	1	12	12	2	11	6621.4164	0.0122
13	2	12	12	1	11	6621.4164	0.0122
13	1	12	12	1	11	6621.4164	0.0122
13	2	12	12	2	11	6621.4164	0.0122
8	6	2	7	5	2	6653.2410	-0.0094
8	3	5	7	2	5	6673.4779	-0.0009
8	4	5	7	3	5	6687.7242	-0.0030
8	5	4	7	4	4	6691.7043	0.0023
8	2	6	7	1	6	6705.4778	0.0012
8	1	7	7	0	7	6719.9765	-0.0098
8	2	7	7	1	7	6719.9765	-0.0257
8	6	3	7	5	3	6785.7065	-0.0053
8	7	2	7	6	2	6988.1523	-0.0055
8	8	0	7	7	0	7238.3254	-0.0049
8	8	1	7	7	1	7239.1603	0.0080
9	6	3	8	5	3	7327.1222	0.0008
9	5	4	8	4	4	7334.3467	0.0053
14	3	12	13	2	11	7462.9931	0.0064
14	2	12	13	3	11	7462.9931	0.0064
14	2	12	13	2	11	7462.9931	0.0064
14	3	12	13	3	11	7462.9931	0.0064
9	4	5	8	3	5	7469.4531	-0.0050
9	3	6	8	2	6	7526.4009	-0.0235
9	4	6	8	3	6	7529.5337	0.0024
9	6	4	8	5	4	7538.7409	0.0042
9	2	7	8	1	7	7548.5953	0.0051
9	3	7	8	2	7	7548.7271	0.0210
9	1	8	8	0	8	7561.5089	0.0044
9	2	8	8	1	8	7561.5089	0.0022
9	7	2	8	6	2	7585.6146	-0.0040
9	7	3	8	6	3	7675.9008	0.0079
9	8	1	8	7	1	7894.7039	-0.0001

Table S7.20. Measured frequencies and residuals (in MHz) for the rotational transitions of the conformer **18j** of muscone.

J'	K'_{-1}	K'_{+1}	J''	K''_{-1}	K''_{+1}	V _{obs}	V _{obs} - V _{calc}
3	2	1	2	1	1	2385.9355	-0.0037
3	1	2	2	0	2	2406.9990	0.0120
3	2	2	2	1	2	2479.0209	0.0119
3	3	0	2	2	0	2551.0274	-0.0012
3	3	1	2	2	1	2598.2379	-0.0084
4	2	2	3	1	2	3175.6810	0.0013
4	3	1	3	2	1	3213.8651	-0.0002
4	1	3	3	0	3	3252.8184	0.0031
4	2	3	3	1	3	3273.7379	0.0025
4	4	0	3	3	0	3451.5432	0.0011
4	4	1	3	3	1	3480.9482	-0.0015
5	2	3	4	1	3	4027.7438	-0.0031
5	4	1	4	3	1	4075.2177	-0.0058
5	1	4	4	0	4	4082.8792	-0.0062
5	2	4	4	1	4	4087.1908	-0.0019
5	3	3	4	2	3	4092.0232	-0.0011
5	5	0	4	4	0	4356.7312	-0.0015
5	5	1	4	4	1	4370.8703	-0.0037
6	4	2	5	3	2	4760.7364	-0.0009
6	3	3	5	2	3	4783.0091	-0.0027
6	2	4	5	1	4	4876.7843	-0.0025
6	3	4	5	2	4	4894.8546	-0.0015
6	4	3	5	3	3	4918.6617	-0.0031
6	5	1	5	4	1	4969.6836	-0.0019
6	5	2	5	4	2	5044.1322	0.0078
6	6	0	5	5	0	5259.4499	-0.0021
6	6	1	5	5	1	5265.2930	-0.0016
7	4	3	6	3	3	5539.3590	0.0001
7	5	2	6	4	2	5601.3712	-0.0016
7	3	4	6	2	4	5650.3843	0.0013
7	4	4	6	3	4	5703.4081	0.0013
7	2	5	6	1	5	5707.6648	0.0022
7	3	5	6	2	5	5711.5398	-0.0075
7	5	3	6	4	3	5757.8045	0.0028
7	6	1	6	5	1	5880.3443	-0.0030
7	6	2	6	5	2	5923.7534	0.0118
7	7	0	6	6	0	6159.8099	0.0018
7	7	1	6	6	1	6162.0197	0.0019
8	5	3	7	4	3	6318.9462	0.0056
8	4	4	7	3	4	6400.4533	0.0111
8	6	2	7	5	2	6481.8182	0.0010
8	3	5	7	2	5	6499.1900	-0.0097
8	5	4	7	4	4	6517.9132	0.0068
8	3	6	7	2	6	6531.8794	-0.0034
8	6	3	7	5	3	6611.5871	0.0066
8	7	1	7	6	1	6790.8130	-0.0028
8	8	0	7	7	0	7058.9691	0.0095
8	8	1	7	7	1	7059.7428	-0.0070
9	6	3	8	5	3	7134.8547	-0.0027
9	5	4	8	4	4	7139.5665	-0.0177
9	4	5	8	3	5	7273.3923	0.0066
9	5	5	8	4	5	7314.8494	-0.0053
9	3	6	8	2	6	7330.3790	0.0071
9	4	6	8	3	6	7333.5348	0.0009
9	6	4	8	5	4	7343.4062	0.0072
9	1	8	8	0	8	7365.3352	-0.0015
9	2	8	8	1	8	7365.3352	-0.0037
9	7	2	8	6	2	7391.8753	-0.0011
9	7	3	8	6	3	7479.7861	0.0084
9	8	1	8	7	1	7696.3770	-0.0129

Table S7.21. Measured frequencies and residuals (in MHz) for the rotational transitions of the conformer **24g** of muscone.

J'	K'_{-1}	K'_{+1}	J''	K''_{-1}	K''_{+1}	V _{obs}	V _{obs} - V _{calc}
3	2	1	2	1	1	2338.5091	-0.0018
4	2	3	3	1	2	2374.0926	0.0018
3	3	0	2	2	0	2519.9081	-0.0004
3	3	1	2	2	1	2566.7665	0.0011
5	1	4	4	2	3	2728.5899	0.0018
5	2	4	4	1	3	2766.2691	-0.0045
4	2	2	3	1	2	3104.9119	-0.0003
4	3	1	3	2	1	3156.8999	0.0002
6	1	5	5	2	4	3181.4625	0.0023
4	1	3	3	0	3	3187.1947	-0.0088
6	2	5	5	1	4	3189.3673	-0.0106
4	2	3	3	1	3	3213.4943	-0.0015
7	1	7	6	0	6	3258.3818	-0.0107
7	0	7	6	1	6	3258.3818	0.0074
4	3	2	3	2	2	3268.4059	-0.0003
4	4	0	3	3	0	3413.9686	0.0015
4	4	1	3	3	1	3441.2147	0.0020
7	1	6	6	2	5	3623.4190	0.0007
7	2	6	6	1	5	3624.8452	0.0007
8	1	8	7	0	7	3697.7688	-0.0088
8	0	8	7	1	7	3697.7688	-0.0064
5	3	2	4	2	2	3870.8656	-0.0008
5	2	3	4	1	3	3939.1566	-0.0004
5	1	4	4	0	4	4004.4022	0.0122
5	2	4	4	1	4	4010.3099	-0.0008
5	4	1	4	3	1	4014.0162	-0.0006
5	3	3	4	2	3	4017.9858	-0.0018
5	4	2	4	3	2	4113.9386	-0.0041
9	1	9	8	0	8	4137.1607	-0.0166
9	0	9	8	1	8	4137.1607	-0.0162
5	5	0	4	4	0	4311.1202	0.0035
5	5	1	4	4	1	4323.3302	0.0026
9	1	8	8	2	7	4502.4579	0.0471
9	2	8	8	1	7	4502.4579	0.0114
10	1	10	9	0	9	4576.5705	-0.0116
10	0	10	9	1	9	4576.5705	-0.0116
6	4	2	5	3	2	4667.9972	-0.0018
6	3	3	5	2	3	4672.5538	-0.0022
6	2	4	5	1	4	4777.4016	-0.0004
6	3	4	5	2	4	4801.8839	0.0002
6	1	5	5	0	5	4812.5498	0.0012
6	2	5	5	1	5	4813.6602	0.0022
6	4	3	5	3	3	4833.0003	-0.0006
6	5	1	5	4	1	4905.5757	-0.0027
10	1	9	9	2	8	4941.7397	0.0180
10	2	9	9	1	8	4941.7397	0.0128
6	5	2	5	4	2	4974.1753	-0.0010
6	6	0	5	5	0	5205.2187	0.0083
6	6	1	5	5	1	5209.9337	0.0031
11	1	10	10	2	9	5381.0546	-0.0042
11	2	10	10	1	9	5381.0546	-0.0049
7	4	3	6	3	3	5413.8871	-0.0044
7	5	2	6	4	2	5506.8606	0.0001
7	3	4	6	2	4	5525.8447	0.0006
7	4	4	6	3	4	5595.7270	-0.0025
7	2	5	6	1	5	5596.2489	0.0015
7	3	5	6	2	5	5602.0248	0.0078
7	1	6	6	0	6	5618.1412	0.0057
7	2	6	6	1	6	5618.3187	-0.0030
7	5	3	6	4	3	5662.9568	0.0009

Appendix IV

7	6	1	6	5	1	5809.9566	-0.0012
7	6	2	6	5	2	5846.8446	-0.0007
7	7	0	6	6	0	6096.9886	-0.0146
7	7	1	6	6	1	6098.6824	0.0042
8	5	3	7	4	3	6186.3443	0.0019
8	4	4	7	3	4	6249.8160	-0.0019
8	3	5	7	2	5	6366.0375	-0.0006
8	4	5	7	3	5	6387.0915	0.0005
8	6	2	7	5	2	6389.1011	-0.0006
8	5	4	7	4	4	6397.9820	0.0023
8	2	6	7	1	6	6405.8632	0.0056
8	3	6	7	2	6	6407.0190	0.0019
8	1	7	7	0	7	6423.0504	0.0146
8	2	7	7	1	7	6423.0504	-0.0144
8	6	3	7	5	3	6509.6538	-0.0018
8	7	1	7	6	1	6711.4851	-0.0037
8	7	2	7	6	2	6728.1530	-0.0112
9	5	4	8	4	4	6970.1170	-0.0074
8	8	0	7	7	0	6987.7420	0.0047
8	8	1	7	7	1	6988.3024	0.0023
9	6	3	8	5	3	7002.8102	-0.0079
9	4	5	8	3	5	7113.7194	0.0005
9	5	5	8	4	5	7172.6427	-0.0055
9	3	6	8	2	6	7185.7331	-0.0004
9	4	6	8	3	6	7190.8074	0.0011
9	2	7	8	1	7	7212.5494	0.0093
9	3	7	8	2	7	7212.7473	-0.0029
9	6	4	8	5	4	7214.1936	-0.0024
9	1	8	8	0	8	7227.7079	0.0075
9	2	8	8	1	8	7227.7079	0.0032
9	7	2	8	6	2	7297.3072	-0.0039
9	7	3	8	6	3	7372.0055	-0.0028
9	8	1	8	7	1	7607.7089	0.0007
9	8	2	8	7	2	7614.4602	-0.0009
10	6	4	9	5	4	7715.9445	0.0108
10	5	5	9	4	5	7834.3146	-0.0035
10	7	3	9	6	3	7868.8724	-0.0011
9	9	0	8	8	0	7878.0481	-0.0041
9	9	1	8	8	1	7878.2437	0.0094
10	6	5	9	5	5	7964.3596	0.0169
10	5	6	9	4	6	7970.7318	0.0037
10	3	7	9	2	7	7996.6308	-0.0224

Table S7.22. Measured frequencies and residuals (in MHz) for the rotational transitions of the conformer **15h** of muscone.

J'	K'_{-1}	K'_{+1}	J''	K''_{-1}	K''_{+1}	V _{obs}	V _{obs} - V _{calc}
3	2	1	2	1	1	2353.2760	0.0024
3	1	2	2	0	2	2369.4829	-0.0064
3	3	0	2	2	0	2535.4592	-0.0037
3	3	1	2	2	1	2582.5282	-0.0010
4	2	2	3	1	2	3124.5458	-0.0012
4	3	1	3	2	1	3176.7505	0.0008
4	2	3	3	1	3	3233.6052	0.0027
4	3	2	3	2	2	3288.7495	0.0007
4	4	0	3	3	0	3434.9540	0.0095
4	4	1	3	3	1	3462.3171	0.0032
5	3	2	4	2	2	3895.3590	-0.0007
5	1	4	4	0	4	4029.4869	0.0134
5	3	3	4	2	3	4043.1227	-0.0016
5	4	2	4	3	2	4139.4933	-0.0001
5	5	0	4	4	0	4337.5363	0.0024
5	5	1	4	4	1	4349.8028	0.0016
6	4	2	5	3	2	4697.4820	-0.0009
6	3	3	5	2	3	4702.0849	-0.0001
6	2	4	5	1	4	4807.3876	0.0013
6	3	4	5	2	4	4831.9688	0.0020
6	1	5	5	0	5	4842.6798	-0.0009
6	2	5	5	1	5	4843.7874	-0.0070
6	4	3	5	3	3	4863.2034	-0.0081
6	5	1	5	4	1	4936.0931	0.0041
6	5	2	5	4	2	5005.0055	0.0062
6	6	0	5	5	0	5237.0539	-0.0022
6	6	1	5	5	1	5241.7956	-0.0028
7	5	2	6	4	2	5541.5063	-0.0060
7	3	4	6	2	4	5560.6213	-0.0053
7	4	4	6	3	4	5630.7854	-0.0109
7	2	5	6	1	5	5631.3299	0.0043
7	3	5	6	2	5	5637.1205	0.0033
7	2	6	6	1	6	5653.5023	0.0091
7	5	3	6	4	3	5698.3140	0.0099
7	6	1	6	5	1	5845.9301	-0.0074
7	6	2	6	5	2	5882.9955	-0.0008
7	7	0	6	6	0	6134.2653	-0.0039
7	7	1	6	6	1	6135.9572	0.0051
8	5	3	7	4	3	6225.5065	0.0053
8	4	4	7	3	4	6289.2829	-0.0081
8	4	5	7	3	5	6427.1439	0.0038
8	6	2	7	5	2	6429.1069	-0.0036
8	5	4	7	4	4	6438.0675	0.0036
8	3	6	7	2	6	6447.1442	-0.0112
8	1	7	7	0	7	6463.2427	-0.0008
8	7	1	7	6	1	6752.9143	-0.0149
8	7	2	7	6	2	6769.6827	-0.0007
9	4	5	8	3	5	7158.4868	-0.0014
9	5	5	8	4	5	7217.6568	0.0108
9	6	4	8	5	4	7259.3557	0.0004
9	7	2	8	6	2	7342.8022	0.0033
9	7	3	8	6	3	7417.8505	0.0057

Table S7.23. Measured frequencies and residuals (in MHz) for the rotational transitions of the conformer **7d** of muscone.

J'	K' ₋₁	K' ₊₁	J''	K'' ₋₁	K'' ₊₁	V _{obs}	V _{obs} - V _{calc}
3	2	1	2	1	1	2485.8642	0.0066
3	1	2	2	0	2	2499.7194	0.0072
3	2	2	2	1	2	2588.5161	0.0043
3	3	0	2	2	0	2677.3144	0.0032
3	3	1	2	2	1	2724.5403	0.0074
4	2	2	3	1	2	3297.6246	0.0073
4	3	1	3	2	1	3356.9927	0.0044
4	2	3	3	1	3	3412.4420	-0.0096
4	3	2	3	2	2	3471.6312	0.0028
4	4	0	3	3	0	3626.2558	-0.0022
4	4	1	3	3	1	3652.8777	-0.0004
5	3	2	4	2	2	4113.7009	0.0066
5	2	3	4	1	3	4180.3016	-0.0014
5	1	4	4	0	4	4251.2228	-0.0034
5	3	3	4	2	3	4267.3808	0.0017
5	4	1	4	3	1	4269.8014	0.0032
5	4	2	4	3	2	4370.2509	0.0001
5	5	0	4	4	0	4577.6163	0.0036
5	5	1	4	4	1	4589.1780	0.0021
6	3	3	5	2	3	4959.6972	-0.0145
6	4	2	5	3	2	4964.0775	0.0000
6	2	4	5	1	4	5070.5924	0.0096
6	3	4	5	2	4	5098.8251	0.0006
6	2	5	5	1	5	5110.9263	-0.0103
6	5	1	5	4	1	5217.7546	-0.0006
6	6	0	5	5	0	5525.6502	-0.0084
6	6	1	5	5	1	5529.9912	-0.0072
7	4	3	6	3	3	5750.6301	-0.0042
7	5	2	6	4	2	5859.7604	-0.0052
7	3	4	6	2	4	5863.0766	0.0037
7	2	5	6	1	5	5940.9160	0.0096
7	4	4	6	3	4	5942.5911	-0.0067
7	3	5	6	2	5	5947.8391	0.0057
7	5	3	6	4	3	6017.0105	0.0096
7	6	1	6	5	1	6176.9878	-0.0004
7	6	2	6	5	2	6211.6014	0.0041
7	7	0	6	6	0	6471.4228	0.0043
7	7	1	6	6	1	6472.9056	-0.0098
8	5	3	7	4	3	6576.7780	-0.0086
8	4	4	7	3	4	6630.9943	-0.0085
8	3	5	7	2	5	6756.4791	-0.0083
8	4	5	7	3	5	6781.5518	-0.0086
8	5	4	7	4	4	6796.1269	-0.0030
8	2	6	7	1	6	6800.9561	0.0002
8	8	0	7	7	0	7416.1743	0.0058
9	6	3	8	5	3	7451.1741	0.0042
9	4	5	8	3	5	7547.3536	0.0185

Table S7.24. Measured frequencies and residuals (in MHz) for the rotational transitions of the conformer **14g** of muscone.

J'	K' ₋₁	K' ₊₁	J''	K'' ₋₁	K'' ₊₁	V _{obs}	V _{obs} - V _{calc}
4	1	3	3	2	2	2301.4224	0.0000
4	1	3	3	2	2	2301.4224	0.0000
3	2	1	2	1	1	2433.7002	-0.0145
5	0	5	4	1	4	2459.1772	0.0010
5	1	5	4	0	4	2460.5995	0.0018
4	2	3	3	1	2	2479.0209	0.0035
4	2	3	3	1	2	2479.0209	0.0035
3	3	1	2	2	0	2608.2046	0.0011
3	3	0	2	2	0	2650.6739	0.0002
3	3	1	2	2	1	2699.7824	0.0077
3	3	0	2	2	1	2742.2486	0.0037
5	1	4	4	2	3	2821.4212	0.0024
5	1	4	4	2	3	2821.4212	0.0024
5	2	4	4	1	3	2875.4424	-0.0058
5	2	4	4	1	3	2875.4424	-0.0058
4	3	2	3	2	1	3076.1459	-0.0042
4	2	2	3	1	2	3219.9632	0.0054
6	1	5	5	2	4	3293.9226	0.0055
6	1	5	5	2	4	3293.9226	0.0055
4	3	1	3	2	1	3296.2648	0.0040
6	2	5	5	1	4	3306.5182	-0.0011
6	2	5	5	1	4	3306.5182	-0.0011
4	2	3	3	1	3	3350.2930	-0.0091
4	3	2	3	2	2	3419.9265	0.0154
5	3	3	4	2	2	3450.3956	-0.0017
4	4	1	3	3	0	3580.6154	0.0031
6	2	4	5	3	3	3594.6566	-0.0115
4	4	0	3	3	0	3596.9276	-0.0182
4	4	1	3	3	1	3623.0789	-0.0036
4	4	0	3	3	1	3639.4191	0.0031
4	3	1	3	2	2	3640.0229	0.0011
7	1	6	6	2	5	3751.4695	-0.0061
7	1	6	6	2	5	3751.4695	-0.0061
7	2	6	6	1	5	3753.9944	0.0033
7	2	6	6	1	5	3753.9944	0.0033
6	3	4	5	2	3	3792.9003	0.0080
8	1	8	7	0	7	3820.0337	-0.0012
8	0	8	7	1	7	3820.0337	0.0040
5	3	2	4	2	2	4020.7622	0.0017
7	2	5	6	3	4	4115.4260	0.0002
5	1	4	4	0	4	4169.0062	0.0000
7	3	5	6	2	4	4175.3558	0.0010
5	3	3	4	2	3	4191.3409	0.0032
8	1	7	7	2	6	4205.4944	-0.0012
8	1	7	7	2	6	4205.4944	-0.0012
8	2	7	7	1	6	4205.9490	-0.0022
8	2	7	7	1	6	4205.9490	-0.0022
5	4	1	4	3	1	4207.4524	0.0062
9	0	9	8	1	8	4273.4544	0.0011
9	1	9	8	0	8	4273.4544	0.0004
5	4	1	4	3	2	4427.5597	0.0028
6	4	3	5	3	2	4476.6174	0.0003
5	5	1	4	4	0	4538.7631	0.0024
5	5	0	4	4	0	4544.3751	0.0027
5	5	1	4	4	1	4555.0999	0.0057
5	5	0	4	4	1	4560.7068	0.0009
8	2	6	7	3	5	4587.8496	-0.0040
8	3	6	7	2	5	4602.4494	-0.0072
9	1	8	8	2	7	4658.9215	0.0468
9	2	8	8	1	7	4658.9215	-0.0304

9	1	8	8	2	7	4658.9232	0.0485
9	2	8	8	1	7	4658.9232	-0.0287
10	0	10	9	1	9	4726.8831	0.0031
10	1	10	9	0	9	4726.8831	0.0030
7	4	4	6	3	3	4783.9197	0.0017
6	3	3	5	2	3	4839.7050	0.0010
6	4	2	5	3	2	4863.3571	0.0047
6	2	4	5	1	4	4964.5880	0.0010
6	3	4	5	2	4	5002.0468	0.0118
6	2	5	5	1	5	5014.9262	-0.0017
9	2	7	8	3	6	5045.1005	-0.0143
6	4	3	5	3	3	5046.9828	0.0024
9	3	7	8	2	6	5048.2335	0.0101
6	5	2	5	4	1	5103.8281	-0.0016
10	1	9	9	2	8	5112.1966	0.0041
10	2	9	9	1	8	5112.1966	-0.0084
10	1	9	9	2	8	5112.1966	0.0041
10	2	9	9	1	8	5112.1966	-0.0084
6	5	1	5	4	1	5155.4820	-0.0123
11	0	11	10	1	10	5180.3067	-0.0026
11	1	11	10	0	10	5180.3067	-0.0026
6	5	2	5	4	2	5220.2227	0.0035
6	5	1	5	4	2	5271.8821	-0.0017
6	6	1	5	5	0	5486.1953	0.0018
6	6	0	5	5	0	5487.9890	-0.0037
6	6	1	5	5	1	5491.8032	-0.0019
6	6	0	5	5	1	5493.6108	0.0065
10	2	8	9	3	7	5498.7693	0.0046
11	1	10	10	2	9	5565.5377	0.0030
11	2	10	10	1	9	5565.5377	0.0010
11	1	10	10	2	9	5565.5377	0.0030
11	2	10	10	1	9	5565.5377	0.0010
7	4	3	6	3	3	5614.2304	0.0048
12	0	12	11	1	11	5633.7391	-0.0010
12	1	12	11	0	11	5633.7391	-0.0010
7	5	2	6	4	2	5759.6326	0.0133
7	2	5	6	1	5	5823.5396	-0.0042
7	4	4	6	3	4	5830.7359	0.0062
7	3	5	6	2	5	5833.4251	0.0026
8	5	4	7	4	3	5842.0524	-0.0001
7	5	3	6	4	3	5922.1474	-0.0034
11	2	9	10	3	8	5951.8130	-0.0101
12	1	11	11	2	10	6018.8874	-0.0153
12	2	11	11	1	10	6018.8874	-0.0156
12	1	11	11	2	10	6018.8886	-0.0141
12	2	11	11	1	10	6018.8886	-0.0144
13	0	13	12	1	12	6087.1627	-0.0091
13	1	13	12	0	12	6087.1627	-0.0091
7	6	2	6	5	1	6091.7258	-0.0026
9	5	5	8	4	4	6096.5221	-0.0055
7	6	1	6	5	1	6111.9379	-0.0101
7	6	2	6	5	2	6143.3998	0.0068
7	5	2	6	4	3	6146.3392	-0.0155
7	6	1	6	5	2	6163.6144	0.0018
12	2	10	11	3	9	6404.9083	0.0109
7	7	1	6	6	0	6428.7730	0.0029
7	7	0	6	6	0	6429.3012	-0.0197
7	7	1	6	6	1	6430.5794	0.0101
7	7	0	6	6	1	6431.1187	-0.0014
8	5	3	7	4	3	6433.3315	0.0155
8	4	4	7	3	4	6467.5942	-0.0064
13	1	12	12	2	11	6472.3055	0.0168
13	2	12	12	1	11	6472.3055	0.0167
13	1	12	12	2	11	6472.3056	0.0169
13	2	12	12	1	11	6472.3056	0.0168

Appendix IV

14	0	14	13	1	13	6540.6014	-0.0023
14	1	14	13	0	13	6540.6014	-0.0023
8	6	3	7	5	2	6593.7790	-0.0040
8	3	5	7	2	5	6613.9041	-0.0043
8	4	5	7	3	5	6649.0792	-0.0004
8	2	6	7	1	6	6669.7904	-0.0100
8	3	6	7	2	6	6672.0139	0.0046
8	5	4	7	4	4	6672.3583	-0.0018
8	6	2	7	5	2	6704.3559	-0.0103
8	7	1	7	6	2	7082.8727	-0.0005
9	5	4	8	4	4	7216.9605	0.0037
8	8	1	7	7	0	7369.5519	0.0072
8	8	0	7	7	1	7370.2616	0.0029
9	5	5	8	4	5	7467.8182	0.0032
9	3	6	8	2	6	7475.0547	-0.0039
9	2	8	8	1	8	7531.4496	-0.0080
9	6	4	8	5	4	7533.2962	0.0012

Table S7.25. Measured frequencies and residuals (in MHz) for the rotational transitions of the conformer **12i** of muscone.

J'	K'_{-1}	K'_{+1}	J''	K''_{-1}	K''_{+1}	V _{obs}	V _{obs} - V _{calc}
3	2	1	2	1	1	2393.5571	-0.0046
3	1	2	2	0	2	2398.7123	-0.0124
3	2	2	2	1	2	2506.2731	0.0096
3	3	0	2	2	0	2613.8051	0.0027
3	3	1	2	2	1	2660.8062	0.0017
4	2	2	3	1	2	3162.3093	0.0016
4	3	1	3	2	1	3245.6790	-0.0004
4	1	3	3	0	3	3254.6451	-0.0006
4	2	3	3	1	3	3294.5853	-0.0030
4	3	2	3	2	2	3366.9873	0.0025
4	4	0	3	3	0	3547.7524	-0.0003
4	4	1	3	3	1	3571.8203	0.0021
5	3	2	4	2	2	3952.2135	0.0012
5	2	3	4	1	3	4008.9218	-0.0004
5	1	4	4	0	4	4097.1508	0.0045
5	2	4	4	1	4	4107.6792	0.0295
5	3	3	4	2	3	4122.7496	0.0001
5	4	1	4	3	1	4147.9112	0.0025
5	4	2	4	3	2	4246.5528	0.0011
5	5	0	4	4	0	4481.9433	-0.0003
5	5	1	4	4	1	4491.4442	-0.0001
6	3	3	5	2	3	4750.1038	0.0030
6	4	2	5	3	2	4786.5204	0.0011
6	2	4	5	1	4	4875.4742	-0.0014
6	1	5	5	0	5	4927.6464	-0.0009
6	2	5	5	1	5	4929.9268	-0.0047
6	4	3	5	3	3	4966.6265	0.0033
6	5	1	5	4	1	5085.2388	-0.0020
6	5	2	5	4	2	5144.2192	0.0014
6	6	0	5	5	0	5412.2976	-0.0007
6	6	1	5	5	1	5415.5539	-0.0023
7	4	3	6	3	3	5515.1363	0.0002
7	3	4	6	2	4	5620.5053	0.0005
7	5	2	6	4	2	5676.6018	-0.0062
7	2	5	6	1	5	5722.1165	-0.0026
7	4	4	6	3	4	5733.3932	-0.0405
7	3	5	6	2	5	5733.7540	-0.0029
7	5	3	6	4	3	5830.9943	0.0100
7	6	1	6	5	1	6028.4012	-0.0013
7	6	2	6	5	2	6055.8292	0.0013
8	5	3	7	4	3	6328.3651	-0.0003
7	7	0	6	6	0	6340.5202	-0.0026
7	7	1	6	6	1	6341.5496	-0.0033
8	4	4	7	3	4	6344.5137	0.0058
8	3	5	7	2	5	6494.3853	0.0016
8	4	5	7	3	5	6535.3053	-0.0013
8	2	6	7	1	6	6555.2071	0.0037
8	3	6	7	2	6	6557.9173	-0.0083
8	5	4	7	4	4	6563.7276	-0.0240
8	1	7	7	0	7	6579.3904	0.0309
8	6	2	7	5	2	6613.4130	-0.0008
8	6	3	7	5	3	6716.4846	0.0062
8	7	1	7	6	1	6965.1744	-0.0002
8	7	2	7	6	2	6976.0281	0.0101
9	5	4	8	4	4	7084.9704	0.0062
9	6	3	8	5	3	7202.4344	-0.0154
9	4	5	8	3	5	7233.9420	0.0044
8	8	0	7	7	0	7267.9036	-0.0086
8	8	1	7	7	1	7268.2133	-0.0080
9	5	5	8	4	5	7341.2268	0.0019

Appendix IV

9	3	6	8	2	6	7343.9041	-0.0077
9	4	6	8	3	6	7355.5281	-0.0084
9	2	7	8	1	7	7383.3193	-0.0106
9	3	7	8	2	7	7383.9042	0.0025
9	6	4	8	5	4	7414.7140	0.0107
9	7	2	8	6	2	7565.6167	0.0073
9	7	3	8	6	3	7619.8048	0.0170
9	8	1	8	7	1	7896.6173	0.0057
9	8	2	8	7	2	7900.4889	-0.0019

Table S7.26. Measured frequencies and residuals (in MHz) for the rotational transitions of the conformer **48b** of muscone.

J'	K' ₋₁	K' ₊₁	J''	K'' ₋₁	K'' ₊₁	V _{obs}	V _{obs} - V _{calc}
3	1	2	2	0	2	2287.0193	0.0050
5	1	5	4	1	4	2347.6873	0.0054
5	0	5	4	0	4	2348.7538	-0.0128
3	3	0	2	2	0	2490.0196	0.0016
3	3	1	2	2	1	2534.5496	0.0033
5	2	4	4	2	3	2686.2663	-0.0049
5	1	4	4	1	3	2719.6040	0.0022
6	1	6	5	1	5	2782.5113	-0.0001
6	0	6	5	0	5	2782.6949	-0.0045
5	3	3	4	3	2	2940.6839	0.0103
4	3	1	3	2	1	3093.7694	0.0023
4	1	3	3	0	3	3102.6142	0.0000
5	2	3	4	2	2	3113.4713	0.0108
6	2	5	5	2	4	3131.4690	0.0014
4	2	3	3	1	3	3140.2448	0.0094
4	3	2	3	2	2	3208.5507	-0.0044
7	1	7	6	1	6	3217.0383	0.0185
7	0	7	6	0	6	3217.0383	-0.0119
5	3	2	4	3	1	3252.2420	-0.0030
4	4	0	3	3	0	3379.2891	0.0017
4	4	1	3	3	1	3402.1333	0.0049
7	2	6	6	2	5	3568.4681	-0.0045
7	1	6	6	1	5	3570.3867	-0.0010
6	4	3	5	4	2	3627.8919	0.0002
8	1	8	7	1	7	3651.4795	-0.0027
8	0	8	7	0	7	3651.4795	-0.0074
5	3	2	4	2	2	3768.2830	0.0002
6	3	3	5	3	2	3874.4747	-0.0052
5	1	4	4	0	4	3905.4494	-0.0073
7	3	5	6	3	4	3909.5717	-0.0010
5	3	3	4	2	3	3929.5144	-0.0001
5	4	1	4	3	1	3952.9013	0.0032
8	2	7	7	2	6	4003.2679	-0.0030
8	1	7	7	1	6	4003.6534	0.0113
5	4	2	4	3	2	4046.3781	-0.0031
9	1	9	8	1	8	4085.9553	0.0123
9	0	9	8	0	8	4085.9553	0.0116
5	5	0	4	4	0	4268.8280	0.0043
5	5	1	4	4	1	4277.8599	0.0025
10	1	10	9	1	9	4520.4052	-0.0017
10	0	10	9	0	9	4520.4052	-0.0018
6	3	3	5	2	3	4529.3009	-0.0013
6	4	2	5	3	2	4563.1673	0.0023
7	4	3	6	4	2	4570.0496	-0.0084
8	4	5	7	4	4	4674.1601	0.0029
6	3	4	5	2	4	4687.3690	0.0076
6	4	3	5	3	3	4733.5950	-0.0044
6	5	1	5	4	1	4845.3067	0.0064
6	5	2	5	4	2	4901.3168	0.0106
11	1	11	10	1	10	4954.8743	0.0014
11	0	11	10	0	10	4954.8743	0.0014
6	6	0	5	5	0	5154.7286	-0.0053
6	6	1	5	5	1	5157.8362	-0.0009
9	3	6	8	3	5	5173.7380	-0.0056
10	3	8	9	3	7	5224.9092	0.0056
10	2	8	9	2	7	5225.4073	0.0064
7	4	3	6	3	3	5258.7484	0.0053
7	3	4	6	2	4	5358.7538	-0.0027
7	5	2	6	4	2	5410.6920	-0.0041
7	4	4	6	3	4	5465.0612	0.0047

Appendix IV

7	3	5	6	2	5	5465.4622	-0.0043
7	2	6	6	1	6	5485.0728	-0.0029
7	5	3	6	4	3	5557.0132	0.0013
7	6	1	6	5	1	5743.3274	0.0016
7	6	2	6	5	2	5769.4187	-0.0046
13	1	13	12	1	12	5823.8048	-0.0026
13	0	13	12	0	12	5823.8048	-0.0026
8	5	3	7	4	3	6033.5963	0.0078
7	7	0	6	6	0	6038.6292	0.0058
7	7	1	6	6	1	6039.6096	0.0034
8	4	4	7	3	4	6049.6642	0.0032
8	4	5	7	3	5	6229.6445	0.0036
8	5	4	7	4	4	6256.3141	0.0093
8	6	2	7	5	2	6302.4897	0.0024
8	7	1	7	6	1	6635.3387	0.0036
8	7	2	7	6	2	6645.6794	0.0063
9	5	4	8	4	4	6755.8304	0.0037
9	6	3	8	5	3	6865.8496	0.0000
8	8	0	7	7	0	6921.7372	0.0180
8	8	1	7	7	1	6922.0068	-0.0077
9	5	5	8	4	5	6997.8982	0.0112
9	7	2	8	6	2	7209.0264	-0.0038
9	7	3	8	6	3	7260.6184	0.0055
10	6	4	9	5	4	7507.8221	0.0093
9	8	1	8	7	1	7522.2971	0.0111
10	5	5	9	4	5	7576.4392	-0.0057
9	9	0	8	8	0	7804.5912	0.0558
9	9	1	8	8	1	7804.5912	-0.0298

Table S7.27. Measured frequencies and residuals (in MHz) for the rotational transitions of the conformer **42g** of muscone.

J'	K' ₋₁	K' ₊₁	J''	K'' ₋₁	K'' ₊₁	V _{obs}	V _{obs} - V _{calc}
3	2	1	2	1	1	2317.6133	0.0022
3	1	2	2	0	2	2320.7864	-0.0097
3	2	2	2	1	2	2424.5024	0.0066
3	3	0	2	2	0	2528.2007	0.0053
3	3	1	2	2	1	2571.9895	0.0037
4	2	2	3	1	2	3060.8163	0.0020
4	3	1	3	2	1	3142.9567	-0.0003
4	1	3	3	0	3	3147.9628	0.0007
4	3	2	3	2	2	3257.1943	0.0033
4	4	0	3	3	0	3430.4415	0.0055
4	4	1	3	3	1	3452.4811	0.0043
5	3	2	4	2	2	3826.8695	-0.0055
5	2	3	4	1	3	3877.6696	-0.0139
5	1	4	4	0	4	3963.0326	-0.0031
5	2	4	4	1	4	3973.5791	0.0062
5	3	3	4	2	3	3988.7990	0.0006
5	4	1	4	3	1	4016.4710	0.0019
5	4	2	4	3	2	4108.0636	-0.0035
5	5	0	4	4	0	4332.5495	0.0002
5	5	1	4	4	1	4341.1052	-0.0007
6	3	3	5	2	3	4596.2784	-0.0036
6	4	2	5	3	2	4636.2241	0.0021
6	2	4	5	1	4	4715.3567	-0.0018
6	4	3	5	3	3	4805.7522	0.0019
6	5	2	5	4	2	4976.2501	-0.0020
6	6	0	5	5	0	5231.0172	-0.0014
6	6	1	5	5	1	5233.9047	-0.0019
7	4	3	6	3	3	5339.3806	-0.0019
7	3	4	6	2	4	5435.6228	0.0096
7	5	2	6	4	2	5499.3630	-0.0009
7	2	5	6	1	5	5534.6921	-0.0004
7	3	5	6	2	5	5546.5560	0.0001
7	5	3	6	4	3	5642.5603	0.0027
7	6	1	6	5	1	5833.0796	0.0003
7	6	2	6	5	2	5857.5915	-0.0043
7	7	0	6	6	0	6127.5283	-0.0019
7	7	1	6	6	1	6128.4246	-0.0048
8	5	3	7	4	3	6129.7613	0.0024
8	4	4	7	3	4	6137.3764	0.0039
8	3	5	7	2	5	6280.8710	0.0078
8	4	5	7	3	5	6322.3310	-0.0062
8	2	6	7	1	6	6340.7970	-0.0016
8	5	4	7	4	4	6351.5971	-0.0086
8	6	3	7	5	3	6499.6165	0.0033
8	7	1	7	6	1	6737.3779	0.0044
8	7	2	7	6	2	6746.9019	0.0025
9	5	4	8	4	4	6857.5300	0.0019
9	6	4	8	5	4	7176.0415	0.0021
9	7	2	8	6	2	7325.3123	-0.0037
10	5	5	9	4	5	7684.4283	-0.0012

Table S7.28. Measured frequencies and residuals (in MHz) for the rotational transitions of the conformer **21c** of muscone.

J'	K' ₋₁	K' ₊₁	J''	K'' ₋₁	K'' ₊₁	V _{obs}	V _{obs} - V _{calc}
3	2	1	2	1	1	2306.4057	-0.0060
3	2	2	2	1	2	2420.2734	0.0102
3	3	0	2	2	0	2533.9871	0.0017
3	3	1	2	2	1	2579.1582	-0.0043
4	2	2	3	1	2	3040.7310	0.0021
4	1	3	3	0	3	3132.6173	0.0006
4	3	1	3	2	1	3134.0757	0.0000
4	2	3	3	1	3	3177.1889	0.0002
4	3	2	3	2	2	3254.1841	0.0000
4	4	0	3	3	0	3442.1020	-0.0169
4	4	1	3	3	1	3464.1717	-0.0029
5	3	2	4	2	2	3804.7022	-0.0161
5	2	3	4	1	3	3853.0423	0.0003
5	1	4	4	0	4	3947.0728	-0.0151
5	2	4	4	1	4	3959.4772	0.0028
5	3	3	4	2	3	3977.4597	-0.0088
5	4	1	4	3	1	4014.1819	0.0031
5	4	2	4	3	2	4108.0636	0.0079
5	5	0	4	4	0	4349.4808	0.0011
5	5	1	4	4	1	4357.7907	-0.0002
6	3	3	5	2	3	4564.2382	0.0032
6	4	2	5	3	2	4617.0818	0.0003
6	2	4	5	1	4	4691.0489	0.0058
6	3	4	5	2	4	4739.9228	0.0010
6	1	5	5	0	5	4748.9069	-0.0019
6	2	5	5	1	5	4751.7561	0.0074
6	4	3	5	3	3	4795.0916	0.0028
6	5	1	5	4	1	4927.3839	-0.0002
6	5	2	5	4	2	4980.6178	-0.0027
6	6	0	5	5	0	5252.9681	0.0033
6	6	1	5	5	1	5255.6915	-0.0006
7	4	3	6	3	3	5305.0576	-0.0114
7	3	4	6	2	4	5400.0784	0.0044
7	5	2	6	4	2	5488.3113	0.0029
7	2	5	6	1	5	5510.7078	-0.0005
7	3	5	6	2	5	5525.0467	-0.0005
7	4	4	6	3	4	5527.9906	-0.0015
7	1	6	6	0	6	5546.1449	0.0068
7	2	6	6	1	6	5546.7371	0.0178
7	5	3	6	4	3	5634.6572	0.0012
7	6	1	6	5	1	5843.5797	0.0050
8	4	4	7	3	4	6092.4923	0.0042
8	5	3	7	4	3	6099.2323	0.0034
7	7	0	6	6	0	6154.4849	0.0054
7	7	1	6	6	1	6155.3157	0.0099
8	3	5	7	2	5	6247.2882	0.0023
8	4	5	7	3	5	6296.8736	0.0041
8	3	6	7	2	6	6319.1556	0.0011
8	5	4	7	4	4	6332.5437	0.0052
8	2	7	7	1	7	6342.0908	-0.0258
8	6	2	7	5	2	6403.9266	0.0021
8	6	3	7	5	3	6496.1546	0.0066
8	7	1	7	6	1	6752.7856	0.0038
8	7	2	7	6	2	6761.6067	-0.0224
9	5	4	8	4	4	6809.8128	0.0009
8	8	0	7	7	0	7055.2535	-0.0047
9	3	6	8	2	6	7070.8594	-0.0081
9	5	5	8	4	5	7074.8894	0.0059
9	1	8	8	0	8	7137.4440	0.0168
9	2	8	8	1	8	7137.4440	-0.0030

9	6	4	8	5	4	7159.5893	-0.0183
9	7	2	8	6	2	7329.7265	0.0086

Table S7.29. Measured frequencies and residuals (in MHz) for the rotational transitions of the conformer **43n** of muscone.

J'	K' ₋₁	K' ₊₁	J''	K'' ₋₁	K'' ₊₁	V _{obs}	V _{obs} - V _{calc}
4	1	3	3	2	2	2273.6185	0.0007
5	0	5	4	1	4	2469.5196	-0.0020
5	1	5	4	0	4	2472.1440	-0.0045
4	2	3	3	1	2	2512.5147	-0.0014
3	3	1	2	2	0	2659.9112	-0.0028
3	3	0	2	2	1	2773.2808	0.0021
5	1	4	4	2	3	2816.2382	0.0009
5	2	3	4	3	2	2879.6090	0.0115
5	2	4	4	1	3	2900.5609	-0.0066
6	0	6	5	1	5	2926.2323	-0.0004
6	1	6	5	0	5	2926.7281	-0.0016
4	3	2	3	2	1	3134.3586	-0.0012
6	1	5	5	2	4	3301.0777	0.0009
6	2	5	5	1	4	3324.0727	0.0014
7	0	7	6	1	6	3382.1526	0.0016
7	1	7	6	0	6	3382.2341	-0.0053
4	3	2	3	2	2	3445.6145	0.0008
5	3	3	4	2	2	3514.9288	0.0007
6	2	4	5	3	3	3552.5588	0.0023
4	3	1	3	2	2	3626.7543	-0.0002
4	4	1	3	3	0	3649.9874	0.0017
4	4	0	3	3	0	3661.1751	-0.0014
4	4	1	3	3	1	3683.0278	0.0093
4	4	0	3	3	1	3694.2111	0.0019
7	1	6	6	2	5	3764.4116	0.0008
7	2	6	6	1	5	3769.7572	-0.0030
8	0	8	7	1	7	3837.9388	0.0092
8	1	8	7	0	7	3837.9388	-0.0059
6	3	4	5	2	3	3851.0583	-0.0016
7	2	5	6	3	4	4107.3183	-0.0082
7	3	4	6	4	3	4157.1414	0.0110
5	4	2	4	3	1	4173.4913	-0.0031
5	3	3	4	2	3	4202.3063	0.0033
7	3	5	6	2	4	4213.6830	-0.0002
8	1	7	7	2	6	4221.6691	0.0011
8	2	7	7	1	6	4222.7952	-0.0003
5	4	1	4	3	1	4257.7450	0.0036
9	0	9	8	1	8	4293.6932	0.0020
9	1	9	8	0	8	4293.6932	-0.0005
5	4	1	4	3	2	4438.8849	0.0028
6	4	3	5	3	2	4575.6542	-0.0027
8	2	6	7	3	5	4596.5996	-0.0095
5	5	1	4	4	0	4624.0122	0.0037
8	3	6	7	2	5	4627.0853	0.0013
5	5	0	4	4	0	4627.4079	0.0069
5	5	0	4	4	1	4638.5989	0.0072
9	1	8	8	2	7	4677.5484	-0.0033
9	2	8	8	1	7	4677.7764	0.0026
10	0	10	9	1	9	4749.4657	0.0113
10	1	10	9	0	9	4749.4657	0.0109
8	3	5	7	4	4	4845.8145	-0.0032
6	4	2	5	3	2	4878.8772	-0.0067
7	4	4	6	3	3	4888.1722	-0.0017
9	3	7	8	2	6	5068.6720	-0.0034
6	4	3	5	3	3	5070.8966	-0.0018
8	4	5	7	3	4	5180.3067	0.0070
6	5	2	5	4	1	5200.6359	0.0016
11	0	11	10	1	10	5205.2187	-0.0018
11	1	11	10	0	10	5205.2187	-0.0019
6	5	1	5	4	1	5233.2464	-0.0026

6	5	1	5	4	2	5317.4990	0.0031
6	4	2	5	3	3	5374.1283	0.0028
9	3	6	8	4	5	5404.8486	-0.0026
10	2	8	9	3	7	5518.3116	-0.0033
10	3	8	9	2	7	5520.0330	0.0002
9	4	6	8	3	5	5524.4198	0.0013
6	6	1	5	5	0	5588.4362	0.0023
11	1	10	10	2	9	5588.8664	0.0040
11	2	10	10	1	9	5588.8664	-0.0035
6	6	1	5	5	1	5591.8225	-0.0039
6	6	0	5	5	1	5592.7905	0.0030
12	0	12	11	1	11	5660.9961	0.0077
12	1	12	11	0	11	5660.9961	0.0077
7	4	4	6	3	4	5836.2798	0.0026
10	3	7	9	4	6	5895.2234	-0.0013
11	2	9	10	3	8	5973.8792	-0.0054
11	3	9	10	2	8	5974.2487	0.0003
8	5	4	7	4	3	5992.7667	0.0067
12	1	11	11	2	10	6044.5425	-0.0023
12	2	11	11	1	10	6044.5425	-0.0036
13	0	13	12	1	12	6116.7682	0.0111
13	1	13	12	0	12	6116.7682	0.0111
7	5	2	6	4	3	6118.8008	-0.0033
7	6	2	6	5	1	6197.5672	0.0019
7	6	1	6	5	1	6208.7401	-0.0064
7	6	2	6	5	2	6230.1804	0.0004
7	6	1	6	5	2	6241.3631	0.0019
9	5	5	8	4	4	6244.3974	-0.0038
12	3	10	11	2	9	6429.3012	-0.0066
13	1	12	12	2	11	6500.2538	0.0035
13	2	12	12	1	11	6500.2538	0.0033
10	5	6	9	4	5	6501.7927	0.0028
7	4	3	6	3	4	6534.8311	-0.0079
7	7	1	6	6	0	6549.1787	0.0081
7	7	0	6	6	0	6549.4277	-0.0031
7	7	0	6	6	1	6550.3943	0.0024
14	0	14	13	1	13	6572.5166	-0.0096
14	1	14	13	0	13	6572.5166	-0.0096
8	6	3	7	5	2	6731.5770	-0.0078
15	0	15	14	1	14	7028.2977	0.0027
15	1	15	14	0	14	7028.2977	0.0027
8	7	2	7	6	1	7172.6427	0.0048
14	3	12	13	2	11	7340.1470	-0.0012
16	0	16	15	1	15	7484.0647	0.0014
16	1	16	15	0	15	7484.0647	0.0014
9	7	3	8	6	2	7758.4241	-0.0131

Table S7.30. Measured frequencies and residuals (in MHz) for the rotational transitions of the conformer **19h** of muscone.

J'	K' ₋₁	K' ₊₁	J''	K'' ₋₁	K'' ₊₁	V _{obs}	V _{obs} - V _{calc}
5	1	5	4	1	4	2390.8419	0.0005
5	0	5	4	0	4	2393.0829	0.0027
3	3	0	2	2	0	2614.2956	-0.0131
5	2	4	4	2	3	2735.7758	0.0011
5	1	4	4	1	3	2788.9805	0.0030
6	1	6	5	1	5	2833.2917	0.0019
6	0	6	5	0	5	2833.7514	-0.0068
5	3	3	4	3	2	2973.9784	0.0016
5	2	3	4	2	2	3174.8878	0.0019
6	2	5	5	2	4	3194.0609	-0.0022
4	3	1	3	2	1	3203.9321	0.0082
6	1	5	5	1	4	3211.5340	0.0008
5	3	2	4	3	1	3255.6459	0.0077
7	0	7	6	0	6	3275.2122	0.0031
4	3	2	3	2	2	3330.4158	0.0063
6	3	4	5	3	3	3499.3992	0.0090
4	4	0	3	3	0	3556.8644	0.0039
4	4	1	3	3	1	3575.7043	0.0006
7	2	6	6	2	5	3640.7917	-0.0006
6	2	4	5	2	3	3643.9209	-0.0009
7	1	6	6	1	5	3645.4271	0.0007
6	4	3	5	4	2	3654.0512	0.0013
8	1	8	7	1	7	3716.8343	0.0080
8	0	8	7	0	7	3716.8343	-0.0090
6	4	2	5	4	1	3838.7930	0.0004
6	4	2	5	4	1	3838.7930	0.0004
5	3	2	4	2	2	3857.8575	0.0029
6	3	3	5	3	2	3918.0668	-0.0017
7	3	5	6	3	4	3985.6713	0.0023
5	3	3	4	2	3	4051.3090	-0.0028
7	2	5	6	2	4	4054.3835	-0.0021
8	2	7	7	2	6	4083.5575	-0.0003
8	1	7	7	1	6	4084.6388	-0.0072
5	4	1	4	3	1	4127.0059	0.0046
9	1	9	8	1	8	4158.5156	-0.0043
9	0	9	8	0	8	4158.5156	-0.0073
5	4	2	4	3	2	4214.9574	-0.0186
8	3	6	7	3	5	4445.5701	-0.0002
8	2	6	7	2	5	4469.2743	-0.0019
7	3	4	6	3	3	4476.4211	0.0038
5	5	0	4	4	0	4496.1039	-0.0085
9	1	8	8	1	7	4525.5430	0.0049
10	1	10	9	1	9	4600.2195	0.0037
10	0	10	9	0	9	4600.2195	0.0032
6	4	2	5	3	2	4710.1601	0.0043
8	4	5	7	4	4	4753.6292	-0.0100
6	3	4	5	2	4	4814.9243	-0.0030
9	3	7	8	3	6	4892.6504	-0.0038
9	2	7	8	2	6	4899.4206	0.0130
8	3	5	7	3	4	4923.6088	0.0014
10	1	9	9	1	8	4966.9077	-0.0088
10	2	9	9	2	8	4966.9077	0.0397
11	1	11	10	1	10	5041.9194	0.0043
11	0	11	10	0	10	5041.9194	0.0042
6	5	1	5	4	1	5078.3315	-0.0037
6	5	2	5	4	2	5121.4357	-0.0047
9	4	6	8	4	5	5240.2809	-0.0067
10	3	8	9	3	7	5335.1726	-0.0044
10	2	8	9	2	7	5336.8865	-0.0024
7	4	3	6	3	3	5369.7207	0.0001

Appendix IV

11	1	10	10	1	9	5408.4306	-0.0204
11	2	10	10	2	9	5408.4306	-0.0108
6	6	0	5	5	0	5431.3063	0.0128
12	1	12	11	1	11	5483.6222	0.0054
12	0	12	11	0	11	5483.6222	0.0054
9	5	5	8	5	4	5486.7747	0.0010
10	3	7	9	3	6	5728.3748	-0.0073
7	5	3	6	4	3	5766.9933	0.0094
11	3	9	10	3	8	5776.5230	-0.0109
12	1	11	11	1	10	5850.0494	0.0009
12	2	11	11	2	10	5850.0494	0.0027
9	6	5	8	6	4	5906.3000	-0.0020
13	1	13	12	1	12	5925.3132	-0.0068
13	0	13	12	0	12	5925.3132	-0.0068
10	5	6	9	5	5	6013.2230	-0.0088
7	6	1	6	5	1	6025.9635	-0.0021
7	6	2	6	5	2	6042.4750	-0.0097
10	4	6	9	4	5	6202.2077	-0.0080
8	5	3	7	4	3	6212.1671	0.0020
12	2	10	11	2	9	6217.8106	-0.0292
12	3	10	11	3	9	6217.8106	0.0593
8	3	5	7	2	5	6302.7491	-0.0053
14	1	14	13	1	13	6367.0248	0.0010
14	0	14	13	0	13	6367.0248	0.0010
8	4	5	7	3	5	6390.0010	0.0061
8	3	6	7	2	6	6411.3204	0.0093
10	6	4	9	6	3	6484.3375	-0.0108
10	5	5	9	5	4	6558.1562	0.0126
12	4	9	11	4	8	6588.2783	-0.0059
12	3	9	11	3	8	6590.5717	0.0123
8	6	3	7	5	3	6664.6121	0.0030

5. APPENDIX V

Table S8.1. Measured frequencies and residuals (in MHz) for the rotational transitions of the conformer **5a** of civetone.

J'	K' ₋₁	K' ₊₁	J''	K'' ₋₁	K'' ₊₁	V _{obs}	V _{obs} - V _{calc}
4	2	2	3	1	2	2622.4065	0.0055
4	2	3	3	1	3	2866.0324	0.0038
3	3	0	2	2	0	2958.3511	0.0027
3	3	1	2	2	1	2965.0440	-0.0081
5	2	3	4	1	3	3044.0707	-0.0004
4	3	1	3	2	1	3363.4952	0.0032
4	3	2	3	2	2	3395.1484	-0.0033
5	2	4	4	1	4	3395.5076	-0.0023
6	2	4	5	1	4	3502.8988	0.0003
5	3	2	4	2	2	3750.8439	-0.0028
5	3	3	4	2	3	3837.4762	-0.0129
6	2	5	5	1	5	3951.0626	0.0094
7	2	5	6	1	5	4006.8009	-0.0005
4	4	0	3	3	0	4062.4849	0.0086
4	4	1	3	3	1	4063.0186	0.0011
6	3	3	5	2	3	4120.2702	0.0006
6	3	4	5	2	4	4296.7091	0.0000
5	4	1	4	3	1	4479.6312	0.0061
7	3	4	6	2	4	4482.6868	0.0009
5	4	2	4	3	2	4483.3047	0.0022
8	2	6	7	1	6	4561.8864	0.0014
7	3	5	6	2	5	4776.7915	-0.0003
8	3	5	7	2	5	4857.0832	0.0002
6	4	2	5	3	2	4891.1244	0.0028
6	4	3	5	3	3	4905.2229	0.0061
8	2	7	7	1	7	5131.0615	-0.0047
5	5	0	4	4	0	5163.6694	0.0223
5	5	1	4	4	1	5163.6694	-0.0136
9	2	7	8	1	7	5171.3186	0.0004
9	3	6	8	2	6	5262.9500	-0.0074
7	4	3	6	3	3	5291.2535	0.0021
7	4	4	6	3	4	5330.9739	-0.0140
6	5	1	5	4	1	5582.6555	0.0086
8	4	4	7	3	4	5673.3265	0.0005
10	3	7	9	2	7	5714.9003	0.0058
9	2	8	8	1	8	5748.5724	0.0042
8	4	5	7	3	5	5764.0633	-0.0011
7	5	2	6	4	2	6000.1859	-0.0042
9	4	5	8	3	5	6033.2804	0.0027
9	4	6	8	3	6	6208.7618	-0.0058
11	3	8	10	2	8	6222.1969	0.0018
6	6	0	5	5	0	6264.5417	-0.0008
6	6	1	5	5	1	6264.5417	-0.0029
8	5	3	7	4	3	6414.5129	-0.0039
8	5	4	7	4	4	6419.9755	0.0025
10	4	7	9	3	7	6669.6815	0.0015
7	6	1	6	5	1	6683.8450	0.0073
7	6	2	6	5	2	6683.8450	-0.0159
11	4	7	10	3	7	6712.7761	0.0124
12	3	9	11	2	9	6790.3077	-0.0019
9	5	4	8	4	4	6822.6355	-0.0149
10	5	5	9	4	5	7219.9859	-0.0060
7	7	0	6	6	0	7365.4066	0.0052
7	7	1	6	6	1	7365.4066	0.0051
8	7	1	7	6	1	7784.7885	0.0009
8	7	2	7	6	2	7784.7885	-0.0006

Table S8.2. Measured frequencies and residuals (in MHz) for the rotational transitions of the conformer **6b** of civetone.

J'	K' ₋₁	K' ₊₁	J''	K'' ₋₁	K'' ₊₁	V _{obs}	V _{obs} - V _{calc}
6	1	6	5	0	5	2579.6968	-0.0016
6	1	5	5	1	4	2852.0878	-0.0087
3	3	0	2	2	0	2943.8644	0.0064
7	1	7	6	0	6	2954.8845	-0.0084
5	2	3	4	1	3	3202.6154	-0.0033
8	0	8	7	1	7	3313.8185	0.0123
8	1	8	7	1	7	3322.3182	0.0116
8	0	8	7	0	7	3330.9471	-0.0052
8	1	8	7	0	7	3339.4554	0.0027
4	3	1	3	2	1	3389.5809	-0.0087
4	3	2	3	2	2	3429.4883	0.0064
5	2	4	4	1	4	3551.2315	0.0023
9	0	9	8	0	8	3725.8215	0.0037
6	2	4	5	1	4	3728.2094	0.0074
5	3	3	4	2	3	3921.6200	-0.0108
4	4	0	3	3	0	4034.6178	0.0052
4	4	1	3	3	1	4035.4481	0.0028
6	3	3	5	2	3	4226.5261	-0.0008
5	4	1	4	3	1	4494.7848	0.0178
5	4	2	4	3	2	4500.3701	-0.0064
7	3	4	6	2	4	4640.8035	0.0046
8	2	6	7	1	6	4939.8833	-0.0158
6	4	2	5	3	2	4946.8752	0.0009
6	4	3	5	3	3	4968.0627	-0.0090
8	3	5	7	2	5	5081.7765	-0.0029
5	5	0	4	4	0	5121.7758	0.0535
5	5	1	4	4	1	5121.7758	-0.0127
7	4	3	6	3	3	5383.4640	-0.0019
8	3	6	7	2	6	5534.5629	0.0061
9	3	6	8	2	6	5568.3452	-0.0121
9	2	7	8	1	7	5630.0445	0.0115
8	4	4	7	3	4	5797.8292	-0.0091
8	4	5	7	3	5	5926.4027	0.0095
7	5	2	6	4	2	6045.2506	-0.0020
7	5	3	6	4	3	6048.0453	-0.0078
10	3	7	9	2	7	6112.3520	0.0053
6	6	0	5	5	0	6208.4346	0.0041
6	6	1	5	5	1	6208.4346	-0.0006
9	4	6	8	3	6	6427.0443	0.0007
8	5	3	7	4	3	6501.0293	-0.0052
8	5	4	7	4	4	6510.8174	-0.0106
7	6	1	6	5	1	6671.7519	0.0225
7	6	2	6	5	2	6671.7519	-0.0285
7	7	0	6	6	0	7295.0906	0.0034
7	7	1	6	6	1	7295.0906	0.0031
9	6	3	8	5	3	7594.8130	-0.0022
9	6	4	8	5	4	7596.0703	0.0039
8	7	1	7	6	1	7758.5138	-0.0012
8	7	2	7	6	2	7758.5138	-0.0053

Table S8.3. Measured frequencies and residuals (in MHz) for the rotational transitions of the conformer **12a** of civetone.

J'	K' ₋₁	K' ₊₁	J''	K'' ₋₁	K'' ₊₁	V _{obs}	V _{obs} - V _{calc}
5	2	3	4	2	2	2365.2626	-0.0053
6	0	6	5	1	5	2383.6899	-0.0004
6	1	6	5	1	5	2413.1362	-0.0065
4	1	3	3	0	3	2449.4288	0.0076
6	2	5	5	2	4	2627.1122	0.0033
4	2	2	3	1	2	2664.4802	-0.0084
6	3	4	5	3	3	2707.6066	-0.0047
6	4	2	5	4	1	2712.3642	0.0029
6	3	3	5	3	2	2760.4737	0.0073
6	1	5	5	1	4	2761.3705	0.0023
7	0	7	6	1	6	2783.1158	0.0035
7	1	7	6	1	6	2797.8351	-0.0009
7	1	7	6	0	6	2827.2921	0.0038
6	2	4	5	2	3	2858.4347	-0.0014
3	3	0	2	2	0	2898.3478	-0.0084
3	3	1	2	2	1	2907.9013	-0.0068
3	3	0	2	2	1	2908.9720	-0.0072
4	2	3	3	1	3	2919.9720	-0.0089
7	2	6	6	2	5	3040.5184	0.0046
5	2	3	4	1	3	3138.0441	0.0016
7	3	5	6	3	4	3156.0798	0.0007
7	1	6	6	1	5	3160.2580	-0.0002
7	4	4	6	4	3	3168.9158	-0.0087
8	0	8	7	1	7	3172.7973	-0.0163
7	4	3	6	4	2	3178.9583	-0.0131
8	1	8	7	1	7	3179.9160	0.0070
8	1	8	7	0	7	3194.6428	0.0102
4	3	2	3	2	1	3320.5519	0.0031
4	3	1	3	2	1	3327.9404	0.0034
7	2	5	6	2	4	3337.6599	0.0000
4	3	2	3	2	2	3372.0002	0.0004
4	3	1	3	2	2	3379.3889	0.0009
8	2	7	7	2	6	3445.1673	-0.0049
5	2	4	4	1	4	3494.2503	0.0158
8	1	7	7	1	6	3538.2294	0.0022
9	0	9	8	1	8	3557.0661	-0.0149
9	1	9	8	1	8	3560.3938	-0.0151
9	0	9	8	0	8	3564.1789	0.0025
9	1	9	8	0	8	3567.5023	-0.0019
8	3	6	7	3	5	3597.9931	0.0024
8	4	5	7	4	4	3629.8125	0.0008
8	4	4	7	4	3	3655.9619	0.0081
6	2	4	5	1	4	3658.9806	-0.0056
5	3	3	4	2	2	3708.0964	0.0044
5	3	2	4	2	2	3736.7812	0.0052
8	3	5	7	3	4	3773.1118	-0.0008
9	2	8	8	2	7	3841.9867	0.0015
5	3	3	4	2	3	3852.6797	-0.0001
5	3	2	4	2	3	3881.3621	-0.0016
9	1	8	8	1	7	3905.4666	-0.0011
10	0	10	9	1	9	3938.5278	0.0166
10	1	10	9	1	9	3940.0456	0.0058
10	0	10	9	0	9	3941.8430	0.0040
9	3	7	8	3	6	4031.3675	-0.0006
6	3	4	5	2	3	4050.4349	-0.0005
9	5	5	8	5	4	4080.2620	0.0050
9	5	4	8	5	3	4084.7398	0.0188
9	4	6	8	4	5	4089.9179	0.0016
6	2	5	5	1	5	4096.8329	-0.0063

6	3	3	5	2	3	4131.9774	0.0029
9	4	5	8	4	4	4147.4301	0.0046
9	2	7	8	2	6	4231.2508	0.0018
10	2	9	9	2	8	4232.4341	0.0003
10	1	9	9	1	8	4271.3948	0.0015
9	3	6	8	3	5	4283.5531	-0.0018
11	0	11	10	1	10	4318.5209	-0.0111
11	1	11	10	1	10	4319.2347	0.0120
11	0	11	10	0	10	4320.0557	-0.0050
7	3	5	6	2	4	4348.0606	-0.0178
6	3	4	5	2	4	4355.4308	-0.0091
5	4	2	4	3	1	4418.8413	0.0075
5	4	1	4	3	1	4419.6308	0.0006
5	4	2	4	3	2	4426.2252	0.0033
5	4	1	4	3	2	4427.0149	-0.0034
10	3	8	9	3	7	4454.9983	-0.0113
7	1	6	6	0	6	4512.1139	-0.0070
7	3	4	6	2	4	4534.8391	0.0025
10	5	6	9	5	5	4545.4483	-0.0011
10	4	7	9	4	6	4546.6980	0.0015
10	2	8	9	2	7	4637.6394	0.0124
11	1	10	10	1	9	4640.3384	0.0067
12	1	12	11	1	11	4698.1956	0.0077
10	3	7	9	3	6	4780.2808	0.0089
6	4	3	5	3	2	4851.6880	-0.0013
6	4	2	5	3	2	4855.6037	-0.0007
11	3	9	10	3	8	4868.6042	-0.0073
8	2	6	7	1	6	4871.9041	-0.0127
6	4	3	5	3	3	4880.3775	0.0042
7	3	5	6	2	5	4884.4069	-0.0032
8	3	5	7	2	5	4970.2889	-0.0004
11	4	8	10	4	7	4997.4853	0.0008
12	2	11	11	2	10	5000.8614	-0.0056
12	1	11	11	1	10	5012.7568	0.0065
5	5	0	4	4	0	5046.5345	0.0522
5	5	1	4	4	1	5046.5345	-0.0305
5	5	1	4	4	0	5046.5345	0.0589
5	5	0	4	4	1	5046.5345	-0.0372
13	1	13	12	1	12	5077.0628	0.0093
13	0	13	12	0	12	5077.2199	-0.0057
11	3	8	10	3	7	5254.9349	0.0017
7	4	4	6	3	4	5341.6809	-0.0057
7	4	3	6	3	4	5355.6455	-0.0029
8	2	7	7	1	7	5371.5474	0.0008
13	2	12	12	2	11	5381.6172	0.0020
13	1	12	12	1	11	5387.7407	-0.0052
9	3	6	8	2	6	5456.9370	-0.0100
12	5	8	11	5	7	5478.4317	0.0103
6	5	2	5	4	2	5495.5333	0.0012
9	2	7	8	1	7	5564.9423	0.0038
8	4	5	7	3	4	5628.6696	0.0086
13	3	11	12	3	10	5668.7709	-0.0182
8	4	4	7	3	4	5668.7709	0.0060
13	2	11	12	2	10	5741.0739	0.0026
8	4	5	7	3	5	5815.4215	0.0023
15	1	15	14	1	14	5834.6889	0.0059
15	0	15	14	0	14	5834.6889	-0.0277
15	0	15	14	1	14	5834.6889	0.0316
15	1	15	14	0	14	5834.6889	-0.0533
7	5	2	6	4	2	5940.6103	0.0052
10	3	7	9	2	7	6005.9564	-0.0136
9	3	7	8	2	7	6028.0914	0.0084
6	6	0	5	5	0	6118.0880	0.0064
6	6	1	5	5	1	6118.0880	0.0001
6	6	1	5	5	0	6118.0880	0.0069

Appendix V

6	6	0	5	5	1	6118.0880	-0.0003
13	3	10	12	3	9	6118.6451	-0.0054
15	2	14	14	2	13	6140.3993	0.0060
16	1	16	15	1	15	6213.4860	0.0013
16	0	16	15	0	15	6213.4860	-0.0133
16	0	16	15	1	15	6213.4860	0.0124
16	1	16	15	0	15	6213.4860	-0.0243
8	5	3	7	4	3	6380.6161	-0.0003
7	6	1	6	5	1	6566.9905	0.0451
7	6	2	6	5	2	6566.9905	-0.0222
17	1	17	16	1	16	6592.2989	0.0129
17	0	17	16	0	16	6592.2989	0.0065
17	0	17	16	1	16	6592.2989	0.0176
17	1	17	16	0	16	6592.2989	0.0018
11	3	8	10	2	8	6623.2756	-0.0006
10	3	8	9	2	8	6641.1199	0.0125
7	7	0	6	6	0	7189.6153	-0.0044
7	7	1	6	6	1	7189.6153	-0.0049
7	7	1	6	6	0	7189.6153	-0.0044
7	7	0	6	6	1	7189.6153	-0.0049
10	5	5	9	4	5	7219.3385	-0.0016
9	6	3	8	5	3	7460.6100	-0.0055
9	6	4	8	5	4	7462.2476	-0.0115

Table S8.4. Measured frequencies and residuals (in MHz) for the rotational transitions of the conformer **6a** of civetone.

J'	K'_{-1}	K'_{+1}	J''	K''_{-1}	K''_{+1}	V _{obs}	V _{obs} - V _{calc}
4	2	2	3	1	2	2586.6345	0.0002
3	3	0	2	2	0	2762.9233	0.0013
3	3	1	2	2	1	2773.1145	0.0079
4	2	3	3	1	3	2831.2279	0.0057
5	2	3	4	1	3	3064.6445	-0.0020
4	3	1	3	2	1	3188.9285	-0.0026
4	3	2	3	2	2	3235.4341	-0.0003
5	2	4	4	1	4	3401.3165	0.0049
6	2	4	5	1	4	3590.9419	-0.0019
5	3	3	4	2	3	3715.1086	-0.0005
4	4	0	3	3	0	3785.7251	0.0044
4	4	1	3	3	1	3786.8553	-0.0024
6	3	3	5	2	3	3990.7551	-0.0032
6	2	5	5	1	5	3998.8491	-0.0006
7	2	5	6	1	5	4173.1161	0.0029
6	3	4	5	2	4	4217.5559	-0.0002
5	4	1	4	3	1	4227.7341	-0.0005
5	4	2	4	3	2	4235.3287	0.0005
7	3	4	6	2	4	4400.3571	-0.0026
7	2	6	6	1	6	4619.8226	0.0100
6	4	2	5	3	2	4659.4604	-0.0012
6	4	3	5	3	3	4687.7356	-0.0023
7	3	5	6	2	5	4746.6259	0.0089
5	5	0	4	4	0	4804.3678	0.0134
5	5	1	4	4	1	4804.4429	-0.0153
8	2	6	7	1	6	4814.6027	0.0001
8	3	5	7	2	5	4847.9992	-0.0023
7	4	3	6	3	3	5072.3902	-0.0014
7	4	4	6	3	4	5148.3701	-0.0041
6	5	1	5	4	1	5249.8732	0.0005
6	5	2	5	4	2	5250.7813	0.0037
8	2	7	7	1	7	5259.0376	-0.0141
8	3	6	7	2	6	5304.0948	-0.0005
9	3	6	8	2	6	5350.0726	-0.0041
8	4	4	7	3	4	5461.7330	-0.0019
9	2	7	8	1	7	5507.4214	0.0004
8	4	5	7	3	5	5622.8536	-0.0007
7	5	2	6	4	2	5692.4739	0.0012
7	5	3	6	4	3	5696.8062	0.0010
6	6	0	5	5	0	5822.4646	0.0035
6	6	1	5	5	1	5822.4646	-0.0050
9	4	5	8	3	5	5835.3891	0.0039
9	3	7	8	2	7	5889.5441	0.0019
9	2	8	8	1	8	5911.2441	0.0045
10	3	7	9	2	7	5915.9607	0.0013
9	4	6	8	3	6	6117.0276	0.0002
8	5	3	7	4	3	6128.3532	0.0015
8	5	4	7	4	4	6143.3102	-0.0008
10	4	6	9	3	6	6216.2988	0.0001
10	2	8	9	1	8	6230.2546	0.0017
7	6	1	6	5	1	6268.6440	0.0408
7	6	2	6	5	2	6268.6440	-0.0507
10	3	8	9	2	8	6500.3371	0.0028
11	3	8	10	2	8	6549.3385	-0.0013
9	5	4	8	4	4	6551.2452	-0.0045
10	2	9	9	1	9	6571.7500	-0.0029
9	5	5	8	4	5	6592.4873	-0.0002
11	4	7	10	3	7	6632.7526	-0.0019
10	4	7	9	3	7	6635.8052	0.0001
8	6	2	7	5	2	6713.6333	0.0010

Appendix V

8	6	3	7	5	3	6714.1640	-0.0002
7	7	0	6	6	0	6840.4980	-0.0001
7	7	1	6	6	1	6840.4980	-0.0008
10	5	5	9	4	5	6953.1594	-0.0021
11	2	9	10	1	9	6958.6090	-0.0263
10	5	6	9	4	6	7048.2193	-0.0074
9	6	3	8	5	3	7156.2860	0.0030
9	6	4	8	5	4	7158.4950	-0.0007
11	4	8	10	3	8	7182.2814	0.0025
8	7	1	7	6	1	7286.8089	0.0045
8	7	2	7	6	2	7286.8089	-0.0038
11	5	6	10	4	6	7328.7201	0.0053
11	5	7	10	4	7	7515.8509	0.0024
12	5	7	11	4	7	7683.3146	0.0038
9	7	2	8	6	2	7732.4668	-0.0092
9	7	3	8	6	3	7732.5458	0.0128
12	4	9	11	3	9	7757.2376	-0.0044
8	8	0	7	7	0	7858.5103	-0.0031
8	8	1	7	7	1	7858.5103	-0.0032

Table S8.5. Measured frequencies and residuals (in MHz) for the rotational transitions of the conformer **11a** of civetone.

J'	K'_{-1}	K'_{+1}	J''	K''_{-1}	K''_{+1}	V _{obs}	V _{obs} - V _{calc}
6	1	6	5	1	5	2373.3840	0.0064
6	0	6	5	0	5	2390.3432	0.0015
4	1	3	3	0	3	2411.5782	0.0143
4	2	2	3	1	2	2536.5047	-0.0018
3	3	0	2	2	0	2653.3161	0.0012
3	3	1	2	2	1	2665.3533	-0.0078
6	1	5	5	1	4	2715.8664	-0.0112
7	1	7	6	1	6	2749.9791	0.0028
7	0	7	6	0	6	2758.2561	-0.0023
4	2	3	3	1	3	2776.7552	0.0027
5	2	3	4	1	3	3029.6730	-0.0011
5	1	4	4	0	4	3066.0605	0.0097
4	3	1	3	2	1	3077.4496	0.0045
7	1	6	6	1	5	3093.2243	-0.0114
8	1	8	7	1	7	3124.4648	-0.0185
8	0	8	7	0	7	3128.2794	0.0060
4	3	2	3	2	2	3131.3315	-0.0004
5	2	4	4	1	4	3352.8473	0.0038
8	1	7	7	1	6	3455.0022	-0.0001
5	3	2	4	2	2	3482.2637	0.0009
9	1	9	8	1	8	3497.9094	0.0137
9	0	9	8	0	8	3499.5632	0.0071
6	2	4	5	1	4	3575.4655	-0.0016
5	3	3	4	2	3	3617.1023	0.0004
4	4	0	3	3	0	3633.2290	0.0032
4	4	1	3	3	1	3634.7687	-0.0039
6	1	5	5	0	5	3757.3575	-0.0019
9	1	8	8	1	7	3814.0294	0.0007
6	3	3	5	2	3	3884.3293	0.0012
6	2	5	5	1	5	3956.3371	-0.0002
5	4	1	4	3	1	4074.7616	-0.0026
5	4	2	4	3	2	4084.9834	-0.0010
6	3	4	5	2	4	4128.2075	-0.0016
7	2	5	6	1	5	4181.0602	-0.0002
7	3	4	6	2	4	4311.6432	-0.0013
6	4	2	5	3	2	4503.3201	-0.0006
6	4	3	5	3	3	4540.6636	0.0000
5	5	0	4	4	0	4608.4367	0.0141
5	5	1	4	4	1	4608.5779	-0.0066
7	3	5	6	2	5	4668.0833	-0.0007
8	3	5	7	2	5	4787.4257	-0.0011
8	2	6	7	1	6	4845.7121	-0.0009
7	4	3	6	3	3	4909.9944	-0.0009
7	4	4	6	3	4	5007.1957	0.0016
6	5	1	5	4	1	5054.5034	0.0035
6	5	2	5	4	2	5055.8953	-0.0066
8	2	7	7	1	7	5224.3097	0.0028
8	3	6	7	2	6	5237.6110	-0.0011
8	4	4	7	3	4	5294.4266	-0.0014
9	3	6	8	2	6	5325.1194	0.0022
8	4	5	7	3	5	5491.0582	-0.0019
7	5	2	6	4	2	5496.6167	0.0185
7	5	3	6	4	3	5503.2408	0.0010
9	2	7	8	1	7	5552.6275	-0.0006
6	6	0	5	5	0	5582.9409	0.0083
6	6	1	5	5	1	5582.9409	-0.0070
9	4	5	8	3	5	5674.1148	0.0019
9	3	7	8	2	7	5835.0070	-0.0048
9	2	8	8	1	8	5877.1647	0.0056
8	5	3	7	4	3	5929.4813	-0.0021

10	3	7	9	2	7	5931.5599	-0.0036
8	5	4	7	4	4	5952.0342	-0.0016
9	4	6	8	3	6	5998.3448	-0.0015
7	6	1	6	5	1	6029.8934	0.0084
7	6	2	6	5	2	6030.0490	0.0013
10	4	6	9	3	6	6079.3774	-0.0020
10	2	8	9	1	8	6274.4634	0.0038
9	5	4	8	4	4	6345.0661	-0.0088
9	5	5	8	4	5	6405.6179	-0.0021
10	3	8	9	2	8	6456.1848	0.0008
8	6	2	7	5	2	6475.3804	0.0015
8	6	3	7	5	3	6476.3117	-0.0061
10	4	7	9	3	7	6533.4063	-0.0050
10	2	9	9	1	9	6536.2736	-0.0094
7	7	0	6	6	0	6557.3441	-0.0040
7	7	1	6	6	1	6557.3441	-0.0053
11	3	8	10	2	8	6604.4313	-0.0060
10	5	5	9	4	5	6735.2939	-0.0013
10	5	6	9	4	6	6869.2412	-0.0097
9	6	3	8	5	3	6917.6126	-0.0062
9	6	4	8	5	4	6921.4741	-0.0097
11	2	9	10	1	9	6989.6447	0.0019
8	7	1	7	6	1	7004.5352	0.0099
8	7	2	7	6	2	7004.5352	-0.0072
12	4	8	11	3	8	7065.5679	0.0038
11	3	9	10	2	9	7095.6338	0.0003
11	5	6	10	4	6	7100.6450	-0.0005
11	2	10	10	1	0	7198.7021	0.0024
12	3	9	11	2	9	7325.7156	0.0011
11	5	7	10	4	7	7349.3531	-0.0013
10	6	4	9	5	4	7353.3171	-0.0037
10	6	5	9	5	5	7365.9798	0.0255
9	7	2	8	6	2	7450.9723	0.0593
9	7	3	8	6	3	7450.9723	-0.0563
8	8	0	7	7	0	7531.7320	-0.0072
8	8	1	7	7	1	7531.7320	-0.0073
12	2	10	11	1	0	7690.4109	0.0013
10	7	3	9	6	3	7895.7488	0.0051
10	7	4	9	6	4	7896.3036	0.0041

Table S8.6. Measured frequencies and residuals (in MHz) for the rotational transitions of the conformer **10d** of civetone.

J'	K' ₋₁	K' ₊₁	J''	K'' ₋₁	K'' ₊₁	V _{obs}	V _{obs} - V _{calc}
4	2	2	3	1	2	2445.5829	-0.0038
3	3	0	2	2	0	2578.5467	-0.0024
5	2	3	4	1	3	2921.4703	-0.0047
4	3	1	3	2	1	2978.7040	0.0101
5	2	4	4	1	4	3246.2887	0.0039
5	3	2	4	2	2	3359.6895	-0.0036
6	2	4	5	1	4	3452.3369	0.0050
5	3	3	4	2	3	3501.5477	-0.0075
4	4	0	3	3	0	3533.6211	0.0043
6	3	3	5	2	3	3740.5596	0.0014
6	2	5	5	1	5	3831.6102	0.0055
5	4	1	4	3	1	3951.8575	-0.0080
5	4	2	4	3	2	3963.2477	0.0062
6	3	4	5	2	4	3993.7079	-0.0019
7	3	4	6	2	4	4150.8215	0.0102
6	4	3	5	3	3	4397.2752	0.0158
7	2	6	6	1	6	4439.2692	0.0136
5	5	1	4	4	1	4483.9029	0.0060
7	3	5	6	2	5	4515.7985	-0.0070
8	3	5	7	2	5	4613.3722	-0.0151
8	2	6	7	1	6	4697.4461	-0.0105
7	4	3	6	3	3	4736.9694	-0.0109
7	4	4	6	3	4	4843.2416	0.0011
6	5	1	5	4	1	4906.9366	-0.0124
6	5	2	5	4	2	4908.5684	-0.0087
8	2	7	7	1	7	5062.9145	0.0072
8	3	6	7	2	6	5068.4020	-0.0018
8	4	4	7	3	4	5096.5071	-0.0007
9	3	6	8	2	6	5141.1152	0.0113
8	4	5	7	3	5	5308.0388	0.0089
7	5	2	6	4	2	5325.7263	-0.0051
7	5	3	6	4	3	5333.4064	-0.0087
9	2	7	8	1	7	5389.0609	-0.0081
6	6	0	5	5	0	5433.0505	0.0084
6	6	1	5	5	1	5433.0505	-0.0101
9	3	7	8	2	7	5649.2264	0.0004
8	5	3	7	4	3	5734.2102	0.0103
10	3	7	9	2	7	5739.9481	-0.0006
8	5	4	7	4	4	5760.1316	-0.0022
9	4	6	8	3	6	5797.8291	0.0022
7	6	1	6	5	1	5857.2750	0.0032
7	6	2	6	5	2	5857.4655	-0.0032
10	2	8	9	1	8	6091.1805	0.0009
9	5	4	8	4	4	6123.5797	-0.0044
9	5	5	8	4	5	6192.5344	0.0003
8	6	2	7	5	2	6279.8810	-0.0011
8	6	3	7	5	3	6281.0212	0.0058
10	4	7	9	3	7	6316.7990	-0.0043
7	7	0	6	6	0	6382.2706	0.0019
7	7	1	6	6	1	6382.2706	0.0002
10	5	5	9	4	5	6486.1325	0.0007
10	5	6	9	4	6	6636.4167	0.0055
9	6	3	8	5	3	6698.8303	-0.0001
9	6	4	8	5	4	6703.4753	-0.0030
9	7	3	8	6	3	7230.5168	-0.0022
8	8	0	7	7	0	7331.4714	0.0032
8	8	1	7	7	1	7331.4714	0.0031

Table S8.7. Measured frequencies and residuals (in MHz) for the rotational transitions of the conformer **1a** of civetone.

J'	K' ₋₁	K' ₊₁	J''	K'' ₋₁	K'' ₊₁	V _{obs}	V _{obs} - V _{calc}
3	2	1	2	1	1	2036.2489	0.0019
4	1	3	3	0	3	2383.9999	-0.0005
4	2	2	3	1	2	2483.5945	-0.0005
3	3	0	2	2	0	2584.4138	0.0022
3	3	1	2	2	1	2597.9015	-0.0006
4	2	3	3	1	3	2724.2209	0.0067
5	2	3	4	1	3	2977.2393	0.0000
4	3	1	3	2	1	2997.3335	0.0003
5	1	4	4	0	4	3037.7041	-0.0033
4	3	2	3	2	2	3056.8248	-0.0013
5	2	4	4	1	4	3296.2397	0.0015
5	3	2	4	2	2	3391.8502	0.0001
6	2	4	5	1	4	3526.9395	0.0009
5	3	3	4	2	3	3537.4257	0.0005
4	4	0	3	3	0	3539.4620	0.0019
4	4	1	3	3	1	3541.3424	0.0007
6	1	5	5	0	5	3724.5523	-0.0006
6	3	3	5	2	3	3789.0065	-0.0005
6	2	5	5	1	5	3895.9082	-0.0003
5	4	1	4	3	1	3970.7242	0.0004
5	4	2	4	3	2	3983.0618	0.0000
6	3	4	5	2	4	4045.3130	-0.0004
7	2	5	6	1	5	4139.3311	-0.0005
7	3	4	6	2	4	4218.9709	-0.0011
6	4	2	5	3	2	4386.9840	-0.0011
7	1	6	6	0	6	4417.7659	0.0020
6	4	3	5	3	3	4431.4485	-0.0008
5	5	0	4	4	0	4489.3962	0.0102
5	5	1	4	4	1	4489.5927	-0.0069
8	3	5	7	2	5	4703.7636	0.0006
7	4	3	6	3	3	4779.5738	-0.0008
8	2	6	7	1	6	4809.7624	0.0029
7	4	4	6	3	4	4892.6720	0.0000
6	5	1	5	4	1	4925.9968	0.0005
6	5	2	5	4	2	4927.8348	-0.0015
8	1	7	7	0	7	5101.9800	0.0019
8	4	4	7	3	4	5152.3188	-0.0025
8	3	6	7	2	6	5152.5169	0.0004
8	2	7	7	1	7	5154.1641	0.0085
9	3	6	8	2	6	5255.3242	0.0006
7	5	2	6	4	2	5357.7341	-0.0006
7	5	3	6	4	3	5366.3830	-0.0008
8	4	5	7	3	5	5373.7605	-0.0002
6	6	0	5	5	0	5438.5080	0.0107
6	6	1	5	5	1	5438.5080	-0.0111
9	2	7	8	1	7	5515.4283	-0.0008
9	4	5	8	3	5	5529.3469	-0.0008
9	3	7	8	2	7	5749.2942	0.0002
9	1	8	8	0	8	5775.0787	0.0037
8	5	3	7	4	3	5778.2248	-0.0029
9	2	8	8	1	8	5800.4219	-0.0024
8	5	4	7	4	4	5807.2332	-0.0018
7	6	1	6	5	1	5876.2016	0.0078
7	6	2	6	5	2	5876.4200	-0.0054
10	3	7	9	2	7	5878.4688	0.0025
9	4	6	8	3	6	5880.8503	-0.0002
10	4	6	9	3	6	5943.9192	0.0005
9	5	4	8	4	4	6178.2531	-0.0125
10	2	8	9	1	8	6227.1481	-0.0001
9	5	5	8	4	5	6254.5933	0.0001

8	6	2	7	5	2	6312.1335	0.0006
8	6	3	7	5	3	6313.4618	-0.0006
10	3	8	9	2	8	6368.8642	-0.0021
7	7	0	6	6	0	6387.4923	0.0012
7	7	1	6	6	1	6387.4923	-0.0009
10	4	7	9	3	7	6417.7897	0.0001
11	4	7	10	3	7	6421.2724	0.0003
10	1	9	9	0	9	6440.2622	0.0042
10	2	9	9	1	9	6451.9269	-0.0054
10	5	5	9	4	5	6550.9118	-0.0007
11	3	8	10	2	8	6565.0079	-0.0057
10	5	6	9	4	6	6714.6528	-0.0009
9	6	3	8	5	3	6744.0460	-0.0011
9	6	4	8	5	4	6749.4762	-0.0017
8	7	1	7	6	1	6825.4762	0.0133
8	7	2	7	6	2	6825.4762	-0.0129
11	5	6	10	4	6	6902.9013	0.0024
11	2	9	10	1	9	6927.1554	0.0016
12	4	8	11	3	8	6974.7404	-0.0007
11	4	8	10	3	8	6985.3977	0.0006
11	3	9	10	2	9	7005.0661	0.0014
11	2	10	10	1	10	7105.9905	-0.0082
10	6	4	9	5	4	7167.7192	0.0000
10	6	5	9	5	5	7185.2731	0.0006
11	5	7	10	4	7	7194.4560	0.0028
12	5	7	11	4	7	7261.1982	0.0065
9	7	2	8	6	2	7262.5234	0.0086
9	7	3	8	6	3	7262.6868	-0.0055
12	3	9	11	2	9	7289.0908	-0.0015
8	8	0	7	7	0	7336.4591	0.0028
8	8	1	7	7	1	7336.4591	0.0026
11	6	5	10	5	5	7576.0676	-0.0013
13	4	9	12	3	9	7607.8538	-0.0024
12	2	10	11	1	10	7612.1947	-0.0006
11	6	6	10	5	6	7623.2902	0.0001
12	3	10	11	2	10	7652.0316	0.0050
13	5	8	12	4	8	7661.8321	0.0018
10	7	3	9	6	3	7697.7110	-0.0005
10	7	4	9	6	4	7698.5602	-0.0004
12	5	8	11	4	8	7700.2592	0.0011
9	8	1	8	7	1	7774.5386	-0.0014
9	8	2	8	7	2	7774.5386	-0.0042

Table S8.8. Measured frequencies and residuals (in MHz) for the rotational transitions of the conformer **2a** of civetone.

J'	K' ₋₁	K' ₊₁	J''	K'' ₋₁	K'' ₊₁	V _{obs}	V _{obs} - V _{calc}
4	2	2	3	1	2	2433.7403	-0.0004
6	2	5	5	2	4	2487.2814	-0.0005
3	3	0	2	2	0	2501.5813	0.0052
3	3	1	2	2	1	2516.5347	0.0030
7	1	7	6	1	6	2601.1782	0.0041
6	3	4	5	3	3	2605.6789	0.0035
7	0	7	6	0	6	2606.3474	0.0002
4	2	3	3	1	3	2669.2355	-0.0127
6	3	3	5	3	2	2715.8664	0.0051
7	2	6	6	2	5	2865.0445	-0.0057
4	3	1	3	2	1	2907.6671	-0.0019
5	2	3	4	1	3	2932.1945	0.0018
7	1	6	6	1	5	2940.5198	0.0173
8	1	8	7	1	7	2953.3075	-0.0095
8	0	8	7	0	7	2955.4459	-0.0049
4	3	2	3	2	2	2972.4578	-0.0001
7	4	4	6	4	3	3066.1400	-0.0078
7	3	4	6	3	3	3220.6847	-0.0065
8	2	7	7	2	6	3232.6127	-0.0137
5	2	4	4	1	4	3239.1535	0.0067
8	1	7	7	1	6	3276.7655	0.0030
5	3	2	4	2	2	3297.5052	0.0003
4	4	0	3	3	0	3425.3482	0.0026
4	4	1	3	3	1	3427.6297	-0.0010
8	3	6	7	3	5	3435.5956	0.0089
5	3	3	4	2	3	3451.7862	-0.0007
6	2	4	5	1	4	3489.3896	0.0004
8	4	5	7	4	4	3509.8741	-0.0008
8	4	4	7	4	3	3589.2791	-0.0054
9	2	8	8	2	7	3592.7757	0.0019
6	3	3	5	2	3	3696.7782	-0.0120
8	3	5	7	3	4	3716.3596	0.0035
6	2	5	5	1	5	3836.2550	0.0039
5	4	1	4	3	1	3850.2163	0.0010
9	4	6	8	4	5	3946.7083	0.0106
10	2	9	9	2	8	3948.2343	0.0112
10	1	9	9	1	8	3958.8813	-0.0026
6	3	4	5	2	4	3960.0229	-0.0006
7	2	5	6	1	5	4110.6069	0.0023
7	3	4	6	2	4	4136.5095	-0.0006
9	3	6	8	3	5	4185.7394	-0.0023
6	4	2	5	3	2	4258.0080	-0.0011
6	4	3	5	3	3	4310.5413	0.0056
5	5	0	4	4	0	4343.6380	-0.0092
5	5	1	4	4	1	4343.9344	0.0038
7	3	5	6	2	5	4499.7580	-0.0024
8	3	5	7	2	5	4636.4234	0.0014
7	4	3	6	3	3	4641.2956	0.0012
7	4	4	6	3	4	4771.0084	0.0003
6	5	1	5	4	1	4774.7702	0.0063
6	5	2	5	4	2	4777.1921	0.0015
8	2	6	7	1	6	4785.6173	-0.0096
8	4	4	7	3	4	5009.8841	-0.0036
8	3	6	7	2	6	5070.2980	0.0011
8	2	7	7	1	7	5085.4172	-0.0151
7	5	2	6	4	2	5199.9005	-0.0014
9	3	6	8	2	6	5206.6382	-0.0007
7	5	3	6	4	3	5211.1908	-0.0053
8	4	5	7	3	5	5253.8644	0.0002
6	6	0	5	5	0	5261.0200	0.0302

6	6	1	5	5	1	5261.0200	-0.0013
12	3	9	11	3	8	5360.7300	-0.0006
9	2	7	8	1	7	5485.9229	0.0025
8	5	3	7	4	3	5611.3885	-0.0001
8	5	4	7	4	4	5648.6488	-0.0008
9	3	7	8	2	7	5667.7925	0.0059
7	6	1	6	5	1	5693.4498	-0.0100
7	6	2	6	5	2	5693.7954	0.0016
9	4	6	8	3	6	5764.9740	-0.0012
10	4	6	9	3	6	5828.6697	0.0069
10	3	7	9	2	7	5848.3727	0.0112
9	5	4	8	4	4	5999.3019	-0.0015
15	3	13	14	3	12	6002.6012	-0.0016
9	5	5	8	4	5	6094.7442	-0.0039
8	6	2	7	5	2	6123.7946	0.0010
8	6	3	7	5	3	6125.7087	0.0106
10	2	8	9	1	8	6183.3545	0.0003
10	3	8	9	2	8	6286.1883	-0.0105
10	4	7	9	3	7	6307.3005	-0.0097
11	4	7	10	3	7	6333.5975	-0.0004
10	5	5	9	4	5	6359.9496	0.0007
11	3	8	10	2	8	6545.1656	0.0099
9	6	3	8	5	3	6549.0958	-0.0009
10	5	6	9	4	6	6556.5832	0.0109
9	6	4	8	5	4	6556.7955	-0.0039
8	7	1	7	6	1	6611.0211	0.0227
8	7	2	7	6	2	6611.0211	-0.0187
11	5	6	10	4	6	6709.1147	0.0008
11	5	6	10	4	6	6709.1147	0.0008
10	6	4	9	5	4	6963.9372	-0.0071
10	6	5	9	5	5	6988.4835	0.0130
9	7	3	8	6	3	7043.0076	-0.0052
12	5	7	11	4	7	7081.9716	-0.0031
12	5	7	11	4	7	7081.9716	-0.0031
8	8	0	7	7	0	7095.3500	-0.0038
8	8	1	7	7	1	7095.3500	-0.0042
12	3	9	11	2	9	7264.3606	-0.0090
11	6	5	10	5	5	7359.6774	0.0033
11	6	6	10	5	6	7424.1425	-0.0015
10	7	3	9	6	3	7472.2405	0.0031
10	7	4	9	6	4	7473.5504	-0.0083
9	8	1	8	7	1	7528.3008	0.0035
9	8	2	8	7	2	7528.3008	-0.0013
12	3	10	11	2	10	7560.1948	0.0075
11	7	4	10	6	4	7897.4548	-0.0094
11	7	5	10	6	5	7902.4134	0.0061
10	8	2	9	7	2	7960.5615	0.0216
10	8	3	9	7	3	7960.5615	-0.0154

Table S8.9. Measured frequencies and residuals (in MHz) for the rotational transitions of the conformer **3a** of civetone.

J'	K'_{-1}	K'_{+1}	J''	K''_{-1}	K''_{+1}	V _{obs}	V _{obs} - V _{calc}
4	2	2	3	1	2	2529.8384	0.0056
3	3	0	2	2	0	2579.3647	-0.0042
3	3	1	2	2	1	2595.3510	-0.0023
4	3	1	3	2	1	3004.8806	0.0026
5	2	3	4	1	3	3054.8128	0.0013
4	3	2	3	2	2	3073.6593	0.0002
5	2	4	4	1	4	3366.9898	-0.0058
5	3	2	4	2	2	3414.5903	0.0005
4	4	0	3	3	0	3530.7010	0.0041
4	4	1	3	3	1	3533.2209	0.0033
5	3	3	4	2	3	3576.7412	-0.0007
6	2	4	5	1	4	3641.3636	0.0146
6	3	3	5	2	3	3836.6527	-0.0038
5	4	1	4	3	1	3975.6601	0.0015
6	2	5	5	1	5	3991.0285	0.0014
5	4	2	4	3	2	3991.9600	-0.0047
6	3	4	5	2	4	4110.2217	0.0019
7	2	5	6	1	5	4294.1861	-0.0017
7	3	4	6	2	4	4303.0695	0.0019
6	4	2	5	3	2	4402.2494	0.0005
6	4	3	5	3	3	4459.5730	0.0006
5	5	0	4	4	0	4476.2684	0.0076
5	5	1	4	4	1	4476.5840	0.0009
7	1	6	6	0	6	4563.6360	-0.0132
7	2	6	6	1	6	4635.8750	-0.0012
7	3	5	6	2	5	4676.5489	0.0002
7	4	3	6	3	3	4803.4939	-0.0004
8	3	5	7	2	5	4833.3394	0.0011
6	5	1	5	4	1	4928.0229	0.0070
6	5	2	5	4	2	4930.7761	0.0066
7	4	4	6	3	4	4943.4627	0.0015
8	2	6	7	1	6	5000.5237	0.0039
8	4	4	7	3	4	5191.9785	0.0005
8	1	7	7	0	7	5259.4303	-0.0027
8	3	6	7	2	6	5274.6550	0.0055
7	5	2	6	4	2	5373.1494	0.0003
7	5	3	6	4	3	5385.9158	0.0008
6	6	0	5	5	0	5420.7679	-0.0062
6	6	1	5	5	1	5420.7679	-0.0432
9	3	6	8	2	6	5437.2365	0.0010
8	4	5	7	3	5	5451.3507	-0.0039
9	4	5	8	3	5	5601.4436	-0.0041
9	2	7	8	1	7	5729.1605	-0.0018
8	5	3	7	4	3	5803.2505	-0.0010
8	5	4	7	4	4	5845.0954	0.0001
7	6	1	6	5	1	5874.0402	0.0032
7	6	2	6	5	2	5874.4318	0.0038
9	3	7	8	2	7	5900.1374	-0.0038
9	2	8	8	1	8	5960.4978	0.0088
9	4	6	8	3	6	5989.1566	-0.0046
10	4	6	9	3	6	6066.0717	-0.0013
10	3	7	9	2	7	6114.2750	0.0008
9	5	4	8	4	4	6207.9960	-0.0026
9	5	5	8	4	5	6314.0464	-0.0007
8	6	2	7	5	2	6324.9361	-0.0007
8	6	3	7	5	3	6327.1641	0.0041
7	7	0	6	6	0	6365.1200	-0.0013
7	7	1	6	6	1	6365.1200	-0.0053
10	2	8	9	1	8	6452.1253	-0.0029
10	3	8	9	2	8	6546.4691	-0.0127

10	4	7	9	3	7	6559.5688	-0.0024
10	5	5	9	4	5	6585.2936	-0.0077
11	4	7	10	3	7	6606.1211	-0.0028
9	6	3	8	5	3	6770.2169	-0.0026
9	6	4	8	5	4	6779.1751	-0.0007
10	5	6	9	4	6	6800.3754	0.0071
8	7	1	7	6	1	6818.7619	-0.0030
8	7	2	7	6	2	6818.8168	0.0020
11	3	8	10	2	8	6844.2152	-0.0050
11	5	6	10	4	6	6955.0984	0.0069
11	2	9	10	1	9	7159.2848	0.0047
11	4	8	10	3	8	7161.5409	0.0035
10	6	4	9	5	4	7203.7916	0.0002
10	6	5	9	5	5	7232.1368	-0.0028
9	7	2	8	6	2	7271.2424	0.0061
9	7	3	8	6	3	7271.5775	0.0060
8	8	0	7	7	0	7309.4321	0.0038
8	8	1	7	7	1	7309.4321	0.0034
11	5	7	10	4	7	7311.6829	-0.0070
12	5	7	11	4	7	7355.9060	0.0112
12	3	9	11	2	9	7591.7480	0.0078
11	6	5	10	5	5	7616.1652	-0.0035
11	6	6	10	5	6	7689.9948	0.0029
10	7	3	9	6	3	7721.2393	-0.0041
10	7	4	9	6	4	7722.8253	-0.0049
9	8	1	8	7	1	7763.2210	0.0026
9	8	2	8	7	2	7763.2210	-0.0033
13	5	8	12	4	8	7823.0562	-0.0124
12	5	8	11	4	8	7853.7083	0.0122

Table S8.10. Measured frequencies and residuals (in MHz) for the rotational transitions of the conformer **20d** of civetone.

J'	K'_{-1}	K'_{+1}	J''	K''_{-1}	K''_{+1}	V _{obs}	V _{obs} - V _{calc}
3	3	0	2	2	0	2703.3466	0.0100
3	3	1	2	2	1	2719.7003	0.0112
4	2	3	3	1	3	2933.0217	0.0075
4	3	1	3	2	1	3166.6187	-0.0091
4	3	2	3	2	2	3236.8495	-0.0046
5	2	3	4	1	3	3254.7567	-0.0108
5	1	4	4	0	4	3350.7348	0.0134
5	3	2	4	2	2	3614.2218	-0.0013
4	4	1	3	3	1	3699.4130	-0.0029
5	3	3	4	2	3	3779.2869	-0.0096
6	2	4	5	1	4	3882.6392	0.0040
6	3	3	5	2	3	4075.0993	-0.0021
6	1	5	5	0	5	4100.5836	0.0110
5	4	1	4	3	1	4179.8158	-0.0034
5	4	2	4	3	2	4196.6376	0.0036
6	3	4	5	2	4	4352.6810	-0.0050
6	4	2	5	3	2	4643.9999	0.0020
5	5	0	4	4	0	4684.4254	0.0035
5	5	1	4	4	1	4684.7609	0.0033
6	4	3	5	3	3	4702.9791	-0.0088
7	4	3	6	3	3	5082.5132	-0.0028
7	4	3	6	3	3	5082.5132	-0.0028
8	3	5	7	2	5	5153.3691	0.0140
6	5	1	5	4	1	5174.4198	0.0110
6	5	2	5	4	2	5177.2821	0.0075
8	2	6	7	1	6	5326.2995	-0.0022
8	3	6	7	2	6	5598.3698	0.0024
7	5	2	6	4	2	5657.5449	-0.0046
7	5	3	6	4	3	5670.8171	-0.0029
6	6	0	5	5	0	5670.9813	0.0283
6	6	1	5	5	1	5670.9813	-0.0105
9	4	5	8	3	5	5957.7669	-0.0075
9	2	7	8	1	7	6096.3986	0.0036
8	5	3	7	4	3	6125.1800	-0.0017
7	6	1	6	5	1	6162.5050	0.0070
7	6	2	6	5	2	6162.9014	-0.0071
8	5	4	7	4	4	6168.5904	-0.0054
9	5	4	8	4	4	6566.8341	-0.0098
8	6	2	7	5	2	6651.6028	0.0043
8	6	3	7	5	3	6653.9220	-0.0092
7	7	0	6	6	0	6657.3126	-0.0045
7	7	1	6	6	1	6657.3126	-0.0087
9	5	5	8	4	5	6676.5172	-0.0050
10	5	6	9	4	6	7202.3719	-0.0050
11	3	8	10	2	8	7293.0831	-0.0167
11	5	6	10	4	6	7388.8856	0.0165
8	8	0	7	7	0	7643.6446	-0.0010
8	8	1	7	7	1	7643.6446	-0.0014
11	5	7	10	4	7	7753.9078	0.0144

Table S8.11. Measured frequencies and residuals (in MHz) for the rotational transitions of the conformer **8a** of civetone.

J'	K'_{-1}	K'_{+1}	J''	K''_{-1}	K''_{+1}	V _{obs}	V _{obs} - V _{calc}
4	2	2	3	2	1	2073.4225	-0.0007
5	3	3	4	3	2	2430.9813	-0.0030
5	4	2	4	4	1	2439.3797	0.0186
5	4	1	4	4	0	2446.0041	0.0122
6	0	6	5	1	5	2455.5170	-0.0071
6	1	6	5	1	5	2458.7629	-0.0047
6	0	6	5	0	5	2464.7508	-0.0013
6	1	6	5	0	5	2467.9826	-0.0130
3	3	1	2	2	0	2540.9034	-0.0048
3	3	0	2	2	0	2546.2685	0.0016
3	3	1	2	2	1	2568.2509	-0.0004
3	3	0	2	2	1	2573.6140	0.0040
5	2	3	4	2	2	2605.3715	0.0025
4	2	2	3	1	2	2617.2808	-0.0010
4	1	3	3	0	3	2619.1569	-0.0004
6	1	5	5	2	4	2657.2698	0.0012
6	2	5	5	2	4	2738.7680	-0.0013
6	1	5	5	1	4	2823.1548	-0.0011
7	0	7	6	1	6	2843.1859	-0.0071
7	1	7	6	1	6	2844.2831	0.0022
7	0	7	6	0	6	2846.4315	-0.0050
7	1	7	6	0	6	2847.5268	0.0025
4	2	3	3	1	3	2847.9515	-0.0023
6	3	4	5	3	3	2904.3742	-0.0013
6	2	5	5	1	4	2904.6559	-0.0007
6	4	3	5	4	2	2939.6865	0.0056
4	3	2	3	2	1	2962.5226	-0.0001
6	4	2	5	4	1	2967.1939	-0.0035
4	3	1	3	2	1	2997.9455	-0.0001
7	2	5	6	3	4	3031.2227	-0.0074
4	3	2	3	2	2	3086.3594	-0.0004
6	3	3	5	3	2	3090.5348	-0.0002
6	2	4	5	2	3	3101.3719	-0.0008
7	1	6	6	2	5	3108.7140	-0.0021
4	3	1	3	2	2	3121.7841	0.0014
7	2	6	6	2	5	3143.9704	-0.0008
7	1	6	6	1	5	3190.2173	0.0005
5	2	3	4	1	3	3207.8253	-0.0015
7	2	6	6	1	5	3225.4727	0.0009
8	0	8	7	1	7	3228.3446	0.0019
8	1	8	7	1	7	3228.6968	0.0012
8	0	8	7	0	7	3229.4249	-0.0057
8	1	8	7	0	7	3229.7803	-0.0031
5	3	3	4	2	2	3320.0872	0.0034
5	1	4	4	0	4	3348.2811	0.0041
7	3	5	6	3	4	3360.4683	0.0013
7	5	3	6	5	2	3429.4883	-0.0002
7	5	2	6	5	1	3435.8348	-0.0011
7	6	3	6	6	2	3435.8348	-0.0011
7	4	4	6	4	3	3437.6993	0.0082
5	3	2	4	2	2	3446.1862	-0.0006
4	4	1	3	3	0	3480.3782	-0.0047
4	4	0	3	3	0	3481.2250	-0.0221
4	4	1	3	3	1	3485.7399	-0.0017
4	4	0	3	3	1	3486.6113	0.0055
5	2	4	4	1	4	3489.6947	0.0009
7	4	3	6	4	2	3516.7759	-0.0037
8	1	7	7	2	6	3524.7501	-0.0053
8	2	7	7	2	6	3538.7349	0.0046
7	2	5	6	2	4	3548.9494	0.0017

8	1	7	7	1	6	3560.0117	0.0013
8	2	7	7	1	6	3573.9824	-0.0030
9	1	9	8	1	8	3612.6915	-0.0137
9	0	9	8	0	8	3612.9464	0.0000
6	3	4	5	2	3	3619.0968	0.0065
5	3	3	4	2	3	3635.8219	0.0006
7	3	4	6	3	3	3651.9054	-0.0011
5	3	2	4	2	3	3761.9271	0.0028
8	3	6	7	3	5	3796.9551	-0.0121
6	2	4	5	1	4	3869.6001	0.0171
7	3	5	6	2	4	3878.1967	0.0121
8	6	3	7	6	2	3913.7997	0.0044
9	1	8	8	2	7	3922.1467	-0.0057
8	4	5	7	4	4	3926.3102	0.0020
9	2	8	8	2	7	3927.3661	-0.0021
6	3	3	5	2	3	3931.3544	0.0016
9	1	8	8	1	7	3936.1267	-0.0006
8	5	4	7	5	3	3937.3785	0.0018
9	2	8	8	1	7	3941.3450	0.0018
5	4	2	4	3	1	3944.1189	-0.0069
8	2	6	7	2	5	3945.0899	0.0001
5	4	1	4	3	1	3951.6215	0.0008
8	5	3	7	5	2	3960.6304	-0.0009
8	6	4	7	6	3	3960.6304	-0.0009
5	4	2	4	3	2	3979.5481	-0.0006
5	4	1	4	3	2	3987.0441	0.0004
10	1	10	9	1	9	3996.5565	-0.0247
10	0	10	9	1	9	3996.5565	0.0099
10	0	10	9	0	9	3996.6790	0.0208
10	1	10	9	0	9	3996.6790	-0.0138
6	1	5	5	0	5	4085.5885	0.0148
8	4	4	7	4	3	4095.7822	0.0004
8	3	6	7	2	5	4126.2095	0.0055
9	2	7	8	3	6	4127.5474	-0.0009
6	2	5	5	1	5	4157.8412	-0.0052
8	3	5	7	3	4	4178.0492	-0.0022
9	3	7	8	3	6	4214.9301	0.0089
6	3	4	5	2	4	4221.4100	-0.0034
9	2	7	8	2	6	4308.6649	0.0024
10	1	9	9	2	8	4311.1113	-0.0010
10	2	9	9	2	8	4312.9800	0.0045
10	1	9	9	1	8	4316.3253	-0.0029
10	2	9	9	1	8	4318.1953	0.0040
6	4	3	5	3	2	4362.1458	0.0035
11	1	11	10	1	10	4380.4321	0.0128
11	0	11	10	0	10	4380.4321	-0.0113
11	1	11	10	0	10	4380.4321	-0.0218
11	0	11	10	1	10	4380.4321	0.0234
9	3	7	8	2	6	4396.0329	-0.0025
6	4	2	5	3	2	4397.1478	-0.0059
9	4	6	8	4	5	4398.9602	0.0007
5	5	1	4	4	0	4409.2827	0.0105
5	5	0	4	4	0	4409.3879	-0.0099
5	5	1	4	4	1	4410.1357	-0.0007
9	6	4	8	6	3	4422.9484	0.0077
9	5	5	8	5	4	4445.0879	-0.0079
7	3	4	6	2	4	4481.8832	-0.0035
6	4	3	5	3	3	4488.2443	-0.0010
9	5	4	8	5	3	4510.6555	0.0057
9	6	5	8	6	4	4510.6555	0.0057
6	4	2	5	3	3	4523.2568	0.0001
10	2	8	9	3	7	4579.9180	0.0000
7	2	5	6	1	5	4595.3832	0.0083
10	3	8	9	3	7	4618.0789	-0.0020
9	3	6	8	3	5	4653.3650	-0.0005

10	2	8	9	2	7	4667.2895	-0.0014
9	4	5	8	4	4	4681.5589	0.0025
11	1	10	10	2	9	4696.6491	-0.0002
11	2	10	10	2	9	4697.2934	0.0005
11	1	10	10	1	9	4698.5155	0.0030
11	2	10	10	1	9	4699.1545	-0.0016
10	3	8	9	2	7	4705.4489	-0.0049
7	4	4	6	3	3	4709.3038	0.0054
12	1	12	11	1	11	4764.2521	0.0022
12	0	12	11	0	11	4764.2521	-0.0052
12	1	12	11	0	11	4764.2521	-0.0084
12	0	12	11	1	11	4764.2521	0.0054
7	1	6	6	0	6	4811.0408	0.0024
7	4	3	6	3	3	4823.3965	-0.0018
7	3	5	6	2	5	4843.1011	-0.0100
10	4	7	9	4	6	4851.5001	-0.0004
6	5	2	5	4	1	4888.9082	0.0001
6	5	1	5	4	1	4890.2515	0.0000
6	5	2	5	4	2	4896.4034	0.0003
6	5	1	5	4	2	4897.7506	0.0041
10	6	5	9	6	4	4936.7829	0.0039
10	5	6	9	5	5	4946.2037	0.0020
8	4	5	7	3	4	4983.6978	-0.0023
11	2	9	10	3	8	4995.7706	-0.0049
11	3	9	10	3	8	5011.3028	-0.0044
7	4	4	6	3	4	5021.5577	-0.0032
11	2	9	10	2	8	5033.9352	-0.0032
11	3	9	10	2	8	5049.4727	0.0026
10	3	7	9	3	6	5070.4959	-0.0014
12	2	11	11	2	10	5081.1449	0.0051
12	1	11	11	1	10	5081.5614	-0.0055
12	2	11	11	1	10	5081.7765	-0.0068
10	5	5	9	5	4	5092.5086	-0.0020
10	6	6	9	6	5	5092.5086	-0.0020
8	3	5	7	2	5	5110.9907	0.0004
7	4	3	6	3	4	5135.6610	0.0002
13	1	13	12	1	12	5148.0760	-0.0055
13	0	13	12	0	12	5148.0760	-0.0077
13	1	13	12	0	12	5148.0760	-0.0087
13	0	13	12	1	12	5148.0760	-0.0045
9	4	6	8	3	5	5204.6136	0.0054
10	4	6	9	4	5	5239.8637	-0.0004
8	4	4	7	3	4	5267.2753	0.0017
11	4	8	10	4	7	5283.1568	0.0002
6	6	0	5	5	0	5335.9217	0.0619
6	6	1	5	5	1	5335.9217	-0.0466
6	6	1	5	5	0	5335.9217	0.0791
6	6	0	5	5	1	5335.9217	-0.0637
8	2	6	7	1	6	5350.2467	-0.0012
7	5	3	6	4	2	5351.1942	-0.0050
7	5	2	6	4	2	5358.8901	0.0001
7	5	3	6	4	3	5386.2128	0.0022
12	2	10	11	3	9	5392.9025	0.0094
7	5	2	6	4	3	5393.9021	0.0006
12	3	10	11	3	9	5398.8967	0.0007
12	3	10	11	2	9	5414.4329	0.0052
11	5	7	10	5	6	5433.6122	0.0023
11	3	8	10	3	7	5439.3501	0.0074
11	6	6	10	6	5	5452.1643	0.0068
8	3	6	7	2	6	5496.1072	0.0001
14	1	14	13	1	13	5531.9137	-0.0019
14	0	14	13	0	13	5531.9137	-0.0025
14	1	14	13	0	13	5531.9137	-0.0028
14	0	14	13	1	13	5531.9137	-0.0016
8	2	7	7	1	7	5537.4937	-0.0058

8	4	5	7	3	5	5587.4033	0.0012
11	4	8	10	3	7	5615.4003	-0.0021
11	5	6	10	5	5	5694.5486	-0.0067
11	6	7	10	6	6	5694.5486	-0.0067
11	4	7	10	4	6	5747.4021	-0.0010
9	4	5	8	3	5	5770.7770	-0.0016
8	5	4	7	4	3	5771.8001	0.0038
13	2	11	12	3	10	5781.5312	-0.0012
13	3	11	12	3	10	5783.7654	0.0031
13	2	11	12	2	10	5787.5407	0.0053
12	3	9	11	3	8	5788.7495	0.0027
13	3	11	12	2	10	5789.7719	0.0067
8	5	3	7	4	3	5802.7412	-0.0005
9	3	6	8	2	6	5819.2633	-0.0027
7	6	2	6	5	1	5819.4228	0.0078
7	6	1	6	5	1	5819.6502	0.0177
7	6	2	6	5	2	5820.7622	0.0038
7	6	1	6	5	2	5820.9669	-0.0090
14	1	13	13	1	12	5848.5648	-0.0263
14	2	13	13	1	12	5848.5648	-0.0494
14	2	13	13	2	12	5848.5648	0.0219
14	1	13	13	2	12	5848.5648	0.0449
8	4	4	7	3	5	5870.9699	-0.0058
12	4	9	11	3	8	5872.4941	0.0158
8	5	4	7	4	4	5885.8974	0.0012
12	5	8	11	5	7	5901.6923	0.0020
15	1	15	14	1	14	5915.7479	-0.0040
15	0	15	14	0	14	5915.7479	-0.0042
15	1	15	14	0	14	5915.7479	-0.0042
15	0	15	14	1	14	5915.7479	-0.0039
8	5	3	7	4	4	5916.8477	0.0060
12	6	7	11	6	6	5963.5651	-0.0016
9	2	7	8	1	7	6098.9032	0.0032
9	5	5	8	4	4	6121.1131	0.0029
13	3	10	12	3	9	6142.8912	0.0064
14	3	12	13	3	11	6167.5217	0.0033
14	2	12	13	2	11	6168.9460	0.0002
9	3	7	8	2	7	6172.2996	0.0017
13	4	10	12	3	9	6179.6358	0.0089
9	4	6	8	3	6	6189.4047	0.0103
12	4	8	11	4	7	6192.6834	-0.0006
9	5	4	8	4	4	6217.6069	-0.0028
15	1	14	14	1	13	6232.2700	0.0014
15	2	14	14	1	13	6232.2700	-0.0060
15	2	14	14	2	13	6232.2700	0.0170
15	1	14	14	2	13	6232.2700	0.0244
9	2	8	8	1	8	6236.1460	-0.0261
7	7	0	6	6	0	6262.0121	0.0072
7	7	1	6	6	1	6262.0121	-0.0077
7	7	1	6	6	0	6262.0121	0.0094
7	7	0	6	6	1	6262.0121	-0.0100
8	6	3	7	5	2	6297.3716	-0.0028
8	6	2	7	5	2	6298.8451	0.0034
16	1	16	15	1	15	6299.5890	-0.0008
16	0	16	15	0	15	6299.5890	-0.0008
16	1	16	15	0	15	6299.5890	-0.0009
16	0	16	15	1	15	6299.5890	-0.0008
8	6	3	7	5	3	6305.0623	-0.0030
8	6	2	7	5	3	6306.5370	0.0045
13	5	9	12	5	8	6347.7923	-0.0048
10	4	6	9	3	6	6357.2758	-0.0013
10	5	6	9	4	5	6385.7496	-0.0060
9	5	5	8	4	5	6404.6850	0.0012
13	6	8	12	6	7	6464.0294	0.0071
14	4	11	13	4	10	6486.5964	0.0096

9	5	4	8	4	5	6501.1798	-0.0035
14	3	11	13	3	10	6508.1329	0.0035
14	4	11	13	3	10	6523.3068	-0.0221
15	3	13	14	3	12	6550.9118	-0.0077
15	2	13	14	2	12	6551.4381	-0.0025
13	4	9	12	4	8	6577.2384	0.0007
10	3	7	9	2	7	6581.1028	0.0021
16	1	15	15	1	14	6615.9918	0.0007
16	2	15	15	2	14	6615.9918	0.0057
16	1	15	15	2	14	6615.9918	0.0080
16	2	15	15	1	14	6615.9918	-0.0016
10	5	5	9	4	5	6628.5610	-0.0030
17	1	17	16	1	16	6683.4333	0.0046
17	0	17	16	0	16	6683.4333	0.0046
17	1	17	16	0	16	6683.4333	0.0046
17	0	17	16	1	16	6683.4333	0.0046
9	4	5	8	3	6	6755.5533	-0.0116
9	6	4	8	5	3	6759.6788	-0.0050
9	6	3	8	5	3	6766.6310	-0.0025
14	5	10	13	5	9	6772.7562	-0.0131
9	6	4	8	5	4	6790.6242	-0.0050
9	6	3	8	5	4	6797.5833	0.0044
10	4	7	9	3	7	6825.9784	0.0047
10	2	8	9	1	8	6830.0750	0.0115
10	3	8	9	2	8	6863.0147	0.0041
15	4	12	14	4	11	6872.5057	-0.0095
10	5	6	9	4	6	6951.9206	-0.0055
18	1	18	17	1	17	7067.2693	0.0011
18	0	18	17	0	17	7067.2693	0.0011
18	1	18	17	0	17	7067.2693	0.0011
18	0	18	17	1	17	7067.2693	0.0011
11	5	6	10	4	6	7083.2653	0.0101
15	5	11	14	5	10	7180.3281	-0.0033
10	6	5	9	5	4	7185.8171	0.0041
8	8	0	7	7	0	7188.0779	-0.0075
8	8	1	7	7	1	7188.0779	-0.0095
10	6	4	9	5	4	7211.5261	0.0032
9	7	2	8	6	2	7229.0501	-0.0001
9	7	3	8	6	3	7230.2512	-0.0115
10	6	5	9	5	5	7282.3120	-0.0005
10	6	4	9	5	5	7308.0138	-0.0086
11	3	8	10	2	8	7353.1495	-0.0031
11	5	7	10	4	7	7534.0525	0.0170
11	6	6	10	5	5	7545.4688	0.0089
11	2	9	10	1	9	7547.6790	0.0052
11	3	9	10	2	9	7561.3437	0.0014
12	5	7	11	4	7	7619.1765	0.0005
11	6	5	10	5	5	7623.5695	0.0038
9	8	1	8	7	1	7672.8964	0.0076
9	8	2	8	7	2	7672.8964	-0.0205
10	7	3	9	6	3	7706.7624	0.0014
10	7	4	9	6	4	7712.3096	-0.0192
11	6	6	10	5	6	7788.2611	-0.0072

Table S8.12. Measured frequencies and residuals (in MHz) for the rotational transitions of the conformer **4a** of civetone.

J'	K'_{-1}	K'_{+1}	J''	K''_{-1}	K''_{+1}	V _{obs}	V _{obs} - V _{calc}
3	3	0	2	2	0	2404.6763	0.0018
3	3	1	2	2	1	2425.9015	-0.0001
4	2	2	3	1	2	2475.3278	-0.0051
4	3	1	3	2	1	2831.4126	0.0060
4	3	2	3	2	2	2916.3835	0.0003
5	3	2	4	2	2	3255.8162	-0.0029
4	4	0	3	3	0	3287.7983	0.0036
4	4	1	3	3	1	3292.2023	0.0028
5	2	4	4	1	4	3301.4491	-0.0027
5	3	3	4	2	3	3436.9840	-0.0015
6	2	4	5	1	4	3664.6353	-0.0016
6	3	3	5	2	3	3716.6553	-0.0065
5	4	1	4	3	1	3732.0747	-0.0019
5	4	2	4	3	2	3759.3695	0.0023
6	4	2	5	3	2	4152.5185	-0.0020
5	5	0	4	4	0	4164.3910	0.0008
5	5	1	4	4	1	4165.1226	-0.0018
7	3	4	6	2	4	4240.5254	0.0035
6	4	3	5	3	3	4241.0523	-0.0009
7	2	5	6	1	5	4353.4650	0.0100
6	5	1	5	4	1	4618.8358	-0.0030
6	5	2	5	4	2	4624.9409	-0.0024
8	3	5	7	2	5	4839.5966	-0.0015
8	4	4	7	3	4	4977.3187	-0.0038
6	6	0	5	5	0	5039.3997	0.0584
6	6	1	5	5	1	5039.3997	-0.0511
7	5	2	6	4	2	5061.2976	-0.0019
8	2	6	7	1	6	5068.1416	-0.0038
7	5	3	6	4	3	5088.3201	-0.0040
8	3	6	7	2	6	5200.8294	0.0060
8	2	7	7	1	7	5240.7157	0.0105
8	4	5	7	3	5	5283.4370	0.0009
9	4	5	8	3	5	5457.6477	0.0081
8	5	3	7	4	3	5479.7065	0.0032
7	6	2	6	5	2	5497.7938	-0.0043
9	3	6	8	2	6	5513.5464	-0.0038
8	5	4	7	4	4	5561.4944	-0.0002
9	2	7	8	1	7	5775.7243	0.0046
9	3	7	8	2	7	5841.6351	0.0080
9	4	6	8	3	6	5854.8304	0.0029
9	5	4	8	4	4	5870.9699	-0.0032
9	2	8	8	1	8	5901.9573	-0.0098
8	6	2	7	5	2	5949.4786	-0.0029
8	6	3	7	5	3	5955.7373	0.0023
10	4	6	9	3	6	6017.8171	-0.0096
9	5	5	8	4	5	6053.3791	-0.0065
10	5	5	9	4	5	6260.8998	0.0038
9	6	3	8	5	3	6391.0175	0.0017
9	6	4	8	5	4	6415.0492	0.0028
10	4	7	9	3	7	6458.9850	-0.0020
10	5	6	9	4	6	6572.8862	-0.0044
11	4	7	10	3	7	6664.0396	-0.0039
11	5	6	10	4	6	6695.4444	0.0130
10	6	4	9	5	4	6810.0801	0.0010
10	6	5	9	5	5	6880.5817	0.0025
11	3	9	10	2	9	7156.9453	-0.0030
11	6	5	10	5	5	7197.7235	-0.0048
12	5	7	11	4	7	7209.1073	-0.0022
12	3	10	11	2	10	7820.9700	0.0023

Table S8.13. Measured frequencies and residuals (in MHz) for the rotational transitions of the conformer **20b** of civetone.

J'	K'_{-1}	K'_{+1}	J''	K''_{-1}	K''_{+1}	V _{obs}	V _{obs} - V _{calc}
3	3	0	2	2	0	2320.4905	-0.0025
3	3	1	2	2	1	2352.8045	0.0029
6	1	6	5	1	5	2404.5435	-0.0116
6	0	6	5	0	5	2405.8821	0.0085
4	2	2	3	1	2	2589.4234	0.0007
6	2	5	5	2	4	2707.0544	0.0071
6	1	5	5	1	4	2741.4397	0.0024
4	3	1	3	2	1	2791.0745	-0.0032
4	3	2	3	2	2	2899.5193	-0.0026
6	3	4	5	3	3	2934.8981	0.0005
6	4	3	5	4	2	3022.5836	-0.0085
7	2	6	6	2	5	3091.0948	0.0038
7	1	6	6	1	5	3103.3161	0.0031
6	2	4	5	2	3	3103.9597	0.0036
6	4	2	5	4	1	3112.1169	-0.0098
8	1	8	7	1	7	3154.2578	0.0540
8	0	8	7	0	7	3154.2578	-0.0263
4	4	0	3	3	0	3165.4948	-0.0014
4	4	1	3	3	1	3175.9100	0.0036
6	3	3	5	3	2	3235.9378	-0.0026
5	2	3	4	1	3	3243.7085	-0.0035
5	3	2	4	2	2	3295.8394	0.0001
7	3	5	6	3	4	3364.0519	0.0086
5	2	4	4	1	4	3427.9006	-0.0013
8	1	7	7	1	6	3472.5557	-0.0055
7	2	5	6	2	4	3477.3417	-0.0073
5	3	3	4	2	3	3485.5755	0.0015
7	4	4	6	4	3	3517.5196	-0.0131
9	1	9	8	1	8	3528.8050	0.0058
9	0	9	8	0	8	3528.8050	-0.0128
7	5	3	6	5	2	3540.3115	0.0129
7	5	2	6	5	1	3573.5847	-0.0038
5	4	1	4	3	1	3637.5496	-0.0043
5	4	2	4	3	2	3694.1144	-0.0003
7	4	3	6	4	2	3724.2112	-0.0004
8	3	6	7	3	5	3768.2360	-0.0010
8	2	6	7	2	5	3823.7003	0.0042
9	2	8	8	2	7	3844.0917	-0.0157
9	1	8	8	1	7	3845.1784	0.0005
6	3	3	5	2	3	3869.4721	-0.0130
10	1	10	9	1	9	3903.3858	0.0019
10	0	10	9	0	9	3903.3858	-0.0024
6	2	4	5	1	4	3961.9583	0.0072
8	4	5	7	4	4	3985.5565	0.0028
5	5	0	4	4	0	4004.5324	0.0062
5	5	1	4	4	1	4007.1629	-0.0015
6	1	5	5	0	5	4090.8481	0.0117
6	4	2	5	3	2	4093.5184	0.0016
6	2	5	5	1	5	4106.5369	0.0041
6	3	4	5	2	4	4110.8456	-0.0037
9	2	7	8	2	6	4177.3633	0.0119
8	3	5	7	3	4	4204.3216	-0.0054
6	4	3	5	3	3	4239.8751	0.0026
11	1	11	10	1	10	4277.9594	-0.0113
11	0	11	10	0	10	4277.9594	-0.0123
6	5	1	5	4	1	4491.3475	-0.0013
6	5	2	5	4	2	4511.5348	0.0014
7	3	4	6	2	4	4524.7987	0.0019
12	1	12	11	1	11	4652.5695	0.0086
12	0	12	11	0	11	4652.5695	0.0084

7	2	5	6	1	5	4697.8728	0.0099
7	3	5	6	2	5	4767.8399	-0.0054
7	1	6	6	0	6	4788.2693	-0.0065
7	4	4	6	3	4	4822.5073	-0.0003
6	6	0	5	5	0	4840.5460	0.0035
6	6	1	5	5	1	4841.1376	0.0030
7	5	2	6	4	2	4952.8012	-0.0094
12	1	11	11	1	10	4967.6621	-0.0110
12	2	11	11	2	10	4967.6621	0.0071
13	1	13	12	1	12	5027.1618	0.0079
13	0	13	12	0	12	5027.1618	0.0079
7	5	3	6	4	3	5029.2334	-0.0065
8	4	4	7	3	4	5145.2522	-0.0086
8	3	5	7	2	5	5251.7812	0.0065
7	6	1	6	5	1	5334.8360	0.0003
7	6	2	6	5	2	5340.6133	0.0001
14	1	14	13	1	13	5401.7451	-0.0037
14	0	14	13	0	13	5401.7451	-0.0037
8	4	5	7	3	5	5444.0353	0.0174
8	3	6	7	2	6	5444.9913	-0.0001
8	1	7	7	0	7	5480.9594	-0.0069
8	5	4	7	4	4	5572.5886	0.0036
7	7	0	6	6	0	5675.7619	0.0810
7	7	1	6	6	1	5675.7619	-0.0427
9	4	5	8	3	5	5799.4796	0.0036
8	6	2	7	5	2	5815.1034	-0.0063
8	6	3	7	5	3	5843.9439	-0.0033
9	5	4	8	4	4	5866.3388	-0.0028
9	3	6	8	2	6	6001.9704	0.0041
9	4	6	8	3	6	6098.4775	-0.0024
9	3	7	8	2	7	6131.9893	0.0023
9	5	5	8	4	5	6151.7204	0.0011
9	1	8	8	0	8	6171.8567	-0.0034
8	7	1	7	6	1	6172.5991	0.0036
8	7	2	7	6	2	6174.0434	-0.0106
9	6	3	8	5	3	6266.5733	0.0070
9	6	4	8	5	4	6359.6355	-0.0106
10	5	5	9	4	5	6418.3914	0.0078
8	8	0	7	7	0	6510.6016	0.0108
8	8	1	7	7	1	6510.6016	-0.0139
10	4	6	9	3	6	6533.6459	0.0028
9	7	2	8	6	2	6663.1993	0.0004
9	7	3	8	6	3	6672.0888	-0.0059
10	6	4	9	5	4	6694.5821	0.0087
10	3	7	9	2	7	6735.4763	-0.0145
10	5	6	9	4	6	6769.9020	0.0002
10	4	7	9	3	7	6775.0713	0.0119
10	7	4	9	6	4	7173.3727	-0.0068
11	5	7	10	4	7	7422.3197	0.0011
11	3	8	10	2	8	7448.9510	-0.0067

Table S8.14. Measured frequencies and residuals (in MHz) for the rotational transitions of the conformer **67b** of civetone.

J'	K' ₋₁	K' ₊₁	J''	K'' ₋₁	K'' ₊₁	V _{obs}	V _{obs} - V _{calc}
3	3	1	2	2	0	2225.2437	-0.0040
3	3	1	2	2	1	2288.5244	0.0000
3	3	0	2	2	1	2313.1534	-0.0040
5	3	3	4	3	2	2546.8793	-0.0225
4	3	2	3	2	1	2617.5820	-0.0028
4	2	2	3	1	2	2642.5746	-0.0051
6	1	5	5	2	4	2721.2364	-0.0014
5	2	3	4	2	2	2721.7595	-0.0018
6	2	5	5	2	4	2726.2356	0.0019
6	1	5	5	1	4	2740.9565	-0.0017
6	2	5	5	1	4	2745.9528	-0.0012
4	3	1	3	2	1	2755.7889	0.0021
4	2	3	3	1	3	2781.4865	0.0016
7	0	7	6	1	6	2785.5746	0.0518
7	1	7	6	1	6	2785.5746	0.0351
7	0	7	6	0	6	2785.5746	-0.0400
7	1	7	6	0	6	2785.5746	-0.0567
4	3	2	3	2	2	2866.2042	-0.0044
5	3	3	4	2	2	2931.5519	0.0111
6	3	4	5	3	3	2994.5886	0.0016
4	3	1	3	2	2	3004.4157	0.0051
4	4	1	3	3	0	3053.6940	-0.0011
4	4	0	3	3	0	3061.5846	0.0038
4	4	1	3	3	1	3078.3377	0.0097
4	4	0	3	3	1	3086.2144	0.0006
7	1	6	6	2	5	3104.3740	-0.0013
7	2	6	6	2	5	3105.5063	-0.0057
7	1	6	6	1	5	3109.3710	-0.0002
7	2	6	6	1	5	3110.5125	0.0047
6	2	4	5	2	3	3118.9356	0.0027
6	4	3	5	4	2	3131.8606	-0.0008
8	0	8	7	1	7	3160.5902	0.0119
8	1	8	7	1	7	3160.5902	0.0089
8	0	8	7	0	7	3160.5902	-0.0049
8	1	8	7	0	7	3160.5902	-0.0078
6	3	4	5	2	3	3204.3686	0.0021
6	4	2	5	4	1	3296.6527	-0.0016
5	3	2	4	2	2	3318.6100	-0.0016
5	2	3	4	1	3	3341.9886	0.0033
6	3	3	5	3	2	3362.8204	0.0065
7	3	5	6	3	4	3407.9440	0.0043
5	1	4	4	0	4	3444.2864	0.0091
5	2	4	4	1	4	3461.6393	0.0042
7	2	5	6	2	4	3466.1804	0.0018
8	2	7	7	2	6	3481.4300	0.0037
8	2	7	7	1	6	3482.5657	0.0028
5	3	3	4	2	3	3486.6113	0.0018
5	4	2	4	3	1	3489.1350	0.0001
7	3	5	6	2	4	3493.3728	-0.0005
9	0	9	8	1	8	3535.6150	0.0044
9	1	9	8	1	8	3535.6150	0.0039
9	0	9	8	0	8	3535.6150	0.0015
9	1	9	8	0	8	3535.6150	0.0010
7	4	4	6	4	3	3620.5976	-0.0087
5	4	2	4	3	2	3627.3383	0.0014
5	4	1	4	3	2	3687.9264	0.0013
7	5	2	6	5	1	3771.5060	0.0054
8	3	6	7	3	5	3798.4142	0.0002
8	2	6	7	2	5	3818.2261	0.0003
6	4	3	5	3	2	3825.2262	0.0005

8	3	6	7	2	5	3825.6086	-0.0001
7	3	4	6	3	3	3837.4762	0.0120
9	1	8	8	2	7	3856.4507	0.0109
9	2	8	8	2	7	3856.4507	-0.0375
9	1	8	8	1	7	3856.6992	0.0187
9	2	8	8	1	7	3856.6992	-0.0297
5	5	1	4	4	0	3868.3022	-0.0002
5	5	0	4	4	0	3870.5628	-0.0004
5	3	2	4	2	3	3873.6963	0.0160
5	5	1	4	4	1	3876.1860	-0.0021
5	5	0	4	4	1	3878.4417	-0.0072
10	0	10	9	1	9	3910.6442	0.0013
10	1	10	9	1	9	3910.6442	0.0012
10	0	10	9	1	9	3910.6442	0.0013
10	1	10	9	0	9	3910.6442	0.0007
6	3	3	5	2	3	3959.6508	-0.0135
6	4	2	5	3	2	4050.6160	0.0091
8	4	5	7	4	4	4069.5550	0.0186
6	2	4	5	1	4	4078.4806	0.0023
7	4	4	6	3	3	4083.0184	0.0003
6	3	4	5	2	4	4144.1811	-0.0105
9	3	7	8	3	6	4177.9306	0.0018
9	2	7	8	2	6	4183.5041	0.0012
9	3	7	8	2	6	4185.3149	0.0031
10	1	9	9	2	8	4231.4282	0.0312
10	2	9	9	2	8	4231.4282	0.0219
10	1	9	9	1	8	4231.4282	-0.0172
10	2	9	9	1	8	4231.4282	-0.0265
11	0	11	10	1	10	4285.6810	0.0031
11	1	11	10	1	10	4285.6810	0.0031
11	0	11	10	0	10	4285.6810	0.0030
11	1	11	10	0	10	4285.6810	0.0030
8	4	5	7	3	4	4315.0941	0.0038
6	5	2	5	4	1	4346.8248	0.0004
6	5	1	5	4	1	4368.8986	-0.0011
6	5	2	5	4	2	4407.4125	-0.0001
6	5	1	5	4	2	4429.4904	0.0025
6	4	2	5	3	3	4437.6746	-0.0031
9	4	6	8	4	5	4482.9380	0.0017
8	4	4	7	4	3	4495.1889	0.0094
9	3	6	8	3	5	4550.2149	-0.0019
10	3	8	9	3	7	4553.6137	0.0056
10	2	8	9	2	7	4554.9971	-0.0076
9	4	6	8	3	5	4583.1502	0.0004
11	1	10	10	2	9	4606.3422	0.0108
11	2	10	10	2	9	4606.3422	0.0090
11	1	10	10	1	9	4606.3422	0.0014
11	2	10	10	1	9	4606.3422	-0.0004
7	4	3	6	3	3	4619.2713	-0.0103
12	0	12	11	1	11	4660.7161	0.0013
12	1	12	11	1	11	4660.7161	0.0013
12	0	12	11	0	11	4660.7161	0.0013
12	1	12	11	0	11	4660.7161	0.0013
6	6	1	5	5	0	4675.3685	-0.0024
6	6	0	5	5	1	4678.2451	0.0073
7	5	3	6	4	2	4736.8181	0.0011
7	2	5	6	1	5	4803.6971	-0.0017
7	4	4	6	3	4	4838.3148	-0.0010
7	5	2	6	4	2	4843.7463	0.0003
10	4	7	9	4	6	4873.0591	0.0020
10	3	7	9	3	6	4896.6046	-0.0104
11	3	9	10	3	8	4928.3477	0.0180
11	3	9	10	2	8	4928.7529	0.0109
9	4	5	8	4	4	4951.9114	-0.0055
7	5	3	6	4	3	4962.1995	0.0014

12	1	11	11	2	10	4981.2872	-0.0004
12	2	11	11	2	10	4981.2872	-0.0007
12	1	11	11	1	10	4981.2872	-0.0022
12	2	11	11	1	10	4981.2872	-0.0025
8	5	4	7	4	3	5017.0095	-0.0018
13	0	13	12	1	12	5035.7581	0.0053
13	1	13	12	1	12	5035.7581	0.0053
13	0	13	12	0	12	5035.7581	0.0053
13	1	13	12	0	12	5035.7581	0.0053
7	5	2	6	4	3	5069.1262	-0.0009
9	5	4	8	5	3	5072.8992	0.0015
7	6	2	6	5	1	5178.1516	0.0031
7	6	1	6	5	2	5207.3627	-0.0002
9	5	5	8	4	4	5223.0804	0.0087
11	4	8	10	4	7	5252.0136	0.0028
11	4	8	10	3	7	5261.3928	0.0068
8	4	4	7	3	4	5276.9989	0.0019
12	3	10	11	3	9	5302.9430	-0.0043
10	4	6	9	4	5	5309.6414	0.0057
8	5	3	7	4	3	5341.8817	-0.0019
13	1	12	12	2	11	5356.2640	-0.0011
13	2	12	12	2	11	5356.2640	-0.0012
13	1	12	12	1	11	5356.2640	-0.0015
13	2	12	12	1	11	5356.2640	-0.0015
7	4	3	6	3	4	5374.5754	-0.0040
14	0	14	13	1	13	5410.7915	0.0001
14	1	14	13	1	13	5410.7915	0.0001
14	0	14	13	0	13	5410.7915	0.0001
14	1	14	13	0	13	5410.7915	0.0001
10	5	6	9	4	5	5420.2013	-0.0201
8	3	5	7	2	5	5426.8945	0.0008
7	7	1	6	6	0	5479.7065	-0.0284
7	7	0	6	6	1	5480.4925	-0.0037
8	4	5	7	3	5	5499.9132	0.0006
8	2	6	7	1	6	5512.5491	-0.0042
8	3	6	7	2	6	5518.7964	-0.0033
8	5	4	7	4	4	5553.2703	-0.0045
12	4	9	11	4	8	5627.0417	-0.0143
8	6	3	7	5	2	5627.4159	0.0024
10	5	5	9	5	4	5627.9969	-0.0024
12	3	9	11	3	8	5628.8845	-0.0110
12	4	9	11	3	8	5629.4765	-0.0027
11	4	7	10	4	6	5634.3674	-0.0057
13	2	11	12	2	10	5677.6471	-0.0081
13	3	11	12	3	10	5677.6471	0.0066
13	3	11	12	2	10	5677.6471	-0.0118
14	1	13	13	2	12	5731.2585	0.0003
14	2	13	13	2	12	5731.2585	0.0003
14	1	13	13	1	12	5731.2585	0.0003
14	2	13	13	1	12	5731.2585	0.0003
8	6	2	7	5	3	5776.9125	0.0017
15	0	15	14	1	14	5785.8278	-0.0022
15	1	15	14	1	14	5785.8278	-0.0022
15	0	15	14	0	14	5785.8278	-0.0022
15	1	15	14	0	14	5785.8278	-0.0022
8	5	3	7	4	4	5878.1574	0.0102
9	5	4	8	4	4	5919.6090	0.0072
9	6	4	8	5	3	5968.9773	0.0040
13	4	10	12	3	9	6001.7774	-0.0047
9	4	5	8	3	5	6014.0426	0.0055
14	2	12	13	2	11	6052.4184	-0.0028
14	3	12	13	3	11	6052.4184	0.0002
14	3	12	13	2	11	6052.4184	-0.0035
11	5	6	10	5	5	6064.2602	0.0099
15	1	14	14	2	13	6106.2637	0.0018

15	2	14	14	2	13	6106.2637	0.0018
15	1	14	14	1	13	6106.2637	0.0018
15	2	14	14	1	13	6106.2637	0.0018
9	3	6	8	2	6	6158.8843	-0.0004
16	0	16	15	1	15	6160.8683	-0.0002
16	1	16	15	1	15	6160.8683	-0.0002
16	0	16	15	0	15	6160.8683	-0.0002
16	1	16	15	0	15	6160.8683	-0.0002
9	4	6	8	3	6	6184.4336	-0.0012
9	5	5	8	4	5	6184.9748	-0.0035
10	6	5	9	5	4	6194.2381	0.0057
9	2	7	8	1	7	6213.7378	0.0038
9	3	7	8	2	7	6215.2959	-0.0063
15	2	13	14	2	12	6427.2610	0.0000
15	3	13	14	3	12	6427.2611	0.0007
15	3	13	14	2	12	6427.2611	0.0000
9	6	3	8	5	4	6457.5513	0.0004
8	4	4	7	3	5	6461.8163	-0.0029
16	1	15	15	2	14	6481.2722	-0.0009
16	2	15	15	2	14	6481.2722	-0.0009
16	1	15	15	1	14	6481.2722	-0.0009
16	2	15	15	1	14	6481.2722	-0.0009
17	0	17	16	1	16	6535.8982	-0.0084
17	1	17	16	1	16	6535.8982	-0.0084
17	0	17	16	0	16	6535.8982	-0.0084
17	1	17	16	0	16	6535.8982	-0.0084
10	5	5	9	4	5	6595.6836	-0.0007
15	4	12	14	4	11	6749.6865	0.0151
10	4	6	9	3	6	6773.4539	-0.0021
17	1	16	16	2	15	6856.3060	0.0167
17	2	16	16	2	15	6856.3060	0.0167
17	1	16	16	1	15	6856.3060	0.0167
17	2	16	16	1	15	6856.3060	0.0167
10	3	7	9	2	7	6871.9994	0.0026
9	9	1	8	8	0	7086.5841	0.0342
9	9	0	8	8	1	7086.5841	-0.0136
17	2	15	16	2	14	7177.0606	-0.0082
10	6	4	9	5	5	7327.4915	-0.0088

Table S8.15. Measured frequencies and residuals (in MHz) for the rotational transitions of the conformer **24c** of civetone.

J'	K' ₋₁	K' ₊₁	J''	K'' ₋₁	K'' ₊₁	V _{obs}	V _{obs} - V _{calc}
6	1	6	5	1	5	2631.4657	0.0010
6	0	6	5	0	5	2631.4657	-0.0030
6	1	6	5	0	5	2631.4657	-0.0033
6	0	6	5	1	5	2631.4657	0.0013
5	2	3	4	2	2	2904.6559	0.0012
7	1	7	6	1	6	3042.9955	-0.0021
7	0	7	6	0	6	3042.9955	-0.0024
7	1	7	6	0	6	3042.9955	-0.0024
7	0	7	6	1	6	3042.9955	-0.0021
7	1	6	6	1	5	3367.5962	-0.0184
7	2	6	6	2	5	3367.5962	0.0246
7	1	6	6	2	5	3367.5962	0.0287
7	2	6	6	1	5	3367.5962	-0.0225
8	1	8	7	1	7	3454.5371	0.0056
8	0	8	7	0	7	3454.5371	0.0056
8	1	8	7	0	7	3454.5371	0.0056
8	0	8	7	1	7	3454.5371	0.0056
7	3	5	6	3	4	3692.2836	0.0274
8	1	7	7	1	6	3779.0535	-0.0020
8	2	7	7	2	6	3779.0535	0.0017
8	1	7	7	2	6	3779.0535	0.0021
8	2	7	7	1	6	3779.0535	-0.0024
9	1	9	8	1	8	3866.0662	0.0002
9	0	9	8	0	8	3866.0662	0.0002
9	1	9	8	0	8	3866.0662	0.0002
9	0	9	8	1	8	3866.0662	0.0002
8	3	6	7	3	5	4104.0764	-0.0049
9	1	8	8	1	7	4190.5505	0.0035
9	2	8	8	2	7	4190.5505	0.0038
9	1	8	8	2	7	4190.5505	0.0039
9	2	8	8	1	7	4190.5505	0.0035
10	1	10	9	1	9	4277.5978	-0.0023
10	0	10	9	0	9	4277.5978	-0.0023
10	0	10	9	0	9	4277.5978	-0.0023
10	1	10	9	0	9	4277.5978	-0.0023
9	3	7	8	3	6	4515.4097	-0.0063
10	1	9	9	1	8	4602.0618	0.0063
10	2	9	9	2	8	4602.0618	0.0064
10	1	9	9	2	8	4602.0618	0.0064
10	2	9	9	1	8	4602.0618	0.0063
11	1	11	10	1	10	4689.1309	-0.0026
11	0	11	10	0	10	4689.1309	-0.0026
11	1	11	10	0	10	4689.1309	-0.0026
11	0	11	10	1	10	4689.1309	-0.0026
10	2	8	9	2	7	4926.7751	-0.0139
10	3	8	9	3	7	4926.7751	-0.0115
11	1	10	10	1	9	5013.5865	0.0146
11	2	10	10	2	9	5013.5865	0.0146
11	1	10	10	2	9	5013.5865	0.0146
11	2	10	10	1	9	5013.5865	0.0146
12	1	12	11	1	11	5100.6655	-0.0001
12	0	12	11	0	11	5100.6655	-0.0001
12	1	12	11	0	11	5100.6655	-0.0001
12	0	12	11	1	11	5100.6655	-0.0001
11	2	9	10	2	8	5338.2097	-0.0031
11	3	9	10	3	8	5338.2097	-0.0029
12	1	11	11	1	10	5425.0680	-0.0242
12	2	11	11	2	10	5425.0680	-0.0242
12	2	11	11	1	10	5425.0680	-0.0242
12	1	11	11	2	10	5425.0680	-0.0242

13	1	13	12	1	12	5512.1923	-0.0040
13	0	13	12	0	12	5512.1923	-0.0040
13	1	13	12	0	12	5512.1923	-0.0040
13	0	13	12	1	12	5512.1923	-0.0040
12	3	10	11	3	9	5749.6646	-0.0085
13	1	12	12	1	11	5836.6163	0.0019
13	2	12	12	1	11	5836.6163	0.0019
13	2	12	12	2	11	5836.6163	0.0019
13	1	12	12	2	11	5836.6163	0.0019
14	1	14	13	1	13	5923.7464	0.0211
14	0	14	13	0	13	5923.7464	0.0211
14	1	14	13	0	13	5923.7464	0.0211
14	0	14	13	1	13	5923.7464	0.0211
13	2	11	12	2	10	6161.1543	0.0006
13	3	11	12	3	10	6161.1543	0.0006
14	1	13	13	1	12	6248.1385	0.0015
14	2	13	13	1	12	6248.1385	0.0015
14	2	13	13	2	12	6248.1385	0.0015
14	1	13	13	2	12	6248.1385	0.0015
15	1	15	14	1	14	6335.2396	-0.0128
15	0	15	14	0	14	6335.2396	-0.0128
15	1	15	14	0	14	6335.2396	-0.0128
15	0	15	14	1	14	6335.2396	-0.0128
14	2	12	13	2	11	6572.6520	0.0055
14	3	12	13	3	11	6572.6520	0.0055
15	1	14	14	1	13	6659.6704	0.0112
15	2	14	14	1	13	6659.6704	0.0112
15	2	14	14	2	13	6659.6704	0.0112
15	1	14	14	2	13	6659.6704	0.0112
18	1	18	17	1	17	7569.8167	-0.0040
18	0	18	17	0	17	7569.8167	-0.0040
18	1	18	17	0	17	7569.8167	-0.0040
18	0	18	17	1	17	7569.8167	-0.0040

Table S8.16. Measured frequencies and residuals (in MHz) for the rotational transitions of the conformer **30a** of civetone.

J'	K'_{-1}	K'_{+1}	J''	K''_{-1}	K''_{+1}	V _{obs}	V _{obs} - V _{calc}
6	1	6	5	1	5	2590.7519	-0.0138
6	0	6	5	0	5	2590.7519	-0.0142
6	1	6	5	0	5	2590.7519	-0.0143
6	0	6	5	1	5	2590.7519	-0.0138
4	2	2	3	1	2	2845.1995	-0.0079
4	3	2	3	2	2	2867.6662	0.0081
4	4	1	3	3	1	2914.7513	-0.0045
7	1	7	6	1	6	2996.7477	-0.0009
7	0	7	6	0	6	2996.7477	-0.0009
7	1	7	6	0	6	2996.7477	-0.0009
7	0	7	6	1	6	2996.7477	-0.0009
7	1	6	6	1	5	3306.4955	0.0030
7	2	6	6	2	5	3306.4955	0.0077
7	1	6	6	2	5	3306.4955	0.0080
7	2	6	6	1	5	3306.4955	0.0027
8	1	8	7	1	7	3402.7265	-0.0053
8	0	8	7	0	7	3402.7265	-0.0053
8	1	8	7	0	7	3402.7265	-0.0053
8	0	8	7	1	7	3402.7265	-0.0053
5	3	2	4	2	2	3546.2693	-0.0041
5	2	3	4	1	3	3572.2479	0.0046
5	4	2	4	3	2	3587.5450	-0.0023
5	5	0	4	4	0	3623.5767	-0.0014
8	1	7	7	1	6	3712.4449	-0.0006
8	2	7	7	2	6	3712.4449	-0.0003
8	1	7	7	2	6	3712.4449	-0.0003
8	2	7	7	1	6	3712.4449	-0.0006
9	1	9	8	1	8	3808.7103	-0.0045
9	0	9	8	0	8	3808.7103	-0.0045
9	1	9	8	0	8	3808.7103	-0.0045
9	0	9	8	1	8	3808.7103	-0.0045
9	1	8	8	1	7	4118.4048	-0.0080
9	2	8	8	2	7	4118.4048	-0.0080
9	1	8	8	2	7	4118.4048	-0.0080
9	2	8	8	1	7	4118.4048	-0.0080
10	1	10	9	1	9	4214.7001	0.0030
10	0	10	9	0	9	4214.7001	0.0030
10	1	10	9	0	9	4214.7001	0.0030
10	0	10	9	1	9	4214.7001	0.0030
6	4	2	5	3	2	4245.5120	-0.0052
6	5	1	5	4	1	4255.4698	0.0003
6	3	3	5	2	3	4280.9530	-0.0012
6	5	2	5	4	2	4309.3574	0.0002
6	6	0	5	5	0	4362.8335	0.0016
6	6	1	5	5	1	4380.7577	0.0044
10	1	9	9	1	8	4524.3913	0.0055
10	2	9	9	2	8	4524.3913	0.0055
10	1	9	9	2	8	4524.3913	0.0055
10	2	9	9	1	8	4524.3913	0.0055
11	1	11	10	1	10	4620.6872	0.0089
11	0	11	10	0	10	4620.6872	0.0089
11	1	11	10	0	10	4620.6872	0.0089
11	0	11	10	1	10	4620.6872	0.0089
11	1	10	10	1	9	4930.3747	0.0134
11	2	10	10	2	9	4930.3747	0.0134
11	1	10	10	2	9	4930.3747	0.0134
11	2	10	10	1	9	4930.3747	0.0134
7	5	2	6	4	2	4945.8308	-0.0142
7	6	1	6	5	1	4978.1647	0.0016
7	4	3	6	3	3	4985.5495	-0.0010

7	5	3	6	4	3	5003.8635	0.0008
7	7	0	6	6	0	5103.6712	-0.0078
7	7	1	6	6	1	5116.0022	-0.0055
12	1	11	11	1	10	5336.3422	0.0044
12	2	11	11	2	10	5336.3422	0.0044
12	1	11	11	2	10	5336.3422	0.0044
12	2	11	11	1	10	5336.3422	0.0044
8	6	2	7	5	2	5649.5238	-0.0024
8	7	1	7	6	1	5707.6886	0.0131
8	4	4	7	3	4	5712.9952	0.0006
8	5	4	7	4	4	5715.8388	0.0058
8	6	3	7	5	3	5719.1217	0.0030
13	1	12	12	1	11	5742.3178	0.0036
13	2	12	12	2	11	5742.3178	0.0036
13	1	12	12	2	11	5742.3178	0.0036
13	2	12	12	1	11	5742.3178	0.0036
8	7	2	7	6	2	5759.7389	0.0022
8	8	0	7	7	0	5844.5859	0.0029
8	8	1	7	7	1	5852.4141	-0.0008
14	1	13	13	1	12	6148.2747	-0.0154
14	2	13	13	2	12	6148.2747	-0.0154
14	1	13	13	2	12	6148.2747	-0.0154
14	2	13	13	1	12	6148.2747	-0.0154
9	7	2	8	6	2	6358.0768	-0.0073
9	6	3	8	5	3	6381.3921	0.0121
9	5	4	8	4	4	6421.0264	0.0015
9	6	4	8	5	4	6427.6015	0.0001
9	5	5	8	4	5	6432.2388	0.0050
9	7	3	8	6	3	6435.8680	-0.0134
9	4	6	8	3	6	6435.9939	-0.0014
9	3	6	8	2	6	6435.9940	0.0065
9	2	7	8	1	7	6438.2889	-0.0003
9	3	7	8	2	7	6438.2889	-0.0004
9	1	8	8	0	8	6439.7653	-0.0016
9	2	8	8	1	8	6439.7653	-0.0016
9	8	1	8	7	1	6443.6902	0.0068
9	8	2	8	7	2	6488.5204	0.0091
9	9	1	8	8	1	6589.6705	0.0002
10	7	3	9	6	3	7075.5279	-0.0026
10	5	6	9	4	6	7148.8702	-0.0099
10	3	7	9	2	7	7152.0360	0.0089
10	10	0	9	9	0	7324.7899	0.0004
10	10	1	9	9	1	7327.4915	-0.0129
11	5	7	10	4	7	7865.2480	0.0021

Table S8.17. Measured frequencies and residuals (in MHz) for the rotational transitions of the conformer **85a** of civetone.

J'	K'_{-1}	K'_{+1}	J''	K''_{-1}	K''_{+1}	V _{obs}	V _{obs} - V _{calc}
5	0	5	4	1	4	2046.7148	0.0038
5	1	5	4	0	4	2046.7148	0.0015
5	1	4	4	2	3	2374.6611	-0.0092
5	2	4	4	1	3	2375.0950	0.0127
4	3	2	3	2	1	2376.2219	-0.0009
6	0	6	5	1	5	2423.2467	-0.0002
6	1	6	5	0	5	2423.2467	-0.0003
5	2	3	4	3	2	2694.6641	-0.0019
5	3	3	4	2	2	2713.9342	0.0027
4	4	1	3	3	0	2734.0476	0.0013
6	1	5	5	2	4	2751.3380	0.0114
6	2	5	5	1	4	2751.3380	-0.0089
7	0	7	6	1	6	2799.7832	0.0000
7	1	7	6	0	6	2799.7832	0.0000
5	3	2	4	4	1	2911.3001	-0.0045
4	4	0	3	3	1	2952.1839	-0.0035
6	2	4	5	3	3	3079.0579	-0.0027
6	3	4	5	2	3	3080.7212	0.0028
5	4	2	4	3	1	3113.8441	0.0055
7	1	6	6	2	5	3127.8431	0.0001
7	2	6	6	1	5	3127.8431	-0.0008
8	0	8	7	1	7	3176.3206	0.0007
8	1	8	7	0	7	3176.3206	0.0007
6	3	3	5	4	2	3388.6798	-0.0020
6	4	3	5	3	2	3433.3963	0.0004
7	3	5	6	2	4	3456.1152	-0.0512
7	2	5	6	3	4	3456.1152	0.0509
5	5	1	4	4	0	3472.7400	0.0026
8	1	7	7	2	6	3504.3649	-0.0003
8	2	7	7	1	6	3504.3649	-0.0003
6	4	2	5	5	1	3539.8083	0.0071
9	0	9	8	1	8	3552.8580	0.0012
9	1	9	8	0	8	3552.8580	0.0012
7	3	4	6	4	3	3783.0203	0.0004
7	4	4	6	3	3	3788.0069	0.0008
8	3	6	7	2	5	3832.5288	-0.0028
8	2	6	7	3	5	3832.5288	0.0025
6	5	2	5	4	1	3859.0179	-0.0010
9	1	8	8	2	7	3880.8931	-0.0001
9	2	8	8	1	7	3880.8931	-0.0001
5	4	1	4	3	2	3903.6407	-0.0057
10	0	10	9	1	9	3929.3940	0.0005
10	1	10	9	0	9	3929.3940	0.0005
7	4	3	6	5	2	4074.6235	0.0040
7	5	2	6	6	1	4144.2973	0.0607
8	3	5	7	4	4	4160.9856	-0.0099
8	4	5	7	3	4	4161.3840	0.0131
7	5	3	6	4	2	4162.5102	-0.0003
9	3	7	8	2	6	4209.0073	0.0034
9	2	7	8	3	6	4209.0073	0.0037
6	6	1	5	5	0	4212.3571	-0.0011
10	1	9	9	2	8	4257.4239	-0.0002
10	2	9	9	1	8	4257.4239	-0.0002
11	0	11	10	1	10	4305.9291	-0.0010
11	1	11	10	0	10	4305.9291	-0.0010
6	6	0	5	5	1	4340.7274	-0.0023
8	4	4	7	5	3	4485.9060	-0.0003
8	5	4	7	4	3	4498.3361	-0.0026
9	4	6	8	3	5	4537.3802	-0.0116
9	3	6	8	4	5	4537.3802	0.0109

10	3	8	9	2	7	4585.5035	-0.0008
10	2	8	9	3	7	4585.5035	-0.0008
7	6	2	6	5	1	4610.8441	0.0000
11	1	10	10	2	9	4633.9566	0.0001
11	2	10	10	1	9	4633.9566	0.0001
12	0	12	11	1	11	4682.4650	-0.0013
12	1	12	11	0	11	4682.4650	-0.0013
8	5	3	7	6	2	4748.9246	0.0080
9	4	5	8	5	4	4866.1465	-0.0035
9	5	5	8	4	4	4867.2797	0.0020
8	6	3	7	5	2	4902.5442	-0.0072
10	4	7	9	3	6	4913.7474	-0.0016
10	3	7	9	4	6	4913.7474	-0.0004
7	7	1	6	6	0	4950.4699	0.0025
11	3	9	10	2	8	4962.0167	-0.0008
11	2	9	10	3	8	4962.0167	-0.0008
6	4	2	5	3	3	4989.9346	0.0077
12	1	11	11	2	10	5010.4910	0.0014
12	2	11	11	1	10	5010.4910	0.0014
7	7	0	6	6	1	5041.6242	-0.0010
13	0	13	12	1	12	5059.0013	-0.0010
13	1	13	12	0	12	5059.0013	-0.0010
9	5	4	8	6	3	5186.6091	-0.0012
9	6	4	8	5	3	5213.6804	-0.0019
7	6	1	6	5	2	5230.2986	-0.0051
10	5	6	9	4	5	5242.4984	-0.0345
10	4	6	9	5	5	5242.4984	0.0446
11	4	8	10	3	7	5290.1860	-0.0016
11	3	8	10	4	7	5290.1860	-0.0015
12	3	10	11	2	9	5338.5371	-0.0003
12	2	10	11	3	9	5338.5371	-0.0003
8	7	2	7	6	1	5367.8562	0.0001
13	1	12	12	2	11	5387.0217	-0.0013
13	2	12	12	1	11	5387.0217	-0.0013
9	6	3	8	7	2	5407.4596	-0.0111
14	0	14	13	1	13	5435.5413	0.0035
14	1	14	13	0	13	5435.5413	0.0035
10	5	5	9	6	4	5571.4581	-0.0043
10	6	5	9	5	4	5574.3922	0.0033
11	5	7	10	4	6	5618.6610	-0.0001
11	4	7	10	5	6	5618.6610	0.0046
9	7	3	8	6	2	5653.5793	0.0026
12	4	9	11	3	8	5666.6577	-0.0040
12	3	9	11	4	8	5666.6577	-0.0040
8	8	1	7	7	0	5685.5664	0.0007
13	3	11	12	2	10	5715.0626	0.0014
13	2	11	12	3	10	5715.0626	0.0014
8	8	0	7	7	1	5747.5872	-0.0034
14	1	13	13	2	12	5763.5535	-0.0029
14	2	13	13	1	12	5763.5535	-0.0029
15	0	15	14	1	14	5812.0685	-0.0044
15	1	15	14	0	14	5812.0685	-0.0044
10	8	2	9	9	1	5813.6341	-0.0143
10	6	4	9	7	3	5883.4386	0.0079
8	7	1	7	6	2	5891.8327	-0.0035
10	7	4	9	6	3	5936.4804	0.0046
11	5	6	10	6	5	5947.8247	-0.0390
11	6	6	10	5	5	5948.1218	0.0207
12	5	8	11	4	7	5994.9846	0.0010
12	4	8	11	5	7	5994.9846	0.0012
13	4	10	12	3	9	6043.1434	-0.0116
13	3	10	12	4	9	6043.1434	-0.0116
10	7	3	9	8	2	6046.1241	0.0165
7	4	3	6	3	4	6061.8988	-0.0016
14	3	12	13	2	11	6091.5870	-0.0003

14	2	12	13	3	11	6091.5870	-0.0003
9	8	2	8	7	1	6127.9887	0.0000
15	1	14	14	2	13	6140.0888	-0.0008
15	2	14	14	1	13	6140.0888	-0.0008
16	0	16	15	1	15	6188.6057	-0.0018
16	1	16	15	0	15	6188.6057	-0.0018
11	6	5	10	7	4	6276.7114	0.0138
8	6	2	7	5	3	6312.8997	0.0007
12	6	7	11	5	6	6323.8071	-0.0062
12	5	7	11	6	6	6323.8071	0.0097
13	5	9	12	4	8	6371.3821	-0.0041
13	4	9	12	5	8	6371.3821	-0.0041
10	8	3	9	7	2	6414.6697	-0.0077
9	9	1	8	8	0	6417.2281	-0.0058
14	4	11	13	3	10	6419.6574	-0.0020
14	3	11	13	4	10	6419.6574	-0.0020
9	9	0	8	8	1	6457.9905	-0.0049
15	3	13	14	2	12	6468.1154	0.0008
15	2	13	14	3	12	6468.1154	0.0008
16	1	15	15	2	14	6516.6156	-0.0070
16	2	15	15	1	14	6516.6156	-0.0070
9	8	1	8	7	2	6555.6641	-0.0030
17	0	17	16	1	16	6565.1501	0.0085
17	1	17	16	0	16	6565.1501	0.0085
11	7	4	10	8	3	6573.9776	0.0071
12	6	6	11	7	5	6653.6672	-0.0024
12	7	6	11	6	5	6654.3017	0.0002
11	8	3	10	9	2	6661.2866	-0.0034
11	8	4	10	7	3	6669.2689	0.0040
13	6	8	12	5	7	6699.9408	0.0008
13	5	8	12	6	7	6699.9408	0.0018
14	5	10	13	4	9	6747.8293	-0.0020
14	4	10	13	5	9	6747.8293	-0.0020
15	4	12	14	3	11	6796.1707	0.0000
15	3	12	14	4	11	6796.1707	0.0000
16	3	14	15	2	13	6844.6393	-0.0034
16	2	14	15	3	13	6844.6393	-0.0034
10	9	2	9	8	1	6888.6681	0.0057
17	1	16	16	2	15	6893.1633	0.0082
17	2	16	16	1	15	6893.1633	0.0082
9	7	2	8	6	3	6960.3044	0.0144
12	7	5	11	8	4	6981.3616	0.0051
12	8	5	11	7	4	6995.7363	-0.0017
14	6	9	13	5	8	7076.2101	-0.0144
14	5	9	13	6	8	7076.2101	-0.0143
15	5	11	14	4	10	7124.2997	-0.0016
15	4	11	14	5	10	7124.2997	-0.0016
10	10	1	9	9	0	7145.7998	-0.0139
10	10	0	9	9	1	7171.8710	-0.0040
11	9	3	10	8	2	7184.3333	0.0109
17	3	15	16	2	14	7221.1723	0.0012
17	2	15	16	3	14	7221.1723	0.0012
10	9	1	9	8	2	7224.5722	0.0041
18	1	17	17	2	16	7269.6967	0.0095
18	2	17	17	1	16	7269.6967	0.0095
19	0	19	18	1	18	7318.2012	-0.0070
19	1	19	18	0	18	7318.2012	-0.0070
14	7	8	13	6	7	7405.1173	0.0058
14	6	8	13	7	7	7405.1173	0.0089
12	9	4	11	8	3	7414.1167	0.0070
9	6	3	8	5	4	7432.6698	-0.0025
15	6	10	14	5	9	7452.5931	0.0019
15	5	10	14	6	9	7452.5931	0.0019
10	8	2	9	7	3	7600.8938	0.0111
11	11	1	10	10	0	7871.9572	-0.0109

11	11	0	10	10	1	7888.2654	-0.0086
11	10	1	10	9	2	7900.7744	-0.0014

6. APPENDIX VI

Table S9.1. Measured frequencies and residuals (in MHz) for the rotational transitions of the conformer **2b** of exaltolide.

J'	K' ₋₁	K' ₊₁	J''	K'' ₋₁	K'' ₊₁	V _{obs}	V _{obs} - V _{calc}
3	2	1	2	1	1	2328.0102	0.0106
3	3	0	2	2	0	2498.4839	-0.0001
3	3	1	2	2	1	2544.5376	0.0049
4	2	2	3	2	1	2652.0276	0.0004
5	3	3	4	3	2	3017.9217	-0.0028
4	2	2	3	1	2	3094.4568	0.0038
4	3	1	3	2	1	3139.2535	-0.0300
5	4	2	4	4	1	3139.2535	0.0070
5	2	3	4	2	2	3169.8111	-0.0018
4	1	3	3	0	3	3172.8818	-0.0064
6	2	5	5	2	4	3184.7824	-0.0006
6	1	5	5	1	4	3189.4880	-0.0005
4	2	3	3	1	3	3196.2128	-0.0042
4	3	2	3	2	2	3246.7559	0.0019
7	1	7	6	1	6	3268.2519	0.0015
7	0	7	6	0	6	3268.2519	-0.0095
4	4	0	3	3	0	3382.6060	0.0017
4	4	1	3	3	1	3410.2014	0.0046
6	3	4	5	3	3	3518.0387	0.0037
6	2	4	5	2	3	3589.4742	-0.0078
7	2	6	6	2	5	3627.3284	-0.0123
7	1	6	6	1	5	3628.1900	0.0031
8	1	8	7	1	7	3709.4962	-0.0032
8	0	8	7	0	7	3709.4962	-0.0047
5	3	2	4	2	2	3856.2252	0.0024
5	2	3	4	1	3	3925.0587	-0.0089
6	3	3	5	3	2	3972.0379	0.0015
7	3	5	6	3	4	3981.3563	0.0003
5	4	1	4	3	1	3986.1911	0.0000
5	2	4	4	1	4	3989.5622	0.0000
5	3	3	4	2	3	3995.7917	0.0065
7	2	5	6	2	4	4002.3425	0.0092
6	4	2	5	4	1	4028.8382	-0.0038
5	4	2	4	3	2	4084.5503	0.0030
9	1	9	8	1	8	4150.7444	-0.0063
9	0	9	8	0	8	4150.7444	-0.0064
5	5	0	4	4	0	4270.4351	0.0037
7	4	4	6	4	3	4280.3538	-0.0034
5	5	1	4	4	1	4283.1879	0.0058
8	3	6	7	3	5	4428.1314	0.0027
7	5	3	6	5	2	4429.1625	-0.0010
8	2	6	7	2	5	4432.8096	-0.0078
7	3	4	6	3	3	4437.2463	0.0041
9	1	8	8	1	7	4509.8112	-0.0087
9	2	8	8	2	7	4509.8112	0.0117
10	1	10	9	1	9	4592.0067	0.0023
10	0	10	9	0	9	4592.0067	0.0023
6	4	2	5	3	2	4646.0743	0.0077
6	3	3	5	2	3	4658.4431	-0.0031
7	4	3	6	4	2	4722.5068	0.0140
6	2	4	5	1	4	4756.4444	-0.0138
8	4	5	7	4	4	4770.3650	0.0024
6	1	5	5	0	5	4787.8980	0.0112
6	2	5	5	1	5	4788.7734	-0.0257
6	4	3	5	3	3	4804.6914	0.0005
8	3	5	7	3	4	4834.6391	0.0050

6	5	1	5	4	1	4866.3650	-0.0002
9	3	7	8	3	6	4869.9856	-0.0045
6	5	2	5	4	2	4936.0629	0.0040
10	1	9	9	1	8	4950.9661	-0.0003
10	2	9	9	2	8	4950.9661	0.0027
11	1	11	10	1	10	5033.2589	-0.0007
11	0	11	10	0	10	5033.2589	-0.0007
6	6	0	5	5	0	5155.5095	0.0114
9	4	6	8	4	5	5228.0755	0.0026
9	3	6	8	3	5	5246.2262	0.0046
8	4	4	7	4	3	5272.9058	-0.0002
10	3	8	9	3	7	5310.9140	-0.0010
11	1	10	10	1	9	5392.1585	0.0033
11	2	10	10	2	9	5392.1585	0.0037
7	4	3	6	3	3	5396.5363	0.0132
7	5	2	6	4	2	5473.9546	0.0006
12	1	12	11	1	11	5474.5160	0.0007
12	0	12	11	0	11	5474.5160	0.0007
7	3	4	6	2	4	5506.2068	0.0004
9	5	5	8	5	4	5544.5494	0.0106
7	4	4	6	3	4	5567.0173	0.0042
7	2	5	6	1	5	5569.3044	0.0014
7	5	3	6	4	3	5627.1584	0.0041
9	4	5	8	4	4	5690.6336	0.0068
11	3	9	10	3	8	5751.8232	0.0133
7	6	1	6	5	1	5760.6079	0.0034
7	6	2	6	5	2	5799.4250	0.0031
12	1	11	11	1	10	5833.3550	-0.0103
12	2	11	11	2	10	5833.3550	-0.0102
13	1	13	12	1	12	5915.7693	-0.0018
13	0	13	12	0	12	5915.7693	-0.0018
10	5	6	9	5	5	6023.4766	-0.0020
7	7	0	6	6	0	6038.2786	-0.0016
7	7	1	6	6	1	6040.1310	-0.0001
9	5	4	8	5	3	6062.4108	-0.0001
10	4	6	9	4	5	6077.3626	-0.0045
8	5	3	7	4	3	6161.6402	0.0011
12	3	10	11	3	9	6192.7945	-0.0026
8	4	4	7	3	4	6232.1831	-0.0037
13	1	12	12	1	11	6274.5938	0.0059
13	2	12	12	2	11	6274.5938	0.0059
8	3	5	7	2	5	6338.5087	0.0015
8	6	2	7	5	2	6342.9447	0.0002
8	4	5	7	3	5	6356.0210	0.0013
14	1	14	13	1	13	6357.0253	-0.0011
14	0	14	13	0	13	6357.0253	-0.0011
8	5	4	7	4	4	6363.6630	0.0043
8	2	6	7	1	6	6373.9455	0.0120
8	6	3	7	5	3	6465.1088	-0.0004
11	5	7	10	5	6	6475.5245	-0.0128
11	4	7	10	4	6	6490.3227	-0.0024
10	5	5	9	5	4	6552.0962	0.0035
8	7	1	7	6	1	6653.1211	-0.0046
8	7	2	7	6	2	6671.2561	-0.0057
14	1	13	13	1	12	6715.8276	0.0093
14	2	13	13	2	12	6715.8276	0.0093
8	8	0	7	7	0	6919.9596	-0.0067
8	8	1	7	7	1	6920.5995	-0.0058
9	5	4	8	4	4	6951.1406	-0.0035
9	6	3	8	5	3	6966.4895	-0.0105
9	4	5	8	3	5	7088.1741	-0.0054
9	4	6	8	3	6	7155.9675	0.0036
9	6	4	8	5	4	7172.6681	-0.0026
9	2	8	8	1	8	7189.8627	0.0067
16	1	16	15	1	15	7239.5323	-0.0026

Appendix VI

16	0	16	15	0	15	7239.5323	-0.0026
9	7	3	8	6	3	7317.8768	-0.0071
9	8	1	8	7	1	7540.5675	-0.0066
10	6	4	9	5	4	7690.1579	0.0018
10	7	3	9	6	3	7817.4711	0.0218
10	4	6	9	3	6	7919.3204	-0.0045
10	6	5	9	5	5	7924.4844	-0.0071
10	2	8	9	1	8	7977.3007	0.0171
10	3	8	9	2	8	7977.3007	-0.0090
10	2	9	9	1	9	7990.0559	-0.0129

Table S9.2. Measured frequencies and residuals (in MHz) for the rotational transitions of the conformer **53a** of exaltolide.

J'	K'_{-1}	K'_{+1}	J''	K''_{-1}	K''_{+1}	V _{obs}	V _{obs} - V _{calc}
3	2	1	2	1	1	2313.2840	-0.0005
3	3	0	2	2	0	2484.7905	0.0044
3	3	1	2	2	1	2528.2939	-0.0043
4	2	2	3	2	1	2652.3492	-0.0016
5	3	3	4	3	2	3036.8612	-0.0128
4	2	2	3	1	2	3070.9078	-0.0095
4	3	1	3	2	1	3121.6527	-0.0013
4	1	3	3	0	3	3148.2522	0.0078
4	2	3	3	1	3	3173.6797	0.0118
5	2	3	4	2	2	3187.2230	-0.0133
4	3	2	3	2	2	3226.0108	0.0011
6	2	5	5	2	4	3239.2920	-0.0063
6	1	5	5	1	4	3244.6444	-0.0070
7	1	7	6	1	6	3356.8916	0.0071
7	0	7	6	0	6	3356.8916	-0.0069
4	4	0	3	3	0	3363.9919	0.0020
4	4	1	3	3	1	3388.9918	0.0043
6	3	4	5	3	3	3550.8888	-0.0034
7	2	6	6	2	5	3696.1420	0.0064
7	1	6	6	1	5	3697.1875	0.0367
8	1	8	7	1	7	3812.2073	-0.0029
8	0	8	7	0	7	3812.2073	-0.0048
5	3	2	4	2	2	3829.8160	0.0049
5	2	3	4	1	3	3892.4781	0.0003
5	1	4	4	0	4	3954.8818	-0.0032
5	2	4	4	1	4	3960.6893	-0.0084
5	4	1	4	3	1	3966.9290	0.0001
5	3	3	4	2	3	3968.3629	0.0026
6	3	3	5	3	2	3977.1974	0.0106
5	4	2	4	3	2	4059.6452	0.0035
5	5	0	4	4	0	4245.8112	0.0004
5	5	1	4	4	1	4256.8771	-0.0012
6	4	2	5	3	2	4618.6748	0.0034
6	3	3	5	2	3	4619.7648	0.0032
6	2	4	5	1	4	4719.0008	-0.0043
10	1	10	9	1	9	4722.8641	-0.0033
10	0	10	9	0	9	4722.8641	-0.0034
6	3	4	5	2	4	4742.9696	-0.0050
6	4	3	5	3	3	4773.2221	0.0029
6	5	1	5	4	1	4844.3694	0.0035
6	5	2	5	4	2	4907.2002	-0.0005
10	1	9	9	1	8	5062.0372	-0.0064
10	2	9	9	2	8	5062.0372	-0.0023
6	6	0	5	5	0	5124.7127	0.0033
11	1	11	10	1	10	5178.1986	-0.0004
11	0	11	10	0	10	5178.1986	-0.0004
7	4	3	6	3	3	5355.6420	-0.0069
7	5	2	6	4	2	5447.4369	0.0027
7	3	4	6	2	4	5459.5564	-0.0020
11	1	10	10	1	9	5517.3039	-0.0011
11	2	10	10	2	9	5517.3039	-0.0006
7	2	5	6	1	5	5527.3404	-0.0141
7	4	4	6	3	4	5527.6252	-0.0003
7	3	5	6	2	5	5533.0901	-0.0022
7	5	3	6	4	3	5592.3942	0.0018
12	1	12	11	1	11	5633.5288	-0.0025
12	0	12	11	0	11	5633.5288	-0.0025
7	6	1	6	5	1	5733.1281	0.0021
7	6	2	6	5	2	5766.4446	0.0004
12	1	11	11	1	10	5972.5938	0.0043

12	2	11	11	2	10	5972.5938	0.0044
7	7	0	6	6	0	6001.4878	0.0048
7	7	1	6	6	1	6002.9612	-0.0061
13	1	13	12	1	12	6088.8681	0.0043
13	0	13	12	0	12	6088.8681	0.0043
8	5	3	7	4	3	6121.7999	-0.0021
8	4	4	7	3	4	6177.3795	0.0014
8	3	5	7	2	5	6288.3068	0.0043
8	4	5	7	3	5	6309.1747	-0.0004
8	6	2	7	5	2	6316.9928	0.0032
8	5	4	7	4	4	6320.5342	0.0028
8	2	6	7	1	6	6326.7832	-0.0042
8	3	6	7	2	6	6327.9628	0.0052
8	6	3	7	5	3	6427.4848	0.0019
13	1	12	12	1	11	6427.8773	-0.0101
13	2	12	12	2	11	6427.8773	-0.0101
14	1	14	13	1	13	6544.2033	0.0073
14	0	14	13	0	13	6544.2033	0.0073
8	7	1	7	6	1	6618.8588	0.0010
8	7	2	7	6	2	6633.7249	0.0009
8	8	0	7	7	0	6877.2865	-0.0087
8	8	1	7	7	1	6877.7988	0.0103
9	5	4	8	4	4	6893.2257	0.0060
9	6	3	8	5	3	6930.2073	0.0022
9	4	5	8	3	5	7027.8553	0.0023
9	5	5	8	4	5	7085.9626	0.0009
9	3	6	8	2	6	7097.5530	-0.0081
9	4	6	8	3	6	7102.6614	-0.0093
9	6	4	8	5	4	7126.9417	0.0060
9	7	2	8	6	2	7209.9213	0.0040
9	7	3	8	6	3	7277.3112	-0.0031
16	1	16	15	1	15	7454.8565	-0.0024
16	0	16	15	0	15	7454.8565	-0.0024
9	8	1	8	7	1	7499.5999	-0.0193
9	8	2	8	7	2	7505.5586	-0.0087
10	6	4	9	5	4	7634.6729	-0.0018
10	5	5	9	4	5	7741.8157	-0.0082
10	7	3	9	6	3	7785.5824	0.0014
10	4	6	9	3	6	7856.4601	-0.0019
10	6	5	9	5	5	7868.9352	0.0086
10	5	6	9	4	6	7873.8173	0.0015
10	3	7	9	2	7	7898.2798	0.0109
10	4	7	9	3	7	7899.3620	0.0044
10	2	8	9	1	8	7918.9784	0.0043

Table S9.3. Measured frequencies and residuals (in MHz) for the rotational transitions of the conformer **49a** of exaltolide.

J'	K'_{-1}	K'_{+1}	J''	K''_{-1}	K''_{+1}	V _{obs}	V _{obs} - V _{calc}
3	2	1	2	1	1	2381.1604	0.0039
3	3	0	2	2	0	2425.9965	-0.0028
3	3	1	2	2	1	2454.3987	0.0007
4	3	1	3	2	1	3178.1623	0.0006
4	2	2	3	1	2	3200.1094	0.0120
4	3	2	3	2	2	3223.5488	-0.0044
4	4	0	3	3	0	3245.0921	0.0083
4	4	1	3	3	1	3275.0939	0.0121
5	4	1	4	3	1	3978.4605	-0.0018
5	3	2	4	2	2	3989.1006	-0.0007
5	2	3	4	1	3	4016.7437	0.0043
5	3	3	4	2	3	4020.0124	0.0058
5	4	2	4	3	2	4032.5291	-0.0007
5	5	0	4	4	0	4070.5146	-0.0016
5	5	1	4	4	1	4097.5389	0.0101
6	4	2	5	3	2	4775.7456	-0.0054
6	5	1	5	4	1	4783.4100	-0.0018
6	3	3	5	2	3	4814.2424	-0.0035
6	4	3	5	3	3	4822.7228	-0.0003
6	2	4	5	1	4	4823.7427	-0.0053
6	3	4	5	2	4	4824.0300	-0.0171
6	1	5	5	0	5	4826.1699	0.0012
6	2	5	5	1	5	4826.1699	-0.0028
6	5	2	5	4	2	4843.5088	0.0018
6	6	0	5	5	0	4900.4733	-0.0011
6	6	1	5	5	1	4921.7335	0.0020
7	5	2	6	4	2	5563.0834	-0.0065
7	6	1	6	5	1	5594.4572	-0.0033
7	4	3	6	3	3	5607.5170	-0.0099
7	3	4	6	2	4	5624.8024	0.0026
7	5	3	6	4	3	5625.7398	0.0165
7	1	6	6	0	6	5630.8215	0.0021
7	2	6	6	1	6	5630.8215	0.0019
7	6	2	6	5	2	5656.7866	0.0034
7	7	0	6	6	0	5732.4893	-0.0028
7	7	1	6	6	1	5747.5099	-0.0001
8	6	2	7	5	2	6353.6252	-0.0035
8	5	3	7	4	3	6395.8352	-0.0070
8	7	1	7	6	1	6412.6828	-0.0012
8	4	4	7	3	4	6424.1067	-0.0003
8	5	4	7	4	4	6426.7529	-0.0044
8	6	3	7	5	3	6429.5951	-0.0003
8	4	5	7	3	5	6430.9951	0.0123
8	2	6	7	1	6	6433.7708	0.0031
8	3	6	7	2	6	6433.7708	0.0017
8	1	7	7	0	7	6435.4396	0.0015
8	2	7	7	1	7	6435.4396	0.0015
8	7	2	7	6	2	6472.5554	-0.0017
8	8	0	7	7	0	6564.7833	-0.0031
8	8	1	7	7	1	6574.5734	-0.0050
9	7	2	8	6	2	7149.0812	0.0115
9	6	3	8	5	3	7179.5828	-0.0055
9	5	4	8	4	4	7220.9820	-0.0055
9	6	4	8	5	4	7227.1524	-0.0002
9	4	5	8	3	5	7231.9536	0.0158
9	5	5	8	4	5	7232.2135	-0.0032
9	7	3	8	6	3	7234.9392	-0.0053
9	3	6	8	2	6	7236.1286	0.0015
9	4	6	8	3	6	7236.1286	-0.0050
9	2	7	8	1	7	7238.5031	-0.0065

Appendix VI

9	3	7	8	2	7	7238.5031	-0.0066
9	8	2	8	7	2	7290.8910	-0.0034
10	7	3	9	6	3	7960.7616	0.0110

Table S9.4. Measured frequencies and residuals (in MHz) for the rotational transitions of the conformer **6c** of exaltolide.

J'	K'_{-1}	K'_{+1}	J''	K''_{-1}	K''_{+1}	V _{obs}	V _{obs} - V _{calc}
3	2	1	2	1	1	2359.4909	-0.0060
3	3	0	2	2	0	2424.8246	-0.0112
3	3	1	2	2	1	2460.1426	-0.0007
4	2	2	3	2	1	2697.3609	0.0043
5	2	4	4	2	3	2727.2773	0.0001
5	1	4	4	1	3	2729.7823	-0.0121
6	1	6	5	1	5	2799.6725	0.0025
6	0	6	5	0	5	2799.6725	0.0007
5	3	3	4	3	2	3069.7263	-0.0003
5	2	3	4	2	2	3123.1689	0.0089
4	3	1	3	2	1	3152.3749	0.0032
6	1	5	5	1	4	3164.5979	0.0169
4	2	2	3	1	2	3171.0800	0.0023
4	3	2	3	2	2	3212.8248	0.0070
7	1	7	6	1	6	3235.8911	-0.0045
7	0	7	6	0	6	3235.8911	-0.0046
4	4	0	3	3	0	3250.9496	-0.0187
4	4	1	3	3	1	3284.7263	-0.0003
5	4	2	4	4	1	3296.9873	0.0074
5	3	2	4	3	1	3492.8508	-0.0005
6	3	4	5	3	3	3526.2886	-0.0120
6	2	4	5	2	3	3535.8856	-0.0032
5	4	1	4	4	0	3549.7452	-0.0066
7	1	6	6	1	5	3600.5716	-0.0112
7	2	6	6	2	5	3600.5716	0.0078
8	1	8	7	1	7	3672.1210	-0.0019
8	0	8	7	0	7	3672.1210	-0.0019
6	4	3	5	4	2	3845.9570	-0.0099
5	3	2	4	2	2	3947.8676	0.0011
6	3	3	5	3	2	3952.8267	0.0012
7	3	5	6	3	4	3965.5277	0.0050
7	2	5	6	2	4	3966.6615	-0.0093
5	2	3	4	1	3	3991.3017	0.0020
5	3	3	4	2	3	3999.3849	0.0017
5	2	4	4	1	4	4001.2696	0.0093
5	4	2	4	3	2	4021.7512	-0.0016
8	1	7	7	1	6	4036.7398	-0.0050
8	2	7	7	2	6	4036.7398	-0.0036
5	5	0	4	4	0	4085.6032	-0.0001
9	1	9	8	1	8	4108.3543	0.0031
9	0	9	8	0	8	4108.3543	0.0031
5	5	1	4	4	1	4112.1926	0.0030
6	4	2	5	4	1	4265.7662	-0.0018
7	4	4	6	4	3	4322.6369	0.0147
7	3	4	6	3	3	4349.3833	0.0040
9	1	8	8	1	7	4472.9329	-0.0072
9	2	8	8	2	7	4472.9329	-0.0071
10	1	10	9	1	9	4544.5829	0.0031
10	0	10	9	0	9	4544.5829	0.0031
6	4	2	5	3	2	4724.7893	0.0069
6	5	1	5	4	1	4760.6575	-0.0063
8	3	5	7	3	4	4770.9445	-0.0046
7	4	3	6	4	2	4783.9346	0.0039
6	2	4	5	1	4	4797.3932	-0.0010
6	4	3	5	3	3	4797.9948	0.0017
6	3	4	5	2	4	4798.4047	-0.0019
6	2	5	5	1	5	4802.1594	-0.0062
6	5	2	5	4	2	4834.3129	-0.0007
9	2	7	8	2	6	4837.8324	-0.0020
9	3	7	8	3	6	4837.8324	0.0074

10	1	9	9	1	8	4909.1487	0.0005
10	2	9	9	2	8	4909.1487	0.0005
6	6	0	5	5	0	4924.3166	0.0021
6	6	1	5	5	1	4942.2726	-0.0006
11	1	11	10	1	10	4980.8086	0.0002
11	0	11	10	0	10	4980.8086	0.0002
8	5	4	7	5	3	5113.9993	0.0056
8	4	4	7	4	3	5174.1338	0.0030
9	4	6	8	4	5	5203.5437	-0.0064
9	3	6	8	3	5	5204.0059	-0.0129
10	2	8	9	2	7	5273.9173	-0.0060
10	3	8	9	3	7	5273.9173	-0.0053
11	1	10	10	1	9	5345.3665	0.0037
11	2	10	10	2	9	5345.3665	0.0037
12	1	12	11	1	11	5417.0393	0.0026
12	0	12	11	0	11	5417.0393	0.0026
7	5	2	6	4	2	5506.6459	0.0030
7	4	3	6	3	3	5555.8895	0.0018
9	4	5	8	4	4	5579.4850	0.0084
7	6	1	6	5	1	5580.8702	-0.0013
7	5	3	6	4	3	5597.9649	-0.0041
7	2	6	6	1	6	5603.0721	0.0128
8	5	3	7	5	2	5604.5317	0.0066
10	3	7	9	3	6	5639.3527	-0.0228
10	4	7	9	4	6	5639.3527	0.0234
7	6	2	6	5	2	5650.8990	0.0000
11	2	9	10	2	8	5710.0653	-0.0013
11	3	9	10	3	8	5710.0653	-0.0013
7	7	0	6	6	0	5763.5968	0.0029
7	7	1	6	6	1	5774.4552	-0.0016
12	1	11	11	1	10	5781.5903	0.0091
12	2	11	11	2	10	5781.5903	0.0091
13	1	13	12	1	12	5853.2651	0.0003
13	0	13	12	0	12	5853.2651	0.0003
9	5	4	8	5	3	6011.4241	-0.0009
11	3	8	10	3	7	6075.2118	0.0001
11	4	8	10	4	7	6075.2118	0.0042
12	2	10	11	2	9	6146.2416	0.0039
12	3	10	11	3	9	6146.2416	0.0039
13	1	12	12	1	11	6217.8005	-0.0010
13	2	12	12	2	11	6217.8005	-0.0010
14	1	14	13	1	13	6289.4889	-0.0034
14	0	14	13	0	13	6289.4889	-0.0034
8	6	2	7	5	2	6296.6000	0.0084
8	5	3	7	4	3	6327.2423	0.0050
8	4	4	7	3	4	6380.6391	0.0000
8	5	4	7	4	4	6389.3398	-0.0006
8	6	3	7	5	3	6400.4444	0.0016
8	2	6	7	1	6	6400.8040	0.0079
8	3	6	7	2	6	6400.8040	-0.0009
8	7	1	7	6	1	6412.3030	-0.0011
8	7	2	7	6	2	6471.6235	0.0016
12	3	9	11	3	8	6511.2115	0.0042
12	4	9	11	4	8	6511.2115	0.0046
13	2	11	12	2	10	6582.4192	-0.0056
13	3	11	12	3	10	6582.4192	-0.0056
8	8	0	7	7	0	6602.0472	-0.0011
8	8	1	7	7	1	6608.1473	0.0017
14	1	13	13	1	12	6654.0279	0.0049
14	2	13	13	2	12	6654.0279	0.0049
15	1	15	14	1	14	6725.7063	-0.0130
15	0	15	14	0	14	6725.7063	-0.0130
9	6	3	8	5	3	7095.7331	-0.0065
9	7	2	8	6	2	7096.9439	-0.0025
16	1	16	15	1	15	7161.9544	0.0088

Appendix VI

16	0	16	15	0	15	7161.9544	0.0088
9	5	4	8	4	4	7164.5321	0.0005
9	6	4	8	5	4	7184.1788	0.0090
9	4	5	8	3	5	7189.1640	-0.0026
9	5	5	8	4	5	7190.4250	-0.0050
9	4	6	8	3	6	7197.4412	-0.0240
9	7	3	8	6	3	7206.4087	0.0013
9	8	2	8	7	2	7296.2677	0.0006
9	9	0	8	8	0	7439.5634	0.0038
9	9	1	8	8	1	7442.8078	-0.0050
10	7	3	9	6	3	7867.1921	-0.0015
10	7	4	9	6	4	7979.7805	0.0014

Table S9.5. Measured frequencies and residuals (in MHz) for the rotational transitions of the conformer **21d** of exaltolide.

J'	K'_{-1}	K'_{+1}	J''	K''_{-1}	K''_{+1}	V _{obs}	V _{obs} - V _{calc}
4	1	3	3	0	3	2345.4484	0.0050
5	1	4	4	0	4	2462.5440	-0.0046
8	1	7	7	0	7	2506.6977	0.0103
8	2	7	7	1	7	2686.2323	0.0067
9	1	8	8	0	8	2812.4902	0.0126
9	2	8	8	1	8	2812.4902	-0.0055
4	2	3	3	1	3	3049.5169	0.0044
5	2	4	4	1	4	3145.1986	0.0005
3	2	1	2	1	1	3157.6046	-0.0068
5	2	3	4	1	3	3176.1881	-0.0018
9	2	7	8	1	7	3177.6554	-0.0133
3	3	0	2	2	0	3195.5167	-0.0004
4	3	1	3	2	1	3205.1348	-0.0090
5	3	2	4	2	2	3233.9690	-0.0037
6	3	3	5	2	3	3319.6101	0.0006
7	3	4	6	2	4	3352.7763	0.0003
8	3	5	7	2	5	3528.7958	0.0114
9	3	6	8	2	6	3563.1287	-0.0033
3	3	1	2	2	1	3689.3180	-0.0005
4	3	2	3	2	2	3689.3180	-0.0007
5	3	3	4	2	3	3904.5542	-0.0009
6	3	4	5	2	4	3964.0747	-0.0017
7	3	5	6	2	5	3973.1582	0.0048
8	3	6	7	2	6	3978.0380	-0.0009
9	3	7	8	2	7	3984.9712	0.0042
4	4	0	3	3	0	3987.8975	0.0051
5	4	1	4	3	1	4003.1286	0.0044
6	4	2	5	3	2	4004.4220	0.0042
8	4	4	7	3	4	4004.6243	-0.0043
9	4	5	8	3	5	4053.3142	-0.0001
10	4	6	9	3	6	4053.3142	0.0224
4	4	1	3	3	1	4057.0034	-0.0057
5	4	2	4	3	2	4127.7342	-0.0072
6	4	3	5	3	3	4127.7342	-0.0072
7	4	4	6	3	4	4184.7732	-0.0007
8	4	5	7	3	5	4204.2884	-0.0093
9	4	6	8	3	6	4419.1312	0.0059
5	5	0	4	4	0	4491.6131	-0.0297
6	5	1	5	4	1	4491.6131	-0.0273
7	5	2	6	4	2	4566.1671	0.0014
9	5	4	8	4	4	4566.1671	0.0014
5	5	1	4	4	1	4681.9924	-0.0003
6	5	2	5	4	2	4734.8382	0.0021
7	5	3	6	4	3	4777.9416	0.0140
8	5	4	7	4	4	4798.7004	-0.0018
9	5	5	8	4	5	4806.5731	0.0059
6	6	0	5	5	0	4807.1976	0.0035
7	6	1	6	5	1	4888.5386	-0.0054
8	6	2	7	5	2	4930.0230	0.0094
9	6	3	8	5	3	4930.0230	0.0096
10	6	4	9	5	4	5004.5986	0.0079
6	6	1	5	5	1	5004.5986	0.0079
7	6	2	6	5	2	5050.0264	-0.0029
8	6	3	7	5	3	5059.8172	-0.0015
9	6	4	8	5	4	5221.7960	-0.0021
10	6	5	9	5	5	5226.2770	-0.0047
7	7	0	6	6	0	5249.4191	-0.0026
8	7	1	7	6	1	5294.4078	-0.0179
7	7	1	6	6	1	5294.4078	0.0012
8	7	2	7	6	2	5368.4057	0.0021

9	7	3	8	6	3	5368.4057	0.0021
8	8	0	7	7	0	5478.5163	0.0019
8	8	1	7	7	1	5571.3615	-0.0022
9	8	1	8	7	1	5591.5955	0.0013
9	8	2	8	7	2	5600.5386	-0.0126
6	1	6	5	1	5	5616.3309	0.0004
6	0	6	5	0	5	5668.7196	0.0054
8	1	8	7	1	7	5728.5161	0.0015
8	0	8	7	0	7	5732.6250	0.0050
9	1	9	8	1	8	5732.6250	0.0072
9	0	9	8	0	8	5881.4451	0.0041
10	1	10	9	1	9	5881.4451	0.0041
10	0	10	9	0	9	5913.3790	0.0065
11	1	11	10	1	10	5917.8206	-0.0018
11	0	11	10	0	10	6170.8957	-0.0010
13	1	13	12	1	12	6170.8957	-0.0008
13	0	13	12	0	12	6299.4355	-0.0026
14	1	14	13	1	13	6319.8713	0.0055
14	0	14	13	0	13	6319.8713	0.0055
15	1	15	14	1	14	6336.1521	0.0018
15	0	15	14	0	14	6385.6355	0.0049
16	1	16	15	1	15	6387.4326	0.0030
16	0	16	15	0	15	6391.4795	-0.0034
6	1	5	5	1	4	6403.7060	0.0678
6	2	5	5	2	4	6411.6600	-0.0034
8	1	7	7	1	6	6411.6600	-0.0059
8	2	7	7	2	6	6433.9855	0.0039
9	1	8	8	1	7	6539.1949	-0.0016
9	2	8	8	2	7	6575.8119	0.0010
10	1	9	9	1	8	6683.6212	-0.0008
10	2	9	9	2	8	6683.6212	-0.0008
11	1	10	10	1	9	6758.2897	-0.0003
11	2	10	10	2	9	6758.2897	-0.0003
14	1	13	13	1	12	6775.2642	0.0010
14	2	13	13	2	12	6777.1611	-0.0036
4	2	2	3	2	1	7013.0237	0.0064
5	2	3	4	2	2	7085.2573	-0.0046
6	2	4	5	2	3	7167.9038	-0.0031
7	2	5	6	2	4	7180.2477	-0.0014
8	2	6	7	2	5	7183.7735	-0.0015
10	2	8	9	2	7	7194.5871	0.0011
10	3	8	9	3	7	7195.2613	0.0043
11	2	9	10	2	8	7196.7075	-0.0062
11	3	9	10	3	8	7196.7075	-0.0062
12	2	10	11	2	9	7206.6148	0.0116
12	3	10	11	3	9	7206.6148	-0.0073
5	3	3	4	3	2	7213.9911	0.0036
6	3	4	5	3	3	7213.9911	0.0033
7	3	5	6	3	4	7261.2257	-0.0076
6	3	3	5	3	2	7409.0149	-0.0018
9	3	6	8	3	5	7428.6515	0.0083
8	4	5	7	4	4	7826.1163	-0.0089
9	4	6	8	4	5	7968.3850	0.0039
8	4	4	7	4	3	7981.5831	0.0002
4	1	3	3	0	3	2345.4484	0.0050
5	1	4	4	0	4	2462.5440	-0.0046
8	1	7	7	0	7	2506.6977	0.0103
8	2	7	7	1	7	2686.2323	0.0067
9	1	8	8	0	8	2812.4902	0.0126
9	2	8	8	1	8	2812.4902	-0.0055

Table S9.6. Measured frequencies and residuals (in MHz) for the rotational transitions of the conformer **4b** of exaltolide.

J'	K' ₋₁	K' ₊₁	J''	K'' ₋₁	K'' ₊₁	V _{obs}	V _{obs} - V _{calc}
3	3	0	2	2	0	2718.8461	0.0090
3	3	1	2	2	1	2749.1799	-0.0011
4	2	2	3	1	2	2894.9909	0.0047
4	2	3	3	1	3	3130.3880	-0.0026
4	3	1	3	2	1	3225.4790	-0.0018
4	3	2	3	2	2	3338.7848	-0.0070
5	2	3	4	1	3	3586.9717	0.0008
4	4	0	3	3	0	3714.8997	0.0010
4	4	1	3	3	1	3722.5720	-0.0031
5	3	2	4	2	2	3746.7866	0.0031
5	3	3	4	2	3	3968.6096	0.0026
5	4	1	4	3	1	4236.4025	-0.0082
5	4	2	4	3	2	4281.7832	-0.0006
6	3	3	5	2	3	4330.1779	-0.0022
6	3	4	5	2	4	4642.0202	0.0010
5	5	0	4	4	0	4703.1090	-0.0015
5	5	1	4	4	1	4704.6638	0.0071
6	4	2	5	3	2	4729.1626	-0.0024
6	4	3	5	3	3	4864.2984	0.0123
7	3	4	6	2	4	4999.1135	0.0077
7	2	5	6	1	5	5188.1893	-0.0075
7	4	3	6	3	3	5221.7960	-0.0013
6	5	1	5	4	1	5239.6388	-0.0004
7	3	5	6	2	5	5355.4775	-0.0024
7	4	4	6	3	4	5481.8238	0.0009
6	6	0	5	5	0	5688.7180	-0.0023
6	6	1	5	5	1	5689.0053	0.0074
7	5	2	6	4	2	5755.3415	0.0045
8	4	4	7	3	4	5769.7927	-0.0021
7	5	3	6	4	3	5807.7284	-0.0005
8	2	6	7	1	6	6018.5232	0.0004
8	3	6	7	2	6	6099.6288	0.0025
8	4	5	7	3	5	6141.2916	-0.0005
7	6	1	6	5	1	6230.5492	-0.0092
7	6	2	6	5	2	6233.3711	-0.0016
8	5	3	7	4	3	6237.7512	-0.0024
8	5	4	7	4	4	6382.1288	-0.0052
9	4	5	8	3	5	6409.0134	0.0061
9	3	6	8	2	6	6594.6430	0.0002
9	5	4	8	4	4	6706.2521	0.0054
8	6	2	7	5	2	6763.5674	-0.0119
8	6	3	7	5	3	6778.5800	-0.0012
9	4	6	8	3	6	6842.4589	-0.0037
9	3	7	8	2	7	6862.9965	0.0001
9	5	5	8	4	5	6987.6830	-0.0007
10	4	6	9	3	6	7151.7760	-0.0046
8	7	1	7	6	1	7217.1265	0.0006
8	7	2	7	6	2	7217.6938	0.0027
9	6	3	8	5	3	7274.9997	-0.0064
9	6	4	8	5	4	7329.4593	0.0060
10	3	7	9	2	7	7445.9340	-0.0030
10	4	7	9	3	7	7578.3134	0.0030
10	3	8	9	2	8	7636.1038	0.0059
8	8	0	7	7	0	7658.6313	0.0076
8	8	1	7	7	1	7658.6313	0.0002
10	6	4	9	5	4	7750.6077	0.0025
11	5	6	10	4	6	7822.0499	-0.0015

Table S9.7. Measured frequencies and residuals (in MHz) for the rotational transitions of the conformer **4a** of exaltolide.

J'	K' ₋₁	K' ₊₁	J''	K'' ₋₁	K'' ₊₁	V _{obs}	V _{obs} - V _{calc}
3	3	0	2	2	0	2767.1855	0.0039
3	3	1	2	2	1	2799.0441	0.0073
4	2	2	3	1	2	2987.3857	-0.0012
4	3	1	3	2	1	3298.4158	0.0037
4	3	2	3	2	2	3415.0630	0.0010
5	2	3	4	1	3	3710.8881	0.0022
4	4	0	3	3	0	3778.2644	0.0042
4	4	1	3	3	1	3786.7212	-0.0005
5	3	2	4	2	2	3849.2183	-0.0021
5	3	3	4	2	3	4072.5837	0.0086
5	4	1	4	3	1	4322.2978	0.0028
5	4	2	4	3	2	4371.5936	-0.0045
6	2	4	5	1	4	4516.2270	-0.0074
6	3	4	5	2	4	4774.3930	0.0056
5	5	0	4	4	0	4781.5255	-0.0062
6	4	2	5	3	2	4838.3524	0.0076
6	4	3	5	3	3	4981.5180	-0.0069
7	3	4	6	2	4	5171.8808	-0.0117
6	5	1	5	4	1	5341.2883	0.0015
7	4	3	6	3	3	5361.0851	0.0042
7	2	5	6	1	5	5368.9442	-0.0064
7	3	5	6	2	5	5515.9797	-0.0032
7	4	4	6	3	4	5628.2898	0.0076
6	6	0	5	5	0	5782.0173	0.0008
6	6	1	5	5	1	5782.3534	0.0015
7	5	2	6	4	2	5878.2935	-0.0014
7	5	3	6	4	3	5937.2386	-0.0051
8	3	5	7	2	5	5970.5821	0.0040
8	4	5	7	3	5	6318.0604	-0.0127
7	6	1	6	5	1	6347.6972	0.0049
7	6	2	6	5	2	6351.0693	-0.0013
8	5	4	7	4	4	6539.8401	-0.0094
9	4	5	8	3	5	6628.3389	0.0115
9	4	6	8	3	6	7049.4595	0.0137
9	6	3	8	5	3	7434.8206	-0.0086

Table S9.8. Measured frequencies and residuals (in MHz) for the rotational transitions of the conformer **7b** of exaltolide.

J'	K' ₋₁	K' ₊₁	J''	K'' ₋₁	K'' ₊₁	V _{obs}	V _{obs} - V _{calc}
3	3	0	2	2	0	2842.7994	-0.0027
3	3	1	2	2	1	2875.6938	0.0051
4	3	1	3	2	1	3404.7899	-0.0066
4	3	2	3	2	2	3523.5946	-0.0058
4	4	0	3	3	0	3878.3776	-0.0048
4	4	1	3	3	1	3887.4006	-0.0055
5	3	2	4	2	2	3989.7496	-0.0008
5	3	3	4	2	3	4213.8506	-0.0072
5	4	1	4	3	1	4451.6323	-0.0117
5	4	2	4	3	2	4503.6915	0.0031
6	3	3	5	2	3	4643.9573	-0.0121
5	5	0	4	4	0	4906.2048	-0.0069
5	5	1	4	4	1	4908.1580	-0.0173
6	3	4	5	2	4	4948.8498	-0.0019
6	4	2	5	3	2	4997.7437	0.0120
6	4	3	5	3	3	5146.2355	0.0057
7	3	4	6	2	4	5387.9317	-0.0047
6	5	1	5	4	1	5495.6115	-0.0102
6	5	2	5	4	2	5511.2267	-0.0065
7	4	3	6	3	3	5555.3754	0.0019
7	4	4	6	3	4	5826.7863	-0.0046
6	6	0	5	5	0	5931.1168	-0.0100
6	6	1	5	5	1	5931.4864	-0.0205
7	5	2	6	4	2	6060.9881	-0.0052
7	5	3	6	4	3	6124.6199	-0.0100
8	4	4	7	3	4	6181.1030	-0.0121
8	3	5	7	2	5	6224.8592	0.0046
8	2	6	7	1	6	6466.2946	0.0033
7	6	1	6	5	1	6526.8817	-0.0117
8	4	5	7	3	5	6551.0530	-0.0001
8	5	4	7	4	4	6760.4372	-0.0101
9	3	7	8	2	7	7346.3307	-0.0085
9	5	5	8	4	5	7431.3231	-0.0120

Table S9.9. Measured frequencies and residuals (in MHz) for the rotational transitions of the conformer **3b** of exaltolide.

J'	K'_{-1}	K'_{+1}	J''	K''_{-1}	K''_{+1}	V _{obs}	V _{obs} - V _{calc}
5	3	3	4	3	2	2650.6835	-0.0069
6	1	6	5	1	5	2722.1310	0.0058
6	0	6	5	0	5	2733.3884	0.0010
5	2	3	4	2	2	2829.8486	0.0034
4	2	2	3	1	2	2922.1520	-0.0050
3	3	0	2	2	0	2948.7554	-0.0003
3	3	1	2	2	1	2968.6909	-0.0116
6	2	5	5	2	4	3018.3509	-0.0030
6	1	5	5	1	4	3137.2630	-0.0044
7	1	7	6	1	6	3150.1558	0.0026
7	0	7	6	0	6	3154.7885	-0.0035
6	4	2	5	4	1	3214.1266	-0.0056
6	3	3	5	3	2	3328.6754	0.0047
4	3	1	3	2	1	3442.5330	-0.0022
4	3	2	3	2	2	3527.1241	-0.0081
5	2	3	4	1	3	3541.4330	-0.0078
7	1	6	6	1	5	3550.2251	0.0023
8	1	8	7	1	7	3576.4158	0.0048
8	0	8	7	0	7	3578.2201	0.0068
7	3	5	6	3	4	3682.7242	0.0074
7	4	4	6	4	3	3740.8839	-0.0083
7	4	3	6	4	2	3792.9164	0.0121
7	2	5	6	2	4	3907.5259	0.0061
5	3	2	4	2	2	3920.6137	-0.0188
7	3	4	6	3	3	3945.2136	0.0009
9	1	9	8	1	8	4001.9112	0.0072
9	0	9	8	0	8	4002.5713	-0.0055
4	4	0	3	3	0	4035.4143	0.0000
4	4	1	3	3	1	4038.7690	0.0025
5	3	3	4	2	3	4115.8776	-0.0039
8	3	6	7	3	5	4174.2567	0.0020
6	2	4	5	1	4	4234.5162	0.0080
8	5	4	7	5	3	4277.0596	-0.0093
8	4	5	7	4	4	4279.9501	0.0054
8	5	3	7	5	2	4289.3452	-0.0069
9	2	8	8	2	7	4349.6618	-0.0018
9	1	8	8	1	7	4369.6313	-0.0051
8	2	6	7	2	5	4377.0196	0.0008
8	4	4	7	4	3	4401.2424	-0.0038
6	3	3	5	2	3	4419.4609	0.0029
10	1	10	9	1	9	4427.0839	-0.0127
10	0	10	9	0	9	4427.3539	0.0133
8	3	5	7	3	4	4541.9569	-0.0039
5	4	1	4	3	1	4551.8397	0.0029
5	4	2	4	3	2	4573.3343	-0.0102
9	3	7	8	3	6	4647.4411	-0.0024
6	3	4	5	2	4	4741.2971	0.0010
10	2	9	9	2	8	4778.8429	0.0018
10	1	9	9	1	8	4787.6408	0.0042
9	2	7	8	2	6	4801.1899	0.0015
9	4	6	8	4	5	4807.9536	-0.0020
9	5	5	8	5	4	4829.6393	-0.0017
9	5	4	8	5	3	4866.0682	-0.0145
7	3	4	6	2	4	4975.7699	-0.0034
9	3	6	8	3	5	5099.2281	-0.0090
10	3	8	9	3	7	5103.9521	-0.0004
5	5	0	4	4	0	5115.0985	0.0034
5	5	1	4	4	1	5115.5479	-0.0031
6	4	3	5	3	3	5119.5874	-0.0082
10	2	8	9	2	7	5201.4930	-0.0006

Appendix VI

11	2	10	10	2	9	5205.4972	-0.0022
12	1	12	11	1	1	5277.2550	0.0205
12	0	12	11	0	1	5277.2550	-0.0096
10	4	7	9	4	6	5319.7589	-0.0034
7	2	6	6	1	6	5372.4478	-0.0014
10	5	6	9	5	5	5380.6372	0.0084
7	3	5	6	2	5	5405.6669	0.0079
7	4	3	6	3	3	5509.3738	0.0077
10	3	7	9	3	6	5605.6387	0.0120
8	3	5	7	2	5	5610.2122	-0.0021
6	5	1	5	4	1	5640.2756	-0.0012
6	5	2	5	4	2	5644.1610	0.0092
10	4	6	9	4	5	5663.2352	-0.0063
7	4	4	6	3	4	5686.7724	0.0045
13	1	13	12	1	2	5702.2900	0.0105
13	0	13	12	0	2	5702.2900	0.0001
8	2	6	7	1	6	5831.5737	0.0171
11	5	7	10	5	6	5924.2252	-0.0116
8	4	4	7	3	4	5965.3992	-0.0004
12	3	10	11	3	9	5981.7337	-0.0001
8	3	6	7	2	6	6106.8129	-0.0063
14	1	14	13	1	3	6127.3176	-0.0077
14	0	14	13	0	3	6127.3176	-0.0112
7	5	2	6	4	2	6156.5754	0.0029
7	5	3	6	4	3	6174.3826	-0.0007
8	4	5	7	3	5	6284.0077	0.0119
9	4	5	8	3	5	6456.6065	0.0104
12	3	9	11	3	8	6463.8173	0.0042
8	5	4	7	4	4	6710.5615	0.0016
10	4	6	9	3	6	7020.6048	0.0043
8	6	3	7	5	3	7247.9861	0.0006
7	7	0	6	6	0	7271.4806	-0.0032
7	7	1	6	6	1	7271.4806	-0.0095
10	5	5	9	4	5	7553.8608	-0.0061
9	6	3	8	5	3	7761.0413	0.0035
5	3	3	4	3	2	2650.6835	-0.0069

7. APPENDIX VII

Table S10.1. Measured frequencies and residuals (in MHz) for the rotational transitions of the conformer **2** of romandolide.

J'	K'_{-1}	K'_{+1}	J''	K''_{-1}	K''_{+1}	V _{obs}	V _{obs} - V _{calc}
3	2	2	2	1	2	2267.7915	-0.0016
5	0	5	4	1	4	2359.2253	0.0023
5	1	5	4	1	4	2366.4493	0.0012
5	0	5	4	0	4	2378.7402	-0.0016
5	1	5	4	0	4	2385.9698	0.0029
5	1	4	4	2	3	2446.5921	-0.0128
3	3	1	2	2	0	2517.1062	0.0009
3	3	0	2	2	0	2521.9566	-0.0010
3	3	1	2	2	1	2541.2420	-0.0007
3	3	0	2	2	1	2546.0926	-0.0024
5	2	4	4	2	3	2580.3343	-0.0010
6	2	4	5	3	2	2666.7759	-0.0103
5	1	4	4	1	3	2681.8291	-0.0003
4	2	2	3	1	2	2712.8161	-0.0002
4	1	3	3	0	3	2719.5020	0.0001
6	2	4	5	3	3	2779.9532	0.0028
6	0	6	5	1	5	2814.8174	0.0015
5	2	4	4	1	3	2815.5575	-0.0023
6	1	6	5	1	5	2817.3101	0.0008
6	0	6	5	0	5	2822.0421	0.0011
6	1	6	5	0	5	2824.5374	0.0030
7	3	4	6	4	2	2876.3452	0.0114
4	2	3	3	1	3	2907.6510	-0.0001
6	1	5	5	2	4	2993.6051	0.0018
4	3	2	3	2	1	2996.1976	0.0017
4	3	1	3	2	1	3028.1738	0.0010
6	2	5	5	2	4	3057.9932	-0.0008
4	3	2	3	2	2	3105.0841	-0.0020
6	1	5	5	1	4	3127.3315	-0.0022
4	3	1	3	2	2	3137.0640	0.0011
7	2	5	6	3	3	3169.0731	0.0026
6	2	5	5	1	4	3191.7245	0.0001
7	0	7	6	1	6	3265.1715	-0.0025
7	1	7	6	1	6	3265.9951	-0.0001
7	0	7	6	0	6	3267.6676	0.0003
7	1	7	6	0	6	3268.4894	0.0008
5	2	3	4	1	3	3340.5557	-0.0002
5	3	3	4	2	2	3419.8394	-0.0002
4	4	1	3	3	0	3434.7033	-0.0010
4	4	0	3	3	0	3435.5078	0.0011
4	4	1	3	3	1	3439.5559	-0.0007
4	4	0	3	3	1	3440.3597	0.0007
7	2	5	6	3	4	3447.0759	-0.0005
5	1	4	4	0	4	3462.7521	-0.0014
7	1	6	6	2	5	3495.6578	0.0020
7	2	6	6	2	5	3522.9560	0.0001
8	2	6	7	3	4	3527.0282	0.0015
5	3	2	4	2	2	3533.0060	0.0022
8	3	5	7	4	3	3556.8549	-0.0003
7	1	6	6	1	5	3560.0462	-0.0003
5	2	4	4	1	4	3576.9662	0.0011
7	2	6	6	1	5	3587.3464	-0.0002
5	3	3	4	2	3	3696.1820	-0.0006
8	0	8	7	1	7	3713.5503	0.0182
8	1	8	7	1	7	3713.7959	0.0022
8	0	8	7	0	7	3714.3520	-0.0014

8	1	8	7	0	7	3714.6179	0.0029
9	2	7	8	3	5	3746.7485	0.0031
6	3	4	5	2	3	3793.4664	0.0008
5	3	2	4	2	3	3809.3502	0.0033
5	4	2	4	3	1	3950.3563	0.0034
5	4	1	4	3	1	3957.2992	0.0007
8	1	7	7	2	6	3968.5071	0.0012
8	2	7	7	2	6	3979.1181	-0.0025
5	4	2	4	3	2	3982.3298	0.0001
5	4	1	4	3	2	3989.2753	-0.0001
8	1	7	7	1	6	3995.8061	0.0002
8	2	7	7	1	6	4006.4158	-0.0049
6	2	4	5	1	4	4029.5265	-0.0016
8	2	6	7	3	5	4060.3199	-0.0011
6	3	3	5	2	3	4071.4722	0.0008
7	3	5	6	2	4	4133.8059	0.0016
9	3	6	8	4	4	4141.4664	-0.0076
9	1	9	8	1	8	4161.2809	0.0094
9	0	9	8	0	8	4161.4432	-0.0086
6	1	5	5	0	5	4211.3456	0.0003
6	2	5	5	1	5	4268.5123	0.0013
6	3	4	5	2	4	4318.4614	-0.0003
5	5	0	4	4	0	4343.1831	0.0042
5	5	1	4	4	1	4343.8588	-0.0029
6	4	3	5	3	2	4425.2309	0.0008
9	1	8	8	2	7	4426.3561	0.0000
9	2	8	8	2	7	4430.2410	-0.0032
9	1	8	8	1	7	4436.9702	-0.0006
9	2	8	8	1	7	4440.8588	-0.0001
6	4	2	5	3	2	4457.5516	0.0006
8	3	6	7	2	5	4466.5598	0.0002
6	4	3	5	3	3	4538.3929	-0.0014
6	4	2	5	3	3	4570.7126	-0.0026
9	2	7	8	3	6	4610.7624	-0.0005
7	3	4	6	2	4	4667.0986	0.0000
7	2	5	6	1	5	4771.9350	0.0002
9	3	7	8	2	6	4820.0312	0.0016
7	4	4	6	3	3	4838.1751	-0.0033
6	5	2	5	4	1	4872.9671	0.0029
6	5	1	5	4	1	4874.2422	0.0009
10	1	9	9	2	8	4877.5672	-0.0019
10	2	9	9	2	8	4878.9315	-0.0011
6	5	2	5	4	2	4879.9099	0.0000
6	5	1	5	4	2	4881.1899	0.0029
10	1	9	9	1	8	4881.4592	0.0020
10	2	9	9	1	8	4882.8331	0.0124
7	4	3	6	3	3	4942.7925	0.0001
7	1	6	6	0	6	4949.3486	-0.0022
7	3	5	6	2	5	4971.6067	-0.0013
7	2	6	6	1	6	4974.1569	-0.0006
11	1	11	10	1	10	5055.9969	0.0087
11	0	11	10	0	10	5055.9969	-0.0086
10	2	8	9	3	7	5112.0101	-0.0021
7	4	4	6	3	4	5116.1843	0.0000
8	4	5	7	3	4	5189.0404	-0.0015
10	3	8	9	2	7	5207.8031	0.0004
11	1	10	10	2	9	5326.1457	-0.0034
11	2	10	10	2	9	5326.6139	0.0024
11	1	10	10	1	9	5327.5104	-0.0022
11	2	10	10	1	9	5327.9765	0.0015
8	3	5	7	2	5	5330.5756	-0.0015
7	5	3	6	4	2	5386.9770	-0.0013
7	5	2	6	4	2	5394.2699	-0.0009
7	5	3	6	4	3	5419.2988	-0.0004
7	5	2	6	4	3	5426.5947	0.0030

8	4	4	7	3	4	5446.4613	0.0025
9	4	6	8	3	5	5495.5919	0.0035
12	0	12	11	1	11	5503.3263	0.0043
12	1	12	11	0	11	5503.3263	-0.0054
12	1	12	11	1	11	5503.3264	0.0022
12	0	12	11	0	11	5503.3264	-0.0031
8	2	6	7	1	6	5536.2713	-0.0019
11	2	9	10	3	8	5583.9260	0.0042
11	3	9	10	2	8	5624.0698	-0.0013
8	3	6	7	2	6	5651.1471	-0.0007
8	1	7	7	0	7	5677.4895	0.0001
8	2	7	7	1	7	5687.2819	-0.0010
8	4	5	7	3	5	5722.3347	-0.0014
12	1	11	11	2	10	5773.7748	-0.0055
12	2	11	11	2	10	5773.9316	-0.0015
12	1	11	11	1	10	5774.2396	-0.0032
12	2	11	11	1	10	5774.4030	0.0075
7	6	2	6	5	1	5782.8423	-0.0085
7	6	1	6	5	1	5783.0686	0.0058
7	6	2	6	5	2	5784.1208	-0.0071
10	4	7	9	3	6	5785.3007	-0.0070
8	5	4	7	4	3	5863.1520	0.0012
8	5	3	7	4	3	5892.3653	-0.0016
13	0	13	12	1	12	5950.6538	-0.0045
13	1	13	12	0	12	5950.6538	-0.0074
13	1	13	12	1	12	5950.6539	-0.0051
13	0	13	12	0	12	5950.6539	-0.0066
8	5	4	7	4	4	5967.7643	-0.0005
8	4	4	7	3	5	5979.7479	-0.0051
8	5	3	7	4	4	5996.9771	-0.0038
9	4	5	8	3	5	6003.8702	-0.0007
12	2	10	11	3	9	6041.1682	-0.0002
12	3	10	11	2	9	6056.9613	0.0002
9	3	6	8	2	6	6060.9039	-0.0022
11	4	8	10	3	7	6090.8201	-0.0006
7	7	1	6	6	1	6155.2304	-0.0076
7	7	0	6	6	0	6155.2304	0.0069
13	1	12	12	1	11	6221.1947	-0.0639
13	2	12	12	2	11	6221.1947	0.0394
9	2	7	8	1	7	6293.4037	-0.0011
8	6	3	7	5	2	6311.1831	-0.0001
8	6	2	7	5	2	6312.6110	0.0002
8	6	3	7	5	3	6318.4737	-0.0020
8	6	2	7	5	3	6319.9076	0.0043
9	3	7	8	2	7	6349.8806	-0.0016
9	4	6	8	3	6	6359.6039	-0.0020
9	5	4	8	4	4	6366.4718	-0.0010
14	0	14	13	1	13	6397.9946	0.0016
14	1	14	13	0	13	6397.9946	0.0008
14	1	14	13	1	13	6397.9946	0.0015
14	0	14	13	0	13	6397.9946	0.0010
9	1	8	8	0	8	6400.1084	0.0016
9	2	8	8	1	8	6403.7303	-0.0030
12	4	9	11	3	8	6436.2702	0.0008
13	2	11	12	3	10	6491.9509	0.0052
13	3	11	12	2	10	6497.8677	-0.0029
8	3	5	7	2	6	6515.1670	0.0017
9	5	5	8	4	5	6533.4292	-0.0040
10	5	6	9	4	5	6615.9896	-0.0061
10	4	6	9	3	6	6633.6121	-0.0016
14	1	13	13	1	12	6668.3822	-0.0182
14	2	13	13	2	12	6668.3822	0.0155
13	4	10	12	3	9	6823.7815	0.0006
9	6	4	8	5	3	6824.9726	-0.0024
9	6	3	8	5	3	6831.7169	0.0003

10	3	7	9	2	7	6833.4118	0.0006
10	5	5	9	4	5	6841.1342	0.0001
15	0	15	14	1	14	6845.3312	0.0050
15	1	15	14	0	14	6845.3312	0.0048
15	1	15	14	1	14	6845.3312	0.0050
15	0	15	14	0	14	6845.3312	0.0048
9	6	4	8	5	4	6854.1935	0.0024
9	6	3	8	5	4	6860.9364	0.0037
11	5	7	10	4	6	6897.1504	0.0054
14	2	12	13	3	11	6940.1462	-0.0091
10	4	7	9	3	7	7026.1880	0.0039
10	2	8	9	1	8	7035.5370	-0.0013
10	3	8	9	2	8	7060.3506	0.0019
8	8	1	7	7	1	7061.0437	0.0014
8	8	0	7	7	0	7061.0437	0.0034
15	1	14	14	2	13	7115.5985	0.0117
15	2	14	14	1	13	7115.5985	-0.0089
15	1	14	14	1	13	7115.5985	-0.0040
15	2	14	14	2	13	7115.5985	0.0068
10	5	6	9	4	6	7124.2784	0.0003
9	7	2	8	6	2	7222.2308	0.0068
9	7	3	8	6	3	7223.3912	-0.0062
16	0	16	15	1	15	7292.6588	0.0013
16	1	16	15	0	15	7292.6588	0.0013
16	1	16	15	1	15	7292.6589	0.0014
16	0	16	15	0	15	7292.6589	0.0014
10	6	5	9	5	4	7305.3320	0.0017
10	6	4	9	5	4	7330.1561	0.0006
11	4	7	10	3	7	7340.5467	0.0006
10	5	5	9	4	6	7349.4227	0.0061
11	5	6	10	4	6	7357.9718	0.0011
10	6	5	9	5	5	7395.7879	0.0011
10	6	4	9	5	5	7420.6065	-0.0056
16	1	15	15	2	14	7562.8331	0.0015
16	2	15	15	1	14	7562.8331	-0.0049
16	1	15	15	1	14	7562.8331	-0.0034
16	2	15	15	2	14	7562.8331	-0.0001
9	8	2	8	7	2	7595.7163	-0.0163
9	8	1	8	7	1	7595.7163	0.0117
11	3	8	10	2	8	7610.6993	0.0006
11	4	8	10	3	8	7716.4268	-0.0023
11	6	6	10	5	5	7725.4555	0.0046
17	0	17	16	1	16	7739.9865	0.0003
17	1	17	16	0	16	7739.9865	0.0003
17	1	17	16	1	16	7739.9865	0.0003
17	0	17	16	0	16	7739.9865	0.0003
11	5	7	10	4	7	7745.4484	-0.0026
10	7	3	9	6	3	7750.4026	-0.0015
10	7	4	9	6	4	7755.7697	-0.0001
11	2	9	10	1	9	7766.7033	0.0019
11	3	9	10	2	9	7776.7868	-0.0019
11	6	5	10	5	5	7800.3275	-0.0011
11	1	10	10	0	10	7838.9383	0.0150
12	5	7	11	4	7	7947.1298	0.0027
11	6	6	10	5	6	7950.5892	-0.0001
9	9	1	8	8	1	7966.8376	0.0012
9	9	0	8	8	0	7966.8376	0.0015

Table S10.2. Measured frequencies and residuals (in MHz) for the rotational transitions of the conformer **30** of romandolide.

J'	K'_{-1}	K'_{+1}	J''	K''_{-1}	K''_{+1}	ν_{obs}	$\nu_{\text{obs}} - \nu_{\text{calc}}$
4	1	3	3	1	2	2101.7310	0.0017
5	1	5	4	1	4	2181.0565	0.0042
5	0	5	4	0	4	2189.8640	-0.0055
4	2	2	3	2	1	2193.5499	0.0082
5	1	5	4	0	4	2194.0649	-0.0019
3	2	2	2	1	2	2219.1809	0.0069
5	1	4	4	2	3	2338.1425	0.0043
3	3	0	2	2	0	2451.7191	-0.0016
3	3	1	2	2	1	2477.3274	0.0007
3	3	0	2	2	1	2485.4148	-0.0051
5	1	4	4	1	3	2530.7102	0.0196
5	3	3	4	3	2	2564.3706	0.0003
5	4	2	4	4	1	2581.7416	-0.0002
6	0	6	5	1	5	2589.3438	0.0000
6	1	6	5	1	5	2590.6058	-0.0022
6	0	6	5	0	5	2593.5402	-0.0009
5	4	1	4	4	0	2593.7270	0.0037
6	1	6	5	0	5	2594.8047	-0.0006
5	2	4	4	1	3	2626.2068	0.0079
4	2	2	3	1	2	2656.1648	-0.0033
5	3	2	4	3	1	2687.6061	0.0118
4	1	3	3	0	3	2697.4918	-0.0002
5	2	3	4	2	2	2739.4924	0.0017
6	1	5	5	2	4	2829.7766	-0.0013
4	2	3	3	1	3	2853.9656	-0.0012
6	2	5	5	2	4	2869.3373	-0.0015
4	3	2	3	2	1	2881.2373	-0.0044
6	1	5	5	1	4	2925.2834	-0.0028
4	3	1	3	2	1	2933.1912	0.0006
6	2	5	5	1	4	2964.8469	-0.0002
7	0	7	6	1	6	2997.9977	-0.0001
7	1	7	6	1	6	2998.3642	0.0027
7	0	7	6	0	6	2999.2623	0.0003
7	1	7	6	0	6	2999.6266	0.0009
4	3	2	3	2	2	3028.6968	0.0003
6	3	4	5	3	3	3055.6221	-0.0006
4	3	1	3	2	2	3080.6458	0.0005
6	4	2	5	4	1	3157.3040	-0.0023
6	2	4	5	2	3	3237.4827	-0.0015
5	3	3	4	2	2	3252.0702	-0.0002
7	1	6	6	2	5	3276.4054	0.0022
6	3	3	5	3	2	3286.0102	-0.0044
7	2	6	6	2	5	3290.8796	-0.0001
5	2	3	4	1	3	3293.9282	-0.0013
7	1	6	6	1	5	3315.9646	0.0004
7	2	6	6	1	5	3330.4422	0.0015
4	4	1	3	3	0	3342.8447	0.0023
4	4	0	3	3	0	3344.4394	0.0010
7	2	5	6	3	4	3345.7777	-0.0110
4	4	1	3	3	1	3350.9364	0.0007
8	0	8	7	1	7	3405.3778	-0.0132
8	1	8	7	1	7	3405.5020	0.0097
8	0	8	7	0	7	3405.7440	-0.0108
8	1	8	7	0	7	3405.8686	0.0126
5	3	2	4	2	2	3427.2439	0.0007
5	1	4	4	0	4	3438.0523	0.0001

5	2	4	4	1	4	3520.5465	0.0004
7	3	5	6	3	4	3524.9950	-0.0018
6	3	4	5	2	3	3568.2023	0.0000
7	6	2	6	6	1	3610.7765	-0.0004
5	3	3	4	2	3	3613.9569	0.0002
7	4	4	6	4	3	3630.6316	0.0028
7	5	3	6	5	2	3632.5427	-0.0050
7	2	5	6	2	4	3676.5073	0.0005
8	1	7	7	2	6	3699.1085	0.0004
8	2	7	7	2	6	3703.9925	0.0009
8	2	7	7	1	6	3718.4695	0.0014
7	4	3	6	4	2	3755.9555	-0.0048
5	3	2	4	2	3	3789.1326	0.0031
9	1	9	8	1	8	3812.4693	0.0343
9	0	9	8	0	8	3812.4693	-0.0394
5	4	2	4	3	1	3824.7408	0.0013
5	4	1	4	3	1	3838.3177	0.0007
7	3	5	6	2	4	3855.7173	0.0024
7	3	4	6	3	3	3856.0963	-0.0037
5	4	2	4	3	2	3876.6890	0.0007
8	3	6	7	3	5	3972.2956	0.0019
6	3	3	5	2	3	3973.7672	0.0002
6	2	4	5	1	4	4000.7221	-0.0010
8	2	6	7	2	5	4069.5190	0.0051
9	1	8	8	2	7	4111.4913	0.0002
9	2	8	8	2	7	4113.0461	-0.0018
9	1	8	8	1	7	4116.3719	-0.0027
9	2	8	8	1	7	4117.9315	0.0001
8	7	2	7	7	1	4123.5965	0.0143
8	7	1	7	7	0	4123.7103	0.0264
8	4	5	7	4	4	4135.3380	-0.0022
8	6	3	7	6	2	4146.4607	-0.0182
8	3	6	7	2	5	4151.5051	0.0033
8	5	4	7	5	3	4169.2942	0.0033
6	1	5	5	0	5	4173.4682	-0.0008
6	2	5	5	1	5	4208.8339	0.0013
8	5	3	7	5	2	4216.8692	-0.0003
10	0	10	9	1	9	4219.3392	0.0175
10	1	10	9	0	9	4219.3392	-0.0173
10	1	10	9	1	9	4219.3393	0.0103
10	0	10	9	0	9	4219.3393	-0.0099
5	5	1	4	4	0	4230.2681	-0.0029
5	5	0	4	4	0	4230.5557	0.0013
5	5	1	4	4	1	4231.8656	-0.0014
5	5	0	4	4	1	4232.1504	0.0000
6	3	4	5	2	4	4235.9309	-0.0020
6	4	3	5	3	2	4246.9551	0.0009
6	4	2	5	3	2	4308.0282	-0.0008
9	2	7	8	3	6	4368.5395	-0.0008
8	4	4	7	4	3	4373.0305	-0.0044
8	3	5	7	3	4	4373.5562	0.0119
9	3	7	8	3	6	4401.5032	0.0051
6	4	3	5	3	3	4422.1270	0.0000
9	2	7	8	2	6	4450.5274	-0.0009
9	3	7	8	2	6	4483.4839	-0.0022
10	1	9	9	2	8	4520.0104	-0.0011
10	2	9	9	2	8	4520.4889	0.0015
10	1	9	9	1	8	4521.5649	-0.0034
10	2	9	9	1	8	4522.0432	-0.0011
7	4	4	6	3	3	4591.5776	0.0091
7	3	4	6	2	4	4592.3813	-0.0015
9	4	6	8	4	5	4617.7117	-0.0070
11	1	11	10	1	10	4626.2187	0.0046
11	0	11	10	0	10	4626.2187	-0.0009
11	0	11	10	1	10	4626.2187	0.0065

11	1	11	10	0	10	4626.2187	-0.0028
9	7	3	8	7	2	4658.2317	-0.0034
9	7	2	8	7	1	4658.9577	-0.0015
9	6	4	8	6	3	4688.0591	0.0042
9	5	5	8	5	4	4700.3268	0.0014
6	5	2	5	4	1	4734.1143	-0.0044
6	5	1	5	4	1	4737.1044	-0.0004
6	5	2	5	4	2	4747.6971	0.0009
6	5	1	5	4	2	4750.6838	0.0015
7	2	5	6	1	5	4751.9399	-0.0038
7	4	3	6	3	3	4777.9744	-0.0003
10	2	8	9	3	7	4806.5632	0.0075
10	3	8	9	3	7	4818.6716	-0.0021
9	5	4	8	5	3	4822.6040	0.0018
9	3	6	8	3	5	4826.2128	0.0091
10	2	8	9	2	7	4839.5133	-0.0002
10	3	8	9	2	7	4851.6341	0.0027
8	4	5	7	3	4	4870.8014	-0.0073
7	3	5	6	2	5	4891.5913	0.0004
7	1	6	6	0	6	4895.8933	0.0013
7	2	6	6	1	6	4909.1025	-0.0018
11	1	10	10	2	9	4927.2483	-0.0013
11	2	10	10	2	9	4927.3924	0.0019
11	1	10	10	1	9	4927.7248	-0.0008
11	2	10	10	1	9	4927.8586	-0.0078
9	4	5	8	4	4	4967.4601	0.0112
7	4	4	6	3	4	4997.1327	-0.0005
12	1	12	11	1	11	5033.1024	0.0026
12	0	12	11	0	11	5033.1024	0.0012
12	0	12	11	1	11	5033.1024	0.0031
12	1	12	11	0	11	5033.1024	0.0007
10	4	7	9	4	6	5076.0298	-0.0002
6	6	0	5	5	0	5114.4767	0.0028
6	6	1	5	5	1	5114.7095	-0.0006
9	4	6	8	3	5	5114.9829	-0.0001
10	7	4	9	7	3	5199.4671	0.0040
10	7	3	9	7	2	5203.0418	-0.0068
7	5	3	6	4	2	5209.3612	0.0012
10	5	6	9	5	5	5216.6720	-0.0053
10	3	7	9	3	6	5221.7456	0.0005
11	2	9	10	3	8	5225.1520	-0.0020
7	5	2	6	4	2	5226.0318	0.0004
11	3	9	10	3	8	5229.3387	0.0017
10	6	5	9	6	4	5232.0873	-0.0024
11	2	9	10	2	8	5237.2697	-0.0022
11	3	9	10	2	8	5241.4570	0.0020
7	5	3	6	4	3	5270.4348	0.0000
7	5	2	6	4	3	5287.1112	0.0050
8	3	5	7	2	5	5289.4185	-0.0018
8	4	4	7	3	4	5294.9097	0.0001
12	2	11	11	2	10	5334.1681	0.0105
10	4	7	9	3	6	5364.8093	0.0000
13	1	13	12	1	12	5439.9871	-0.0002
13	0	13	12	0	12	5439.9871	-0.0006
13	0	13	12	1	12	5439.9871	-0.0001
13	1	13	12	0	12	5439.9871	-0.0007
8	2	6	7	1	6	5505.4918	-0.0017
10	4	6	9	4	5	5507.2972	0.0020
11	4	8	10	4	7	5513.1392	-0.0067
8	3	6	7	2	6	5573.0042	-0.0007
11	3	8	10	3	7	5594.1224	0.0032
8	4	5	7	3	5	5607.4747	-0.0019
8	1	7	7	0	7	5610.2136	-0.0010
8	2	7	7	1	7	5614.7331	-0.0013
8	5	4	7	4	3	5622.6906	-0.0001

7	6	1	6	5	1	5625.5230	0.0016
7	6	2	6	5	2	5627.9166	0.0006
12	2	10	11	3	9	5635.7278	0.0018
12	3	10	11	3	9	5637.1041	0.0008
12	3	10	11	2	9	5641.2898	0.0035
11	4	8	10	3	7	5656.2044	-0.0057
8	5	3	7	4	3	5686.9416	0.0009
11	5	7	10	5	6	5711.0261	-0.0039
13	1	12	12	1	11	5740.9248	-0.0188
13	2	12	12	2	11	5740.9248	0.0104
13	1	12	12	2	11	5740.9248	0.0218
13	2	12	12	1	11	5740.9248	-0.0303
11	7	5	10	7	4	5746.6525	0.0027
11	7	4	10	7	3	5760.3624	0.0065
11	6	6	10	6	5	5771.8844	-0.0007
8	5	4	7	4	4	5809.0970	0.0001
14	1	14	13	1	13	5846.8750	-0.0012
14	0	14	13	0	13	5846.8750	-0.0013
14	0	14	13	1	13	5846.8750	-0.0011
14	1	14	13	0	13	5846.8750	-0.0013
8	5	3	7	4	4	5873.3744	0.0275
9	4	5	8	3	5	5888.8122	-0.0019
12	4	9	11	4	8	5934.9168	0.0026
9	5	5	8	4	4	5949.9819	0.0007
12	3	9	11	3	8	5972.5108	0.0009
11	4	7	10	4	6	5977.3351	-0.0036
7	7	0	6	6	0	5997.9177	0.0238
7	7	1	6	6	1	5997.9177	-0.0159
13	2	11	12	3	10	6043.3868	0.0019
13	3	11	12	3	10	6043.8250	0.0032
13	2	11	12	2	10	6044.7497	-0.0124
13	3	11	12	2	10	6045.2037	0.0047
9	3	6	8	2	6	6046.1088	-0.0013
11	5	6	10	5	5	6071.8975	0.0079
8	6	2	7	5	2	6129.0923	0.0014
9	5	4	8	4	4	6136.5063	-0.0017
8	6	3	7	5	3	6141.8473	0.0000
14	1	13	13	1	12	6147.6970	-0.0029
14	2	13	13	2	12	6147.6970	0.0054
14	1	13	13	2	12	6147.6970	0.0086
14	2	13	13	1	12	6147.6970	-0.0061
12	5	8	11	5	7	6180.1396	-0.0015
10	5	6	9	4	5	6199.2143	0.0047
9	2	7	8	1	7	6242.4360	-0.0012
9	4	6	8	3	6	6252.8999	-0.0016
15	1	15	14	1	14	6253.7622	-0.0034
15	0	15	14	0	14	6253.7622	-0.0034
15	0	15	14	1	14	6253.7622	-0.0033
15	1	15	14	0	14	6253.7622	-0.0034
9	3	7	8	2	7	6270.5104	-0.0010
12	7	6	11	7	5	6296.9339	-0.0085
12	6	7	11	6	6	6298.6451	0.0004
9	1	8	8	0	8	6320.8364	0.0019
9	2	8	8	1	8	6322.2868	-0.0032
12	7	5	11	7	4	6339.2741	-0.0265
13	4	10	12	4	9	6347.5612	0.0069
13	3	10	12	3	9	6363.0263	0.0034
13	4	10	12	3	9	6372.0377	-0.0118
9	5	5	8	4	5	6374.0798	-0.0024
12	4	8	11	4	7	6380.1323	-0.0310
14	2	12	13	3	11	6450.1329	-0.0002
14	3	12	13	3	11	6450.2680	0.0004
14	2	12	13	2	11	6450.5661	-0.0039
14	3	12	13	2	11	6450.7053	0.0008
8	7	1	7	6	1	6510.2636	0.0070

8	7	2	7	6	2	6510.7358	-0.0031
15	1	14	14	1	13	6554.4919	-0.0017
15	2	14	14	2	13	6554.4919	0.0006
15	1	14	14	2	13	6554.4919	0.0015
15	2	14	14	1	13	6554.4919	-0.0026
10	4	6	9	3	6	6569.9030	-0.0026
9	6	3	8	5	3	6614.3653	0.0005
10	5	5	9	4	5	6623.1041	-0.0006
13	5	9	12	5	8	6625.5604	-0.0054
12	5	7	11	5	6	6636.5459	-0.0005
9	6	4	8	5	4	6660.6061	-0.0052
13	4	9	12	4	8	6746.5365	0.0033
14	4	11	13	4	10	6755.7340	0.0000
14	3	11	13	3	10	6761.5974	-0.0031
14	4	11	13	3	10	6764.7608	0.0002
13	6	8	12	6	7	6804.2753	0.0013
10	3	7	9	2	7	6817.3281	0.0012
13	7	7	12	7	6	6844.4249	0.0214
15	2	13	14	2	12	6856.7330	-0.0706
15	3	13	14	3	12	6856.7330	0.0235
8	8	0	7	7	0	6881.2122	0.0074
8	8	1	7	7	1	6881.2122	0.0010
10	4	7	9	3	7	6927.4335	0.0001
13	7	6	12	7	5	6951.4809	-0.0152
16	1	15	15	1	14	6961.3086	-0.0012
16	2	15	15	2	14	6961.3086	-0.0005
16	1	15	15	2	14	6961.3086	-0.0003
16	2	15	15	1	14	6961.3086	-0.0014
10	2	8	9	1	8	6965.5684	-0.0077
10	5	6	9	4	6	6973.0430	0.0023
10	3	8	9	2	8	6976.1364	-0.0008
9	7	2	8	6	2	7019.4174	0.0042
9	7	3	8	6	3	7022.4959	0.0009
10	1	9	9	0	9	7029.9122	0.0181
10	2	9	9	1	9	7030.3408	-0.0017
14	5	10	13	5	9	7052.5677	0.0070
17	1	17	16	1	16	7067.5537	0.0103
17	0	17	16	0	16	7067.5537	0.0103
17	0	17	16	1	16	7067.5537	0.0103
17	1	17	16	0	16	7067.5537	0.0103
10	6	4	9	5	4	7069.4190	0.0010
13	5	8	12	5	7	7127.5742	0.0019
15	4	12	14	4	11	7162.1685	0.0146
15	3	12	14	3	11	7164.2522	0.0006
15	4	12	14	3	11	7165.3348	0.0208
11	5	6	10	4	6	7187.6989	-0.0002
10	6	5	9	5	5	7192.3754	-0.0002
16	2	14	15	2	13	7263.2395	-0.0069
16	3	14	15	3	13	7263.2395	0.0216
16	3	14	15	2	13	7263.2395	-0.0188
14	6	9	13	6	8	7284.1208	-0.0084
11	4	7	10	3	7	7325.4992	0.0000
17	1	16	16	1	15	7368.1424	0.0018
17	2	16	16	2	15	7368.1424	0.0019
17	1	16	16	2	15	7368.1424	0.0020
17	2	16	16	1	15	7368.1424	0.0017
14	7	8	13	7	7	7380.6030	0.0024
15	5	11	14	5	10	7467.6800	0.0001
18	0	18	17	1	17	7474.4347	0.0037
18	1	18	17	0	17	7474.4347	0.0037
18	1	18	17	1	17	7474.4347	0.0037
18	0	18	17	0	17	7474.4347	0.0037
11	6	5	10	5	5	7503.0081	-0.0062
10	7	3	9	6	3	7520.3218	0.0033
10	7	4	9	6	4	7533.9060	0.0028

Appendix VII

14	5	9	13	5	8	7542.6113	0.0050
16	4	13	15	4	12	7568.0941	0.0160
16	4	13	15	3	12	7569.1414	0.0009
11	3	8	10	2	8	7571.9314	-0.0012
14	7	7	13	7	6	7599.6743	0.0133
11	5	7	10	4	7	7608.0388	-0.0019
11	4	8	10	3	8	7621.9025	-0.0031
17	2	15	16	2	14	7669.8014	-0.0045
17	3	16	16	3	14	7669.8014	0.0074
17	3	15	16	2	14	7669.8014	-0.0079
17	2	15	16	3	14	7669.8014	0.0074
11	2	9	10	1	9	7681.2806	0.0010
11	3	9	10	2	9	7684.9880	0.0012
11	1	10	10	0	10	7738.2804	0.0100
11	2	10	10	1	10	7738.3986	-0.0054
11	6	6	10	5	6	7747.5827	-0.0007
9	9	0	8	8	0	7764.4901	0.0045
9	9	1	8	8	1	7764.4901	0.0035
18	1	17	17	1	16	7774.9712	-0.0102
18	2	17	17	2	16	7774.9712	-0.0102
18	1	17	17	2	16	7774.9712	-0.0102
18	2	17	17	1	16	7774.9712	-0.0103
12	5	7	11	4	7	7846.9054	-0.0015
19	0	19	18	1	18	7881.3186	0.0015
19	1	19	18	0	18	7881.3186	0.0015
19	1	19	18	1	18	7881.3186	0.0015
19	0	19	18	0	18	7881.3186	0.0015
15	7	9	14	7	8	7896.9436	0.0067
10	8	2	9	7	2	7905.0812	0.0047
10	8	3	9	7	3	7905.7450	0.0005
12	6	6	11	5	6	7960.4580	0.0024

Table S10.3. Measured frequencies and residuals (in MHz) for the rotational transitions of the conformer **3** of romandolide.

J'	K'_{-1}	K'_{+1}	J''	K''_{-1}	K''_{+1}	V _{obs}	V _{obs} - V _{calc}
5	1	5	4	1	4	2285.4607	-0.0071
5	0	5	4	0	4	2309.0475	-0.0037
5	1	5	4	0	4	2330.2983	-0.0023
5	2	4	4	2	3	2460.4428	-0.0026
5	3	3	4	3	2	2522.5549	0.0031
5	1	4	4	1	3	2571.3862	0.0010
3	3	1	2	2	0	2589.8783	0.0060
3	3	0	2	2	1	2605.7568	-0.0091
4	3	3	3	2	3	2637.0281	-0.0016
4	2	2	3	1	2	2637.0285	-0.0012
5	2	3	4	2	2	2640.9757	-0.0009
6	0	6	5	1	5	2715.8048	0.0011
6	1	6	5	1	5	2725.1673	0.0063
6	0	6	5	0	5	2737.0550	0.0019
6	1	6	5	0	5	2746.4100	-0.0004
6	1	5	5	2	4	2766.6864	-0.0163
4	2	3	3	1	3	2844.2383	0.0187
6	1	5	5	1	4	3027.0569	0.0003
6	4	3	5	4	2	3034.7293	-0.0052
4	3	2	3	2	1	3059.1889	-0.0024
4	3	1	3	2	1	3072.3901	-0.0028
4	3	1	3	2	2	3138.3321	0.0027
7	0	7	6	1	6	3157.9447	-0.0041
7	1	7	6	1	6	3161.8734	0.0021
7	0	7	6	0	6	3167.3047	-0.0015
7	1	7	6	0	6	3171.2141	-0.0145
6	2	4	5	2	3	3173.7351	-0.0016
6	2	5	5	1	4	3189.1069	-0.0040
5	2	3	4	1	3	3190.2166	-0.0007
5	1	4	4	0	4	3248.1419	-0.0013
7	1	6	6	2	5	3297.1671	0.0093
7	2	6	6	2	5	3387.0644	-0.0008
7	1	6	6	1	5	3459.2155	0.0034
5	2	4	4	1	4	3463.6523	-0.0120
5	3	3	4	2	2	3487.6467	-0.0011
7	3	5	6	3	4	3519.8254	0.0009
4	4	1	3	3	0	3535.6554	0.0004
4	4	0	3	3	0	3535.8807	0.0030
5	3	2	4	2	2	3537.4748	0.0056
5	4	3	4	3	3	3537.4748	0.0056
4	4	1	3	3	1	3537.5924	-0.0028
4	4	0	3	3	1	3537.8181	0.0002
7	5	2	6	5	1	3539.2353	-0.0067
7	4	4	6	4	3	3548.6972	-0.0038
8	0	8	7	1	7	3595.3696	-0.0016
8	1	8	7	1	7	3596.9572	-0.0019
8	0	8	7	0	7	3599.2927	-0.0009
8	1	8	7	0	7	3600.8903	0.0088
5	3	3	4	2	3	3665.5840	-0.0107
7	2	5	6	2	4	3684.0627	-0.0021
5	3	2	4	2	3	3715.4247	0.0086
8	1	7	7	2	6	3791.2107	0.0003
6	2	4	5	1	4	3792.5751	0.0064
8	2	7	7	2	6	3836.6496	0.0011
6	3	4	5	2	3	3871.6030	0.0127
8	1	7	7	1	6	3881.1170	-0.0008
8	2	7	7	1	6	3926.5515	-0.0044
8	3	6	7	3	5	4004.6979	-0.0027
5	4	2	4	3	1	4030.4836	-0.0122
9	0	9	8	1	8	4030.6271	-0.0034

9	1	9	8	1	8	4031.2571	0.0002
9	0	9	8	0	8	4032.2174	-0.0011
5	4	1	4	3	1	4032.4679	0.0042
9	1	9	8	0	8	4032.8465	0.0017
5	4	1	4	3	2	4045.6647	-0.0006
8	5	3	7	5	2	4058.9030	0.0055
8	4	5	7	4	4	4061.3861	-0.0019
8	2	6	7	2	5	4165.6510	0.0012
7	3	5	6	2	4	4217.6577	-0.0204
6	3	4	5	2	4	4230.0705	0.0021
9	2	7	8	3	6	4243.1647	0.0044
9	1	8	8	2	7	4258.1475	-0.0042
9	2	8	8	2	7	4279.5959	-0.0052
9	1	8	8	1	7	4303.5900	0.0001
9	2	8	8	1	7	4325.0314	-0.0078
10	0	10	9	1	9	4464.9536	-0.0067
10	1	10	9	1	9	4465.1980	-0.0044
10	0	10	9	0	9	4465.5865	-0.0001
10	1	10	9	0	9	4465.8381	0.0093
9	3	7	8	3	6	4478.2265	-0.0004
7	3	4	6	2	4	4505.4623	-0.0036
6	4	3	5	3	2	4506.0562	-0.0024
6	4	2	5	3	2	4515.5786	-0.0010
6	5	3	5	4	3	4515.5786	-0.0010
6	4	3	5	3	3	4555.8897	0.0097
6	4	2	5	3	3	4565.4045	0.0035
9	4	6	8	4	5	4569.3340	0.0206
9	5	4	8	5	3	4587.2422	-0.0079
9	2	7	8	2	6	4615.8282	0.0038
10	1	9	9	2	8	4708.5125	0.0002
10	2	9	9	2	8	4718.1517	0.0007
10	1	9	9	1	8	4729.9652	0.0036
10	2	9	9	1	8	4739.5975	-0.0028
10	2	8	9	3	7	4806.2343	-0.0026
7	3	5	6	2	5	4821.1382	0.0023
9	3	7	8	2	6	4850.8959	0.0049
11	1	11	10	1	10	4899.0193	0.0173
11	0	11	10	0	10	4899.1516	-0.0005
10	3	8	9	3	7	4940.4972	-0.0002
6	5	2	5	4	1	4976.5888	0.0004
7	4	3	6	3	3	4977.9322	0.0041
6	5	2	5	4	2	4978.5573	0.0010
6	5	1	5	4	2	4978.8128	0.0062
10	2	8	9	2	7	5041.3006	-0.0029
8	3	5	7	2	5	5053.3543	-0.0006
10	4	7	9	4	6	5069.0372	0.0027
7	4	4	6	3	4	5079.6498	-0.0121
7	4	3	6	3	4	5112.6865	-0.0100
10	5	5	9	5	4	5128.7970	0.0026
11	2	10	10	2	9	5154.1184	-0.0033
11	1	10	10	1	9	5159.5891	0.0037
11	2	10	10	1	9	5163.7559	-0.0045
10	3	8	9	2	7	5175.5604	-0.0035
10	4	6	9	4	5	5260.1470	0.0081
11	2	9	10	3	8	5322.3416	0.0060
12	0	12	11	1	11	5332.7173	0.0065
12	1	12	11	0	11	5332.8248	-0.0127
8	4	5	7	3	4	5333.4383	0.0007
11	3	9	10	3	8	5392.9019	0.0021
6	6	0	5	5	0	5414.2414	0.0116
6	6	1	5	5	1	5414.2414	-0.0093
8	4	4	7	3	4	5424.1005	-0.0080
11	2	9	10	2	8	5456.5999	0.0039
7	5	3	6	4	2	5472.3268	0.0012
7	5	2	6	4	2	5473.7997	0.0066

7	6	3	6	5	3	5473.7997	0.0066
7	5	3	6	4	3	5481.8467	0.0001
7	5	2	6	4	3	5483.3153	0.0012
11	3	9	10	2	8	5527.1668	0.0066
11	4	8	10	4	7	5557.9095	-0.0041
12	1	11	11	2	10	5586.9981	0.0130
12	2	11	11	2	10	5588.7535	0.0111
12	1	11	11	1	10	5591.1589	-0.0011
12	2	11	11	1	10	5592.9163	-0.0011
8	4	5	7	3	5	5621.2304	0.0050
9	3	6	8	2	6	5659.9328	0.0009
11	5	6	10	5	5	5688.3659	0.0043
8	4	4	7	3	5	5711.8884	-0.0079
13	1	13	12	1	12	5766.4829	0.0144
13	0	13	12	0	12	5766.4829	-0.0074
13	0	13	12	1	12	5766.4832	0.0275
13	1	13	12	0	12	5766.4832	-0.0199
12	2	10	11	3	9	5802.8624	0.0156
12	3	10	11	3	9	5837.6587	0.0023
9	4	5	8	3	5	5876.6045	-0.0065
8	5	4	7	4	3	5954.3439	0.0045
8	5	3	7	4	3	5960.4738	-0.0022
8	5	4	7	4	4	5987.3748	0.0008
13	2	12	12	2	11	6022.7184	-0.0085
13	1	12	12	1	11	6023.7586	-0.0028
13	2	12	12	1	11	6024.4748	-0.0095
12	4	9	11	4	8	6034.5909	-0.0181
14	0	14	13	1	13	6200.1900	0.0097
14	1	14	13	0	13	6200.1900	-0.0079
14	1	14	13	1	13	6200.1901	0.0051
14	0	14	13	0	13	6200.1901	-0.0031
11	4	8	10	3	7	6240.9834	0.0067
12	5	7	11	5	6	6266.3809	-0.0060
13	3	11	12	3	10	6277.1986	0.0238
13	2	11	12	2	10	6295.6141	0.0061
13	3	11	12	2	10	6311.9598	-0.0246
7	7	0	6	6	0	6352.9214	-0.0040
7	7	1	6	6	1	6352.9214	-0.0060
9	5	5	8	4	4	6408.3312	-0.0001
8	6	2	7	5	2	6417.4526	0.0073
8	7	3	7	6	3	6417.4526	0.0073
8	6	3	7	5	3	6418.7149	0.0003
9	5	4	8	4	4	6428.7051	0.0033
14	1	13	13	2	12	6456.1414	-0.0101
14	2	13	13	2	12	6456.4494	0.0062
14	1	13	13	1	12	6456.8753	0.0009
9	5	5	8	4	5	6498.9769	-0.0253
13	4	10	12	4	9	6499.2368	-0.0112
15	1	15	14	1	14	6633.9056	0.0063
15	0	15	14	0	14	6633.9056	0.0033
15	0	15	14	1	14	6633.9056	0.0081
15	1	15	14	0	14	6633.9056	0.0016
14	3	12	13	3	11	6713.5153	0.0080
14	2	12	13	2	11	6722.4434	-0.0117
8	7	1	7	6	1	6855.5904	0.0054
8	7	2	7	6	2	6855.5904	-0.0204
15	2	14	14	2	13	6890.0875	0.0244
15	1	14	14	1	13	6890.2437	0.0047
9	6	3	8	5	3	6914.5485	-0.0002
14	4	11	13	4	10	6953.2798	0.0053
10	5	5	9	4	6	7078.8584	0.0048
15	2	13	14	2	12	7152.2665	-0.0014
8	8	0	7	7	0	7291.5932	0.0011
8	8	1	7	7	1	7291.5932	0.0009
16	1	15	15	1	14	7323.6804	-0.0494

Appendix VII

16	2	15	15	2	14	7323.6804	0.0211
16	1	15	15	2	14	7323.6814	0.0675
16	2	15	15	1	14	7323.6814	-0.0938
10	6	4	9	5	4	7404.0548	0.0164
17	1	17	16	1	16	7501.3044	-0.0193
17	0	17	16	0	16	7501.3044	-0.0197
16	2	14	15	2	13	7583.7357	-0.0156
17	1	16	16	2	15	7757.2845	0.0433
17	2	16	16	1	15	7757.2845	-0.0197
17	1	16	16	1	15	7757.2867	0.0001
17	2	16	16	2	15	7757.2867	0.0279
9	8	1	8	7	1	7794.3513	0.0015
9	8	2	8	7	2	7794.3513	-0.0012

Table S10.4. Measured frequencies and residuals (in MHz) for the rotational transitions of the conformer **9** of romandolide.

J'	K'_{-1}	K'_{+1}	J''	K''_{-1}	K''_{+1}	V _{obs}	V _{obs} - V _{calc}
3	3	0	2	2	0	2470.1751	0.0055
3	3	1	2	2	1	2482.3084	0.0092
5	0	5	4	1	4	2562.7172	0.0161
4	2	2	3	1	2	2703.8252	-0.0031
4	2	3	3	1	3	2866.2715	0.0004
4	3	1	3	2	1	3006.3152	0.0017
4	3	2	3	2	2	3057.4836	-0.0021
6	0	6	5	1	5	3067.7926	0.0002
6	1	6	5	0	5	3082.3357	-0.0154
6	1	5	5	2	4	3162.5293	0.0071
5	2	3	4	1	3	3316.4804	-0.0022
4	4	1	3	3	0	3354.2770	-0.0173
4	4	0	3	3	0	3354.6241	-0.0005
4	4	1	3	3	1	3356.7100	0.0018
4	4	0	3	3	1	3357.0488	0.0103
5	1	4	4	0	4	3392.4439	-0.0118
6	2	5	5	1	4	3404.3596	0.0062
5	3	2	4	2	2	3533.7712	0.0006
7	0	7	6	1	6	3567.0013	0.0035
7	1	7	6	0	6	3572.6608	0.0030
5	3	3	4	2	3	3650.9809	-0.0004
7	1	6	6	2	5	3718.7247	-0.0009
7	2	6	6	1	5	3847.4956	-0.0020
5	4	1	4	3	1	3904.1806	-0.0001
5	4	2	4	3	2	3917.5104	0.0021
6	2	4	5	1	4	3973.3703	-0.0045
8	0	8	7	1	7	4063.5994	-0.0021
8	1	8	7	0	7	4065.7059	-0.0018
6	3	3	5	2	3	4074.8700	0.0034
6	1	5	5	0	5	4123.0542	-0.0029
5	5	0	4	4	0	4234.8912	0.0020
5	5	1	4	4	0	4234.8912	0.0428
5	5	1	4	4	1	4235.1887	0.0100
5	5	0	4	4	1	4235.1887	-0.0307
6	3	4	5	2	4	4266.5057	0.0001
6	4	2	5	3	2	4439.6512	-0.0005
6	4	3	5	3	3	4485.5316	-0.0007
9	0	9	8	1	8	4559.1542	0.0053
9	1	9	8	0	8	4559.9125	0.0043
7	3	4	6	2	4	4651.2471	0.0002
7	2	5	6	1	5	4675.9911	-0.0043
9	2	8	8	1	7	4785.0667	0.0061
6	5	1	5	4	1	4789.8310	0.0029
6	5	2	5	4	2	4792.2833	-0.0002
7	1	6	6	0	6	4849.9176	-0.0137
7	2	6	6	1	6	4888.1926	-0.0110
7	3	5	6	2	5	4905.2898	0.0048
7	4	3	6	3	3	4958.0671	0.0005
10	1	10	9	0	9	5054.5461	-0.0142
7	4	4	6	3	4	5066.3905	-0.0021
10	2	9	9	1	8	5271.2705	0.0020
8	3	5	7	2	5	5274.7476	0.0015
7	5	2	6	4	2	5339.2247	0.0009
7	5	3	6	4	3	5350.4740	0.0006
8	2	6	7	1	6	5410.8628	0.0037
8	4	4	7	3	4	5473.1483	-0.0005
11	1	11	10	0	10	5549.3841	0.0017
8	3	6	7	2	6	5565.8451	-0.0028
8	1	7	7	0	7	5568.2735	0.0026
8	2	7	7	1	7	5585.7000	-0.0039

8	4	5	7	3	5	5665.5380	0.0104
7	6	1	6	5	1	5670.5446	0.0138
7	6	2	6	5	2	5670.9006	-0.0093
11	1	10	10	2	9	5757.8570	0.0022
8	5	3	7	4	3	5876.3242	-0.0024
8	5	4	7	4	4	5912.4673	-0.0041
7	7	0	6	6	0	5993.6075	0.0037
7	7	1	6	6	1	5993.6075	-0.0005
7	7	1	6	6	0	5993.6075	0.0042
7	7	0	6	6	1	5993.6075	-0.0010
9	4	5	8	3	5	6011.3073	-0.0038
12	0	12	11	1	11	6044.2511	0.0164
12	1	12	11	0	11	6044.2511	-0.0150
9	2	7	8	1	7	6154.0481	0.0026
8	6	2	7	5	2	6224.7607	0.0027
8	6	3	7	5	3	6226.8923	-0.0044
9	3	7	8	2	7	6244.3827	0.0028
9	1	8	8	0	8	6280.2210	0.0067
9	4	6	8	3	6	6286.6267	-0.0070
9	2	8	8	1	8	6287.6190	-0.0048
9	5	4	8	4	4	6394.3065	0.0005
9	5	5	8	4	5	6482.9527	-0.0077
13	0	13	12	1	12	6539.1699	0.0103
13	1	13	12	0	12	6539.1699	-0.0003
8	7	1	7	6	1	6550.1662	0.0251
10	4	6	9	3	6	6594.3165	-0.0021
10	3	7	9	2	7	6674.6004	-0.0041
9	6	3	8	5	3	6774.1514	-0.0045
9	6	4	8	5	4	6782.6573	-0.0122
8	8	0	7	7	0	6872.8671	0.0024
8	8	1	7	7	1	6872.8671	0.0019
8	8	1	7	7	0	6872.8671	0.0024
8	8	0	7	7	1	6872.8671	0.0018
10	2	8	9	1	8	6889.2133	0.0024
10	5	5	9	4	5	6896.0934	-0.0063
10	4	7	9	3	7	6930.7559	-0.0071
10	3	8	9	2	8	6935.8351	0.0123
10	1	9	9	0	9	6988.5827	0.0062
9	7	2	8	6	2	7105.7157	-0.0099
11	4	7	10	3	7	7233.2261	0.0017
10	6	4	9	5	4	7313.4667	-0.0069
10	6	5	9	5	5	7339.9225	-0.0032
11	5	6	10	4	6	7402.5055	-0.0003
11	3	8	10	2	8	7426.2655	0.0036
9	8	1	8	7	1	7429.5193	0.0014
9	8	2	8	7	2	7429.5193	-0.0054
15	0	15	14	1	14	7528.9852	0.0001
15	1	15	14	0	14	7528.9853	-0.0009
11	4	8	10	3	8	7596.1559	0.0063
11	2	9	10	1	9	7613.2750	0.0034
10	7	3	9	6	3	7659.2384	-0.0041
10	7	4	9	6	4	7660.8708	-0.0186
11	5	7	10	4	7	7671.7779	-0.0080
11	1	10	10	0	10	7695.1434	0.0071
9	9	0	8	8	0	7752.1142	-0.0001
9	9	1	8	8	1	7752.1142	-0.0001
11	6	5	10	5	5	7835.3149	-0.0047
11	6	6	10	5	6	7902.1984	-0.0078
12	5	7	11	4	7	7942.4980	0.0088
10	8	2	9	7	2	7985.5873	0.0184

Table S10.5. Measured frequencies and residuals (in MHz) for the rotational transitions of the conformer **48** of romandolide.

J'	K'_{-1}	K'_{+1}	J''	K''_{-1}	K''_{+1}	V _{obs}	V _{obs} - V _{calc}
6	0	6	5	1	5	2247.5335	0.0085
3	2	2	2	1	2	2248.4640	0.0267
6	1	6	5	0	5	2338.9891	0.0024
4	2	3	3	1	2	2394.4320	0.0029
4	2	2	3	1	2	2518.8282	-0.0022
8	2	6	7	3	5	2555.0682	-0.0105
7	1	6	6	2	5	2609.2957	-0.0035
7	0	7	6	1	6	2627.4603	-0.0005
7	1	7	6	0	6	2676.2177	-0.0012
5	2	4	4	1	3	2693.2641	-0.0017
3	3	1	2	2	0	2754.7117	-0.0006
3	3	0	2	2	0	2755.5659	-0.0056
4	2	3	3	1	3	2756.2190	0.0057
3	3	1	2	2	1	2763.7651	-0.0010
3	3	0	2	2	1	2764.6246	-0.0007
5	2	3	4	1	3	2957.7283	-0.0019
6	2	5	5	1	4	2969.8824	-0.0060
8	0	8	7	1	7	2997.6312	0.0020
8	1	8	7	0	7	3022.4427	0.0002
8	1	7	7	2	6	3085.8103	0.0144
9	2	7	8	3	6	3152.3968	-0.0059
4	3	2	3	2	1	3154.4893	-0.0009
4	3	1	3	2	1	3160.4280	0.0015
4	3	2	3	2	2	3198.4842	-0.0042
7	2	6	6	1	5	3235.1257	-0.0020
5	2	4	4	1	4	3291.7251	-0.0064
9	0	9	8	1	8	3362.1384	0.0000
9	1	9	8	0	8	3374.3476	-0.0013
6	2	4	5	1	4	3438.5986	-0.0023
11	3	8	10	4	7	3486.2349	-0.0378
8	2	7	7	1	6	3503.0931	0.0001
5	3	3	4	2	2	3523.2349	0.0000
9	1	8	8	2	7	3528.2474	0.0005
5	3	2	4	2	2	3546.3649	0.0019
5	3	3	4	2	3	3647.6269	-0.0094
10	0	10	9	1	9	3723.5869	-0.0027
10	1	10	9	0	9	3729.4475	-0.0016
10	2	8	9	3	7	3730.3025	0.0051
4	4	1	3	3	0	3779.0271	0.0151
4	4	0	3	3	1	3779.9165	-0.0221
9	2	8	8	1	7	3786.3405	0.0000
6	3	4	5	2	3	3851.7100	-0.0003
6	2	5	5	1	5	3853.3677	0.0162
6	3	3	5	2	3	3917.8759	-0.0009
10	1	9	9	2	8	3940.8737	0.0049
7	2	5	6	1	5	3968.8612	-0.0039
11	0	11	10	1	10	4083.4671	-0.0018
11	1	11	10	0	10	4086.2290	0.0027
10	2	9	9	1	8	4090.5753	-0.0031
6	3	4	5	2	4	4116.1766	0.0021
7	3	5	6	2	4	4139.2711	-0.0013
12	3	9	11	4	8	4149.7940	0.0029
5	4	2	4	3	1	4197.1068	-0.0006
5	4	1	4	3	1	4197.7109	0.0014
5	4	2	4	3	2	4203.0410	-0.0028
5	4	1	4	3	2	4203.6431	-0.0027
11	2	9	10	3	8	4273.2542	-0.0020
11	1	10	10	2	9	4331.6285	0.0026
8	3	6	7	2	5	4391.6972	0.0027
11	2	10	10	1	9	4414.1727	-0.0047

7	2	6	6	1	6	4438.1276	-0.0038
12	0	12	11	1	11	4442.5677	-0.0026
12	0	12	11	1	11	4442.5677	-0.0026
12	1	12	11	0	11	4443.8463	-0.0017
8	2	6	7	1	6	4553.7643	-0.0001
6	4	3	5	3	2	4605.7064	-0.0040
7	3	5	6	2	5	4607.9758	-0.0090
6	4	2	5	3	2	4608.6740	-0.0018
9	3	7	8	2	6	4618.4355	-0.0137
6	4	3	5	3	3	4628.8266	-0.0120
6	4	2	5	3	3	4631.8041	0.0001
8	3	5	7	2	5	4692.1212	0.0149
12	1	11	11	2	10	4708.1926	0.0018
12	2	10	11	3	9	4772.4231	0.0012
13	3	10	12	4	9	4797.3394	-0.0009
5	5	1	4	4	0	4799.1415	0.0362
5	5	0	4	4	1	4799.1415	-0.0361
5	5	0	4	4	0	4799.1415	0.0314
5	5	1	4	4	1	4799.1415	-0.0313
13	0	13	12	1	12	4801.2991	0.0005
13	1	13	12	0	12	4801.8837	0.0007
10	3	8	9	2	7	4832.1375	0.0067
7	4	4	6	3	3	4994.2394	-0.0045
7	4	3	6	3	3	5004.8585	0.0050
8	2	7	7	1	7	5042.0258	0.0261
11	3	9	10	2	8	5048.1102	0.0022
7	4	4	6	3	4	5060.4081	-0.0023
7	4	3	6	3	4	5071.0170	-0.0031
13	1	12	12	2	11	5076.2824	-0.0012
13	2	12	12	1	11	5098.8209	-0.0001
8	3	6	7	2	6	5125.4325	0.0005
9	3	6	8	2	6	5135.3230	0.0076
14	1	14	13	0	13	5160.1201	0.0035
9	2	7	8	1	7	5192.0405	0.0017
6	5	2	5	4	1	5220.2536	0.0034
6	5	1	5	4	2	5220.8967	-0.0078
13	2	11	12	3	10	5228.5025	0.0034
12	3	10	11	2	9	5281.6987	0.0016
8	4	5	7	3	4	5349.1667	-0.0001
8	4	4	7	3	4	5379.8039	-0.0008
14	3	11	13	4	10	5409.9843	0.0137
14	1	13	13	2	12	5439.6181	0.0001
14	2	13	13	1	12	5450.9426	-0.0028
8	4	5	7	3	5	5502.2176	-0.0105
15	0	15	14	1	14	5518.3254	0.0002
15	1	15	14	0	14	5518.4459	0.0021
8	4	4	7	3	5	5532.8614	-0.0045
13	3	11	12	2	10	5542.9797	0.0013
10	3	7	9	2	7	5633.3244	0.0029
7	5	3	6	4	2	5639.1244	-0.0025
7	5	3	6	4	3	5642.0867	-0.0055
7	5	2	6	4	3	5642.3977	-0.0050
14	2	12	13	3	11	5649.3651	0.0080
9	4	6	8	3	5	5658.9684	-0.0027
9	2	8	8	1	8	5660.3744	0.0099
9	3	7	8	2	7	5669.1130	-0.0076
9	4	5	8	3	5	5734.1719	-0.0005
15	1	14	14	2	13	5800.4061	0.0007
15	2	14	14	1	13	5805.9917	0.0025
6	6	1	5	5	0	5818.7630	0.0022
6	6	0	5	5	1	5818.7630	-0.0029
6	6	0	5	5	0	5818.7630	0.0019
6	6	1	5	5	1	5818.7630	-0.0026
14	3	12	13	2	11	5833.5683	-0.0089
16	1	16	15	0	15	5876.8145	0.0001

10	4	7	9	3	6	5919.8197	-0.0044
15	3	12	14	4	11	5973.5975	-0.0016
8	5	4	7	4	4	6063.1981	0.0042
8	5	3	7	4	4	6064.5206	0.0031
10	4	6	9	3	6	6081.0909	-0.0036
15	3	13	14	2	12	6148.5762	0.0183
16	1	15	15	2	14	6159.8809	-0.0036
16	2	15	15	1	14	6162.5959	0.0031
11	3	8	10	2	8	6192.6668	0.0012
17	0	17	16	1	16	6235.1890	0.0082
17	1	17	16	0	16	6235.1890	-0.0151
10	3	8	9	2	8	6237.8316	0.0024
7	6	2	6	5	2	6240.4027	-0.0316
7	6	2	6	5	1	6240.4038	0.0218
7	6	1	6	5	1	6240.4038	0.0177
12	4	9	11	3	8	6320.4917	-0.0047
16	2	14	15	3	13	6424.6067	0.0053
10	4	7	9	3	7	6436.6918	0.0016
11	4	7	10	3	7	6443.7068	0.0251
9	5	5	8	4	4	6454.7800	-0.0016
16	3	14	15	2	13	6480.8012	0.0051
9	5	5	8	4	5	6485.4260	0.0065
13	4	10	12	3	9	6485.6785	0.0038
9	5	4	8	4	5	6489.9423	-0.0017
17	1	16	16	2	15	6518.7197	0.0026
17	2	16	16	1	15	6520.0156	0.0027
18	0	18	17	1	17	6593.5953	0.0043
18	1	18	17	0	17	6593.5953	-0.0059
14	4	11	13	3	10	6649.2318	0.0033
8	6	3	7	5	2	6661.1536	-0.0015
8	6	2	7	5	2	6661.1536	-0.0301
8	6	2	7	5	3	6661.5019	0.0077
8	6	3	7	5	3	6661.5019	0.0363
17	2	15	16	3	14	6794.2955	-0.0098
15	4	12	14	3	11	6829.0132	-0.0117
7	7	1	6	6	0	6838.3689	0.0031
7	7	0	6	6	1	6838.3689	0.0027
7	7	0	6	6	0	6838.3689	0.0030
7	7	1	6	6	1	6838.3689	0.0027
11	4	8	10	3	8	6937.8746	-0.0079
19	0	19	18	1	18	6951.9890	-0.0066
19	1	19	18	0	18	6951.9890	-0.0111
9	6	4	8	5	3	7080.1448	0.0021
9	6	3	8	5	3	7080.2651	-0.0188
8	7	2	7	6	1	7260.1224	0.0071
8	7	1	7	6	2	7260.1224	0.0026
8	7	1	7	6	1	7260.1224	0.0068
8	7	2	7	6	2	7260.1224	0.0030
20	0	20	19	1	19	7310.4019	0.0064
20	1	20	19	0	19	7310.4019	0.0045
11	5	7	10	4	7	7344.8381	-0.0004
21	0	21	20	1	20	7668.7972	0.0062
21	1	21	20	0	20	7668.7972	0.0054
8	8	1	7	7	0	7857.9541	-0.0020
8	8	0	7	7	1	7857.9541	-0.0020
8	8	0	7	7	0	7857.9541	-0.0020
8	8	1	7	7	1	7857.9541	-0.0020
20	3	18	19	2	17	7882.8576	-0.0128
11	6	6	10	5	6	7917.9377	-0.0033

Table S10.6. Measured frequencies and residuals (in MHz) for the rotational transitions of the conformer **50** of romandolide.

J'	K'_{-1}	K'_{+1}	J''	K''_{-1}	K''_{+1}	V _{obs}	V _{obs} - V _{calc}
5	1	5	4	0	4	2325.9496	0.0155
3	2	2	2	1	2	2328.0236	-0.0004
6	0	6	5	1	5	2568.3970	0.0019
4	2	2	3	1	2	2665.4985	0.0005
6	1	6	5	0	5	2712.2395	-0.0029
3	3	0	2	2	0	2843.5693	0.0076
3	3	1	2	2	1	2847.9741	0.0011
4	2	3	3	1	3	2855.3055	-0.0135
5	1	4	4	0	4	2961.2750	-0.0140
5	2	4	4	1	3	2975.7313	0.0142
7	0	7	6	1	6	3018.1473	0.0018
7	1	7	6	0	6	3106.3912	0.0017
5	2	3	4	1	3	3124.4168	-0.0012
4	3	2	3	2	1	3296.9460	-0.0063
4	3	1	3	2	1	3299.2438	0.0018
4	3	2	3	2	2	3320.2818	-0.0025
6	2	5	5	1	4	3335.2293	-0.0091
5	2	4	4	1	4	3403.0270	0.0049
8	0	8	7	1	7	3457.3026	0.0011
8	1	8	7	0	7	3508.9638	-0.0084
6	1	5	5	0	5	3587.9361	0.0032
6	2	4	5	1	4	3608.8136	0.0024
7	2	6	6	1	5	3681.1714	-0.0134
5	3	3	4	2	2	3733.2372	0.0012
5	3	2	4	2	2	3742.2686	-0.0003
5	3	3	4	2	3	3800.8450	0.0015
9	0	9	8	1	8	3889.1156	0.0030
4	4	0	3	3	0	3891.0506	0.0121
4	4	1	3	3	1	3891.3312	-0.0177
9	1	9	8	0	8	3918.3341	0.0032
6	2	5	5	1	5	3970.5913	-0.0021
8	2	7	7	1	6	4020.6729	0.0045
7	2	5	6	1	5	4125.1944	-0.0020
6	3	4	5	2	3	4144.2791	-0.0007
6	3	3	5	2	3	4170.7189	0.0017
7	1	6	6	0	6	4245.7145	0.0019
6	3	4	5	2	4	4292.9822	0.0015
10	0	10	9	1	9	4316.2479	0.0071
10	1	10	9	0	9	4332.3386	0.0046
5	4	1	4	3	1	4354.9236	0.0048
5	4	2	4	3	2	4357.0372	-0.0014
9	2	8	8	1	7	4362.3759	0.0004
10	1	9	9	2	8	4406.9326	0.0030
7	3	5	6	2	4	4526.1311	-0.0047
7	2	6	6	1	6	4556.8767	0.0013
7	3	4	6	2	4	4589.5921	0.0006
8	2	6	7	1	6	4678.4402	-0.0093
11	1	11	10	0	10	4749.2468	0.0118
7	3	5	6	2	5	4799.7070	-0.0017
6	4	2	5	3	2	4815.3696	0.0010
6	4	3	5	3	3	4823.5576	-0.0013
8	1	7	7	0	7	4924.0408	-0.0074
5	5	0	4	4	0	4936.5284	0.0072
5	5	1	4	4	1	4936.5284	-0.0108
8	3	5	7	2	5	5010.5653	0.0045
11	2	10	10	1	9	5081.1718	0.0054
12	0	12	11	1	11	5163.2300	0.0007
12	1	12	11	0	11	5167.8399	-0.0019
7	4	3	6	3	3	5268.7905	-0.0034
9	2	7	8	1	7	5272.1440	-0.0037

7	4	4	6	3	4	5292.1742	-0.0077
8	3	6	7	2	6	5323.4241	-0.0012
12	1	11	11	2	10	5341.6320	-0.0043
6	5	1	5	4	1	5401.5018	-0.0067
6	5	2	5	4	2	5401.6799	0.0124
9	3	6	8	2	6	5447.9614	0.0036
12	2	11	11	1	10	5463.4304	0.0160
13	0	13	12	1	12	5584.9761	-0.0210
13	1	13	12	0	12	5587.4180	0.0034
9	1	8	8	0	8	5610.4500	-0.0005
9	1	8	8	0	8	5610.4500	-0.0005
8	4	4	7	3	4	5710.5233	-0.0013
8	4	4	7	3	4	5710.5233	-0.0013
8	4	5	7	3	5	5765.0070	-0.0024
8	4	5	7	3	5	5765.0070	-0.0023
9	2	8	8	1	8	5777.4579	0.0064
9	2	8	8	1	8	5777.4579	0.0064
13	1	12	12	2	11	5785.9881	-0.0125
13	2	12	12	1	11	5858.5559	-0.0128
7	5	2	6	4	2	5865.6493	0.0287
9	3	7	8	2	7	5865.6493	-0.0595
7	5	2	6	4	2	5865.6493	0.0287
7	5	3	6	4	3	5866.3876	-0.0109
10	2	8	9	1	8	5906.5936	-0.0061
6	6	0	5	5	0	5981.8410	0.0025
6	6	1	5	5	1	5981.8410	0.0016
14	0	14	13	1	13	6006.2648	-0.0019
14	1	14	13	0	13	6007.5246	0.0047
9	4	6	8	3	6	6244.8416	-0.0081
10	1	9	9	0	9	6295.2661	-0.0025
8	5	3	7	4	3	6327.8486	0.0027
8	5	4	7	4	4	6330.6163	-0.0022
10	2	9	9	1	9	6406.4324	0.0039
11	3	8	10	2	8	6418.4886	-0.0039
10	3	8	9	2	8	6427.1969	0.0042
7	6	1	6	5	1	6447.0052	0.0069
7	6	2	6	5	2	6447.0052	-0.0033
10	4	6	9	3	6	6545.5920	0.0015
11	2	9	10	1	9	6576.2782	-0.0016
15	1	14	14	2	13	6650.1869	0.0061
15	2	14	14	1	13	6674.0912	0.0044
10	4	7	9	3	7	6734.9006	-0.0016
9	5	4	8	4	4	6786.5031	0.0021
9	5	5	8	4	5	6794.5081	-0.0062
8	6	2	7	5	2	6911.7585	-0.0018
8	6	3	7	5	3	6911.8340	0.0135
11	4	7	10	3	7	6943.9351	-0.0084
12	3	9	11	2	9	6966.1585	-0.0074
11	1	10	10	0	10	6973.7663	-0.0009
11	3	9	10	2	9	7007.5235	0.0102
7	7	0	6	6	0	7027.1335	0.0018
7	7	1	6	6	1	7027.1335	0.0017
11	2	10	10	1	10	7044.1073	0.0062
11	4	8	10	3	8	7238.3514	0.0065
10	5	5	9	4	5	7238.9399	-0.0021
10	5	6	9	4	6	7258.7747	-0.0031
12	2	10	11	1	10	7269.7868	0.0189
12	4	8	11	3	8	7343.8287	-0.0043
8	7	1	7	6	1	7492.3449	-0.0033
8	7	2	7	6	2	7492.3449	-0.0039
13	3	10	12	2	10	7560.4872	-0.0078
12	3	10	11	2	10	7605.3555	0.0013
11	5	6	10	4	6	7681.4334	0.0186
11	5	7	10	4	7	7724.7714	-0.0070
12	4	9	11	3	9	7757.9302	-0.0013

Appendix VII

13	4	9	12	3	9	7761.0101	-0.0031
10	6	4	9	5	4	7838.4542	0.0044
9	7	2	8	6	2	7957.3098	-0.0020
9	7	3	8	6	3	7957.3098	-0.0061

8. APPENDIX VIII

Table S11.1. Measured frequencies and residuals (in MHz) for the rotational transitions of the conformer **1** of helvetolide.

J'	K' ₋₁	K' ₊₁	J''	K'' ₋₁	K'' ₊₁	V _{obs}	V _{obs} -V _{calc}
4	2	2	3	1	2	2404.7342	0.0018
4	3	1	3	2	1	2537.5916	0.0006
4	3	2	3	2	2	2623.2711	-0.0004
4	4	1	3	3	1	2821.2520	-0.0004
5	2	3	4	1	3	3020.3752	0.0002
5	3	2	4	2	2	3039.1258	0.0013
5	3	3	4	2	3	3182.4777	0.0015
5	4	1	4	3	1	3277.1173	-0.0038
5	4	2	4	3	2	3326.4779	-0.0002
8	2	7	7	2	6	3462.1652	-0.0063
8	1	7	7	1	6	3464.0750	-0.0068
5	5	0	4	4	0	3550.6263	0.0005
5	5	1	4	4	1	3553.2548	0.0000
6	3	3	5	2	3	3597.1640	0.0009
9	1	9	8	1	8	3603.1878	0.0128
9	0	9	8	0	8	3603.1878	0.0049
9	0	9	8	1	8	3603.1878	0.0148
9	1	9	8	0	8	3603.1878	0.0029
6	2	4	5	1	4	3680.5043	0.0007
6	4	2	5	3	2	3735.5982	0.0002
6	3	4	5	2	4	3771.9766	0.0010
9	2	8	8	2	7	3849.1924	0.0086
9	1	8	8	1	7	3849.6858	0.0048
6	4	3	5	3	3	3855.2802	-0.0034
10	1	10	9	1	9	3989.8625	-0.0064
10	0	10	9	0	9	3989.8625	-0.0080
10	0	10	9	1	9	3989.8625	-0.0060
10	1	10	9	0	9	3989.8625	-0.0084
6	5	1	5	4	1	4027.1200	-0.0016
6	5	2	5	4	2	4046.6680	0.0008
7	3	4	6	2	4	4219.2279	0.0011
7	4	3	6	3	3	4229.2317	-0.0008
10	2	9	9	2	8	4235.8471	0.0097
10	1	9	9	1	8	4235.9727	0.0131
6	6	0	5	5	0	4286.9517	0.0014
6	6	1	5	5	1	4287.5923	-0.0014
7	2	5	6	1	5	4345.6801	-0.0006
11	0	11	10	1	10	4376.5600	-0.0040
11	1	11	10	0	10	4376.5600	-0.0045
11	1	11	10	1	10	4376.5601	-0.0039
11	0	11	10	0	10	4376.5601	-0.0043
7	3	5	6	2	5	4384.5123	0.0001
7	4	4	6	3	4	4414.1629	0.0003
7	5	2	6	4	2	4482.7552	0.0009
7	5	3	6	4	3	4552.7763	-0.0017
11	2	10	10	2	9	4622.4416	0.0079
11	1	10	10	1	9	4622.4416	-0.0209
12	1	12	11	1	11	4763.2672	0.0067
12	0	12	11	0	11	4763.2672	0.0066
12	0	12	11	1	11	4763.2672	0.0067
12	1	12	11	0	11	4763.2672	0.0066
7	6	1	6	5	1	4770.2100	-0.0015
7	6	2	6	5	2	4776.3646	0.0009
8	4	4	7	3	4	4786.3071	0.0005
8	3	5	7	2	5	4889.0798	0.0049
8	5	3	7	4	3	4930.9795	-0.0004
8	2	6	7	1	6	4996.9500	0.0014

8	4	5	7	3	5	5003.0095	0.0007
8	3	6	7	2	6	5010.4326	-0.0017
7	7	0	6	6	0	5022.4519	-0.0027
7	7	1	6	6	1	5022.6050	0.0041
8	5	4	7	4	4	5081.6448	-0.0008
8	6	2	7	5	2	5240.0295	-0.0005
8	6	3	7	5	3	5269.6323	0.0010
13	1	12	12	2	11	5395.6642	-0.0057
13	2	12	12	1	11	5395.6642	-0.0079
9	4	5	8	3	5	5414.1241	-0.0107
9	5	4	8	4	4	5417.1667	0.0006
8	7	1	7	6	1	5508.3205	0.0010
8	7	2	7	6	2	5510.0177	-0.0002
14	0	14	13	1	13	5536.6610	0.0068
14	1	14	13	0	13	5536.6610	0.0068
9	3	6	8	2	6	5564.3042	-0.0010
9	4	6	8	3	6	5615.3874	-0.0007
9	2	7	8	1	7	5638.0449	-0.0029
9	5	5	8	4	5	5640.1907	0.0024
9	3	7	8	2	7	5642.1730	-0.0045
9	6	3	8	5	3	5686.0465	-0.0010
8	8	0	7	7	0	5757.7461	0.0151
8	8	1	7	7	1	5757.7461	-0.0166
9	6	4	8	5	4	5775.4648	0.0007
14	1	13	13	2	12	5782.3069	-0.0078
14	2	13	13	1	12	5782.3069	-0.0083
15	0	15	14	1	14	5923.3472	-0.0031
15	1	15	14	0	14	5923.3472	-0.0031
10	5	5	9	4	5	5973.1498	0.0016
9	7	2	8	6	2	5987.7904	0.0004
9	7	3	8	6	3	5997.8893	0.0012
10	4	6	9	3	6	6093.2712	0.0000
10	6	4	9	5	4	6124.3773	-0.0015
15	1	14	14	2	13	6168.9716	0.0009
15	2	14	14	1	13	6168.9716	0.0008
10	3	7	9	2	7	6223.1240	-0.0014
10	5	6	9	4	6	6228.8267	-0.0001
10	4	7	9	3	7	6242.0021	-0.0038
9	8	1	8	7	1	6244.5110	-0.0007
10	2	8	9	1	8	6274.5605	0.0013
10	3	8	9	2	8	6275.7174	-0.0044
10	6	5	9	5	5	6303.9259	0.0033
10	7	3	9	6	3	6450.6870	-0.0001
10	7	4	9	6	4	6490.2082	-0.0003
9	9	0	8	8	0	6492.9443	0.0031
9	9	1	8	8	1	6492.9443	-0.0036
16	1	15	15	2	14	6555.6231	-0.0111
16	2	15	15	1	14	6555.6231	-0.0111
11	6	5	10	5	5	6603.4688	0.0007
11	5	6	10	4	6	6606.2025	0.0035
17	0	17	16	1	16	6696.7481	0.0094
17	1	17	16	0	16	6696.7481	0.0094
10	8	2	9	7	2	6728.2030	0.0012
10	8	3	9	7	3	6731.2274	0.0003
11	4	7	10	3	7	6778.2970	0.0011
11	5	7	10	4	7	6841.5542	-0.0028
11	6	6	10	5	6	6862.1171	0.0023
11	3	8	10	2	8	6868.9114	-0.0056
11	4	8	10	3	8	6875.0718	-0.0062
11	7	4	10	6	4	6887.3884	0.0040
11	3	9	10	2	9	6909.4920	-0.0159
11	7	5	10	6	5	6995.2316	-0.0004
12	6	6	11	5	6	7158.2415	0.0002
11	8	3	10	7	3	7203.3977	0.0009
11	8	4	10	7	4	7217.6690	0.0001

Appendix VIII

10	10	0	9	9	0	7228.1275	0.0013
10	10	1	9	9	1	7228.1275	0.0000
12	5	7	11	4	7	7294.1627	0.0034
12	7	5	11	6	5	7316.2107	-0.0019
12	6	7	11	5	7	7450.7534	0.0018
11	9	2	10	8	2	7465.4659	0.0042
11	9	3	10	8	3	7466.2933	-0.0005
12	5	8	11	4	8	7469.2512	-0.0010
12	3	9	11	2	9	7508.3146	0.0057
12	4	9	11	3	9	7510.1558	0.0002
12	7	6	11	6	6	7523.0466	-0.0005
12	2	10	11	1	10	7543.0465	0.0285
12	8	4	11	7	4	7659.3790	0.0023
12	8	5	11	7	5	7708.6436	-0.0012
11	10	1	10	9	1	7715.4349	0.0104
11	10	2	10	9	2	7715.4349	-0.0134
13	7	6	12	6	6	7788.4740	-0.0055
13	6	7	12	5	7	7796.0632	0.0009
12	9	3	11	8	3	7946.4956	0.0026
12	9	4	11	8	4	7951.0284	-0.0056
13	5	8	12	4	8	7988.6747	-0.0013

Table S11.2. Measured frequencies and residuals (in MHz) for the rotational transitions of the conformer **2** of helvetolide.

J'	K'_{-1}	K'_{+1}	J''	K''_{-1}	K''_{+1}	V _{obs}	V _{obs} - V _{calc}
5	1	4	4	1	3	2340.0369	-0.0018
4	2	2	3	1	2	2407.3103	-0.0066
6	0	6	5	1	5	2450.8833	0.0050
6	1	6	5	1	5	2451.1671	-0.0022
6	0	6	5	0	5	2452.0817	0.0030
6	1	6	5	0	5	2452.3756	0.0058
4	3	1	3	2	1	2556.2952	-0.0007
5	2	3	4	2	2	2561.9664	0.0020
5	3	2	4	3	1	2563.2328	0.0002
4	3	2	3	2	2	2641.5415	-0.0036
6	1	5	5	2	4	2676.5116	0.0071
6	2	5	5	2	4	2688.5027	-0.0004
6	1	5	5	1	4	2713.2183	-0.0031
6	2	5	5	1	4	2725.2175	-0.0025
6	2	4	5	3	3	2725.7442	-0.0147
7	0	7	6	1	6	2839.4825	0.0494
7	1	7	6	1	6	2839.4825	-0.0181
7	0	7	6	0	6	2839.7466	0.0224
7	1	7	6	0	6	2839.7466	-0.0451
4	4	0	3	3	0	2842.8147	-0.0086
4	4	1	3	3	1	2851.4103	-0.0058
6	2	4	5	2	3	2998.8344	0.0005
6	4	2	5	4	1	3017.5238	-0.0028
5	2	3	4	1	3	3017.8132	0.0027
5	3	2	4	2	2	3050.6479	-0.0007
7	1	6	6	2	5	3079.9015	-0.0069
7	2	6	6	2	5	3083.4009	-0.0020
7	1	6	6	1	5	3091.9104	0.0034
7	2	6	6	1	5	3095.4008	-0.0008
6	3	3	5	3	2	3111.2058	-0.0047
6	3	4	5	2	3	3143.0494	0.0222
5	3	3	4	2	3	3197.5275	0.0093
8	0	8	7	1	7	3227.6429	0.0473
8	1	8	7	1	7	3227.6429	0.0322
8	0	8	7	0	7	3227.6429	-0.0202
8	1	8	7	0	7	3227.6429	-0.0354
7	2	5	6	3	4	3238.5129	-0.0008
5	4	2	4	3	1	3284.1440	0.0016
5	4	1	4	3	1	3307.9174	-0.0006
5	4	2	4	3	2	3353.9473	0.0000
7	2	5	6	2	4	3382.7040	-0.0031
7	3	5	6	2	4	3443.4964	-0.0030
8	1	7	7	2	6	3472.6729	0.0007
8	2	7	7	2	6	3473.6142	-0.0018
7	5	2	6	5	1	3473.7894	0.0012
8	1	7	7	1	6	3476.1667	-0.0001
8	2	7	7	1	6	3477.1064	-0.0041
5	5	1	4	4	0	3589.6712	0.0003
5	5	0	4	4	0	3590.3325	0.0020
5	5	1	4	4	1	3592.5731	-0.0033
7	4	3	6	4	2	3594.2890	0.0043
6	3	3	5	2	3	3599.8937	-0.0009
7	3	4	6	3	3	3612.1627	0.0045
9	0	9	8	1	8	3615.6789	0.0100
9	1	9	8	1	8	3615.6789	0.0067
9	0	9	8	0	8	3615.6789	-0.0052
9	1	9	8	0	8	3615.6789	-0.0085
6	4	3	5	3	2	3663.1435	0.0088
6	2	4	5	1	4	3676.6045	-0.0013
8	3	5	7	4	4	3685.7352	0.0016

8	2	6	7	3	5	3687.6078	-0.0043
8	2	6	7	2	5	3748.4033	-0.0011
6	4	2	5	3	2	3762.2106	-0.0015
8	3	6	7	2	5	3769.9359	-0.0076
6	3	4	5	2	4	3784.0808	-0.0014
9	1	8	8	2	7	3861.9109	0.0067
9	2	8	8	2	7	3862.1454	-0.0003
9	1	8	8	1	7	3862.8405	-0.0075
9	2	8	8	1	7	3863.0931	0.0035
6	4	3	5	3	3	3878.7457	0.0017
8	6	2	7	6	1	3944.7343	0.0024
7	4	4	6	3	3	3975.9919	0.0020
10	0	10	9	1	9	4003.7320	0.0063
10	1	10	9	1	9	4003.7320	0.0056
10	0	10	9	0	9	4003.7320	0.0030
10	1	10	9	0	9	4003.7320	0.0022
8	5	3	7	5	2	4037.4770	0.0025
8	3	5	7	3	4	4049.5673	0.0020
6	5	2	5	4	1	4060.1683	0.0133
6	5	1	5	4	1	4066.9007	-0.0055
6	5	2	5	4	2	4083.9259	-0.0047
9	2	7	8	3	6	4099.5855	-0.0020
9	2	7	8	2	6	4121.1268	0.0003
9	3	7	8	2	6	4127.9256	-0.0028
8	4	4	7	4	3	4155.8718	0.0019
7	3	4	6	2	4	4213.2280	0.0091
9	3	6	8	4	5	4230.8404	0.0065
7	4	3	6	3	3	4245.2970	0.0107
8	4	5	7	3	4	4247.5833	0.0061
10	2	9	9	2	8	4250.1790	-0.0165
10	1	9	9	1	8	4250.3923	0.0146
10	2	9	9	1	8	4250.3923	-0.0448
6	6	1	5	5	0	4335.2691	-0.0020
6	6	0	5	5	0	4335.4242	0.0129
6	6	1	5	5	1	4335.9244	-0.0063
7	2	5	6	1	5	4346.1166	0.0253
11	0	11	10	1	10	4391.7831	0.0020
11	1	11	10	1	10	4391.7831	0.0018
11	0	11	10	0	10	4391.7831	0.0013
11	1	11	10	0	10	4391.7831	0.0011
7	3	5	6	2	5	4394.8922	0.0072
9	7	2	8	7	1	4424.3018	0.0012
9	3	6	8	3	5	4428.8415	-0.0043
7	4	4	6	3	4	4432.8600	0.0027
9	6	3	8	6	2	4485.2255	-0.0009
7	5	3	6	4	2	4487.3952	-0.0075
10	2	8	9	3	7	4495.3702	0.0026
10	2	8	9	2	7	4502.1933	0.0238
10	3	8	9	2	7	4504.1583	0.0027
9	4	6	8	3	5	4516.6607	-0.0033
7	5	2	6	4	2	4523.1727	0.0049
7	5	3	6	4	3	4586.4673	-0.0128
9	5	4	8	5	3	4627.8174	-0.0011
11	1	10	10	2	9	4638.1560	0.0210
11	2	10	10	2	9	4638.1560	0.0069
11	1	10	10	1	9	4638.1560	-0.0384
11	2	10	10	1	9	4638.1560	-0.0525
10	4	6	9	5	5	4646.5288	-0.0082
9	4	5	8	4	4	4664.4432	-0.0009
10	3	7	9	4	6	4699.1296	0.0068
12	0	12	11	1	11	4779.8363	-0.0010
12	1	12	11	1	11	4779.8363	-0.0011
12	0	12	11	0	11	4779.8363	-0.0012
12	1	12	11	0	11	4779.8363	-0.0012
10	3	7	9	3	6	4786.9412	0.0002

8	4	4	7	3	4	4788.9909	-0.0071
7	6	2	6	5	1	4816.4338	0.0001
7	6	1	6	5	1	4818.1499	-0.0003
10	4	7	9	3	6	4819.9596	0.0004
7	6	2	6	5	2	4823.1831	-0.0019
8	5	4	7	4	3	4840.7421	0.0021
8	3	5	7	2	5	4880.0976	0.0204
11	2	9	10	3	8	4885.3333	-0.0033
11	2	9	10	2	8	4887.3183	-0.0043
8	5	3	7	4	3	4966.3585	0.0009
8	2	6	7	1	6	5002.5749	-0.0139
8	4	5	7	3	5	5017.3043	0.0074
12	1	11	11	2	10	5026.1177	0.0156
12	2	11	11	2	10	5026.1177	0.0124
12	1	11	11	1	10	5026.1177	0.0015
12	2	11	11	1	10	5026.1177	-0.0018
10	6	4	9	6	3	5060.3382	-0.0004
10	4	6	9	4	5	5102.9098	-0.0016
8	5	4	7	4	4	5110.0365	0.0000
11	3	8	10	4	7	5120.0948	-0.0011
9	5	5	8	4	4	5120.8291	0.0104
11	3	8	10	3	7	5153.1226	0.0085
11	4	8	10	3	7	5164.2201	0.0240
13	0	13	12	1	12	5167.8962	0.0023
13	1	13	12	1	12	5167.8962	0.0023
13	0	13	12	0	12	5167.8962	0.0023
13	1	13	12	0	12	5167.8962	0.0023
10	5	5	9	5	4	5201.9146	-0.0009
11	4	7	10	5	6	5223.1758	-0.0024
12	2	10	11	3	9	5273.5448	-0.0055
12	2	10	11	2	9	5274.1006	0.0026
8	6	3	7	5	2	5278.1485	-0.0157
10	5	6	9	4	5	5357.7200	-0.0041
9	4	5	8	3	5	5403.8780	0.0012
9	5	4	8	4	4	5438.2993	-0.0069
11	4	7	10	4	6	5477.9678	-0.0230
11	7	4	10	7	3	5500.0636	-0.0016
12	3	9	11	3	8	5530.2641	0.0051
12	4	9	11	3	8	5533.6937	-0.0021
9	3	6	8	2	6	5560.4941	-0.0245
8	7	1	7	6	1	5564.7297	0.0054
8	7	2	7	6	2	5566.0350	-0.0002
11	5	7	10	4	6	5595.5766	-0.0136
9	4	6	8	3	6	5626.7980	0.0002
9	2	7	8	1	7	5647.5490	0.0005
13	2	11	12	2	10	5661.4716	-0.0203
9	5	5	8	4	5	5662.2354	-0.0040
11	6	5	10	6	4	5662.8674	0.0097
9	6	4	8	5	3	5689.6962	0.0019
11	5	6	10	5	5	5718.2088	-0.0022
9	6	3	8	5	3	5736.8523	0.0066
14	2	13	13	2	12	5802.0737	0.0004
14	1	13	13	1	12	5802.0737	-0.0002
14	2	13	13	1	12	5802.0737	-0.0004
14	1	13	13	2	12	5802.0778	0.0046
9	6	4	8	5	4	5815.3112	-0.0006
8	8	0	7	7	0	5823.9104	0.0074
8	8	1	7	7	1	5823.9104	-0.0155
12	4	8	11	4	7	5828.5384	0.0111
12	5	8	11	4	7	5874.8623	0.0081
13	3	10	12	4	9	5909.9318	-0.0024
13	3	10	12	3	9	5913.3660	-0.0050
13	4	10	12	3	9	5914.3898	0.0139
15	0	15	14	1	14	5944.0057	-0.0001
15	1	15	14	1	14	5944.0057	-0.0001

15	0	15	14	0	14	5944.0057	-0.0001
15	1	15	14	0	14	5944.0057	-0.0001
10	5	5	9	4	5	5975.7790	0.0014
10	6	5	9	5	4	6019.6208	-0.0091
9	7	2	8	6	2	6044.2920	-0.0010
14	2	12	13	2	11	6049.1229	-0.0182
14	3	12	13	2	11	6049.1231	-0.0271
14	2	12	13	3	11	6049.1231	0.0188
9	7	3	8	6	3	6052.2263	0.0037
10	4	6	9	3	6	6077.9459	0.0035
12	7	5	11	7	4	6085.2002	0.0016
12	5	7	11	5	6	6158.3492	-0.0020
10	6	4	9	5	4	6169.3597	-0.0062
13	4	9	12	4	8	6187.7312	-0.0006
15	1	14	14	2	13	6190.0758	-0.0022
15	2	14	14	2	13	6190.0758	-0.0023
15	1	14	14	1	13	6190.0758	-0.0024
15	2	14	14	1	13	6190.0758	-0.0024
13	5	9	12	4	8	6204.0548	0.0027
10	3	7	9	2	7	6226.3373	0.0042
10	5	6	9	4	6	6244.9372	0.0003
12	6	6	11	6	5	6248.8102	0.0027
10	4	7	9	3	7	6252.5474	-0.0021
10	2	8	9	1	8	6286.8633	-0.0067
14	3	11	13	4	10	6298.0539	0.0103
14	3	11	13	3	10	6299.0478	-0.0007
14	4	11	13	3	10	6299.3264	-0.0027
9	8	1	8	7	1	6309.6447	0.0117
9	8	2	8	7	2	6309.9495	0.0019
16	0	16	15	1	15	6332.0632	0.0031
16	1	16	15	1	15	6332.0632	0.0031
16	0	16	15	0	15	6332.0632	0.0031
16	1	16	15	0	15	6332.0632	0.0031
10	6	5	9	5	5	6337.1121	-0.0054
15	2	13	14	2	12	6436.9091	-0.0041
15	2	13	14	3	12	6436.9091	0.0050
15	3	13	14	2	12	6436.9092	-0.0062
10	7	3	9	6	3	6509.5698	-0.0018
13	5	8	12	5	7	6529.7409	-0.0021
10	7	4	9	6	4	6541.5347	-0.0160
14	4	10	13	5	9	6544.0982	-0.0060
14	4	10	13	4	9	6560.4220	-0.0024
16	1	15	15	2	14	6578.0908	-0.0001
16	2	15	15	2	14	6578.0908	-0.0001
16	1	15	15	1	14	6578.0908	-0.0001
16	2	15	15	1	14	6578.0908	-0.0002
11	5	6	10	4	6	6591.0844	0.0073
11	6	5	10	5	5	6630.3045	-0.0036
15	3	12	14	3	11	6685.7985	0.0115
13	7	6	12	7	5	6698.8421	-0.0009
17	0	17	16	1	16	6720.1219	0.0091
17	1	17	16	1	16	6720.1219	0.0091
17	0	17	16	0	16	6720.1219	0.0091
17	1	17	16	0	16	6720.1219	0.0091
11	4	7	10	3	7	6768.9967	0.0044
13	6	7	12	6	6	6773.0458	-0.0055
10	8	2	9	7	2	6792.7438	0.0064
16	2	14	15	2	13	6824.7430	-0.0117
16	2	14	15	3	13	6824.7430	-0.0095
16	3	14	15	2	13	6824.7432	-0.0120
11	5	7	10	4	7	6853.5850	0.0115
14	5	9	13	5	8	6872.8757	0.0023
11	3	8	10	2	8	6877.2711	-0.0066
15	4	11	14	4	10	6941.0414	-0.0066
11	7	4	10	6	4	6949.3025	0.0043

17	1	16	16	2	15	6966.1100	0.0011
17	2	16	16	2	15	6966.1100	0.0011
17	1	16	16	1	15	6966.1100	0.0011
17	2	16	16	1	15	6966.1100	0.0011
18	0	18	17	1	17	7108.1622	-0.0015
18	1	18	17	1	17	7108.1622	-0.0015
18	0	18	17	0	17	7108.1622	-0.0015
18	1	18	17	0	17	7108.1622	-0.0015
12	6	6	11	5	6	7160.8977	-0.0070
17	2	15	16	2	14	7212.6387	-0.0015
17	2	15	16	3	14	7212.6387	-0.0009
17	3	15	16	2	14	7212.6389	-0.0014
14	6	8	13	6	7	7215.4998	-0.0020
15	5	10	14	5	9	7224.8070	-0.0014
12	5	7	11	4	7	7271.4355	-0.0019
11	8	4	10	7	4	7279.5714	-0.0034
14	7	7	13	7	6	7296.1923	-0.0060
16	4	12	15	5	11	7323.6855	0.0026
16	4	12	15	4	11	7325.3163	0.0037
18	1	17	17	2	16	7354.1354	0.0053
18	2	17	17	2	16	7354.1354	0.0053
18	1	17	17	1	16	7354.1354	0.0053
18	2	17	17	1	16	7354.1354	0.0053
17	3	14	16	3	13	7460.4531	0.0052
12	6	7	11	5	7	7468.4393	0.0106
12	5	8	11	4	8	7479.6375	-0.0129
19	0	19	18	1	18	7496.1980	-0.0146
19	1	19	18	1	18	7496.1980	-0.0146
19	0	19	18	0	18	7496.1980	-0.0146
19	1	19	18	0	18	7496.1980	-0.0146
12	3	9	11	2	9	7520.2113	-0.0028
12	2	10	11	1	10	7559.7332	0.0147
12	7	6	11	6	6	7560.9929	0.0006
15	6	9	14	6	8	7583.7899	0.0135
16	5	11	15	5	10	7592.6121	0.0220
17	4	13	16	4	12	7711.1693	-0.0047
19	1	18	18	2	17	7742.1558	0.0030
19	2	18	18	2	17	7742.1558	0.0030
19	1	18	18	1	17	7742.1558	0.0030
19	2	18	18	1	17	7742.1558	0.0030
13	6	7	12	5	7	7775.6064	0.0015
15	7	8	14	7	7	7828.6865	0.0152
18	3	15	17	3	14	7848.0361	-0.0044
20	0	20	19	1	19	7884.2681	0.0089
20	1	20	19	1	19	7884.2681	0.0089
20	0	20	19	0	19	7884.2681	0.0089
20	1	20	19	0	19	7884.2681	0.0089
16	6	10	15	6	9	7919.7197	-0.0078
13	5	8	12	4	8	7972.6365	-0.0166
19	2	17	18	2	16	7988.4908	-0.0006
19	2	17	18	3	16	7988.4908	-0.0005
19	3	17	18	2	16	7988.4911	-0.0003

Table S11.3. Measured frequencies and residuals (in MHz) for the rotational transitions of the conformer **37** of helvetolide.

J'	K'_{-1}	K'_{+1}	J''	K''_{-1}	K''_{+1}	V _{obs}	V _{obs} - V _{calc}
4	2	2	3	1	2	2456.9621	0.0015
4	1	3	3	0	3	2474.7259	0.0074
6	0	6	5	1	5	2590.3510	-0.0002
6	1	6	5	1	5	2591.9415	-0.0049
6	0	6	5	0	5	2595.2322	0.0005
5	2	3	4	2	2	2595.7425	0.0066
6	1	6	5	0	5	2596.8287	0.0018
4	2	3	3	1	3	2621.5522	0.0037
4	3	2	3	2	1	2675.7625	0.0017
4	3	1	3	2	1	2708.4949	-0.0043
6	1	5	5	2	4	2761.5717	-0.0049
4	3	2	3	2	2	2779.1581	-0.0009
7	3	4	6	4	3	2789.6513	-0.0065
6	1	5	5	1	4	2859.8704	-0.0060
6	2	5	5	1	4	2904.4481	-0.0043
6	3	4	5	3	3	2940.7407	0.0032
6	4	3	5	4	2	2974.3626	0.0134
7	0	7	6	1	6	3004.9090	0.0013
7	1	7	6	1	6	3005.4099	0.0043
7	0	7	6	0	6	3006.5005	-0.0025
7	1	7	6	0	6	3007.0046	0.0038
5	2	3	4	1	3	3036.9484	-0.0011
4	4	1	3	3	0	3050.2413	-0.0012
4	4	0	3	3	0	3051.1340	-0.0003
4	4	1	3	3	1	3055.2587	-0.0002
4	4	0	3	3	1	3056.1509	0.0003
5	3	3	4	2	2	3064.3675	-0.0007
6	2	4	5	2	3	3086.9726	0.0130
5	1	4	4	0	4	3147.9966	-0.0036
5	3	2	4	2	2	3178.1207	0.0005
7	2	5	6	3	4	3214.4757	-0.0004
7	1	6	6	2	5	3214.6502	0.0011
5	2	4	4	1	4	3232.3558	-0.0135
7	1	6	6	1	5	3259.2277	0.0026
5	3	3	4	2	3	3323.2312	-0.0057
7	3	5	6	3	4	3405.1832	-0.0055
6	3	4	5	2	3	3409.3696	-0.0002
8	0	8	7	1	7	3418.0588	-0.0058
8	1	8	7	1	7	3418.2310	0.0161
8	0	8	7	0	7	3418.5507	-0.0118
8	1	8	7	0	7	3418.7223	0.0095
8	3	5	7	4	4	3470.0731	-0.0021
7	4	4	6	4	3	3474.5200	-0.0059
7	5	2	6	5	1	3478.4968	-0.0034
5	4	2	4	3	1	3522.3965	-0.0031
5	4	1	4	3	1	3530.0707	0.0006
7	2	5	6	2	4	3536.8847	-0.0016
5	4	2	4	3	2	3555.1369	-0.0012
5	4	1	4	3	2	3562.8045	-0.0040
8	1	7	7	2	6	3644.9123	-0.0003
8	2	7	7	2	6	3651.4362	-0.0188
8	1	7	7	1	6	3662.7164	-0.0096
8	2	7	7	1	6	3669.2687	0.0003
6	2	4	5	1	4	3671.2233	0.0016
6	3	3	5	2	3	3682.2865	0.0011
7	3	5	6	2	4	3727.5989	0.0000
8	2	6	7	3	5	3757.3241	0.0086
6	1	5	5	0	5	3822.0349	-0.0059
9	1	9	8	1	8	3830.8053	-0.0002
9	0	9	8	1	8	3830.8053	0.0441

9	0	9	8	0	8	3830.9241	0.0126
9	1	9	8	0	8	3830.9241	-0.0317
8	3	6	7	3	5	3853.5801	0.0005
5	5	1	4	4	1	3855.8730	-0.0139
6	2	5	5	1	5	3861.7625	0.0262
6	3	4	5	2	4	3895.3310	-0.0011
8	2	6	7	2	5	3948.0241	-0.0041
6	4	3	5	3	2	3954.4074	-0.0007
8	4	5	7	4	4	3965.1386	-0.0100
6	4	2	5	3	2	3989.6640	-0.0011
8	5	3	7	5	2	4006.6545	-0.0006
8	3	6	7	2	5	4044.2952	0.0029
9	1	8	8	2	7	4064.2657	-0.0005
9	2	8	8	2	7	4066.5362	0.0032
6	4	3	5	3	3	4068.1605	0.0005
9	1	8	8	1	7	4070.8097	0.0011
9	2	8	8	1	7	4073.0737	-0.0018
6	4	2	5	3	3	4103.4152	-0.0019
7	3	4	6	2	4	4239.4908	0.0002
10	1	10	9	1	9	4243.3468	0.0159
10	0	10	9	0	9	4243.3468	-0.0155
10	0	10	9	1	9	4243.3468	0.0287
10	1	10	9	0	9	4243.3468	-0.0283
9	2	7	8	3	6	4245.1587	0.0080
7	4	4	6	3	3	4329.0336	0.0007
6	5	1	5	4	1	4342.9763	0.0009
7	2	5	6	1	5	4348.2304	-0.0012
6	5	2	5	4	2	4349.1288	0.0008
9	3	7	8	2	6	4383.9820	-0.0083
7	4	3	6	3	3	4440.6998	0.0023
9	4	6	8	4	5	4441.1512	-0.0079
10	1	9	9	2	8	4479.0988	-0.0064
10	1	9	9	1	8	4481.3870	0.0150
10	2	9	9	1	8	4482.1242	-0.0003
7	1	6	6	0	6	4486.0274	-0.0068
7	3	5	6	2	5	4494.3627	-0.0055
9	5	4	8	5	3	4558.0403	-0.0002
7	4	4	6	3	4	4601.9493	0.0009
8	4	5	7	3	4	4650.0173	0.0007
11	1	11	10	1	10	4655.8483	0.0082
11	0	11	10	0	10	4655.8483	-0.0009
11	0	11	10	1	10	4655.8483	0.0118
11	1	11	10	0	10	4655.8483	-0.0046
6	6	0	5	5	0	4657.6386	-0.0233
6	6	1	5	5	1	4657.8043	0.0209
10	2	8	9	3	7	4694.2953	0.0138
10	3	8	9	3	7	4711.4245	0.0135
7	4	3	6	3	4	4713.6106	-0.0024
10	3	7	9	4	6	4726.6963	0.0014
10	2	8	9	2	7	4736.8500	-0.0070
10	3	8	9	2	7	4753.9885	0.0020
7	5	2	6	4	2	4819.5447	0.0049
7	5	3	6	4	3	4846.2001	-0.0001
8	3	5	7	2	5	4857.5503	0.0028
11	1	10	10	2	9	4892.2682	-0.0048
8	4	4	7	3	4	4916.5240	0.0018
9	4	6	8	3	5	4936.2314	-0.0011
8	2	6	7	1	6	5037.0452	0.0105
12	1	12	11	1	11	5068.3515	0.0045
12	0	12	11	0	11	5068.3515	0.0019
12	0	12	11	1	11	5068.3515	0.0055
12	1	12	11	0	11	5068.3515	0.0008
8	3	6	7	2	6	5115.4836	-0.0018
11	2	9	10	3	8	5122.2829	-0.0009
11	3	9	10	3	8	5128.7308	-0.0002

11	2	9	10	2	8	5139.3993	-0.0140
8	1	7	7	0	7	5142.2473	-0.0099
11	3	9	10	2	8	5145.8581	-0.0024
7	6	1	6	5	1	5148.2680	0.0021
7	6	2	6	5	2	5149.5006	-0.0121
8	4	5	7	3	5	5161.9065	-0.0018
10	4	7	9	3	6	5214.9952	-0.0019
11	3	8	10	4	7	5259.0351	-0.0099
8	5	3	7	4	3	5275.2625	0.0010
12	1	11	11	2	10	5304.8866	0.0012
12	2	11	11	1	10	5305.2037	0.0010
11	4	8	10	4	7	5342.5957	0.0075
8	5	4	7	4	4	5352.9627	0.0021
8	4	4	7	3	5	5428.4106	-0.0033
9	4	5	8	3	5	5445.7301	0.0067
7	7	0	6	6	0	5459.8839	0.0039
7	7	1	6	6	1	5459.8839	-0.0145
13	1	13	12	1	12	5480.8595	0.0048
13	0	13	12	0	12	5480.8595	0.0041
13	0	13	12	1	12	5480.8595	0.0051
13	1	13	12	0	12	5480.8595	0.0038
11	4	8	10	3	7	5515.9953	0.0075
9	3	6	8	2	6	5530.8492	-0.0001
12	2	10	11	3	9	5540.5042	-0.0057
12	2	10	11	2	9	5546.9509	-0.0063
12	3	10	11	2	9	5549.2623	-0.0048
8	6	2	7	5	2	5634.4422	0.0007
8	6	3	7	5	3	5641.2234	-0.0016
9	5	4	8	4	4	5713.3120	-0.0004
11	5	6	10	5	5	5714.6303	0.0150
9	2	7	8	1	7	5715.7170	-0.0066
13	1	12	12	1	11	5717.3937	-0.0208
13	2	12	12	2	11	5717.3937	0.0316
13	1	12	12	2	11	5717.3937	0.0548
13	2	12	12	1	11	5717.3937	-0.0440
12	3	9	11	4	8	5735.5176	0.0010
9	4	6	8	3	6	5749.4859	-0.0019
9	3	7	8	2	7	5751.7573	0.0007
12	4	9	11	4	8	5771.8355	0.0084
9	1	8	8	0	8	5794.4980	-0.0054
9	2	8	8	1	8	5796.6421	0.0222
12	4	9	11	3	8	5855.3610	-0.0093
9	5	5	8	4	5	5877.0689	-0.0005
14	1	14	13	1	13	5893.3664	0.0032
14	0	14	13	0	13	5893.3664	0.0030
14	0	14	13	1	13	5893.3664	0.0033
14	1	14	13	0	13	5893.3664	0.0030
13	2	11	12	3	10	5954.7326	-0.0057
13	3	11	12	3	10	5955.5362	0.0014
13	2	11	12	2	10	5957.0518	0.0036
13	3	11	12	2	10	5957.8335	-0.0112
10	4	6	9	3	6	6041.1724	0.0026
9	6	3	8	5	3	6109.5462	0.0047
14	1	13	13	1	12	6129.7828	-0.0020
14	2	13	13	2	12	6129.7828	0.0142
14	1	13	13	2	12	6129.7828	0.0212
14	2	13	13	1	12	6129.7828	-0.0089
9	6	4	8	5	4	6135.0265	-0.0005
10	5	5	9	4	5	6162.9136	0.0041
13	3	10	12	4	9	6177.4674	-0.0001
13	4	10	12	3	9	6228.4234	-0.0088
10	3	7	9	2	7	6231.0348	0.0028
8	8	0	7	7	0	6262.0304	-0.0013
8	8	1	7	7	1	6262.0304	-0.0040
12	5	7	11	5	6	6270.0962	0.0002

15	1	15	14	1	14	6305.8793	0.0074
15	0	15	14	0	14	6305.8793	0.0073
15	0	15	14	1	14	6305.8793	0.0074
15	1	15	14	0	14	6305.8793	0.0073
10	4	7	9	3	7	6361.8548	-0.0013
14	2	12	13	3	11	6367.5093	-0.0017
14	2	12	13	2	11	6368.2989	-0.0086
14	3	12	13	2	11	6368.5713	-0.0025
10	3	8	9	2	8	6396.6272	-0.0074
10	5	6	9	4	6	6425.3034	0.0020
9	7	2	8	6	2	6440.6981	0.0149
9	7	3	8	6	3	6442.1443	-0.0046
10	1	9	9	0	9	6444.9530	-0.0108
10	2	9	9	1	9	6445.6640	-0.0081
15	1	14	14	1	13	6542.1882	-0.0081
15	1	14	14	1	13	6542.1882	-0.0081
15	2	14	14	2	13	6542.1882	-0.0032
10	6	4	9	5	4	6563.8568	0.0019
14	3	11	13	4	10	6601.7625	-0.0012
14	4	11	13	3	10	6622.0139	-0.0031
10	6	5	9	5	5	6635.8406	0.0017
11	5	6	10	4	6	6660.7545	0.0060
11	4	7	10	3	7	6702.5488	0.0011
16	1	16	15	1	15	6718.3883	0.0079
16	0	16	15	0	15	6718.3883	0.0079
16	0	16	15	1	15	6718.3883	0.0079
16	1	16	15	0	15	6718.3883	0.0079
9	8	1	8	7	1	6753.6686	0.0229
9	8	2	8	7	2	6753.6686	-0.0151
15	2	13	14	3	12	6779.8142	-0.0153
15	3	13	14	2	12	6780.1804	-0.0021
10	7	3	9	6	3	6925.3884	0.0064
11	3	8	10	2	8	6926.6177	-0.0020
10	7	4	9	6	4	6931.9981	0.0023
16	1	15	15	1	14	6954.6418	0.0106
16	2	15	15	2	14	6954.6418	0.0121
11	4	8	10	3	8	6993.0314	-0.0019
11	6	5	10	5	5	6994.4612	0.0057
11	5	7	10	4	7	7001.1685	0.0044
15	3	12	14	4	11	7018.1638	-0.0051
11	2	9	10	1	9	7039.7973	-0.0159
11	3	9	10	2	9	7045.4929	-0.0150
9	9	0	8	8	0	7064.1600	-0.0009
9	9	1	8	8	1	7064.1600	-0.0012
17	1	17	16	1	16	7130.8943	0.0063
17	0	17	16	0	16	7130.8943	0.0063
17	0	17	16	1	16	7130.8943	0.0063
17	1	17	16	0	16	7130.8943	0.0063
11	6	6	10	5	6	7150.9334	0.0055
12	5	7	11	4	7	7227.8763	0.0072
17	1	16	16	1	15	7367.0825	0.0021
17	2	16	16	2	15	7367.0825	0.0025
11	7	4	10	6	4	7399.6252	0.0034
12	4	8	11	3	8	7407.5837	0.0072
11	7	5	10	6	5	7422.5850	0.0002
16	3	13	15	4	12	7431.4332	-0.0073
16	4	13	15	3	12	7434.2152	-0.0011
18	1	18	17	1	17	7543.3995	0.0050
18	0	18	17	0	17	7543.3995	0.0050
18	0	18	17	1	17	7543.3995	0.0050
18	1	18	17	0	17	7543.3995	0.0050
10	9	1	9	8	1	7555.8896	0.0020
10	9	2	9	8	2	7555.8896	-0.0041
12	5	8	11	4	8	7603.8359	-0.0008
17	2	15	16	2	14	7604.2990	-0.0102

Appendix VIII

17	3	15	16	3	14	7604.2990	0.0088
17	2	15	16	3	14	7604.2990	0.0175
17	3	15	16	2	14	7604.2990	-0.0189
12	3	9	11	2	9	7606.2589	-0.0072
12	4	9	11	3	9	7636.1341	0.0047
12	6	7	11	5	7	7687.8090	0.0014
12	3	10	11	2	10	7695.8039	-0.0091
18	1	17	17	1	16	7779.5285	-0.0106
18	2	17	17	2	16	7779.5285	-0.0105
17	3	14	16	4	13	7843.6388	0.0068
17	4	14	16	3	13	7844.5864	-0.0206
12	7	5	11	6	5	7854.1445	0.0069
10	10	0	9	9	0	7866.2742	-0.0014
10	10	1	9	9	1	7866.2742	-0.0014
13	5	8	12	4	8	7869.4488	0.0109
13	6	7	12	5	7	7888.1853	0.0110
12	7	6	11	6	6	7917.9809	0.0069
19	1	19	18	1	18	7955.9085	0.0090
19	0	19	18	0	18	7955.9085	0.0090
19	0	19	18	1	18	7955.9085	0.0090
19	1	19	18	0	18	7955.9085	0.0090

Table S11.4. Measured frequencies and residuals (in MHz) for the rotational transitions of the conformer **34** of helvetolide.

J'	K'_{-1}	K'_{+1}	J''	K''_{-1}	K''_{+1}	V _{obs}	V _{obs} - V _{calc}
5	1	4	4	1	3	2372.4969	0.0013
4	2	2	3	1	2	2392.5721	0.0012
6	0	6	5	1	5	2512.0041	-0.0009
6	1	6	5	0	5	2529.5074	0.0049
6	1	5	5	2	4	2605.4870	0.0060
4	3	2	3	2	1	2715.0941	0.0034
6	1	5	5	1	4	2784.7596	0.0113
4	3	2	3	2	2	2785.4802	0.0036
6	3	4	5	3	3	2806.3701	-0.0045
6	5	1	5	5	0	2811.7691	0.0101
6	4	3	5	4	2	2820.8540	0.0100
6	2	5	5	1	4	2886.5411	-0.0129
5	2	3	4	1	3	2917.4893	-0.0015
7	0	7	6	1	6	2918.1426	0.0176
7	1	7	6	1	6	2920.0447	-0.0040
7	0	7	6	0	6	2923.1450	0.0011
7	1	7	6	0	6	2925.0654	-0.0021
7	1	6	6	2	5	3076.5595	-0.0119
5	3	3	4	2	2	3105.5813	0.0063
4	4	1	3	3	0	3115.2712	-0.0023
4	4	0	3	3	0	3115.6024	0.0064
4	4	1	3	3	1	3117.7096	0.0032
4	4	0	3	3	1	3118.0349	0.0059
7	2	6	6	2	5	3127.6807	-0.0002
5	3	2	4	2	2	3166.1891	-0.0081
7	1	6	6	1	5	3178.3725	-0.0046
7	3	5	6	3	4	3261.5849	-0.0104
5	3	3	4	2	3	3291.2896	0.0017
7	4	4	6	4	3	3298.1795	-0.0042
8	0	8	7	1	7	3321.1912	-0.0065
8	1	8	7	1	7	3321.9103	0.0001
8	1	8	7	0	7	3323.8367	0.0029
7	2	5	6	2	4	3406.7384	0.0060
6	3	4	5	2	3	3454.8557	0.0052
8	2	6	7	3	5	3472.5008	0.0075
6	2	4	5	1	4	3489.7138	0.0017
8	1	7	7	2	6	3516.7718	0.0069
8	2	7	7	2	6	3540.1711	0.0068
8	1	7	7	1	6	3567.8765	0.0020
8	1	7	7	1	6	3567.8765	0.0020
5	4	2	4	3	1	3572.5149	0.0042
5	4	1	4	3	1	3575.3681	0.0253
5	4	2	4	3	2	3588.8914	-0.0117
5	4	1	4	3	2	3591.7368	0.0016
6	3	3	5	2	3	3613.5428	0.0044
8	3	6	7	3	5	3705.7358	0.0101
9	0	9	8	1	8	3722.9969	-0.0093
9	1	9	8	1	8	3723.2559	-0.0076
9	0	9	8	0	8	3723.7179	-0.0008
9	1	9	8	0	8	3723.9778	0.0018
8	4	5	7	4	4	3772.5265	-0.0034
8	5	3	7	5	2	3777.8469	0.0003
6	3	4	5	2	4	3820.5731	-0.0052
8	2	6	7	2	5	3837.4940	0.0044
9	1	8	8	2	7	3937.1581	-0.0026
5	5	0	4	4	0	3940.3893	-0.0067
5	5	0	4	4	1	3940.7037	-0.0149
5	5	1	4	4	1	3940.7037	0.0237
9	2	8	8	2	7	3947.1964	-0.0050
9	1	8	8	1	7	3960.5673	0.0072

9	2	8	8	1	7	3970.6010	0.0003
6	4	3	5	3	2	4006.8359	-0.0024
6	4	2	5	3	2	4020.3800	-0.0009
6	4	3	5	3	3	4067.4709	0.0104
6	4	2	5	3	3	4081.0018	-0.0013
7	3	4	6	2	4	4097.2650	-0.0108
7	2	5	6	1	5	4111.6967	0.0004
10	0	10	9	1	9	4124.3111	-0.0118
10	1	10	9	0	9	4124.6837	0.0125
9	3	7	8	3	6	4138.1426	0.0052
9	2	7	8	2	6	4238.9638	-0.0015
9	4	6	8	4	5	4239.9703	-0.0085
9	5	4	8	5	3	4275.6019	-0.0032
10	1	9	9	2	8	4346.8990	-0.0002
10	2	9	9	2	9	4361.0533	0.0014
10	2	9	9	1	8	4361.0533	0.0014
9	3	7	8	2	6	4371.3643	-0.0055
7	3	5	6	2	5	4374.8815	-0.0054
7	4	4	6	3	3	4400.5838	0.0021
6	5	2	5	4	1	4405.2699	0.0020
6	5	1	5	4	1	4405.6872	0.0028
6	5	2	5	4	2	4408.1067	0.0067
6	5	1	5	4	2	4408.5261	0.0096
7	4	3	6	3	3	4446.5998	-0.0049
10	2	8	9	3	7	4492.0567	-0.0012
11	1	11	10	1	10	4525.5441	0.0545
11	0	11	10	0	10	4525.5441	-0.0049
11	0	11	10	1	10	4525.5441	0.0862
11	1	11	10	0	10	4525.5441	-0.0366
7	4	4	6	3	4	4559.2765	0.0068
10	3	8	9	3	7	4559.8197	-0.0066
10	2	8	9	2	7	4624.4616	-0.0008
8	3	5	7	2	5	4630.9302	-0.0076
10	3	8	9	2	7	4692.2289	-0.0018
10	4	7	9	4	6	4697.2100	0.0018
8	4	5	7	3	4	4744.6576	0.0004
11	1	10	10	2	9	4751.5270	0.0023
11	1	10	10	1	9	4755.6333	-0.0035
6	6	0	5	5	0	4764.3626	0.0272
6	6	1	5	5	1	4764.3626	-0.0071
8	2	6	7	1	6	4770.7958	-0.0130
10	5	5	9	5	4	4789.9566	-0.0021
7	5	3	6	4	2	4862.9614	-0.0018
7	5	2	6	4	2	4865.3771	-0.0081
8	4	4	7	3	4	4866.7156	-0.0168
7	5	3	6	4	3	4876.5119	0.0061
12	1	12	11	1	11	4926.5501	0.0104
12	0	12	11	0	11	4926.5501	-0.0104
12	0	12	11	1	11	4926.5501	0.0213
12	1	12	11	0	11	4926.5501	-0.0213
11	2	9	10	3	8	4940.9606	0.0061
8	1	7	7	0	7	4950.6290	0.0093
8	3	6	7	2	6	4952.9287	-0.0029
11	2	9	10	2	8	5008.7187	-0.0041
11	3	9	10	2	8	5040.7699	0.0011
8	4	5	7	3	5	5070.2026	-0.0017
12	1	11	11	2	10	5153.8979	-0.0014
12	2	11	11	2	10	5154.5257	0.0011
12	1	11	11	1	10	5155.5302	0.0051
12	2	11	11	1	10	5156.1486	-0.0018
8	4	4	7	3	5	5192.2833	0.0038
9	3	6	8	2	6	5220.9473	-0.0018
7	6	1	6	5	1	5230.8816	-0.0194
7	6	2	6	5	2	5231.2803	0.0182
8	5	4	7	4	3	5302.5675	0.0000

9	4	5	8	3	5	5308.2982	-0.0015
9	4	5	8	4	6	5308.3000	0.0003
8	5	3	7	4	3	5312.5527	-0.0151
11	5	6	10	5	5	5323.6697	0.0043
13	1	13	12	1	12	5327.5816	0.0000
13	0	13	12	0	12	5327.5816	-0.0072
13	0	13	12	1	12	5327.5816	0.0037
13	1	13	12	0	12	5327.5816	-0.0109
8	5	4	7	4	4	5348.5869	-0.0036
8	5	3	7	4	4	5358.5935	0.0027
12	2	10	11	3	9	5366.0132	0.0037
12	3	10	11	3	9	5380.2887	-0.0212
12	2	10	11	2	9	5398.0529	-0.0026
12	3	10	11	2	9	5412.3631	0.0072
9	2	7	8	1	7	5441.8900	-0.0096
9	3	7	8	2	7	5550.8960	-0.0087
13	1	12	12	2	11	5555.3392	-0.0146
13	2	12	12	2	11	5555.5914	0.0024
13	2	12	12	1	11	5556.2169	0.0027
12	4	9	11	4	8	5574.8178	-0.0005
7	7	0	6	6	0	5588.1431	0.0060
7	7	1	6	6	1	5588.1431	0.0021
9	4	6	8	3	6	5604.4585	0.0011
8	6	2	7	5	2	5695.4696	0.0018
8	6	3	7	5	3	5697.4991	-0.0123
9	5	5	8	4	4	5707.0595	0.0024
14	1	14	13	1	13	5728.6165	-0.0040
14	0	14	13	0	13	5728.6165	-0.0065
14	0	14	13	1	13	5728.6165	-0.0028
14	1	14	13	0	13	5728.6165	-0.0077
9	5	4	8	4	4	5739.5981	0.0073
13	2	11	12	3	10	5777.9928	0.0011
13	3	11	12	3	10	5784.1047	0.0030
13	2	11	12	2	10	5792.2970	0.0049
10	4	6	9	4	7	5795.8506	-0.0053
10	4	6	9	3	6	5795.8506	-0.0053
13	3	11	12	2	10	5798.4013	-0.0008
9	5	5	8	4	5	5829.1402	0.0079
9	5	4	8	4	5	5861.6595	-0.0065
10	3	7	9	2	7	5864.3454	-0.0059
14	1	13	13	2	12	5956.4566	-0.0040
14	1	13	13	1	12	5956.6826	-0.0131
14	2	13	13	1	12	5956.7650	-0.0175
13	4	10	12	4	9	5996.2574	-0.0078
8	7	1	7	5	1	6055.0446	-0.0313
8	7	2	7	6	2	6055.0447	-0.0243
10	5	6	9	4	5	6060.1032	0.0009
10	2	8	9	1	8	6105.8178	0.0159
10	5	5	9	4	5	6147.5912	0.0035
13	4	10	12	3	9	6150.4398	0.0181
9	6	3	8	5	3	6155.2266	0.0069
9	6	4	8	5	4	6163.3981	0.0035
10	3	8	9	2	8	6163.5254	-0.0042
10	4	7	9	3	7	6163.5254	-0.0028
14	3	12	13	3	11	6186.0431	-0.0033
14	2	12	13	2	11	6189.6234	-0.0097
14	3	12	13	2	11	6192.1762	0.0199
11	4	7	10	4	8	6342.6301	0.0091
11	4	7	10	3	7	6342.6301	0.0091
15	1	14	14	1	13	6357.5257	-0.0107
15	2	14	14	2	13	6357.5257	0.0445
15	1	14	14	2	13	6357.5257	0.0761
15	2	14	14	1	13	6357.5257	-0.0423
14	3	11	13	4	10	6370.4821	0.0048
14	4	11	13	4	10	6409.0337	0.0101

10	5	5	9	4	6	6411.6458	-0.0002
8	8	0	7	7	0	6411.9131	0.0034
8	8	1	7	7	1	6411.9131	0.0030
14	4	11	13	3	10	6488.8413	-0.0035
9	7	2	8	6	2	6520.9167	-0.0161
9	7	3	8	6	3	6521.2761	0.0189
16	1	16	15	1	15	6530.6857	-0.0069
16	0	16	15	1	15	6530.6857	-0.0068
16	1	16	15	0	15	6530.6857	-0.0073
16	0	16	15	0	15	6530.6857	-0.0072
11	3	8	10	2	8	6541.7970	0.0020
11	5	6	10	4	6	6556.1915	-0.0047
15	2	13	14	3	12	6586.1375	0.0071
15	3	13	14	3	12	6587.1454	0.0013
15	2	13	14	2	12	6588.6577	0.0041
15	3	13	14	2	12	6589.6604	-0.0070
10	6	4	9	5	4	6604.9122	-0.0019
12	5	8	11	4	7	6609.8306	0.0072
10	6	5	9	5	5	6630.5111	0.0030
11	4	8	10	3	8	6745.9426	-0.0054
11	2	9	10	1	9	6757.5849	0.0000
16	1	15	15	1	14	6758.4254	-0.0133
16	2	15	15	2	14	6758.4254	0.0069
16	1	15	15	2	14	6758.4254	0.0183
16	2	15	15	1	14	6758.4254	-0.0246
11	3	9	10	2	9	6785.5340	0.0152
15	3	12	14	4	11	6798.1795	-0.0020
15	4	12	14	3	11	6854.3798	-0.0135
9	8	1	8	6	1	6878.9098	-0.0041
9	8	2	8	7	2	6878.9098	-0.0032
17	1	17	16	1	16	6931.7318	0.0069
17	0	17	16	0	16	6931.7318	0.0068
17	0	17	16	1	16	6931.7318	0.0069
17	1	17	16	0	16	6931.7318	0.0067
10	7	3	9	6	3	6984.7669	0.0013
10	7	4	9	6	4	6986.2938	-0.0003
16	2	14	15	3	13	6987.4937	-0.0232
16	3	14	15	3	13	6987.9117	-0.0033
16	2	14	15	2	13	6988.5431	0.0124
16	3	14	15	2	13	6988.9266	-0.0022
11	6	6	10	5	6	7102.3214	-0.0178
17	1	16	16	1	15	7159.3705	-0.0031
17	2	16	16	2	15	7159.3705	0.0042
17	1	16	16	2	15	7159.3705	0.0083
17	2	16	16	1	15	7159.3705	-0.0071
16	4	13	15	4	12	7219.1165	-0.0059
12	3	9	11	2	9	7225.6686	0.0133
9	9	0	8	8	0	7235.6708	0.0016
9	9	1	8	8	1	7235.6708	0.0015
16	4	13	15	3	12	7236.7900	0.0020
18	1	18	17	1	17	7332.7537	-0.0003
18	0	18	17	0	17	7332.7537	-0.0003
18	0	18	17	1	17	7332.7537	-0.0003
18	1	18	17	0	17	7332.7537	-0.0003
10	8	2	9	7	2	7345.3037	0.0195
10	8	3	9	7	3	7345.3037	-0.0273
12	4	9	11	3	9	7347.7548	-0.0110
11	7	4	10	6	4	7444.4687	-0.0004
12	6	6	11	5	6	7445.1610	-0.0110
11	7	5	10	6	5	7450.1261	0.0012
18	1	17	17	1	16	7560.3279	0.0011
18	2	17	17	2	16	7560.3279	0.0037
18	1	17	17	2	16	7560.3279	0.0051
18	2	17	17	1	16	7560.3279	-0.0003
10	9	1	9	8	1	7702.7152	-0.0075

Appendix VIII

10	9	2	9	8	2	7702.7152	-0.0082
11	8	3	10	7	3	7810.4967	0.0274
11	8	4	10	7	4	7810.7388	0.0171
19	1	18	18	2	17	7961.2927	0.0034
19	2	18	18	1	17	7961.2927	0.0015

Table S11.5. Measured frequencies and residuals (in MHz) for the rotational transitions of the conformer **12** of helvetolide.

J'	K'_{-1}	K'_{+1}	J''	K''_{-1}	K''_{+1}	V _{obs}	V _{obs} - V _{calc}
6	1	6	5	1	5	2610.3219	0.0076
6	0	6	5	0	5	2611.4111	-0.0156
6	2	5	5	2	4	2817.5963	0.0023
4	4	0	3	3	0	2837.1105	-0.0012
4	4	1	3	3	1	2843.6641	0.0006
6	1	5	5	1	4	2844.6667	-0.0130
7	1	7	6	1	6	3027.6502	-0.0052
7	0	7	6	0	6	3027.9463	-0.0036
6	2	4	5	2	3	3090.7716	0.0044
6	3	3	5	3	2	3168.6116	-0.0010
7	2	6	6	2	5	3241.9740	0.0077
7	1	6	6	1	5	3252.1128	-0.0048
5	4	1	4	3	1	3320.2336	-0.0018
5	4	2	4	3	2	3356.6111	-0.0057
8	1	8	7	1	7	3444.7620	0.0268
8	0	8	7	0	7	3444.7620	-0.0473
7	2	5	6	2	4	3512.0081	-0.0002
5	5	0	4	4	0	3579.9409	0.0021
8	2	7	7	2	6	3661.5522	0.0023
8	1	7	7	1	6	3664.8532	0.0082
7	3	4	6	3	3	3692.6566	-0.0181
6	4	2	5	3	2	3790.0382	-0.0062
6	4	3	5	3	3	3887.4937	-0.0044
8	2	6	7	2	5	3910.4609	0.0016
6	5	1	5	4	1	4073.2088	0.0004
9	2	8	8	2	7	4079.2420	0.0076
9	1	8	8	1	7	4080.2121	-0.0009
8	3	5	7	3	4	4166.3041	0.0096
7	4	3	6	3	3	4276.9368	0.0015
10	1	10	9	1	9	4278.7544	0.0023
10	0	10	9	0	9	4278.7544	-0.0020
9	2	7	8	2	6	4311.6087	0.0054
6	6	0	5	5	0	4320.7946	0.0028
10	2	9	9	2	8	4496.3076	-0.0019
10	1	9	9	1	8	4496.5708	-0.0122
7	5	2	6	4	2	4549.8581	-0.0120
9	3	6	8	3	5	4587.5082	0.0207
11	1	11	10	1	10	4695.7558	0.0030
11	0	11	10	0	10	4695.7558	0.0020
10	2	8	9	2	7	4720.5269	0.0084
8	4	4	7	3	4	4812.5800	0.0048
7	6	1	6	5	1	4818.7419	-0.0060
7	6	2	6	5	2	4822.0601	-0.0100
11	1	10	10	1	9	4913.2712	-0.0358
11	2	10	10	2	9	4913.2712	0.0373
10	3	7	9	3	6	4980.3361	-0.0144
7	7	0	6	6	0	5061.0945	-0.0076
12	1	12	11	1	11	5112.7589	0.0051
12	0	12	11	0	11	5112.7589	0.0049
8	5	4	7	4	4	5125.8604	0.0076
11	2	9	10	2	8	5134.0197	0.0159
8	6	2	7	5	2	5308.1852	0.0139
12	1	11	11	1	10	5330.1430	-0.0178
12	2	11	11	2	10	5330.1430	0.0011
11	3	8	10	3	7	5374.5586	-0.0045
9	4	5	8	3	5	5410.0449	0.0023
9	5	4	8	4	4	5483.6518	-0.0015
13	1	13	12	1	12	5529.7553	0.0008
13	0	13	12	0	12	5529.7553	0.0008
12	2	10	11	2	9	5549.4665	0.0101

Appendix VIII

8	7	1	7	6	1	5560.6348	0.0095
8	7	2	7	6	2	5561.4131	-0.0094
9	5	5	8	4	5	5677.7778	-0.0027
13	1	12	12	1	11	5747.0662	-0.0022
13	2	12	12	2	11	5747.0662	0.0026
12	3	9	11	3	8	5778.7280	0.0027
9	6	3	8	5	3	5778.9786	0.0050
8	8	0	7	7	0	5801.2777	0.0011
8	8	1	7	7	1	5801.2777	-0.0116
9	6	4	8	5	4	5835.2372	0.0122
14	1	14	13	1	13	5946.7599	0.0057
14	0	14	13	0	13	5946.7599	0.0057
13	2	11	12	2	10	5965.6727	-0.0163
10	5	5	9	4	5	6007.5889	-0.0132
9	7	2	8	6	2	6056.3914	0.0027
9	7	3	8	6	3	6061.3078	-0.0038
10	4	6	9	3	6	6066.3946	-0.0077
14	1	13	13	1	12	6163.9981	-0.0039
14	2	13	13	2	12	6163.9981	-0.0027
13	3	10	12	3	9	6189.6234	0.0068
10	6	4	9	5	4	6230.2682	0.0100
15	1	15	14	1	14	6363.7587	0.0064
15	0	15	14	0	14	6363.7587	0.0064
10	7	4	9	6	4	6562.6682	-0.0014
15	1	14	14	1	13	6580.9494	-0.0006
15	2	14	14	2	13	6580.9494	-0.0004
11	6	5	10	5	5	6691.0930	0.0063
11	4	7	10	3	7	6752.1704	0.0005
16	1	16	15	1	15	6780.7540	0.0057
16	0	16	15	0	15	6780.7540	0.0057
15	2	13	14	2	12	6798.9239	-0.0168
16	1	15	15	1	14	6997.9011	-0.0054
16	2	15	15	2	14	6997.9011	-0.0054
17	1	17	16	1	16	7197.7540	0.0123
17	0	17	16	0	16	7197.7540	0.0123
12	6	6	11	5	6	7202.3918	0.0030
16	2	14	15	2	13	7215.7115	-0.0072
12	4	8	11	3	8	7431.6538	0.0073
18	1	17	17	1	16	7831.8251	-0.0067
18	2	17	17	2	16	7831.8251	-0.0067

Table S11.6. Measured frequencies and residuals (in MHz) for the rotational transitions of the conformer **19** of helvetolide.

J'	K'_{-1}	K'_{+1}	J''	K''_{-1}	K''_{+1}	V _{obs}	V _{obs} - V _{calc}
6	1	6	5	0	5	2339.6722	-0.0084
6	0	6	5	1	5	2339.6722	0.0004
7	1	7	6	0	6	2706.8374	-0.0013
7	0	7	6	1	6	2706.8374	-0.0005
8	1	8	7	0	7	3074.0024	-0.0017
8	0	8	7	1	7	3074.0024	-0.0017
8	1	7	7	2	6	3347.3840	0.0081
8	2	7	7	1	6	3347.3840	-0.0018
9	1	9	8	0	8	3441.1728	0.0015
9	0	9	8	1	8	3441.1728	0.0015
9	1	8	8	2	7	3714.5028	0.0035
9	2	8	8	1	7	3714.5028	0.0026
10	1	10	9	0	9	3808.3381	-0.0009
10	0	10	9	1	9	3808.3381	-0.0009
10	1	9	9	2	8	4081.6415	0.0040
10	2	9	9	1	8	4081.6415	0.0039
11	1	11	10	0	10	4175.5060	-0.0004
11	0	11	10	1	10	4175.5060	-0.0004
11	1	10	10	2	9	4448.7896	0.0044
11	2	10	10	1	9	4448.7896	0.0043
12	1	12	11	0	11	4542.6681	-0.0053
12	0	12	11	1	11	4542.6681	-0.0053
12	1	11	11	2	10	4815.9454	0.0070
12	2	11	11	1	10	4815.9454	0.0070
13	1	13	12	0	12	4909.8397	0.0002
13	0	13	12	1	12	4909.8397	0.0002
12	2	10	11	3	9	5089.3830	-0.0006
13	1	12	12	2	11	5183.0893	-0.0053
13	2	12	12	1	11	5183.0893	-0.0053
14	1	14	13	0	13	5277.0170	0.0123
14	0	14	13	1	13	5277.0170	0.0123
13	3	11	12	2	10	5456.4843	-0.0070
14	1	13	13	2	12	5550.2476	-0.0047
14	2	13	13	1	12	5550.2476	-0.0047
15	1	15	14	0	14	5644.1654	-0.0035
15	0	15	14	1	14	5644.1654	-0.0035
14	2	12	13	3	11	5823.6141	-0.0001
14	3	12	13	2	11	5823.6141	-0.0001
15	1	14	14	2	13	5917.4116	0.0008
15	2	14	14	1	13	5917.4116	0.0008
16	1	16	15	0	15	6011.3305	-0.0013
16	0	16	15	1	15	6011.3305	-0.0013
15	2	13	14	3	12	6190.7534	0.0067
15	3	13	14	2	12	6190.7534	0.0067
16	1	15	15	2	14	6284.5630	-0.0062
16	2	15	15	1	14	6284.5630	-0.0062
17	1	17	16	0	16	6378.4821	-0.0112
17	0	17	16	1	16	6378.4821	-0.0112
16	2	14	15	3	13	6557.8803	-0.0051
16	3	14	15	2	13	6557.8803	-0.0051
17	1	16	16	2	15	6651.7334	0.0062
17	2	16	16	1	15	6651.7334	0.0062
18	1	18	17	0	17	6745.6632	0.0097
18	0	18	17	1	17	6745.6632	0.0097

